http://researchcommons.waikato.ac.nz/

Research Commons at the University of Waikato

Copyright Statement:

The digital copy of this thesis is protected by the Copyright Act 1994 (New Zealand).

The thesis may be consulted by you, provided you comply with the provisions of the Act and the following conditions of use:

- Any use you make of these documents or images must be for research or private study purposes only, and you may not make them available to any other person.
- Authors control the copyright of their thesis. You will recognise the author's right to be identified as the author of the thesis, and due acknowledgement will be made to the author where appropriate.
- You will obtain the author's permission before publishing any material from the thesis.

Calcium Phosphate Precipitation from Whey Permeate

A thesis
submitted in partial fulfilment
of the requirements for the degree
of
Doctor of Philosophy in Chemistry
at
The University of Waikato
by

NATALIA N. PANOVA

The University of Waikato
Te Whare Wānanga o Waikato

2001

ABSTRACT

Currently the New Zealand Dairy Industry manufactures a very successful milk calcium product known as ALAMIN™ by the precipitation of calcium phosphates (CaP) from various heated whey permeate streams. The main scientific *objective* of the study described in this thesis was to seek a detailed insight into the fundamental chemistry of the calcium phosphate precipitation process from whey permeates.

To achieve this scientific objective, the project involved the use of a combination of the theoretical, computer-based speciation calculations, experimental bench-scale calcium phosphate precipitation and application of a large suite of chemical, spectroscopic and microscopic instrumental techniques for analysing the as received whey permeates and commercial ALAMIN™ samples, as well as products of bench-scale precipitation reactions from whey permeate and laboratory-prepared solutions modelling whey permeate. An extensive literature search of calcium phosphate precipitation was also carried out.

Equilibrium Speciation Calculations which predicted precipitation and ion speciations as a function of pH in a complex ionic medium modelling various whey permeate media were used to investigate the influence of several components, i.e. lactate, citrate, sulphate, Mg^{2+} and Ca:P molar ratio on the extent of precipitation of calcium phosphate solids in the system. The ion speciation program also modelled the effect of seasonal variations in the whey permeate by varying the concentrations of certain components while keeping others constant. In general, the fundamental component influencing yield of calcium phosphate solids in the permeate was found to be the free Ca^{2+} ion, the concentration of which was sensitive to pH, citrate, lactate, and sulfate concentration as well as Ca:P molar ratio.

To provide an experimental dimension to these ion speciation studies, a simulated lactic whey ultrafiltrate (SLWUF) buffer which mimicked lactic whey permeate was developed and its precipitation chemistry studied under pH-stat control at pH 6.8 and 25°C. In conjunction with the pH-stat studies, Ca ISE studies were also undertaken to provide

additional scientific data on the systems. In general, the experimental work effectively confirmed most of the trends predicted by the ion speciation calculations with regard to the effects on free calcium ion by other components in the simulated buffer. The most important finding on the chemistry of calcium phosphate precipitation from the simulated lactic whey ultrafiltrate buffer was that the precipitation product proceeds via the well documented *phase transformation process* from an initially amorphous structurally ill-defined solid through to the final microcrystalline non-stoichiometric hydroxyapatite.

Bench-scale precipitation work which incorporated laser light scattering analysis, Ca ISE, FTIR, TEM and ICP-OES/AAS analysis executed on the actual whey permeates effectively proved that calcium phosphate precipitation from the (heated) whey permeate exhibited a similar phase transformation chemistry to that observed with the simulated lactic whey ultrafiltrate (SLWUF) buffer. Agitation rate data and laser light scattering of precipitation from lactic whey permeates coupled with a Log-Normal distribution analysis of the Malvern (*Mastersizer*) particle size data revealed an increase of aggregation with time and with increases in agitation rate. The Log-Normal analysis suggested that 2-3 distinct particle populations were present throughout the precipitation reaction. Other characterisation work on the commercial ALAMIN^{TM} solids proved that it was a poorly crystalline insoluble non-stoichiometric hydroxyapatite material which co-deposits with a small amount of citrate and protein. This agrees with the precipitation work conducted on precipitates from SLWUF buffers which also show co-deposition with citrate. An additional finding was that lactic whey permeates exhibited less buffering capacity than sulfuric acid whey permeates due to the presence of higher concentrations of citrate in the latter. Concerns about inclusions of calcium sulfate solid phases in the commercial sulfuric acid whey-derived ALAMIN^{TM} were found to be unnecessary due to the experimental confirmation that these phases were not present to any great extent in the final product, a fact backed up by theoretical speciation calculations and ICP-OES analysis.

In general, this study illustrates the successful application of both theoretical speciation calculations and experimental work to make sense of the chemistry occurring in a naturally complex system which is potentially of great value to the New Zealand Dairy Industry.

ACKNOWLEDGMENTS

I would like to express my sincere appreciation and gratitude to my Chief Supervisor, Dr. Michael R. Mucalo for his continued guidance and tremendous support over the last three years and also to my Co-Supervisor Professor Brian K. Nicholson (The University of Waikato) for the constant support and attention to the GRIF related progress.

I am also grateful to Dr. Kevin Pearce of New Zealand Dairy Research Institute for the advice on computer speciation calculations, designed to lactic whey permeate systems and also for recommendations on treatment of experimental Malvern (*Mastersizer*) data by Log-Normal distribution analyses, for the analyses of Ca-electrode measurement data and for discussion on the mechanism of particle flocculation as a function of agitation rate.

The Foundation for Research, Science and Technology is also gratefully acknowledged for financial assistance in the form of a GRIF.

I am also very grateful to Dr. Andrew (Buck) Rogers of New Zealand Dairy Research Institute for the discussion of results and assistance in the pH-stat experimental work on calcium phosphate precipitation from Simulated Lactic Whey Ultrafiltrate (SLWUF) buffer solutions.

Dr. Motekaitis (Texas A&M University) is thanked for the supply of the SPEXY-C computer program used for calculating speciation plots.

For information relating to ALAMIN™ specifications, I would like to thank Heather Lukin of the New Zealand Dairy Board.

Dr. Skelte Anema of New Zealand Dairy Research Institute is thanked for the provision of research results on the measurement of zeta potentials. I would also like to express my appreciation to Dr. Steve Haylock of New Zealand Dairy Research Institute for information coming out of the Calcium Platform Reviews.

Personal thanks must also go to Mr. Neil Gatland of Whey Products (NZ), Dr. Richard Archer, Mr. Steve Smith and Mr. Conrad Heron of Kiwi Co-operative Dairies Ltd for information relating to the manufacture of ALAMIN™.

The staff at Anchor Products Edgecumbe, in particular, Rachel Mc Cormack, Hana Weka and Palatasa Havea are also warmly acknowledged for the provision of valuable analysis data relating to the sulfuric acid whey permeate and washed and unwashed ALAMIN™ cake and commercial ALAMIN™ powder.

I would also like to thank Katrina Roberts of New Zealand Dairy Research Institute for the discussion of the bench-scale optimisation of ALAMIN™ precipitation conditions.

The University of Waikato Chemistry Department and main library staff are also acknowledged for space and facilities provided as well as the provision of the numerous interloans required to complete the literature review.

I am also grateful to Catherine Hobbis of the University of Auckland Chemistry Department (XPS), Dave Wild and Alf Harris of the Waikato Microscope Unit at MIRINZ Food Technology and Research as well as NZDRI staff in Palmerston North (TEM, SEM/EDX, LSCM), Kay Card at Industrial Research Ltd, Lower Hutt (further EDX work), Yuanji Zhang, Department of Technology, University of Waikato (XRD), Dr. Nick Kim, University of Waikato Chemistry Department (AAS), Jannine Sims, University of Waikato Chemistry Department (FTIR), Wendy Jackson, University of Waikato Chemistry Department (ESMS), Helen Turner and Steve Cooke, University of Waikato Earth Sciences Department (Malvern *Mastersizer*).

Personal thanks also go to Brett Loper for his assistance with computer issues, Craig R. Bullen for his discussions on Transmission (TEM) and Scanning Electron Microscopy (SEM) images and to David Foster and Reece Harrison for their discussions on ICP-OES elemental analyses, applied to lactic whey permeates and sera.

CONTENTS

Abstract ii
Acknowledgments iv
Contents vi
List of Figures xiv
List of Tables xxiii
List of Abbreviations xxvi

CHAPTER 1: GENERAL AND BACKGROUND INFORMATION

1.1 The Interest in Calcium Phosphate in the New Zealand Dairy Industry 1
1.2 Production of Calcium Phosphate in the New Zealand Dairy Industry 2
1.2.1 Production of Lactic and Mineral Acid Whey (Prior to Ultrafiltration) 2
1.2.1(a) Lactic Casein Wheys 2
1.2.1(b) Mineral Acid Wheys 3
1.2.2 Typical Composition of Whey and the Process of Ultrafiltration 4
1.3 A Summary of the Precipitation of Calcium Phosphate from Ultrafiltered Whey Permeates in New Zealand Dairy Industry 7
1.4 Purpose and Objectives 9

CHAPTER 2: LITERATURE REVIEW OF THE CHEMISTRY OF CALCIUM PHOSPHATE AND ITS PRECIPITATION FROM AQUEOUS SOLUTION

2.1 Introduction 11
2.2 Composition of Calcium Phosphate Compounds 11
2.3 A General Word on Calcium Phosphate Phases: Apatitic versus Non-Apatitic 13
2.4 Descriptions of discrete Calcium Phosphate Phases of relevance to ALAMIN™ 13
2.4.1 Hydroxyapatite: $Ca_{10}(PO_4)_6(OH)_2$ 13
2.4.2 Tricalcium Phosphate: $Ca_3(PO_4)_2$ 15
2.4.3 Octacalcium Phosphate: $Ca_8H_2(PO_4)_6.5H_2O$ 15
2.4.4 Brushite (DCPD): $CaHPO_4.2H_2O$ and Monetite (DCPA): $CaHPO_4$ 17
2.4.5 Amorphous Calcium Phosphate (ACP) 18

2.5 Nature of Calcium Phosphate in Milk 19

2.6 Introduction to Calcium Phosphate Precipitation from Aqueous Solution 23

2.7 General Tends observed in the Precipitation of Calcium Phosphate 24

2.7.1 Cornerstone Study by Eanes et al. 24

2.7.2 Further Studies by Eanes et al. with Microscopic Evidence of the Intermediate Calcium Phosphate Phases 25

2.7.2(a) Freshly Precipitated Solid 26

2.7.2(b) Solids left to Mature or "Age" 26

2.8 Introduction to Various Concepts and Terminology associated with Calcium Phosphate Compounds and their Precipitation from Aqueous Solutions 27

2.9 Supersaturation and Solubility Products of Sparingly Soluble Salts 27

2.9.1 Solubility Products 27

2.9.2 Definition of Supersaturation 28

2.9.3 A General Word on Nucleation 28

2.9.4 Thermodynamics and Seeded versus Unseeded Nucleation 29

2.10 Solubilities and Supersaturation in Ca^{2+}- and Inorganic Phosphate-Containing Solutions 29

2.10.1 Ion Products and K_{sp} values of the Various Calcium Phosphate Phases 29

2.10.2 Phase Transformations and Ostwald's Law of Stages in Precipitating Calcium Phosphate Suspensions 30

2.11 Influences on the Chemistry of Calcium Phosphate Precipitation from Aqueous Solution 31

2.12 Effect of pH and Temperature 31

2.12.1 Study by van Kemenade et al. 31

2.12.1(a) Solubility Isotherms for the Calcium Phosphate Phases 31

2.12.1(b) Hydroxide Uptake as a Function of Time 34

2.12.2 High pH versus Low pH Precipitation 36

2.12.3 Thermodynamic Analysis of the Transitional Phases in the Precipitation of Calcium Phosphate 37

2.12.4 Effect of Temperature 39

2.13 Effect of Supersaturation 39

2.13.1 Introduction 39

2.13.2 General Trends and Definitions of Terms 40

2.13.3 Experiments at "High" Supersaturation 41

2.13.4 Experiments at "Low" Supersaturation 42

2.13.5 Summary of the "High" and "Low" Supersaturation Limits which define whether or not ACP forms as an Intermediate Phase 43

2.14 Influence of Ionic Strength 45

2.14.1 Formal Definition of Ionic Strength 45

2.14.2 Ionic Strength and its Effect on Calcium Phosphate Precipitation 46

2.14.3 Effect of Different Alkali Metal Cations 47

2.15 Influence of Seeding 48

2.15.1 Homogeneous versus Heterogeneous Nucleation 48

2.15.2 Experiments involving the Seeded Growth of Calcium Phosphate from the Literature 48

2.15.3 Effect of Seed Characteristics on Calcium Phosphate Precipitation 49

2.16 Influence of Additives and Impurities 51

2.16.1 Categorisation of the Effects that Additives and Impurities may have on Calcium Phosphate Precipitates and the Precipitation Reaction 51

2.16.2 The First Effect: Effects of Substitutions of Hydroxyapatite Lattice Ions (Ca^{2+}, PO_4^{3-}, OH^-) for other Cations or Anions 52

2.16.2(a) Carbonate (CO_3^{2-}) 52

2.16.2(b) Other Anions 53

2.16.2(c) Cations 54

2.16.3 The Second Effect: Effects of Impurities and Additives on the Precipitation Reaction of Calcium Phosphate 54

2.16.3(a) Effect of Biological Macromolecules 54

2.16.3(b) Effect of Dietary Fibre Substances 56

2.16.3(c) Effect of Citric, Acetic and Lactic Acids 56

2.16.3(d) Effect of Casein 58

2.16.3(e) Effect of Magnesium Ion 60

2.17 Ion Speciation in the Whey Permeate and the Need for Simulated Milk Ultrafiltrate (SMUF) Buffers 61

2.17.1 Ionic Components present in Milk and Lactic Casein Whey Permeate 61

2.17.2 Calculation of the Ion Speciation in Complex Ionic Solutions 62

2.17.3 The Relevant Ion Species in Whey UF-Permeate and their Quantification: The SPE Program 64

2.17.4 The Need for Simulated Ultrafiltrate Permeate Solutions as an Experimental Model for the Real Whey Permeate System 65

2.18 Solid State Interconversions of Calcium Phosphate Compounds 66

CHAPTER 3: TECHNIQUES FOR STUDYING ALAMIN™ AND WHEY PERMEATES

3.1 X-ray Diffraction (XRD) 67

3.2 Scanning Electron Microscopy/Energy Dispersive X-ray Analysis (SEM/EDX) Aspects 68

3.3 Transmission Electron Microscopy (TEM) 69

3.4 Fourier Transform Infrared Spectroscopy (FTIR) 70

3.5 X-ray Photoelectron Spectroscopy (XPS) 70

3.6 Light Scattering Methods for Determination of Particle Sizes 72

3.7 Electrospray Mass Spectrometry (ESMS) 73

3.8 Atomic Absorption Spectroscopy (AAS) 75

3.9 Inductively Coupled Plasma (Optical Emission/ Mass) Spectroscopy (ICP-OES/MS) 75

3.10 pH-Stat Method 76

3.11 Calcium Ion-Selective Electrode (ISE) Measurements 77

CHAPTER 4: INVESTIGATION OF SIMULATED LACTIC WHEY ULTRAFILTRATE (SLWUF) BUFFERS AS A MODEL FOR NATURAL WHEY PERMEATES

4.1 Computer Speciation Calculations 78

4.1.1 Algorithm employed for performing the Computer Speciation Calculations 79

4.1.2 Ion Speciation and Chemical Equilibria occurring in the Multicomponent Systems 79

4.1.3 Corrections to the K values for Ionic Strength 81

4.1.4 Basic Introduction to the Thermodynamics of Precipitation (and Dissolution) of Sparingly Soluble Salts from Supersaturated Solutions 82

4.2 The Use of SPE to Model Precipitation from SLWUF Buffers 83

4.2.1 Construction of the Input File 83

4.2.2 Results and Discussion 85

4.2.2(a) Ion/Molecular Speciation and Solid Formation 85

4.2.2(b) Impact of varying Ca:P Molar Ratios on the Precipitation of Calcium Phosphate from the SLWUF Buffer 90

4.2.2(c) Impact of varying Citrate Concentration on the Precipitation of Calcium Phosphate from the SLWUF Buffer 91

4.2.2(d) Impact of Magnesium Concentrationon the Precipitation of Calcium Phosphate from the SLWUF Buffer 93

4.3 pH-Stat Controlled Experimental Work for Confirmation of Trends predicted by Computer Speciation Calculations 95

4.3.1 Preparation of SLWUF Buffers 95

4.3.2 Precipitation of Solids from the SLWUF Buffers under pH-stat Control 98

4.3.2(a) Experimental 98

4.3.2(b) Results: Hydroxide Uptake as a Function of Time 100

4.3.3 Influence of the Different Ca:P Molar Ratios in the SLWUF Buffer 101

4.3.4 Influence of Citrate Concentration in the SLWUF Buffer 102

4.3.5 Influence of Magnesium Concentration in the SLWUF Buffer 103

4.3.6 Influence of pH in the SLWUF Buffer 105

4.4 Determination of Free Reactive Calcium Ion in the SLWUF Filtrates using a Calcium Ion-Selective Electrode (ISE) 106

4.4.1 Calcium Ion-Selective Electrode Calibration 107

4.4.2. Calcium Ion-Selective Electrode (ISE) Measurements 109

4.4.2(a) Free Calcium Concentration as a Function of Time during the Precipitation under pH-stat controlled Conditions 109

4.4.2(b) Influence of Phosphate Level in the SLWUF Buffer as a Function of pH, set-up for CaP Precipitation under pH-stat controlled Conditions 111

4.4.2(c) Influence of Citrate Level in the SLWUF Buffers 112

4.5 Fourier Transform Infrared Spectroscopy (FTIR) Analyses of the CaP Precipitates, obtained from SLWUF Buffers 113

4.6 Scanning Electron Microscopy (SEM) 123

CHAPTER 5: CHEMICAL SPECIATION CALCULATIONS OF THE PRECIPITATION OF CALCIUM PHOSPHATE USING CONCENTRATION DATA FROM THE COMMERCIAL PROCESS

5.1 Computer Speciation Calculations of the Precipitation of Calcium Phosphate using Concentration Data for a Commercial Lactic Whey Permeate 129

5.1.1 Construction of the Input File 129

5.1.2 Results and Discussion 131

5.1.2(a) Speciation Plots of dissolved Molecular and Ionic Species 131

5.1.2(b) Solid Phases predicted to form in a Lactic Whey Permeate, as calculated by SPE 134

5.1.2(c) Influence of varying Ca:P Molar Ratios on the Precipitation of Calcium Phosphate, as calculated by SPE 135

5.1.2(d) Influence of varying Citrate Concentration on the Precipitation of Calcium Phosphate, as calculated by SPE 138

5.1.2(e) Titration Curve Calculations 140

5.2 Computer Speciation Calculations of the Precipitation of Calcium Phosphate using Concentration Data for a Commercial Sulfuric Acid Whey Permeate 143

5.2.1 Previous Experimental Work on Systems involving Precipitation of Calcium Sulfate 143

5.2.2 Construction of the Input File 144

5.2.3 Results and Discussion 148

5.2.3(a) Ion and Molecular Speciation 148

5.2.3(b) Solids Formation, as calculated by SPE 153

5.2.3(c) Titration Curve Calculations 157

5.2.3(d) Impact of varying Citrate Concentration on the Precipitation of Calcium Phosphate 159

5.2.3(e) Impact of varying Ca:P Molar Ratios on the Precipitation of Calcium Phosphate 166

5.2.3(f) Impact of varying Sulfate Concentration on the Precipitation of Calcium Phosphate 170

CHAPTER 6: CHARACTERISATION OF WHEY PERMEATE AND ALAMIN™ POWDER FROM VARIOUS SOURCES

6.1 Characterisation of the Commercial Lactic Whey Permeate and ALAMIN™ Powder by Chemical, Spectroscopic and Microscopic Techniques 173

6.1.1 Atomic Absorption Spectroscopy (AAS) Analysis of Ca Concentration in the Commercial Lactic Whey Permeate 173

6.1.2 Chemical Analysis of the Commercial Lactic Whey Permeate by ICP-OES 175

6.1.3 Electrospray Mass Spectrometric Analysis (ESMS) of the Commercial Lactic Whey Permeate 178

6.1.4 Fourier Transform Infrared Spectroscopy (FTIR) Analyses of the Commercial ALAMIN™ Powder, produced from Lactic Whey Permeate 183

6.1.4(a) Assignment of Peaks in the 500-1200 cm^{-1} Region 183

6.1.4(b) Assignment of other Non-phosphate related Peaks in the 4000-1300 cm^{-1} Region 187

6.1.4(c) FTIR Spectra of the Other Commercial Products of Potential Use as ALAMIN™ Supplements 189

6.1.5 Scanning Electron Microscopy (SEM) and Transmission Electron Microscopy (TEM) of the Commercial ALAMIN™ Powder, produced from Lactic Whey Permeate 191

6.1.5(a) Particle Morphology 193

6.1.5(b) SEM Analysis of Other Commercial Products 197

6.1.5(c) Energy Dispersive X-ray Analysis (EDX) of ALAMIN™ Powder 203

6.1.6 X-Ray Photoelectron Spectroscopy (XPS) of the Commercial ALAMIN™ Powder, produced from Lactic Whey Permeate 205

6.1.7 X-ray Diffraction (XRD) Investigation of ALAMIN™ Powder, produced from Lactic Whey Permeate 210

6.1.7(a) Phase Identification of ALAMIN™ Powder 210

6.1.7(b) Crystallite Sizes of ALAMIN™ Powder 213

6.1.8 Malvern (*Mastersizer*) Determination of Particle Sizes on Various Grades of Commercial ALAMIN™ Powders, produced from Lactic Whey Permeate 215

6.1.9 Differential Scanning Calorimetric Analysis (DSC) of ALAMIN™ Powder 217

6.2 Characterisation of the Commercial Sulfuric Acid Whey Permeate and ALAMIN™ Powder by Chemical, Spectroscopic and Microscopic Techniques 222

6.2.1 Fourier Transform Infrared Spectroscopy (FTIR) Analyses 222

6.2.2 Scanning Electron Microscopy Characterisation of ALAMIN™ Solids, produced from Sulfuric Acid Whey Permeate 229

6.2.3 Chemical Analysis of ALAMIN™ Powders and Cakes by ICP-OES 229

CHAPTER 7: CHEMISTRY OF CALCIUM PHOSPHATE PRECIPITATION FROM WHEY PERMEATES

7.1 Bench-Scale Experimental Investigation of the Precipitation of Calcium Phosphate from Whey Permeates 236

7.1.1 The Precipitation Reaction: Experimental Procedure 236

7.1.2 pH Study of the Precipitation Process from Whey Permeates 239

7.1.2(a) Results of the pH Study of the Precipitation Process from Lactic Whey Permeate 239

7.1.2(b) Results of the pH Study of the Precipitation Process from Sulfuric Acid Whey Permeate 239

7.1.3 Atomic Absorption Spectroscopy (AAS) Study of Ca Concentration in the Whey Permeate Sera obtained after Precipitation of Calcium Phosphate 241

7.1.4 Chemical Analysis of Serum by ICP-OES 243

7.1.5 Fourier Transform Infrared Spectroscopy (FTIR) Analyses of the Precipitated CaP Solids 245

7.1.6 Scanning Electron Microscopy (SEM)/Transmission Electron Microscopy (TEM) Analyses of the Precipitated CaP Solids 247

7.1.6(a) SEM Studies of Calcium Phosphate Precipitates 247

7.1.6(b) TEM Studies of Calcium Phosphate Precipitates 249

7.1.7 Free Ca^{2+} ion Measurements in Reacting Whey Permeates using a Calcium Ion-Selective Electrode (ISE) Method 251

7.1.8 Electrospray Mass Spectrometry of Serum (ESMS) 255

7.1.9 X-ray Diffraction Study of the Precipitated CaP Solids 258

7.2 Aqueous ALAMIN™ Suspension Study 260

7.3 Measurement of Adsorption Isotherms of Whey Proteins on the Surface of Commercially Synthesised (Pure) Hydroxyapatite 268

7.4 Malvern Laser (*Mastersizer*) Determination of the Particle Sizes over the Course of Precipitation Reaction 271

7.4.1 Effect of Agitation Rate on CaP Particle Sizes 272

7.4.1(a) The Influence of Agitation Rate on the Particle of CaP Precipitated from Heated Whey Permeates 273

7.4.1(b) Flocculation Kinetics 273

7.4.1(c) Additional Malvern Particle Size Analyses at more Vigorous Agitation Rates 276

7.4.2 Log-Normal Distribution Analyses of the Particle Size Distributions 280

7.4.2(a) Log-Normal Distribution Analysis 280

7.4.2(b) Log-Normal Analyses of the Experimental Malvern Particle Distribution Curves for Precipitation Experiments conducted with varying Agitation Rates 281

7.4.2(c) Log-Normal Analyses of the Experimental Malvern Particle Distribution Curves in a given Precipitation Experiment as a Function of the Precipitation Time 282

CHAPTER 8: CONCLUSIONS

8.1 Review and Evaluations of Objectives 287

8.2 Recommendations for Further Study 298

REFERENCES 300

APPENDICES 311

REVIEWS, CONFERENCE ABSTRACTS AND PUBLICATIONS ARISING FROM THE WORK 325

LIST OF FIGURES

Figure 1-1: A schematic representation of the ultrafiltration process of whey 6

Figure 1-2: General flow chart of the commercial calcium phosphate precipitation process from lactic and mineral acid whey UF-permeates 7

Figure 2-1: Structure of OCP with superimposed unit cells for OCP and HAP 16

Figure 2-2: Schematic showing where the structural transformation of 2 OCP layers to 4 unit cells of HAP takes place 17

Figure 2-3: Schematic representation of a casein micelle and a submicelle 20

Figure 2-4: Hairy casein micelle model 22

Figure 2-5: Solubility isotherms of HAP, OCP and DCPD at 25°C (solid lines) and 37°C (dotted lines) as log P(total) versus pH 33

Figure 2-6: Typical relaxation curves (from pH- stat experiments) for precipitation of: a) a pure phase forming successively; b) two phases forming successively and c) two phases forming simultaneously over a certain period 35

Figure 2-7: Crystal growth of calcium phosphate in the presence of sodium chloride 47

Figure 2-8: Schematic for the mechanism of the stabilisation of amorphous calcium phosphate by adenosine triphosphate 55

Figure 3-1: Schematic representation of the Malvern Laser Particle Sizer 73

Figure 3-2: Schematic representation of the processes occurring in ESMS 74

Figure 4-1: Flow chart giving the basic outline of the algorithm employed for carrying out the SPE computer speciation calculations 80

Figure 4-2: SPE calculated concentration-pH plot showing the general distribution of the dominant free ions, complex ions and solid species over the pH range 3-9 in the "standard" SLWUF buffer solution 86

Figure 4-3: SPE calculated distribution of the main soluble and insoluble species in the "standard" SLWUF buffer solution at pH=6.8 87

Figure 4-4: SPE calculated distribution of the main soluble and insoluble species in the "standard" SLWUF buffer solution at pH=4.6 88

Figure 4-5: SPE calculated distribution of the $Ca(Lac)^+$ ion species as a function of the citrate concentration (0, 4 and 8 mM) in the SLWUF buffer 88

Figure 4-6: SPE calculated concentration-pH plot showing the pH region over which $CaCit^-$ ion is stable for concentrations of citrate in the SLWUF buffer from 2-8 mM 89

Figure 4-7: Predicted concentration of free calcium ion ($[Ca^{2+}_{(aq)}]$) in the SLWUF buffer for three different Ca: P molar ratios: 1.00, 1.28 and 1.50 90

Figure 4-8: SPE calculated concentration of free calcium ions ($[Ca^{2+}_{(aq)}]$) as a function of the citrate level in the SLWUF buffer solutions for citrate levels varying from 2-8 mM 91

Figure 4-9: Predicted concentration-pH plot showing the impact of varying citrate ion concentration in the SLWUF buffer on solid CaP yield ($Ca_{(S)}=Ca_{[OCP]} + Ca_{[BRUSHITE]}$) for citrate concentrations varying from 0-8 mM 92

Figure 4-10: SPE calculated concentration-pH plot, showing citrate influence on the solid brushite and OCP formation in the SLWUF system 93

Figure 4-11: SPE calculated concentration-pH plot showing the level of free Mg^{2+} ions, $MgCit^-$ ions and $MgHPO_4$ molecules in the "standard" SLWUF buffer solution (Ca:Mg molar ratio=9.7) at pH 3-9 94

Figure 4-12: SPE calculated concentration-pH plot showing the distribution of $MgCit^-$ and $MgHPO_4$ species with a different Ca:Mg ratios (9.7-for "standard" and 3.1 for Mg-enriched SLWUF system) 94

Figure 4-13: A photograph of the computer-controlled pH-stat instrument setup 99

Figure 4-14: The typical relaxation profile curve for precipitation of CaP at T=25°C and pH=6.8 from the "standard" SLWUF buffer solution 100

Figure 4-15: pH-stat relaxation profile curves for the precipitation of CaP at 25°C and pH=6.8 from the SLWUF buffer solutions with a different Ca:P molar ratios 101

Figure 4-16: pH-stat relaxation profile curves for the precipitation of CaP at T=25°C and pH=6.8 from the SLWUF solutions with a different citrate concentration from 0 to 8 mM 103

Figure 4-17: pH-stat relaxation profile curves for the precipitation of CaP at T=25°C and pH=6.8 from the SLWUF buffer solutions with a different Ca:Mg molar ratios 104

Figure 4-18: pH-stat relaxation profile curves for the precipitation of CaP at T=25°C and pH=6.8 from the "standard" SLWUF buffer solutions at different pH 105

Figure 4-19: Typical calibration curve of $Log[Ca^{2+}]$ versus E (mV) axis at T=25°C 108

Figure 4-20: The typical curve of free calcium ion ($[Ca^{2+}_{(aq)}]$) concentration left in the filtrates as a function of time after precipitation was initiated from the "standard" SLWUF buffer solution at T=25°C and pH=6.8 110

Figure 4-21: Concentration of free Ca^{2+} ion as a function of pH for the precipitation of CaP at 25°C for varying levels of total phosphate (24, 28 and 30 mM) in the SLWUF buffer solutions measured by the Ca ISE method 112

Figure 4-22: Concentration of free Ca^{2+} ion as a function of citrate concentration (mM) in the SLWUF buffer solutions at pH=4.6 and T=25°C, measured using the Ca ISE method 113

Figure 4-23: Comparison of the FTIR spectrum of CaP precipitate, collected from the pH-stat precipitation process from the "standard" SLWUF buffer at T=25°C and pH=6.0, with FTIR spectrum of Brushite 115

Figure 4-24: Comparison of the FTIR spectrum of CaP precipitate, collected from the pH-stat precipitation process from the "standard" SLWUF buffer at T=25°C and pH=4.3, with FTIR spectrum of commercial (Fluka) Hydroxyapatite 116

Figure 4-25: Comparison of the FTIR spectrum of CaP precipitate, collected from the pH-stat precipitation process from the "standard" SLWUF buffer at T=25°C and pH=6.8, with FTIR spectrum of Brushite 117

Figure 4-26: FTIR spectra of the CaP precipitates, collected from the pH-stat precipitation process from the "standard" SLWUF buffer at T=25°C and pH=6.8 at different stages of the precipitation process 118

Figure 4-27: Comparison of the FTIR spectra of CaP precipitates, collected from pH-stat precipitation process from the SLWUF buffer (with 2 and 8 mM citrate) at T=25°C and pH=6.0 with FTIR spectrum of Ca_3Cit_2 120

Figure 4-28: The outline of the adsorption of the COO^- groups of Cit^{3-} ion on the (100) face of the hydroxyapatite 121

Figure 4-29: SEM micrographs of the freeze-dried CaP precipitates formed from the "standard" SLWUF buffer solution at T=25°C and pH=6.8: a) amorphous phase (precipitation time 10 min); b) brushite crystals in the amorphous phase (precipitation time 25 min) 124

Figure 4-30: SEM micrographs of the freeze-dried CaP precipitates formed from the "standard" SLWUF buffer at T=25°C and pH=6.8: a) *intermediate stage* (precipitation time 35 min); b) final stage (precipitation time 60 min) 125

Figure 4-31: SEM micrographs of the freeze-dried CaP precipitates formed from the "standard" SLWUF buffer solution at T=25°C and pH=6.0 (precipitation time 40 min) 127

Figure 4-32: SEM micrographs of the freeze-dried CaP precipitates formed from the "standard" SLWUF buffer solution at T=25°C and pH=6.0 (precipitation time 10 min) 128

Figure 5-1: SPE calculated concentration-pH plot showing the general distribution of the dominant free ions, complex ions and solid species over the pH range 2-8 in lactic whey permeate at T=25°C 131

Figure 5-2: SPE calculated concentration-pH plot showing the concentration of lactate-containing species over the pH range 2-10 in lactic whey permeate at T=25°C 132

Figure 5-3: SPE calculated concentration-pH plot showing the distribution of calcium-containing species and CaP solids over the pH 2-12 in lactic whey permeate at T=25°C 133

Figure 5-4: SPE calculated concentration-pH plot showing the distribution of $CaLac^{+}$ species over pH 2-8 at T=25°C at the different lactate level in lactic whey permeate 134

Figure 5-5: SPE calculated concentration-pH plot showing the distribution of free Ca^{2+} ions over the pH 6-7 at T=25°C and at varying Ca:P molar ratios (1:1 -30 mM Ca^{2+} and 30 mM PO_4^{3-}; 1.25:1 -30 mM Ca^{2+} and 24 mM PO_4^{3-}; 1:1.25 -30 mM Ca^{2+} and 37.5 mM PO_4^{3-}) in the lactic whey permeate 136

Figure 5-6: SPE calculated pH-stability regions for the formation of Brushite and OCP phases in the lactic whey permeate for varying Ca:P molar ratios (1.25:1 and 1:1) 137

Figure 5-7: SPE calculated pH-stability regions for the citrate-containing species in the lactic whey permeate system (with 8 mM citrate) 138

Figure 5-8: SPE calculated pH-stability diagram, representing the formation of the OCP in lactic whey permeate system for the citrate concentration varying from 0 to 8 mM 139

Figure 5-9: SPE calculated concentration-pH diagram, representing the impact of varying citrate ion concentration on the CaP yield as ($Ca_{(S)}$=$Ca_{[OCP]}$ + $Ca_{[BRUSHITE]}$) in the lactic whey permeate for citrate concentration from 0 to 8 mM 139

Figure 5-10: SPE calculated titre NaOH-pH curve for a lactic permeate at T=25°C for pH range from 4.6-9.0 141

Figure 5-11: SPE calculated titre NaOH-pH curve for lactic whey permeate at T=25°C for pH 5.0-8.0 for the varying citrate concentration (2 and 8 mM) 142

Figure 5-12: SPE calculated general distribution of the main ion species and solid phases over the pH range 3-8 in sulfuric acid whey permeate 149

Figure 5-13: SPE calculated distribution of the dominant ion and molecular species over the pH range 3-8 in sulfuric acid whey permeate 150

Figure 5-14: SPE calculated: a) an overall distribution and b) Mg-containing species over pH 3-12 in sulfuric acid whey permeate (enlarged scale) 152

Figure 5-15: SPE predicted distribution of the precipitated solid phases over the pH range 2-8 in sulfuric acid whey permeate 155

Figure 5-16: SPE calculated diagram showing the coexistence of 3 phases: 1) Gypsum - 2) Ardealite - 3) Brushite phases over the pH range 2-7 (enlarged scale) 155

Figure 5-17: Comparison of the crystal structure of Gypsum ($CaSO_4.2H_2O$), Brushite ($CaHPO_4.2H_2O$) and Ardealite ($Ca_2HPO_4SO_4.4H_2O$) projected along the c axis 156

Figure 5-18: SPE calculated titre NaOH-pH curve for the sulfuric acid whey permeate 158

Figure 5-19: SPE calculated distribution of: a) calcium-magnesium-citrate containing species and b) titration curve for the sulfuric acid whey permeate 160

Figure 5-20: SPE calculated distribution of calcium-citrate containing species as a function of pH for the sulfuric acid whey permeate 161

Figure 5-21: SPE calculated distribution of calcium citrate solid ($Ca_3Cit_2.6H_2O$) as a function of pH for the sulfuric acid whey permeate 161

Figure 5-22: SPE calculated influence of the citrate concentration on the Brushite (Br) and OCP formation for a series of citrate concentrations from 0 mM to 9 mM in the sulfuric acid whey permeate 163

Figure 5-23: Impact of citric acid on the overall yield in the sulfuric acid whey permeate over the pH range 4.6-9.6 164

Figure 5-24: Impact of the citrate concentration on the Gypsum and Ardealite formation for a series of citrate concentrations from 0 mM to 9 mM over pH 3.6-5.6 164

Figure 5-25: Comparison of the free Ca^{2+} level and solid formation (Gypsum - Ardealite - Brushite and Octacalcium phosphate) for the typical sulfuric acid whey permeate with 7 mM and without citrate 165

Figure 5-26: Impact of citrate concentration (0-9 mM) on the Brushite (Br) and Octacalcium phosphate (OCP) formation 165

Figure 5-27: Distribution of free Ca^{2+} and SO_4^{2-} ions depending on the Ca:P molar ratio from 1.24:1 to 1:1.24 over the pH range 2-8 in the sulfuric acid whey permeate 167

Figure 5-28: The effect of increasing Ca:P molar ratio on levels of free Ca^{2+} ions 168

Figure 5-29: Impact of Ca:P molar ratio (from 1.24:1 to 1:1.24) on Brushite and OCP 168

Figure 5-30: Influence of Ca:P molar ratio on: a) Gypsum and b) Ardealite formation Ca:P molar ratios were varied from 1.24:1 to 1:1.24 169

Figure 5-31: Distribution of ion and solid species depending on Ca:S ratio: a) main species and b) zoomed fragment, showing the formation of Gypsum, Ardealite and Citrate ($Ca_3Cit_2.6H_2O$) as well as molecular $CaSO_4$ and $MgSO_4$ levels 171

Figure 6-1: The AAS calibration plot for the standard solutions with varying Ca^{2+} concentration (0-30 ppm) 174

Figure 6-2: Negative ion mode ESMS spectrum (- 25 V) for the commercial as received lactic whey UF-permeate 179

Figure 6-3: Positive ion mode ESMS spectrum (+ 25 V) for the commercial as received lactic whey UF-permeate 181

Figure 6-4: Expansion of positive ion mode ESMS spectrum (+ 25 V) region from m/z 17 to 25 for the commercial as received lactic whey UF-permeate 182

Figure 6-5: FTIR spectrum of the typical commercial lactic ALAMIN™ powder 184

Figure 6-6: Comparison of the FTIR spectra of commercial lactic ALAMIN™ powder (1) with *Fluka*-brand hydroxyapatite (2): a) region showing "Peak 1" and b) (inset) region showing "Peak 5" 185

Figure 6-7: FTIR spectra of the typical commercial lactic ALAMIN™ powder and different calcium phosphates 186

Figure 6-8: Comparison of the FTIR spectrum of commercial lactic ALAMIN™ powder with FTIR spectra of Ca_3Cit_2 and Na_3Cit 188

Figure 6-9: FTIR spectra of KBr disks of the whey proteins: a) FTIR spectrum of β-lactalbumin and α-lactoglobulin mixture (85 and 9 %) and b) FTIR spectrum of β-lactalbumin and α-lactoglobulin mixture (13 and 69 %) 190

Figure 6-10: FTIR spectra of: a) LACPRODAN and b) LACTOVAL powders 192

Figure 6-11: SEM micrographs of the commercial lactic ALAMIN™ powder: a) typical particle at the magnification x 1 300 and b) at the magnification x 20 000 194

Figure 6-12: SEM micrographs of the commercial lactic ALAMIN™ powder (*finest fraction*): a) typical particle at the magnification x 6 000 and b) at the magnification x 20 000 195

Figure 6-13: SEM micrographs of the commercial lactic ALAMIN™ powder: a) typical particle at the magnification x 6 000 and b) at the magnification x 20 000 196

Figure 6-14: SEM micrographs of *Fluka*-brand HAP powder: a) typical particle at the magnification x 4 500 and b) surface of particle at the magnification x 25 000 198

Figure 6-15: SEM micrographs of *BABI*-brand HAP powder: a) typical particle at the magnification x 3 500 and b) surface of the particle at magnification x 25 000 199

Figure 6-16: TEM micrograph of the cross-section of commercial lactic ALAMIN™ powder (finest fraction) at the magnification x 18 3000 200

Figure 6-17: SEM micrographs of LACPRODAN powder: a) typical particle at the magnification x 2 500 and b) at the magnification x 299 201

Figure 6-18: SEM micrographs of LACTOVAL powder:
a) typical particle at the magnification x 4 000 and
b) at the magnification x 300 202

Figure 6-19: Photograph of the XPS spectrometer employing a hemispherical electron energy analyzer and a non-monochromatic X-ray source 205

Figure 6-20: Typical XPS wide-scan spectrum of the commercial lactic ALAMIN™ powder 207

Figure 6-21: Typical XPS narrow-scan spectra of the commercial lactic ALAMIN™ powder in the region: a) C 1s and b) N 1s 209

Figure 6-22: XRD patterns of the commercial lactic ALAMIN™ powder 211

Figure 6-23: Schematic of the crystal structure of hydroxyapatite 212

Figure 6-24: Stacked plot of XRD patterns of the commercial lactic ALAMIN™ powder as a function of temperature (T=200, 400, 595 and 800°C) 214

Figure 6-25: Typical DSC curves for the commercial heated from 25 to 640°C ALAMIN™ powders, derived from: a) lactic whey permeate; b) sulfuric acid whey permeate 219

Figure 6-26: DSC curves for: a) lactose and b) citric acid, heated from 25 to 640°C 221

Figure 6-27: FTIR spectrum of the commercial sulfuric acid ALAMIN™ powder 223

Figure 6-28: FTIR spectrum of the commercial sulfuric acid derived a) washed and b) unwashed CaP cake 224

Figure 6-29: FTIR spectrum of naturally occurring gypsum (geological sample) 226

Figure 6-30: FTIR spectrum of calcium sulfate hemihydrate ($CaSO_4.1/2H_2O$) 227

Figure 6-31: FTIR spectrum of anhydrous $CaSO_4$ 228

Figure 6-32: SEM micrographs of unwashed CaP cake powder at the magnification of: a) x 350 and b) x 450 230

Figure 6-33: SEM micrographs of: a) unwashed and b) washed CaP powder, produced from the sulfuric acid whey permeate 231

Figure 6-34: SEM micrographs of the sulfuric acid ALAMIN™ powder:
a) typical particles at magnification x 1 500 and b) at magnification x 4 000 232

Figure 7-1: Flow chart for the experimental bench-scale precipitation reaction of calcium phosphate from the commercial whey UF-permeate 237

Figure 7-2: Apparatus used for the experimental bench-scale precipitation reaction of CaP from the commercial whey UF-permeate 238

Figure 7-3: Change in pH over the reaction time for CaP precipitation process from heated (T=75°C) lactic whey UF-permeate 240

Figure 7-4: pH as a function of the reaction time for heated (T=75°C) whey permeates:
a) sulfuric acid whey permeate; b) lactic whey permeate 241

Figure 7-5: Concentration of the Ca^{2+} as a function of the reaction time, as measured by Atomic Absorption Spectroscopy 243

Figure 7-6: FTIR spectra of the CaP solids, collected after: a) 3 min; b) 15 min; c) 30 min after the onset of thespontaneous precipitation process from lactic whey permeate 246

Figure 7-7: SEM micrographs of the vacuum dried CaP precipitate, isolated from the precipitating lactic whey permeate 30 minutes after base addition: a) typical particle at magnification x 3 000; b) at magnification x 15 000 248

Figure 7-8: TEM micrograph of the CaP solid, isolated from the precipitating lactic whey permeate 5 minutes after base addition (magnification x 228 000) 250

Figure 7-9: TEM micrograph of the CaP solid, isolated from the precipitating lactic whey permeate 20 minutes after base addition (magnification x 120 000) 252

Figure 7-10: TEM micrograph of the CaP solid, isolated from the precipitating lactic whey permeate 30 minutes after base addition (magnification x 30 000) 253

Figure 7-11: Free Ca^{2+} ion concentration in the sera after NaOH addition as measured by a Ca ISE method (expanded) 254

Figure 7-12: Negative ion mode ESMS spectrum (- 25 V) for the lactic whey permeate serum, collected 2 min after the onset of CaP precipitation process 257

Figure 7-13: Positive ion mode ESMS spectrum (+ 25 V) for the lactic whey permeate serum, collected 2 min after the onset of CaP precipitation process 259

Figure 7-14: Comparison of XRD patterns: a) for CaP precipitate, collected at the final stage of the precipitation process (30 min) with b) for fine nanocrystalline HAP (*BABI*-brand) 261

Figure 7-15: FTIR spectrum recorded of the lactic ALAMIN™ solid: a) before and b) after CO_2 gas treatment in the IR band at 1320-1540 cm^{-1} 264

Figure 7-16: SEM micrographs of the typical CaP particle, derived from lactic ALAMIN™ suspension after CO_2 gas treatment: a) at the magnification x 2000; b) at the magnification x 5 000 265

Figure 7-17: SEM micrographs of the ALAMIN™ powder, enriched by casein (10 %): a) typical particle at the magnification x 450; b) it's surface at the magnification x 4 000 267

Figure 7-18: Adsorption isotherm for whey proteins (β-lactoglobulin/α-lactalbumin of weight ratio 9.4) on the surface of *Fluka*-hydroxyapatite powder particles at T=25°C 269

Figure 7-19: Schematic representation of the variation of charge with pH for a protein 270

Figure 7-20: Schematic representation of the surface charge of hydroxyapatite in the crystal state: a) hydroxyapatite particle; b) expanded area of hydroxyapatite; c) crystal unit cell of hydroxyapatite 271

Figure 7-21: Schematic of the cooperative adsorption between protein and surface 271

Figure 7-22: Reaction vessel illustrating the agitator propellers used in the agitation rate precipitation experiments 272

Figure 7-23: Malvern particle size distributions for the precipitation of CaP from lactic whey permeate at T=75°C and W=100 rpm as a function of the reaction time: a) initial (1 min); b) 5 min; c) 30 min 274

Figure 7-24: Plot of D[4, 3] versus reaction time (after initiation of precipitation) for precipitation of CaP from lactic whey permeate at T=75°C at an agitation rate, W=100 rpm 275

Figure 7-25: Relationship between Malvern-determined particle diameter D[4, 3] of CaP particles and the agitation rate (W) during the precipitation from lactic whey permeate 276

Figure 7-26: Malvern particle size distributions for the precipitation of CaP from lactic whey permeate at T=75°C at varying agitation rates (W): a) increase in W from 34 to 300 rpm; b) increase in W from 300 to 1000 rpm 277

Figure 7-27: Stress acting on an aggregates: a) shearing stress; b) normal stress 278

Figure 7-28: Schematic diagram showing: a) mixing; b) adsorption; c) re-arrangement of the adsorbed chains to give an equilibrium conformation of particles; d) collisions between destabilised particles to form flocs and e) break-up of flocs 280

Figure 7-29: 2 Log-Normal populations fitted to the experimental Malvern particle size distribution curves: a) Log scale plot; b) Linear scale plot 283

Figure7-30: 3 Log-Normal populations fitted to the experimental Malvern particle size distribution curves: a) Log scale plot; b) Linear scale plot 284

Figure 7-31: 2 Log-Normal populations fitted to the experimental Malvern particle size distributions curves: a) Log scale plot; b) Linear scale plot 285

Figure 8-1: General scheme showing the phase transformation of calcium phosphate precipitating from lactic whey permeate solution 297

LIST OF TABLES

Table 1-1: Composition of a typical whey 4

Table 1-2: A breakdown of the whey proteins of bovine milk 5

Table 2-1: Compositions of some calcium phosphates most closely associated with ALAMIN™ production 12

Table 2-2: Abbreviations for the various apatites which ALAMIN™ could fall under 14

Table 2-3: Typical salt composition of bovine milk 19

Table 2-4: Phases that may precipitate out of a metastable, supersaturated solution of calcium ions and inorganic phosphate 30

Table 2-5: Precipitating sequences observed (on the basis of electron micrographs) from the study by van Kemenade et al. 34

Table 2-6: Comparative degrees of supersaturation relative to hydroxyapatite and amorphous calcium phosphate (ACP) in systems from which hydroxyapatite formed 44

Table 4-1: Basic chemical components defining the medium and their concentrations in SLWUF buffer, as contained in the input file used in SPE program 83

Table 4-2: *Log (β)* values and stoichiometric coefficients for the basic chemical components, dissolved complex ion species and *Log* K_{sp} values for insoluble CaP solid phases at T=25°C in the Fortran-formatted input file SPE program for the lactic whey permeate system 84

Table 4-3: "Standard" Simulated Lactic Whey Ultrafiltrate (SLWUF) buffer composition (citrate - 2 mM) 96

Table 4-4: Additives for the SLWUF buffer solutions with different Ca:P ratios, based on SLWUF buffer, containing a basic 2 mM citrate concentration (assuming 1L total volume) 97

Table 4-5: Additives for the SLWUF buffer solutions with different citrate concentration (assuming 1L total volume) 98

Table 4-6: Additives for the SLWUF buffers with different magnesium concentrations, based on 2 mM citrate solution (assuming 1L total volume) 98

Table 4-7: Standard solutions of $CaCl_2$ in KCl with ionic strength I=0.1 (estimated ionic strength in whey permeates) that were used for the calibration of the Calcium ISE at T=25°C 107

Table 4-8: Experimental data for Ca ISE measurements during the time-course of the precipitation process from SLWUF buffer solutions 109

Table 5-1: Basic chemical components defining the medium and their concentrations in a lactic whey permeate, as contained in the input file of SPE program 130

Table 5-2: Typical compositional data for a lactic whey permeate 130

Table 5-3: SPE calculated CaP yield as ($Ca_{(S)}$=$Ca_{[OCP]}$ + $Ca_{[BRUSHITE]}$) in the lactic whey permeate for the citrate concentration from 0 to 8 mM 140

Table 5-4: Typical compositional data for a sulfuric acid whey permeate 144

Table 5-5: Sulfuric whey permeate composition at the end of season 145

Table 5-6: The formation constants for the whey permeate species at I=0.1 as used in the SPE calculations 146

Table 5-7: *Log* K_{sp} values at I=0.1 for all the possible solid phases 147

Table 5-8: SPE calculated yield of solid OCP formation 162

Table 5-9: SPE calculated overall yield of solid (Brushite + OCP) formation in the sulfuric acid whey permeate for citrate concentration from 0 to 8 mM 162

Table 5-10: Free Ca^{2+} content depending on the Ca:P molar ratio at pH 6.4, 6.6 and 6.8 166

Table 5-11: Overall Ca yield and Ca concentration depending on the Ca:P molar ratio over the pH 6.4, 6.6 and 6.8 166

Table 6-1: ICP-OES parameters for the all ion determinations 175

Table 6-2: Characteristic wavelengths, used for the ICP-OES measurements 176

Table 6-3: ICP-OES data of the chemical composition for a typical commercial whey permeate. Data from three replicate measurements plus the average of these are given 177

Table 6-4: Comparison of Ca:P molar ratios, determined by EDX and ICP for the commercial ALAMIN™ powders 204

Table 6-5: XPS operational parameters for the wide scan spectrum 206

Table 6-6: XPS operational parameters for the narrow scan spectrum 206

Table 6-7: XPS peaks analysis for the commercial lactic ALAMIN™ powder 208

Table 6-8: Comparison XRD data of commercial lactic ALAMIN™ powder and crystals of HAP and OCP 212

Table 6-9: Data from XRD analysis: width at half height ($\beta_{½}$) of the 002 diffraction peak and crystallite size, *D* 214

Table 6-10: Typical Malvern (*Mastersizer*) parameters, used for ALAMIN ™ particle size measurements 216

Table 6-11: Malvern (*Mastersizer*) particle size data on various grades of as received commercial ALAMIN™ powders, produced from lactic whey permeate 217

Table 6-12: Positions of the DSC thermogram peaks for commercial ALAMIN™, LACPRODAN and LACTOVAL powders 218

Table 6-13: Positions of the DSC thermogram peaks for the whey proteins, lactose and citric acid 220

Table 6-14: Fundamental vibrational frequencies (Nakamoto, 1986) of the tetrahedral five-atom molecules SO_4^{2-} and PO_4^{3-} (in cm^{-1}) in FTIR spectra 225

Table 6-15: Chemical ICP-OES analyses of acid-digested samples of the sulfuric acid whey permeate-derived washed and unwashed CaP cake (and also washed lactic CaP cake and ALAMIN™ powder) 233

Table 6-16: Colorimetric (for P) and ICP-OES analyses of acid digested samples of the sulfuric acid whey permeate-derived washed and unwashed CaP cake (and also washed lactic CaP cake and ALAMIN™ powder) 234

Table 7-1: ICP-OES data of the chemical composition of the serum, derived from the lactic whey permeate after removal of the CaP precipitate obtained at T=75°C and pH=6.8 245

Table 7-2: The particle size of ALAMIN™ powder before/after bubbling of CO_2 gas through the aqueous suspension. pH before/after bubbling is also given in parentheses 263

Table 7-3: Malvern (*Mastersizer*) determined final particle sizes in CaP slurries precipitated from lactic whey permeate 273

Table 7-4: Overall Malvern Laser (*Mastersizer*) particle distribution curve fitting data as a function of agitation rates $W \leq 300$ rpm for the precipitation of calcium phosphate (reaction time=30 min) from lactic whey permeate 282

LIST OF ABBREVIATIONS

°C	degrees Celsius
AAS	atomic absorption spectroscopy
ACP	amorphous calcium phosphate
Ard	ardealite
C	concentration
CaP	calcium phosphate
Ca-ISE	calcium ion-selective electrode
CCP	colloidal calcium phosphate
cit, citr	citrate
DSC	differential scanning calorimetry
DCPD	dicalcium phosphate dihydrate (brushite)
EDTA	ethylenediaminetetraacetic acid
EDX	energy dispersive X-ray
ESMS	electrospray mass spectrometry
ICP-OES	inductively coupled plasma optical emission spectroscopy
FTIR	Fourier transform infrared
g	gram
GRIF	Graduate Research in Industry Fellowship
Gyp	gypsum
HAP	hydroxyapatite
Lac	lactate
lactic ALAMIN™	ALAMIN™ manufactured from lactic whey UF-permeate
MCP	micellar calcium phosphate
min	minutes
mL	millilitre
M	mol L^{-1}, moles per liter
mM	mmol L^{-1} =1000 x mol L^{-1}
NZDRI	New Zealand Dairy Research Institute

OCP	octacalcium phosphate
ppm	parts per million
rpm	revolutions per minute
SEM	scanning electron microscopy
SLWUF	simulated lactic whey ultrafiltrate
sulfuric acid ALAMIN™	ALAMIN™ manufactured from sulfuric acid whey UF-permeate
TEM	transmission electron microscopy
TCP	tricalcium phosphate
UV/Vis	ultraviolet/visible
UF	ultrafiltration
UF-permeate	whey permeate fraction that passes through the UF membrane
XPS	X-ray photoelectron spectroscopy
XRD	X-ray diffraction

CHAPTER ONE

GENERAL AND BACKGROUND INFORMATION

1.1 The Interest in Calcium Phosphate in the New Zealand Dairy Industry

Calcium phosphate is an important mineral constituent of many dairy products. Calcium as a dietary supplement has a very high profile in today's health conscious world and its inclusion in products consumed on a daily basis by consumers is thus keenly sought after. The adult human body contains about 1200 g of calcium which amounts to about 1.5-2% of body weight (Holt, 1997). Of this amount, 99% occurs in bone and teeth where it is present as a calcium phosphate compound providing strength and structure. The remaining 1% is found in extracellular fluids and intracellular structures and cell membranes. Calcium is implicated in many regulatory functions in the body, such as maintenance of normal heart beat, blood coagulation, hormone secretion, nerve conduction, muscle contraction and activation of enzymes. Cow's milk and dairy-based products are recognised as being excellent sources of dietary calcium.

In endeavouring to provide calcium-enhanced products to their customers, it has been a practice of some food manufacturers worldwide to supplement the natural calcium level in their products by artificial means by addition, for instance, of calcium carbonate. Today's consumers, however, increasingly demand that the ingredients comprising the products they ingest be "naturally" derived (Sime, 1998) which presents a challenge to the providers of calcium supplemented foods. The New Zealand Dairy Industry has met this challenge by developing an industrial process to prepare a highly successful calcium-containing product known commercially as ALAMIN™ which is in the form of calcium phosphate derived via precipitation from UF (ultrafiltration) whey permeates. This process is currently of major interest in the New Zealand Dairy Industry due to the high demand for the ALAMIN™ product from overseas clients who add this ingredient to their dairy-based products. The process, moreover, yields a value-added product from whey permeates.

Calcium phosphate was long regarded as a nuisance product during the processing of whey permeates to extract lactose and whey proteins (Brothersen et al., 1982; Daufin et al., 1993). Lactose, for instance, can be removed from whey by the so-called Steffen process where a calcium salt (e.g. calcium oxide) is added to precipitate the lactose. However, it is known that any added calcium will also precipitate large amounts of phosphate so giving an impure precipitate, thus the suggestion was made by Brothersen (Brothersen et al., 1982) that calcium phosphate be recovered by precipitation from whey permeates (before extraction of lactose) at a pH at which lactose would not precipitate (pH < 8). Furthermore, it was commented that calcium phosphate recovered in this way could be useful as a food supplement.

It is interesting to note that little rigorous scientific attention internationally has been directed to studying the precipitation of calcium phosphate from whey permeates. The paper by Brothersen (Brothersen et al., 1982) described a precipitation process which differed quite significantly from the present ALAMIN™ production process in that *extra* calcium, in the form of calcium oxide, was being added to the whey permeates in order to precipitate out calcium phosphates whereas only *permeate-derived calcium* is being removed in the New Zealand Dairy Industry process.

1.2 Production of Calcium Phosphate in the New Zealand Dairy Industry

1.2.1 Production of Lactic and Mineral Acid Whey (Prior to Ultrafiltration)

1.2.1(a) Lactic Casein Wheys

The primary function of the casein starter (a defined mixture of bacteria) is to reliably produce lactic acid from lactose which is present in the whey. A secondary function is to produce CO_2 gas which acts a little like baking powder in the casein curd. The resulting more open curd is easier to handle, wash and dry. The CO_2 gas production involves the metabolism of citrate.

Starter bacteria are subject to phage attack, a viral infection that kills them. A single phage particle infects a single bacterial cell, multiplies and then bursts the cell liberating many more phage particles which infect further bacterial cells. This can lead

to a slowing or complete cessation of acid production. Phages evolve quickly and new ones are constantly appearing. To ensure consistent starter growth and acid production rates, NZ starters are composed of a defined mixture of different strains. The strains within a single starter are chosen for having no presently active phages, and for being unrelated so that if a phage does appear, some strains will remain uninfected and acid production will continue.

An important issue with regard to the lactic whey permeates is the citrate and lactate level and the effect it has on precipitation (see section 2.17: "Ion Speciation in the Whey Permeate and the Need for Simulated Milk Ultrafiltrate (SMUF) Buffers"). In milk, citrate concentration is *ca.* 9 mM. It is believed that most citrate is used up during casein making, depending on how quickly the pH falls. The bacteria responsible are only active at higher pH values. In the lactic wheys and permeates used for calcium phosphate precipitation, the citrate levels have not been reliably determined and need to be on freshly generated whey permeates in order to gain insights into the true level of citrate at time of precipitation reaction. The level of citrate has a direct influence on availability of free calcium for the precipitation reaction (this has been dealt with in Chapter 4). Lactate levels may also influence levels of free calcium although the association complex of lactate with calcium is less stable relative to that of citrate with calcium. Citric acid test kits based on enzymic conversion of: 1) citrate to oxaloacetate + acetate, 2) oxaloacetate + NADH conversion to malate + NAD^+, and 3) UV absorbance determination of the $NADH/NAD^+$ are available. The detection limit for the assay is 0.5 mg L^{-1} citric acid. Free calcium ions will reduce the rate of the enzymic reactions and carbonate needs to be removed by degassing acid solutions. Diluted samples, preferably containing about 15-30 mg L^{-1} citric acid, need to be clear, colourless (at 340 nm) and at near neutral pH.

1.2.1(b) Mineral Acid Wheys

The separation of the casein curd from the whey destined for ultrafiltration is achieved via a simple acid precipitation process where hydrochloric or sulfuric acid can be used to achieve the final pH. The composition of this whey is different from that of lactic whey and is dominated by chloride or sulfate ion with lactate being at much lower levels. Citrate levels are significantly higher in these wheys relative to lactic wheys since bacterial starters (which consumes the citrate) are not used.

1.2.2 Typical Composition of Whey and the Process of Ultrafiltration

The typical composition of whey is summarised in Table 1-1. A more detailed breakdown of the proteins that are present in bovine milk whey (and which are largely separated from the permeate by ultrafiltration before any precipitation of calcium phosphate takes place in the permeate) is summarised in Table 1-2.

Table 1-1: Composition of a typical whey (Marshall, 1982).

Analysis (weighted seasonal average)	Composition ($g\ L^{-1}$) Cheese whey	Composition ($g\ L^{-1}$) Lactic whey
Total solids	67	64
Protein (total nitrogen-non-protein nitrogen)*6.38	6.2	5.8
Non-protein nitrogen	0.27	0.4
Lactose	52.4	44.3
Minerals (as ash)	5.2	7.5
Milk-fat	0.2	0.3
Phosphate	0.5	2
Calcium	0.4	1.6
Sulfate	0.6	0.5
Magnesium	0.08	0.1
Sodium	0.5	0.51
Potassium	1.5	1.4
Chloride	1.0	0.9
Lactate (conjugate base of lactic acid)	2.0	6.4
pH	5.9	4.6

Table 1-2: A breakdown of the whey proteins of bovine milk (Marshall, 1982).

Whey protein	Approximate proportion of skim milk protein (%)	Approximate concentration in whey (g L^{-1})	Proportion of total whey protein (%)	Isoelectric point (pH)
β-lactoglobulin	7-12	3	50	5.35-5.49
α-lactalbumin	2-5	0.7	12	4.2-4.5
Immunoglobulins	1.9-3.3	0.6	10	5.5-8.3
Bovine serum albumin	0.7-1.3	0.3	5	5.13
Proteose peptone fraction	2-6	1.4[a]	23	
Total whey proteins	15-22	6	100	

[a] Includes proteose-peptones, residual casein and a number of minor proteins

Ultrafiltration (UF) is a physicochemical separation technique in which a pressurised solution flows over a porous membrane. The commercial process of ultrafiltration allows the selective pressure-driven separation of whey proteins from CaP salts, lactose and water in varying proportions under the mild conditions of temperature and pH (Marshall, 1982, Hobman, 1992).

Figure 1-1 is a schematic representation of the ultrafiltration of whey. Ultrafiltration retains in the *retentate* flow any insoluble substances or solutes larger than 20 000 Da molecular weight. The rest of the whey stream is passed through the membrane, driven by the applied pressure to the *permeate flow*. The membrane will let through water and some low molecular weight solutes but will retain the bulk of the whey protein. There is, however, a small amount of protein leakage past the membrane. Permeates after UF contain approximately 0.3 % protein.

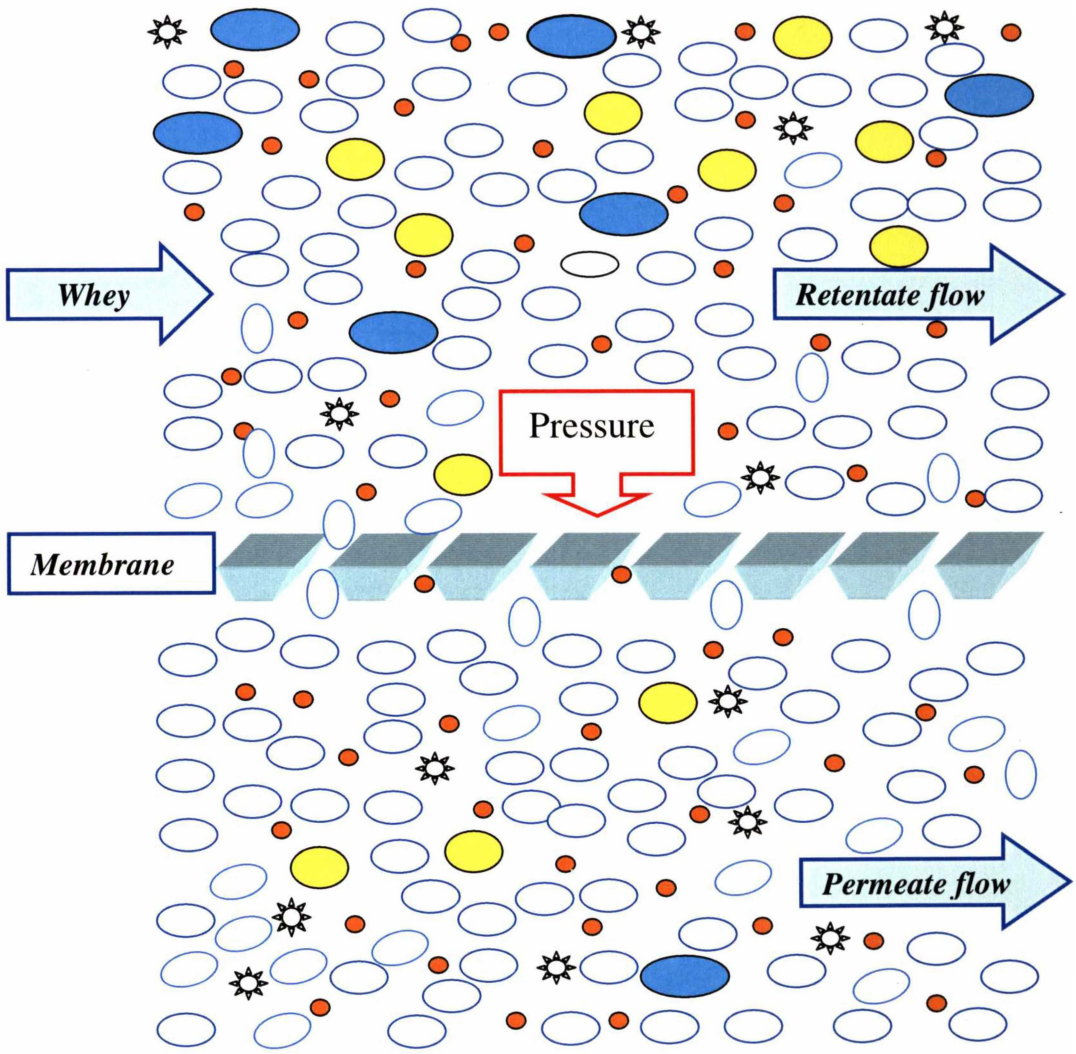

Figure 1-1: A schematic representation of the ultrafiltration process of whey.

1.3 A Summary of the Precipitation of Calcium Phosphate from Ultrafiltered Whey Permeates in New Zealand Dairy Industry

Figure 1-2 is a general scheme representing the flow chart of the commercial calcium phosphate precipitation process from lactic and mineral acid whey UF-permeates:

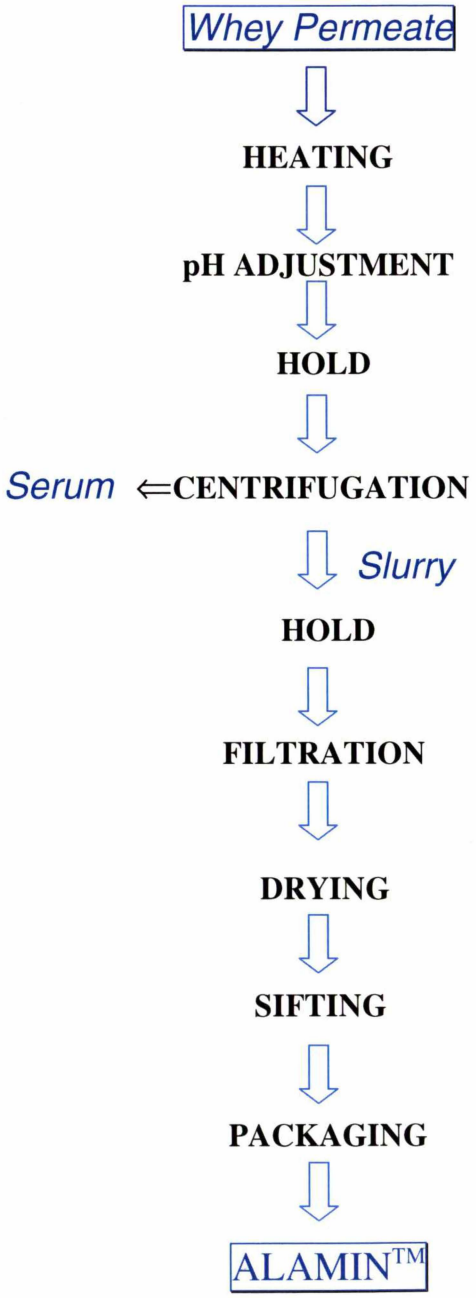

Figure 1-2: General flow chart of the commercial calcium phosphate precipitation process from lactic and mineral acid whey UF-permeates.

Whey permeate from the UF process is heated and made alkaline by addition of a base solution to adjust pH (Figure 1-2). The resultant suspension containing precipitated calcium phosphate is then held to allow the CaP crystals to grow and stabilize. The solid phase of the suspension is then recovered by centrifugation with the liquid phase (serum) sent on for further processing. The solid phase recovered by centrifugation is further concentrated by filtration and then the concentrated solids (CaP cake) fed to the drier. This CaP cake is then broken up mechanically before being passed into a drier with the emerging dried calcium phosphate powder being collected, sorted according to size, blended and packaged.

Currie (Currie, 1990) reported on a study of the optimisation of the primary extraction of calcium phosphate from lactic whey UF-permeate as part of a Diploma of Applied Science investigation. By using a bench-scale bath vacuum filtration vessel employed for carrying out initial trials to assess the feasibility of filter presses in the commercial processes, Currie established that pressure filtration (with various filter cloths) would be a useful way of separating precipitated calcium phosphate.

A massive amount of literature pertaining to calcium phosphate chemistry exists spanning a large number of broad areas such as biomaterials, precipitation and biomineralisation. Much research in dairy chemistry-based groups has concentrated on the so-called "colloidal calcium phosphate" (CCP) or "micellar calcium phosphate" (MCP) phase which has been demonstrated to be the amorphous calcium phosphate phase present in natural milk encased in casein micelles (see section 2.5: "Nature of Calcium Phosphate in Milk"). In this form, the amorphous calcium phosphate has been claimed to be responsible for the bioavailability of calcium in milk as, upon ingestion, the calcium is easily released from casein micelles in the acidic environment of the stomach, dissolved and absorbed into the body.

The CCP phase in milk is not of direct relevance to the ALAMIN^{TM} production process since the micellar casein-calcium phosphate structure comprising the CCP is destroyed (and all of the calcium and inorganic phosphate released into aqueous solution) during the process of acidification of skim milks to pH 4.6 by bacterial starters or sulfuric acid addition. However, the existence of CCP in milk and the mode by which it is colloidally

stabilised may be of interest in investigations into achieving long term stability of suspended ALAMIN™ powders in products which are purposefully manufactured to have an extended shelf life such as ultra-heat treated milk.

1.4 Purpose and Objectives

An important recommendation from the previous ALAMIN™ investigations was that more fundamental aspects of the chemistry of the system be investigated at the PhD level with regard to the speciation existing in the sulfuric acid permeate and the effects it has on the precipitation process. Originally this GRIF-based project on investigation of calcium phosphate precipitation from the commercial lactic whey permeate was suggested by Dr. Richard Archer.

The purpose of this work was investigation of calcium phosphate precipitation chemistry in order to improve the commercial product quality of ALAMIN™ powder:

- To perform the computer speciation calculations for the provision of information on the *chemistry of the precipitation*. Questions that were hoped to be answered by the chemical speciation program were:
  - What phases are involved in the calcium phosphate precipitation process?
  - What are the impacts of Ca:P molar ratio, citrate and sulfate concentration on the yield of the precipitated calcium phosphate solids?
  - What ion and molecular species occur in the lactic and sulfuric acid whey permeates?
  - What is the influence of pH on the precipitation process?
- To analyse the influence of components in the lactic and sulfuric acid whey UF-permeates, by investigation of the precipitation process from simulated whey permeate solutions which act as models of the ionic salt media in the actual lactic and sulfuric acid whey permeates.

- To investigate the formation and flocculation process of calcium phosphate phases, precipitated from heated industrial whey permeates. Questions that were hoped to be answered by this investigation were:

  - How fast do the calcium phosphate particles grow during the precipitation process?
  - What is the mechanism of aggregation of the particles?
  - What is the influence of the agitation rate on the flocculation process?
  - Do any distinct populations of particles develop during the precipitation process which influence particle size and shape?

- To characterise the ALAMIN^{TM} powder and commercial whey UF-permeates with a wide range of techniques such as: X-ray Diffraction (XRD), Scanning Electron Microscopy/ Energy Dispersive X-ray analysis (SEM/ EDX), Transmission Electron Microscopy (TEM), Fourier Transform Infrared Spectroscopy (FTIR), X-ray Photoelectron Spectroscopy (XPS), Malvern (*Mastersizer*) Laser Light Scattering analysis, Electrospray Mass Spectrometry (ESMS), Atomic Absorption Spectroscopy (AAS), Inductively Coupled Plasma Spectroscopy (ICP-OES), pH-stat method, Calcium Ion-Selective Electrode (ISE) method, UV-Visible Spectroscopy and Differential Scanning Calorimetry.

CHAPTER TWO

LITERATURE REVIEW OF THE CHEMISTRY OF CALCIUM PHOSPHATE AND ITS PRECIPITATION FROM AQUEOUS SOLUTION

2.1 Introduction

"Calcium phosphate" is a very general term used to refer to a large and complex range of solid compounds which contain Ca^{2+} and PO_4^{3-} ions as a basic component of their structure. To anyone involved in the manufacture of ALAMIN™ in the New Zealand Dairy Industry, it is very tempting to assume that the calcium phosphate compound being produced by precipitation, behaves like a simple substance when in fact the chemistry surrounding its transformation in solution is far from trivial, and in fact, exceedingly complex. It is the aim of this section of the review to provide a basic introduction to the nature of the calcium phosphate phases which are most likely involved in the ALAMIN™ production process and to explain the fundamental chemistry of calcium phosphate compounds when they form by precipitation from solution. Chapter 3 will provide a rudimentary introduction to the instrumental techniques that can be used to probe the nature of ALAMIN™ and the whey permeate from which it is derived.

2.2 Composition of Calcium Phosphate Compounds

Table 2-1 is a summary of the calcium phosphate phases that are believed to be most closely associated with the production of ALAMIN™. They are listed in order of decreasing Ca:P (calcium to phosphorus) ratio which is often used as a qualitative means of identifying the particular phase. A more correct term for calcium phosphate compounds is "calcium orthophosphates" (Elliot, 1994) which are formally defined as salts of phosphoric acid, H_3PO_4 and, can thus form compounds that contain $H_2PO_4^-$, HPO_4^{2-}or PO_4^{3-} ions. Calcium orthophosphates are very important in nature as they are the principal mineral constituent of bones and teeth in humans that are built up by biomineralisation processes (Mann, 1988) in which Ca^{2+} and phosphate ions are transported to a calcification region in the body (Posner, 1961) where local conditions are favourable towards precipitation of calcium phosphate compounds.

Collagen in natural bone tissue provides the platform or scaffold on which calcification occurs but for maintenance of healthy bone tissue, a steady supply of the basic building blocks, viz., Ca^{2+} and phosphate ions must be made available from physiological (body) fluids, which explains the enthusiasm on the part of consumers in ingesting products enriched with calcium. If the supply of calcium in the body fluids is insufficient, bone resorption can occur where the body dissolves bone tissue to redress the balance.

Table 2-1: Compositions of some calcium phosphates most closely associated with ALAMIN™ production (Elliot, 1994).

Structural Formula	Ca:P ratio	Common Name	Formula Abbreviation
$Ca_{10}(PO_4)_6(OH)_2$	1.67	Hydroxyapatite[a]	HAP[a]
$Ca_3(PO_4)_2$	1.50	Tricalcium phosphate[b]	TCP
$Ca_{10-2x}H_{2x}(PO_4)_6(OH)_2$ or "$Ca_3(PO_4)_2.2H_2O$" or "$Ca_9(PO_4)_6$"	1.18-1.50	Amorphous calcium phosphate[c]	ACP
$Ca_8H_2(PO_4)_6.5H_2O$	1.33	Octacalcium phosphate	OCP
$CaHPO_4.2H_2O$	1.00	Dicalcium phosphate dihydrate (Brushite)	DCPD
$CaHPO_4$	1.00	Dicalcium phosphate (Monetite)	DCP

[a] There are many other subclassifications under the general heading of "hydroxyapatite" (see Table 2-2);

[b] For this compound, crystalline phases labelled as: α, β, and γ phases also exist;

[c] The structure of amorphous calcium phosphate cannot be determined by XRD due to its non-crystalline nature.

2.3 A General Word on Calcium Phosphate Phases: Apatitic versus Non-apatitic

Calcium orthophosphate compounds are all white solids with most being sparingly soluble in water but dissolving completely in mineral acids. The following is a more detailed description of some calcium orthophosphate phases that have some relevance to ALAMIN™. In general, the calcium orthophosphates, TCP, OCP, DCPD, and DCP are classified as *non-apatitic* phosphates whereas HAP is classified as an *apatitic* phosphate. Apatites are a large family of compounds which are characterised by the general structural formula, $Ca_{10}(PO_4)_6X_2$ where X can be F^- ion (fluorapatite), OH^- ion (hydroxyapatite) or a Cl^- ion (chlorapatite), for instance. The name "apatite" had been coined by a German mineralogist called Werner from a Greek word *apatos* meaning to deceive, because it was frequently confused with other minerals occurring in nature. The choice of this name for the apatite family of compounds was very prescient in that the apatite structure is remarkably tolerant of a wide range of ionic substitutions in its crystal structure. The Ca^{2+} ion, for instance, can be partly or completely replaced by Ba^{2+}, Sr^{2+} or Pb^{2+} ions and PO_4^{3-} by CO_3^{2-}. Carbonate-substituted calcium hydroxy apatites comprise the natural bone in our bodies. This property within the apatite family of compounds considerably complicates the chemistry of these compounds.

2.4 Descriptions of discrete Calcium Phosphate Phases of relevance to ALAMIN™

2.4.1 Hydroxyapatite: $Ca_{10}(PO_4)_6(OH)_2$

Hydroxyapatite is just one of the family of apatites. This is the phase which has the greatest relevance to ALAMIN™ since it is the thermodynamically most stable phase (at basic pH) to form by precipitation from solution and thus represents essentially the final ALAMIN™ product. The term "hydroxyapatite", however, is a gross oversimplification of what the ALAMIN™ could represent. Table 2-2 explains the abbreviations for the various subclassifications of apatites. ALAMIN™ could fit into any of these categories depending on the conditions under which it was synthesised. The compositional variation that "hydroxyapatite" compounds could have is due to the hospitable nature of the apatite structure which can undergo a variety of substitutions with various cations and anions from solution.

Table 2-2: Abbreviations for the various apatites which ALAMIN™ could fall under (Elliot, 1994).

Generalised Abbreviation	Explanation
OHAP, HAP	Hydroxyapatite, $Ca_{10}(PO_4)_6(OH)_2$
s-OHAP s-HAP	Stoichiometric HAP. Used when emphasis is required that the compound has a chemical compositions corresponding to the ideal formula, $Ca_{10}(PO_4)_6(OH)_2$
ns-OHAP, ns-HAP	Non-stoichiometric hydroxyapatite (carbonate free). Indicates that the chemical analysis shows or would show a departure from that of s-HAP. This may involve lattice H_2O, HPO_4^{2-}, Ca^{2+}, and/ or $2OH^-$ replaced by O^{2-}
Ca-def OHAP, Ca-def HAP	A precipitated apatitic calcium phosphate (carbonate free) with a Ca:P molar ratio in the range 1.66-1.50 or less. Compounds that might contain interlayers of OCP are included
BCaP	Precipitated basic apatitic calcium phosphate with an uncertain composition which may include CO_3^{2-} or HCO_3^- ions
A-CO_3AP	A-type carbonate apatite, ideally $Ca_{10}(PO_4)_6CO_3$ where carbonate is substituted into the OH^- position of the HAP structure
B-CO_3AP	B-type carbonate apatite, i.e. a carbonate-containing apatite in which the PO_4^{3-} ions are replaced by CO_3^{2-} ions
AB-CO_3AP	Carbonate-containing apatite in which both of the above substitutions take place
CO_3AP	Any carbonate-containing apatite

In general, ALAMIN™ could best be described as a Ca-deficient apatite. The chemistry of HAP is extremely complex because when it is made by precipitation from solution, the apatitic products formed can have Ca:P molar ratios that can vary from 1.50-1.66 and sometimes even outside this range. The precipitates depending on their state of development can be of submicron (small, almost colloidal) dimensions so that their surface chemistry becomes very important. These factors add a dimension of complexity to the preparation and study of HAP precipitates since the thermal stability of the precipitates (especially BCaP's) is very low so that variable amounts of water, acid phosphate, and carbonate contaminants are all lost in a complex manner on heating. Thus in the drying of ALAMIN™ such factors could be of relevance.

2.4.2 Tricalcium Phosphate: $Ca_3(PO_4)_2$

The chemistry surrounding these particular phases of calcium phosphate are complex and various structural phases exist labelled as α, β, and γ phases that are not relevant to production of ALAMIN™ and so will not be discussed. The TCP phase which is of possibly closest relevance to ALAMIN™ is that referred to as "whitlockite". This is defined as a TCP structure containing an indeterminate level of Mg^{2+} and HPO_4^{2-} ions in its structure. Given that whey contains a low level of Mg^{2+} ion (see Table 1-1), whitlockite may be of some relevance. Whitlockite is defined as the phase of TCP which is precipitated from aqueous solution when Mg^{2+} ion has been deliberately added to solution (Rowles et al., 1968). The pH for formation of well-crystallised whitlockite phases by precipitation is usually in the range of 5-6 (Rowles et al., 1968; LeGeros et al., 1989) which indicates that it is necessary for HPO_4^{2-} ions to be present for incorporation into the whitlockite lattice. The TCP crystal form is rhombohedral in nature.

2.4.3 Octacalcium Phosphate: $Ca_8H_2(PO_4)_6.5H_2O$

The typical appearance of OCP is as thin blade-like crystals. These can often form quite beautiful spherulitic growths if the crystals grow by radiating from a common origin. Florette-type (flower like) morphology has also been used to describe the nature of OCP crystals In solution, OCP often occurs as a transient intermediate in the precipitation of more thermodynamically stable HAP as well as biological apatites (e.g. bone and teeth).

UNIVERSITY OF WAIKATO
LIBRARY

The reason for this is because OCP can nucleate and grow more easily than HAP and this has a considerable amount of importance in understanding biomineralisation in the body and also possibly the growth of calcium phosphate particles in whey permeate after addition of sodium hydroxide. Octacalcium phosphate once formed can provide a "platform" on which hydroxyapatite can grow. This is shown in Figure 2-1 which is a schematic representation of the crystal structure of OCP. The large parallelogram drawn below represents the unit cell making up the OCP structure and the rhombus drawn at the upper right represents the unit cell for HAP. Figure 2-1 shows that if the structure of HAP were to "sit" on the OCP structure, there would be close correspondence of 2 oxygen atoms on "P6" of OCP and 4 pairs of Ca^{2+} ions on Ca (5), Ca (7) and Ca (6) and Ca (8) with O atoms and Ca^{2+} ions on the HAP lattice.

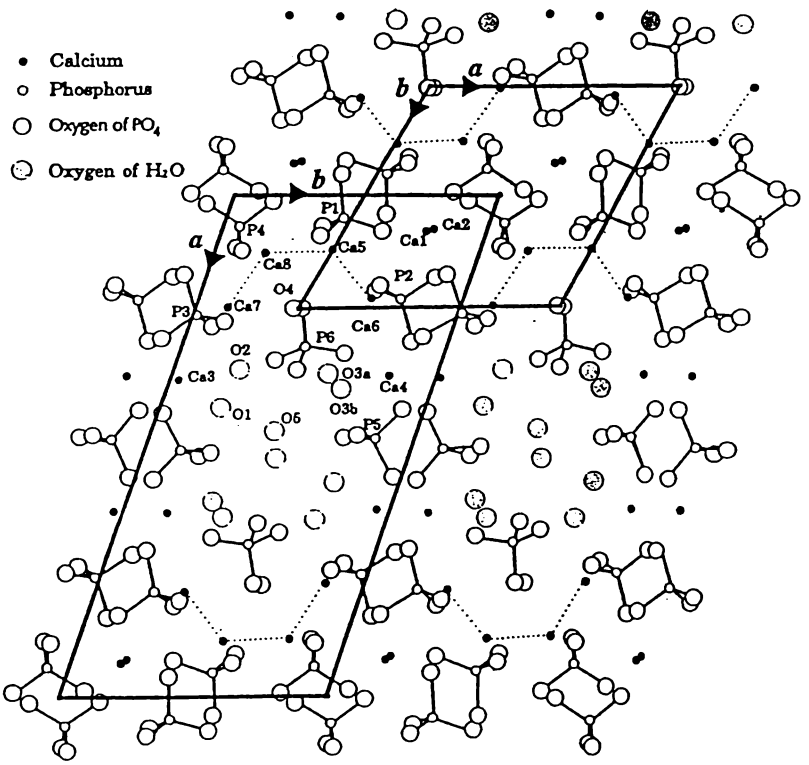

Figure 2-1: Structure of OCP with superimposed unit cells for OCP and HAP shown (Elliot, 1994).

The proposed hydrolysis mechanism of two OCP layers to four unit cells of HAP structure (Tung, 1998) is depicted in Figure 2-2:

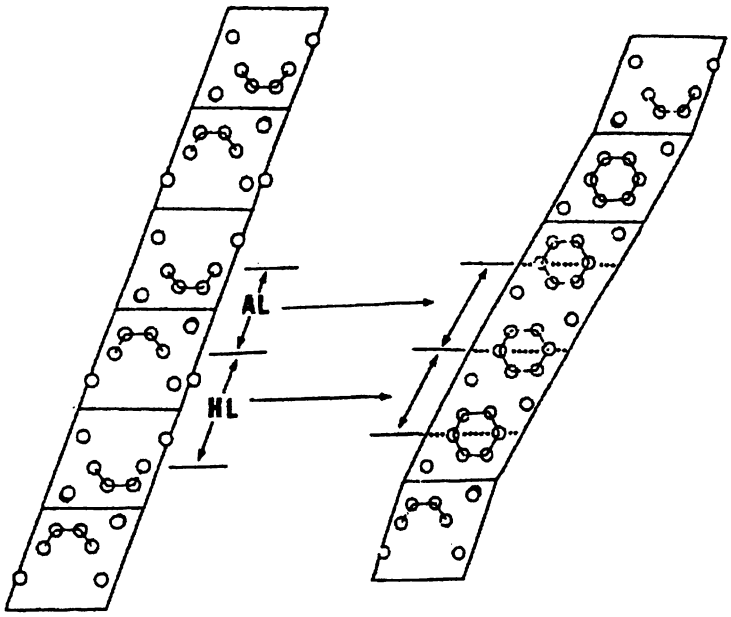

a) b)

Figure 2-2: Schematic showing where the structural transformation of 2 OCP layers to 4 unit cells of HAP takes place. The HL (hydrated layer) of OCP becomes the AL (apatitic layer) in HAP. Only the Ca ions are shown: a) three unit cells of OCP and b) four unit cells of HAP and two 1/2 unit cells of OCP (Tung, 1998).

2.4.4 Brushite: (DCPD) $CaHPO_4.2H_2O$ and Monetite (DCPA): $CaHPO_4$

Brushite (also known as DCPD or "dicalcium phosphate dihydrate") occurs as a hydrated compound and like OCP is also one of the transient intermediates in the precipitation of HAP. It is regarded as an "acid phosphate" since it contains HPO_4^{2-} groups and has been proposed as an intermediate in apatitic mineralisation and dissolution processes (bone mineralisation), dissolution of tooth enamel in acids, and during fluoride treatment of teeth. The formation of DCPD by direct precipitation in solution is favoured at acidic pH values (4-5). The crystal form of DCPD is characteristically plate-like or prismatic. DCPA ("dicalcium phosphate anhydrous") or monetite is simply the anhydrous form of DCPD and can be formed by dehydration of DCPD. Its formation by precipitation is difficult since the hydrated DCPD structure is thermodynamically favoured and so this is not regarded as a particularly relevant intermediate phase in the formation of ALAMIN™, at least not in aqueous solution.

2.4.5 Amorphous Calcium Phosphate (ACP)

This is a very important phase since it often occurs as a transient species during the formation of calcium phosphates by precipitation in aqueous solution. ACP is often prepared in the process of rapid precipitation reactions (Elliot, 1994). The nature of ACP is extremely complex given that changes in conditions can alter the properties of the solid formed. When precipitating from solution, there is often a lag time before initial formation of ACP which is highly sensitive to solution composition. In general, higher initial Ca:P molar ratios, higher temperatures, higher pH values or presence of pyrophosphate, fluoride, magnesium or carbonate can reduce this induction time. The lag time is increased by presence of citrate, poly-L-glutamic acid or polyacrylate. The ACP is of particular scientific relevance to the formation of ALAMIN™ as some of the abovementioned variables amongst others (e.g. temperature, pH, presence of carbonate, citrate, lactate, magnesium, and initial Ca:P molar ratios) are important factors in the ALAMIN™ production process.

The chemical composition of ACP depends critically on washing. A study of ACP precipitates formed in the pH range 6.6-10.6 varied in Ca:P molar ratio from 1.18-1.50 after freeze-drying of the precipitate (Termine et al., 1972). However, washing of the precipitates before freeze-drying gave Ca:P ratios of 1.50±0.03. In fact at pH 6.6, washing considerably reduced the percentage of the total phosphorus present as acid phosphate from 33 to 18 %. Opinions appear to differ on why washing brings about this change. The most obvious reason would be the washing away of soluble surface-adsorbed phases or occluded Ca^{2+} ions. These observations, which were made in the case of ACP precipitating from an aqueous solution, may have some relevance to the precipitation of calcium phosphate from whey permeates especially if some of the solid still contains material in the ACP state. The transformation properties of ACP are very interesting and also very relevant in the case of ALAMIN™. Generally, it has been found that moist ACP converts (in the absence of an aqueous phase) to "non-stoichiometric HAP" at room temperature in 24 hours. Even vacuum dried samples convert to apatite over a period of months at ambient temperature (Puech et al., 1982). In the presence of a bulk aqueous phase at alkaline pH, the usual product of hydrolysis of ACP is HAP or non-stoichiometric HAP. ACP has been shown to be stable to transformation when

prepared in solutions at high pH, high ionic strength solutions rich in Ca^{2+} ions relative to HPO_4^{2-} ions, or low in initial supersaturation or temperature. ACP is also stable in the presence of poly-L-glutamate, polyacrylate, phosvitin, casein, large amounts of protein polysaccharides, or in the presence of small amounts of Mg^{2+}, $P_2O_7^{4-}$, CO_3^{2-}, or F^- ions (Termine et al., 1970). High magnification electron micrographs of ACP have revealed this phase to consist of spherical particles with diameters in the range of 20-120 nm without structure (Nylen et al., 1963). The particles are smaller if prepared under conditions of high supersaturation and/or pH; for a given pH, higher temperatures give larger particles (Blumenthal et al., 1972).

2.5 Nature of Calcium Phosphate in Milk

It is of interest to consider briefly the nature of calcium phosphate in cow's milk as this is the origin of all the calcium and the inorganic phosphate present in the whey permeate after removal of casein by precipitation at pH 4.6. Milk is a complex colloidal dispersion containing fat globules, casein micelles (which contain the amorphous or "colloidal calcium phosphate") and whey proteins in an aqueous solution of lactose, minerals and a few other minor compounds (Holt, 1997). The typical salt composition of bovine milk is given in Table 2-3 (Holt, 1985)

Table 2-3: Typical salt composition of bovine milk (Holt, 1985).

Component	Concentration (mM)
Ca^{2+}	30.1
Mg^{2+}	5.1
Na^+	25.5
K^+	36.8
P_i (inorganic phosphate)	20.9
Citrate	9.8
Cl^-	30.3

Table 2-3 shows that calcium and inorganic phosphate are present in relatively high concentrations in cow's milk. Approximately one third of the calcium can be regarded as "free" Ca (i.e. present in the aqueous media of milk) whilst the remainder is bound

largely to the casein phosphoproteins, partly as a calcium phosphate salt and partly as calcium caseinate (Holt, 1981). The calcium phosphate phase has often been referred as "micellar calcium phosphate" or MCP because of its close association with casein micelles in the milk. The first representation of casein micelle structure shown in Figure 2-3 is that of the "casein sub-micelle" model. It has evolved from several earlier models (Walstra et al., 1984, Schmidt 1982).

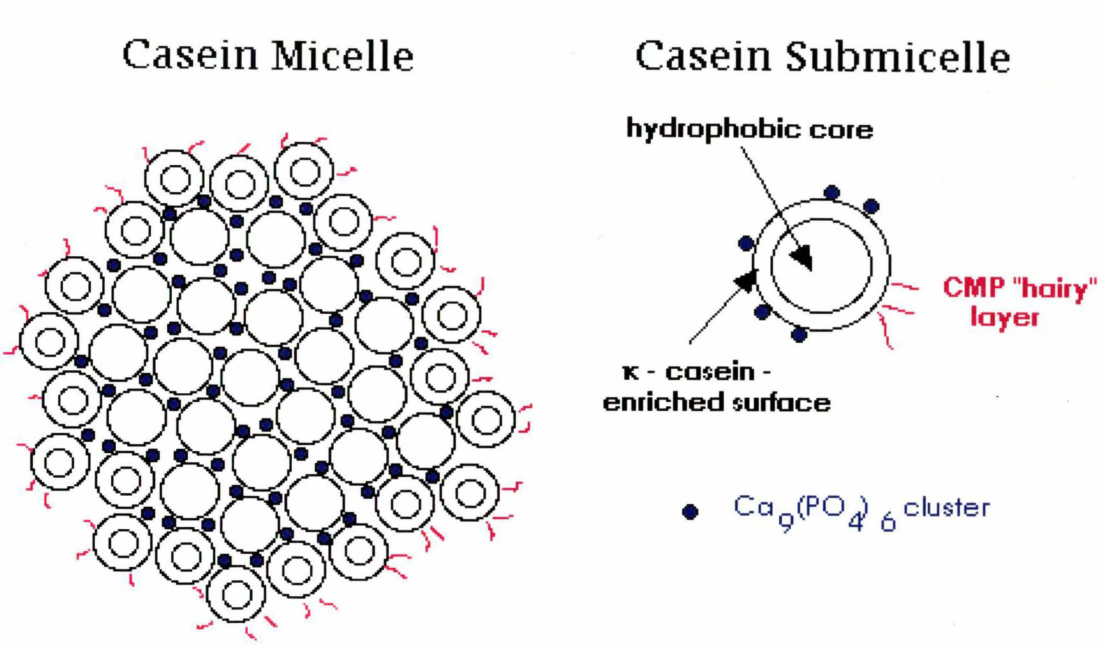

Figure 2-3: Schematic representation of a casein micelle and a submicelle (Walstra et al., 1984, Schmidt, 1982). Submicelles are to a first approximation considered to be spherical.

Much research effort worldwide has been directed towards an unequivocal characterisation of the MCP phase in milk but this has largely been hampered by the fact that it is difficult to distinguish between calcium bound directly to the casein phosphoproteins and calcium which is part of the MCP. Experimental attempts to measure the Ca:P ratio of the MCP, which is traditionally used to characterise CaP phases (see Table 2-1), have led to values of 1.40-1.62 and assertions (occasionally on the basis of other experimental data such as heat calorimetry measurements) that the calcium phosphate phase is Brushite (DCPD) or TCP or even HAP (Evenhuis et al., 1957; Chaplin, 1984; Holt, 1982; Holt et al., 1989; Lyster, 1979). Doubt, however, must be cast on these values for the Ca:P ratio because of the uncertainty in the amount of caseinate calcium and in particular, the intimate association with casein phosphopeptides.

Pyne and McGann (Pyne et al., 1960) have suggested that the mineralised regions of calcium phosphate in milk are accompanied by co-deposited calcium citrate which contributes partly to the Ca portion of the overall measured Ca:P_i ratio (P_i=inorganic phosphate ion). However, Holt et al. (Holt et al., 1989) challenged this philosophy and showed that if caseinate-associated phosphorus (designated by the symbol, P_o) is allowed for in the Ca:P calculation (i.e. if Ca:(P_o+P_i) ratios are calculated), the Ca:P ratio is found to be close to 1.0 suggesting that the MCP could be approximately described by an acidic-type *brushite* (DCPD) phase. Holt (Holt, 1997) has suggested an empirical formula for the calcium phosphate phase present in the MCP to be:

$$Ca(HPO_4)_{0.7}(PO_4)_{0.2}(H_2O)_x$$

The empirical composition for an entire MCP cluster can then be deduced on the basis of the above as a complex of about 50 empirical formulae with four or five calcium caseinate polypeptide chains:

$$[Ca(HPO_4)_{0.7}(PO_4)_{0.2}(H_2O)_x]_{50}[Ca_{2.5}Mg_{0.5}SerP_4\text{-}Casein]_5$$

Infrared spectra of MCP prepared as per the procedure of Holt (Holt et al., 1989) clearly confirms the existence of amorphous-type calcium phosphate in the micelles (Nelson et al., 1989). The amorphous nature of MCP renders the use of such techniques as X-ray diffractometry impossible since the technique is suitable only for unequivocal identification of crystalline phases. However, more sophisticated structural techniques (which require access to a synchrotron source of X-ray radiation) such as extended X-ray absorption fine structure (EXAFS) and X-ray absorption near edge spectroscopy (XANES) have shown that spectra of MCP from cow's milk and brushite are very similar indicating that the MCP is brushite-like in character. The picture that evolves from such work is one where the MCP consists of a domain of calcium phosphate which has formed by nucleation of calcium on the phosphate moieties of the phosphoserine and phosphothreonine residues from the casein proteins (Holt, 1982). In recent studies (Holt et al., 1996a), the "hairy casein micelle" model has evolved as a suggestion for the structure of casein micelles in an attempt to explain some of the "remarkable aspects" of

milk such as its property of withstanding moderate heat treatment without coagulation as well as its ability to maintain levels of ionic calcium and inorganic phosphate in solution at high supersaturation without spontaneous precipitation occurring. The hairy casein micelle model (Figure 2-4) consists of an open structure of polypeptide chains crosslinked by CaP nanoclusters in its core and an external region of low segment density which is known as the "hairy layer", which protects the CaP nanoclusters from coagulation by a steric or "crowding" effect.

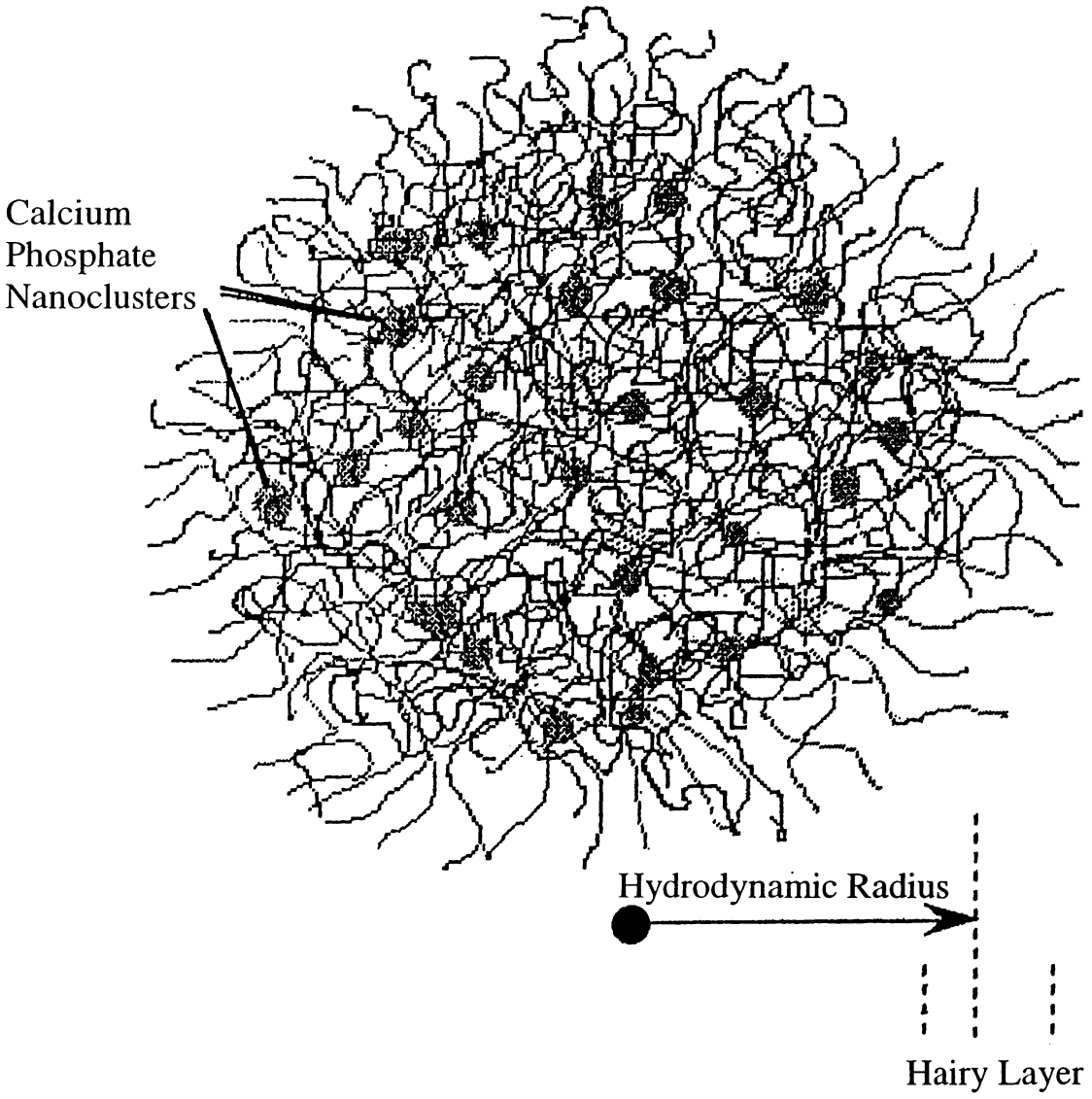

Figure 2-4: Hairy casein micelle model (Holt et al., 1996a). Calcium phosphate nanoclusters are shown as grey circles.

This structure of the MCP is destroyed upon acidification to pH 4.6 with all bound calcium and inorganic phosphate being released into the whey. However, the remarkable property exhibited by casein with respect to stabilising amorphous clusters of calcium phosphate in milk should be kept in mind when considering the addition of calcium phosphate powders to dairy media for supplementing the calcium level. A problem with the addition of calcium phosphate powders to various dairy media such as ultra-heat treated (UHT) milk has been their varying properties with respect to suspendibility in solution. Stabilisation could, in theory, be achieved by addition of protein or protein-like substances.

2.6 Introduction to Calcium Phosphate Precipitation from Aqueous Solution

The study of the precipitation of calcium phosphates from aqueous solutions has been a subject of intense research by a large number of authors (Eanes et al., 1965a, 1965b, 1968, 1973, 1976, 1977; van Kemenade et al., 1987, 1989; Feenstra et al., 1979, 1981; Heughebaert et al., 1984; Inskeep et al., 1988; Koutsoukos et al., 1980, 1981; Tenhuisen et al., 1994; Boskey et al., 1976; Holt et al., 1996b; Cheng et al., 1983; Nelson et al., 1986; Aoba et al., 1984; Moreno et al., 1968; Nancollas et al., 1974; Tomazic et al., 1975; Ishikawa et al., 1993a; Wong et al., 1993; Madsen et al., 1991; Schmidt et al., 1987a, 1987b; Abbona et al., 1990 and many more). The greater part of these studies have been carried out under controlled conditions where criteria such as maintaining constant compositions of calcium, phosphate and hydroxide and using carefully pre-grown and characterised hydroxyapatite seed crystals have been followed. The studies can be basically grouped into two types: *homogeneous* (unseeded) precipitation of calcium phosphate and *heterogeneous* (seeded) precipitation of calcium phosphate. Both areas will be discussed in this chapter since the unseeded and seeded processes are of relevance to the production of calcium phosphate by precipitation from natural whey permeates.

Careful, scientifically rigorous studies of the precipitation of calcium phosphate phases from natural whey permeate solutions are, in contrast, very few in number in the international chemical literature (Pouliot et al., 1991; Goldmann et al., 1992), hence the

interest by the New Zealand Dairy Industry in carrying out a fundamental study into the chemistry of calcium phosphate precipitation from the commercial whey UF-permeates.

2.7 General Trends observed in the Precipitation of Calcium Phosphate

2.7.1 Cornerstone Study by Eanes et al.

The paper by Eanes et al. (Eanes et al., 1965a) effectively laid the cornerstone for the intense period of research into the precipitation of calcium phosphate from aqueous solutions that followed in the 1970's-1990's. The paper was an X-ray diffraction/ titrimetric and spectrophotometric study of the "intermediate states in the (homogeneous) precipitation of hydroxyapatite". In the experiments, which were performed in closed systems to prevent absorption of CO_2, an initial Ca:P (solution) molar ratio of 1.71 was used at pH 10.5 and at a temperature of 25°C. In the study, it was reported that when the calcium phosphate precipitates, the first solid product to emerge is not hydroxyapatite, but an unstable amorphous solid, which is commonly referred to as "amorphous calcium phosphate". This amorphous solid (which gives a broad featureless signal with X-ray diffraction) usually has a measured Ca:P molar ratio of *ca.* 1.5 regardless of the calcium salt used to achieve the ACP (Eanes et al., 1965a). Once formed, the ACP gradually converts to a crystalline solid (apatitic) calcium phosphate in the solution. This is shown experimentally by the gradual appearance of a broad X-ray diffraction pattern typical of apatitic calcium phosphate and an increase in the measured Ca/P molar ratio towards 1.67 which is the value expected for hydroxyapatite ($Ca_{10}(PO_4)_6(OH)_2$). An increase in the degree of crystallinity is also observed (Eanes et al., 1965b).

Three stages in the precipitation were noted in the 1965 study. The first stage was the rapid formation of the ACP, the second stage was its slow (over a period of hours) transformation to a poorly crystallised apatite, and the third stage, which commences relatively rapidly after the second stage, is characterised by a slowly increasing degree in crystallinity of the apatitic precipitate which can extend over weeks in the solution. Later authors ascribed the second stage to an OCP (or DCPD) intermediate on which apatite growth commenced almost immediately. The process of the ACP to hydroxyapatite

conversion in solution was described as "autocatalytic" meaning that the emerging hydroxyapatite crystals act as sites for heterogeneous nucleation of more hydroxyapatite. In other words once the "foundation" (in the form of ACP) is formed, a more crystalline phase begins to form on it and as the small crystallites form, they themselves form the "foundation pegs" for even more hydroxyapatite to grow, and so on, so that the rate of conversion is accelerated as more hydroxyapatite is formed. It is important that the ACP be in water when this occurs as the process occurs by stages of initial dissolution and reprecipitation (i.e. it is solution mediated). A highly simplified and crude scheme, which describes the separation of calcium phosphate from solution by precipitation, can be given as:

$$Ca^{2+} + P_i \Rightarrow (\text{minutes}) \Rightarrow (2)\ ACP \Rightarrow (\text{minutes / hours}) \Rightarrow$$

$$(3)\ DCPD\ /\ OCP \Rightarrow (\text{hours / days})\ (4)\ HAP$$

where P_i is a very broad term referring to "inorganic phosphate ion" in solution. The above scheme can be affected by many variables such as pH, concentration, supersaturation, temperature and additives. In some cases, completely different phases of calcium phosphate can form whilst in others (for instance, when additives such as Mg^{2+} are included), the amorphous intermediate phase can be stabilised and prevented from converting to a crystalline substance.

2.7.2 Further Studies by Eanes et al. with Microscopic Evidence of the Intermediate Calcium Phosphate Phases

Eanes et al. (Eanes et al., 1973) performed a very illustrative transmission electron microscopic study showing the formation of the initially amorphous calcium phosphate and its transformation to crystalline apatite. Precipitates generated from a) mixing of 10.4 mM $CaCl_2$ and Na_2HPO_4 solutions in 0.15 M TRIS buffer (adjusted to pH 7.40 with HCl) and b) mixing of an unbuffered solution of 8.0 mM $CaCl_2$ and a 60 mM $NaHCO_3$-buffered solution of 3.4 mM Na_2HPO_4 (with background ionic strength of 0.15 M NaCl) were used. Solid precipitates were taken at various stages and lyophilised (freeze-dried) to minimise side-effects caused by drying processes.

2.7.2 (a) Freshly Precipitated Solids

Electron micrographs from freshly precipitated preparations revealed the existence of two morphological types: low contrast spherules and high contrast disks and spheres. These were identified as amorphous calcium phosphate. The true nature of the ACP precipitate was postulated to be a very loosely organised, highly hydrated, colloidal aggregate when it was present in solution, which is believed to collapse into disk-like and sphere-like shapes when it is brought into contact with the grid membrane on which samples are mounted for transmission electron microscopic analysis. A colloidal suspension is one which consists of many sub-microscopic particles in the 1 nm to 1 μm size range that are not visible to the naked eye.

2.7.2(b) Solids left to Mature or "Age"

The study by Eanes (Eanes et al., 1973) showed convincingly the evolution of an initially formed amorphous phase into a more crystalline apatitic phase. The ACP was seen as a "necessary" precursor to the formation of hydroxyapatite in solution. As more apatitic crystals grow, they create secondary sites for the growth of even more crystals. The amorphous calcium phosphate "foundation" eventually dissolves away and is replaced by a mat of semi-crystalline apatitic phase. The progress of the conversion can also be followed by light scattering since a solution containing this precipitate becomes increasingly more "turbid" and so blocks light. It is believed that the precipitation of calcium phosphate from whey permeates also proceeds through an intermediate ACP phase.

What was also apparent from Eanes study (Eanes et al., 1973) was that electron micrographs of solids allowed to "age" revealed that the "borders" of the high contrast ACP spherules began to be randomly punctuated with small bodies of crystals which became large and more numerous in appearance as the precipitate was allowed to mature. At the same time, the X-ray diffraction patterns of the solid were observed to resemble poorly crystallised apatite. Electron micrographs of precipitates allowed to age for 300 minutes after the initial formation showed the initial spherules to be completely clustered with plate-like crystals (Eanes et al., 1973).

2.8 Introduction to Various Concepts and Terminology associated with Calcium Phosphate Compounds and their Precipitation from Aqueous Solutions

It is necessary to introduce some concepts and terminology that are widely used by researchers in the field of calcium phosphate and its precipitation from aqueous solution before discussing the factors which influence the process.

2.9 Supersaturation and Solubility Products of Sparingly Soluble Salts

2.9.1 Solubility Products

Sparingly soluble salts are those which can only be dissolved to a limited extent in water (Atkins, 1996). The calcium phosphates are well known for their very limited solubility in aqueous solutions (Moreno et al., 1968; McDowell et al., 1971). In chemistry, physical constants can be used to provide a relative index of insolubilities of various compounds to describe the relative insolubility of various compounds. These are formulated and measured from the equilibrium that exists between a sparingly soluble ionic compound (e.g. $Ca(OH)_2$), and its ions in solution, viz.,

$$Ca(OH)_2 \rightleftharpoons Ca^{2+}_{(aq)} + 2OH^-_{(aq)}$$

The equilibrium constant for this solubility equilibrium is called K_{sp}, the solubility product or solubility constant (Atkins, 1996). This can be related to the *activities* of the ionic species in solution, viz.,

$$K_{sp} = a(Ca^{2+})\, a(OH^-)^2$$

where a is the activity of an ionic species in solution. Activities of ionic species are basically referred to as "effective concentrations" defined for experimental purposes and which account (in an empirical sense) for ion-ion interactions in solution. Activity of calcium ion, for instance, is given by $a(Ca^{2+}) = f_{Ca}{}^{2+}[Ca^{2+}]$, where $f_{Ca}{}^{2+}$ = the activity coefficient of the calcium ion and $[Ca^{2+}]$ = the concentration of the calcium ion in M. K_{sp} values for various inorganic solids have been compiled in the chemical literature. The smaller the value of K_{sp}, the more insoluble the salt. For example, the K_{sp} value for Bi_2S_3,

an very insoluble sulfide compound, is 1.0×10^{-97}, whereas the K_{sp} value for $Ca(OH)_2$ is 5.5×10^{-6} indicating it is a much more soluble salt.

2.9.2 Definition of Supersaturation

Values of K_{sp} can be used to predict whether solutions of ions at certain concentrations when mixed will spontaneously precipitate solid. This will tend to occur if the IP (ion product) given by the expression for K_{sp} exceeds the value for K_{sp}. Often so-called metastable solutions can exist where the IP exceeds the K_{sp} value for an insoluble salt with no precipitation of solid occurring. Such solutions are said to be supersaturated with respect to the particular phase in question. Thus in equation form, supersaturation is defined by the symbol β, and a solution is said to be supersaturated with respect to a solid phase if (Wong et al., 1993):

$$\beta = \frac{IP}{K_{sp}} > 1$$

Other papers may also use the symbol, Π, to denote supersaturation (Feenstra et al., 1979). In addition, a slightly modified expression for supersaturation (called S_{CaP}) is used which is defined later (see 2.13.2: "General Trends and Definitions of Terms").

2.9.3 A General Word on Nucleation

The basic principles of nucleation underlie many important processes that occur in science, technology and nature when phase transitions are occurring (Toschev, 1973).

Nucleation can be defined as the formation of small embryonic clusters which necessarily precedes a general macroscopic phase transition. In nature, when rain falls from the sky, small nucleating water droplets must form on small dust particles in the atmosphere before they grow to become a larger raindrop. The same principle operates for deposition of solid, small clusters of material must first form before bulk crystallisation occurs.

2.9.4 Thermodynamics and Seeded versus Unseeded Nucleation

During nucleation the smallest molecular aggregates (embryos) of a crystalline phase is formed. The overall free energy goes through a maximum at some critical size r^*. Embryos in solution will tend to decrease their overall free energy by changing their size. Those smaller than the critical size achieve this by redissolving, and those larger than r* will continue to grow. The size of the nucleus (critical radius, r^*) will govern its survival and further growth (if $r > r^*$) or its destruction (if $r < r^*$). Nucleation may proceed via *homogeneous* pathways whereby nuclei are produced in a short "burst" in the bulk of the solution when a certain critical supersaturation level is reached. The alternative type of nucleation is known as *heterogeneous* nucleation whereby growth of the solid phase from supersaturated solutions begins to occur on seed crystals added to the solution.

2.10 Solubilities and Supersaturation in Ca^{2+}- and Inorganic Phosphate-Containing Solutions

2.10.1 Ion Products and K_{sp} values of the Various Calcium Phosphate Phases

Nucleation and precipitation from calcium and inorganic phosphate-containing solutions is generally complicated by the fact that the solution may be supersaturated with respect to more than one calcium phosphate solid phase. Table 2-4 (Feenstra et al., 1979) lists the common CaP phases that may precipitate out of aqueous solution as well as their K_{sp} values. In principle, the same phases may precipitate out of the whey permeate in the commercial precipitation process upon addition of hydroxide ion. The IP values for the various calcium phosphate phases are:

$$IP_{DCPD} = [Ca^{2+}]f_2[HPO_4^{2-}]f_2$$

$$IP_{OCP} = ([Ca^{2+}]f_2)^4(PO_4^{3-})f_3)^3[H^+]f_1$$

$$IP_{TCP} = ([Ca^{2+}]f_2)^3(PO_4^{3-})f_3)^2$$

$$IP_{HAP} = \frac{([Ca^{2+}]f_2)^5(PO_4^{3-})f_3)^3 K_w}{[H^+]f_1}$$

where f_x represents the activity coefficient of a z valent ion (M^{z+} or N^{z-}).

Table 2-4: Phases that may precipitate out of a metastable, supersaturated solution of calcium ions and inorganic phosphate (from Feenstra et al., 1979).

Calcium Phosphate Phase	Solubility Product (K_{sp}), M
Dicalcium phosphate dihydrate (DCPD) $CaHPO_4.2H_2O$	2.1×10^{-7} $(M)^2$
Tricalcium phosphate (TCP) $Ca_3(PO_4)_2$	1.15×10^{-29} $(M)^5$
Octacalcium phosphate (OCP) $Ca_8H_2(PO_4)_6$	1.25×10^{-47} $(M)^8$ (expressed for the "monomer unit" $Ca_4H(PO_4)_3$)
Hydroxyapatite (HAP) $Ca_{10}(PO_4)_6(OH)_2$	6.3×10^{-59} $(M)^9$ (expressed for the "monomer unit" $Ca_5(PO_4)_3(OH)$)

2.10.2 Phase Transformations and Ostwald's Law of Stages in Precipitating Calcium Phosphate Suspensions

Earlier, it was shown in Eanes's studies (Eanes et al., 1965a, 1965b, 1968, 1973, 1976, 1977) that the development of an apatitic-like solid from a precipitating calcium phosphate suspension is preceded by 2 intermediate stages. The behaviour of calcium phosphate as it precipitates from aqueous solution is said to follow the Ostwald rule of stages, a famous rule formulated by Ostwald (Ostwald, 1897) who was the first person to study precipitation processes in highly supersaturated solutions. The rule asserts (Feenstra, 1979) that the phase which is precipitating first is not the most thermodynamically stable phase but rather a metastable phase which is "thrown together" rapidly at the initial stages of the reaction due to its relative ease of formation. The initially formed phase then transforms over time into more stable phases and eventually reaches the most thermodynamically stable phase which constitutes the end product. In the case of calcium phosphate precipitation, the initial *amorphous* phase produced is metastable and transforms eventually into hydroxyapatite which is the thermodynamically most stable calcium phosphate compound. In the particular early study by Eanes et al. (1965a) which was conducted at pH 10.5, the second intermediate stage referred vaguely

to as "apatitic", has been shown on the basis of later work by other researchers to be OCP (Tomazic et al., 1975; Eanes et al., 1977; Meyer et al., 1978; Madsen et al., 1991). This phase is penultimate to HAP in thermodynamic stability.

It is important to note, however, that the conditions under which the precipitation of calcium phosphate is carried out can greatly affect the system with respect to the intermediates and products that result. In general, changes in pH, temperature, initial supersaturation, seeding concentration, solution components (e.g. proteins and milk-derived inorganic and organic species such as citrate and lactate and lactose), ionic strength, and ion speciation can have a vast effect on the character of intermediates and phases produced, yields, and speed of reaction. Given that whey can vary in its overall composition, it is critical to the smooth running of the commercial calcium phosphate production process that there be a thorough understanding of how changes in conditions influence the precipitation reaction.

2.11 Influences on the Chemistry of Calcium Phosphate Precipitation from Aqueous Solution

In this section the influences of various factors on calcium phosphate precipitation will be covered. These have been broken down into the following subheadings: effect of pH, effect of supersaturation, effect of temperature, influence of ionic strength, influence of seeding concentration, and influence of additives/impurities. Although an attempt has been made to separate these effects as an aid to understanding how they might affect the commercial CaP production process, it should be understood that there will be a large degree of overlap between these areas and that the most pragmatic approach is to consider the overall situation in order to gain insights.

2.12 Effect of pH and Temperature

2.12.1 Study by van Kemenade et al.

2.12.1(a) Solubility Isotherms for the Calcium Phosphate Phases

The pH at which the calcium phosphate precipitates can have a profound effect on the precipitating sequence of the phases that precede the final apatitic product. A key study by van Kemenade et al. (van Kemenade et al., 1987) has looked into the formation of the

three important calcium phosphate solids (DCPD, OCP, HAP) as well as ACP as a function of pH and supersaturation. In agreement with the numerous studies by Eanes et al. (see earlier), van Kemenade noted that the formation of HAP was always found to be preceded by one or more precursor phases. Direct and homogeneous formation of HAP was never observed under the experimental conditions used.

As calcium phosphate precipitates out a number of precursor intermediates before HAP is produced, most previous literature-sourced studies on calcium phosphate precipitation calculate and display "solubility isotherms" of the various precursor calcium phosphate phases to HAP (including HAP itself). Figure 2-5 illustrates the solubility isotherms of HAP, OCP and DCPD as reported by van Kemenade et al. (van Kemenade et al., 1987) at temperatures of 25°C and 37°C. These are plots of $\log_{10}P_T$ vs. pH (P_T = total initial phosphate concentration). The isotherms are of constant saturation equal to 1. Above the lines, precipitation can occur but may not either because another phase does so in preference or because it has no accessible mechanism of precipitation. In the particular experiments carried out by van Kemenade et al., an ionic strength of 0.15 M and total calcium / phosphorus molar ration (Ca:P) of 1.16 was used. In addition a *constant* (pH-stat controlled) pH (6.0, 6.7, 7.4) was used during precipitation experiments under these conditions, the phases of DCPA and whitlockite are not found.

Inspection of the solubility isotherms in Figure 2-5 (from van Kemenade et al.) and comparison with the curves produced in other studies on calcium phosphate precipitation run under slightly different experimental conditions (Koutsoukos et al., 1980; Feenstra et al., 1979), reveal some differences (e.g. under some conditions, formation of TCP should be theoretically possible) but essentially the behaviour of the medium with respect to the various solid calcium phosphate phases is very similar. HAP is regarded as the thermodynamically most stable phase since it has the lowest solubility of all the calcium phosphates compared on the curve. At a pH of 6.7 and a temperature of 26°C, the isothermal curves for OCP and DCPD intersect. This means that above pH 6.7, DCPD has the higher solubility and is therefore less stable than OCP. At a lower pH, the stability order is OCP < DCPD < HAP. The Ostwald rule would, therefore, predict a change in precipitating sequence at about pH 6.7 at a temperature of 26°C. In the case of precipitation of calcium phosphate from whey permeates, this may be of consequence,

were the reaction to be carried out at 26°C. However, the precipitation is carried out at elevated temperatures and so there is a temperature effect.

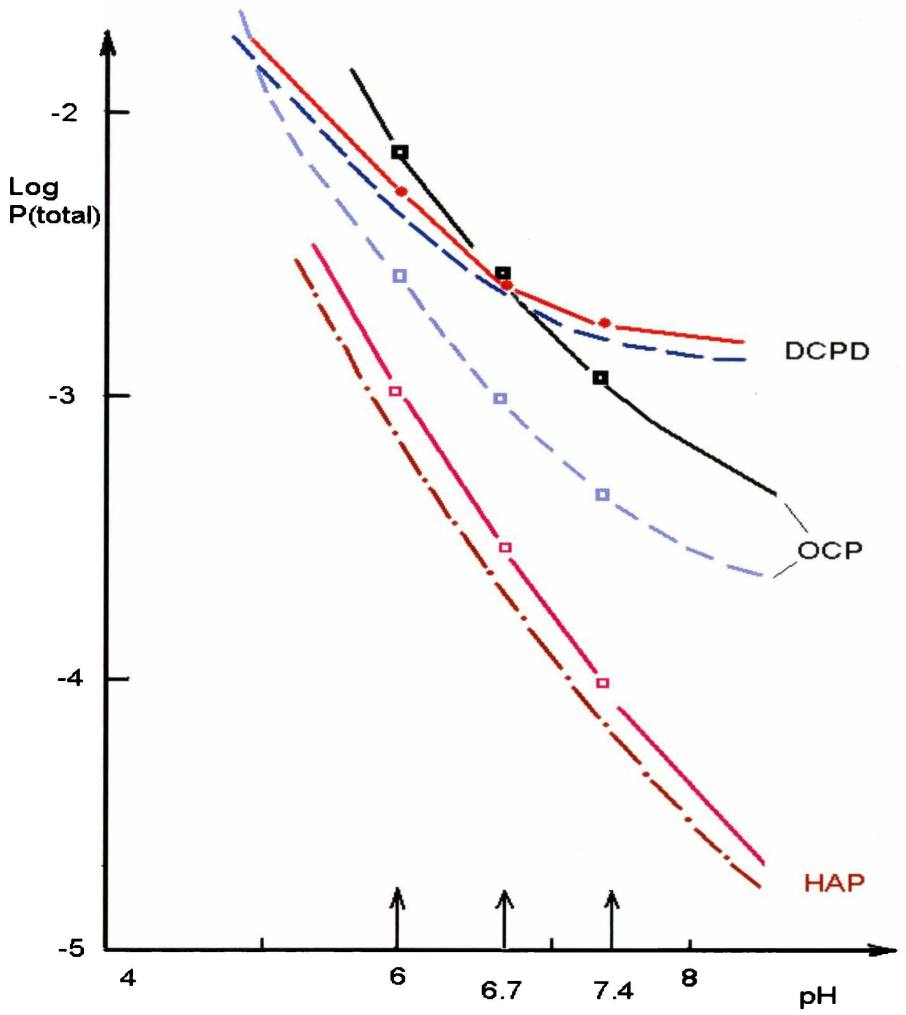

Figure 2-5: Solubility isotherms of HAP, OCP and DCPD at 25°C (solid lines) and 37°C (dotted lines) as log P(total) versus pH. P(total) is the total phosphate concentration (M) in solution. The Ca:P molar ratio 1.16 and ionic strength 0.15 (from van Kemenade et al., 1987).

Inspection of the solubility curves at 37°C in Figure 2-5 shows a shift of the solubility curves for all phases to lower pH with a consequent shift to lower pH of the intersection point of the DCPD and OCP curves. This effectively keeps the relative stability of the phases in the sequence DCPD < OCP < HAP at lower pH values. This is likely to be the sequence for the precipitating whey permeates although DCPD has not yet been observed as an intermediate phase. In van Kemenade's study (van Kemenade et al., 1987), the

information from the solubility isotherms was effectively supported by the observed precipitation sequence which was deduced by examination of electron micrographs of the precipitating solids. Table 2-5 summarises the precipitating sequence observed.

Table 2-5: Precipitating sequences observed (on the basis of electron micrographs) from the study by van Kemenade et al. (van Kemenade et al., 1987). For a broad description of experimental conditions, see caption to Figure 2-5 (solubility curves).

pH	T (°C)	Precipitating sequence
6.0	26	OCP => DCPD => HAP
6.7	26	DCPD = OCP => HAP
7.4	26	ACP => OCP => HAP
6.7	37	DCPD => OCP => HAP

In general, the experiments proved (by way of electron microscopy) that Ostwald's law of stages was being followed. Of particular note in van Kemenade's study was the reversal of sequence for OCP and DCPD at pH 6.0 and 6.7 at 26°C, which is in accordance with the solubility isotherms (see Figure 2-5). However, it was noted that at pH 7.4, instead of DCPD appearing as the first precipitated phase, a much less stable ACP (amorphous calcium phosphate) precipitate was postulated to occur. This was deduced from the complete absence of plate-like DCPD crystals in electron micrographs obtained from precipitates over all the supersaturation levels trialed. The electron micrograph of the precipitate from the pH 7.4 reaction performed at high supersaturation was distinctly apatitic in its morphology and had a measured Ca:P molar ratio from EDX analysis (see Chapter 3 for details of this instrumental technique) of 1.57-1.65 confirming it was a calcium deficient apatite.

2.12.1(b) Hydroxide Uptake as a Function of Time

Van Kemenade et al. (Van Kemenade et al., 1987) displayed diagnostic graphical data (see Figure 2-6) which relate hydroxide uptake as a function of time after precipitation of calcium phosphate begins to occur.

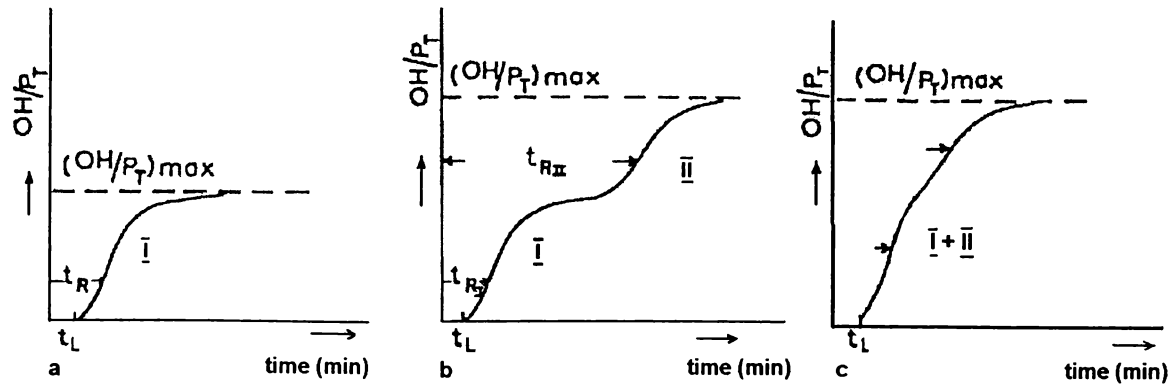

Figure 2-6: Typical relaxation curves (from pH-stat experiments) for precipitation of: a) a pure phase forming successively; b) two phases forming successively and c) two phases forming simultaneously over a certain period. Precipitation parameters are the relaxation time, t_R, defined at inflection points of the S-shaped curves, the lagtime (t_L), and the maximum amount of base uptake (OH/P_T). In curve c arrows point to inflection points which cannot be interpreted as separate relaxation times (from van Kemenade et al., 1987).

These curves (Figure 2-6) are plotted as total base uptake (given by OH/P_T; P_T = total phosphate) versus time. They are called "relaxation" curves as they demonstrate how a metastable supersaturated solution achieves greater stability by "relaxing" from an initial high-energy state by precipitation of a solid phase.

The "relaxation" of supersaturated calcium phosphate solutions tends to follow curves (b) and (c) in Figure 2-6. The "inflection" points indicated in curves are evidence for separate phases forming. This is because of the nucleation and growth kinetics of the different calcium phosphate phases occurring. Unbuffered precipitation reactions involving calcium phosphate exhibit a drop in pH as the reaction proceeds due to ongoing formation of a basic apatitic phase, which requires the uptake of hydroxide. This can be expressed in chemical equation form for each of the precursor phases and hydroxyapatite (Brown et al., 1984):

$$1)\ DCPD \Rightarrow OCP$$

$$6CaHPO_4 2H_2O + Ca^{2+} + 4OH^- \Rightarrow Ca_8H_2(PO_4)_6 5H_2O + 11H_2O$$

$$2)\ OCP \Rightarrow HAP$$

$$Ca_8H_2(PO_4)_6 5H_2O + 2Ca^{2+} + 4OH^- \Rightarrow Ca_5(PO_4)_3 OH + 7H_2O$$

It should also be noted that there will also be more than one phase change occurring at once. Thus, in cases where ACP is a precursor and is forming OCP as a secondary intermediate, there will also be simultaneous formation of HAP on top of the nascent OCP phase. The ability of OCP as a template for apatitic overgrowth has already been mentioned earlier in this review (Elliot, 1994).

2.12.2 High pH versus Low pH Precipitation

A paper by Pouliot et al. (Pouliot et al., 1991) on induction of calcium phosphate precipitation in sweet whey permeate claimed improved yields at pH= 8.0 (as opposed to pH 6.6) though only in the presence of added DCPD seeds. Unfortunately, fundamental studies on calcium phosphate precipitation give little or no information on "yield" in terms of a particular solid phase, given that the character of the solids is changing constantly throughout the reaction. However, it has already been shown in previous work (see earlier) by van Kemenade et al., (van Kemenade et al., 1987) that conducting the precipitation at pH 7.4 at a temperature of 25°C leads to a change in the intermediate solid phase produced from a DCPD/OCP-like intermediate to an ACP/OCP-like intermediate which then converts to an apatitic solid. Thus, an obvious consequence of altering pH is to change the mechanism of the precipitation reaction by changing the nature of the intermediary solid phase.

It has been reported by both van Kemenade et al. (van Kemenade et al., 1987) and by Heughebaert et al. (Heughebaert et al., 1984) that OCP will be the first phase to appear and grow at pH 6.0 (van Kemenade reported their result at a temperature of 26°C and Heughebaert reported their results for growth of OCP on OCP seed crystals at 37°C).

Thus, assuming a similar precipitation sequence at 70°C (there is a strong possibility that DCPD could be the so-called "seeding" phase formed in pH adjustment to pH 5.5-5.8 since this phase is generally stable at pH < 6.5), OCP crystals could well be formed that could then develop via DCPD into the typical apatitic calcium phosphate phase upon adjustment to pH 6.7. The previous research on the actual sequence of precipitation of the unstable precursor phases to HAP can be very difficult to interpret (i.e. in terms of comparisons with the whey permeate from which ALAMIN™ is derived) due to the wide variety of conditions under which calcium phosphate has been grown, as reported in the literature studies.

2.12.3 Thermodynamic Analysis of the Transitional Phases in the Precipitation of Calcium Phosphate

Meyer et al. (Meyer et al., 1978) provide an excellent explanation for what happens to the mechanism of the precipitation reaction as precipitation is conducted at increasing pH. Unseeded precipitation reactions over the pH range 7-9 were performed and the data collected. Most of the data collected with regard to changes in calcium, phosphate and hydroxide concentrations with time indicated discontinuities in the plotted curves indicating phase transitions from an initial amorphous phase through to a secondary crystalline phase and finally the (apatitic) end product which developed after conversion of the secondary phase. The thermodynamic stabilities of the experimental solutions with respect to a solution in equilibrium with the well-defined pure crystalline calcium phosphate phases HAP, TCP, OCP and DCPD were then determined at each point corresponding to a sampling time during the precipitation sequence using the equation for the free energy of transfer of material from a supersaturated solution to a saturated solution (ΔG):

$$\Delta G = -2.303 \frac{RT}{n} \log \frac{IP}{K_{sp}}$$

where R is the ideal gas constant (8.314 J K^{-1} mol^{-1}), T is absolute temperature in K and n is the number of ionic terms in the activity product (IP) expression.

The ΔG calculations serve two purposes: Firstly, when plotted versus time, they show how the calcium phosphate ion products (IP) in solution vary during the course of the precipitation experiments. Secondly, the ΔG values indicate the thermodynamic stability of the experimental solutions compared to solutions in thermodynamic equilibrium with the particular phase in question (e.g. HAP, TCP, OCP, DCPD). Any calculated ΔG values at or near zero, suggest the possibility that the solution phase may be in equilibrium with the solid phase for which a solubility product (K_{sp}) is known. If the ΔG curves consistently flatten out at this point (i.e. where ΔG=0) at the beginning, or the end, of an apparent phase transition in spite of a wide variation of experimental conditions, then the evidence for a specific solid phase being an intermediate is particularly strong. Meyer et al. (Meyer et al., 1978) thus illustrated a series of plots of ΔG versus time for a) the entire reaction and b) for the course of the reaction beginning with the start and the end of only the secondary (first formed crystalline solid after the initial amorphous solid) transition. The ΔG values were generated for each of the phases DCPD, OCP, TCP and HAP and the results compared. In brief, all plots showed that as the precipitation reaction was performed at higher pH, the duration of the amorphous-crystalline transition period *became longer* whilst the secondary transition to an apatitic phase occurred much more rapidly.

Meyer et al.'s studies indicate, furthermore, that the solution phase in equilibrium with the first formed phase is very likely to be OCP. This was deduced from the observation that the ΔG curves for the secondary transition flatten at a point very near to but slightly above the ΔG=0 line. A further interesting observation was that at the end of the secondary transition, a phase which was more basic and apatitic in nature but with a composition corresponding roughly to TCP had formed. This is an interesting observation as it would explain the experimentally observed Ca:P ratio of 1.50 that is often found for initially formed precipitates. TCP is then postulated to convert to HAP by further uptake of calcium and hydroxide ions from solution. Thus in summary, the sequence of events occurring as deduced from the thermodynamic analysis of Meyer et al. is:

1) *Amorphous Phase* ⇒ 2) " *Acid*" *Crystalline (OCP) Phase* ⇒

3) " *Basic*" *TCP – like phase* ⇒ 4) *HAP*

The strongest evidence for the crystalline phase associated with the secondary transition being an "acidic" OCP-like compound was the speed of the conversion of the OCP-like precipitate to TCP/HAP. At pH 7.00, 193 minutes were required for the secondary transformation to TCP/HAP to take place while at pH > 8.80, the transformation was too rapid for an accurate measurement to be taken.

2.12.4 Effect of Temperature

In general, most soluble inorganic salt compounds like sodium chloride, for instance, exhibit increasing solubility in water as temperature is increased. The same trend applies for relatively insoluble substances in water. HAP is an unusual solid in that it exhibits the opposite trend. It becomes more insoluble in water as temperature is increased. This property of HAP coupled with the high supersaturation of calcium phosphate phases in the whey permeates ensures a rapid precipitation of solid when pH is increased in the heated permeates at 75°C.

Pouliot et al. (Pouliot et al., 1991) conducted a study into the precipitation of calcium phosphate from sweet cheese whey and found that only a gel and not a granular crystalline precipitate of calcium phosphate could be obtained at pH 7.5-8.0. Much more satisfactory results were obtained at pH 8.0 and a higher temperature of 50°C in the presence of DCPD seeds.

2.13 Effect of Supersaturation

2.13.1 Introduction

The degree of supersaturation or metastability of solution has been found to be a very important factor in influencing calcium phosphate precipitation. Although the specific effect of supersaturation cannot be fully separated from those of pH, specific concentrations of calcium and inorganic phosphate, ionic strength, temperature and the presence of heteronuclei (seeds), many authors (Nancollas et al., 1974; Boskey et al, 1976; Koutsoukos et al., 1980; Feenstra et al., 1979; van Kemenade et al., 1987; Abbona et al., 1990) have discussed the effects of low, medium and high supersaturation media

on the precipitation of calcium phosphate. Given, under many conditions, HAP formation is preceded by a number of other less thermodynamically stable, more soluble calcium phosphate phases, a solution will have different values of supersaturation (or undersaturation) depending on which calcium phosphate phase it is referenced to (i.e. in terms of its K_{sp} value). For example, a solution with certain, initial values of total calcium and inorganic phosphate may be supersaturated with respect to HAP, OCP and TCP but undersaturated with respect to DCPD (see Table 2-4). Other solutions may be supersaturated with respect to all the calcium phosphate phases. Solutions with these differing initial conditions (prior to any precipitation experiment) will behave differently.

2.13.2 General Trends and Definitions of Terms

In general, two regimes of precipitation behaviour have been identified. For precipitation of calcium phosphate in solutions with "high" supersaturation, an amorphous calcium phosphate (which subsequently transforms to hydroxyapatite via intermediate phases such as OCP, for instance) is initially formed. Precipitating solutions with "low" supersaturation, on the other hand, appear to form hydroxyapatite directly, albeit, several hours after mixing.

Before discussing the work of previous authors, it is necessary to define some terms frequently used that define the supersaturation level. The "degree of supersaturation "

$$S_{\text{CaP}} = \frac{IP - K_{sp}}{K_{sp}}$$

with respect to each of the calcium phosphate phases has already been defined earlier and given the symbol, β, however some authors have also defined a somewhat modified expression for supersaturation which is given the symbol, S_{CaP} (Nancollas et al., 1974; Boskey et al., 1976). A term (S_{Ca}) is also used which relates to the free calcium ionic concentration:

$$S_{Ca} = \frac{[Ca^{2+}]_t - [Ca^{2+}]_{eq}}{[Ca^{2+}]_{eq}}$$

where $[Ca^{2+}]_t$ = the ionic calcium concentration at the beginning of a given experiment and $[Ca^{2+}]_{eq}$ = the ionic calcium concentration value at equilibrium (Boskey et al., 1976).

2.13.3 Experiments at "High" Supersaturation

Nancollas et al. (Nancollas et al., 1974) performed a "high" supersaturation (seeded) experiment in which total ionic calcium and phosphate concentrations were initially 1.562 and 0.973 mM (ionic strength = 6.73 mM). At these concentrations, the solution was supersaturated with respect to all four calcium phosphate phases, DCPD, OCP, TCP and HAP. The corresponding S_{CaP} values were 0.66, 1.60×10^2, 1.17×10^3 and 1.23×10^{11} for DCPD, OCP, TCP and HAP respectively. S_{Ca} values were 0.24, 1.1, 3.4 and 43.6 for DCPD, OCP, TCP and HAP respectively. In the precipitation experiment, Nancollas et al. calculated $\Delta[Ca]/\Delta[P]$, where $\Delta[Ca]$ and $\Delta[P]$ were calculated as differences in concentration between initial concentrations and concentrations after a specific time, t.

In the high supersaturation seeded experiments, it was found that $\Delta[Ca]/\Delta[P]$ attained a relatively constant value of *ca.* 1.50 after 30 minutes of reaction. X-ray diffractograms of the material (grown on the seeds) indicated only HAP seed material initially. Calculations based on X-ray diffractograms with respect to the degree of crystallinity indicated an initial drop in crystallinity until about 5 hours after which point crystallinity increased. All of these results were interpreted by Nancollas et al. as suggesting that in the early stages of HAP-seeded growth, an amorphous phase is formed which subsequently undergoes conversion to a crystalline material with an apatitic X-ray diffractogram pattern. This behaviour is comparable to that for unseeded precipitation of calcium phosphate as shown in the work by Eanes et al. (Eanes et al., 1965a, 1965b, 1973). Nancollas et al. (Nancollas et al., 1974) furthermore demonstrated (by controlled dissolution of the nascent precipitates at pH 7.4 and measurement of dissolved $\Delta[Ca]/\Delta[P]$ in their study that one of the intermediate, unstable phases formed was OCP.

Nancollas et al. emphasised in his study that the intermediate phases formed and then redissolved over time to provide calcium and phosphate for formation of the thermodynamically more stable phases of TCP and HAP.

Van Kemenade et al. (van Kemenade et al., 1987) performed an extensive study of calcium phosphate precipitation at different pH, temperatures and levels of supersaturation as discussed earlier. Unfortunately, the supersaturation values were not reported for defining the regions of "high", "moderate" and "low" supersaturation. At high supersaturation and pH 7.4, HAP was produced via conversion of an intermediate OCP phase. In most studies conducted by van Kemenade et al., HAP was reported as a final product which was reached via dissolution/reprecipitation of intermediate OCP and DCPD phases.

2.13.4 Experiments at "Low" Supersaturation

Boskey et al. (Boskey et al., 1976) performed a study on precipitation of HAP from unseeded solutions at low supersaturation. After a certain induction period of 13-35 minutes following mixing calcium and phosphate solutions, Boskey et al. detected no solids in transmission electron micrographs of withdrawn samples. After the induction time, "dot-like" material was observed, which was approximately 25 Å in diameter which gave a featureless X-ray diffractogram pattern, as expected for an amorphous compound such as ACP. After 24 hours, long, microcrystalline particles were observed which gave a much sharper X-ray diffraction pattern that was identical to that for hydroxyapatite. Changes in the solution calcium (Δ[Ca]) and phosphate (Δ[P]) concentrations in solution during crystal growth in the low supersaturation solutions consistently gave $\Delta[Ca]/\Delta[P]$ ratios of 1.67. Calculations of the number of hydroxyapatite particles produced as a function of time after nucleation began, showed that after 120 minutes, no new particles were forming and that existing nuclei were simply growing in size (ripening). On first appearance, this leads one to think that HAP forms directly but according to some researchers, it does not. Due to the low supersaturation, nuclei formed initially are far fewer in number and hence their influence on composition small enough to be undetectable, hence giving the impression of direct nucleation. In other studies by Boskey et al. the calculated supersaturations with respect to HAP were much higher and

consequently, an amorphous precursor (ACP) or OCP was observed to occur (see Table 2-6).

In the paper by Nancollas et al. (Nancollas et al., 1974) on seeded growth of HAP at various supersaturations, it was stated that under conditions of low supersaturation, the calcium phosphates with the lower Ca:P ratios such as DCPD, OCP and TCP, cannot form and, therefore, their hypothetical dissolution (were these solid phases to form) would not contribute to the overall $\Delta[Ca]/\Delta[P]$ ratios.

2.13.5 Summary of the "High" and "Low" Supersaturation Limits which define whether or not ACP forms as an Intermediate Phase

Many previous calcium phosphate precipitation studies do not give a clearly defined threshold for the "high" supersaturation level at which an amorphous intermediate phase is expected to precipitate out of solution. However, Abbona et al. (Abbona et al., 1990) state that if the supersaturation with respect to HAP is $> 10^{12}$ (using the expression for β_{HAP} rather than for S_{CaP}), ACP precipitates. This agrees with Boskey et al. (Boskey et al., 1976) who stated that S_{CaP} values of 10^{12} and 10^{14} with respect to HAP would necessarily give ACP as an initial phase (see Table 2-6). In contrast, solutions with S_{CaP} values of 10^{7} are expected to give hydroxyapatite "directly" (i.e. apparently directly). In other studies (e.g. Feenstra et al., 1979), the supersaturation level with respect to HAP is not stated but appears to be 3.5×10^{10}.

Indeed, in the study by van Kemenade et al. (van Kemenade et al., 1987) it is stated that direct formation of HAP is never observed over the range of low, moderate and high supersaturation levels studies and that it formation is necessarily preceded by some intermediate amorphous or crystalline (either OCP or DCPD) phase which then acts as a "template" or foundation on which HAP can nucleate and grow by dissolution/ reprecipitation processes. Thus, there is clearly some confusion and controversy in the literature about what effect supersaturation has on the mechanism of calcium phosphate precipitation.

Table 2-6: Comparative degrees of supersaturation relative to hydroxyapatite and amorphous calcium phosphate (ACP) in systems from which hydroxyapatite formed (from Boskey et al., 1976).

Total calcium (mM)	Total phosphate (mM)	S_{CaP}	S_{Ca}(HAP)	S_{Ca}(ACP)	First precipitate observed	Reference
0.50	0.50	9.0×10^{5}	22	-0.7	HAP dots	Boskey et al. 1976
1.33	1.00	8.9×10^{8}	44	-0.1	HAP dots	Boskey et al. 1976
1.67	1.00	2.4×10^{9}	47	0.3	HAP dots	Boskey et al. 1976
1.562 3	0.973 3	1.2×10^{11} 6×10^{11}	43.6	10^{-3}	ACP ACP	Nancollas et al., 1974 Brecevic et al., 1972
1.2	20	1×10^{18}			OCP	Furedi-Millhofer et al., 1971
12.0	10.8	1×10^{22}	500	7	ACP	Boskey et al., 1973

Van Kemenade (van Kemenade et al., 1987) also made a particularly relevant observation with respect to the phosphate level in precipitating systems of calcium phosphate. The relaxation times (see Figure 2-6) and lag times before precipitation "takes off" were found to increase sharply as initial phosphate concentration was decreased from 6 to 4 mM. The kinetic precipitation boundary was found by extrapolation to be about 3.9 mM phosphate in a system precipitating at pH 6.7, 26°C, ionic strength 0.15 M, and Ca:P ratio 1.16. In the precipitation of calcium phosphate from whey permeates, the Ca:P molar ratio is *ca.* 1.30 meaning that calcium is in excess and phosphate is the limiting reagent. An increase in extent of precipitation and hence yield could thus be realised by the addition of phosphate from an external source.

2.14 Influence of Ionic Strength

2.14.1 Formal Definition of Ionic Strength

"Ionic strength" refers to the background ionic "environment" existing in an aqueous solution. The ionic environment includes not only ions that are participating in reactions in the medium but also inert spectator ions. In aqueous solution chemistry, ionic strength can be calculated and described numerically by making a summation of all the ions present in the solution. This is achieved by multiplying the concentrations of all ions present by the square of the charge on the ion (e.g. +1, -1, +2 etc). Ionic strength is commonly denoted by the symbol "*I*" although some texts also use "μ". The expression for calculating it can thus be expressed as:

$$I = \frac{1}{2}\sum_i c_i z_i^2$$

where c_i and z_i are the concentration and charge respectively of ion i in the medium.

Ionic strength is used to calculate activities of ions or "effective concentrations" of ions in solution (these are used in calculations of IP, see 2.10.1: "Ion Products and K_{sp} values of the Various Calcium Phosphate Phases"). Activity coefficients of ions in dilute and semi-dilute solutions are well understood and can be calculated from fundamental principles. The coefficients, f_i, depend on the ionic strength and can be calculated using the Debye Huckel limiting law:

$$\log_{10} f_i = -z_i^2 B\sqrt{I}$$

where $B = 0.51$ at 25°C if the solvent involved is water and z_i is the atomic charge on the ion.

Often the above expression does not provide a satisfactory estimate of the activity coefficient if the ionic strength is high (e.g. if $I > 0.06$ M), in which case the Davies equation is used to calculate values of the activity coefficients.

This expression is frequently used by researchers in the calculation of activity coefficients in studies on calcium phosphate precipitation. The Davies equation (Davies, 1962) is:

$$\log_{10} f_i = -0.5 z_i^2 \left\{ \frac{\sqrt{I}}{1+\sqrt{I}} - 0.3\, I \right\}$$

2.14.2 Ionic Strength and its Effect on Calcium Phosphate Precipitation

Previous calcium phosphate research has not devoted much attention to investigations of the effect of ionic strength on the overall precipitation reaction. In previous studies, ionic strength has generally been in the range of 0.015-0.16 M. Nancollas et al. (Nancollas et al., 1974) is the only author to make a systematic study of the effect of ionic strength on the hydroxyapatite-seeded growth of calcium phosphate. After demonstrating that the type of base used (e.g. NaOH, KOH, LiOH, CsOH or aqueous ammonia) did not affect the rates of the reaction or the mechanism, Nancollas et al. then showed that the effect of adding "neutral" electrolytes (e.g. LiCl, NaCl, KCl, CsCl, NH_4Cl) was significant. This is illustrated in Figure 2-7 which describes crystal growth of calcium phosphate in the presence of increasing concentrations of NaCl.

It was postulated by Nancollas et al. that the added electrolyte may affect reaction rates by inducing coagulation of the amorphous calcium phosphate precursor in a manner similar to classical colloid coagulation. Added electrolyte may also serve to effectively reduce the supersaturation level in the solution by reducing the values of the activity coefficients of the reacting ions in solution. As can be seen from Figure 2-7, the "discontinuity"characteristic of phase changes occurring in solution as a function of precipitation time (see Figure 2-6 from earlier) is consistent with the proposal that NaCl is reducing the driving force for the reaction. At an ionic strength of 0.15 M, DCPD and OCP do not form. It is the formation (and simultaneous dissolution) of these phases that give rise to the typically observed "discontinuities" on the [Ca] versus time curves.

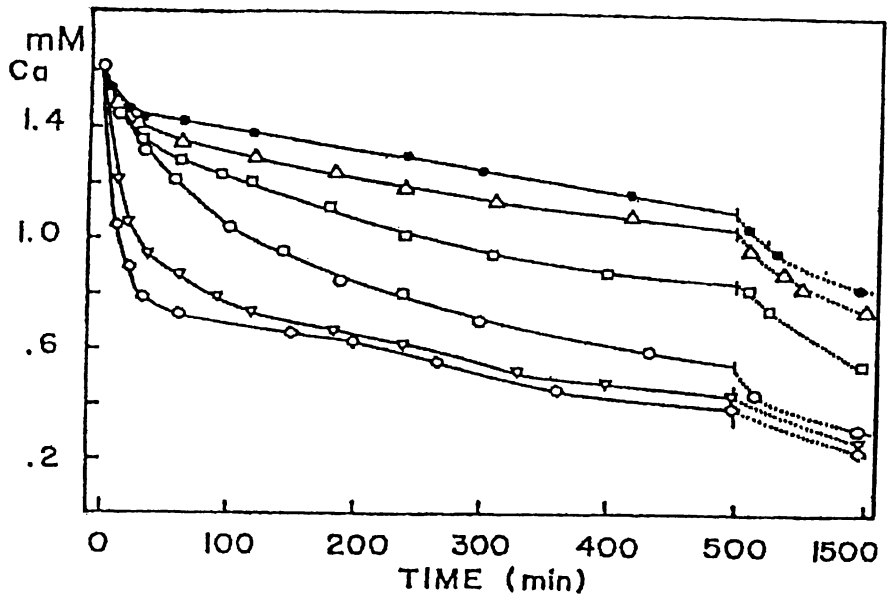

Figure 2-7: Crystal growth of calcium phosphate in the presence of sodium chloride. Plots of total calcium concentration as a function of time: ◊-0 mM NaCl, ▽-10 mM NaCl, ○-50 mM NaCl, □-150 mM NaCl, •-700 mM NaCl (from Nancollas et al., 1974).

2.14.3 Effect of Different Alkali Metal Cations

Nancollas et al. (Nancollas et al., 1974) performed seeded calcium phosphate precipitation experiments in 0.15 M lithium, sodium, potassium, caesium and ammonium chlorides. A marked effect was observed on the crystallisation on changing the alkali metal cation. Toward the end of the reaction (1000 minutes) the extent of crystal growth increases in the order KCl < CsCl < NH_4Cl < LiCl < NaCl. The greatest differences were found between the potassium and sodium chlorides which are of particular importance in biological systems. For instance, after 1000 minutes of growth, 60% of the calcium is precipitated in the NaCl system whereas only 40% has deposited in the presence of KCl. Nancollas et al. also found that the sodium ion could become incorporated into the apatite structure whereas potassium ion was only reversibly adsorbed on the surface of the solid. The reason for potassium ion being a greater retarder of calcium phosphate crystallisation relative to sodium was postulated to be due to the different pzc (points of zero charge) values of HAP in the presence of sodium and potassium chloride at the

different pH values. Point of zero charge refers to the pH at which the net charge on the HAP particles residing in aqueous solution are effectively zero (this is related to zeta potential). The pzc for HAP in the presence of NaCl occurs at pH 7.5 and at pH 8.4 in the presence of KCl. Thus at pH 7.4 (which was the pH at which Nancollas et al. carried out their calcium phosphate precipitation experiment), the nascent HAP surface in the precipitating reaction medium would be appreciably positively charged in the KCl solution so leading to a lower rate of crystallisation.

2.15 Influence of Seeding

2.15.1 Homogeneous versus Heterogeneous Nucleation

The idea of seeding has become an important issue in the precipitation of calcium phosphate and it is thus appropriate to discuss the fundamentals of seeding in precipitation reactions. Crystallisation may be induced in metastable, supersaturated solutions by inoculating with seed crystals (Koutsoukos et al, 1981). In unseeded homogeneous nucleation, the crystals of the precipitated material are usually most effective as seeds, although crystallisation may also take place on the surfaces of crystals of either pre-added crystals of the precipitating phase or on the surface of crystals of completely different materials which offer a good crystal lattice match to the substance being precipitated. This is referred to as heterogeneous nucleation.

2.15.2 Experiments involving the Seeded Growth of Calcium Phosphate from the Literature

Nancollas et al. (Nancollas et al., 1974) commented that studies on spontaneous precipitation of calcium phosphate are often beset by reproducibility problems due to the uncertainty as to whether solutions undergoing "spontaneous" precipitation are totally free of foreign seed nucleating particles which can have a significant impact on rates of the precipitation reaction. Koutsoukos et al. (Koutsoukos et al., 1980) have claimed that attempts to predict results from industrial precipitation processes can frequently lead to overdesign of plants and expensive pilot plant studies.

In the chemical literature, the most careful, rigorous bench work reported on determination the rates of reaction in systems involving calcium phosphate precipitation have been conducted using carefully prepared and characterised calcium phosphate (HAP, DCPD or even OCP) seed materials. Experiments involving growth on well-defined seed materials have been shown to be highly reproducible so that studies can be made on the effects of factors such as the level of supersaturation, seed morphology and the presence of foreign ions. Koutsoukos et al. (Koutsoukos et al., 1980) have also reported an experimental technique for studying calcium phosphate precipitation under conditions of constant composition whereby pH in the precipitating solution is carefully controlled by means of a pH-stat. To prevent the precipitous decrease in concentrations of lattice ions (viz., Ca^{2+} and inorganic phosphate), an autoburette dispensed solutions containing these species (including inert electrolyte in order to maintain ionic strength at a constant level) in response to a glass electrode which was sensitive to changes in solution pH. This approach has been shown to yield highly reproducible and precise results.

2.15.3 Effect of Seed Characteristics on Calcium Phosphate Precipitation

Eanes (Eanes, 1976) conducted studies on formation of calcium phosphates on apatite seeds from supersaturated (with respect to ACP) solutions and found that under conditions where ACP would normally precipitate spontaneously, apatite seeds reduced the amount of free ACP formed with a large fraction of the solution Ca and inorganic phosphate removed from the solution depositing directly on the apatite seeds. It was found that if seed concentration was increased to a sufficiently high level (>0.5 mg mL^{-1}), ACP formation was not observed. Thus it is apparent that seeding can directly alter the mechanism of the precipitation reaction occurring in supersaturated solutions.

In general, Eanes found that the initial ACP formation event in seeded solutions was followed by seed-induced formation of new apatite crystals accompanied by further losses in solution Ca and inorganic phosphate. Loss of Ca and inorganic phosphate was proportional to the amount of seed added. Aoba et al. (Aoba et al., 1984) showed a linear correlation between rate of precipitation and seeding surface area for precipitations at 37°C using HAP seeds prepared at 65°C. Although, it was found that initial precipitation

rate *per* square metre of seed was the same for different surface area apatite seeds, small crystals were discovered to produce a more rapid decline in pH (indicating faster precipitation) compared to larger crystals. Thus, it is clear that seed surface area is an important variable in any seeded precipitation process and is an important factor to bear in mind for the whey permeate precipitation process.

Aoba et al. (Aoba et al., 1984) also suggested that seed geometry may influence the rate of precipitation of calcium phosphate. In general, this would manifest itself by the preferential deposition of calcium phosphate on one crystal plane relative to another. This is a difficult aspect to examine closely in bench scale studies since very quantitative data on the geometry of the crystals as well as kinetic measurement would be needed. Such studies could well involve the use of carefully pregrown single crystals of a particular geometry which would be difficult and time consuming to use and, ultimately not practical to use in an industrial setting such as recovery of calcium phosphate from whey UF-permeates in the New Zealand Dairy Industry.

Nancollas et al. (Nancollas et al., 1974) found that the degree of supersaturation affected the mechanism of calcium phosphate formation on apatite seeds with high supersaturations resulting in the formation of an ACP precursor phase which converted to OCP and then to HAP, and low supersaturations leading to direct formation of HAP on the seed crystals.

In their studies on induction of calcium phosphate precipitation from sweet whey (initially at pH 5.90 and stored at 4°C before use), Pouliot et al. (Pouliot et al., 1991) found that seeding with DCPD at pH 8.0 (achieved by base addition) and a temperature of 50°C induced extensive precipitation of an apatitic calcium phosphate. In contrast, unseeded whey permeate gave very unsatisfactory precipitation results.

DCPD crystals have very characteristic plate-like morphology and thus their initial formation as seeds with subsequent overgrowth of apatitic calcium phosphate could well explain larger particle sizes. Indeed, the paper by Pouliot et al. (Pouliot et al., 1991) shows electron micrographs which illustrate clearly the association of an apatitic phase

with platey DCPD seeds. The DCPD may also undergo hydrolysis itself to HAP (Fulmer et al., 1998).

2.16 Influence of Additives and Impurities

2.16.1 Categorisation of the Effects that Additives and Impurities may have on Calcium Phosphate Precipitates and the Precipitation Reaction

In general, two fundamental effects or consequences can arise from having "impurities" or "additives" present in media where calcium phosphate precipitation is occurring. For the sake of clarity, one may define impurities or additives as any substance that is different from the main lattice ion components making up hydroxyapatite phase (i.e. substances other than Ca^{2+}, inorganic phosphate, or OH^-).

The first effect is on the composition or "integrity" of the apatitic precipitate itself. Changes due to phase transformations notwithstanding, the presence of various impurity ionic components can lead to incorporation of these ionic components into the crystal lattice of the hydroxyapatite. This arises from the fact that the apatite-like crystal lattice is a very "hospitable" lattice. It can easily undergo substitutions under suitable conditions of lattice ions (e.g. Ca^{2+}, PO_4^{3-} and OH^-) for other cations or anions. The best known example of this is carbonate (CO_3^{2-}) which can substitute either for -OH (type A substitution) or for PO_4^{3-} (type B substitution). This has a noticeable effect on the properties of the precipitate. It is important to note that lattice-bound foreign components should be distinguished from surface-bound components. The latter type of impurity cation/anion has no effect on structural properties of the solid (LeGeros et al., 1993).

The second major effect of additives or impurities is on the precipitation reaction itself and the nature of the calcium phosphate phase that separates from solution (i.e. DCPD, OCP, TCP or HAP). The effects can arise from a number of solution-mediated processes such as adsorption of the impurity substances on specific crystal faces of the precipitating calcium phosphate phases that can retard the growth of one phase and consequently favour the formation of another calcium phosphate phase.

Alternatively, additives may have the capability of sequestering or holding Ca^{2+} ions in the form of chemical complexes in solution (e.g. citrate ion (Cit^{3-})) is able to complex Ca^{2+} ion as $[Ca(Cit)]^-$ in solution.

The complexation of the calcium makes this species less reactive to precipitation and so can increase the induction time (which is the time for appreciable precipitation and hence calcium loss from solution to occur) for the precipitation reaction. Additives may also affect the growth of nuclei in solution once they are formed so that suspensions consisting of particles of colloidal dimensions may form instead. Examples of studies from the literature will be discussed briefly in order to illustrate these factors in more detail.

2.16.2 The First Effect: Effects of Substitutions of Hydroxyapatite Lattice Ions (Ca^{2+}, PO_4^{3-}, OH^-) for other Cations or Anions

There are numerous studies in the literature (Elliot, 1994) where apatite compounds have been prepared in the presence of anions and cations which can substitute into the apatite crystal lattice. For the sake of this chapter, only those of relevance to the ALAMIN™ production process will be discussed.

2.16.2(a) Carbonate (CO_3^{2-})

The effects of carbonate incorporation in the hydroxyapatite crystal lattice via type A and type B substitutions as described earlier have been well documented in the literature. In particular, type A and type B-substituted carbonate has opposite effects on the lattice structure of the hydroxyapatite unit. Increasing carbonate incorporation is known to have a noticeable effect on the shapes and sizes of apatitic crystals (LeGeros et al., 1993). If sodium carbonate is incorporated into apatitic structures (i.e. in a coupled manner with carbonate-for-phosphate anion and sodium-for-calcium cation substitutions), the shape of the carbonate apatite crystals change from acicular crystals to rods to equi-axed crystals with increasing carbonate content.

Carbonate incorporation into the hydroxyapatite lattice can also influence the solubility of the HAP. Carbonate-substituted apatites are recognised as being much more soluble than carbonate-free apatites (LeGeros et al., 1983). Crystallinity in hydroxyapatite compounds is also known to be reduced by the introduction of carbonate into the structure such that a more amorphous compound results. Carbonate could be incorporated deliberately into the calcium phosphate precipitate in order to produce a "softer" product bearing in mind, however, that some yield loss could occur due to the greater expected solubility of the carbonated apatite product. An excellent example of semi-crystalline carbonated apatite is bone which is more broadly classified as a biological apatite. The generalised composition (see below) of biological apatites is a good illustration of how hospitable the apatite lattice is towards substitution of foreign cations and anions:

$$(Ca, M)_{10}(PO_4, CO_3, Y)_6(OH, F, Cl)_2$$

where M represents other minor (e.g. magnesium, sodium, potassium etc) and trace elements (e.g. strontium, barium, lead); Y represents acid phosphate, HPO_4^{2-}, sulfates, borates, vanadates, etc. In calcium phosphate compounds, the presence of carbonate can be readily detected by such simple techniques as FTIR spectroscopy.

2.16.2(b) Other Anions

Other anions that may be incorporated into the hydroxyapatite lattice are Cl^- and F^- anions. Fluoride ion incorporation is of particular interest as this decreases the solubility of hydroxyapatite. This is caused by smaller size of the F^- ion which means it can fit more "snugly" into the hydroxyapatite crystal lattice. In fact, in a completely F-substituted hydroxyapatite lattice (i.e. $Ca_{10}(PO_4)_6F_2$) the crystal structure becomes overall more closely packed and is said to "degenerate" upon substitution with larger Cl^- or OH^- ions into a more open (and hence more unstable structure). The change in solubility properties of hydroxyapatite compounds upon introduction of fluoride into the medium is of interest to the ALAMIN™ production process, if an increase in yield is being considered. However, the inevitable incorporation of fluoride in the product may not be a desirable outcome.

2.16.2(c) Cations

It has already been mentioned earlier (see 2.14: "Influence of Ionic Strength") that sodium ion can become incorporated into the calcium phosphate product (Nancollas et al., 1974) whereas potassium ion only reversibly adsorbs to the surface of the solid. Hydroxyapatite is also highly susceptible to substitution of lattice Ca^{2+} by cadmium ions (Cd^{2+}). In fact, substitution can occur to such an extent that an entirely new phase of cadmium phosphate may be created (Aoki, 1994). This means it is imperative to keep a check on levels of heavy metal ions in the production process.

The cation that has the most significant effect on the formation of calcium phosphate compounds is the magnesium ion. Magnesium has been identified as having two main effects in calcium phosphate chemistry: 1) on the mechanism of the calcium phosphate precipitation reaction (by prolonging the lifetime of the intermediate amorphous calcium phosphate precipitate; see later) and 2) by changing the nature of the precipitating calcium phosphate phase. 1) and 2) are intertwined effects. In so far as 2) is concerned, the presence of magnesium can lead to a TCP-like phase precipitating out of solution which is a Ca-Mg-containing calcium phosphate known as "whitlockite". This has been described earlier in the review when descriptions of the discrete calcium phosphate phases of relevance to ALAMIN™ were given (see 2.4: "Descriptions of Discrete Calcium Phosphate Phases of relevance to ALAMIN™").

Bachra et al. (Bachra et al., 1965) showed that apatitic calcium phosphate precipitation was "disturbed" when magnesium ion was included in the solution. In general, apatitic precipitates were more poorly crystallised in the presence of magnesium than without. Further details of the effect of magnesium and studies in which this has been investigated (Eanes et al., 1981; Bachra et al., 1965; Abbona et al., 1990) are given below.

2.16.3 The Second Effect: Effects of Impurities and Additives on the Precipitation Reaction of Calcium Phosphate

2.16.3(a) Effect of Biological Macromolecules

The presence of impurity substances can affect the precipitation product by adsorbing on the emerging crystallites in such a way as to retard or influence growth or maturation.

Nature provides extreme but beautiful examples of these "controlled nucleation processes" in biomineralisation where precise arrays of inorganic crystals are deposited in various, highly specific shapes such as seashells (calcium carbonate) and bones (carbonated hydroxyapatite). Organic macromolecules (Mann, 1988) play a key role in regulation of mineralised growth in living organisms. Often they function as a platform on which crystal growth can be initiated and then directs the extent of its growth. In humans, collagen is the primary organic "matrix" which, along with other substances, directs the growth of bone.

The following diagram (Figure 2-8) from Posner et al. (Posner et al., 1984) illustrates how substances in nature can stabilise ACP and prevent it from growing to form HAP. In Figure 2-8, ATP is known as "adenosine triphosphate", an important biological molecule which regulates bone growth by stabilising ACP (Blumenthal et al., 1975a). It is said to behave very much like pyrophosphate anion ($P_2O_7^{4-}$) which is well known for its ability to inhibit apatite growth. Other biological molecules studied have also been found to interact with HAP.

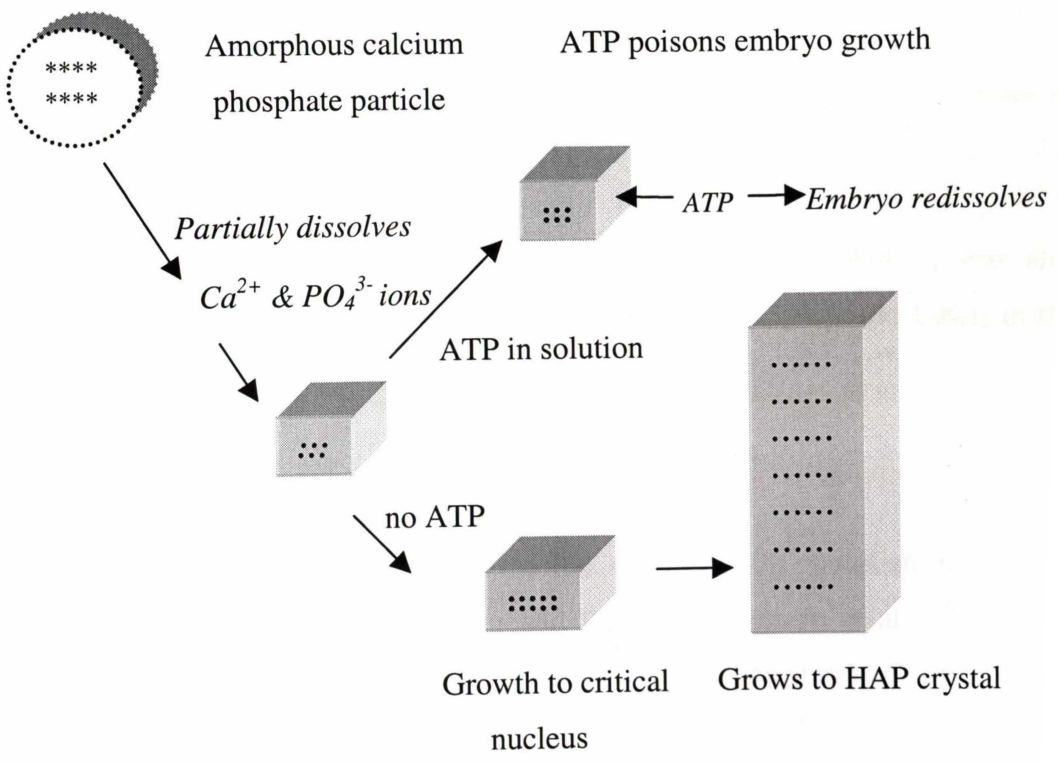

Figure 2-8: Schematic for the mechanism of the stabilisation of amorphous calcium phosphate by adenosine triphosphate (from Posner et al., 1984).

Some of these are of vital importance in nature such as salivary macromolecules which maintain human saliva in a supersaturated state with respect to the dental mineral in teeth (which is a calcium hydroxyapatite) and avoids crystal growth on the tooth surfaces or spontaneous precipitation in the salivary secretion (Moreno et al., 1984). Proteins such as bovine serum albumin may also slow down HAP growth from ACP (Blumenthal et al., 1975b).

2.16.3(b) Effect of Dietary Fibre Substances

Numerous studies using additives of more relevance to the ALAMIN™ precipitation process have been conducted to deduce the effect on calcium phosphate precipitation. Yamamoto et al. (Yamamoto et al., 1992) studied the effect of alginate, a dietary fibre possessing acidic groups and known inhibitors of HAP formation such as poly-L-glutamate and proteoglycan, on calcium phosphate precipitation at pH 7.4 using a Na_2HPO_4/NaH_2PO_4 buffer and $CaCl_2$. In general, alginate was found to increase the induction time for the precipitation of HAP to take place. However, it was found that HAP precipitation was not prevented so much as delayed by the presence of alginate.

Pach et al. (Pach et al., 1996) studied calcium phosphate precipitation in the presence of potato starch, hydroxyethyl cellulose and colloidal silica. Potato starch was found to alter the morphology and nucleation of HAP drastically. The starch was believed to provide nucleation sites for the deposition of crystallites. A fibre-like morphology was also observed for HAP precipitated at pH 7.4 from reaction of $NH_4H_2PO_4$ and $CaCl_2$ in the presence of 1% colloidal potato starch.

2.16.3(c) Effect of Citric, Acetic and Lactic Acids

Other additives of more direct relevance to the industrial calcium phosphate production process have been examined by Tenhuisen and Brown (Tenhuisen et al., 1994) who investigated the effects of citric and acetic acids on the kinetics (rate) of formation of calcium-deficient hydroxyapatite at physiological temperatures (38°C) using a variety of techniques such as isothermal calorimetry (heat evolution measurements), solution chemistry, scanning electron microscopy, surface area measurements and infrared spectroscopy. This study was conducted on a cement-like HAP formation reaction which

is frequently used for clinical purposes to prepare bone-like material. The reaction studied was an acid-base reaction involving tetracalcium phosphate and monetite, which produced a calcium-deficient apatite.

$$6CaHPO_4 + 3Ca_4(PO_4)O \Rightarrow 2Ca_9HPO_4(PO_4)_5OH + H_2O$$

Since HAP is the thermodynamically most stable phase to form, heat is evolved in its formation from higher energy states. The heat evolution curves showed that the heat evolved depended very much on the acid (citric or acetic) present in the aqueous medium. Citric acid (17-150 mM) was found to retard the formation of HAP by the above reaction significantly. For HAP formation in deionised water, the time for the reaction to approach completion was < 10 hours while in 150 mM citric acid, it took *ca.* 75 hours. The level of citrate in the reaction medium reported by Tenhuisen and Brown (Tenhuisen et al., 1994) was not high enough to precipitate the $Ca_3(Cit)_2$ but was believed to adsorb on the surfaces of the reacting tetracalcium phosphate and monetite. Citrates have been reported to adsorb on a variety of calcium phosphates (Brecevic et al., 1979; Myers, 1987). In the study by Tenhuisen and Brown, the "hollow-shell-like"morphology of HAP precipitates as observed in electron micrographs suggested citrate adsorption on the reactants. Citrate adsorption on the reactants was postulated to block dissolution sites on the tetracalcium phosphate so leading to the slower reactions observed. When citrate becomes exhausted from solution (via eventual adsorption and/or incorporation on/into the HAP product as demonstrated in the study), the dissolution of the reactants then accelerates and the reaction "takes off" after the lengthy induction period. The induction period is caused not only by the propensity of the citrate to adsorb on the reactants but also on the ability of citrate to complex free calcium in solution so lowering the reactivity of the calcium towards precipitation as HAP.

The IR spectra of HAP prepared in the presence of citric acid in the study are extremely interesting as they reveal a broad and weak peak at *ca.* 1425 cm^{-1} which has been assigned to carboxyl group stretching of citrate adsorbed on the surface of the HAP product. The spectrum does not resemble that for crystalline $Ca_3(Cit)_2$ and is in fact much broader in peak shape. This has been interpreted as indicating that the citrate is in a state of structural disorder which are environmental effects said to be caused by molecular

interactions in the range of a few nanometres (such as what occurs when the material is adsorbed and not a discrete crystalline compound).

The study by Tenhuisen and Brown (Tenhuisen et al., 1994) also discussed the influence of acetic acid on HAP formation from tetracalcium phosphate and monetite. Acetic acid was found to accelerate the formation of HAP (relative to distilled water mediated reactions). As acetic acid concentration increased, dissolution of the reactants increased and so reaction to form HAP increased indicating that the acceleration in the case of the HAP formation reaction in the presence of acetic acid was primarily a pH phenomenon.

In the chemical literature, studies probing the effect of lactate on HAP appear to have been restricted to dental areas where the effect of lactic acid on the formation of artificial caries lesions has been investigated (Hoppenbrouwers et al., 1988). It is anticipated that the role of lactate in the whey permeate medium used in the commercial calcium phosphate production process will become clearer from the ion speciation studies as described later in Chapters 4 and 5.

2.16.3(d) Effect of Casein

A number of authors (Holt et al., 1996b; Schmidt et al., 1987b; van Kemenade et al., 1989) have studied the effect of the various caseins on calcium phosphate precipitation. The role of casein in the maintenance of calcium phosphate stability and the high supersaturation of calcium in cow's milk is well known (see earlier sections on discussion of micellar calcium phosphate). Thus it is not at all surprising that casein would have a significant influence on the precipitation of calcium phosphate. Moreover, HAP is commonly used as a chromatographic support material to separate the different caseins (Sleigh et al., 1979). The study by Schmidt et al. (Schmidt et al., 1987b) is of particular relevance to the commercial calcium phosphate precipitation because whole casein, phosphopeptides and other various proteins from several whey preparations were investigated for their HAP inhibition properties. Calcium phosphate formation was studied over a wide pH range from 5.8 to 7.3. At the lower end of the pH scale, DCPD was normally observed with OCP at the higher pH end. It was found that proteins like bovine serum albumin and phosvitin accelerated the precipitation of calcium phosphate whereas β-lactoglobulin had no effect (cf α-lactalbumin which is known to complex Ca^{2+}

ion). Whole casein was found to have a high inhibitory action. The fat, phospholipids and lipoproteins from cheese whey have no apparent inhibitory properties. Acidified whey preparation (AWP) was found to inhibit calcium phosphate precipitation. In general, it was found that of the various caseins trialled, viz., β- and κ-casein, κ-casein had no apparent inhibitory effect, whereas β-casein (identified by its active peptide fragment in acidified whey preparations) was found to have an inhibitive effect possibly via adsorption of the inhibitor molecules via their phosphoserine residues, to the surface of the calcium phosphate nuclei thus preventing further growth.

Similar work to that of Schmidt et al. (Schmidt et al., 1987b) has been carried out by van Kemenade et al. (van Kemenade et al., 1989) on the influence of casein on the precipitation of the precursor phases to HAP, viz., DCPD and OCP. It was found (in contrast to Schmidt's study) that all caseins had a strong retarding effect on the rate of HAP crystal formation. Moreover, it was discovered that individual α_{s1} and β-caseins induced extensive formation of DCPD at the expense of OCP, whereas in the presence of κ-casein, DCPD levels are low. It was suggested that simple selective adsorption of α_{s1} and β-caseins to the DCPD and OCP phases was not solely responsible for the preferred growth of DCPD at the cost of OCP. An additional process, namely, increased aggregation of solid DCPD clusters caused by adsorption of α_{s1} and β-caseins was also found to occur. Such adsorption processes tend to reduce charge by electrostatic interactions so leading to aggregation. Indeed, the fact that "colloidal calcium phosphate" plays a cementing role in the casein micelle in milk and induces aggregation of casein submicelles into stable micelles due to electrostatic interactions, was taken as further evidence for this type of mechanism operating in the casein-calcium phosphate system studied by van Kemenade et al (van Kemenade et al., 1989). It has also been shown that casein adsorption is strongest for DCPD and weakest for HAP which supports evidence from earlier studies that the amorphous calcium phosphate phase present in milk is actually closely related to DCPD (see 2.5: "Nature of Calcium Phosphate in Milk").

The casein structure in the case of the α_{s1} and β-caseins is regarded as being very open and flexible since after binding to one calcium phosphate particle they can adsorb to another particle via a process known as "bridging". The α_{s1} and β-caseins are also known to have >1 phosphoserine residue (the chemical anchoring "hook" for calcium phosphate

particles) whereas κ-casein only has one phosphoserine residue. It is thus notable that van Kemenade et al. (van Kemenade et al., 1989) only found α_{s1} and β-caseins to induce this aggregation of DCPD but not κ-caseins. This difference in behaviour for κ-casein as observed in the study by van Kemenade et al., was interpreted as being related to its different function in milk casein micelles where it exists on the outer layer of the casein micelle acting as a hairy layer which prevents the casein micelle from aggregating in milk.

Further work carried out in 1996 by Holt et al. (Holt et al., 1996b), confirmed studies on inhibitory properties of casein. It was found that β-casein phosphopeptides could modulate the precipitation of calcium phosphate from undersaturated solutions by forming amorphous DCPD nanoclusters in a similar fashion as would be observed in milk. Holt et al.'s study suggested that a short casein phosphopeptide at a concentration of 10^{-3} M can act to form a stable population of calcium phosphate nanoclusters, so preventing uncontrolled precipitation from even a grossly supersaturated solution.

2.16.3(e) Effect of Magnesium Ion

Finally, it is appropriate to review the important effect of magnesium ion on the precipitation of calcium phosphate. In the lactic whey permeate the amount of magnesium present is roughly one tenth the concentration of that of the calcium. This corresponds approximately to a molar ratio Mg:Ca of 0.12. Magnesium ion is known to have a significant effect on the stability of the ACP precursor (see 2.4.5: "Amorphous Calcium Phosphate (ACP)"). Thus the precipitation of calcium phosphate from the commercial whey permeate could be affected by the presence of magnesium. Effects of magnesium are summarised below.

Magnesium ion is most associated with preserving or prolonging the lifetime of the intermediate ACP state (Boskey et al., 1974; Eanes et al., 1981; Abbona et al., 1990). Boskey et al. (Boskey et al., 1974) observed that when the Mg:Ca molar ratio in the system exceeded 0.2, no conversion of ACP to HAP was observed (at pH=8). For a Mg:Ca molar ratio in the range of 0.004 to 0.04 (as found in bones and teeth), the induction period of the amorphous-to-crystalline (HAP) transformation increased with

increasing magnesium concentration. In terms of the various stages of the calcium phosphate precipitation reaction, magnesium was found to affect primarily the induction period (in which no change in crystallinity is observed) and not the rapid proliferation period where crystallisation to HAP occurs via an autocatalytic process exhibiting first order kinetics.

In the study by Abbona et al. (Abbona et al., 1990), amorphous precipitates were reported to survive transformation to crystalline phases in systems in which the molar Mg:Ca ratio was > 4.0. The majority of their precipitation reactions were performed below pH 8 and spanned the pH range 5.81-7.77 (initial/final pH values included, viz., before/after precipitation reactions). Compared with the study by Boskey et al. (Boskey et al., 1974), only solutions with Mg:Ca molar ratios < 0.4 could yield HAP. Solutions with molar ratios of Mg:Ca > 0.4 were said to "block" HAP nucleation with even whitlockite not forming due to the supersaturation level with respect to this compound not being sufficiently high.

Abbona et al. (Abbona et al., 1990) claim that solutions containing < 2.0 mM magnesium have no effect on the precipitating phase. However, other authors (Bachra et al., 1969) have claimed magnesium levels as low as 1.0 mM can delay nucleation with levels of 10 mM magnesium inhibiting conversion altogether. Caution must be exercised in comparing results of different authors as quite frequently different conditions have been employed in each experiment. It is also important not to consider the effects of magnesium in isolation as Mg and Ca levels are not the sole parameter to control the conversion of the amorphous precursor to HAP but rather a combination of parameters such as concentration, additives, pH and temperature.

2.17 Ion Speciation in the Whey Permeate and the Need for Simulated Milk Ultrafiltrate (SMUF) Buffers

2.17.1 Ionic Components Present in Milk and Lactic Casein Whey Permeate

Milk and consequently the whey permeate derived from milk is a complex ionic medium consisting not only of ionic calcium and inorganic phosphate but also numerous other ionic and non-ionic species all of which have the potential to interact with each other and

so affect the level of "free" calcium and "free" phosphate available for the precipitation reaction of calcium phosphate. In Chapter 1, Table 1-1 listed some of the important ionic components in lactic casein whey (Marshall, 1982). Important ionic constituents are: K, Na, Ca, Mg, Cl, inorganic phosphate (P_i), and sulfate. Lactic casein whey has a considerably higher ionic calcium level than does sweet whey from cheddar cheese.

Lactose is an important constituent in all wheys, be they rennet, lactic casein, mineral acid casein or sweet (cheddar cheese) whey. In the lactic casein whey where acidity has been formed by the action of starter bacteria, the lactose concentration is reduced with a corresponding increase in the concentration of organic acids (generally lactic acid).

2.17.2 Calculation of the Ion Speciation in Complex Ionic Solutions

Ion speciation refers to the way in which ions are distributed in a solution. "Free" calcium in whey permeate, for example, is described as calcium ion which simply exists in solution as an aquated calcium ion or "$Ca^{2+}_{(aq)}$". It is "free" calcium that reacts with phosphate ions to produce the calcium phosphate precipitate in solution. However, not all calcium in the whey permeate will exist in this form. Some may exist in equilibrium with a complexed form such as a citrate (Cit^{3-}) or lactate (Lac^-) complex (e.g. $[Ca\text{-}Cit]^-$ or $[Ca\text{-}Lac]^+$ or even as an ion pair with HPO_4^{2-} (i.e. $CaHPO_4$). The extent of complexation or (soluble) ion pair formation will depend on the equilibrium constant for the formation of the complex in solution. For example consider the equilibrium between Ca^{2+} and Lac^- to form the complex $[Ca\text{-}Lac]^+$:

$$Ca^{2+} + Lac^- \overset{K}{\rightleftharpoons} [Ca - Lac]^+$$

K is the equilibrium (association) constant that governs the position of the equilibrium between these two species. Since there are many anions that could potentially complex or ion-pair with Ca^{2+}, these all need to be taken into account so that the whey permeate will consist of many simultaneous equilibria. Thus, at a certain pH, calcium ions will be distributed as various complexes with lactate, citrate, sulfate etc.

The problem then consists of describing these simultaneous equilibria mathematically so that the relative amounts of speciation can be quantified. This can be quite a daunting and in fact an impossible exercise if done by hand. Thus, computer programs equipped to handle calculations involving many simultaneous equilibria must be employed.

Holt et al. (Holt et al., 1981) has calculated the ion equilibria present in milk diffusate and compared results with that of experiment. In that particular study, the most important components of milk diffusate were regarded to be K^+, Na^+, Ca^{2+}, Mg^{2+}, Cl^-, citrate (Cit^{3-}), inorganic phosphate (P_i), sulfate, carbonate, and phosphate esters consisting mainly of sugar phosphates such as glucose-1-phosphate (Glc-1-P), galactose-1-phosphate (Gal-1-P), fructose-6-phosphate (Fr-6-P) as well as N-acetylglucosamine-1-P. A group of various negative ions which contribute about 10 mM of negative charges in a normal milk diffusate are treated as an acetate ion ($RCOO^-$) for simplicity's sake.

Mass balance equations were constructed by Holt et al. for the purpose of calculating equilibrium concentrations of the various free ions and complexes thereof. The mass balance equation for calcium, for instance, consists of a sum of the concentrations of the various complexes together with the free ion concentration [Ca^{2+}], viz.,

$$[Ca]_{total} = [Ca^{2+}] + [CaPO_4^-] + [CaHPO_4] + [CaH_2PO_4^+] +$$
$$[Ca-Glc-1-P] + [CaH-Glc-1-P^+] + [Ca-Cit^-] +$$
$$[CaH-Cit] + [CaH_2-Cit^+] + [CaSO_4] + [CaHSO_4^+] +$$
$$[CaCO_3] + [CaHCO_3^+] + [CaCl^+] + [CaRCOO^+]$$

Once these mass balance equations are deduced, association constants can be used to express the concentrations of the various species in terms of [Ca^{2+}], [H^+], [HPO_4^{2-}], etc. For example, in the study by Holt et al. (Holt et al., 1981):

$$[CaH_2PO_4^+] = [Ca^{2+}][HPO_4^{2-}][H^+]K_{CaH_2PO_4^+} \cdot K_{H_2PO_4^-}$$

Similar expressions can be constructed for other complexes such as $CaCl^+$, $CaPO_4^+$ etc, using association constants which can be obtained from an appropriate database.

A NIST database exist with values for critical stability (association or equilibrium) constants that can be referred to (Smith et al., 1998). Mass balance equations for various species (e.g. citrate, sulfate, chloride etc) are then solved using $[H^+]$ as a fixed quantity (obtained from a pH measurement), and initial trial values of $[Ca^{2+}]$, $[Mg^{2+}]$ and ionic strength. The concentrations of all complexes are then computed and a revised estimate of ionic strength made. The new value of ionic strength is then used in a second cycle and so on until successive estimates of ionic strength differ by <1%. The computation of these is tedious and thus requires a computer. Feenstra et al. (Feenstra et al., 1979) have reported a detailed procedure for calculating concentrations in the case of many simultaneous equilibria.

2.17.3 The Relevant Ion Species in Whey UF-Permeate and their Quantification: The SPE Program

In the whey permeate, the important ionic species that could influence the concentrations of free calcium and inorganic phosphate are (besides the species of calcium and inorganic phosphate themselves): citrate, lactate, carbonate, and magnesium. Although the bulk of whey proteins are removed by ultrafiltration, residual proteins such as α-lactalbumin or β-lactoglobulin may also potentially bind calcium, especially α-lactalbumin (Kronman et al., 1981). The distribution of calcium and phosphate between citrate and lactate especially, can affect the level of free calcium in solution that is available for precipitation. A program known as SPE has been obtained which has been written by Martell et al. (Martell et al., 1992). This program (see Chapter 4) provides the mathematical algorithms for computing ion speciation in complex ionic solutions as a function of pH when the initial/typical concentrations for species such as phosphate, citrate, lactate, carbonate, magnesium and calcium and hydrogen ion are inputted together with the association constants for the various complexes that can form. In addition, the SPE program can account for solubility equilibria, i.e. equilibria between a sparingly soluble solid and its dissolved components. Thus, K_{sp} values (see earlier) for the various sparingly soluble calcium phosphate phases (e.g., HAP, OCP, TCP and DCPD as well as $CaCO_3$) can also be entered into the SPE program. The program can be instructed to "simulate" precipitation of one or all of the solid phases. In addition, "titration curves" can be generated to show what the $[OH^-]$ versus pH profile looks like

when the solid phases are forming in solution. The output of the SPE program can be presented in various ways, i.e. as list of numbers, for instance in spreadsheets, but the most useful way for presenting the results of the ion speciation calculations is as a plot showing how a particular ion (e.g. Ca^{2+}) is distributed (as complex ions and solids) in the system as a function of pH. Thus, the SPE program can give much useful information on the behaviour of the reacting whey permeate system as a function of pH. It should, however, be noted that these calculations represent how the system will behave in a thermodynamic sense and does not take into account "kinetic" effects such as, for instance, the occurrence of phase transformations by Ostwald's law of stages.

2.17.4 The Need for Simulated Ultrafiltrate Permeate Solutions as an Experimental Model for the Real Whey Permeate System

Dairy media are extremely complex in nature and it is thus difficult to understand fully the role of specific ionic components in a particular process under study (e.g. precipitation) due to the interplay of all the components in the media. Ion speciation programs such as SPE (see 2.17.3: "The Relevant Ion Species in Whey UF-Permeate and their Quantification: SPE Program) can offer some theoretical insights into the behaviour of a precipitating system but it is important that these trends be backed up by real results obtained from carefully controlled precipitation experiments. It has often been useful to study simplified systems of milk constituents in order to gain a better insight into problems in dairy technology. This offers opportunities for experimental control and for determining the participation of individual components which are not possible with natural dairy-derived media such as milk diffusate or whey permeates. Similar solutions have been made which simulate physiological body fluid ("simulated body fluid" or SBF). These are used for studying calcium phosphate growth on various pre-treated substrates which is of relevance in biomineralisation or bone growth studies (Mucalo et al., 1995a; Mucalo et al., 1995b; Mucalo et al., 1995c).

Jenness and Koop (Jenness et al., 1962) prepared a synthetic lactose-free "milk salt" solution (consisting of inorganic salts of phosphates, citrates, calcium, magnesium, carbonate, and chlorides) and performed a study in order to compare the properties with those of actual milk ultrafiltrate. This type of milk salt solution has often been referred to as a "simulated milk ultrafiltrate or "SMUF" buffer in the dairy science literature.

In order to better understand the influence of components in the commercial lactic and mineral acid UF whey permeates, it is necessary to design SMUF-like buffers which are good synthetic models of the ionic salt media in the actual whey permeates. In the actual permeates, the concentrations of ionic components will never be at a precisely constant level due to seasonal variations. Composing a SMUF-like buffer allows precise experimental control on the levels of ionic impurities such as lactate, citrate or sulfate ions. In addition, non-ionic components such as lactose (Jenness et al., 1962) can be added in order to elucidate the effects of these components on precipitation of calcium phosphate. In the present study, a SMUF-like buffer has been designed and given the acronym "SLWUF" or simulated lactic whey "ultrafiltrate" buffer (see Chapter 4). These buffers can be used to provide information on the effects of calcium, phosphate, lactate, citrate and protein levels.

2.18 Solid State Interconversions of Calcium Phosphate Compounds

Earlier, it was explained that the intermediate phases (e.g. ACP, OCP etc) do not interconvert to apatitic phases if they are isolated quickly from the aqueous precipitating medium and dried. If the calcium phosphate precipitate is unwashed and then fed into a drier, it is highly likely that residual traces of lactose and proteins which will adsorb strongly to the calcium phosphate particles will cause caking of the solids. The calcium phosphate phases can also exhibit some sensitivity to thermal treatments. Heating of some calcium phosphate compounds can lead to some solid state phase interconversions caused mostly by the dehydration or dehydroxylation of the calcium phosphate compounds.

Hydroxyapatite (HAP) is known to dehydroxylate and undergo a phase change to TCP at a temperature of 1300-1460°C (Ruys et al., 1992). However, it has been shown by many researchers that HAP begins to lose its hydroxyl groups at a much lower temperature (e.g. 770°C) than that at which the phase change occurs. These temperatures are well above the temperature at which the ALAMIN™ powder is dried, so that dehydroxylation of HAP to form TCP is not likely to occur.

CHAPTER THREE
TECHNIQUES FOR STUDYING ALAMIN™ AND WHEY PERMEATES

Many different techniques were used for studying ALAMIN and the whey permeate from which it was derived. All of these are conventional spectroscopic and microscopic techniques used in practice today and hence only brief details of each are given.

3.1 X-ray Diffraction (XRD)

This technique, which forms the basis of X-ray crystallography, is usually employed for providing an unequivocal identification of the phase of a crystalline solid. Since X-ray radiation has wavelengths comparable to the spacing of atoms in crystals (~0.1 nm), it is diffracted by crystal lattices and produces a characteristic intensity pattern which can be interpreted to produce a detailed picture of the position of atoms in the crystalline solid being irradiated (Atkins, 1998).

It is usual in industry, for instance, to analyse samples as received in powder form rather than as single crystals in order to obtain some idea of the identity of the solid phase. In such cases, the sample consists of a random collection of tiny crystals often of mixed phases and a powder X-ray diffractogram can be obtained and analysed by the instrument to give a diffraction pattern which can subsequently be compared to a database of X-ray diffraction patterns of known compounds in order to establish the identity of the solid phase (s) in the powder. The technique is non-destructive and can be applied directly to powder samples such as ALAMIN™ simply by mounting the solid on a glass slide and placing in the instrument. The technique has been used widely for calcium phosphates in past studies (Slosarczyk et al., 1996; Boskey et al., 1976; Nancollas et al., 1974; Kieswetter et al., 1994 to name a few). Powder XRD will only give meaningful results if the solid is crystalline in character. "Amorphous" substances (i.e. non-crystalline solids whose structures do not consist of regular arrays of atoms) will not give X-ray diffractograms and poorly crystalline powders will give poorly defined or "broad" X-ray diffractograms. The technique can in principle be applied to ALAMIN™ although it should be borne in mind that this substance possesses poor crystallinity so that data from

the XRD may well be limited unless the sample is crystallised further by heating to 600-700°C.

In general, phase identity where the sample is reasonably crystalline can be unequivocally determined. If a mixture of phases is produced (e.g. TCP and HAP), the mass fractions of each phase can, in theory, be calculated by integration of peak areas of characteristic peaks due to the individual phases as long these peaks are well separated (Ishikawa et al., 1993b). Eanes (Eanes et al., 1965b) estimated mean crystallite size of hydroxyapatite crystals in their precipitation study by measuring the peak width at half maximum of the 002 diffraction peak (at *ca.* 26° 2θ) and using the Scherrer formula:

$$D = \frac{57.3\,K\lambda}{\beta_{1/2}\cos\theta}$$

where D is the dimension (lengthwise) of an apatite crystallite, K is the crystal shape factor constant (0.9), $\beta_{1/2}$ is the width at half height of the 002 peak, λ is the X-ray wavelength in Ångstroms, and θ is the angle at which the 002 diffraction peak occurs (13°). The same treatment could be carried out for ALAMIN™ crystals since the 002 diffraction peak is a well separated and distinct feature in the XRD. For poorly crystalline samples, however, it is important to note that the error in estimating the crystallite size would be very large due to poor resolution caused by noise in the 002 diffraction peak. Eanes et al. (Eanes et al., 1965b) found that, during the amorphous-to-crystalline conversion of the ACP to precipitates with apatitic character, the mean crystal size remained essentially unchanged. This implied that the apatitic crystal nuclei once formed, grow so rapidly to their final size that at any given point during the conversion the majority of crystals present are fully developed. The formula also assumes a perfect single crystal hence any numerical data obtained from powders must be interpreted in light of this.

3.2 Scanning Electron Microscopy/Energy Dispersive X-ray Analysis (SEM/EDX)

In a SEM instrument, images are formed by the collection and amplification of electrons backscattered or emitted from the surface of a bulk specimen when a high-energy

electron beam is scanned across its surface. A magnified image is formed and the SEM can be used in the same way essentially as an optical microscope except that its resolution is vastly superior. This technique has commonly been employed for observing the particle morphology in investigations of the precipitation of calcium phosphates from aqueous solution (Abbona et al., 1990; Feenstra et al., 1979; Boskey et al., 1976; van Kemenade et al., 1989; Mucalo et al, 1995a; Mucalo et al., 1995b; Christoffersen et al., 1989; Tomazic et al., 1975; Nelson et al., 1986; Heughebaert et al., 1984; Koutsoukos et al., 1980 and many others).

Energy dispersive X-ray analysis or EDX is the quantitative analysis arm of the SEM instrument. In a standard EDX microanalysis (Bowen et al., 1975), the count rate on an area of the sample is measured for a specific element (e.g. the Ca Kα X-ray peak). This is then compared to the count rate of a standard of a pure element or a pure alloy whose composition is accurately known. The ratio of the intensities from the unknown and the standard, k, is the basic experimental measurement. This number leads to a value of the % elemental composition of the sample. The most useful information that can come from EDX analyses of ALAMIN^{TM} is the Ca:P molar ratio which is often used in calcium phosphate chemistry as a qualitative means of phase identification (see Table 2-1 in Chapter 2). There is, however, a certain amount of statistical error inherent in the measurement of k due to the random nature of the emission of electrons from the gun, and hence the emission of X-rays from the specimen. For a practitioner in the area of SEM using EDX-measured values to determine the Ca:P molar ratios, it is good practice to regard these ratios to be correct to within ±10%.

3.3 Transmission Electron Microscopy (TEM)

The TEM is, in principle, similar to the light microscope but differs in that it uses a beam of electrons instead of visible light for image formation. In addition, the much shorter wavelength of the electron compared to that of visible light enables a much higher resolution to be achieved that in turn permits much higher magnification without loss of detail (England, 1991; Bowen et al., 1975). TEM gives an image based on the *transmission* of electrons through a layer of specimen deposited on a semi-transparent substrate. The image thus created is a 2-dimensional one which clearly shows the shapes

of particles outlined against the transparent grid. Particle sizes can be measured directly from the TEM micrographs to give a particle size distribution.

The rapid way of sample preparation involves the deposition of the particles from aqueous solution, for instance to be examined on a collodion-film-coated circular copper grid which is 1-2 mm in diameter. The dispersed solid sample can then be observed on the grid by TEM since the carbon comprising the collodion film is of sufficiently low atomic weight to permit transmission of electrons thus giving a bright background contrast.

The more labour intensive method of preparing samples for TEM analysis is by embedding the sample in epoxy resin. Thin sections of the embedded sample in the epoxy resin are then cut using an ultramicrotome which is equipped with a diamond knife. These thin sections containing the embedded sample can then be viewed on the TEM. ALAMIN™ particle morphology can be readily visualised with this technique although it would be recommended for observation of very fine particles especially phases which are isolated from solution and which are relatively amorphous.

3.4 Fourier Transform Infrared Spectroscopy (FTIR)

IR spectroscopy is a powerful tool for the characterisation of specific *functional groups* within a molecule (e.g. $-OH^-$, $-PO_4^{3-}$, $-CO_3^{2-}$, -COOH, $-NH_2$ groups etc). Infrared spectra of molecules are recorded with an IR spectrometer. The spectral output of an IR spectrum is a plot of absorbance versus wavelength in wavenumbers (cm^{-1}).

For the investigation of solid samples as in the case of commercial ALAMIN™ particles, the well-known KBr disk method is used which involves dispersing of the sample in a KBr matrix under pressure.

3.5 X-ray Photoelectron Spectroscopy (XPS)

X-ray photoelectron spectroscopy is for determining the chemical nature of the surfaces of metals, glass, ceramics, polymers and many other types of materials (Barr, 1994; Konishi et al., 1987; Moulder et al., 1995). This surface sensitive technique is based on

the Einstein Photoelectric Effect in which photons of sufficiently short wavelengths are used to ionise atoms or molecules in irradiated materials. The fundamental principle upon which XPS is based is that photoelectrons escape from the surface of a sample (enclosed in a high vacuum) that is subjected to an X-ray beam usually consisting of Mg Kα X-rays. The electrons escape into the vacuum of the instrument and can be picked up by a detector where they can be analysed in terms of their kinetic energies to provide information on the *binding energy* of the electron in the atom in which it was originally resident. When an X-ray irradiates the atoms on the surface of a sample, electrons from different orbitals (energy levels) in the atom are ejected. These all have unique binding energies which can be used to trace the orbital from which the electron was ejected.

The output from an XPS is thus a trace of counts versus binding energy and will contain peaks corresponding to the various core electrons in the material being investigated. The XPS of hydroxyapatite (Konishi et al., 1987), for instance shows electrons ejected that correspond to the various core electrons from calcium, phosphorus and oxygen. These peaks, however, do not correspond to the photoelectrons originating from the *bulk* of the specimen but from the *surface*. The reason for this is that only electrons residing in atoms within the first few atomic or molecular layers (~100 Å) will encounter the least encumbrances and escape from the surface with practically unchanged kinetic energy (after being excited by the X-ray radiation). This is referred to as *elastic scattering* and it is these electrons that give the "peaks" in the spectrum. Although the original irradiating X-rays are capable of penetrating many micrometres below the surface of the sample so exciting many electrons in these levels, the electrons generated deeper below the surface than about 100 Å collide with other structural atoms in the sample so losing their energy *(inelastic scattering)*. The net result is that these inelastically scattered electrons are not detected as "photoelectrons" but instead appear as a stepped background in the spectrum. This makes XPS a surface-specific technique.

Sample preparation is relatively simple. A metal stub containing the sample dispersed as a powder (in the case of ALAMIN^{TM}) on a piece of double-sided sticky tape is used. A wide scan is obtained first to assess what material is present and then a narrow scan over one of the peaks is acquired to get better resolution and fine structure that can yield important information. XPS, in addition to be a surface specific technique, is also a

chemically sensitive technique. This means the binding energies of electrons from the various atoms will differ slightly if the chemical environment of the surface atom is different. Thus, metal atoms on the surface of materials can be detected in their different oxidation states.

In the case of ALAMIN™, XPS can be used primarily for detecting the presence of various groups adsorbed to the surface of the particles. Thus it could be used as a qualitative means of ascertaining the amount of protein at the surface of the ALAMIN™ particles. It may also show other elements such as the presence of sodium. Thus this technique could be of potential use in studies relating to colloidal stabilisation of suspended ALAMIN™ by various additives.

3.6 Light Scattering Methods for Determination of Particle Sizes

The Malvern *Mastersizer* uses laser diffraction size analysis, which is based on the principle that particles of a given size diffract light through a given angle, the angle increasing with decreasing particle size. A narrow beam of monochromatic light (the laser) is passed through a suspension, and the diffracted light is focused onto a multi-element ring detector (see Figure 3-1). The detector senses the angular distribution of scattered light intensity. A lens, placed between the illuminated sample with the detector at its focal point, focuses the undiffracted light to a point at the centre of the detector. This leaves only the surrounding diffraction pattern, which does not vary with particle movement. Thus, a stream of particles can be passed through the beam to generate a stable diffraction pattern (Singer et al., 1988, Allen, 1981).

The particles dispersed in the solvent scatter light so producing a unique light scattering intensity characteristic of the angle of observation. In simple terms, the particles scatter light so that the measured energy on the detector has a peak at a favoured scattering angle which is related to the particle diameter. Therefore, large particles have peak energies in small angles of scatter and vice versa. The scattered laser light from the sample is detected by the receiver of the optical measurement unit. These data from the receiver are transmitted to the computer system where the Malvern operating software calculates the size distribution.

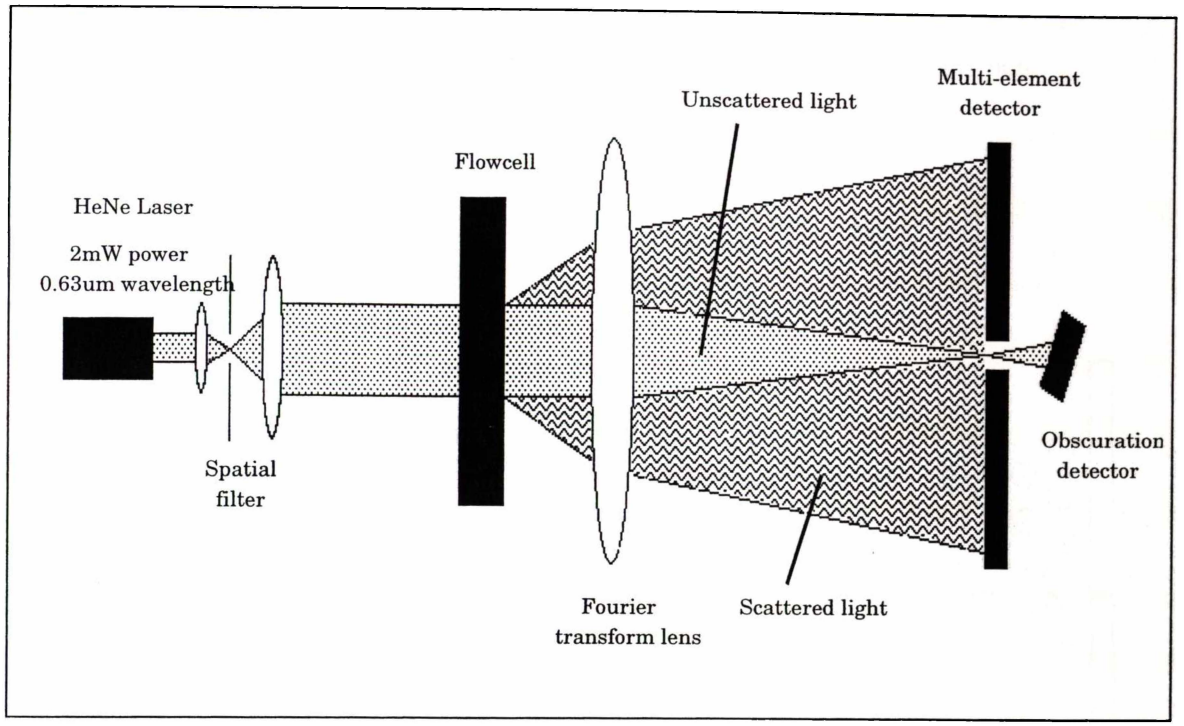

Figure 3-1: Schematic representation of the Malvern Laser Particle Sizer (from Reference Manual, Mastersizer, Malvern Instruments Ltd, 1996).

3.7 Electrospray Mass Spectrometry (ESMS)

ESMS is a relatively new form of mass spectrometry having only been introduced during the 1980's (Cole, 1997). Most conventional forms of mass spectrometry (the use of an instrument to detect masses of ions and molecules) involve applying some high energy process in order to achieve the energetically unfavourable process of conversion of an ion in solution to an ion in the gas phase where it can then be analysed. The act of doing this to an ion is enough to lead to side processes such as net ionisation (creation of ions from neutral molecules) and fragmentation of ions (Kebarle et al., 1993). Such processes can frustrate the determination of the mass of the parent molecular ion (the original ion being analysed). ESMS, in contrast, is regarded (Kebarle et al., 1993) as the "purest" form of transfer of ions from solution to the gas phase; little if any extra internal energy (during the transfer to the gas phase) is imparted to the ions so that the ion "survives" mostly intact for analysis. In ESMS, a large range of ion types can be transferred from solution to the gas phase such as Na^+, Cl^-, organic protonated bases, Ca^{2+}, Sr^{2+}, and Ba^{2+} as well as doubly and triply charged transition metal and lanthanide ions and complexes thereof; bio-organic ions such as multiply protonated peptides and proteins of molecular

mass 100,000 Da; and multiply deprotonated, negatively charged nucleic acids. Figure 3-2 is a schematic representation of the processes occurring in an ESMS experiment.

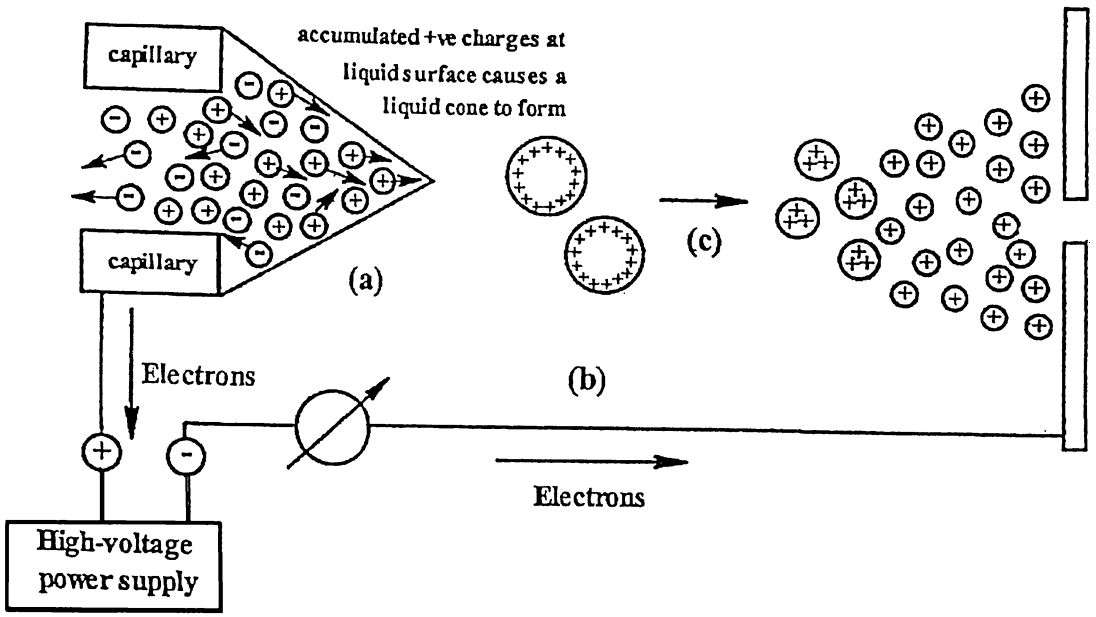

Figure 3-2: Schematic representation of the processes occurring in ESMS (Kebarle et al., 1993).

The aqueous sample mixed with a dipolar solvent such as methanol or acetonitrile. Small background concentrations of salts (e.g. NaCl) are required in the solution for adequate conductivity. This solution is drawn to a charged metal capillary tip. The very high electric field imposed by the power supply within the instrument causes an enrichment of positive electrolyte ions within the solution at the meniscus of the solution at the metal capillary tip. The net charge is pulled downfield, expanding the meniscus into a cone that emits a fine mist of positively charged droplets. Solvent evaporation reduces the volume of the droplets at constant charge, leading to eventual breaking apart of the droplets. These droplets contain the ions, which are reduced at a cathode, and the resultant ion current produces the ion signal observed.

The technique of ESMS provides a quick analysis of *solutions of ions* and could thus be regarded as a potential analytical technique for characterisation of the whey permeate. The wet chemical analysis of this multicomponent solution is chemically and procedurally complicated with separate analyses required for lactate, citrate, calcium, magnesium etc. The development of a rapid and easy analytical or qualitative identification method for the whey permeate is thus desirable.

3.8 Atomic Absorption Spectroscopy (AAS)

AAS is used routinely for quantitative elemental analyses In brief the solution to be analysed is aspirated into the instrument where, it is drawn into the burner flame undergoing a conversion from salt particles to an atomic vapour. A process of equilibrium between molecular, atomic and ionised atomic vapours then occurs. The bias of this depends on such factors as flame temperature, flame speed, solution composition and other factors.

The standard procedure for analysing a sample involves the preparation of accurately known concentrations of solutions to be analysed (e.g. Ca^{2+}). The solutions are then aspirated into the instrument and a calibration curve obtained. The solution with unknown concentration is then introduced and its concentration determined by interpolation in the AAS software of the previously obtained calibration curve. Solid samples such as ALAMIN™ are dissolved completely in acid to yield homogeneous solutions prior to analysis.

3.9 Inductively Coupled (Optical Emission/Mass) Spectroscopy (ICP-OES/MS)

ICP-OES/MS techniques are an alternative, more expensive method to AAS for determining the concentrations of various elements in solution or in a compound. Generally, ICP methods involve the use of a plasma into which samples are aspirated in a similar manner to AAS. The plasma torch consists of three accurately aligned concentric tubes of fused-silica placed in a water cooled induction coil of an radio-frequency generator. A plasma is initiated by a brief spark discharge into the gas stream. In the induction coil region electrons from the spark provide a path for energy transfer between the coil and argon and a self-containing plasma is established. The basic difference

between the plasma torch and the flame burner in AAS is the temperature in the "hot zone". Whereas AAS flame hot zones can have temperatures from 1850-4780 K, ICP plasmas are thermally very hot and spectrally very intense with equilibrium temperatures of about 9000-10,000 K. Because of these much higher temperatures and the inert atmosphere of the ICP plasma discharge, some of the difficulties found in flame AAS techniques are not present in the ICP method.

Chemical interferences such as the well known CaP compound formation in the AAS flame (see section 3.8) are negligible in the plasma, since any compound is likely to be atomised completely during their passage through the hot pathway in the centre of the plasma discharge. Addition of EDTA or other such chemical complexing agents is thus not necessary. The "matrix" effect, as known in AAS is also not a problem in ICP methods. The only major problem is selecting an appropriate wavelength of the analyte element which is not spectrally interfered with by other elements present in the plasma. In general, the favourable properties of the ICP technique make it a valuable method for analysing elements with a greater degree of sensitivity than AAS methods.

3.10 pH-Stat Method

The advantage of the pH-stat experimental work is its ability to probe kinetic aspects of a reaction under controlled pH conditions. A computer-controlled pH-stat method allows measurement of the volume of NaOH needed to maintain pH at a certain value. During the precipitation time, the demand on hydroxide will differ depending on what state the reaction is at hence this will be illustrated in any output from this technique at constant temperature. Usually a spreadsheet package associated with a pH-stat unit allows collation of the data in an easy to analyse format.

The whey permeate systems under study in this thesis exhibit a large degree of natural variability with regard to concentrations of inorganic and organic components. This can cause problems when trying to establish trends or isolating a specific substance as being the sole cause for a given effect. Simulated milk ultrafiltrate (SMUF) buffers provide the model solutions that can be used to provide experimental evidence for the influence of specific components on calcium phosphate precipitation such as lactose, lactate, citrate etc. The SMUF-type solutions offer a system in which a greater level of experimental

control is achievable because of the known composition of the model solutions and the ability to "perturb" the system by the addition of known amounts of "additives". In the present study, buffers simulating the lactic whey permeate were formulated and these have been very successfully studied by pH-stat methods in order to gain insights into the chemical behaviour of the whey permeate with regard to precipitation (see Chapter 4).

3.11 Calcium Ion-Selective Electrode (ISE) Measurements

The level of calcium ions corresponding to the measured potential, E can be expressed using the Nernst equation:

$$E = E^{o} + (RT / zF) \ln a_{Ca^{2+}}$$

where $E°$ is the standard electrode potential, R is the ideal gas constant, z is the number of electrons per ion involved in the electrode reaction (+2), F is the Faraday constant, $a_{Ca}{}^{2+}$ is activity of the calcium ion. The calcium ion activity, $a_{Ca}{}^{2+}$, is related to concentration $c_{Ca}{}^{2+}$ by following equation:

$$a_{Ca^{2+}} = f_{Ca^{2+}} c_{Ca^{2+}}$$

where $f_{Ca}{}^{2+}$ is activity coefficient. In very dilute solutions $f_{Ca}{}^{2+}$ is approximately equal to 1, hence, $a_{Ca}{}^{2+} \approx c_{Ca}{}^{2+}$.

Ion-selective electrodes have been widely used for several years for quantitative analysis Calcium ion electrodes are very useful for following free calcium ion concentrations in dairy fluids and especially in media such as milk where there is an equilibrium between casein micelles and free calcium in the aqueous solution surrounding the micelle. In media involving many simultaneous equilibria between calcium and other species, the method is of use in deducing reactivity of calcium ion to CaP precipitation. Under the conditions of constant, moderately high ionic strength found in many cheeses, conditions of the calcium ion activity coefficients are constant and the electrical potential of a calcium ion electrode is directly related to the logarithm of the concentration of free calcium ions Log[Ca^{2+}]. Thus free calcium ion concentrations can be conveniently determined in cheese using a suitably calibrated calcium ion-selective electrode (Pearce, 1997).

CHAPTER FOUR

INVESTIGATION OF SIMULATED LACTIC WHEY ULTRAFILTRATE (SLWUF) BUFFERS AS A MODEL FOR NATURAL WHEY PERMEATES

In this Chapter, computer speciation calculations were performed to predict, using published acidity, stability and solubility constants, the equilibrium distribution of ionic species and occurrence of precipitating phases in simulated lactic whey ultrafiltrate (SLWUF) buffers which were designed specifically for this study (see section 2.17.4: "The Need for Simulated Ultrafiltrate Permeate Solutions as an Experimental Model for real Whey Permeate System") as a function of pH. Bench scale experimental work on precipitation from SLWUF buffer solutions has been carried out to confirm the trends predicted by these speciation calculations. The rationale for the design of the SLWUF buffer was primarily to model the behaviour of the lactic acid whey permeate as used in the proprietary process. During the project, the chronological order of research activity in this area was firstly a computer speciation study using some actual industrial compositional data on the whey permeate based on previous chemical analyses. These produced some interesting trends that were of relevance to the precipitation of calcium phosphate from such media. In particular, allowance was made in the program for the natural variation in concentrations of components in the whey permeate. Secondly in this project, an actual simulated buffer solution was designed to allow experimental confirmation of the trends predicted by the speciation calculations. However, the design of this involved some simplifications (e.g. the omission of lactose and protein) and in addition the concentrations of this simulated buffer were not exactly the same as in the industrial permeate. Chapter 4 deals primarily with the SLWUF buffer and the speciation calculations performed (plus experimental confirmation of trends) using the strictly defined compositions of this buffer.

4.1 Computer Speciation Calculation

In order to gain a theoretical and comprehensive understanding of calcium phosphate (CaP) precipitation from whey permeate solutions, ion speciation calculations were carried out using commercial "*SPE*" software, written by Martell and Motekaitis (Martell et al., 1992). Using data for the stability and solubility constants we can predict the ion distributions over a wide pH interval from pH 2 to 12. This program can also estimate formation of various solid inorganic phases such as calcium phosphates,

lactates and citrates. Therefore, we can predict the influence of solution sulfate and citrate concentrations on the yield of the separated solids expected from the whey permeate solutions. Thus, the SPE (actually a modified version called "SPEXY-C.exe" was used) program can give much useful information on the behaviour of the reacting whey permeate system as a function of pH. However, it should be noted that these calculations represent how the system will behave in a thermodynamic sense and does not take into account kinetic effects such as the phase transformations, that are known to occur in freshly precipitated CaP. Iterative calculations were performed to determine the distribution of solid and solution species in a reactive simulated whey permeate medium as a function of pH, using input data based on actual compositional data for a typical lactic whey permeate and a mineral acid whey permeate. The calculations were used to predict the expected yields of solids in a typical precipitation and to estimate the effects of the presence of citrate and sulfate ions as well as the impact induced by changing the Ca:P molar ratio in the permeate. Computer speciation calculations can be set up to produce equilibrium calculations for more than 32 ionic and molecular species and 7 solid phases.

4.1.1 Algorithm employed for performing the Computer Speciation Calculations

The algorithm illustrated in Figure 4-1, summarises the stepwise methodology employed in the speciation calculations.

4.1.2 Ion Speciation and Chemical Equilibria occurring in the Multicomponent Systems

Whey permeate is a complex system consisting of many simultaneous equilibria. At a certain pH, "Ca" for instance, will be distributed as a component in various complexes involving lactate, citrate, sulfate etc. The problem then consists of describing these simultaneous equilibria mathematically so that the relative amounts of speciation can be quantified. Applied computer programs "SPEXY-C" equipped to handle calculations involving many simultaneous equilibria must be employed (Ure et al., 1994). In the original milk system before acidification one third of the Ca is present in the serum phase as free Ca^{2+} or complexed predominantly by citrate and phosphate (Holt, 1997). Ca^{2+} bound in small complexes like $CaCit^{-}$ and $CaHPO_4$ are expected to be in rapid exchange with free Ca^{2+} in solution, whereas "colloidal Ca" (Ca bound in the calcium micelles) is only partially exchanged over the time scale of a few days.

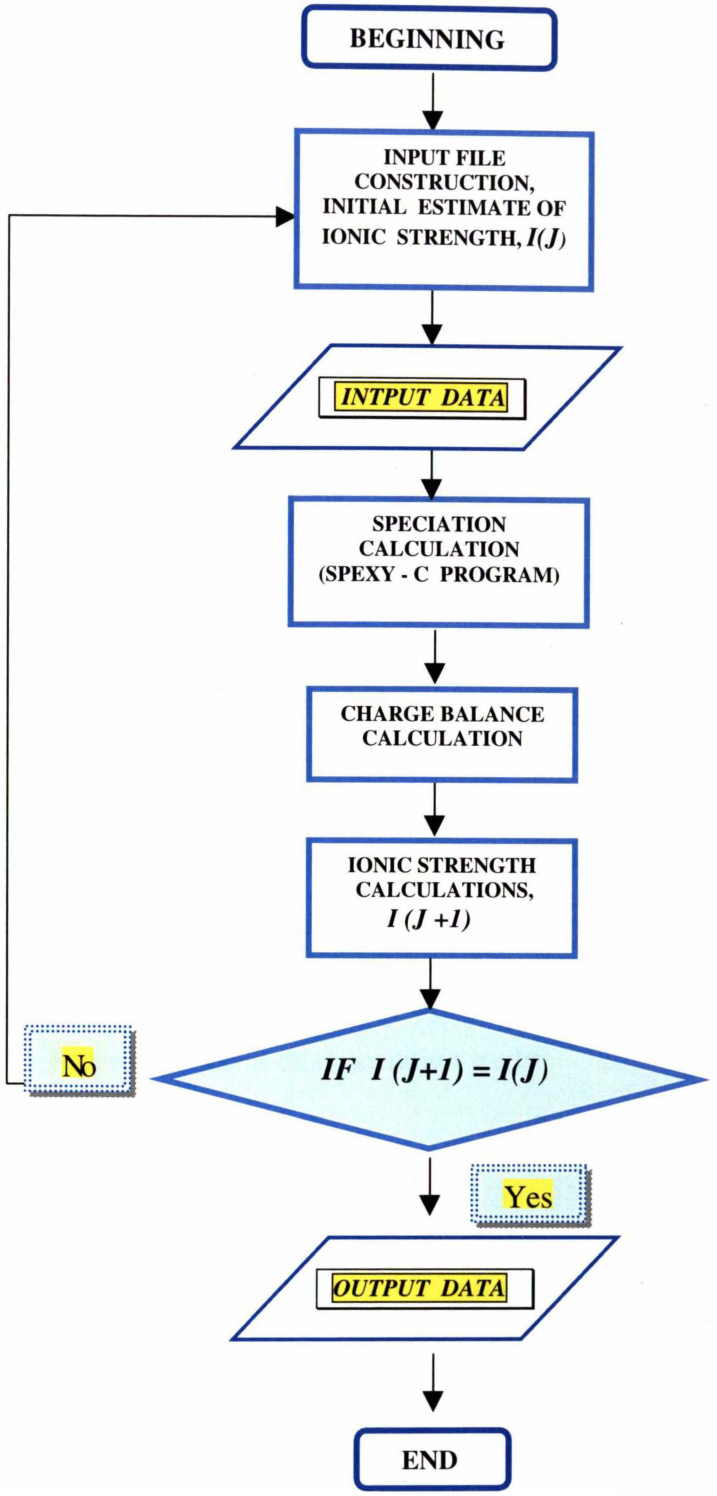

Figure 4-1: Flow chart giving the basic outline of the algorithm employed for carrying out the SPE computer speciation calculations.

Acidification of the milk to pH 4.6 and removal of casein liberates all the calcium plus other ionic components such as citrate, lactate, phosphate, magnesium etc to give a complex solution in which there will be various ion-ion interactions. In such a system,

the total "calcium" ([Ca]) can be determined by summing up all the concentrations of ion complexes that involve calcium. Similar expressions can be deduced for [P], [Mg] etc. For example:

$$[Ca]_{total} = [Ca^{2+}] + [CaCit^{-}] + [CaHPO_4] + [CaOH^{+}] + [CaLac^{-}] \ldots$$
$$[P]_{total} = [H_2PO_4^{-}] + [HPO_4^{2-}] + [CaHPO_4] + [MgHPO_4] \ldots$$
$$[Mg]_{total} = [Mg^{2+}] + [MgCit^{-}] + [MgHPO_4] + [MgOH^{+}] \ldots$$
$$[Cit]_{total} = [Cit^{3-}] + [H_2Cit^{-}] + [HCit^{2-}] + [MgCit^{-}] + [CaCit^{-}] \ldots$$

As there are many anions that could potentially complex or ion-pair with Ca^{2+} (or Mg^{2+} etc), these all need to be taken into account. The extent of complexation or soluble ion-pair formation will depend on the equilibrium constant for the formation of the complex in solution, e.g. consider the equilibrium between Ca^{2+} and citrate (Cit^{3-}) to form complex [Ca-Cit]$^{-}$:

$$Ca^{2+} + Cit^{3-} \overset{K}{\rightleftharpoons} [Ca - Cit]^{-}$$

K (equilibrium constant) values have been determined in the literature from various experiments. Stability constants from NIST database #46 (Smith et al., 1998) were the primary source of data that were used in this speciation study.

4.1.3 Corrections to the K values for Ionic Strength

The value of stability constant *K* (see 2.17.2: "Calculation of the Ion Speciation in Complex Ionic Solutions") is dependent on the ionic strength of the medium. The "stepwise" stability constant *K* will change with the ionic strength *I* of the medium in which the complexation reaction is occurring. Literature values of *K* can often be quoted along with the ionic strength value (e.g. $I = 0.05$, 0.1 M). For values of *I* intermediate to these values, e.g. ($I = 0.12$ M), an interpolation method based on empirical extended Debye-Hückel equations can be used. In this equation "overall" stability constants (*log β*) are computed by summing "stepwise" *K* values. This is the value that the SPE program makes use of in its calculations. The groundwork for this empirical equation was performed by Dr. Kevin Pearce (Pearce, 1998). In essence, the procedure involves the use of an arbitrary, two-parameter (these being *a* and *c*) Debye - Hückel - type equation:

$$Log\beta_I = LogK_0 - a\sum_i z_i^2 A\frac{I^{\frac{1}{2}}}{(1+1.5I^{\frac{1}{2}})} + cI + LogK'$$

In this equation I is the ionic strength, $\log \beta_I$ is the β value at ionic strength I, $LogK_0$ is the thermodynamic K value at zero ionic strength, A is a constant specific to aqueous systems and is equal to 0.5115 at 25°C, $\sum_i z_i^2$ is calculated from the charges on the stepwise equilibrium solution species, a and c are found from graphical regression programs or are given arbitrary values, and $log\ K'$ is defined as the stepwise constant values at ionic strength I. All data are for 25°C as there is a paucity of data for stability constants at higher temperatures.

4.1.4 Basic Introduction to the Thermodynamics of Precipitation (and Dissolution) of Sparingly Soluble Salts from Supersaturated Solutions

Precipitation of calcium phosphate from an aqueous solution tends to occur when the solution becomes supersaturated with respect to the calcium phosphate compound. Dissolution of the compound, on the other hand, takes place when the surrounding aqueous solution is undersaturated with respect to that compound. Driving forces controlling dissolution and precipitation reactions are related to respective supersaturation or undersaturation levels defined with regard to the thermodynamic solubility product (K_{sp}). This describes the equilibrium state between the precipitated calcium phosphate solid and the components comprising the solid phase dissolved in aqueous solution. For example, the precipitation of brushite from reaction between Ca^{2+} and HPO_4^{2-} ions in aqueous solution can be described by the following equation:

$$Ca^{2+}_{(aq)} + HPO_4^{2-}{}_{(aq)} + 2H_2O \overset{K_{sp}}{\rightleftharpoons} CaHPO_4.2H_2O_{(s)}$$

Where K_{sp} is the solubility product of brushite. Values of K_{sp} have been extensively tabulated for many thousands of compounds. Values of K_{sp} from NIST database #46 (Smith et al., 1998) were used in this study. In common with the complex ion stability constants used for determining dissolved species, the SPE program uses "overall" formation constants ("*Log β*") values for precipitating solid phases, which were

corrected for ionic strength using the procedure outlined in the last section. For the purpose of this study, initial K_{sp} values corrected for ionic strengths of 0.1 M were used. As the program computes a more refined value of I, the K_{sp} and other thermodynamic constants were adjusted accordingly.

In these calculations, the formation of the calcium phosphate phases, brushite and octacalcium phosphate (these being precursor phases of the final phase, HAP) were "allowed" in order to illustrate the "phase transformations" that can occur in the solids precipitating from whey permeate. The formation of the compound, hydroxyapatite (HAP) was not included due to the failure of the SPE program to arrive at a convergent iteration (see Algorithm in Figure 4-1) when this compound was taken into account. The reason for this is due to HAP's high thermodynamic stability, which results in its dominating the species distribution diagram and suppressing all other solids. Use of brushite and octacalcium phosphate in the calculations is considered to be justifiable for predicting yields, as these compounds are direct precursors to the final HAP product.

4.2 The Use of SPE to Model Precipitation from SLWUF Buffers

4.2.1 Construction of the Input File

The Fortran-compiled SPE program input file comprised 1) the concentration values of the basic chemical components in the model system (expressed as mmol/50 mL in Table 4-1) and 2) the *log* β values and stoichiometric coefficients for the basic chemical components, dissolved complex ion species and insoluble calcium-containing solids (see data in Table 4-2).

Table 4-1: Basic chemical components defining the medium and their concentrations in SLWUF buffer, as contained in the input file used in the SPE program.

Component	PO_4^{3-}	$Citrate^{3-}$	$Lactate^{-}$	Mg^{2+}	Ca^{2+}
Concentration, (mmol/50 mL)	1.21	0.1	3.5	0.16	1.55

Table 4-2: *Log (β)* values and stoichiometric coefficients for the basic chemical components, dissolved complex ion species and *Log* K_{sp} values for insoluble CaP solid phases at T=25°C in the Fortran-formatted input file SPE program for the lactic whey permeate system.

Species	*Log (β)* at *I=0.1*	*Stoichiometric coefficients*
PO_4^{3-}	0.0	0101 0200 0300 0400 0500 0600 0700
HPO_4^{2-}	11.52	0101 0200 0300 0400 0500 0600 0701
$H_2PO_4^-$	18.23	0101 0200 0300 0400 0500 0600 0702
H_3PO_4	20.29	0101 0200 0300 0400 0500 0600 0703
$CaHPO_4$	13.39	0101 0200 0300 0400 0500 0601 0701
$CaH_2PO_4^+$	19.26	0101 0200 0300 0400 0500 0601 0702
Cit^{3-}	0.0	0100 0201 0300 0400 0500 0600 0700
$HCit^{2-}$	5.66	0100 0201 0300 0400 0500 0600 0701
H_2Cit^-	10.0	0100 0201 0300 0400 0500 0600 0702
H_3Cit	12.89	0100 0201 0300 0400 0500 0600 0703
$CaCit^-$	3.56	0100 0201 0300 0400 0500 0601 0700
$CaHCit$	7.65	0100 0201 0300 0400 0500 0601 0701
CaH_2Cit^+	12.10	0100 0201 0300 0400 0500 0601 0702
Lac^-	0.0	0100 0200 0301 0400 0500 0600 0700
$HLac$	3.66	0100 0200 0301 0400 0500 0600 0701
$CaLac^+$	1.07	0100 0200 0301 0400 0500 0601 0700
$Ca(Lac)_2$	2.00	0100 0200 0302 0400 0500 0601 0700
Mg^{2+}	0.0	0100 0200 0300 0400 0501 0600 0700
$MgCit^-$	3.43	0100 0201 0300 0400 0501 0600 0700
$MgHCit$	7.29	0100 0201 0300 0400 0501 0600 0701
MgH_2Cit^+	11.8	0100 0201 0300 0400 0501 0600 0702
$MgHPO_4$	13.53	0101 0200 0300 0400 0501 0600 0701
$MgOH^-$	-11.61	0100 0200 0300 0400 0501 0600 07-1
Ca^{2+}	0.0	0100 0200 0300 0400 0500 0601 0700
$CaOH^+$	-12.91	0100 0200 0300 0400 0500 0601 07-1
CO_3^{2-}	0.0	0100 0200 0300 0401 0500 0600 0700
HCO_3^-	9.87	0100 0200 0300 0401 0500 0600 0701
H_2CO_3	15.99	0100 0200 0300 0401 0500 0600 0702
$CaCO_3$	2.32	0100 0200 0300 0401 0500 0601 0700
$CaHCO_3^+$	10.70	0100 0200 0300 0401 0500 0601 0701
H^+	0.0	0100 0200 0300 0400 0500 0600 0701
OH^-	-13.78	0100 0200 0300 0400 0500 0600 07-1
Solids	*Log* K_{sp} at *I=0.1*	*Stoichiometric coefficients*
OCP	-42.25	0103 0200 0300 0400 0500 0604 0701
Brushite	-17.44	0101 0200 0300 0400 0500 0601 0701
Ca_3Cit_2	-14.2	0100 0202 0300 0400 0500 0603 0700
$Ca(Lac)_2$	-3.34	0100 0200 0302 0400 0500 0601 0700
HAP	-38.78	0103 0200 0300 0400 0500 0605 07-1

4.2.2 Results and Discussion

4.2.2(a) Ion /Molecular Speciation and Solid Formation

A plot of the concentration of the various dissolved and solid species forming in the "standard" SLWUF buffer as a function of pH between pH 3-9 is shown (see Figure 4-2). A description of the significant ion and molecular species can be given as follows:

Ca^{2+} - free calcium ion concentration ($[Ca^{2+}_{(aq)}]$), the overall level of which is influenced strongly by the formation of calcium containing species, in particularly CaP solids.

CaLac^{+}- an ionic complex formed from free Ca^{2+} and lactate^{-} ions, with the maximum concentration at low pH 4.3.

$H_2PO_4^-$ - is a result of the equilibrium distribution of species of phosphoric acid (H_3PO_4, HPO_4^{2-} and PO_4^{3-}). This is the important form at the permeate pH of 4.6.

CaCit^{-} - in the pH region 4-7, is the complex ion formed between Ca^{2+} and Cit^{3-} ions. The maximum concentration of this complex is predicted to be at pH 5.6. This complex is a significant binding agent of free calcium. It ties up the calcium in solution in a form which makes it less available for the precipitation reaction between calcium ion and phosphate ion.

At low pH range 3.0-4.3 calcium ions ($[Ca^{2+}_{(aq)}]$) are partially bound with phosphate ions in the molecular complex ($CaH_2PO_4)^+$.

The general trends in the distribution of an ion, molecular and solid species in the "standard" SLWUF buffer model solution, calculated by SPE program are as follows (see Figure 4-2):

As pH increases, free calcium ion (Ca^{2+}) decreases from a maximum of *ca.* 22 mM at pH 3 to nearly zero at a pH of 9. This is due to the increasing incorporation of Ca^{2+} in various solid calcium phosphate phases such as brushite and OCP as pH is increased.

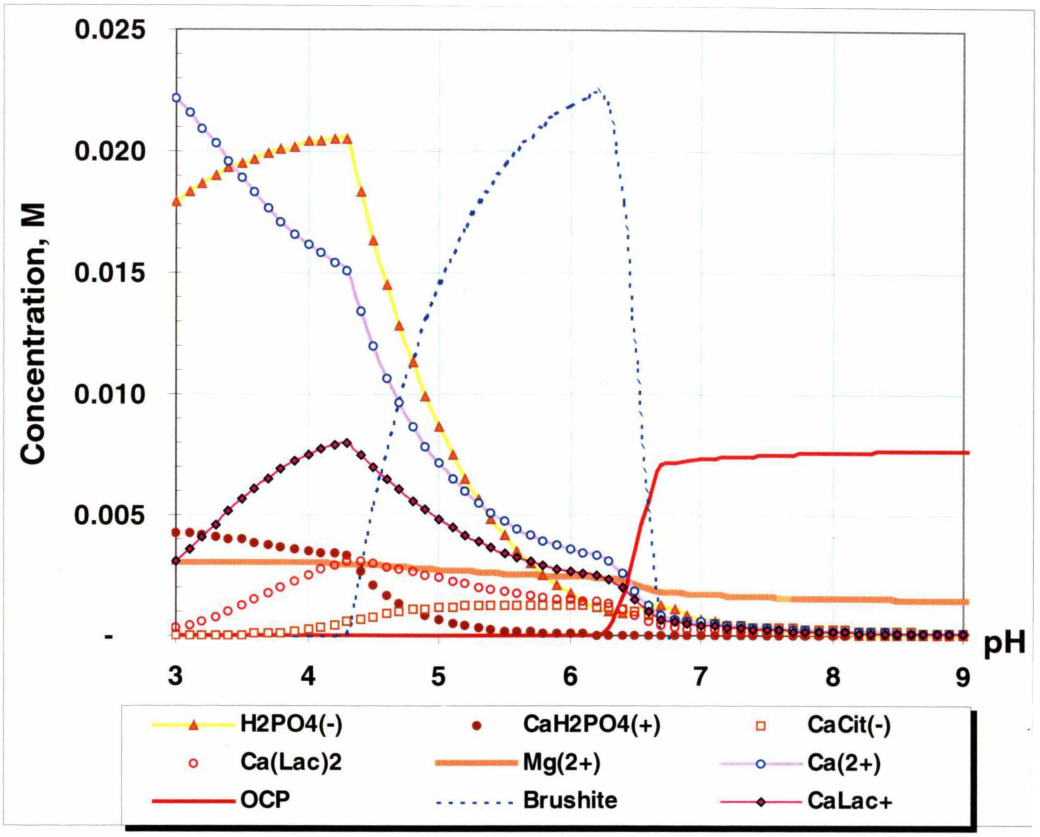

Figure 4-2: SPE calculated concentration-pH plot showing the general distribution of the dominant free ions, complex ions and solid species over the pH range 3-9 in the "standard" SLWUF buffer solution.

At the low pH (≤ 3), the concentration of free Ca^{2+} is not at its maximum value of 31 mM due to its involvement in other complexation equilibria with citrate, lactate and $H_2PO_4^-$. Inorganic phosphate ion at low pH (3-4.5) is mainly present as $H_2PO_4^-$ ion, as expected from its pK_a2 value of 2.06 at *I=0.1* M. Only moderate formation of the molecular complex ion $CaH_2PO_4^+$ occurs over this pH range. Above pH 4.5, the level of free inorganic phosphate ion species in solution drops sharply due to its involvement in brushite formation which is dominant over the pH range 4.5-6.8. For this reason, free HPO_4^{2-} ion is not a significant species over this pH range.

In the speciation calculations, brushite is the first solid phase to form under conditions of thermodynamic equilibrium in the SLWUF buffer and is stable over a pH range of 4.5-6.5. Above pH 6.5, octacalcium phosphate (OCP) is the thermodynamically more stable phase meaning its formation dominates in the speciation distribution pie graph (see Figure 4-3) and the majority of calcium and phosphate in the medium is consumed in forming this solid. OCP is well known as a precursor to HAP phase formation (Elliot, 1994).

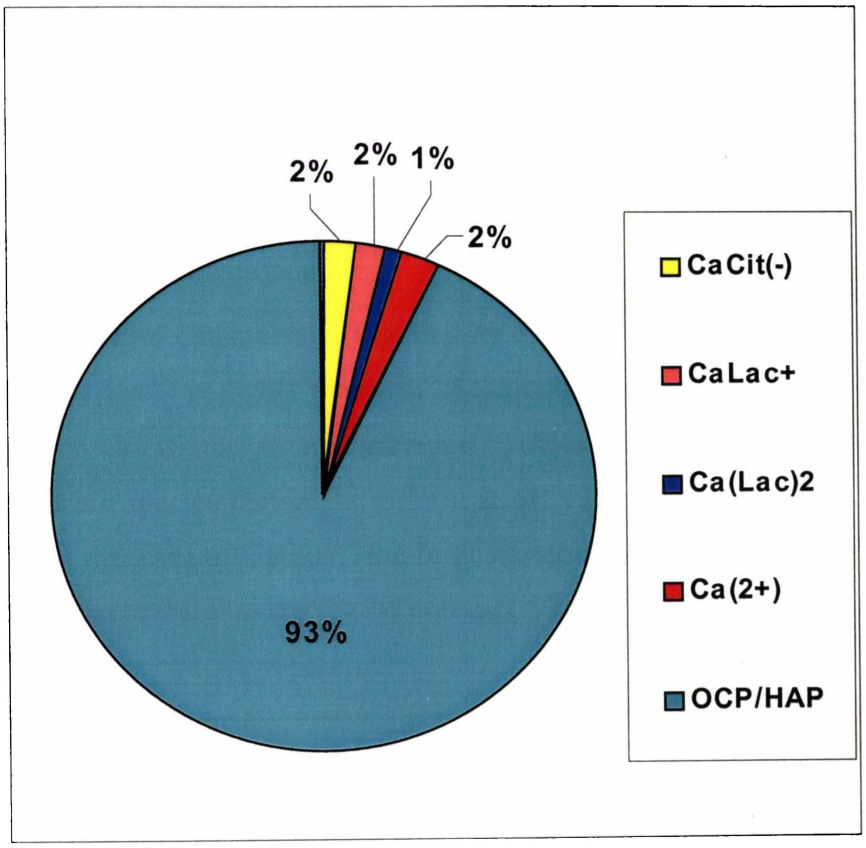

Figure 4-3: SPE calculated distribution of the main soluble and insoluble species in the "standard" SLWUF buffer solution at pH=6.8.

As stated above and shown below in Figure 4-4, SPE calculations predict that the brushite phase will be a significant phase at pH 4.6:

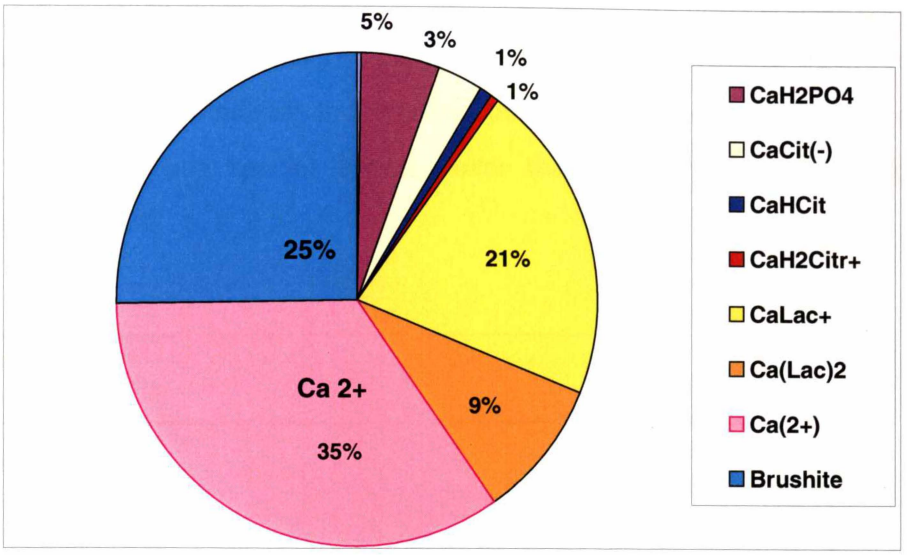

Figure 4-4: SPE calculated distribution of the main soluble and insoluble species in the "standard" SLWUF buffer solution at pH=4.6.

SPE calculations also demonstrate (Figure 4-4) that at pH=4.6 the concentration of the ion complex $Ca(Lac)^+$ is higher than that of the complex formed between calcium ion and citrate, viz, $CaCit^-$ ion. As was previously shown in Figure 4-2, $Ca(Lac)^+$ ion and $Ca(Lac)_2$ ions are species that begin to form at pH values below 4.3. SPE calculations also show that the level of $Ca(Lac)^+$ ion in this system generally depends on the citrate concentration due to the complex $CaCit^-$ (see next Figure 4-5).

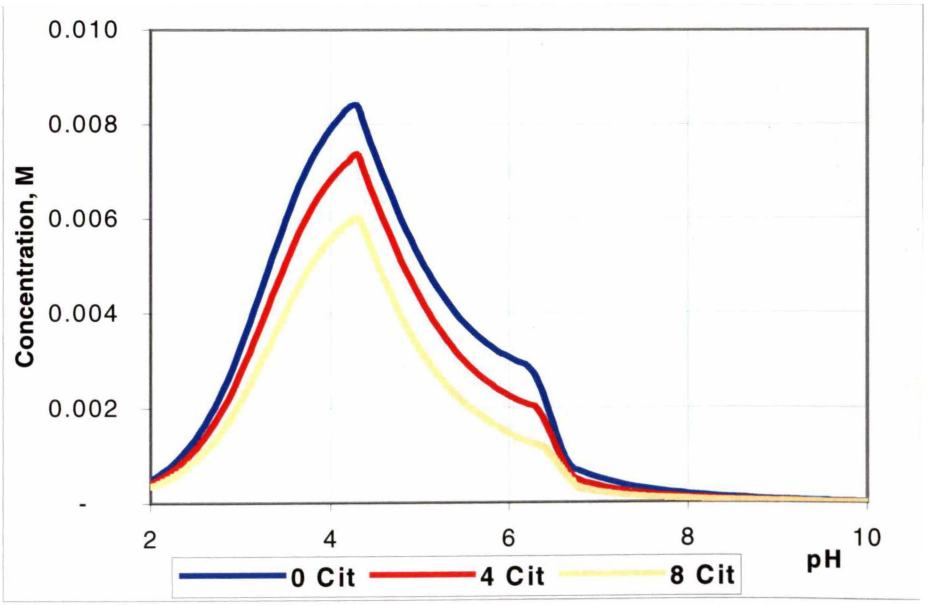

Figure 4-5: SPE calculated distribution of the $Ca(Lac)^+$ ion species as a function of the citrate concentration (0, 4 and 8 mM) in the SLWUF buffer.

Thermodynamic considerations, however, predict that citrate ion plays a more significant role in the SLWUF buffer. In general, citrate is a moderate chelating agent for free calcium ion because of its tendency to form the $CaCit^-$ ion complex. As it was shown in Figure 4-6, the $CaCit^-$ ion species appears over the pH range 3-9 and reached a maximum at *ca.* pH 5.8.

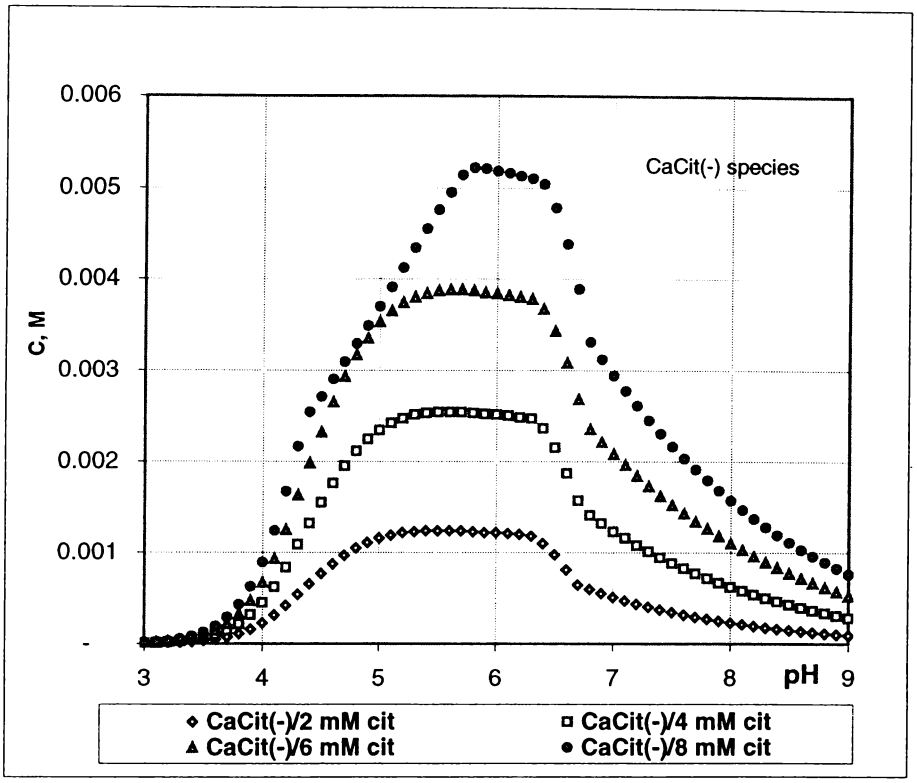

Figure 4-6: SPE calculated concentration - pH plot showing the pH region over which $CaCit^-$ ion is stable for concentration of citrate in the SLWUF buffer from 2-8 mM.

The maximum in $CaCit^-$ ion formation occurs near to the maximum predicted for solid brushite formation and thus has a significant effect on the formation of solid calcium phosphate phases by restricting the amount of reactive free Ca^{2+} available for precipitation. In this system, solid calcium citrate (Ca_2Cit_3) is also predicted to form, although its formation in the "standard" SLWUF buffers where citrate concentration is low (2 mM) is negligible. SPE calculations show that the solid Ca_2Cit_3 is predicted to form in significant amounts when the concentration of the citrate in the SLWUF buffer exceed 6 mM. More details on citrate and lactate influences are given in Chapter 5.

4.2.2(b) Impact of varying Ca:P Molar Ratios on the Precipitation of Calcium Phosphate from the SLWUF Buffer

Increasing or decreasing the phosphate concentrations in the medium (and hence reducing or increasing the Ca:P molar ratio) was found primarily to affect the concentration of free calcium in the medium. In general, a Ca:P molar ratio of 1:1, which is lower than in the "standard" SLWUF buffer formulation (where Ca:P molar ratio=1.28), leads to greater utilisation of free calcium over all pH regions with consequent higher yields of precipitated calcium phosphate solid. Figure 4-7 is an illustration of this general trend and shows that the concentration of the free calcium ions decreases in the following order of Ca:P molar ratios 1.5 > 1.28 > 1.0.

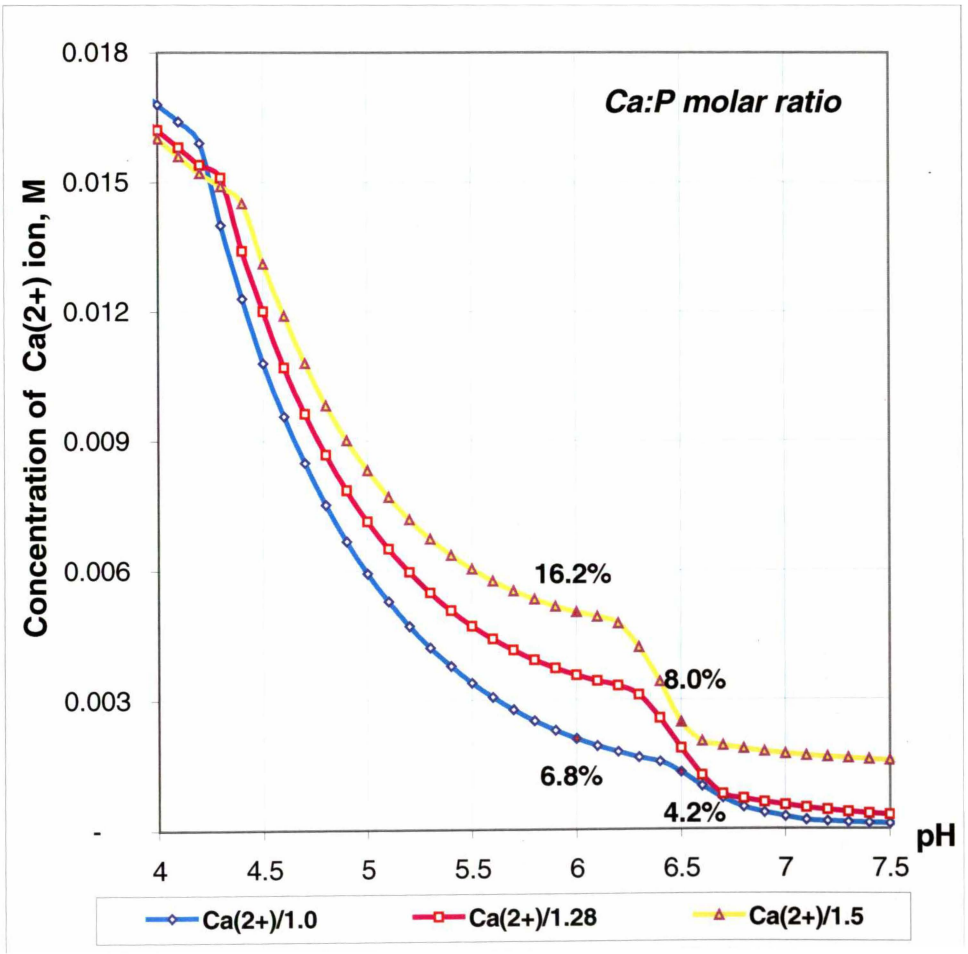

Figure 4-7: Predicted concentration of free calcium ion ($[Ca^{2+}_{(aq)}]$) in the SLWUF buffer for three different Ca:P molar ratios: 1.00, 1.28 and 1.50 (1.28=Ca:P molar ratio in "standard" SLWUF buffer). Percentage values refer to the % of total Ca (31 mM) left in the SLWUF buffer at pH 6.0 and 6.5 as $[Ca^{2+}_{(aq)}]$ ion after precipitation.

For example, at pH 6.0 for Ca:P molar ratios of 1.5 and 1.0, the level of free calcium ion ($[Ca^{2+}_{(aq)}]$ left after precipitation from SLWUF medium) differs by over 9 % for the two cases (100%=31mM Ca^{2+}). As pH increases, the difference in free calcium ion concentration between Ca:P molar ratios of 1.0 and 1.5 decreases to 3.8 % (pH=6.5). Overall, these results indicate clearly that phosphate is a limiting reagent in the precipitation of calcium phosphate solids from the SLWUF buffer and an increase in phosphate level would, in theory, increase the yields of solids from such media, which is important from an industrial point of view.

4.2.2(c) Impact of varying Citrate Concentration on the Precipitation of Calcium Phosphate from the SLWUF Buffer

The main effect of citrate ion in the SLWUF buffer is its ability to act as a moderate binding agent for free calcium ion. The chelate $CaCit^-$ is thermodynamically predicted to form over the pH range 4-8. The predicted concentration of this complex increases as citrate concentration is increased from 2-8 mM resulting in a decrease in the amount of free calcium in the medium (see Figure 4-8).

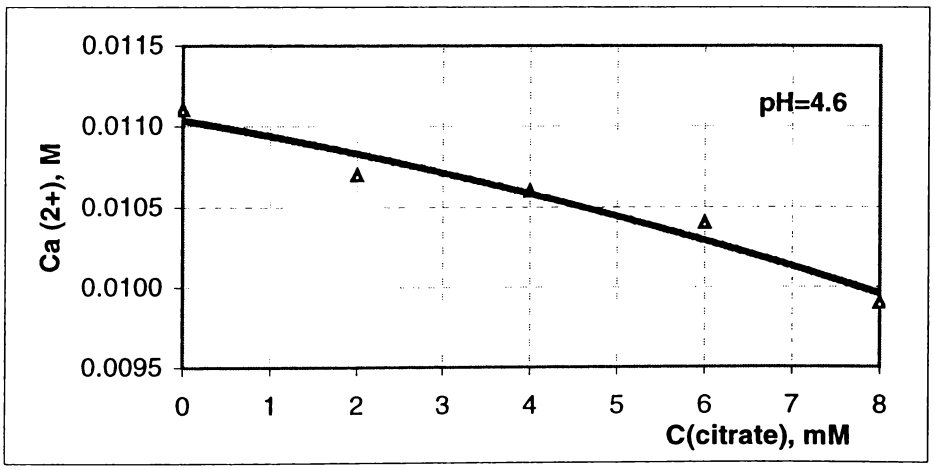

Figure 4-8: SPE calculated concentration of free calcium ions ($[Ca^{2+}_{(aq)}]$) in the SLWUF buffer solutions for citrate levels varying from 2-8 mM.

This has a consequence on the onset of the predicted formation of the predicted brushite and OCP solids. Figure 4-9 is a plot of the percentage yield versus pH for the total yield of solid Ca in the form of brushite and OCP ($Ca_{(S)} = Ca_{[OCP]} + Ca_{[BRUSHITE]}$).

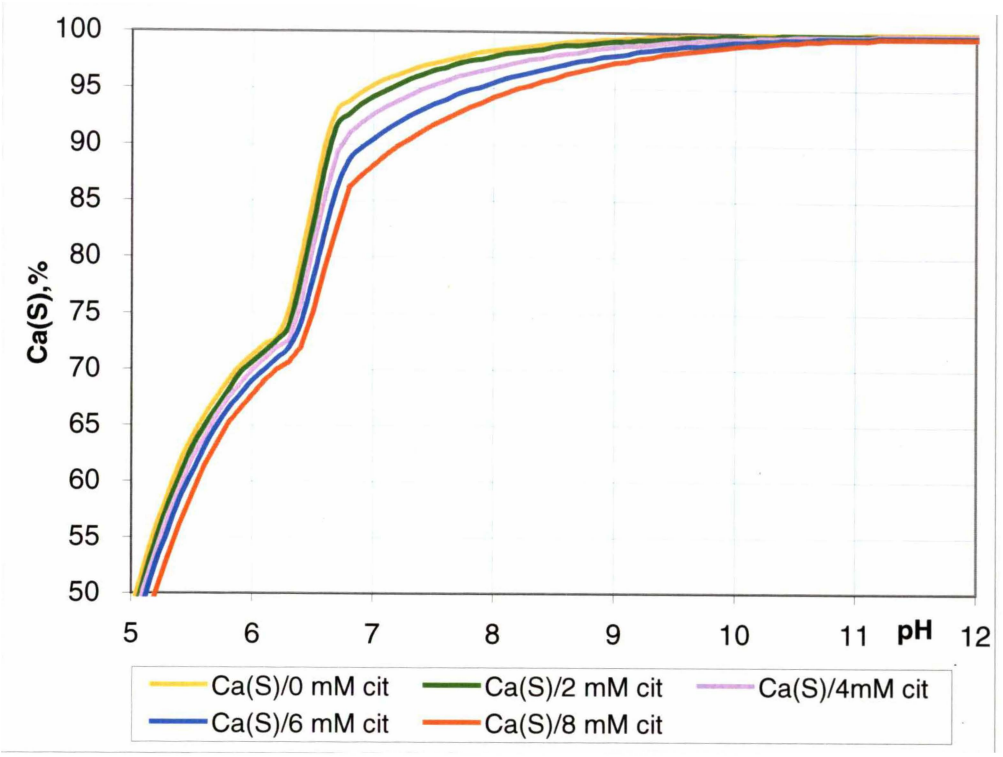

Figure 4-9: Predicted concentration - pH plot showing the impact of varying citrate ion concentration in the SLWUF buffer on solid CaP yield ($Ca_{(S)} = Ca_{[OCP]} + Ca_{[BRUSHITE]}$) for citrate concentrations varying from 0-8 mM.

It is clear that increasing levels of citrate reduce the yield of solid precipitated. The difference in solid yield between precipitation from an 8 mM and 0 mM citrate is at its greatest over the pH range 6.5-6.8 where OCP is beginning to form. For example, at pH=6.8, the difference in precipitation yield approaches 8%.

Citrate is therefore acting as an inhibitor of calcium phosphate formation which is well known experimentally from previous studies (Tenhuisen and Brown, 1994). The following Figure 4-10 illustrates that an increased level of citrate in the SLWUF buffer can extend the pH-stability region of brushite and hence delay the formation of the OCP solid phase.

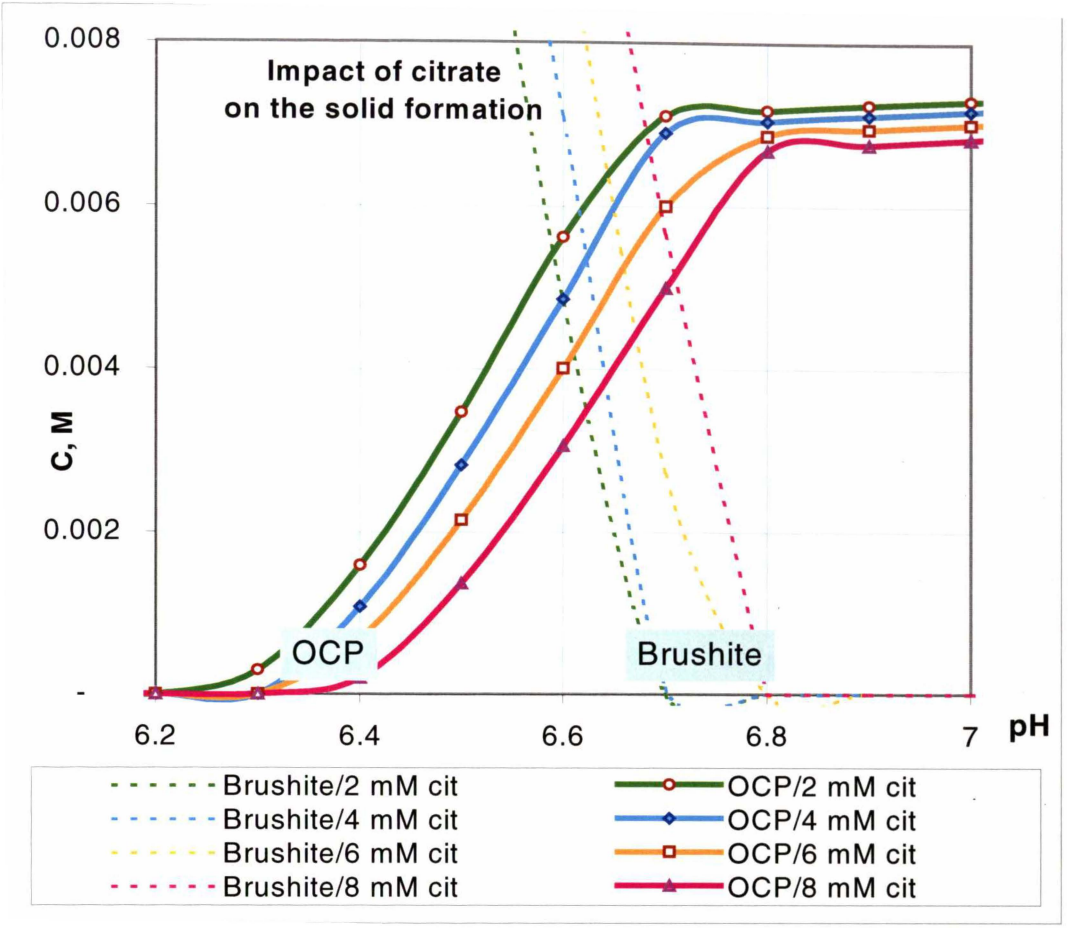

Figure 4-10: SPE calculated concentration - pH plot, showing citrate influence on the solid brushite and OCP formation in the SLWUF buffer.

So, an increase in the citrate level in the SLWUF causes a delay in OCP formation and extends the stability region of the brushite. This delay is proportional to the concentration of citrate in the SLWUF.

4.2.2(d) Impact of Magnesium Concentration on the Precipitation of Calcium Phosphate from the SLWUF Buffer

Speciation calculations were also performed on the SLWUF system in which the concentration of magnesium ion was varied while keeping other components constant (see Figures 4-11 and 4-12). The concentration of the Mg^{2+} ion in a "standard" SLWUF buffer system (which most closely resembles actual lactic whey permeate) is 3.2 mM (Ca:Mg molar ratio=9.7). Over the pH region 3-9 (see Figure 4-11) Mg^{2+} ions were merely distributed in the SLWUF medium as $MgCit^-$ and $MgHPO_4$ species. This has the effect of releasing more free calcium ion for reaction due to competition of the

magnesium for citrate. Increasing the magnesium ion concentration simply increased the levels of the $MgCit^-$ and $MgHPO_4$ species (see Figure 4-12).

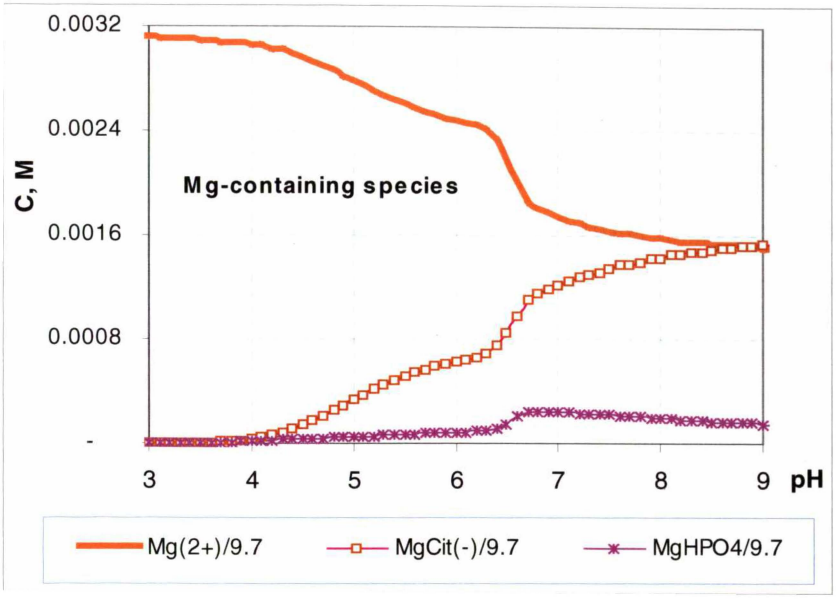

Figure 4-11: SPE calculated concentration-pH plot showing the level of free Mg^{2+} ions, $MgCit^-$ ions and $MgHPO_4$ molecules in the "standard" SLWUF buffer solution (Ca:Mg molar ratio = 9.7) at pH 3-9.

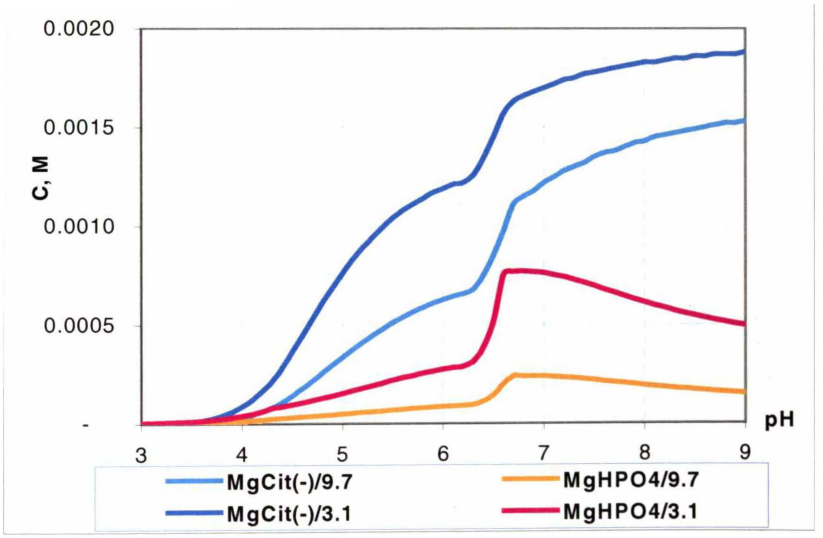

Figure 4-12: SPE calculated concentration-pH plot showing the distribution of the $MgCit^-$ and species with a different Ca:Mg molar ratios (9.7- for "standard" and 3.1 for Mg-enriched SLWUF system).

However, it is well known from previous research that Mg^{2+}ion has a far more profound influence than suggested by the SPE program in that it influences the kinetics of the phase transformation.

4.3 pH-Stat Controlled Experimental Work for Confirmation of Trends predicted by Computer Speciation Calculations

pH-stat controlled experimental work was undertaken to provide the experimental evidence of the trends, predicted for Simulated Lactic Whey Ultrafiltrate (SLWUF) buffer solutions, by SPE chemical calculations. For this purpose, the SLWUF buffer which had been previously subjected to speciation calculations in an earlier section of this chapter was actually formulated (see Table 4-3) to simulate a typical lactic whey derived permeate as would be obtained if the majority of whey proteins had been removed by an ultrafiltration process. The important industrial link to these studies is that they quantify the effect that various species can have on the characteristics of calcium phosphate precipitates. SLWUF buffers were also prepared with differing levels of citrate, phosphate, lactate and magnesium levels. These were prepared in order to gain insights into the effects of concentration variation on the precipitation and solution chemistry occurring in these solutions. The rationale behind this was because the actual lactic whey permeate used in the proprietary process can often vary considerably from batch to batch and from day to day so that an understanding of the complex interactions occurring in the permeate streams was needed.

4.3.1 Preparation of SLWUF Buffers

Experimental. Doubly distilled water was used for the preparation of solutions in all cases. Reagents employed in the preparation of solutions were Analytical Grade and used without further purification. The "standard" simulated lactic whey ultrafiltrate buffer (SLWUF) buffer solution used in this study was based upon the recipe reported in 1962 by Jenness and Koops (Jenness and Koops, 1962) and was prepared by combination of two solutions "A" and "B" containing preweighed amounts of the ionic components listed in Table 4-3. Solution "A" is made by adding two mol equivalents of HCl (1.0 M) to a suspension of $MgCO_3$ and $CaCO_3$. Calcium lactate is then added, dissolved and the resulting solution degassed N_2 (for 20 min.) and subsequently filtered to remove any particulate matter. The pH at this stage of the preparation is usually < 5.0. The remaining components in the SLWUF preparation recipe which make up solution "B" (see Table 4-3) are dissolved in water (*ca.* 200 mL) and filtered. The pH of solution "B" at this stage is usually in the range of 4.6-5.0. Solution "B" is then added slowly with stirring to solution "A" and the resultant solution made up to 1 L with

Table 4-3: "Standard" Simulated Lactic Whey Ultrafiltrates (SLWUF) buffer composition (citrate -2 mM).

Component		g L^{-1}	Ca (mM)	Mg (mM)	PO_4 (mM)	SO_4 (mM)	Cl (mM)	Na (mM)	K (mM)	Citrate (mM)	Lactate (mM)
Solution "A"											
$CaCO_3$		1.0	10								
$Ca(Lactate)_2.4H_2O$		4.58	21.0								42.0
$MgCO_3$		0.27		3.2							
HCl (1M)		26.8 mL					26.8				
Solution "B"											
KH_2PO_4		3.3			24.2				24.2		
$K_3(Citrate).H_2O$		0.65							6	2	
$Na_3(Citrate).2H_2O$		0									
K_2CO_3		0.03							0.61		
K_2SO_4		0.19				1.1			2.2		
KOH (1M)		5.29							5.29		
NaOH (1M)		16						16			
Lactic acid		2.5									28
Total	(g L^{-1})		1.24	0.08	2.3	0.106	0.95	0.368	1.50	0.378	6.2
	mM		31	3.2	24.2	1.1	26.8	16	38.3	2.0	70

Protein and lactose are not included.

degassed doubly distilled water with extra lactic acid added if necessary to adjust to pH 4.6. The solution was then either used immediately or else stored in plastic polyethylene bottles in the fridge until needed for pH-stat precipitation experiments. Slightly altered formulations of the "standard" SLWUF buffer were also prepared and used for studying precipitation. These were solutions in which one or more of the components had been changed in order to simulate the seasonal variability expected in natural whey permeates and its consequent effects on calcium phosphate precipitation. Tables 4-4 to 4-6 summarise the altered formulations that were prepared for experiments. In general, changes to three of the fundamental components comprising the "standard" SLWUF formulation were made: a) Ca:P molar ratio (see Table 4-4). This was varied in the SLWUF from a ratio of *ca.* 1:1 to 1:1.55 by changing the amount of phosphate salts added with the Ca:P molar ratio in the "standard" SLWUF buffer formulation being defined as 1.29:1, a value close to the ratio expected in natural whey permeates, b) Citrate concentrations (see Table 4-5). These were varied from 0-8 mM with 2 mM being defined arbitrarily as the normal level of citrate in the "standard" SLWUF buffer permeate and c) Ca:Mg molar ratio (see Table 4-6). SLWUF buffers were in which the Ca:Mg molar ratio was 9.7:1 (corresponding to 3.2 mM Mg^{2+} defined as being the normal level of Mg^{2+} ion in the "standard" SLWUF formulation), 7.6:1 corresponding to 4.1 mM Mg^{2+}, and 3.1:1 corresponding to 10 mM of Mg^{2+}.

Table 4-4: Additives for the SLWUF buffer solutions with different Ca:P ratios, based on a SLWUF buffer, containing a basic 2 mM citrate concentration (assuming 1 L total volume).

Component*	20 mM phosphate	24 mM phosphate	28 mM phosphate	30 mM phosphate
K_2HPO_4, g	2.72	3.30	3.80	4.00
K_3(Citrate).H_2O, g	0.65	0.65	0.65	0.65
KOH (1M), mL	9.49	5.29	1.49	0.51
NaOH (1M), mL	16.00	16.00	16.00	16.00
Lactic acid, mL	ca. 3	ca. 2.5	ca. 2	ca. 1.5

Table 4-5: Additives for the SLWUF buffer solutions with different citrate concentration (assuming 1 L total volume).

Component*	0 mM Citrate	2 mM Citrate	4 mM Citrate	6 mM Citrate	8 mM Citrate
$K_3(Citrate).H_2O$, g	0	0.65	1.23	1.23	1.23
$Na_3(Citrate).2H_2O$, g	0	0	0.06	0.66	1.24
KOH (1M), mL	9.6	5.29	0	0	0
NaOH (1M), mL	16.0	16.0	15.4	7. 0	3.3
Lactic acid, mL	ca. 3	ca. 2.5	ca. 2	ca. 1.5	ca. 1

Table 4-6: Additives for the SLWUF buffers with different magnesium concentrations, based on a 2 mM citrate solution (assuming 1 L total volume).

Component**	3.2 mM Mg^{2+}	4.1 mM Mg^{2+}	10.0 mM Mg^{2+}
$MgCO_3$, g	0.27	0.35	0.84

*All changes in the Tables 4-4 and 4-5 relate to "Solution B".

**Changes in Table 4-6 relate to "Solution A" (see also Table 4-3). All other component concentrations involved in the preparation protocol for the SLWUF buffer solutions were kept the same.

4.3.2 Precipitation of Solids from the SLWUF Buffers under pH-stat Control

The objective of the pH-stat experimental work was to study the kinetics of the precipitation reaction from SLWUF buffer solutions by measurement of the volume of added NaOH solution needed to keep pH constant in the reaction medium during the period. The pH-stat controlled experiments were carried out by performing the calcium phosphate precipitation at fixed pH-values in the range 6.0-7.2.

4.3.2(a) Experimental

All pH-stat controlled precipitation experiments were carried out under an atmosphere of nitrogen in a jacketed cell (54 x 80 mm) heated to the required temperature by way of

a thermostated water bath accurate to within ±0.2°C. In order to compare results with the SPE calculated speciation study (see section 4.2: "Use of SPE to Model Precipitation from SLWUF Buffers"), all precipitation experiments were performed at 25°C. pH measurements were made using either an Orion Ross Sure Flow combined electrode or a Radiometer combined electrode calibrated (using a 2-point calibration) at the reaction temperature with IUPAC 6.865 and 4.005 buffers. The pH was monitored and adjusted using a Radiometer 290 PHM pH-stat controller. The resulting data were collected and displayed using the spreadsheet package accompanying the pH-stat (version 1.1 X9649). Throughout experiments the pH stayed constant to within ±0.004 pH units. Figure 4-13 is a photograph of the computer-controlled pH-stat instrument setup:

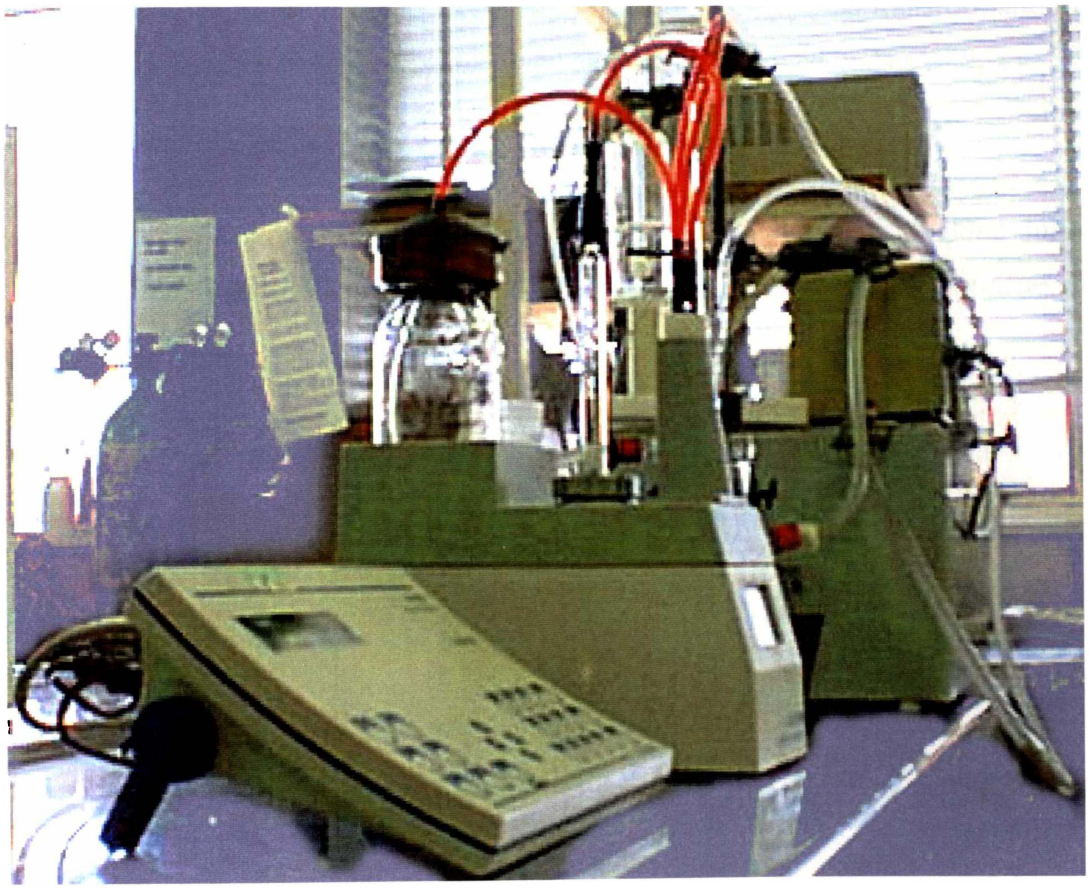

Figure 4-13: A photograph of the computer-controlled pH-stat instrument setup.

A typical experiment involved pH-jumping a stirred (using a 24 mm coated teflon magnetic stirring flea) solution of SLWUF buffer (110 g) by rapidly injecting a pre-weighed volume of NaOH (3.75 M) so that the reaction solution could be brought as close to the designated pH value as quickly as possible (the reason for this was because

the pH-stat controller did not have the ability to bring the SLWUF mixture instantaneously to the required pH). The pH-stat controller was then switched on and allowed to take over the maintenance of pH at a constant value by the automatic addition of 0.1 M NaOH solution (in this study: the fixed pH values studied ranged from 6 to 7.2). Stable pH readings were generally obtained in 1-2 minutes after pH jumping. Precipitation times (measured as time after pH jumping) were usually 30-60 minutes. Occasionally precipitation times less than this maximum time were studied when information on unstable solid phase intermediates appearing before the final apatitic precipitation product was desired.

Precipitated solids were filtered, sucked dry for 30 seconds and then cooled rapidly by pouring liquid nitrogen on them to arrest any possible further phase transformation of the solid. Solid samples were then freeze-dried and stored in sealed vials.

4.3.2(b) Results: Hydroxide Uptake as a Function of Time

Figure 4-14 illustrates the typical plot for the volume of NaOH solution added during the precipitation from the "standard" SLWUF buffer as a function of time after pH jumping (60 minutes):

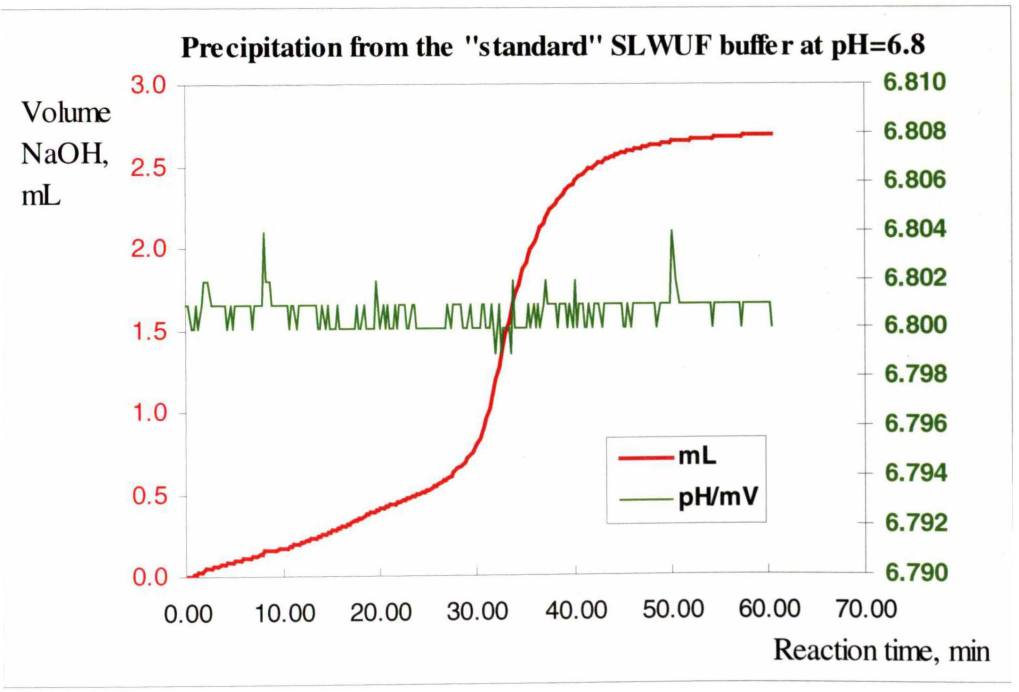

Figure 4-14: The typical relaxation profile curve for precipitation of CaP at T=25°C and pH=6.8 from the "standard" SLWUF buffer solution.

As a rule, a sigmoidal type curve for hydroxide uptake as a function of time was observed during the precipitation process from the SLWUF buffer solutions at T=25°C and pH=6.8. This sigmoidal type profile is interpreted as being representative of the three well-known distinct stages of the precipitation, these being: 1) the induction period, 2) the autocatalytic stage and 3) the final stage, involving maturation of the apatitic solid (Eanes, 1965; van Kemenade et. al., 1987). As such the curve is able to provide kinetic information on the calcium phosphate precipitation reaction and can sow the influence of various additives and conditions.

4.3.3 Influence of the Different Ca:P Molar Ratios in the SLWUF Buffer

In order to study the influence of the different Ca:P molar ratios in SLWUF buffers on the CaP precipitation process, the pH-stat controlled experimental work was performed at the same experimental conditions as described earlier (see section *4.3.2(a): "Experimental"*).

Results. Figure 4-15 illustrates the comparison of the relaxation profile curves for the precipitation CaP reaction at 25°C and pH=6.8 from SLWUF buffer solutions with different phosphate levels of 20, 24 and 30 mM (see Table 4-6) corresponding to Ca:P

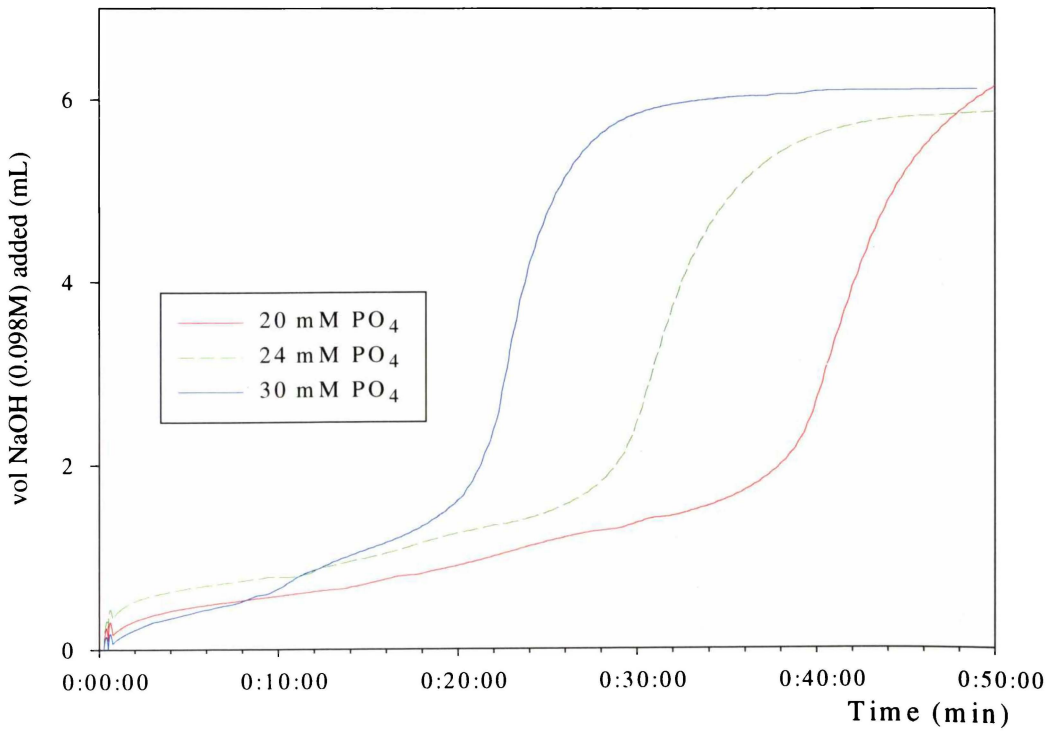

Figure 4-15: pH-stat relaxation profile curves for the precipitation of CaP at T=25°C and pH=6.8 from the SLWUF buffer solutions with a different Ca:P molar ratios.

molar ratios of 1.55, 1.29 and 1.1. The comparison of the relaxation profiles (Figure 4-15) shows that CaP precipitation reaction from SLWUF buffers with the highest level of phosphate (30 mM) proceeds faster than the buffer with the lowest phosphate level (20 mM). Hence this shows that the addition of extra phosphate leads to greater utilisation of phosphate.

This is clearly in agreement with what was predicted from the speciation calculations when the effect of extra phosphate addition to the SLWUF was being modelled and hence provides experimental proof for the predicted trend. So phosphate can be considered as an accelerating reagent for CaP precipitation in SLWUF buffers which is important from a kinetics point of view.

4.3.4 Influence of Citrate Concentration in the SLWUF Buffer

Experimental. SLWUF buffer solutions with citrate concentrations from 0-8 mM, i.e.: 0, 2, 4, 6 and 8 mM, were prepared in accordance with the protocol, shown in Tables 4-3 and 4-4. A series of pH-stat controlled experiments was carried out at pH=6.8 and T=25°C, following the procedure mentioned previously (see section *4.3.2(a): "Experimental"*).

Results. Experimental pH-stat relaxation curves for the precipitation of CaP at T=25°C and pH=6.8 from SLWUF solutions with different citrate concentrations are shown in Figure 4-16. These curves show the significant influence of citrate, as an inhibitor of the CaP precipitation process from SLWUF buffers. For example, when no citrate is present, CaP precipitation from the SLWUF at T=25°C is complete after only 35 minutes.

In contrast, the precipitation from the SLWUF buffer solution containing 8 mM citrate takes more than five hours to reach a state of completion (this being the flattening out of the pH-stat curve signifying formation of the apatitic phase). This is clearly in good agreement with the predictions made previously using the SPE program. Citrate presence obviously suppresses the formation of calcium phosphate solids due to its chelating ability which reduces the level of reactive free calcium ion in solution.

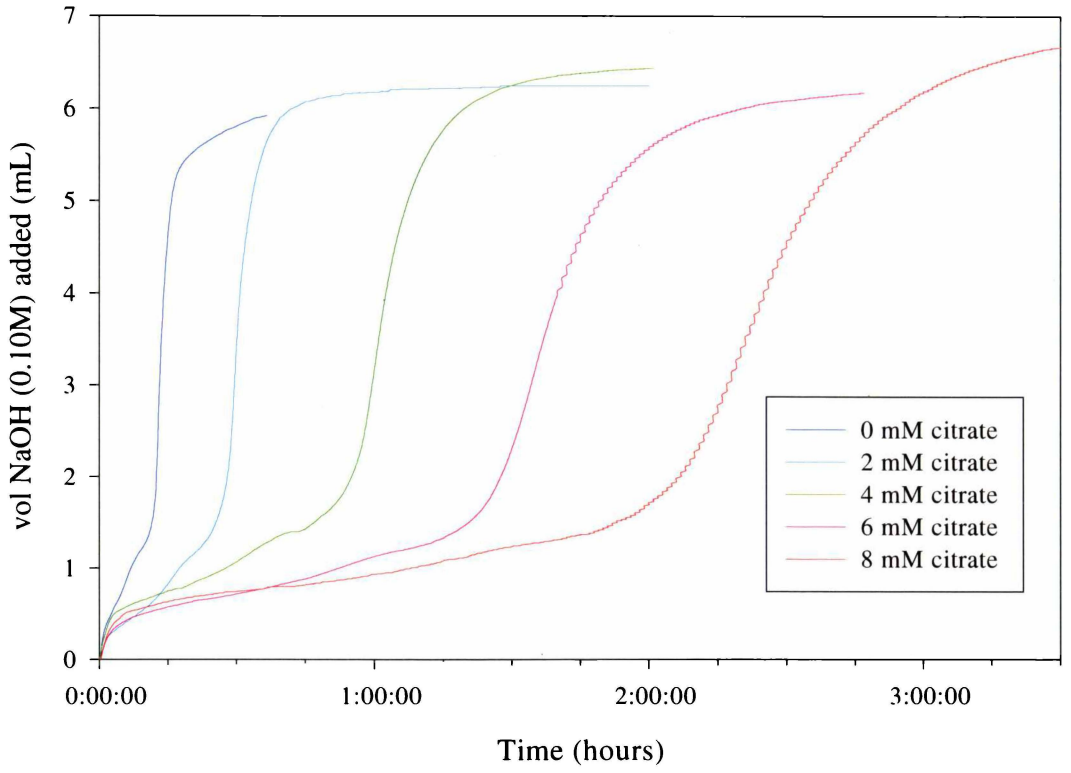

Figure 4-16: pH-stat relaxation profile curves for the precipitation of CaP at T=25°C and pH=6.8 from the SLWUF solutions with a different citrate concentration from 0 to 8 mM.

4.3.5 Influence of Magnesium Concentration in the SLWUF Buffer

Experimental. In order to determine the influence of varying magnesium concentration in the permeate, three SLWUF buffer solutions with different magnesium concentrations were prepared, using $MgCO_3$ as the magnesium source (see Table 4-6). These consisted of buffers in which the concentration of magnesium ion was 3.2 mM, 4.1 mM and 10 mM. This corresponded to Ca:Mg molar ratios of 9.7, 7.6 and 3.1 respectively. Of these solutions, the buffer with 3.2 mM magnesium ion corresponded to the "standard" SLWUF buffer solution.

Results. The pH-stat results for this work are shown below (see Figure 4-17). They show that magnesium has a strong influence on the shapes of the pH-stat profiles. For the "standard" SLWUF buffer solution with 3.2 mM of Mg ion (Ca:Mg molar ratio=9.7)

the precipitation process required *ca.*1 hour, while for the SLWUF buffer solution with 10 mM of Mg (Ca:Mg ratio=3.1) the precipitation reaction was not complete for more than two hours after pH jumping.

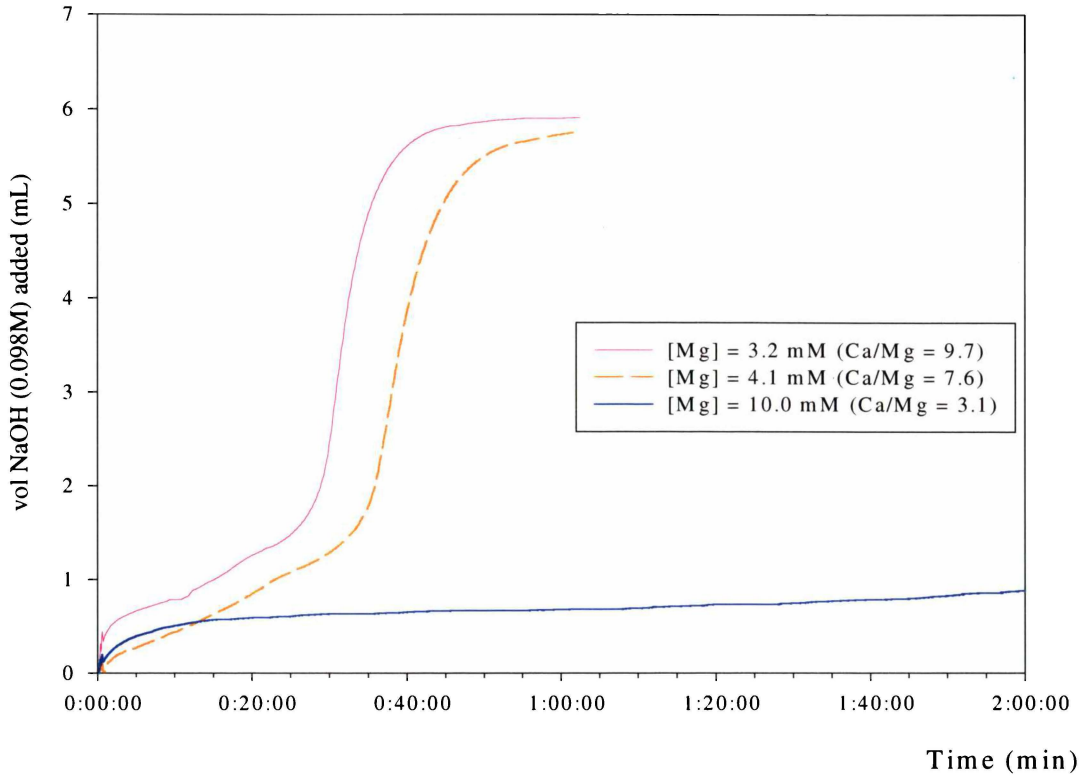

Figure 4-17: pH-stat relaxation profile curves for the precipitation of CaP at T=25°C and pH=6.8 from the SLWUF buffer solutions with a different Ca:Mg molar ratios.

From a kinetic point of view, the pH-stat experimental data show the significant impact of magnesium as an inhibitor of the precipitation process from SLWUF buffers. The inhibition arises from the well known role of magnesium ion as a stabiliser of the ACP intermediate as has been shown extensively by previous workers (Boskey et al., 1974; Eanes et al., 1981; Abbona et al., 1990). This is thus not in agreement with what was predicted from the SPE calculations as this program knows nothing of the magnesium inhibition of calcium phosphate precipitation. It is not known how much the magnesium level in the whey permeate varies during the season but it is clear that magnesium levels would have a significant impact on the industrial precipitation process were they to become significant.

4.3.6 Influence of pH in the SLWUF Buffer

Experimental. pH-stat controlled work was performed with the "standard" SLWUF buffer solution using the usual experimental protocol for the pH-stat experiments (see Table 4-3) to show the impact of pH on the kinetics of the precipitation of calcium phosphate. A series of pH-stat controlled experiments was carried out at 25°C at pH values of 6.4, 6.8 and 7.2 (see section *4.3.2 (a): "Experimental"*).

Results. Experimental pH-stat relaxation curves for the precipitation of CaP at 25°C and pH=6.8 from "standard" SLWUF buffer at different pH are shown in Figure 4-18. These curves show the significant influence of pH on the kinetics of the precipitation process from standard SLWUF buffers: for example, precipitation from a SLWUF solution at pH 6.4 requires only 20 minutes before completion of the reaction, while precipitation from SLWUF buffer solution at pH 6.8 requires 60 minutes.

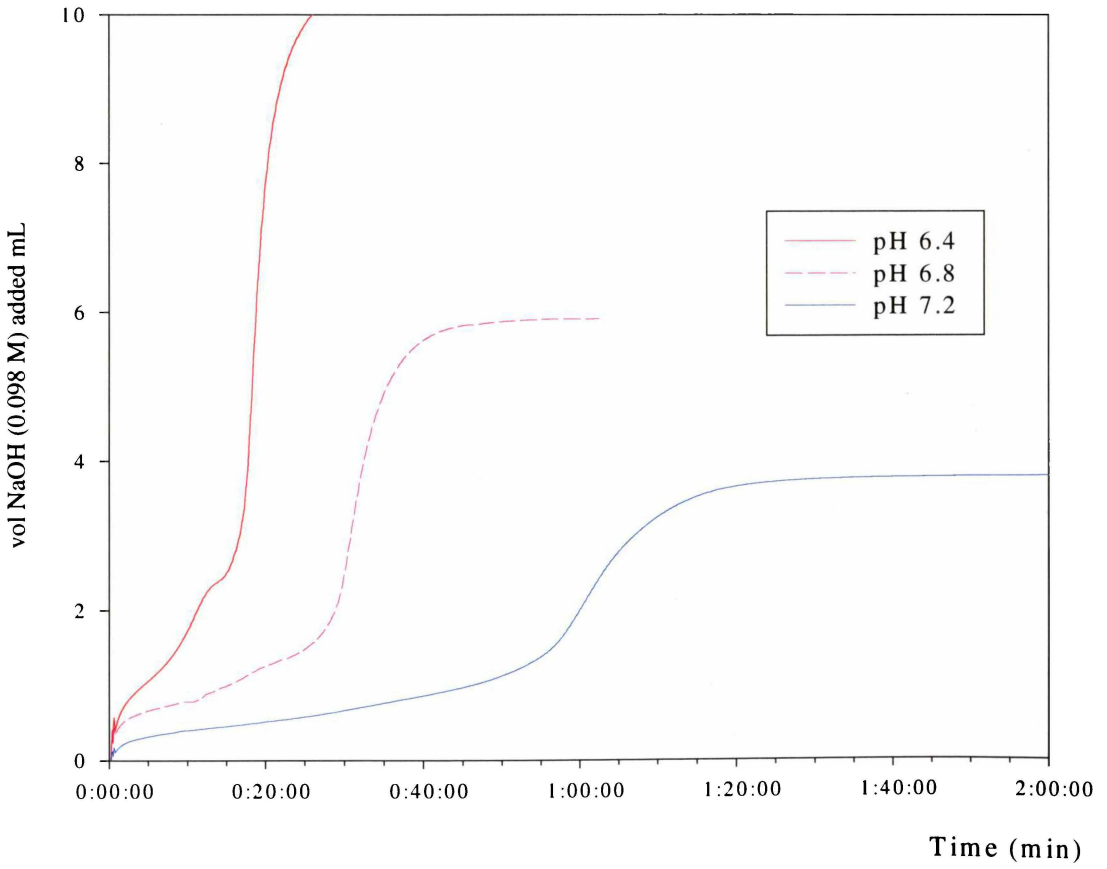

Figure 4-18: pH-stat relaxation profile curves for the precipitation of CaP at T=25°C and pH=6.8 from the "standard" SLWUF buffer solutions at different pH.

At pH 7.2, the reaction takes two hours to complete. This indicates that increasing the pH at which the precipitation takes place changes the mechanism of the reaction by influencing the lifetime of the intermediate amorphous phase ACP. Also it has already been shown in previous work by van Kemenade et al., (van Kemenade et al., 1987) that conducting the precipitation at pH 7.4 at temperature of 25°C leads to a change in the intermediate solid phase produces from a DCPD/OCP like intermediate to an ACP/OCP like intermediate which then converts to an apatitic solid. The reason for this delayed onset of final apatitic solid formation as pH is increased has been covered theoretically by the work of Meyer et al. (Meyer et al., 1978), described in Chapter 2 (section 2.12.3: "Thermodynamic Analysis of the Transitional Phases in the Precipitation of Calcium Phosphate") where a thermodynamic analysis of the transitional phases in the precipitation of calcium phosphate is given. These showed that when precipitation is carried out at higher pH, the duration of the amorphous-crystalline transition period in the development of the calcium phosphate precipitate becomes longer whilst the secondary transition to the apatitic phase occurred much more rapidly. Hence in the case of the SLWUF buffer, the different pH studies show that the ACP intermediate has an increased lifetime at high pH.

4.4 Determination of Free Reactive Calcium Ion in the SLWUF Filtrates using a Calcium Ion-Selective Electrode (ISE)

Calcium Ion-Selective Electrode (ISE) experimental work was undertaken along with the aforementioned pH-stat experimental data to provide experimental evidence for confirmation of the trends (in calcium ion concentration as a function of pH), predicted for SLWUF buffer solutions, by SPE calculations (see section 4.2: "The Use of SPE to Model Precipitation from SLWUF Buffers"). The Ca ISE experiments were performed in conjunction with a pH-stat experimental run on the filtrates of the SLWUF buffers after the precipitation and filtering off of the CaP precipitates. The reason for this will be given later (see section 4.4.2(a): "Free Calcium Concentration as a Function of Time during Precipitation under pH-stat controlled Conditions"). A calcium ion-selective electrode technique was employed as the analytical method for quantitative determining the concentration of free Ca^{2+} ion (Calcium Electrode, Operating Instructions, 1998). The calcium ion electrode (ISE25Ca by Radiometer Analytical) is a PVC membrane electrode as customarily used for direct measurements of calcium ions in aqueous solutions in combination with a (Radiometer) REF201 Ag/AgCl reference electrode.

4.4.1 Calcium Ion-Selective Electrode (ISE) Calibration

Experimental. The calcium ion-selective electrode (ISE25Ca) was calibrated against known concentrations of $CaCl_2$ in KCl of the same ionic strength (I=0.1 M) as believed to exist in actual whey permeate. Nine standard solutions of $CaCl_2$ in KCl were prepared, using KCl (0.1 M) as a background electrolyte in the range of Ca concentration 0.0001-0.033 M (see Table 4-7). Milli-Q water was used for preparing all solutions with a specific resistivity equal to 17.5 MΩ cm).

Table 4-7: Standard solutions of $CaCl_2$ in KCl with ionic strength I=0.1 M (estimated ionic strength in whey permeates) that were used for the calibration of the Calcium ISE at T=25°C.

C (Ca^{2+}), M	No	Ionic Strength, I M	Volume KCl (0.1 M), mL	Volume $CaCl_2$ (0.0333 M), mL
0.0333	1	0.1	0	100
0.030	2	0.1	10	90
0.025	3	0.1	25	75
0.020	4	0.1	40	60
0.015	5	0.1	45	55
0.010	6	0.1	70	30
0.005	7	0.1	85	15
0.001	8	0.1	97	3
0.0001	9	0.1	99.7	0.3

The calibration curve (see Figure 4-19) of Log_{10} [Ca^{2+}] versus E (mV) axis is linear in shape thus showing a Nernstian response for the electrode.

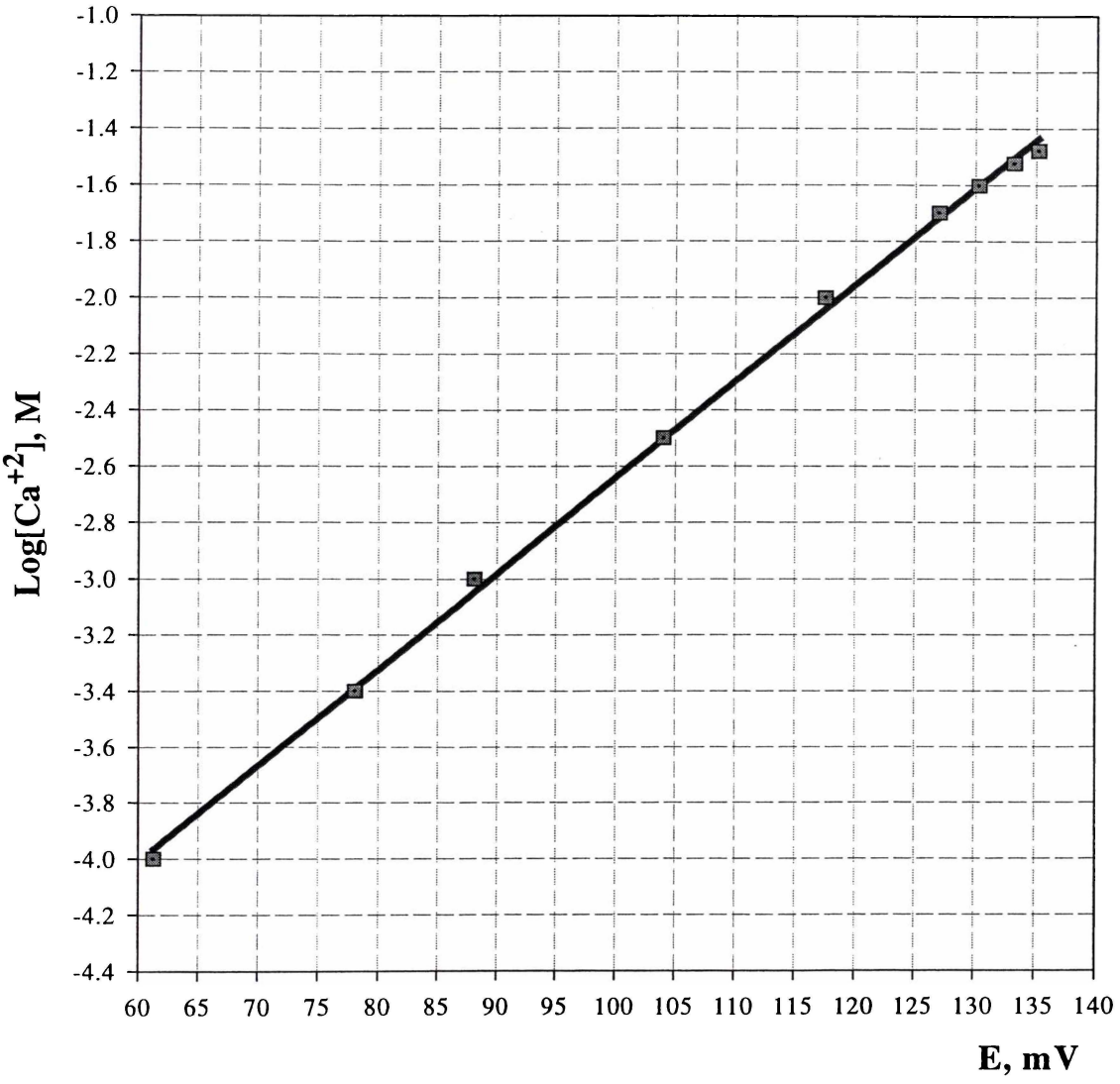

Figure 4-19: Typical calibration curve of Log [Ca^{2+}] versus E (mV) axis at T=25°C.

4.4.2 Calcium Ion-Selective Electrode (ISE) Measurements

4.4.2(a) Free Calcium Concentration as a Function of Time during the Precipitation under pH-stat controlled Conditions

Calcium ion-selective electrode (ISE) measurements were carried out on the standard SLWUF (2 mM citrate) filtrate solutions to determine the trends in free calcium ion concentrations left in the filtrates as a function of time after base addition to stimulate precipitation. In a typical precipitation experiment, carried out at 25°C under pH-stat controlled conditions (see section 4.3.2: "Precipitation of Solids from the SLWUF Buffers under pH-stat Control"), NaOH was added to adjust the pH to 6.8. For times of 5, 15, 30, 35, 40 and 60 minutes after base addition the resultant slurries were placed in an ice-water bath with the CaP precipitates being separated off using sintered glass funnels. Each of the filtrates so obtained was then analysed by the Ca ISE at 25°C to determine the concentration of free calcium ion remaining after the precipitation process (Table 4-8). Calcium phosphate solids, isolated from above time-course experiments were freeze-dried for further investigation by SEM and FTIR techniques. Ca ISE measurements on actual precipitating solutions (i.e. when there is a mixture of solid and liquid present) did not yield sensible results due to the fouling of the Ca ISE membrane surface with solids. This caused the Ca ISE to give a constant reading regardless of time of precipitation. The measurement of filtrates approach as described above was thus adopted. The mV readings obtained from the Ca ISE electrode had an estimated error based on observation of ±0.5 mV, which translated into a concentration error of *ca.* ±3.5%.

Table 4-8: Experimental data for Ca ISE measurements during the time-course of the precipitation process from the SLWUF buffer solutions.

Time, min	E, mV	Ca^{2+}, mM
5.0	102.0	3.01
15.0	102.0	3.01
30.0	101.0	2.78
35.0	95.0	1.74
40.0	85.0	0.79
60.0	82.0	0.63

Figure 4-20 illustrates the change in free calcium ion concentration left in the filtrate as a function of time after precipitation was initiated from the "standard" SLWUF buffer solution at T=25°C. The "zero time" point for free calcium in the SLWUF buffer before base addition has not been included in order to allow a clearer illustration of the trend in free calcium ion remaining in the filtrates as a function of time after precipitation.

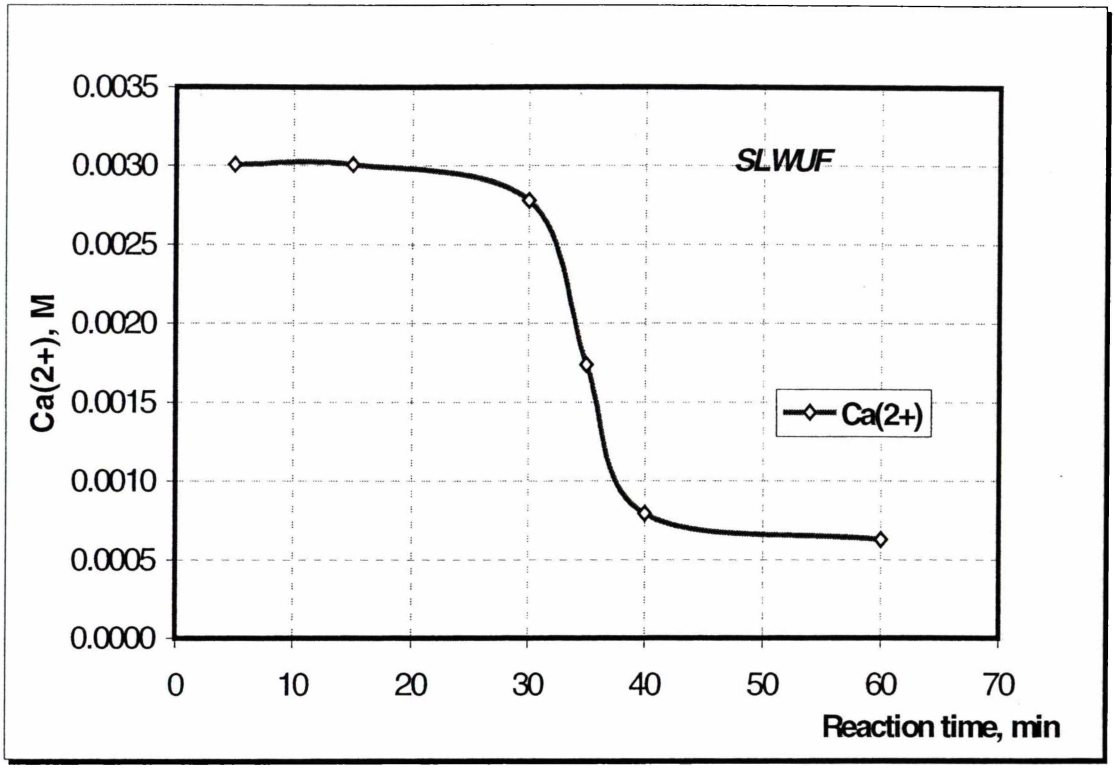

Figure 4-20: The typical curve of free calcium ion ($[Ca^{2+}_{(aq)}]$) concentration left in the filtrates as a function of time after precipitation was initiated from the "standard" SLWUF buffer solution at T=25°C and pH=6.8.

In general, a sigmoidal type curve, as shown in Figure 4-20 was obtained. This mirrors the typical relaxation profile curve of volume NaOH added versus time obtained from pH-stat controlled experiments for precipitation of CaP at T=25°C and pH=6.8 from "standard" SLWUF buffer solutions, as was previously demonstrated in Figure 4-14 (section *4.3.2(b) Results: Hydroxide Uptake as a Function of Time*). It shows that initially calcium is being taken up to form part of the amorphous calcium phosphate precipitate. As the precipitate undergoes phase transformation into the apatitic solid (hydroxyapatite) extra calcium is taken up from the solution very rapidly during the autocatalytic stage where ACP converts into HAP. Over this stage the consumption of

base added increases also as shown in the pH-stat experiments due to the liberation of protons in the phase transformation process.

4.4.2(b) Influence of Phosphate Level in the SLWUF Buffer as a Function of pH, set-up for CaP Precipitation under pH-stat controlled Conditions

Experimental. Experimental work was also performed to study the influence of phosphate concentration in SLWUF buffers on the free Ca^{2+}ion concentration left in the solutions after the precipitation process had been completed. This was done to test the predictions made by the speciation calculations relating to the amount of calcium utilisation at the different phosphate levels. For this purpose, SLWUF buffer solutions with different phosphate concentrations of 24, 28 and 32 mM were prepared (see Table 4-4) while keeping the same calcium concentration at 31 mM. In the "standard" SLWUF buffer, the concentration of Ca^{2+} is 31 mM and the phosphate concentration is 24 mM.

Experimental work was carried out under pH-stat-controlled conditions at pH values of 6.0, 6.2, 6.4, 6.6, 6.8 and 7.2 at a temperature of 25°C. 40 minutes after precipitation was initiated, CaP solids were separated off using sintered glass funnels. Ca ISE measurements were then carried out on the filtrates at 25°C in the same thermally jacketed cell as used in pH-stat experiments (dimensions 54 x 80 mm).

Results. These experimental data (Figure 4-21) demonstrate that: 1) the concentration of free Ca^{2+} ion decreases with increasing pH as predicted by the computer speciation calculations (see *4.2.2(b): "Impact of varying Ca:P Molar Ratios on the Precipitation of Calcium Phosphate from the SLWUF Buffer"*), 2) an increase of the phosphate level from 24 to 30 mM leads to a reduction in the free Ca ion concentration left in the solution after the precipitation at any given pH. This is also in agreement with the computer speciation calculations (see Figure 4-7), performed for SLWUF buffers with different Ca:P molar ratios.

It is thus clear that the addition of extra phosphate to the SLWUF buffer solutions enhances calcium phosphate precipitation, and hence decreases the level of free Ca^{2+} ion in the solution (Figure 4-21):

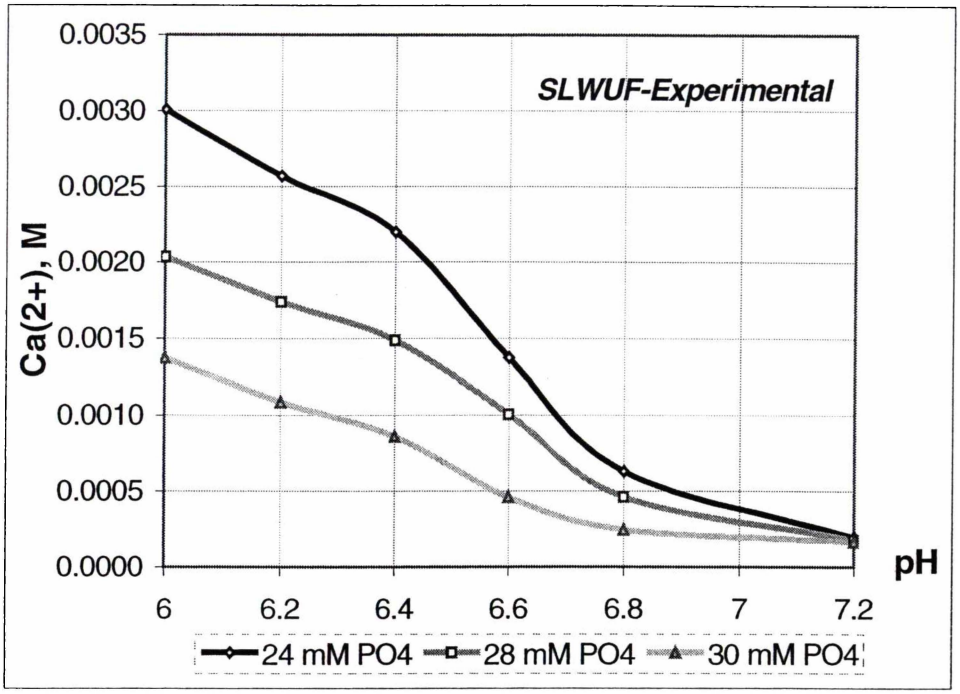

Figure 4-21: Concentration of free Ca^{2+} ion as a function of pH for the precipitation of CaP at 25°C for varying levels of total phosphate (24, 28 and 30 mM) in the SLWUF buffer solutions measured by the Ca ISE method.

This lends experimental weight to the prediction from the speciation calculations that phosphate is a limiting reagent for the CaP precipitation process occurring in the SLWUF buffer solutions.

4.4.2(b) Influence of Citrate Level in the SLWUF Buffers

Experimental. Five simulated whey permeates solutions with a different citrate concentrations were prepared (0, 2, 4, 6 and 8 mM citrate) in accordance with the protocol given in Table 4-5 to investigate the impact of citrate concentration on the free Ca^{2+} ion level in the SLWUF buffer solutions. Ca ISE measurements were performed at T=25°C on freshly prepared SLWUF buffer solutions. In these experiments, no CaP precipitation was undertaken. It was merely desired to measure free calcium ion concentrations in the SLWUF buffers at pH 4.6.

Results. Ca ISE measurements on the SLWUF buffer at pH 4.6 show that the concentration of free Ca^{2+} ion gradually decreased from 7 mM for the SLWUF buffer with 0 mM citrate to 4.4 mM for the SLWUF buffer containing the maximum amount of citrate studied (i.e. 8 mM, see Figure 4-22). This is hence in agreement with the computer speciation calculations for the concentration of free Ca^{2+} as a function of the citrate level in the SLWUF system at pH=4.6 which show the same decreasing trend for free Ca^{2+} ion with increasing citrate level in the SLWUF buffer (see Figure 4-8).

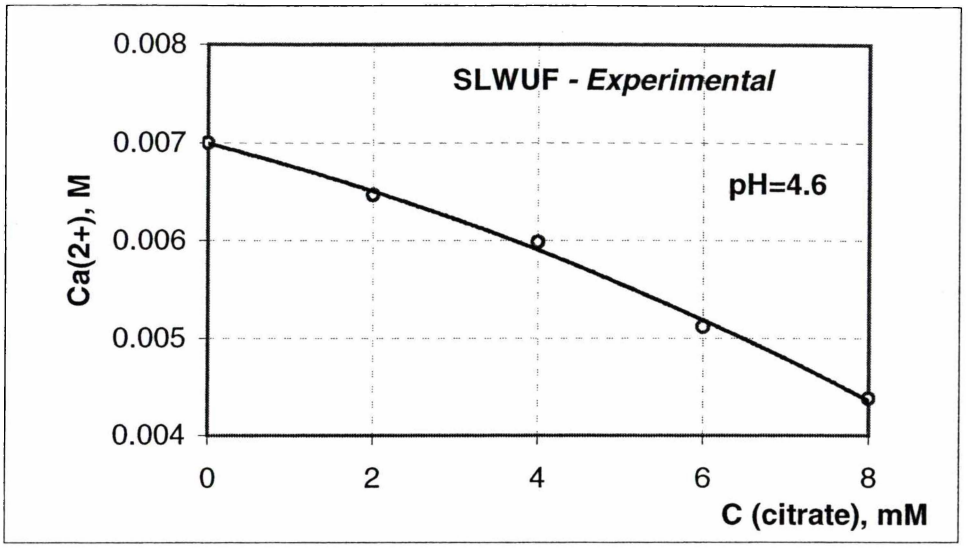

Figure 4-22: Concentration of free Ca^{2+} ion calcium ions as a function of citrate concentration (mM) in the SLWUF buffer solutions at pH=4.6 and T=25°C, measured using the Ca ISE method.

4.5 Fourier Transform Infrared Spectroscopy (FTIR) Analyses of the CaP Precipitates, obtained from SLWUF Buffers

Experimental. KBr disks (prepared from oven-dried BDH grade KBr) of the precipitated and freeze-dried CaP solids generated from pH-stat experiments (at different pH 6.0, 6.8 and 7.2) were prepared (loading of calcium phosphate in the KBr disk was 0.27 wt.% where wt.% = (w(sample)/w(KBr)x100%) to study the effect of pH, different citrate, magnesium and phosphate concentrations on CaP phase formation in the SLWUF buffers. FTIR spectra were recorded on a Digilab FTS-40 FTIR Spectrometer. 16 scans were acquired between 4000-400 cm^{-1} at 4 cm^{-1} resolution.

Results: Effect of pH at which the pH-stat controlled precipitation of CaP from the SLWUF buffer takes place

Figures 4-23 and 4-24 show FTIR spectra of CaP solids, collected at pH=6.0 and pH=6.8 after the precipitation was completed (the pH-stat controlled precipitation took 40 minutes). pH-stat runs carried out at pH less than the "industrial pH" value of 6.8 (i.e. pH=6.0) produced a final CaP solid which was composed predominantly of brushite crystals (Figure 4-23) with some contamination by an amorphous-like CaP phase. This was evident from comparison with the FTIR of the CaP phase with that of pure brushite which shows some differences. At one stage of the research involving pH-stat studies of SLWUF buffers, it was serendipitously observed (Rogers et al., 1998) that some white solid had deposited in a freshly prepared "standard" SLWUF buffer solution at a measured pH equal to 4.3 (presumably via premature nucleation). FTIR spectra of this isolated solid showed the unmistakable IR signature of a reasonably pure brushite phase (see Figure 4-25). SEM micrographs taken of this substance showed the plate like morphology which suggests of brushite crystals. This is in agreement with the computer speciation calculations (see section 4.2: "The Use of SPE to Model Precipitation from SLWUF Buffers"), that predict the formation of the brushite phase in the pH range 4.3-6.5 (see Figures 4-3 and 4-5). It also agrees with work previously reported by other researchers in the field of calcium phosphate precipitation from aqueous media (van Kemenade et al., 1987, Abbona et al., 1990). In contrast the pH-stat runs carried out at the "industrial pH" value of 6.8 produced a CaP solid (see Figure 4-24) which gave IR spectroscopic features more akin to HAP.

When pH-stat controlled experiments of CaP precipitation from the SLWUF buffer at pH 6.8 as a function of time after initiation of precipitation (after pH jumping) was carried out, samples of CaP solid were collected at various stages of the precipitation as defined on the typical pH-stat profile for CaP precipitation (see Figure 4-14). This involved rapid arrest of the CaP precipitation reaction by addition of liquid nitrogen followed by rapid filtration and freeze drying (no washing was carried out) for 48 hours. This ensured little opportunity for any amorphous intermediates to phase transform *during* the isolation process so avoiding the obtaining of a false result. IR spectra were obtained in the usual manner using prepared KBr disks.

Figure 4-26 shows a stacked plot of some selected FTIR spectra obtained at various stages of the precipitation reaction performed at pH 6.8. They show the phase changes

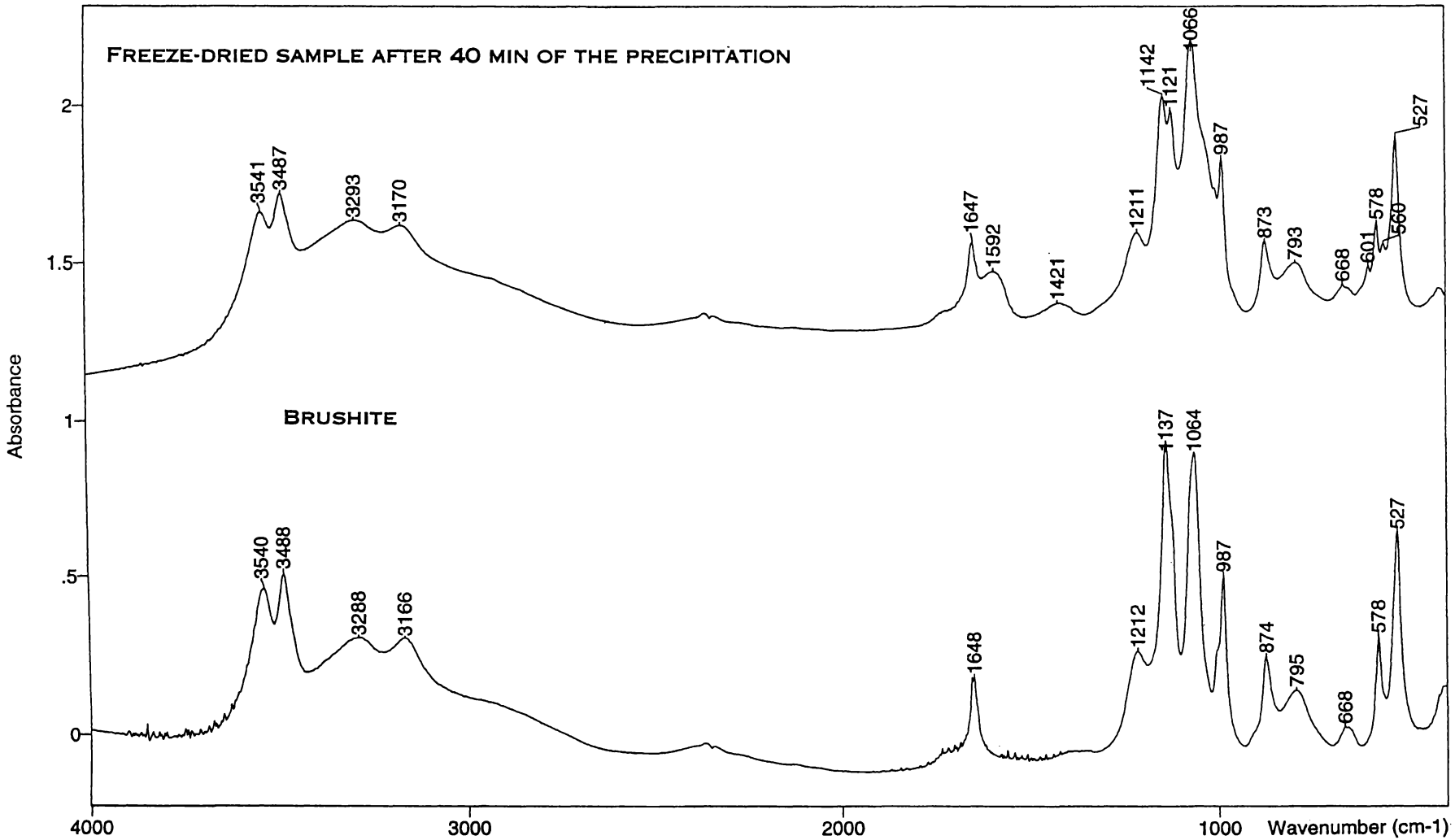

Figure 4-23: Comparison of the FTIR spectrum of CaP precipitate, collected from the pH-stat precipitation process from the "standard" SLWUF buffer at T=25°C and pH=6.0, with FTIR spectrum of Brushite.

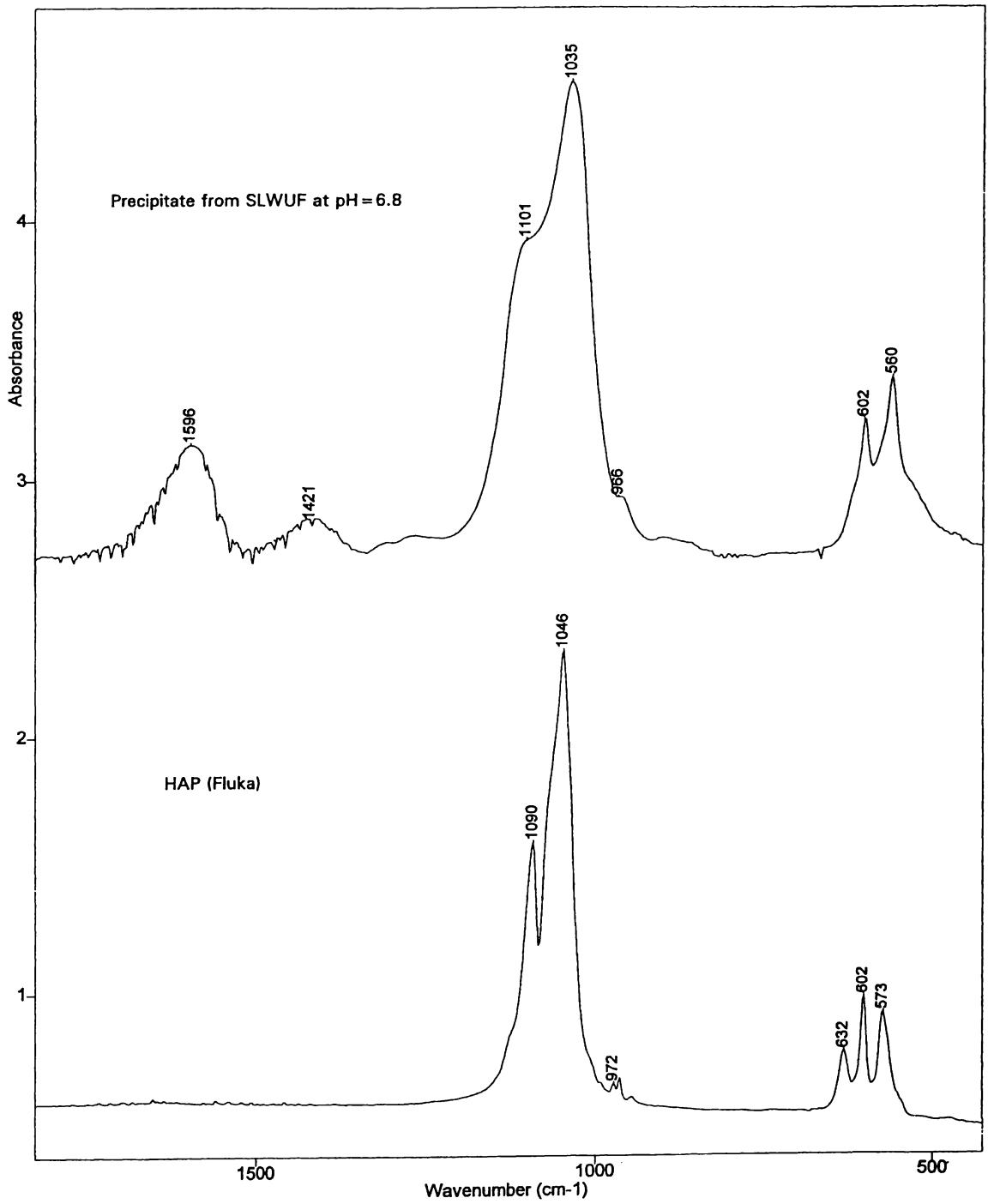

Figure 4-24: Comparison of the FTIR spectrum of CaP precipitate, collected from the pH-stat precipitation process from the "standard" SLWUF buffer at T=25°C and pH=6.8 with FTIR spectrum of commercial (*Fluka*) Hydroxyapatite.

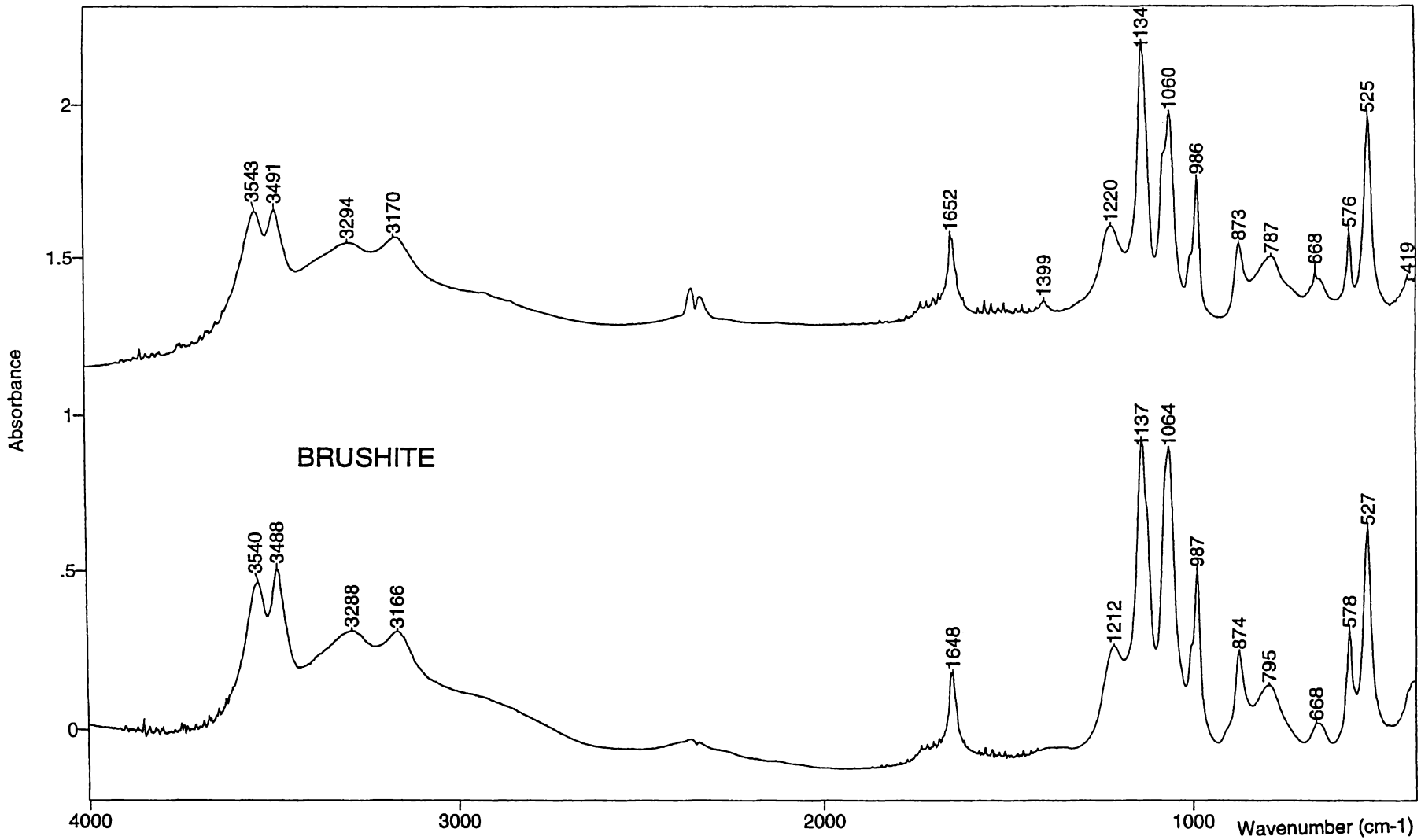

Figure 4-25: Comparison of the FTIR spectrum of CaP precipitate, collected from the pH-stat precipitation process from the "standard" SLWUF buffer at T=25°C and pH=4.3, with FTIR spectrum of Brushite.

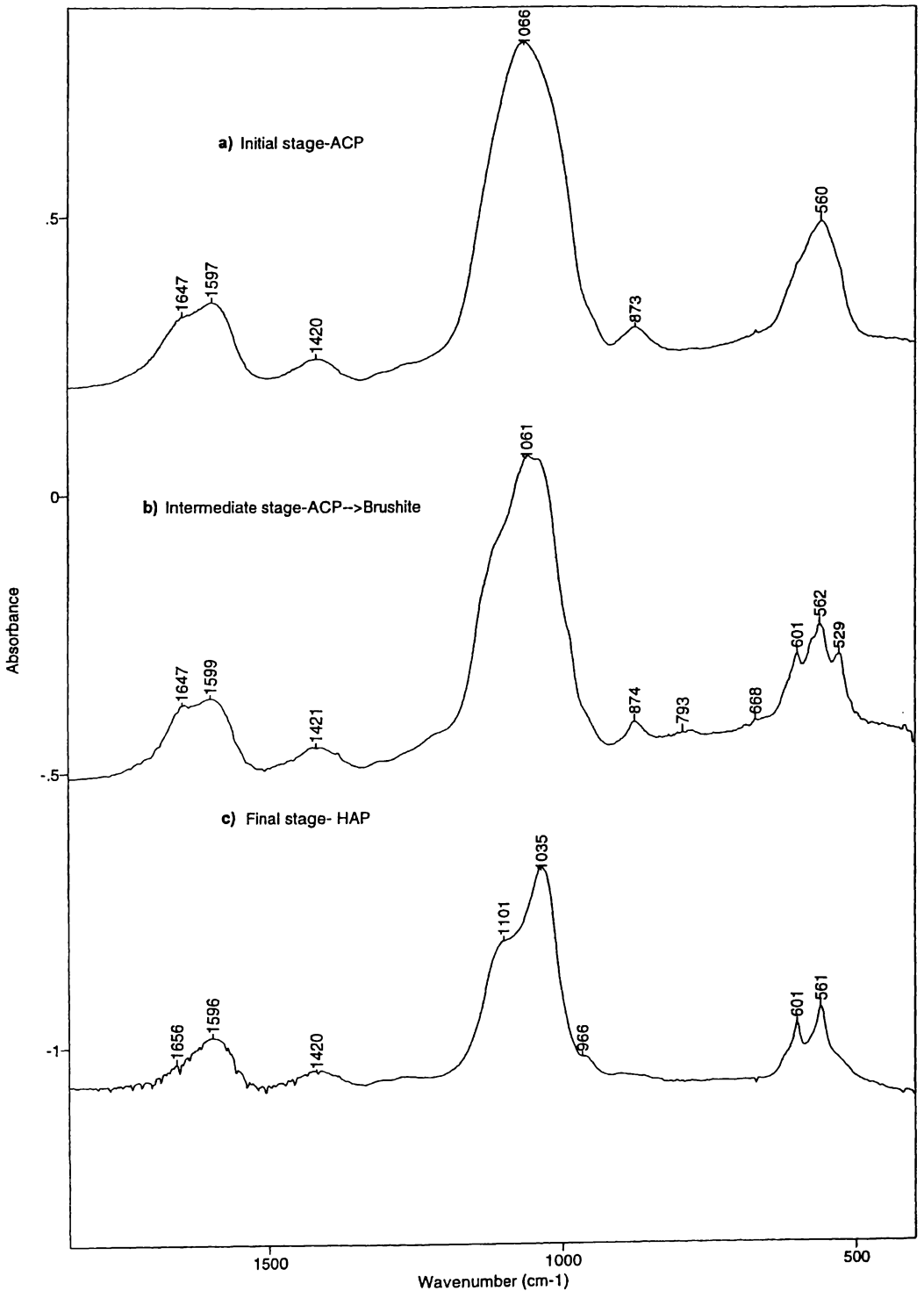

Figure 4-26: FTIR spectra of the CaP precipitates, collected from pH-stat precipitation process from the "standard" SLWUF buffer at T=25°C and pH=6.8 at different stages of the precipitation process.

the precipitate undergoes during the various stages of the precipitation reaction. The general results as gleaned from the FTIR analysis of the precipitates are as follows:

a) IR spectra, obtained for the precipitate at the *initial stage* of the precipitation reaction (CaP samples isolated 1, 5, 10, 15 and 20-22 min after precipitation was initiated) show characteristic broad spectral features at 560 ± 2 and 1066 ± 4 cm^{-1} which have been assigned (Nakamoto, 1986) to the stretching and bending fundamentals of the $-PO_4$ unit (see Figure 4-26(a) which is an FRIR spectrum of the precipitate isolated after 10 minutes of reaction time). The broad and structureless (unsplit) nature of the 560 and 1066 cm^{-1} peaks is typical of an amorphous calcium phosphate phase (ACP) for which the PO_4^{3-} unit behaves spectroscopically like an isolated structural unit in the solid (unlike HAP which exhibits splitting in its 560 cm^{-1} peak due the chemically asymmetric environment of the PO_4^{3-} unit in the HAP lattice). Additional features at 1647, 1597 and 1420 cm^{-1} are due to traces of *moisture* and citrate present in the solid.

b) IR spectra of the CaP solids in the *intermediate* (viz., autocatalytic) stage of the precipitation reaction (25-40 minutes) appear to exhibit in the IR features which are characteristic of the following CaP phases: ACP (dominant contributor), brushite (minor contributor especially as gauged by peaks at 874, 793 and 529 cm^{-1}) and HAP (minor contributor as gauged by the peaks at 601 and 562 cm^{-1} (see Figure 4-26(b)). This clearly shows the precipitate to be in a state of flux between phase transformations given the various phases co-existing in this sample.

c) Lastly, IR spectra of CaP solid isolated at the so-called *final* stage of the precipitation process (precipitation time > 40 min., where the pH-stat curve (Figure 4-14) flattens out) clearly resemble that of an apatite-like phase, viz., HAP (see Figure 4-26(c)). In general, this appears to be different from the FTIR spectra of commercial (Fluka) HAP (see Figure 4-24) which is more crystalline and contains spectral features at 3527 cm^{-1} (not shown in Figure 4-24) and 632 cm^{-1} due to lattice OH-associated vibrations. The HAP produced in the precipitation from SLWUF at pH 6.8 does not contain these features and gives overall broader IR peaks because it is a poorly crystallised hydroxyapatite which probably has a Ca:P molar ratio lower than that dictated by stoichiometry (i.e. 1.67).

As was mentioned above, peaks at 1420 and 1596 cm^{-1} observed in IR spectra of CaP precipitates, are due to vibrations associated with the citrate molecule (see Figure 4-27).

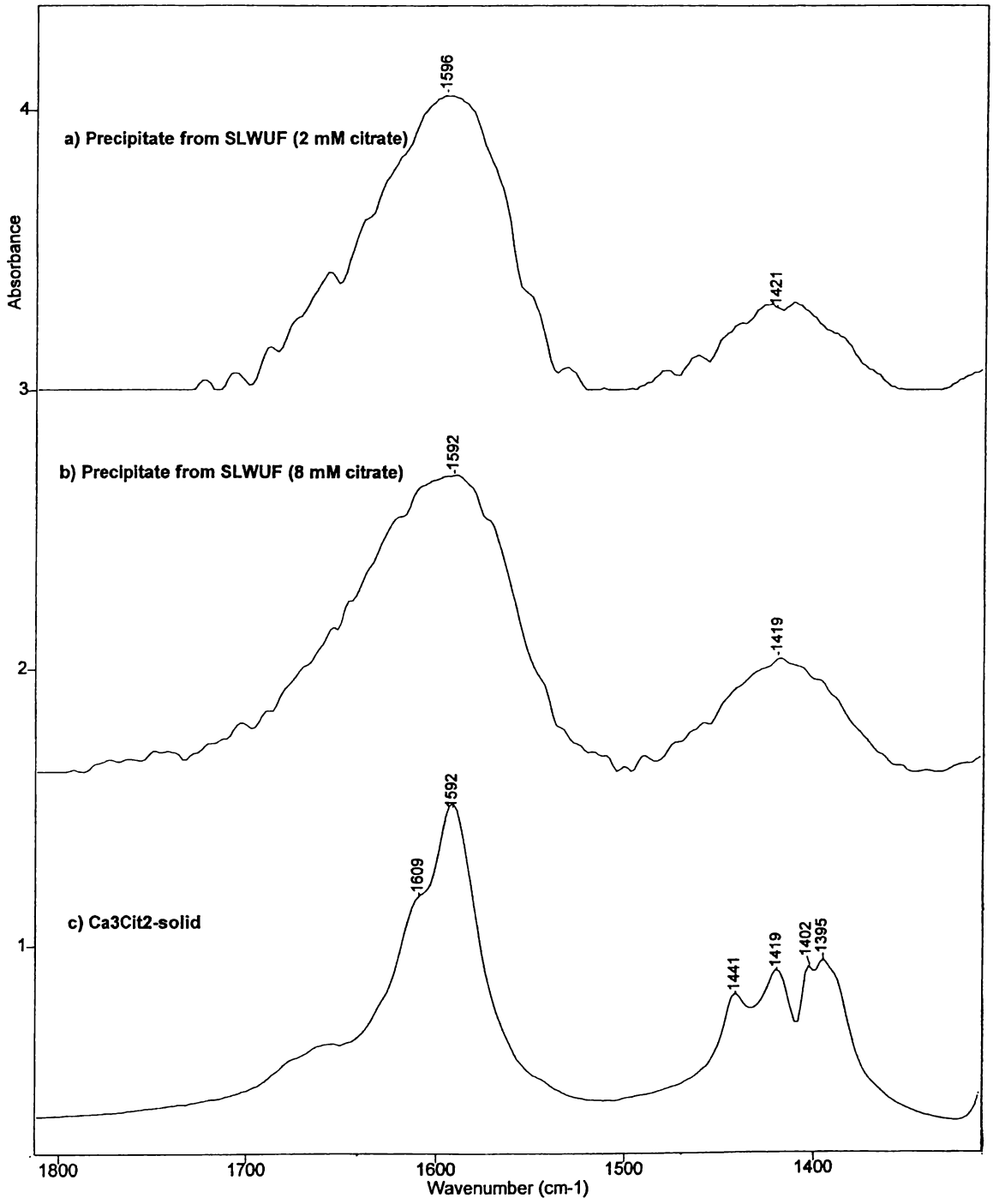

Figure 4-27: Comparison of the FTIR spectra of CaP precipitates, collected from pH-stat precipitation process from the SLWUF buffer (with 2 and 8 mM citrate) at T=25°C and pH=6.0 with FTIR spectrum of Ca_3Cit_2.

This implies that citrate from the SLWUF buffer has a tendency to co-deposit with the precipitated CaP solid due possibly to some affinity of citrate for the HAP surface. In fact, previous researchers (López-Macipe et al., 1998; Rhee et al., 2000) have conducted studies to show that citrate does have an affinity for HAP due to its ability to adsorb on the HAP surface. López-Macipe produced a schematic diagram illustrating the way in which the citrate anion (Cit^{3-}) can adsorb to the (100) face of a HAP crystal. This is shown in Figure 4-28.

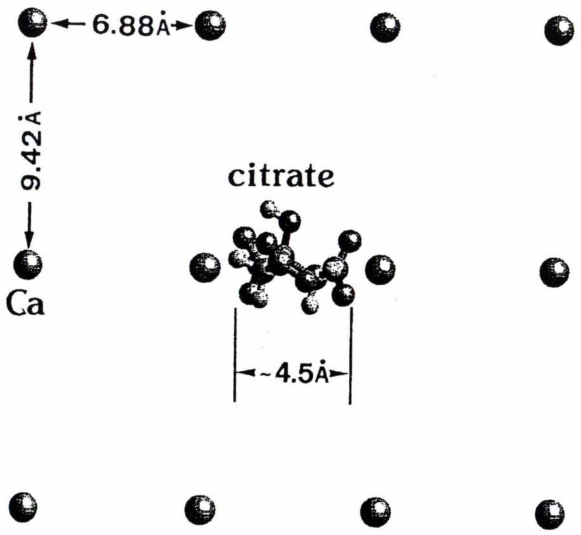

Figure 4-28: The outline of the adsorption of the COO^- groups of Cit^{3-} ion on the (100) face of the hydroxyapatite (from López-Macipe et al., 1998).

In contrast Rhee et al. (Rhee et al., 2000) in their studies on HAP formation on cellulose cloth have given a schematic on how citric acid can stimulate nucleation. The pK_a3 of citric acid is 6.4 and hence at pH 6.8, an appreciable amount of tricitrate ion will exist in solution. Citric acid ($C_6H_8O_7$) binds via its negatively charged carboxyl head groups to calcium ions in the solution and form a "HAP embryo", as shown below:

at pH 6.8

(i)

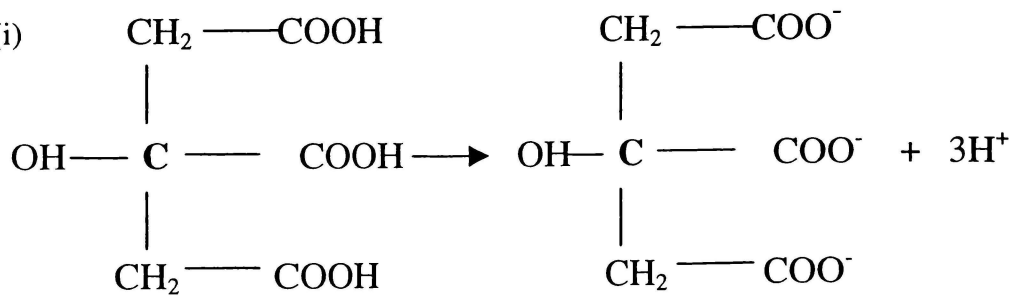

(ii)

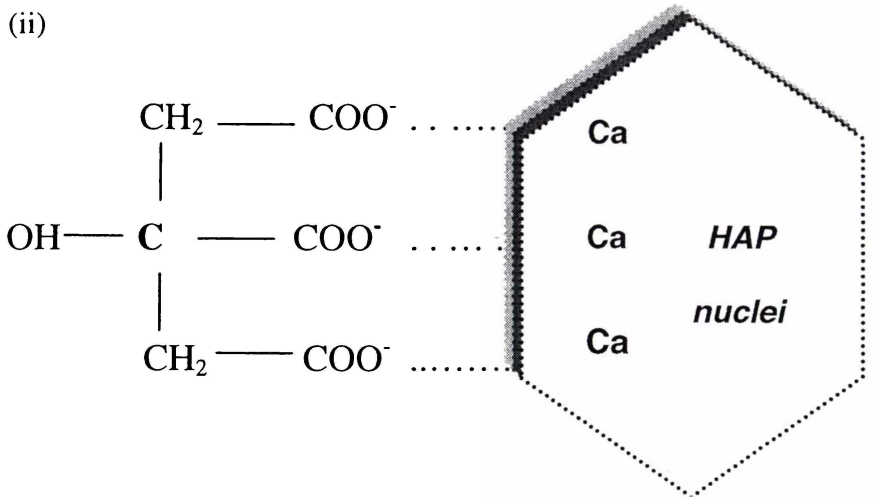

It was of interest to compare FTIR spectra of the CaP solids, precipitated from SLWUF buffers with different citrate concentrations in order to check whether citrate was surface adsorbing on the CaP solids. For this purpose, KBr discs of the CaP precipitated from SLWUF buffers under pH-stat controlled conditions (pH=6.8) with varying citrate level (0-8 mM), were prepared with identical weight percentage values (0.26-0.27 wt. %). FTIR spectra were acquired and after 2-point baseline corrections, the intensity of two IR peaks in the resultant spectra were ratioed, viz., I (1402 cm^{-1}) : I (1035 cm^{-1}), i.e., the ratio of the 1402 cm^{-1} citrate associated peak to the 1035 cm^{-1} P-O associated peak. The reason for this ratioing was to *normalise* the intensity of the citrate-associated peak to that of the phosphate peak in the same spectrum. In this way, any possible intensity differences in the citrate peak (caused for instance by non-uniform distribution of the CaP compound in the pellet) could be minimised. This ratio for the CaP was found to be 0.0562 (precipitated from SLWUF with 0 mM citrate), 0.164 (SLWUF with 2 mM citrate) 0.150 (SLWUF with 4 mM citrate), 0.179 (SLWUF with 6 mM citrate) and reaching the maximum value 0.199 (SLWUF with 8 mM citrate). This trend seems to indicate that an increase in citrate uptake is occurring on the CaP solid as the citrate "background" concentration in the whey permeate increases. Some of the data exhibited a little scatter (e.g. the result for 2 mM citrate sample, which was higher than the value for 4 mM citrate sample) but in general, increased citrate adsorption is probably occurring. This is supported by studies by López-Macipe et al. who have published Langmuir adsorption isotherms for citrate adsorbed onto hydroxyapatite (López-Macipe et al., 1998).

IR spectra were also acquired of other SLWUF-derived CaP precipitates in which phosphate and magnesium level was varied in order to see if there would be any changes to the calcium phosphate phase produced from such media. However, all CaP precipitates isolated (in the final stage when the apatitic phase had been produced) were identical to each other as gauged from their FTIR spectra which showed the typical features of an apatite-like phase.

4.6 Scanning Electron Microscopy (SEM)

Experimental. SEM microscopy was employed in conjunction with the pH-stat experimental work and calcium ISE measurements to investigate the morphology of the CaP precipitates isolated from the SLWUF buffer. CaP precipitates, collected from the different stages of the precipitation from SLWUF buffers under pH-stat controlled conditions were frozen with liquid nitrogen and then freeze-dried. Scanning electron micrographs were acquired using a *Hitachi S4000 Scanning Eelectron Microscope.* SEM micrographs were obtained with an accelerating voltage of 5 kV at varying magnifications. Calcium phosphate is an insulator and thus has to be coated with a conductive layer to carry away the negative electrical charge that builds up on the sample by adsorption of electrons from the primary electron beam. To avoid charging, a small amount of the precipitated CaP powder was placed on double-sided sticky conductive carbon tape which was affixed to the top of the sample stubs. The samples were then placed into a *Hitachi E1030 Ion Sputter Coater.* When the vacuum reached 20 Pa, the chamber was purged with Argon gas and a coating of Pt-Pd (20 nanometres) was sputtered onto the sample. The specimen stub with coated particles of the CaP precipitated powder was subsequently mounted onto a sample holder and placed atop the stage of the specimen chamber of the SEM instrument, which was under a vacuum of $2x10^{-7}$ Pa.

Results. Figure 4-29(a) illustrates an SEM micrograph of CaP precipitates formed in the *initial* stage of the precipitation process from "standard" SLWUF buffers under pH-stat controlled conditions at T=25°C and pH=6.8. In general, the morphology is typical of the "caviar-like" morphology of amorphous CaP material.

Figures 4-29(b) and 4-30 (a) illustrate the material obtained in the *intermediate* stage of the precipitation process in which there appears to be a coexistence of amorphous CaP, plate-like brushite crystals and hydroxyapatite.

a)

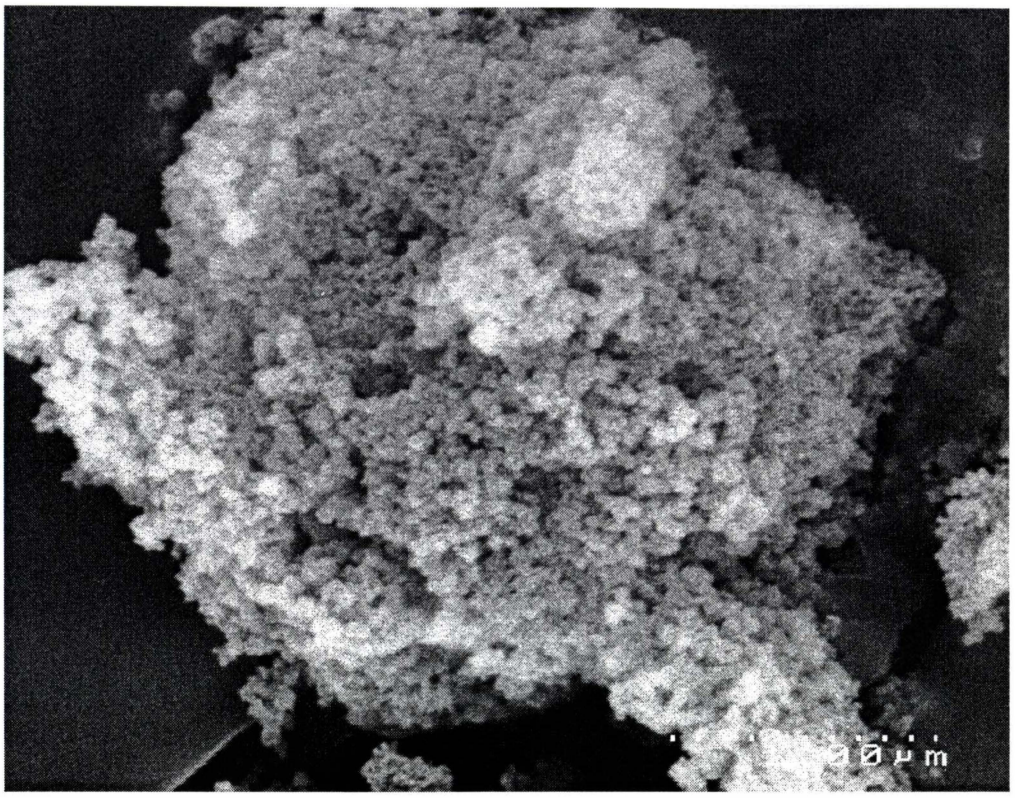

b)

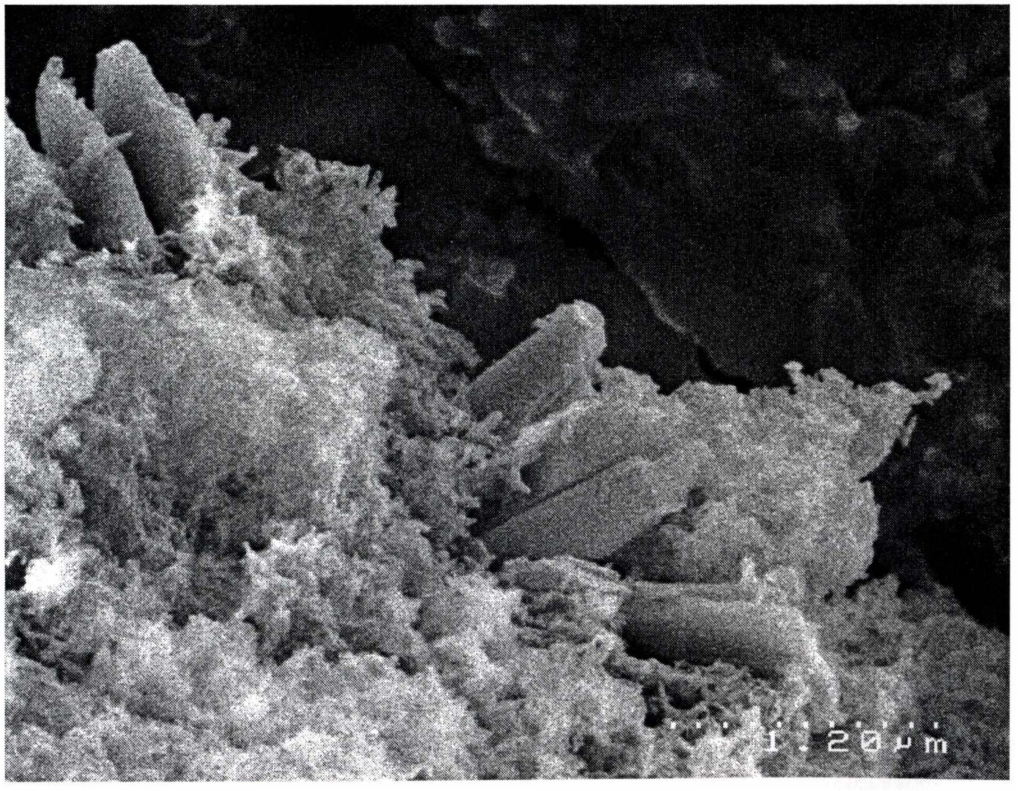

Figure 4-29: SEM micrographs of the freeze-dried CaP precipitates formed from the "standard" SLWUF buffer solution at T=25°C and pH=6.8: a) amorphous phase (precipitation time 10 min); b) brushite crystals in the amorphous phase (precipitation time 25 min).

a)

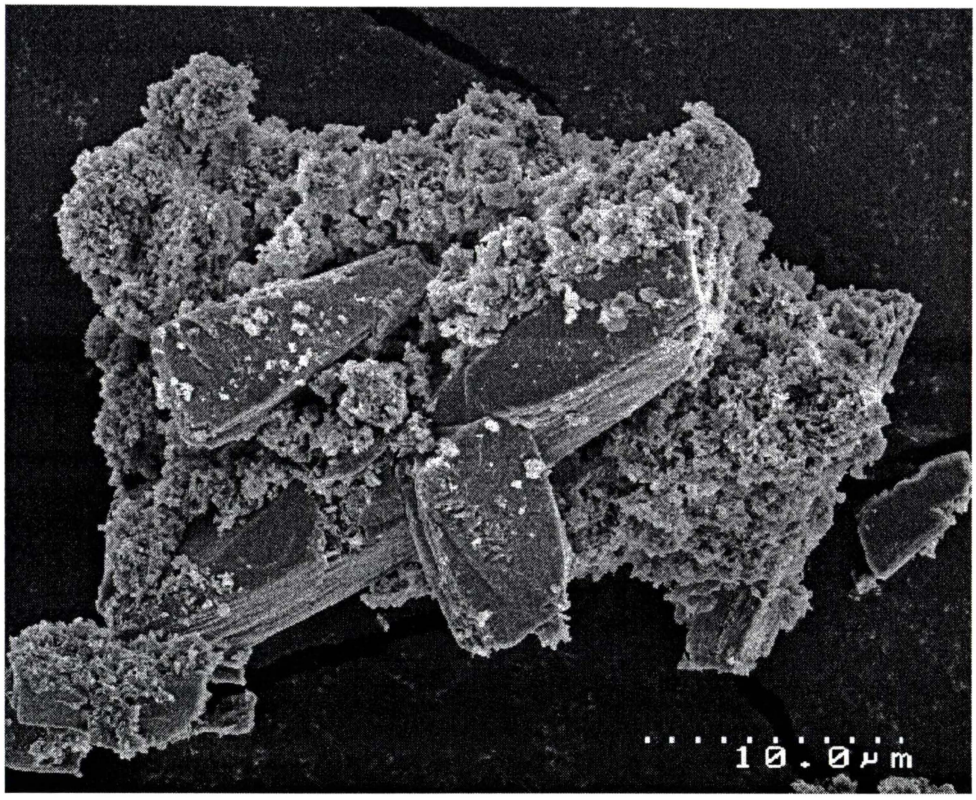

b)

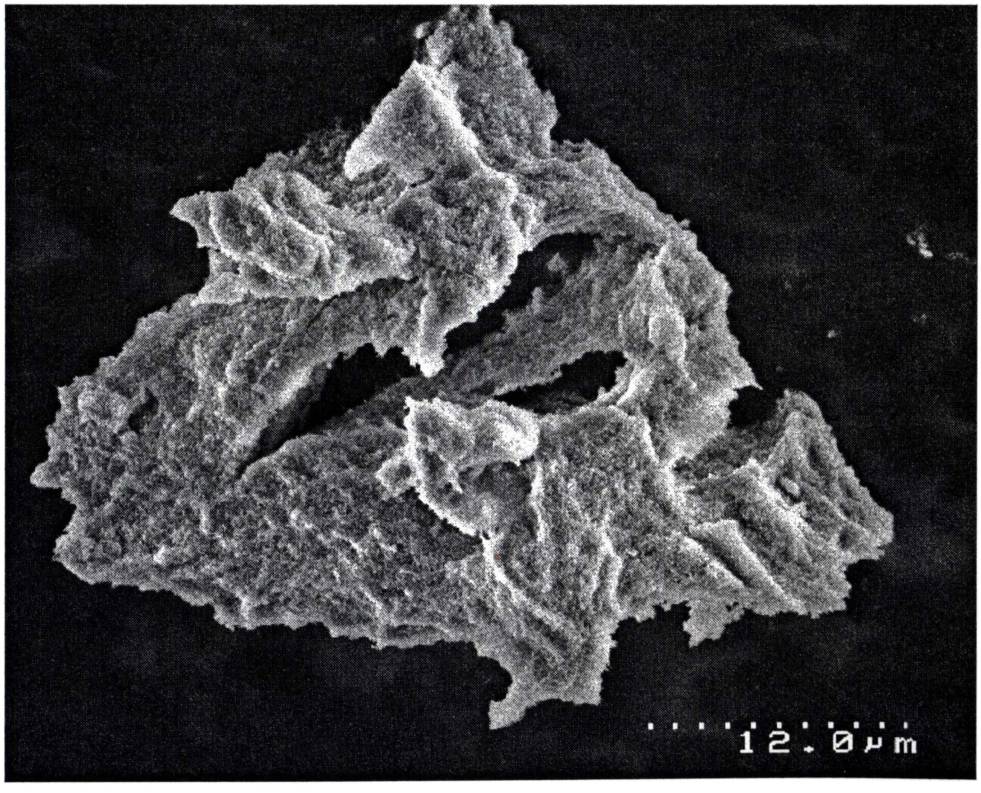

Figure 4-30: SEM micrographs of the freeze-dried CaP precipitates formed from the "standard" SLWUF buffer solution at T=25°C and pH=6.8: a) *intermediate stage* (precipitation time 35 min); b) *final stage* (precipitation time 60 min).

The scanning electron micrographs suggest that the brushite-like crystals are dissolving and being replaced by the fine HAP crystals.

Scanning electron micrographs of CaP material obtained in the *final* stage of the precipitation process from "standard" SLWUF buffers (pH-stat controlled conditions at T=25°C and pH=6.8) show predominantly the small crystals characteristic of apatite as confirmed by XRD analysis of the precipitates (see Figure 4-30(b)).

Scanning electron micrographs were also carried out on *final* products obtained after pH-stat runs carried out at the lower pH of 6.0 during 40 minutes. These were composed predominantly of dendritic brushite crystals (see Figure 4-31), surrounded by what looked like amorphous CaP material.

The brushite crystals seemed to form at the corners of amorphous particles beginning to phase transform to brushite, as shown by scanning electron micrographs (see Figure 4-32), demonstrating the initial phase of brushite crystals formation at lower pH of 6.0 (precipitation time 10 min). Mullin (Mullin, 1993) has reported that the development of crystal dendrites preferentially occurs at the particle corners which are not blocked by impurities.

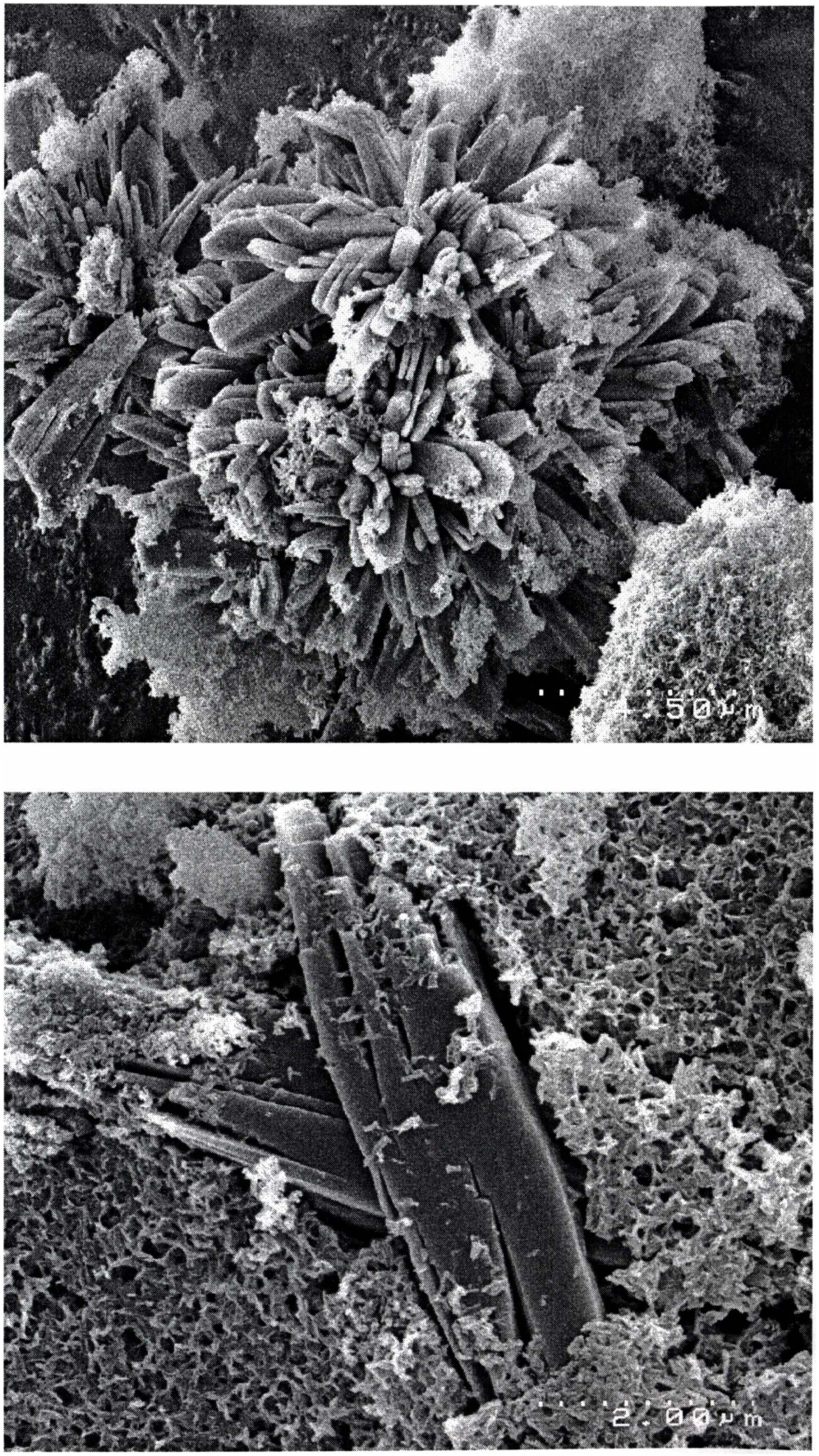

Figure 4-31: SEM micrographs of the freeze-dried CaP precipitates formed from the "standard" SLWUF buffer solution at T=25°C and pH=6.0 (precipitation time 40 min).

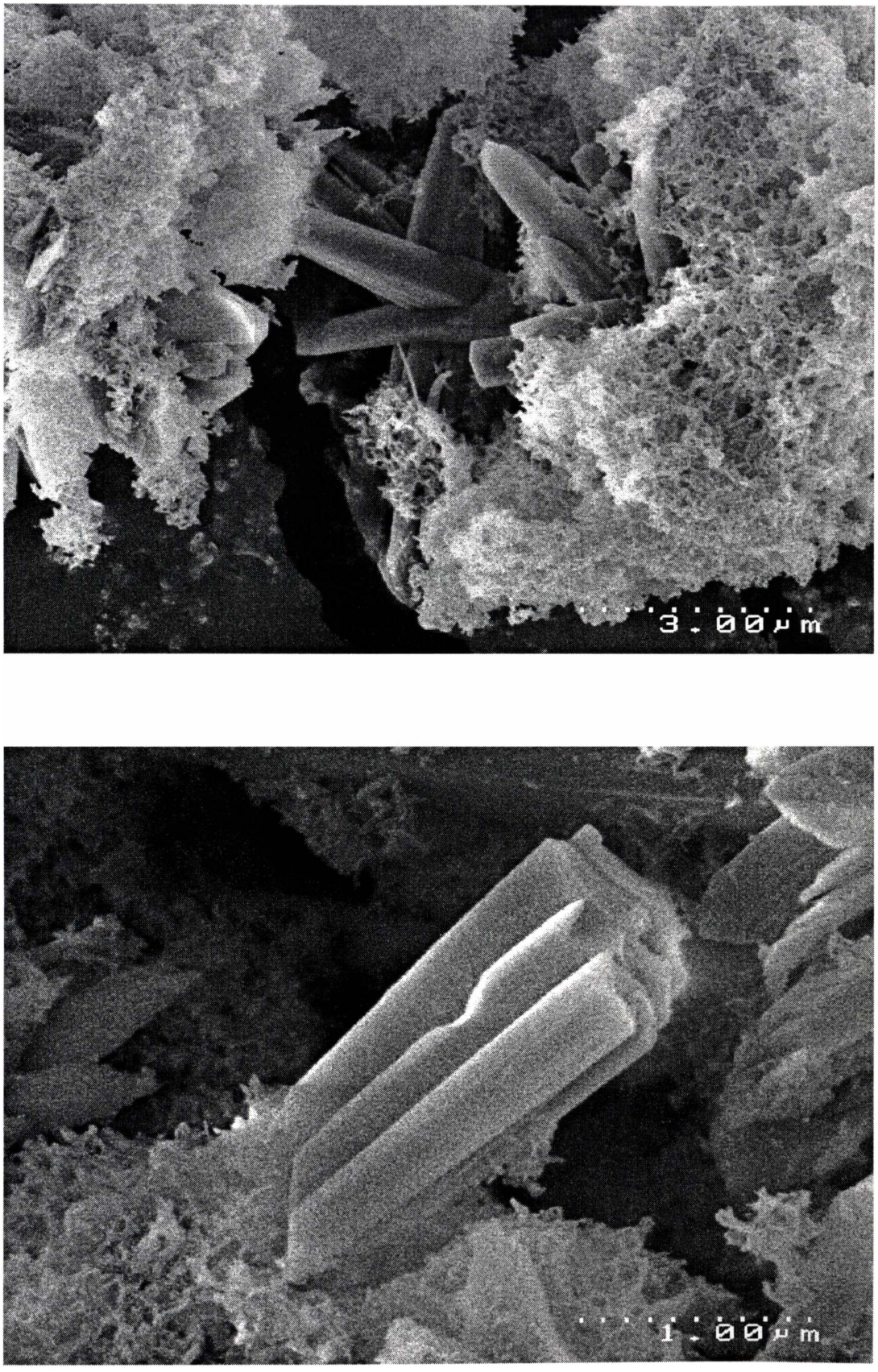

Figure 4-32: SEM micrographs of the freeze-dried CaP precipitates formed from the "standard" SLWUF buffer solution at T=25°C and pH=6.0 (precipitation time 10 min).

CHAPTER FIVE

CHEMICAL SPECIATION CALCULATIONS OF THE PRECIPITATION OF CALCIUM PHOSPHATE USING CONCENTRATION DATA FROM THE COMMERCIAL PROCESS

In Chapter 4, the results of various computer speciation calculations of the multicomponent equilibria in lactic simulated whey permeate ultrafiltrate buffer solutions (SLWUF) were discussed with respect to their effect on the precipitation of calcium phosphate (CaP). In this chapter, the computer speciation calculations have been extended using the concentration data of whey permeates used in the precipitation of calcium phosphate from lactic and sulfuric acid whey permeates. The first half of Chapter 5, on the other hand, is a separate speciation calculation using actual data specific to a commercial lactic whey permeate. Although the trends are practically identical in some respects to the trends discussed in Chapter 4, some aspects of the results of the calculations have been dealt with in greater depth than in Chapter 4 such as the influences of citrate and lactate.

5.1 Computer Speciation Calculations of the Precipitation of Calcium Phosphate using Concentration Data for a Commercial Lactic Whey Permeate

5.1.1 Construction of the Input File

As in Chapter 4, an input file (see Algorithm in Figure 4-1) into which concentrations expressed as mmol in 50 mL were entered for various anionic and cationic species, was constructed. These represent the fundamental ionic components of the system.

In general, the same list of fundamental ionic components as used in SLWUF calculation were used in these calculations, except that the concentrations were specific to the lactic whey permeate. The values used in the input file are given in Table 5-1, which represents the composition of the typical lactic whey permeate in mid-season (data on which these values are based are given in Table 5-2).

Table 5-1: Basic chemical components defining the medium and their concentrations in a lactic whey permeate, as contained in the input file of SPE program.

Component	PO_4^{3-}	$Citrate^{3-}$	$Lactate^{-}$	Mg^{2+}	Ca^{2+}
Concentration, (mmol/50 mL)	1.20	0.10	2.865	0.185	1.50

Table 5-2: Typical compositional data for a lactic whey permeate (proprietary information).

Component	Concentration, mM	Concentration, ppm	Mr, g mol^{-1}
Ca^{2+}	30	1202.4	40.08
P (in PO_4^{3-})	24	743.3	30.97
Lactate	57.3	5101.4	89.03
Mg^{2+}	3.7	89.9	24.31
Cl^{-}	26.8	950.1	35.45
Na^{+}	16.0	367.8	22.99
K^{+}	37.9	1481.9	39.10
Citrate	2.0	378.2	189.10

The major differences between the data given in Table 5-1 and that given in Table 4-1 is that in Table 5-1, the lactate level is lower, the magnesium level is higher, and the calcium level is lower than in the SPE calculation carried out for the SLWUF buffer. The Ca:P molar ratio for the basic set of components defined in Table 5-1 is 1.25:1 in contrast to 1.28:1 for the SLWUF buffer. For the speciation calculation, involving lactic whey permeate, *Log (β)* values and stoichiometric coefficients for the basic chemical components and dissolved complex ion species as well as *Log* K_{sp} values for any solid phases at T=25°C and ionic strength *I=0.1*, as summarised in the Table 4-2 (see section 4.2.1: "Construction of the Input File"), were used in the Fortran-formatted input file of SPE program.

5.1.2 Results and Discussion

5.1.2(a) Speciation Plots of dissolved Molecular and Ionic Species

Figure 5-1 depicts the SPE calculated general distribution of fundamental components, dominant free ions, complex ions, dissolved molecular species and insoluble species over the pH range 2-8 for an ionic composition corresponding to the lactic whey permeate. It is obvious that this distribution is very similar to that described in Chapter 4.

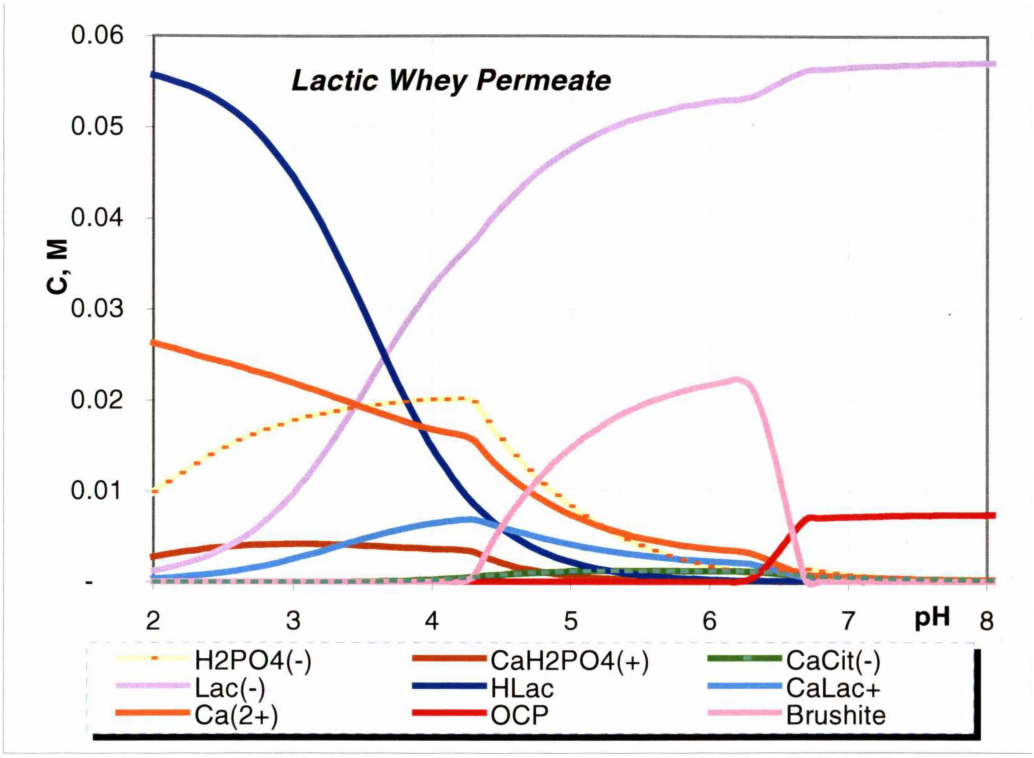

Figure 5-1: SPE calculated concentration-pH plot showing the general distribution of the dominant free ions, complex ions and solid species over the pH range 2-8 in lactic whey permeate at T=25°C.

As pH increases, free calcium ion (Ca^{2+}) decreases from a maximum of *ca.* 26 mM at pH 2 to zero by the time pH 8 is reached. At pH 4.3 free calcium ion (Ca^{2+}) exhibit a "kink". This is due to the increasing incorporation of Ca^{2+} in solid calcium phosphate phases such a brushite ($CaHPO_4.2H_2O$), which starts to form from pH 4.4 and transforms to OCP ($Ca_8H_2(PO_4)_6.5H_2O$) phase from pH 6.3.

The origin of the lactic acid in the whey permeate is as a result of the conversion of the lactose to the lactic acid by the action of the starter. This conversion occurs quantitatively as one mole of lactose yields four moles of lactic acid:

$$C_{12}H_{22}O_{11} + H_2O \rightleftharpoons 4\,C_3H_6O_3$$

Figure 5-1 also includes in the same diagram, the influence of lactate and shows the variation in the speciation of lactate from being mostly in the form of lactic acid below pH 3 to being in the form of the lactate ion above pH 4. The plots in general show the general low importance of lactate in any chemical equilibria in the permeate apart from $Ca(Lac)^+$ species or $Ca(Lac)_2$ species (see Figure 5-2 below). In Chapter 4, no experimental evidence was ever obtained for the existence of solid species such as $Ca(Lac)_2$ for instance due to its high solubility in the medium relative to calcium phosphate phases. Despite this, it was of interest to see how lactate could influence chemical equilibria in the lactic whey permeate given its prominent levels (see data in Table 5-2).

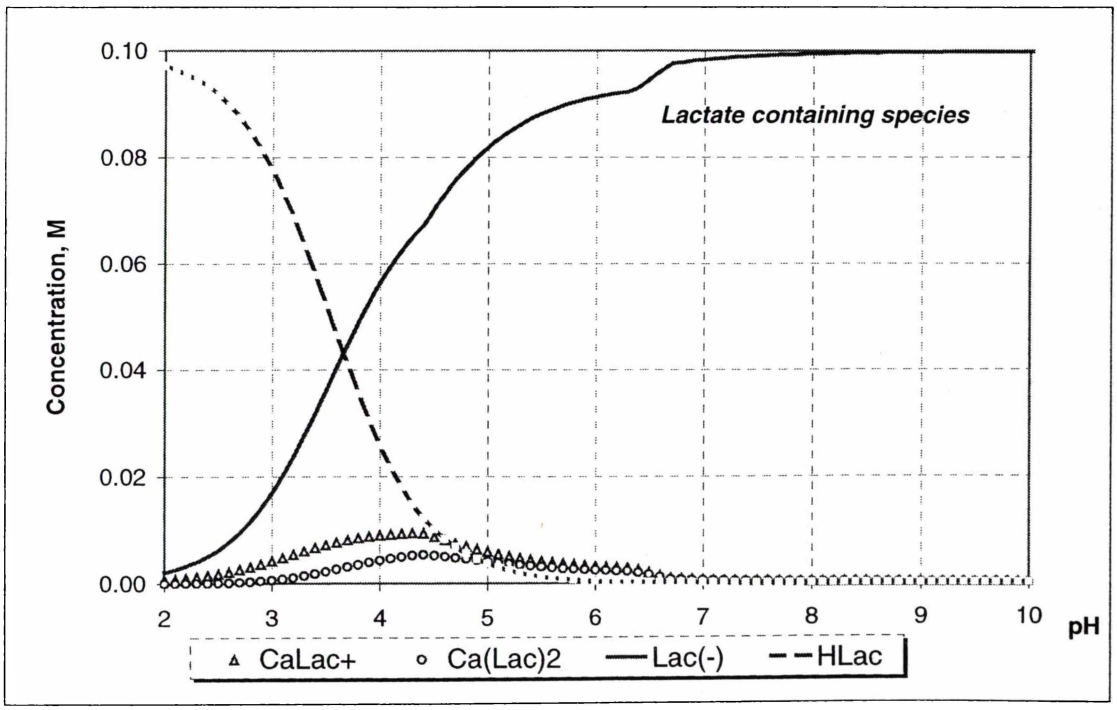

Figure 5-2: SPE calculated concentration-pH plot showing the concentration of lactate-containing species over the pH range 2-10 in lactic whey permeate at T=25°C.

For this purpose, the concentration of the lactate in the permeate was made to vary in the SPE program input file from 25 to 100 mM while keeping other concentrations the

same (in the SLWUF this was not entirely possible due to the interdependence of lactate and citrate in the composition.

What was found in these investigations that the dominant calcium-lactate containing species is ions $Ca(Lac)^+$ (Figure 5-3), which has some influence on the profile of the free Ca^{2+} distribution curve over the pH range from 2-6.5. The amount of the $Ca(Lac)^+$ complex increases proportionally with the lactate concentration in the medium (see Figure 5-4).

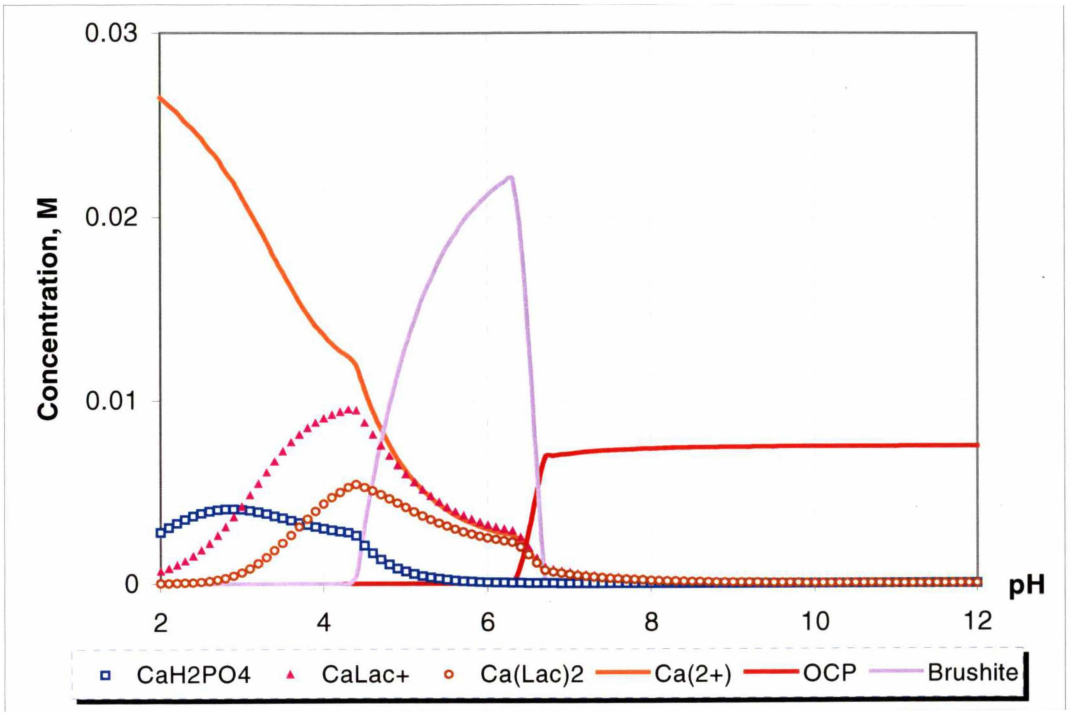

Figure 5-3: SPE calculated concentration-pH plot showing the distribution of calcium-containing species and CaP solids over the pH 2-12 in lactic whey permeate at T=25°C.

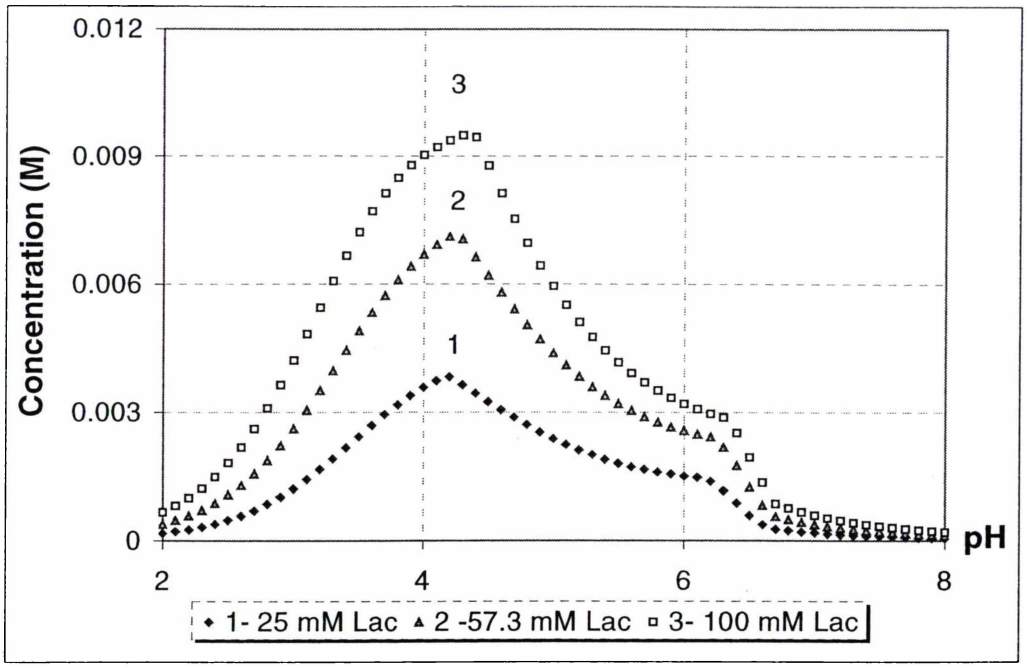

Figure 5-4: SPE calculated concentration-pH plot showing the distribution of $CaLac^+$ species over pH 2-8 at T=25°C at the different lactate level in lactic whey permeate.

5.1.2(b) Solid Phases predicted to form in a Lactic Whey Permeate, as calculated by SPE

Calcium Lactate ($CaLac_2$) and Calcium Citrate ($Ca_3Cit_2.6H_2O$) Formation. As shown in Chapter 4 and in the previous discussion, computer speciation calculations show that little to no solid calcium lactate forms at all, even at when high concentrations of the lactate (100 mM) are made to exist in the lactic whey permeate. Calcium citrate ($Ca_3Cit_2.6H_2O$) which is predicted to form over the pH range 4.5-6.5 will only appear in significant amounts if the concentration of citrate in the medium exceeds 8 mM.

Brushite Formation. Brushite ($CaHPO_4.2H_2O$), as previously shown in Chapter 4, is the dominant solid phase forming in the SLWUF buffer over the pH range 4.3-6.7 as was depicted in Figure 5-3 (see *4.2.2(a): "Ion/Molecular Speciation and Solid Formation"*).

Octacalcium Phosphate or Hydroxyapatite Formation. As demonstrated in Chapter 4, the calculations for this composition also show that octacalcium phosphate ($Ca_8H_2(PO_4)_6.5H_2O$) is the major precipitating phase occurring after pH 6.2 and it continues to form over the rest of the pH region up to pH 12 (see Figure 5-3). In reality,

it is known in real calcium phosphate precipitating systems that this is not true and that HAP is the dominant phase at more basic pH. However, given the constraints of the program, we can only use the OCP result as an indirect indicator of this dominance at higher pH. If hydroxyapatite (HAP) is actually included in the SPE calculation as an allowed solid phase, the general output from the program is such that it completely dominates after pH 5 in the calculation thus affording limited information on precursor phases to HAP (these being brushite and OCP). Since brushite and OCP are direct precursors to HAP, following the formation (and hence yields) of these solids is a justifiable approach to gaining information about the likely phase transformations occurring in the reacting system as a function of pH.

Brushite-Octacalcium Phosphate Formation. As mentioned earlier, brushite formation begins at pH 4.3 and reaches a maximum concentration of 22.3 mM at pH 6.2. After this point the concentration of brushite drops sharply and octacalcium phosphate formation (see Figure 5-3) begins with consumption of brushite and extra free calcium ions ($[Ca^{2+}_{(aq)}]$) from the medium.

$$6CaHPO_4.2H_2O_{(s)}+2Ca^{2+}_{(aq)} \rightleftharpoons Ca_8H_2(PO_4)_6.5H_2O_{(s)}+4H^{+}_{(aq)}+7H_2O$$

These phases are, as mentioned previously, the precursor phases to the final thermodynamically most stable apatitic (hydroxyapatite) solid corresponding to ALAMIN™ powder and thus the SPE calculations provide an indirect demonstration of the phase transformation of the precipitating solids.

5.1.2(c) Influence of varying Ca:P Molar Ratios on the Precipitation of Calcium Phosphate, as calculated by SPE

The Ca:P molar ratios in the lactic whey permeate system were varied from 1.25:1 to 1:1.25, with the concentration of Ca^{2+} ion kept constant at 30 mM. The concentration of PO_4^{3-} was varied from 24 to 37.5 mM. Plots of Ca^{2+} concentration versus pH (Figure 5-5) indicate that the precipitation reaction is more complete at pH 6.8 than at pH 6.4.

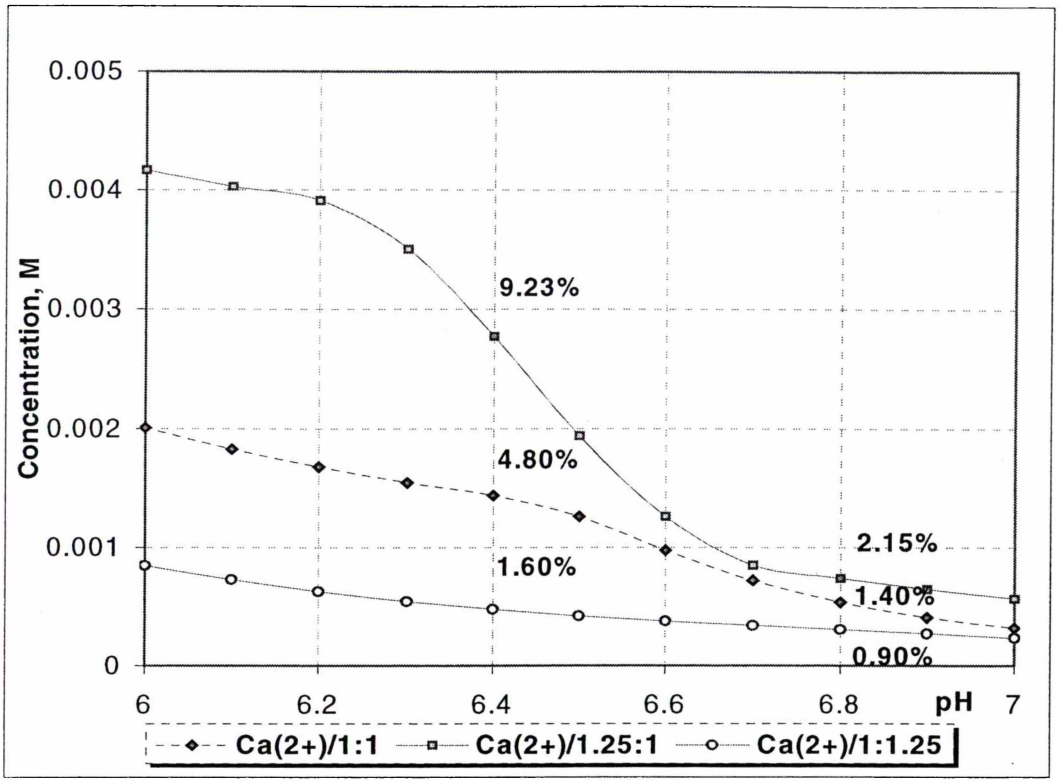

Figure 5-5: SPE calculated concentration-pH plot showing the distribution of free Ca^{2+} ions over the pH 6-7 at T=25°C and at varying Ca:P molar ratios (1:1 -30 mM Ca^{2+} and 30 mM PO_4^{3-}; 1.25:1 -30 mM Ca^{2+} and 24 mM PO_4^{3-}; 1:1.25 -30 mM Ca^{2+} and 37.5 mM PO_4^{3-}) in the lactic whey permeate.

For example, for a ratio of Ca:P=1.25:1 (actual ratio in the natural lactic whey permeate), the amount of Ca^{2+} ion remaining in solution after precipitation is only 2.15% at pH of 6.8, whereas at pH 6.4, the amount of Ca^{2+} ion remaining in solution is 9.23% of the total. Plots of Ca^{2+} ion concentration versus pH (see Figure 5-5) indicate, that adding the extra phosphate leads to increase the Ca precipitation from whey permeate solution: from 9.2% to 1.6% at pH 6.4 and from 2.15% to 0.9% at pH 6.8. This confirms that phosphate is limitary (or lacking) ion in the CaP precipitation process from natural lactic whey permeate. This is an identical trend as found for the SLWUF buffers in Chapter 4 and was proven experimentally using Ca ISE measurements.

In common with the SLWUF buffer system, the SPE calculations indicate that an increase of phosphate concentration causes an extension of the region of pH stability for brushite formation as well as an increase in its concentration (see Figure 5-6):

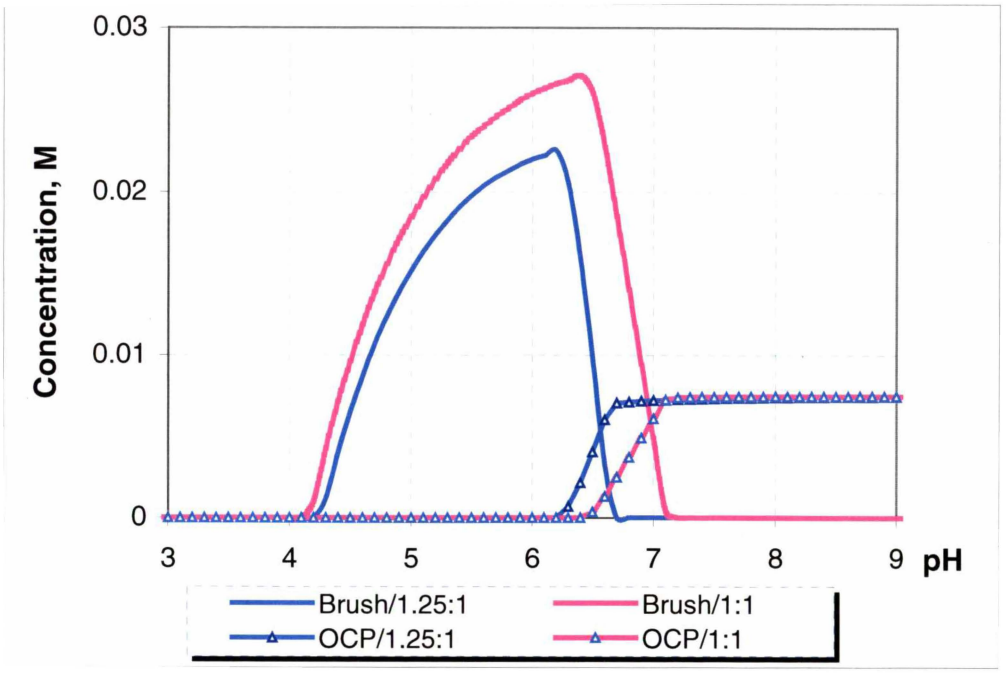

Figure 5-6: SPE calculated pH-stability regions for the formation of Brushite and OCP phases in the lactic whey permeate for varying Ca:P molar ratios (1.25:1 and 1:1).

Moreover, this causes a delay in OCP formation, starting from pH ≥ 6.5 for Ca:P molar ratio1:1, instead of pH ≥ 6.3 for the normal Ca:P molar ratio 1.25:1 (see Figure 5-6). In Chapter 4, it was shown that varying the citrate ion concentration in the SLWUF caused changes in the pH stability regions for brushite and OCP. By the same token, when Ca:P molar ratio is varied in a lactic whey permeate composition, similar changes in the pH stability region for OCP and brushite occur. The common effect in both cases is the change in free calcium ion concentration that results in the medium. Hence the changes in the pH stability regions of both brushite and OCP can be said to arise from changes to the free calcium ion concentration in the medium.

5.1.2(d) Influence of varying Citrate Concentration on the Precipitation of Calcium Phosphate, as calculated by SPE

For the investigation of the citrate influence in the lactic whey permeate the concentration of the citrate was varied from 0-8 mM, while keeping concentrations of other components in the lactic whey permeate the same. The results were predictably similar to those found in Chapter 4 for the SLWUF buffer. However for clarification of these trends, a detailed figure showing the speciation of citrate in the permeate is included here. It shows that at low pH (2-4), the CaH_2Cit^+ species is dominant while at higher pH values (4.5-7.5) the main calcium-citrate containing species is $CaCit^-$, as shown in Figure 5.7:

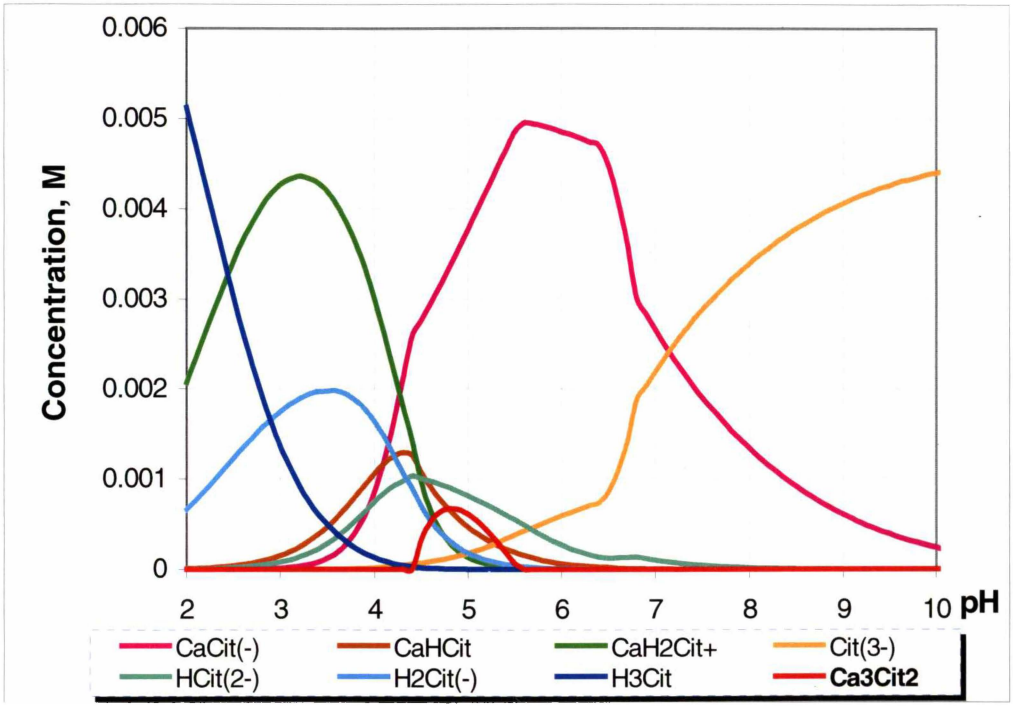

Figure 5-7: SPE calculated pH-stability regions for the citrate-containing species in the lactic whey permeate system (with 8 mM citrate).

In general, the concentration of the dominant calcium-citrate species $CaCit^-$ was proportionally increased with an increase of the citrate level in the medium. The maximum concentration (4.95 mM) of this species occurs at pH 5.6. The same tendency was observed in the calculations performed for the SLWUF buffer system (see Figure 4-6 in *4.2.2(a): "Ion/Molecular Speciation and Solid Formation"*). After pH 5.6, the level of this complex decreases precipitously as formation of the insoluble Ca-P-containing phases sets in. As a result, the dissociation of this $CaCit^-$ complex causes a sharp increase in the Cit^{3-} anion concentration over the pH range 6.4-6.8 (see Figure 5-7).

The following diagram (see Figure 5-8) illustrates the trends in CaP (OCP) formation as a function of citrate concentration in the lactic whey permeate. In general, citrate causes a decrease in the concentration of the OCP solid due to competition for Ca^{2+} by citrate (to form $CaCit^-$) in the pH range 6.2-6.8. In effect, a delay in OCP formation is caused by the higher citrate concentration. As a consequence the total CaP yield (calculated as ($Ca_{(S)}$=$Ca_{[OCP]}$ + $Ca_{[BRUSHITE]}$)) decreases (see Figure 5-9).

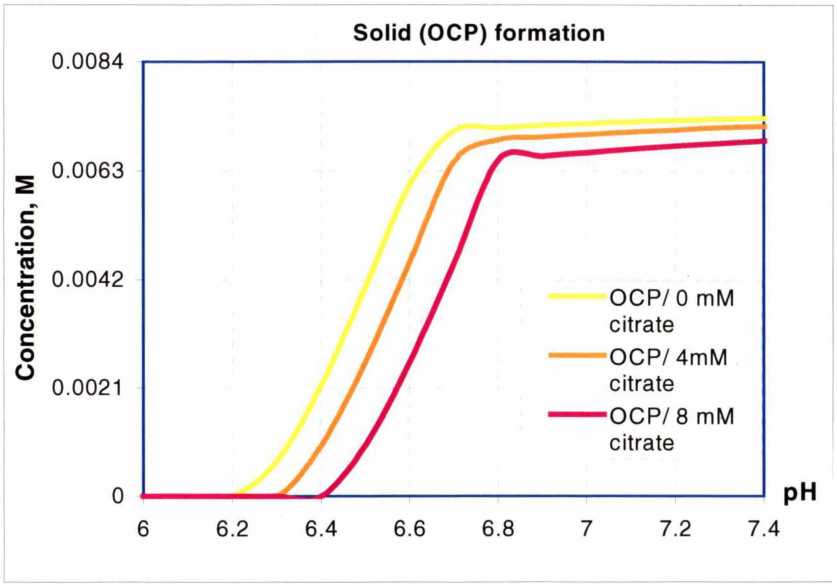

Figure 5-8: SPE calculated pH-stability diagram, representing the formation of the OCP in the lactic whey permeate system for citrate concentration varying from 0 to 8 mM.

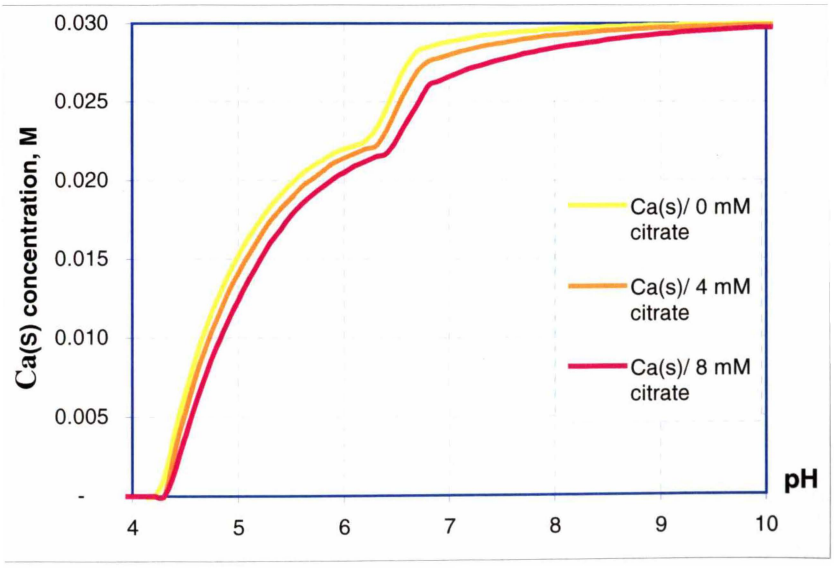

Figure 5-9: SPE calculated concentration-pH diagram, representing the impact of varying citrate ion concentration on the CaP yield as ($Ca_{(S)}$=$Ca_{[OCP]}$ + $Ca_{[BRUSHITE]}$) in the lactic whey permeate for citrate concentration from 0 to 8 mM.

The following Table 5-3 summarises the effect of the citrate concentration on the CaP yield:

Table 5-3: SPE calculated CaP yield as ($Ca_{(S)}=Ca_{[OCP]} + Ca_{[BRUSHITE]}$) in the lactic whey permeate for the citrate concentration from 0 to 8 mM.

Concentration of citrate in lactic whey permeate	Total yield $Ca_{(S)}$, at pH=6.5		Total yield $Ca_{(S)}$, at pH=6.8	
mM	mM	%	mM	%
0	2.610	100.00	2.85	100.00
4	2.460	94.25	2.76	96.80
8	2.258	86.50	2.60	91.22

From these results, it is obvious that the presence of citrate causes a delay in CaP formation, which becomes more pronounced as citrate concentration increases in the pH 6.4-6.8 region (see Figure 5-9 and Table 5-3). In general, the higher concentration of citrate present in lactic whey permeate results in the lower CaP yield in this pH region. At pH = 6.5 the effect of citrate on the CaP yield is more pronounced than it is at pH 6.8 due probably to the higher level of free calcium available at this lower pH. In general, it can be stated that citrate has an overall suppressing effect on CaP precipitation in the system.

5.1.2(e) Titration Curve Calculations

The SPE program is capable of predicting "titration curves" for systems under study. In other words, it is possible to follow the NaOH titre in M as pH is increased from 4.6 to 9.0. The use of titre in units of molarity appears to be an idiosyncratic feature of the *SPE* program whereby concentrations of NaOH required to cause the pH changes illustrated are calculated for the 50 mL solution modelled in SPE. The acid base titration curve can be calculated by SPE by calculating the net charge at each pH value ($=\Sigma c_i z_i$) and assuming electroneutrality is restored by appropriate acid (HCl) or base (NaOH) addition (this forms the charge balance portion of the algorithm in Figure 4.1). As a consequence of this ionic strength can then be calculated. The SPE calculated titration curve (see Figure 5-10) illustrates the "caustic demand" versus pH. In general, Figure 5-10 shows that caustic demand increases steadily from pH 4.6 (original permeate pH) to 6.2.

If Figure 5-10 (region I) is compared with the ion-speciation plots given in Figure 5-1, the gradual increase in caustic demand can be associated with the formation of brushite which rapidly consumes HPO_4^{2-} ion produced by the deprotonation of $H_2PO_4^-$. This can be shown by the equations below:

$$H_2PO_4^-{}_{(aq)} + OH^-{}_{(aq)} \rightleftharpoons HPO_4^{2-}{}_{(aq)} + H_2O$$

$$Ca^{2+}{}_{(aq)} + HPO_4^{2-}{}_{(aq)} + 2H_2O \rightleftharpoons CaHPO_4.2H_2O_{(s)}$$

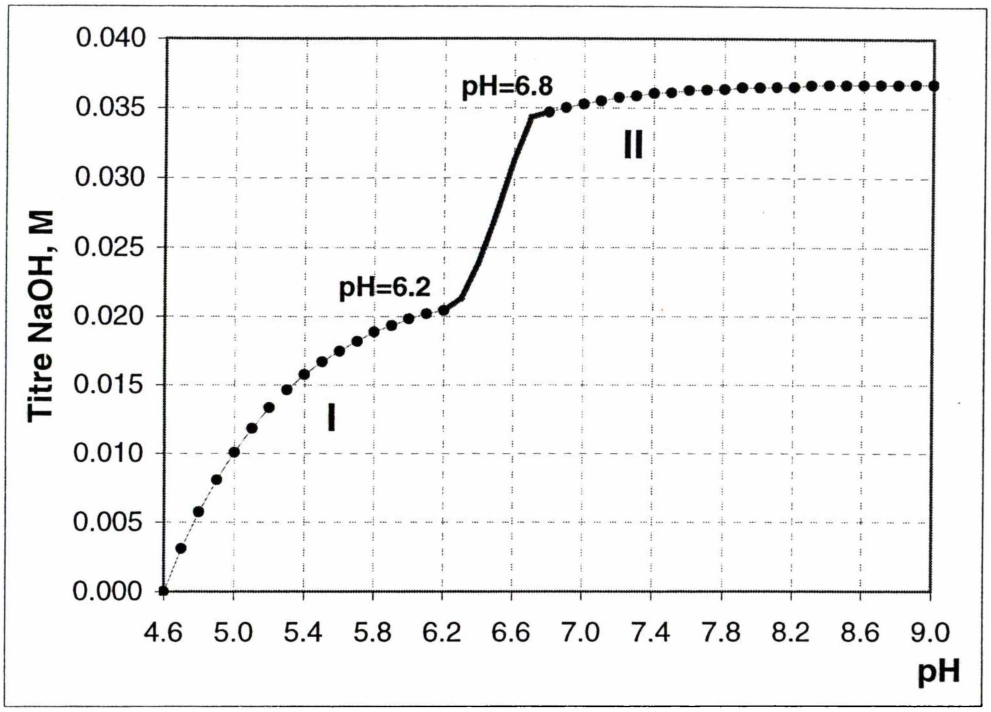

Figure 5-10: SPE calculated titre NaOH-pH curve for a lactic whey permeate at T=25°C for pH range from 4.6-9.0.

In the pH region from 6.2 to 6.8 the caustic demand shows a sharp increase though with pH exhibiting a limited increase of 0.6 pH units. The reason for this is believed to be due to the many possible chemical processes acting simultaneously to prevent the pH from increasing sharply (i.e. are acting to buffer the pH of the medium) in this pH region. One of these processes is the important phase transformation of brushite to OCP (see equation below) which results in the net production of excess protons which serves to neutralise the alkalinity of the medium.

$$6CaHPO_4.2H_2O_{(s)} + 2Ca^{2+}{}_{(aq)} \rightleftharpoons Ca_8H_2(PO_4)_6.5H_2O_{(s)} + 4H^+{}_{(aq)} + 7H_2O$$

One example of the processes occurring in the pH region 6.2-6.8, is OCP formation which increases sharply after pH 6.4. Other processes that contribute to caustic demand

in this pH region are mostly associated with *citrate-associated* acid-base equilibria (citric acid undergoes its third deprotonation step, pK_a3, in this region, see structure below) as well as complexation of citrate species by free calcium ion. This process will require the consumption of hydroxide and will thus compete with the phase transformation process which is at the same time liberating excess protons (that will become neutralised by base):

$$^{-}OOCCH_2\text{-}\underset{\underset{COOH}{|}}{\overset{\overset{OH}{|}}{C}}\text{-}CH_2COO^{-} \rightleftharpoons {}^{-}OOCCH_2\text{-}\underset{\underset{COO^{-}}{|}}{\overset{\overset{OH}{|}}{C}}\text{-}CH_2COO^{-} + H^{+}$$

After pH 6.8 (region II, Figure 5-10) there is only a slight increase in caustic demand with rising pH which can be understood in terms of the steady state formation of OCP from phase transformation of brushite which liberates protons that become neutralised by base so offsetting any sharp increase in pH. Figure 5-11 shows the influence of varying citric acid concentrations (2 and 8 mM) on the titre of NaOH for lactic whey permeate.

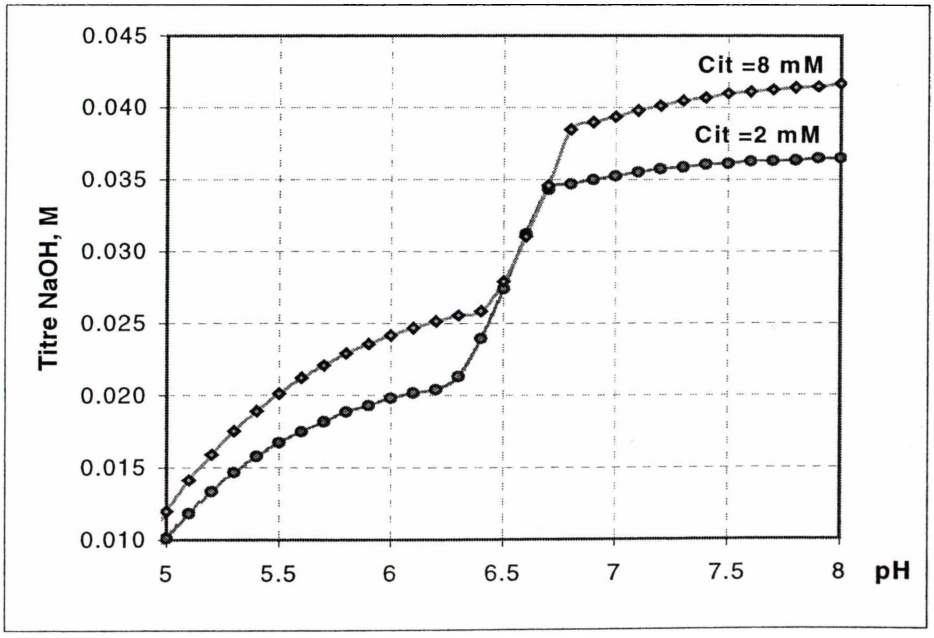

Figure 5-11: SPE calculated titre NaOH-pH curve for lactic whey permeate at T=25°C for pH range from 5.0-8.0 for the varying citrate concentration (2 and 8 mM).

Predictably, an increased caustic demand is found when citrate concentration is made to increase in the lactic whey permeate media. This is merely due to increases in the amount of citrate that need neutralising by base.

5.2 Computer Speciation Calculations of the Precipitation of Calcium Phosphate using Concentration Data for a Commercial Sulfuric Acid Whey Permeate

This section represents the results of the application of chemical speciation calculations to the industrial precipitation of calcium phosphate from sulfuric acid whey permeate. This is different from the lactic whey permeates modelled by SPE in Chapters 4 and 5 as there is an appreciable amount of sulfate in this buffer which can influence precipitation. As stated, sulfate content in sulfuric acid whey permeate is significantly higher compared to the very low levels present in lactic acid whey permeate due purely to the use of sulfuric acid for acidification of the whey. It was thus of interest to see if calcium sulfate would theoretically co-precipitate out with the calcium phosphate in such a permeate hence the need for speciation calculations.

5.2.1 Previous Experimental Work on Systems involving Precipitation of Calcium Sulfate

Since calcium sulfate is thought to be a possible precipitating phase in the industrial calcium phosphate precipitation process, it is of interest to review some previous work on precipitation of calcium sulfate. Much work on the precipitation of calcium sulphate with a focus on certain industrial processes involving this solid have been reported (Packter, 1974; Kazak et al., 1981; Mile et al., 1982, etc.). For example, the Wet-Process for the production of phosphoric acid is based on the digestion of calcium phosphate with sulphuric acid and proceeds according to the following reaction:

$$Ca_3(PO_4)_2 + 3H_2SO_4 \longrightarrow 3\ "CaSO_4" + 2H_3PO_4$$

in which, depending on reaction conditions, the "$CaSO_4$" either precipitates as the dihydrate ($CaSO_4.2H_2O$) or the hemihydrate ($CaSO_4.1/2H_2O$). In general, a large quantity of the dihydrate known also as gypsum is produced as a byproduct of the phosphoric acid manufacturing process (Adami et al., 1968; Bespalov et al., 1994). It is used to make the familiar product "Plaster of Paris". The conditions necessary for the precipitation of phosphate - free gypsum in media rich in phosphoric acid are described in (Adami et al., 1968). There are three variants to the hemihydrate process (Bűchner et al., 1989):

1) Calcium sulfate precipitates out immediately as the hemihydrate and is filtered off.
2) Calcium sulfate precipitates out initially as the dihydrate and is then recrystallized to the hemihydrate.
3) Calcium sulfate precipitates out initially as hemihydrate and is then recrystallized to the dihydrate.

The recrystallization can be carried out either by filtering off the calcium sulfate or *in situ.* This literature shows how calcium sulfate formation is important at low pH (i.e. 3.5-4.5) which is relevant to the present study of expected solid phases precipitating from the sulfuric acid whey permeate. In fact there are many factors, including the presence of trace impurities (Sarig et al., 1982), which influence the size and crystal habit of gypsum ($CaSO_4.2H_2O$) crystals, as formed in the phoshporic acid wet process.

5.2.2 Construction of the Input File

The SPE program contains an input file into which concentrations expressed as mmoles in 50 mL can be entered for various anionic and cationic species, which represent the fundamental ionic components of the system. In general, the important ionic constituents present in *sulfuric acid whey permeate* are: K^+, Na^+, Ca^{2+}, Mg^{2+}, Cl^-, inorganic phosphate and sulfate. The values used in the input file are based on the following data given in Table 5-4, which represents the composition of a typical sulfuric acid whey permeate in mid-season.

Table 5-4: Typical compositional data for a sulfuric acid whey permeate[1].

Component	Concentration, mM	Concentration, ppm
Ca^{2+}	26.0	1042.1
PO_4^{3-}	21.0	650.4
SO_4^{2-}	23.0	737.6
Mg^{2+}	3.45	83.9
Na^+	16.3	374
K^+	28.9	1132
Citrate	7.0	1330
Lactate	0.045	4.0

[1]proprietary information

In comparison with a lactic whey permeate, sulfuric acid whey permeate in mid-season has relatively high sulfate content, while the calcium level is relatively lower (see Appendix A1). The chemical composition of sulfuric acid whey permeate depends on the time of the season. It has been shown that the calcium level in the whey permeate decreases towards the end of the season and the sulfate content increases (see Table 5-5 below). In mid-season the Ca:P molar ratio in the sulfuric acid whey permeate is 1.24 according to data in Table 5-4. The Ca:S molar ratio in this permeate is 1.13. In contrast, toward the end of the season the Ca:P molar ratio is 1.19 with the Ca:S ratio being 0.91. Thus in late season, the sulfate level is slightly in excess of the calcium level (see Table 5-5).

Table 5-5: Sulfuric whey permeate composition at the end of season[1]

Component	Concentration, mM	Concentration, ppm
Ca^{2+}	21.5	863
PO_4^{3-}	18.0	556
SO_4^{2-}	23.5	753
Mg^{2+}	3.6	87.9
Na^{+}	16.3	374
K^{+}	28.9	1132

[1]late May 1998, proprietary information.

Schematically, the seasonal variation in calcium, sulfate and phosphate ions can be represented as follows:

Mid-season

========== Ca (26 mM)
========== S (23 mM)
========== P (21 mM)

Late season

========== S (23.5 mM)
========== Ca (21.5 mM)
========== P (18.0 mM)

If the CaP precipitate (cake) is not washed, the levels of sulfate are analysed to be 10000 ppm. When the cake is washed, the sulfate is around 4000 ppm. There were also difficulties with the sulfate assaying procedure as phosphate may chemically interfere with sulfate determination by gravimetric analysis based on $BaSO_4$ precipitation due to $Ba_3(PO_4)_2$ co-precipitation.

The following table (Table 5-6) summarises the overall *(Log β_I)* values for the whey permeate and were used in the SPE program.

Table 5-6: The formation constants for the whey permeate species at *I=0.1M* as used in the SPE calculations (data from NIST database # 46 (Smith et al., 1998)).

Species	*Log (β_I)* at *I = 0.1M*
HPO_4^{2-}	11.52
$H_2PO_4^-$	18.23
H_3PO_4	20.15
$CaHPO_4$	13.14
$Ca_2HPO_4^+$	18.83
$HCit^{2-}$	5.65
H_2Cit^-	10.0
H_3Cit	12.9
$CaCit^-$	3.45
CaHCit	7.72
CaH_2Cit^+	11.0
HLac	3.66
$CaLac^+$	1.07
$Ca(Lac)_2$	1.62
$MgOH^+$	11.88
$MgCit^-$	12.82
MgHCit	7.50
MgH_2Cit^+	10.7
$MgHPO_4$	13.17
$CaOH^+$	12.82
HCO_3^-	9.91
$CaCO_3$	2.38
$CaHCO_3^+$	10.68
OH^-	13.78
HSO_4^-	1.54
$CaSO_4$	1.48
$MgSO_4$	1.48

The following Table 5-7 summarises the *Log* K_{sp} values for all the possible solid phases of calcium phosphate (4 different phases), sulfate, lactate, carbonate, and citrate that may precipitate from the whey permeate upon adjustment of pH with sodium hydroxide.

Table 5-7: *Log* K_{sp} values at $I = 0.1M$ for all the possible solid phases.

Molecular Formula	Name	*Log* K_{sp} at $I = 0.1M$
$CaHPO_4.2H_2O$	Dicalcium phosphate dihydrate (Brushite)	17.30
$Ca_3(PO_4)_2$	Tricalcium phosphate (TCP)	25.17
$Ca_8H_2(PO_4)_6$	Octacalcium phosphate (OCP)	42.36
$Ca_{10}(PO_4)_6(OH)_2$	Hydroxyapatite (HAP)	38.78
$CaSO_4.2H_2O$[1]	Calcium sulphate dihydrate (Gypsum)	3.78
$Ca_3Cit_2.6H_2O$	Calcium citrate	14.2
$CaCO_3$	Calcium carbonate	7.66
$Ca_2HPO_4SO_4.4H_2O$[1]	Ardealite (Ard)	21.34[2]

[1]These *Log* K_{sp} values were used only for the calculations of the sulfuric acid whey permeate.

[2]*Log* K_{sp} for the Ardealite was estimated from the SPE calculation.

Variation of the input file for investigating changes in the sulfuric whey permeate and their effect on ion speciation and precipitation of solids

The numbers representing concentrations of the basic ionic components in the whey permeate that were entered into the input file (see earlier) were varied over certain ranges (as in the calculations performed in Chapter 4 and 5) in order to deduce the

effects on ion speciation and solid formation in the whey permeate. These are summarised below: in all cases the concentration of calcium ion was kept constant at 26 mM.

(i) Citrate Concentration

The concentration of citrate in a typical mid-season sulfuric acid whey permeate is 7.0 mM (see Table 5-4). However for the purpose of the calculations, the citrate level was varied from 0-9 mM with all other ion concentrations kept constant. This was to investigate the effect of citrate on the total yields of precipitated calcium phosphate solid (brushite and octacalcium phosphate).

(ii) Phosphate Concentration

The concentration of phosphate in a typical mid-season sulfuric acid whey permeate is 21 mM. The molar Ca:P ratio in a typical permeate is thus 1.24:1. Calculations were performed using phosphate concentrations which varied from 21-32.2 mM such that the molar Ca:P ratio varied from 1.24:1 to 1:1.24.

(iii) Sulfate Concentration

The concentration of sulfate in a typical mid-season sulfuric acid whey permeate is 23 mM. This corresponds to a molar Ca:S ratio of 1.13. Calculations were performed using sulfate concentrations that were varied such that the molar Ca:S ratio varied from 1.13 to 0.90. This was to mimic the conditions occurring in late season when the sulfate level in the whey permeate is relatively high (see Table 5-5).

5.2.3 Results and Discussion

5.2.3(a) Ion and Molecular Speciation

The following Figures 5-12 and 5-13 represents SPE calculated the general distribution of the main ionic and molecular species as well as solid phases forming in the sulfuric acid whey permeate as a function of pH.

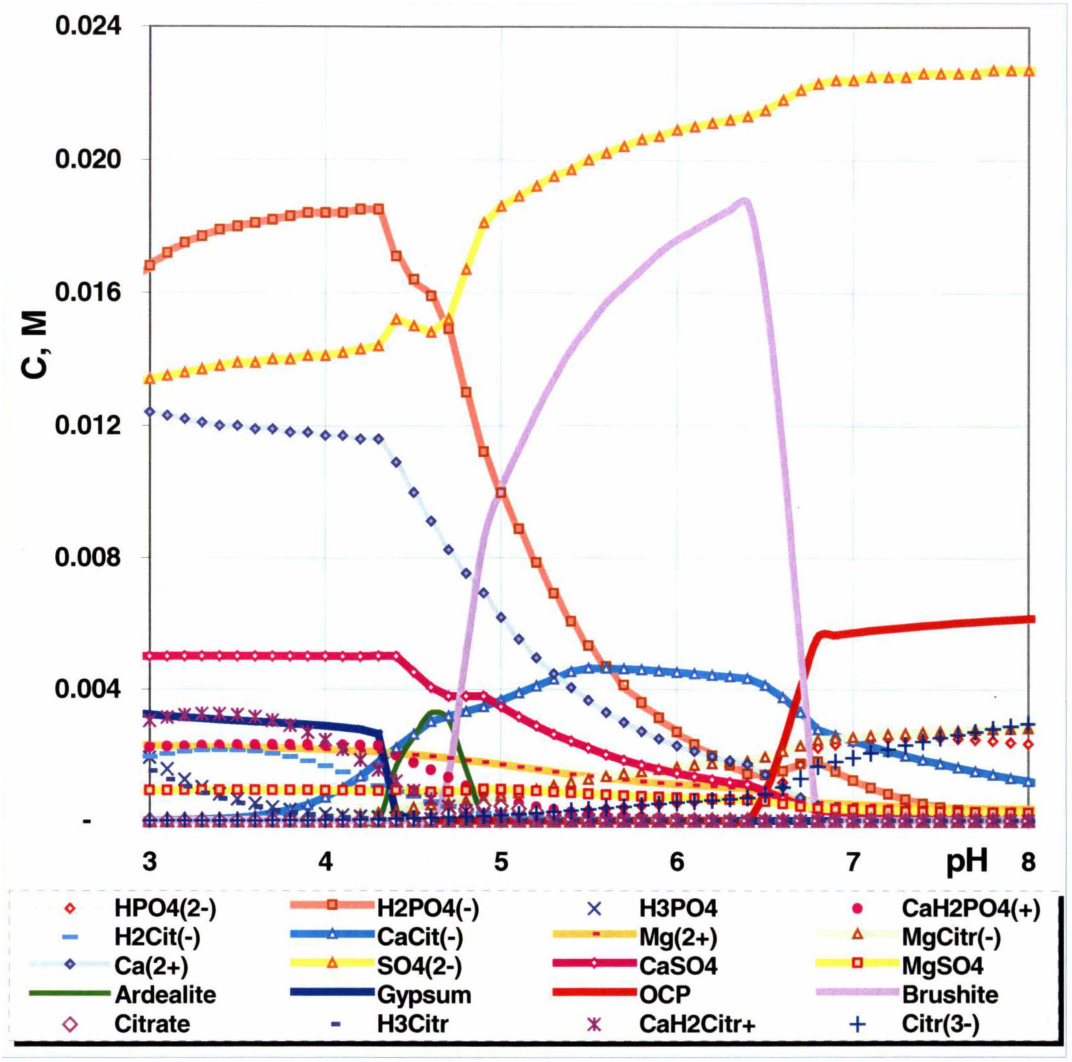

Figure 5-12: SPE calculated general distribution of the main ion species and solid phases over the pH range 3-8 in sulfuric acid whey permeate.

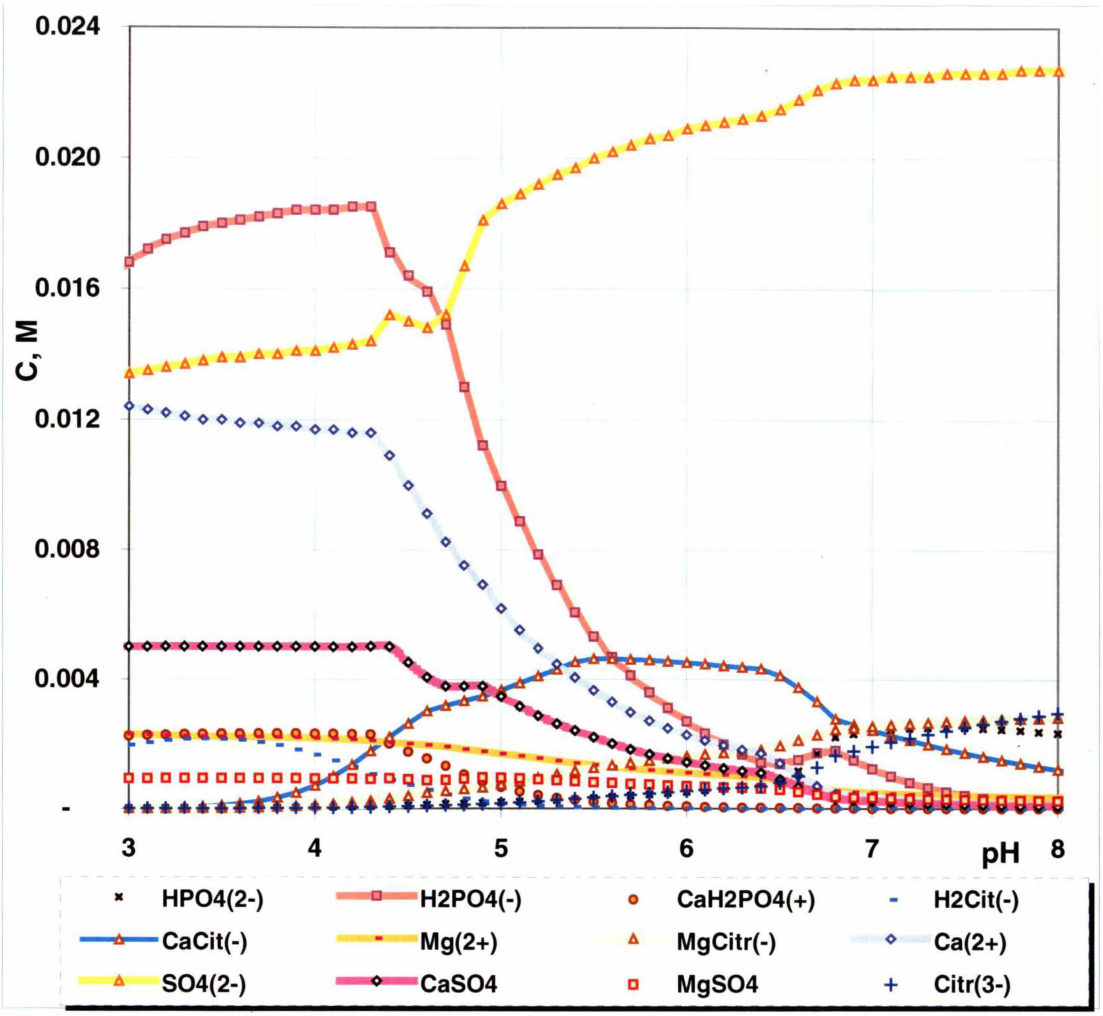

Figure 5-13: SPE calculated distribution of the dominant ion and molecular species over the pH range 3-8 in sulfuric acid whey permeate.

SPE calculations (see Figures 5-12 and 5-13) illustrates that the dominant ion and molecular species in sulfuric acid whey permeate are as follows:

$H_2PO_4^-$ - as a result of the equilibrium distribution of species of phosphoric acid (H_3PO_4, HPO_4^{2-} and PO_4^{3-}).

Ca^{2+} - free calcium ion concentration, the level of which depends on the formation of calcium containing species, especially CaP solids as well as the complex between Ca^{2+} and Cit^{3-} (i.e. $CaCit^-$) which are the main consumers of Ca^{2+} as pH increases.

SO_4^{2-} - sulfate ion concentration in the permeate gradually increases as a result of the dissolution of the calcium sulfate-containing solids (gypsum and ardealite) which are *predicted* to be present as solid phases at pH < 5. Dissolved SO_4^{2-} reaches a constant level after pH 6.8 implying that almost all possible solid phases containing sulfate have passed into solution by this pH.

$CaCit^-$ - In the pH region 4-7, complex ion formation between Ca^{2+} and Cit^{3-} ion to form $CaCit^-$ is important. The maximum concentration of this complex is predicted to be at pH 5.8. This complex is a significant binding agent of free calcium. It ties up the calcium in solution in a form, which makes it less available for the direct precipitation reaction between calcium ion and phosphate ion.

$CaSO_{4\,(aq)}$ (and ***$MgSO_{4(aq)}$***) - These refer to soluble ion-pair species or "undissociated molecular form" of calcium sulfate and magnesium sulfate. These form by straight combination of the calcium and sulfate ions to form a soluble compound (Aoki et al., 1979) in solution:

$$Ca^{2+}_{(aq)} + SO_4{}^{2-}_{(aq)} \rightleftharpoons \underset{\textbf{\textit{undissociated}}}{CaSO_{4\,(aq)}} \rightleftharpoons CaSO_4.n\,H_2O_{\,(s)}$$

$$Mg^{2+}_{(aq)} + SO_4{}^{2-}_{(aq)} \rightleftharpoons \underset{\textbf{\textit{undissociated}}}{MgSO_{4\,(aq)}}$$

In fact, it has been commented that the trapping of the liquid media (which will contain various dissolved components) inside forming crystals aggregates can be an undesirable phenomenon in various technological processes (Yaminskii et al, 1991). This could possibly be a scenario in the precipitation of calcium phosphate from APE sulfuric whey permeate whereby sulfate or even "soluble" calcium sulfate ($CaSO_{4(aq)}$) from the sulfate-rich media is becoming incorporated to a small extent in porous aggregates making up the calcium phosphate cake.

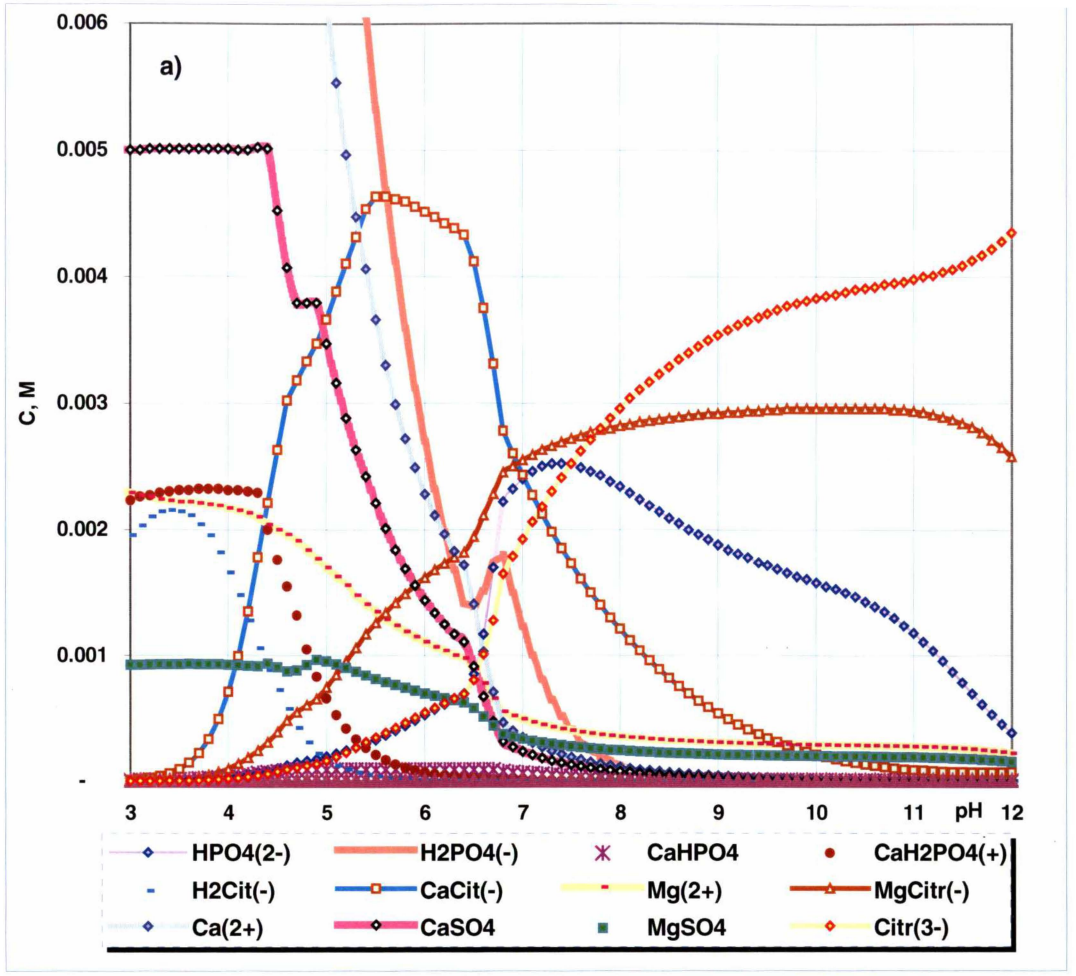

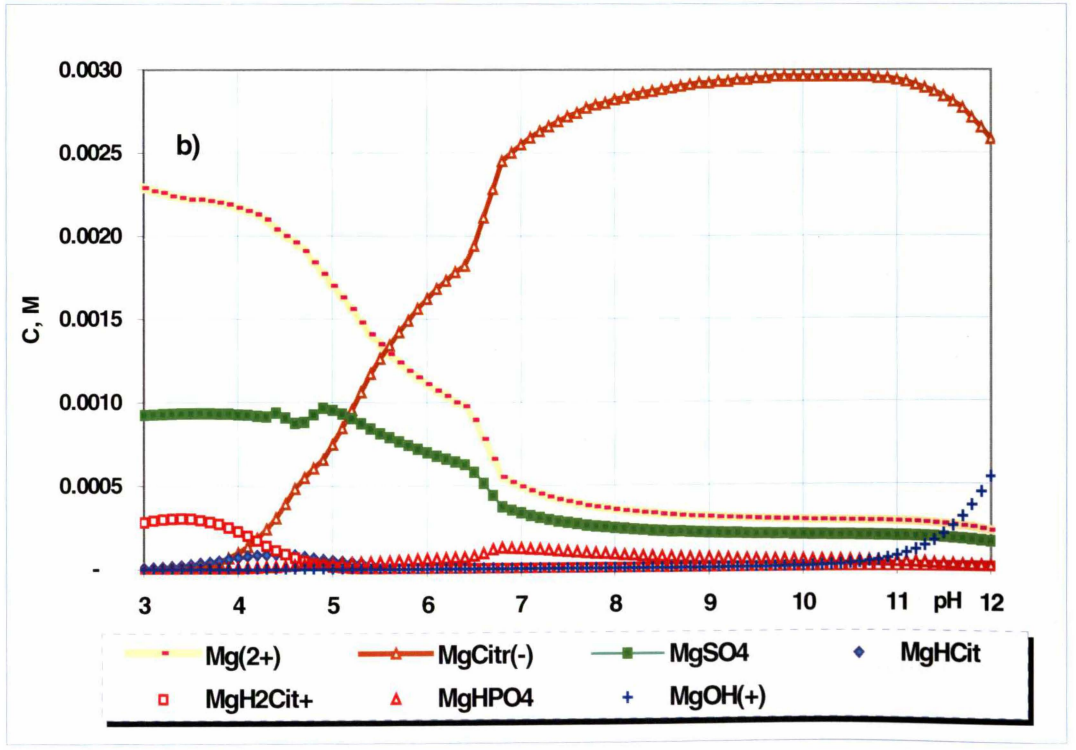

Figure 5-14: SPE calculated: a) an overall distribution and b) Mg-containing species over the pH range 3-12 in sulfuric acid whey permeate (enlarged scale).

5.2.3(b) Solids Formation, as calculated by SPE

SPE calculations predict the formation of the following thermodynamically favoured phases:

(a) Gypsum ($CaSO_4.2H_2O$)

This solid phase appears to be important over the pH region 2-4.4 (see Figure 5-15). Thus it should be stressed that this solid phase is only important in the low pH region. In fact, this is the way "chemical" gypsum is manufactured. It is formed as a precipitated by-product by the so-called "Wet Process" which involves the dissolution of apatite to form phosphoric acid (Adami et al., 1968; Berry, 1972). This is quite a relevant observation because it indicates that gypsum formation in the sulfuric acid whey permeate at usual pH values is not a dominant phase at all. The extent of its formation appears to be influenced by the citrate concentration, the sulfate concentration, and the Ca:P molar ratio in the permeate (see later discussion). It was observed previously (Hamdona et al., 1993; Sarig et al., 1982; Budz et al., 1998) that there are many factors, including the presence of some metal ions and trace impurities, which influence the formation of gypsum ($CaSO_4.2H_2O$).

(b) Ardealite ($Ca_2HPO_4SO_4.4H_2O$)

This hypothetical mixed calcium sulfate-calcium phosphate phase appears to form in the low pH region over a very narrow range from 4.4-4.9 (see Figures 5-15 and 5-16). It is also influenced by citrate and sulfate concentrations as well as Ca:P ratio (see later discussion for a fuller description of this phase and the factors affecting its formation). As was reported in the literature (Balenzano et al., 1984), the chemical date for ardealite are very close to the ideal composition of a double salt "$CaSO_4.CaHPO_4.4H_2O$".

(c) Brushite ($CaHPO_4.2H_2O$) and Calcium Citrate ($Ca_3Cit_2.6H_2O$)

The precipitation of this calcium phosphate compound, which is a major solid phase and one of the precursor solid phases to HAP (Mucalo et al., 1998) is dominant over the pH region 4.7-6.7 (see Figures 5-12 and 5-15). A far more minor phase, this being calcium citrate ($Ca_3Cit_2.6H_2O$) is also forming over this pH region.

(d) Octacalcium phosphate ($Ca_8H_2(PO_4)_6.5H_2O$) or Hydroxyapatite ($Ca_5(PO_4)_3OH$)

Octacalcium phosphate is a major precipitating phase occurring after pH 6.5 and predominating over the rest of the pH region up to pH 12 (see Figure 5-12). When hydroxyapatite is actually included in the calculation as an allowed solid phase, it (as observed in other SPE calculations) completely dominates after pH 5 in the calculation thus affording limited information on precursor phases to HAP (these being brushite and OCP). This is the reason that this compound is considered separately from the SPE calculations. Since brushite and OCP are direct precursors to HAP, following the formation (and hence yields) of these solids is a justifiable approach to gaining information about the likely phase transformations occurring in the reacting system as a function of pH.

Coexistence of Gypsum - Ardealite - Brushite

In general, at low pH 2-5, the following calcium sulfate and calcium phosphate/sulfate mixed solid phases are thermodynamically possible as precipitation products from the APE sulfuric acid whey permeate solutions (see Figures 5-11 and 5-13): Firstly, *Gypsum* ($CaSO_4.2H_2O$) which generally (Adami et al., 1968) forms in very acidic conditions, forms in the whey permeate at pH 2.0-4.4. Its concentration in the medium will depend significantly on the free sulfate concentration as well as the concentrations of citrate and also the Ca:P molar ratio (see 5.2.3(e): "Impact of varying Ca:P Molar Ratios on the Precipitation of Calcium Phosphate"). Secondly, Ardealite ($Ca_2HPO_4SO_4.4H_2O$) can form (see Figures 5-15 and 5-16). Ardealite has actually been synthesised and crystals analysed by single crystal and powder X-ray diffraction method (Aslanian et al., 1982; Sakae, 1978).

Ardealite is an intermediate member of the gypsum-brushite isodimorphous series. The similarity in both the chemical composition and structures of gypsum - $CaSO_4.2H_2O$ and brushite - $CaHPO_4.2H_2O$ (Balenzano et al., 1984) mean that solid-solid solutions of combinations of the two compounds may exist over the complete range of compositions between two minerals.

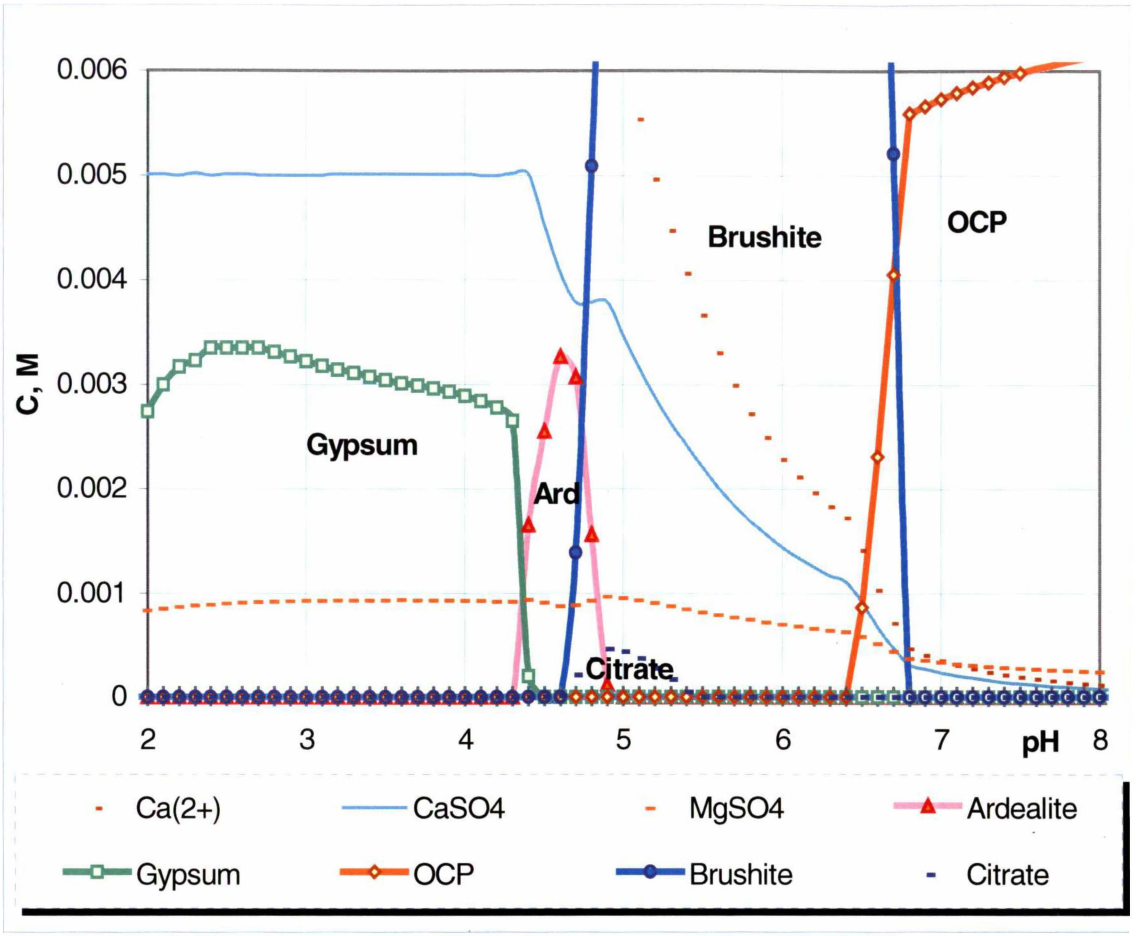

Figure 5-15: SPE predicted distribution of the precipitated solid phases over the pH range 2-8 in the sulfuric acid whey permeate.

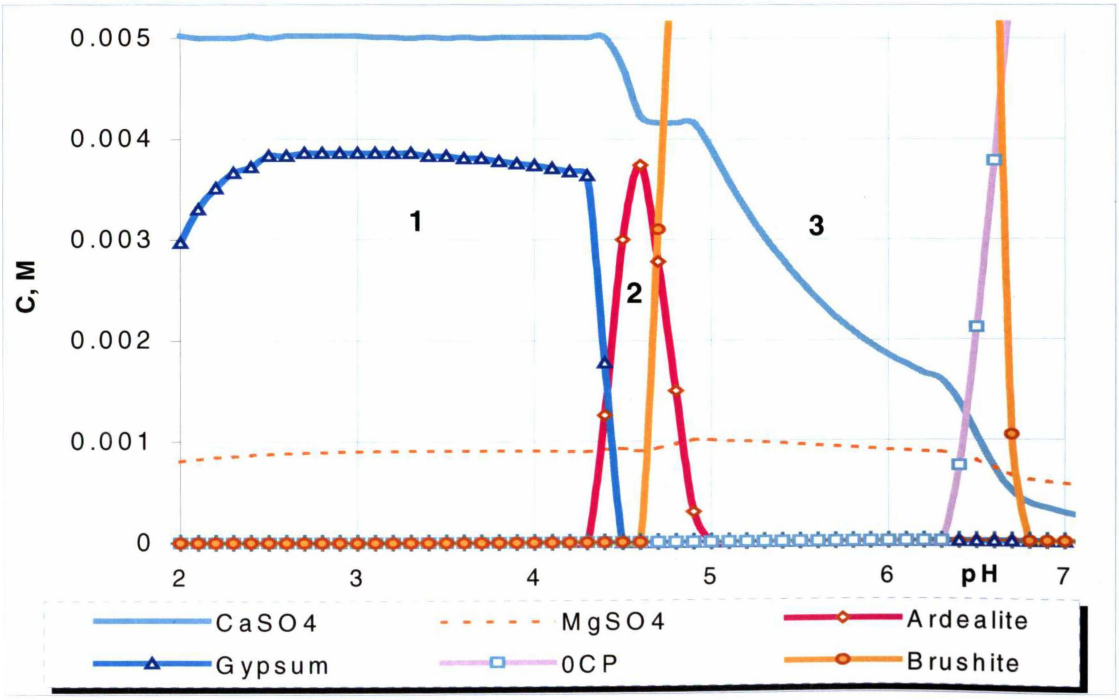

Figure 5-16: SPE calculated diagram showing the coexistence of 3 phases: 1) Gypsum – 2) Ardealite – 3) Brushite over the pH range 2-7 (enlarged scale).

The synthetic calcium phosphate-sulfate hydrate, ardealite, was observed (Sakae et al., 1978) to possess a sheet-structure analogous to that of brushite and gypsum but with a different mode of sheet stacking. The lattice parameters of ardealite crystals are similar in value to those exhibited by gypsum and brushite crystals except in the "cell *b*" dimension (see Figure 5-17).

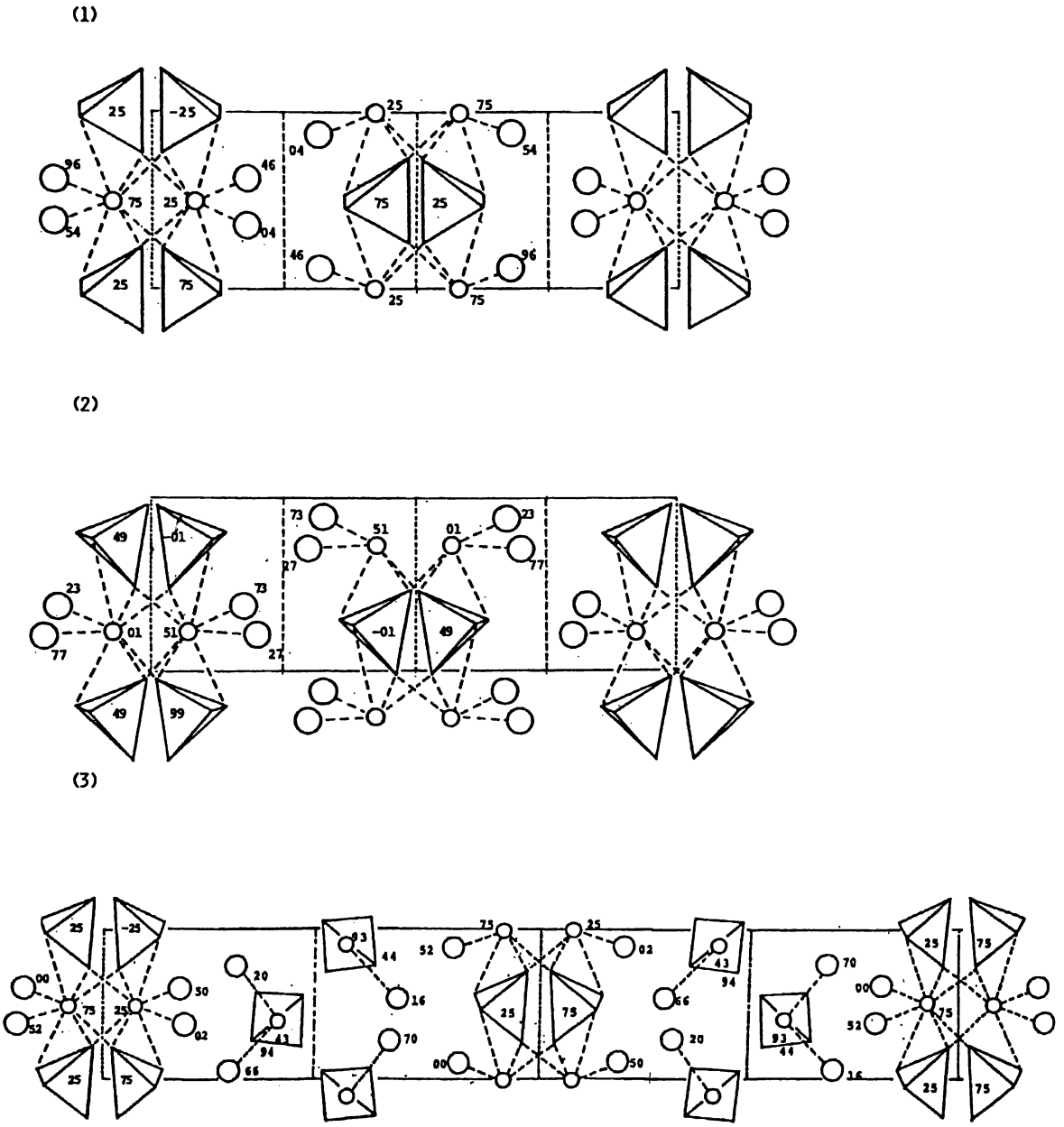

Figure 5-17: Comparison of the crystal structure of Gypsum ($CaSO_4.2H_2O$), Brushite ($CaHPO_4.2H_2O$) and Ardealite ($Ca_2HPO_4SO_4.4H_2O$) projected along the *c* axis (Sakae et al., 1978): (1) $CaSO_4.2H_2O$, (2) $CaHPO_4.2H_2O$, and (3) $Ca_2HPO_4SO_4.4H_2O$. Large circles represent water molecules and small circles represent calcium atoms. Numbers are the *z* coordinates of the tetrahedra, calcium and water sites.

It should be noted that in the commercial ALAMIN™ powder, the presence of ardealite has not ever been observed by IR spectra of the solids, as it would (if it does form and owing to the narrow pH region, 4.4-4.9 over which it forms) dissolve before the onset of brushite formation at pH 4.7.

Brushite-Octacalcium Phosphate Formation

As mentioned earlier and as seen in other whey systems, brushite formation begins at pH 4.7 and reaches a maximum at pH 6.4. After pH 6.5 brushite formation drops sharply and OCP formation begins (see Figure 5-12). These phases are, as mentioned previously, the precursor phases to the final thermodynamically most stable apatitic (HAP) solid corresponding to ALAMIN™ powder and thus the SPE calculations provide an indirect demonstration of the phase transformation of the precipitating solid occurring in the commercial precipitation region. The concentrations of these precursor phases (brushite and OCP) will vary depending on levels of sulfate and citrate anions as well as the Ca:P molar ratio in whey permeate. In the typical sulfuric whey permeate *brushite* is the calcium phosphate which has been formed at the initial stages of the precipitation process (pH 4.7-6.7, C_{max}=18.5 mM at pH_{max}=6.3). The next CaP phase to form after the brushite phase is predictably OCP (pH 6.5-12, final C_{max} =6.48 mM).

5.2.3(c) Titration Curve Calculations

Figure 5-18 illustrates the calculated titration curve showing the progress of base addition to the sulfuric acid whey permeate as a function of pH. As plotted, this effectively represents a calculated "Caustic Demand Curve" as was described for the lactic whey permeate calculation earlier in this chapter. In general, Figure 5-18 demonstrates that caustic demand increases steadily from pH 4.6 (original permeate pH) to 6.4. If Figure 5-18 (region I) is compared with the ion-speciation plots given in Figure 5-12, the gradual increase in caustic demand can be associated with the formation of brushite which begins at pH 4.7 and rapidly consumes HPO_4^{2-} ion produced by the deprotonation of $H_2PO_4^-$.

In the pH region 6.4-6.8 (Figure 5-18) the caustic demand shows a sharp increase though with pH exhibiting a limited increase of 0.4 pH units. This is a region in which many possible chemical processes are acting simultaneously to prevent the pH from

increasing sharply (i.e. are acting to buffer the pH of the medium). One of these processes is the important phase transformation of brushite to OCP which results in the net production of excess protons which serves to neutralise the alkalinity of the medium.

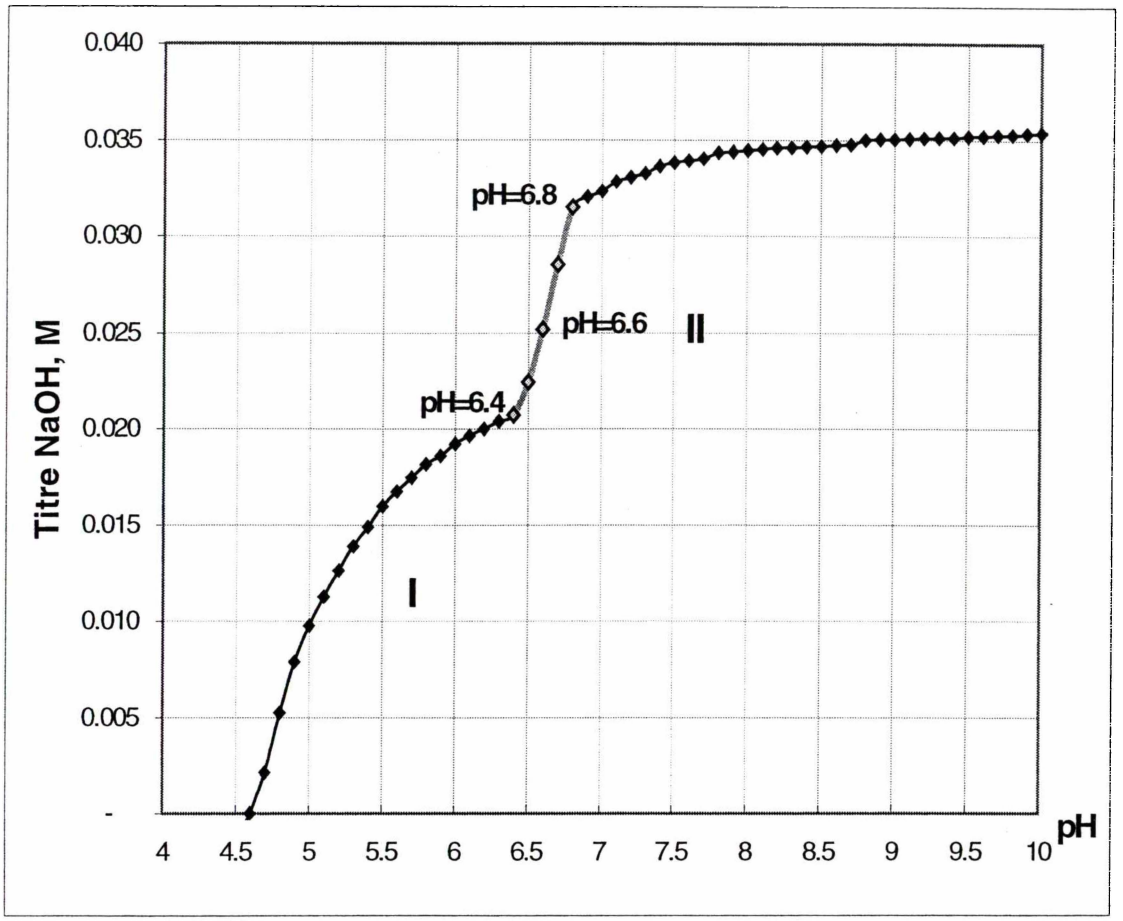

Figure 5-18: SPE calculated titre NaOH-pH curve for the sulfuric acid whey permeate.

The sharp increase in OCP formation over the pH region 6.4-6.8 will thus be a significant contributor to caustic demand. Nevertheless, in this pH region, there are other processes which will contribute to caustic demand. These processes are mostly associated with citric acid-associated acid-base equilibria as well as complexation of citrate species by free calcium ion. The same tendency has been previously observed for lactic whey permeate system (see 5.1.2(e): "Titration Curve Calculations").

After pH 6.8 (region II, Figure 5-18) there is only a slight increase in caustic demand with rising pH which can be understood in terms of a steady state formation of OCP from phase transformation of brushite which liberates protons that become neutralised by base so offsetting any sharp increase in pH.

5.2.3(d) *Impact of varying Citrate Concentration on the Precipitation of Calcium Phosphate*

The most important citrate species occurring in the sulfuric whey permeate and their effect on the yields of precipitated solids can be summarised below. Many of these trends are mirrored in the calculations performed on the SLWUF buffer and the lactic whey permeate.

1. The dominant calcium-citrate containing complex ion is $CaCit^-$ from pH 4-8 (see Figure 5-19 below). The level of this species in the permeate depends on the concentration of citrate (this being Cit^{3-}) in the sulfuric whey permeate medium. When this concentration is varied (by changing the value in the input file used in the SPE program) from 0-9 mM Cit^{3-}, the level of $CaCit^-$ increases proportionally (see Figure 5-20). This complex exhibits a maximum in its formation at *ca.* pH 5.6 when the calculations are done using typical permeate concentrations.

2. In contrast, solid (precipitated) calcium citrate ($Ca_3Cit_2.6H_2O$) is predicted to occur over a pH range of 4.4-5.7 in the typical permeate. Its formation was only observed if the concentration of Cit^{3-} was ≥ 6 mM (see Figure 5-21).

The formation of calcium citrate complexes has a significant impact on the yields of precipitated solids from the whey permeate. This is because the Cit^{3-} anion sequesters free calcium ion from solution as a complex and thus competes with the precipitation reaction which requires free calcium to combine with phosphate anions to give solids. In addition, the levels of the $CaCit^-$ complex are at their highest in the vicinity of the commercial precipitation region (pH 6.4-6.8). Table 5-8 and Figure 5-22 summarises the effect of citrate concentration on the yield of OCP in the pH range 6.4-7.0. The data in Tables 5-8 and 5-9 corresponding to 7 mM Cit^{3-} represent the typical level of citrate in the sulfuric acid whey permeate.

It has recently been found (Marković et al., 1993) that OCP solids can be prepared whereby citrate anion can be incorporated into the crystal lattice of the OCP structure to form octacalcium phosphate carboxylates. This observation is in itself interesting given HAP in ALAMIN™ may well evolve from a short-lived OCP precursor and may explain the ubiquitous citrate presence in the solids. Citrate however cannot enter the HAP lattice (it is too big) and instead it adsorbs to the surface of HAP crystals as shown by López-Macipe et al. (López-Macipe et al., 1998).

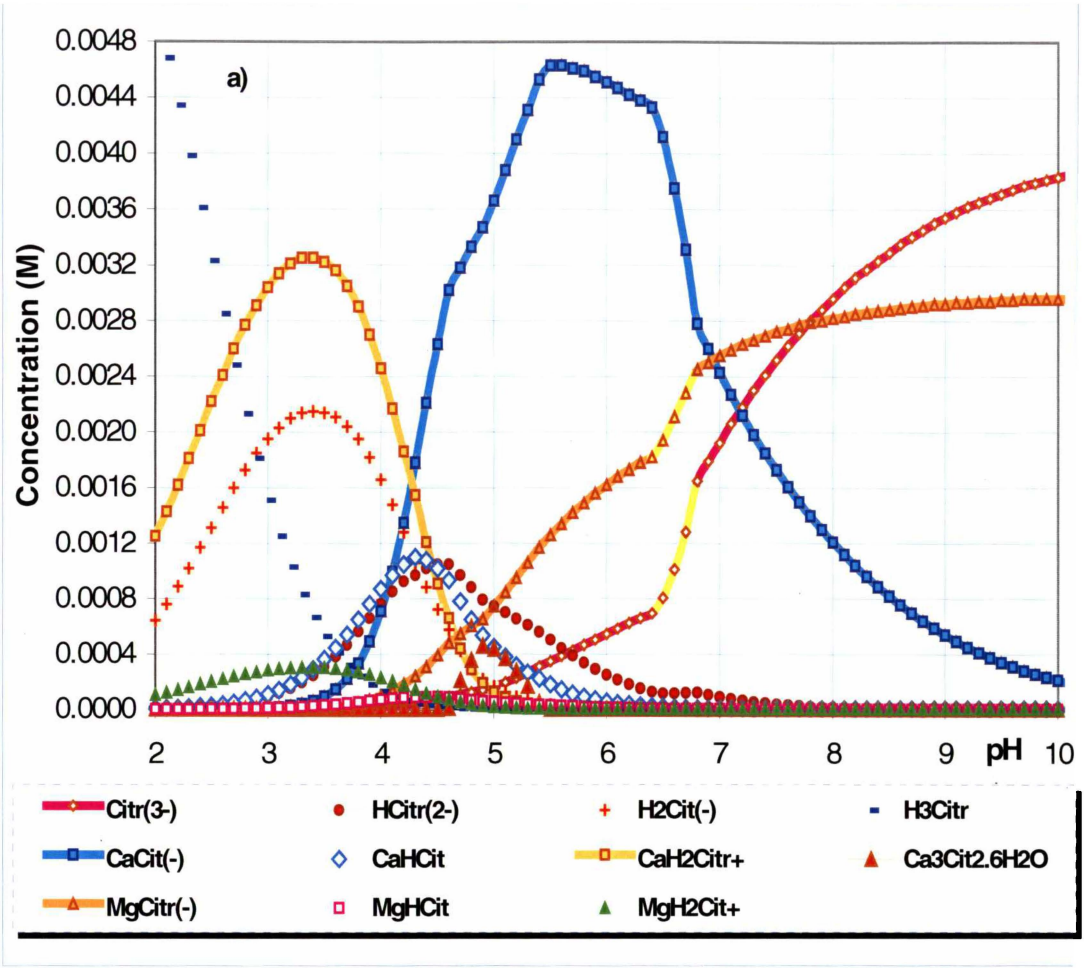

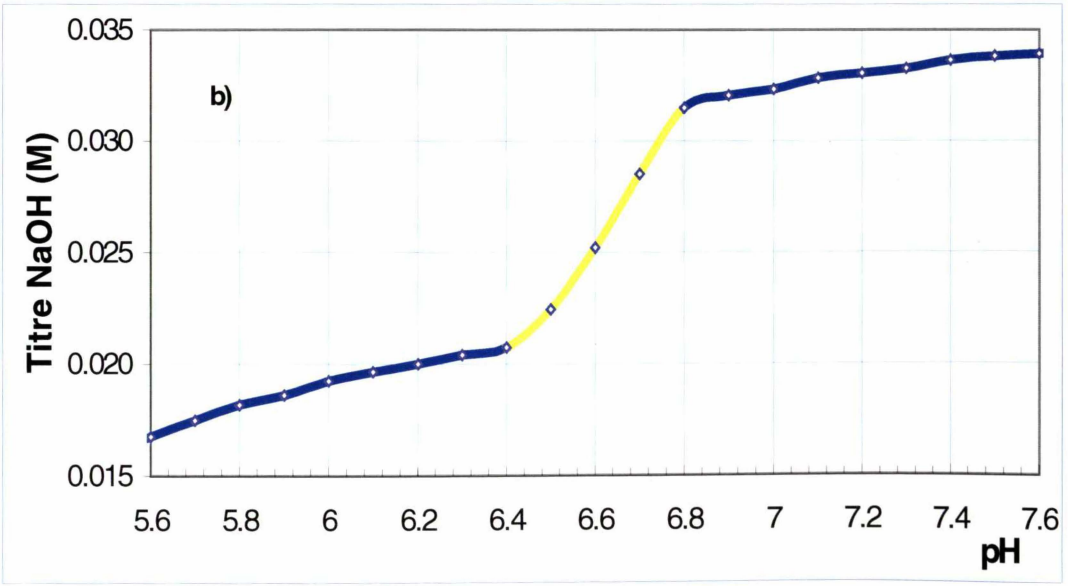

Figure 5-19: SPE calculated distribution of: a) calcium-magnesium-citrate containing species and b) titration curve for the sulfuric acid whey permeate.

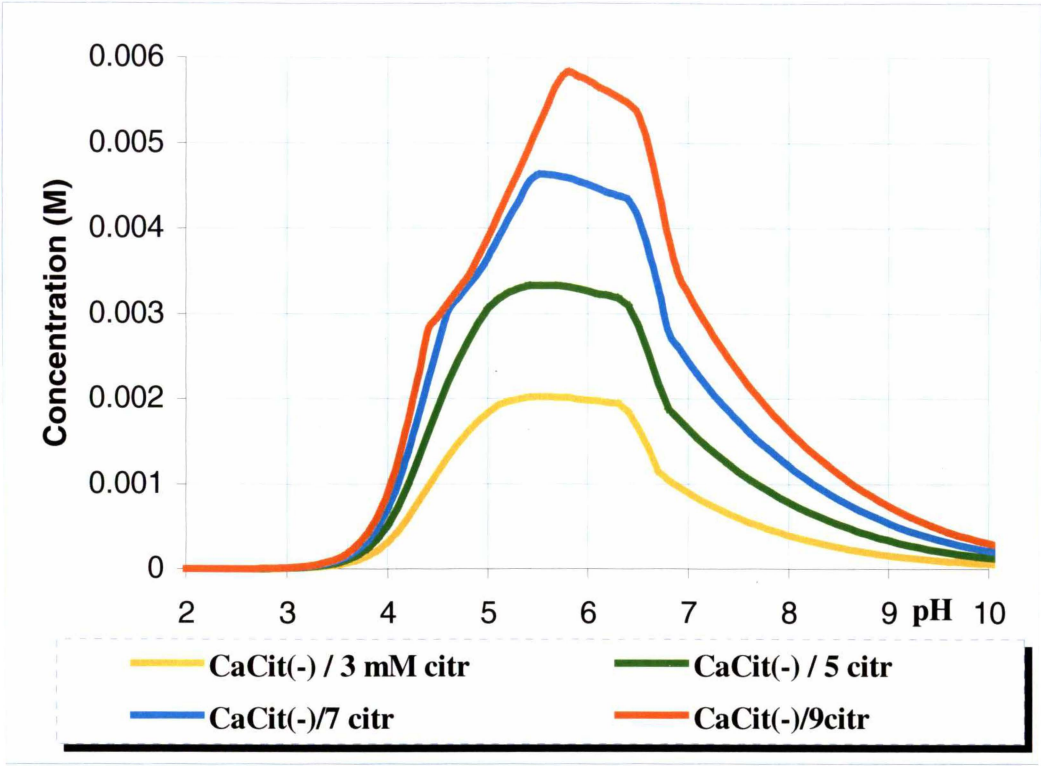

Figure 5-20: SPE calculated distribution of calcium-citrate containing species as a function of pH for the sulfuric acid whey permeate.

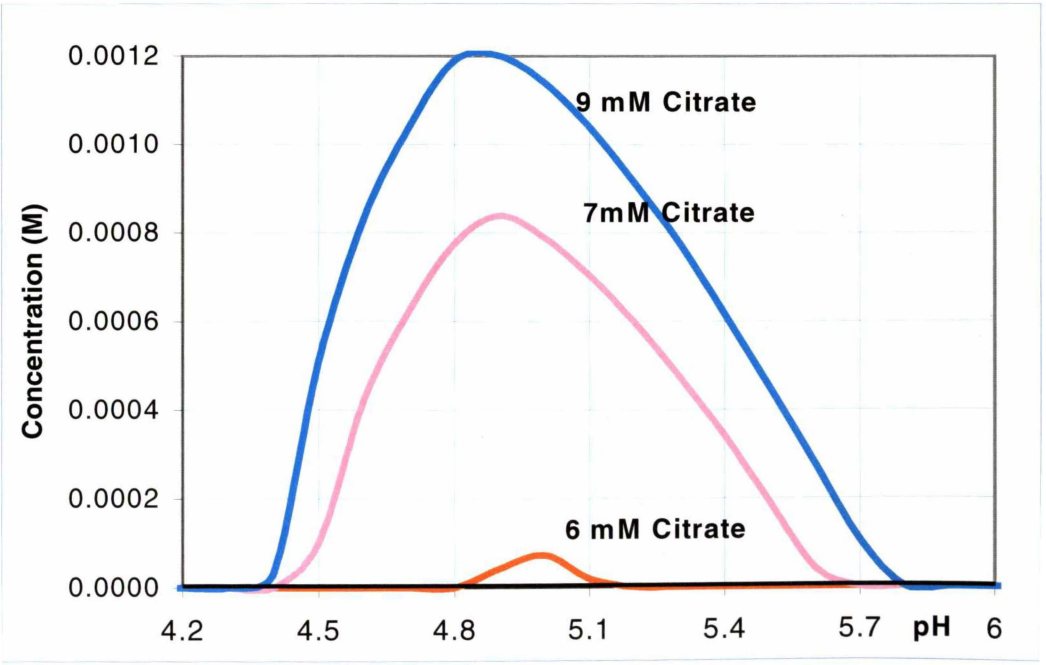

Figure 5-21: SPE calculated distribution of calcium citrate solid ($Ca_3Cit_2.6H_2O$) as a function of pH for the sulfuric acid whey permeate.

Table 5-8: SPE calculated yield of OCP solid formation.

pH	Yield of OCP solid (mM)				
	0 mM Citrate	3 mM Citrate	5 mM Citrate	7 mM Citrate	9 mM Citrate
6.4	2.04	0.97	0.47	0.0	0.0
6.6	5.42	4.19	3.29	2.31	1.45
6.8	6.18	5.97	5.79	5.59	5.11
7.0	6.26	6.07	5.91	5.73	5.54

From the data in Table 5-8 it is clear that citrate inhibits the formation of OCP. In fact, it is obvious that the presence of citrate causes a delay in OCP formation, which becomes more pronounced as citrate concentration increases. For instance, at pH 6.3, OCP begins forming when there is no citrate at all in the medium. However, at citrate concentrations of 4 mM, OCP formation does not occur till pH 6.4 and at even higher concentrations of citrate (8 mM), it does not occur until pH 6.5. The following Table 5-9 shows the SPE calculated overall yield of CaP solid (Brushite + OCP) as a function of citrate concentration.

Table 5-9: SPE calculated overall yield of solid (Brushite + OCP) formation in the sulfuric acid whey permeate for citrate concentration from 0 to 8 mM.

pH	Overall yield of solid (mM)				
	0 mM Citrate	3 mM Citrate	5 mM Citrate	7 mM Citrate	9 mM Citrate
6.4	21.5	20.2	19.5	18.7	18.1
6.6	23.9	22.6	21.6	20.4	19.4
6.8	24.7	23.9	23.2	22.4	21.3
7.0	25.0	24.3	23.6	22.9	22.2

In general, citrate extends the brushite stability region to higher pH and thus delays OCP formation as can be seen in Figure 5-22. This was also observed in the speciation calculations for the SLWUF buffers and the lactic whey permeate.

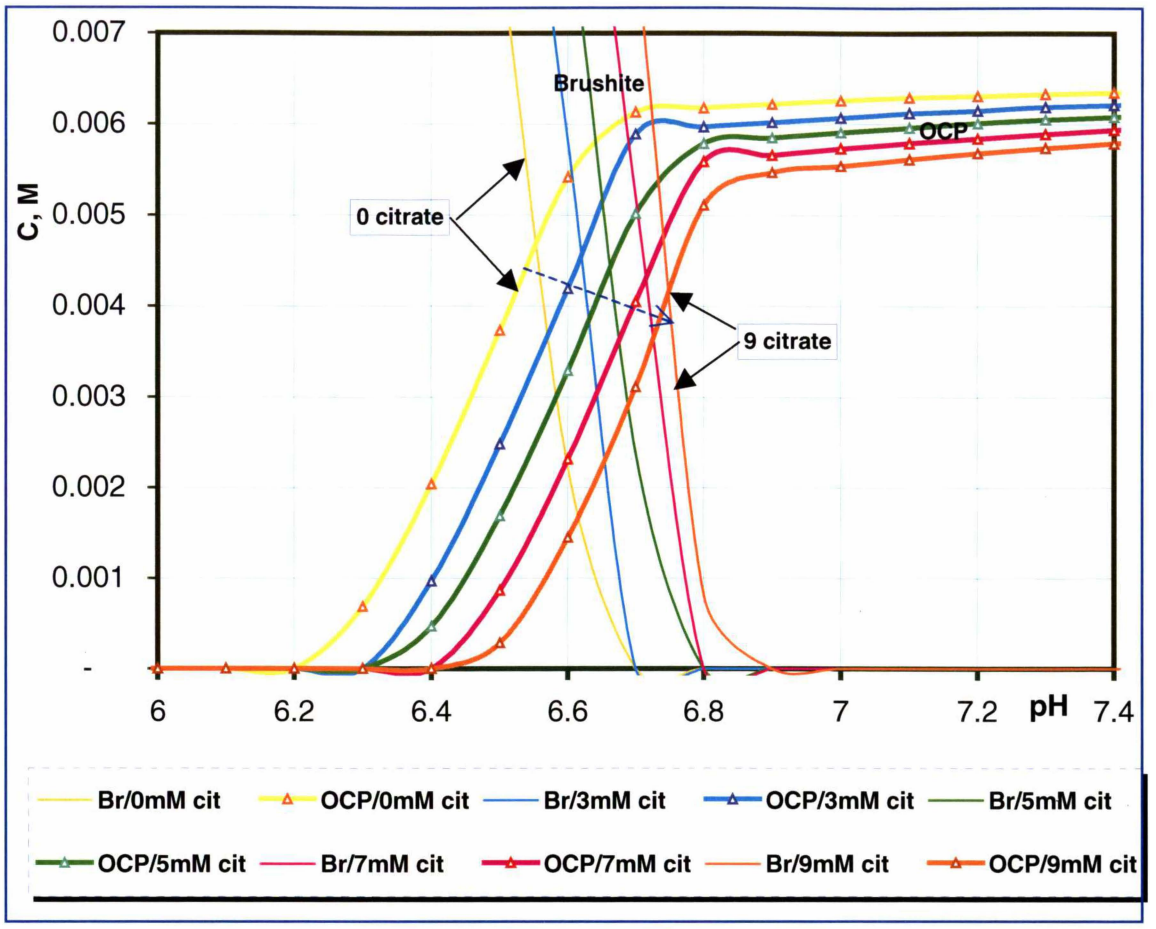

Figure 5-22: SPE calculated influence of the citrate concentration on the Brushite (Br) and OCP formation for a series of citrate concentrations from 0 mM to 9 mM in the sulfuric acid whey permeate. Colour coding has been used to distinguish the curves generated for the different citrate concentrations.

Figure 5-23 functions as a better indicator of the overall effect of citrate on the yields of precipitated CaP solids as a function of pH and citrate concentration in that it shows the total yield of solids (Brushite + OCP) forming and the inhibitory effects of citrate in the medium.

Effects of Citrate on Gypsum and Ardealite Concentrations. It is also of interest to show the inhibitory effect of citrate on the formation of solid phases occurring at lower pH values such as gypsum and ardealite. Figures 5-24 and 5-25 summarise the effect of citrate on these phases. In general, in common with the CaP phases, the presence of citrate leads to lower levels of these solid compounds in the overall product distribution. In essence, citrate presence in the permeate globally suppresses free calcium in the medium over the entire pH range 2-12 so that less calcium is available for participation in solid phases such as calcium phosphates and calcium sulfates (Figures 5-25 and 5-26).

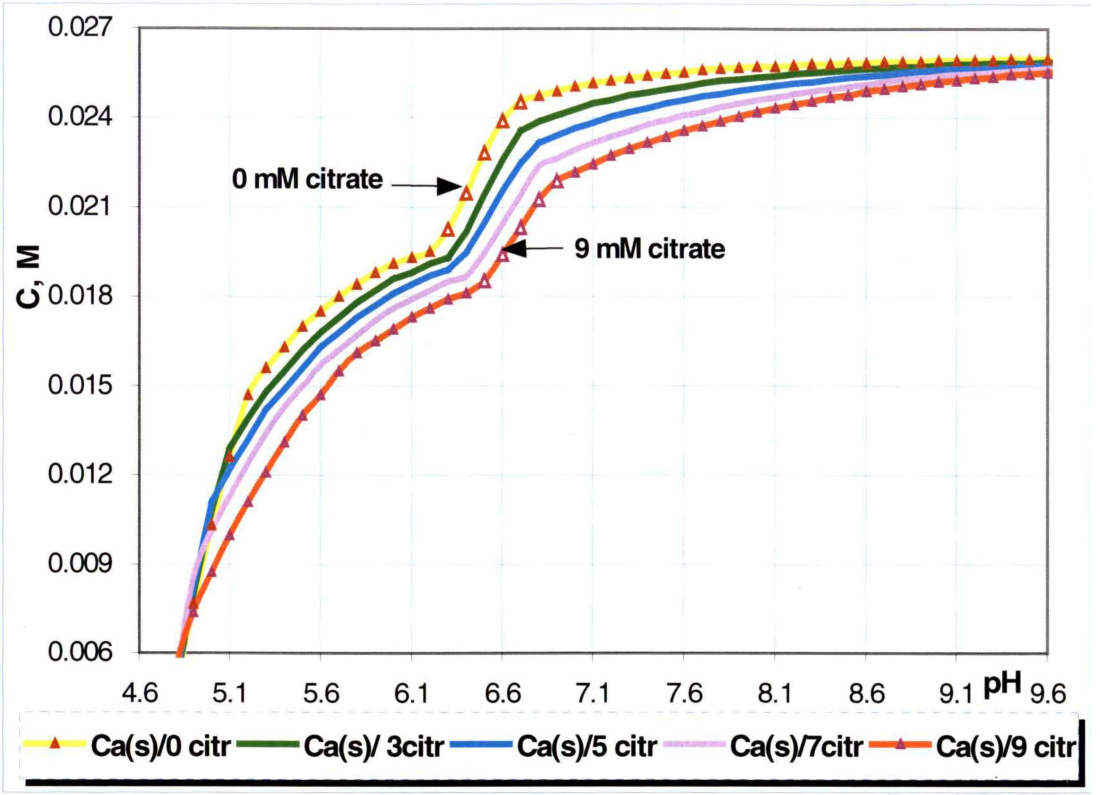

Figure 5-23: Impact of citric acid on the overall yield in the sulfuric acid whey permeate over the pH range 4.6-9.6.

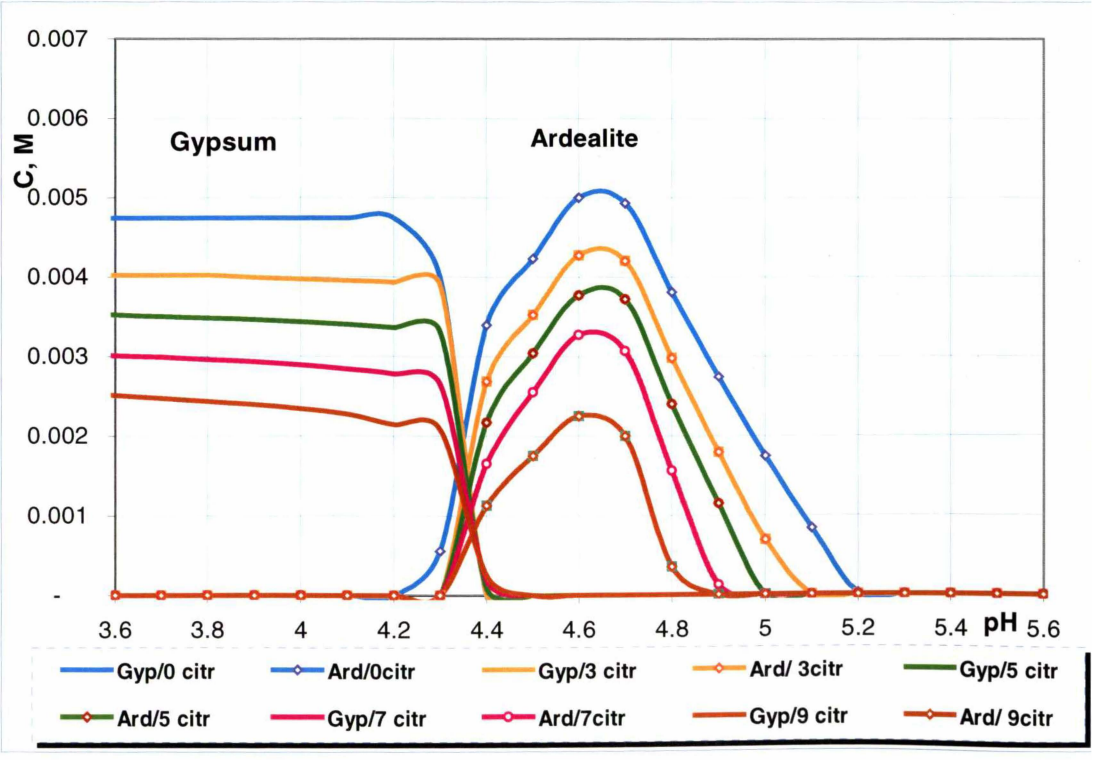

Figure 5-24: Impact of the citrate concentration on the Gypsum and Ardealite formation for a series of citrate concentrations from 0 mM to 9 mM over pH 3.6-5.6.

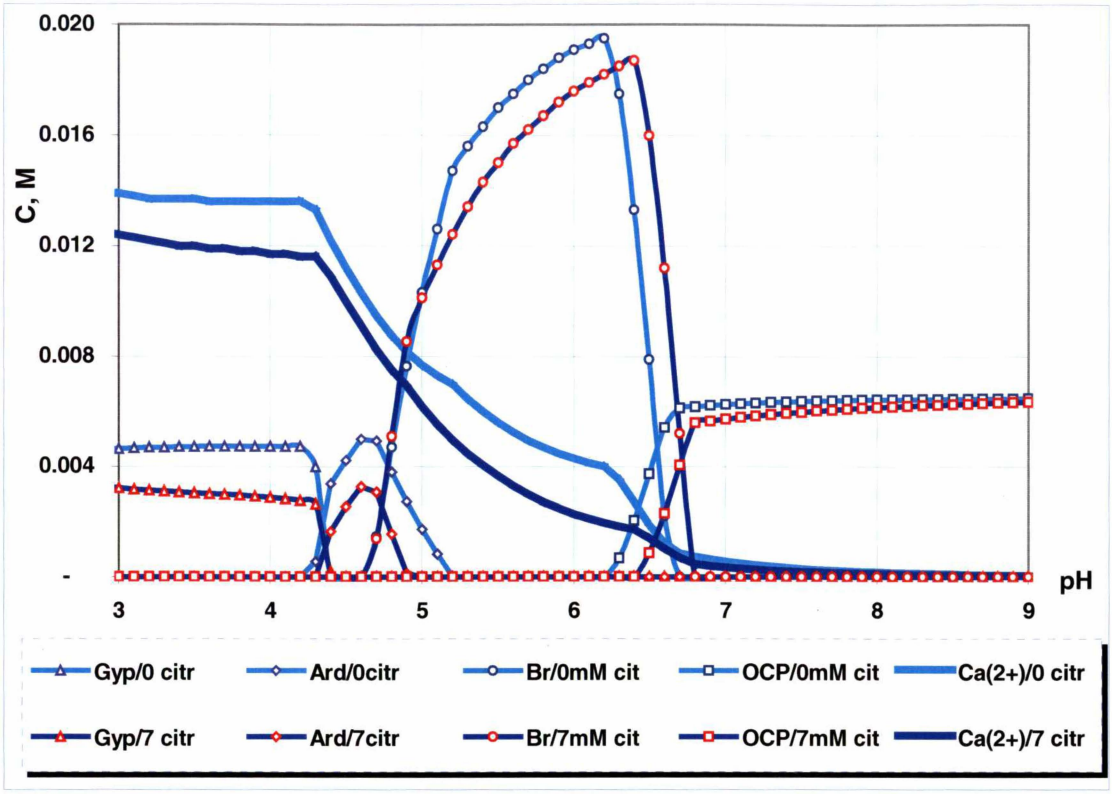

Figure 5-25: Comparison of the free Ca^{2+} level and solid formation (Gypsum-Ardealite-Brushite and Octacalcium phosphate) for the typical sulfuric acid whey permeate with 7 mM and without citrate.

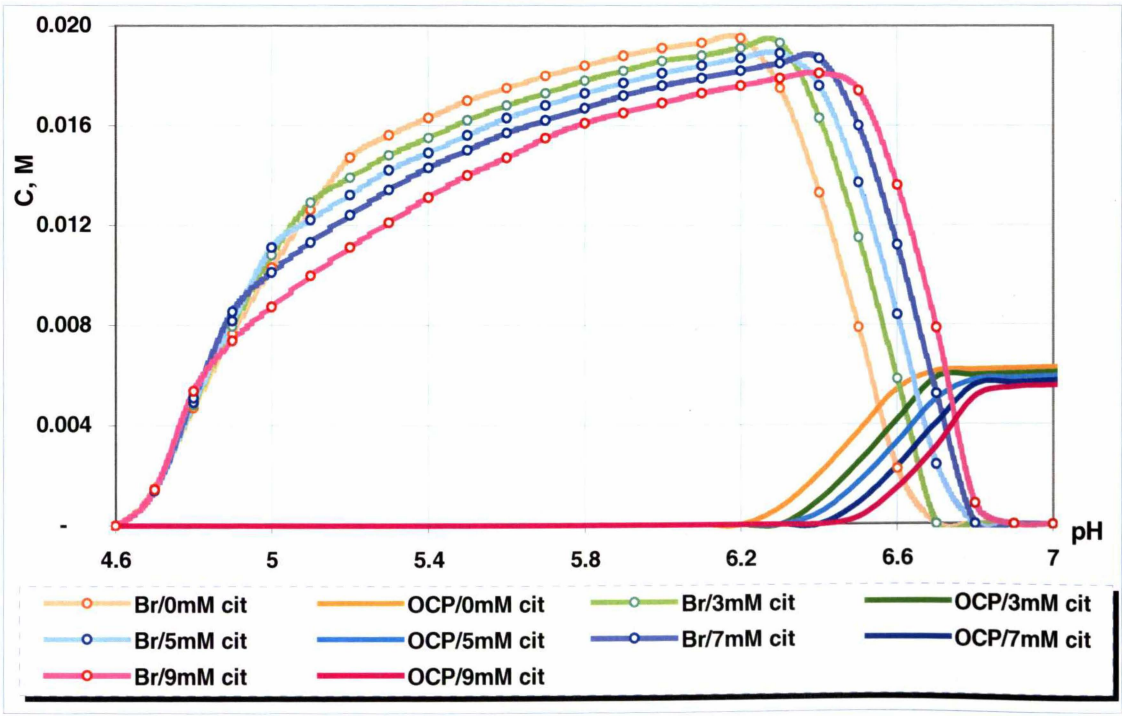

Figure 5-26: Impact of citrate concentration (0-9 mM) on the Brushite (Br) and Octacalcium phosphate (OCP) formation.

5.2.3(e) Impact of varying Ca:P Molar Ratios on the Precipitation of Calcium Phosphate

Figure 5-27 illustrates the concentrations of free calcium (Ca^{2+}) and sulfate (SO_4^{2-}) ion in the permeate as a function of pH and Ca:P molar ratio. The figures shows three sets of data pertaining to when the Ca:P molar ratio was set to 1.24:1 (typical level where calcium is in excess), 1:1 (equimolar amounts of calcium and phosphate) and 1:1.24 (phosphate in excess). Table 5-10 summarises the consequences of changing the Ca:P molar ratio on the levels of free calcium in the whey permeate. It can be seen that increasing the phosphate level with respect to the calcium level in the medium leads to a lower amount of free calcium remaining in the medium after precipitation. In effect, the increase in phosphate causes a more efficient utilisation of calcium in the precipitation process and hence leads to an increase in yield of precipitated solid (see Table 5-11). The level of free calcium remaining after precipitation is dependent on pH; higher levels of free calcium remain at lower pH values. For example, for a Ca:P molar ratio of 1:1.24, the level of free calcium remaining after precipitation at pH 6.4 is only 1.5% (of the total calcium present in the system, 26 mM) whilst at pH 6.8, the level of calcium remaining is only 1.0% of the total (see Table 5-10 and Figures 5-27 and 5-28 for clarification).

Table 5-10: Free Ca^{2+} content depending on the Ca:P molar ratio at pH 6.4, 6.6 and 6.8.

Ca:P molar ratio	% of total Ca^{2+} in system remaining in solution after precipitation			Absolute Ca^{2+} concentration, mM, after precipitation		
	pH			pH		
	6.4	6.6	6.8	6.4	6.6	6.8
1.24 : 1	6.7	4.0	1.8	1.73	1.03	0.47
1 : 1	3.1	2.5	1.6	0.79	0.66	0.42
1 : 1.24	1.5	1.2	1.0	0.40	0.31	0.26

Table 5-11: Overall Ca yield and Ca concentration depending on the Ca:P molar ratio over the pH 6.4, 6.6 and 6.8.

Ca:P molar ratio	Overall Ca (Brushite and OCP) yield (in % of max Ca yield (26 mM))			Overall Ca (Brushite and OCP) concentration in mM		
	pH			pH		
	6.4	6.6	6.8	6.4	6.6	6.8
1.24 : 1	71.9	78.5	86.1	18.7	20.4	22.4
1 : 1	81.5	83.1	86.5	21.2	21.6	22.5
1 : 1.24	86.5	88.1	89.6	22.5	22.9	23.3

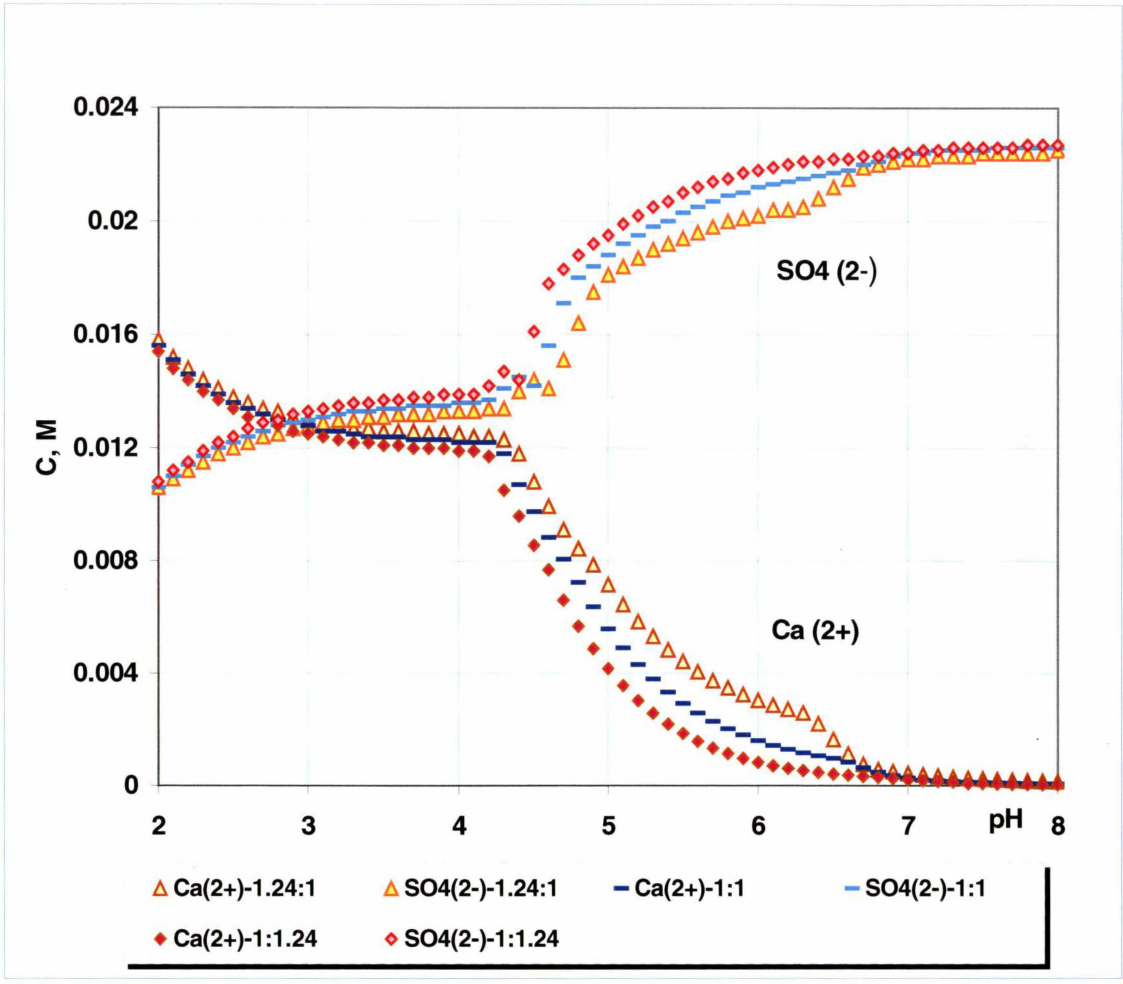

Figure 5-27: Distribution of free Ca^{2+} and SO_4^{2-} ions depending on the Ca:P molar ratio from 1.24:1 to 1:1.24 over the pH range 2 to 8 in the sulfuric acid whey permeate.

In general, these results show that phosphate ion is a limiting reagent in the precipitation of calcium phosphate from sulfuric acid whey permeates (as they are in lactic acid whey permeates), thus increasing the level of phosphate by artificial means may lead to the realisation of increased yields of solids.

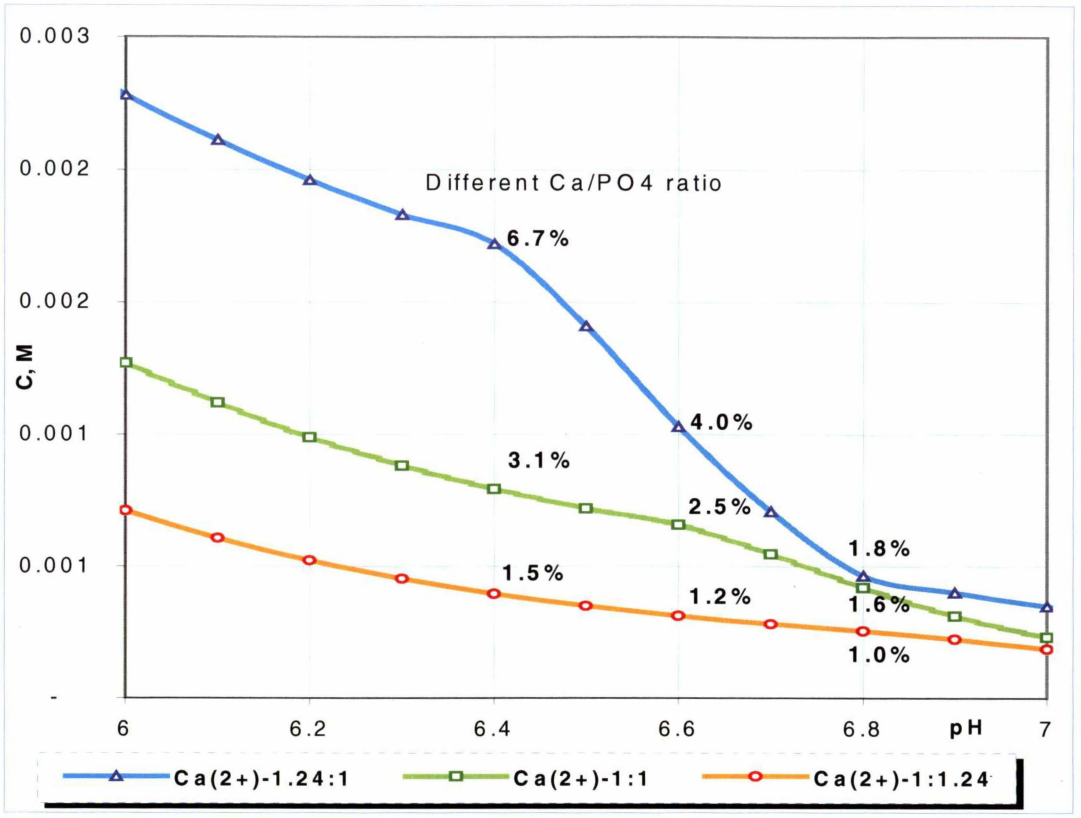

Figure 5-28: The effect of increasing Ca:P molar ratio on levels of free Ca^{2+} ions.

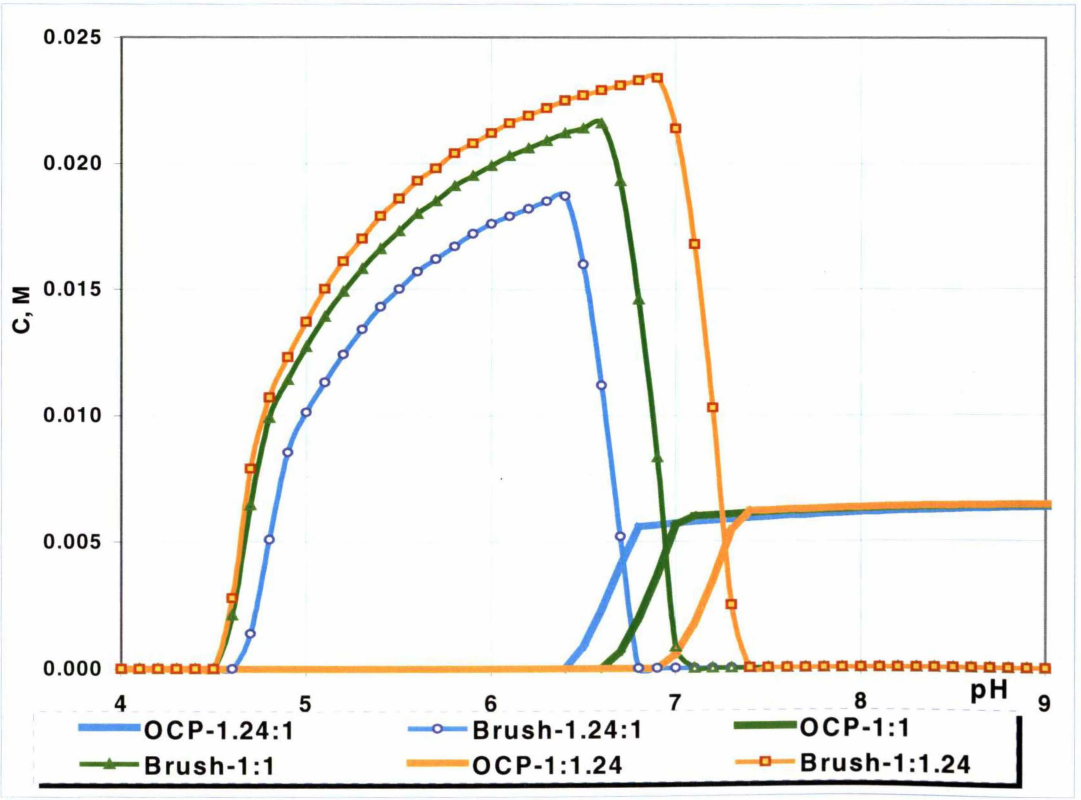

Figure 5-29: Impact of Ca:P molar ratio (from 1.24:1 to 1:1.24) on Brushite and OCP.

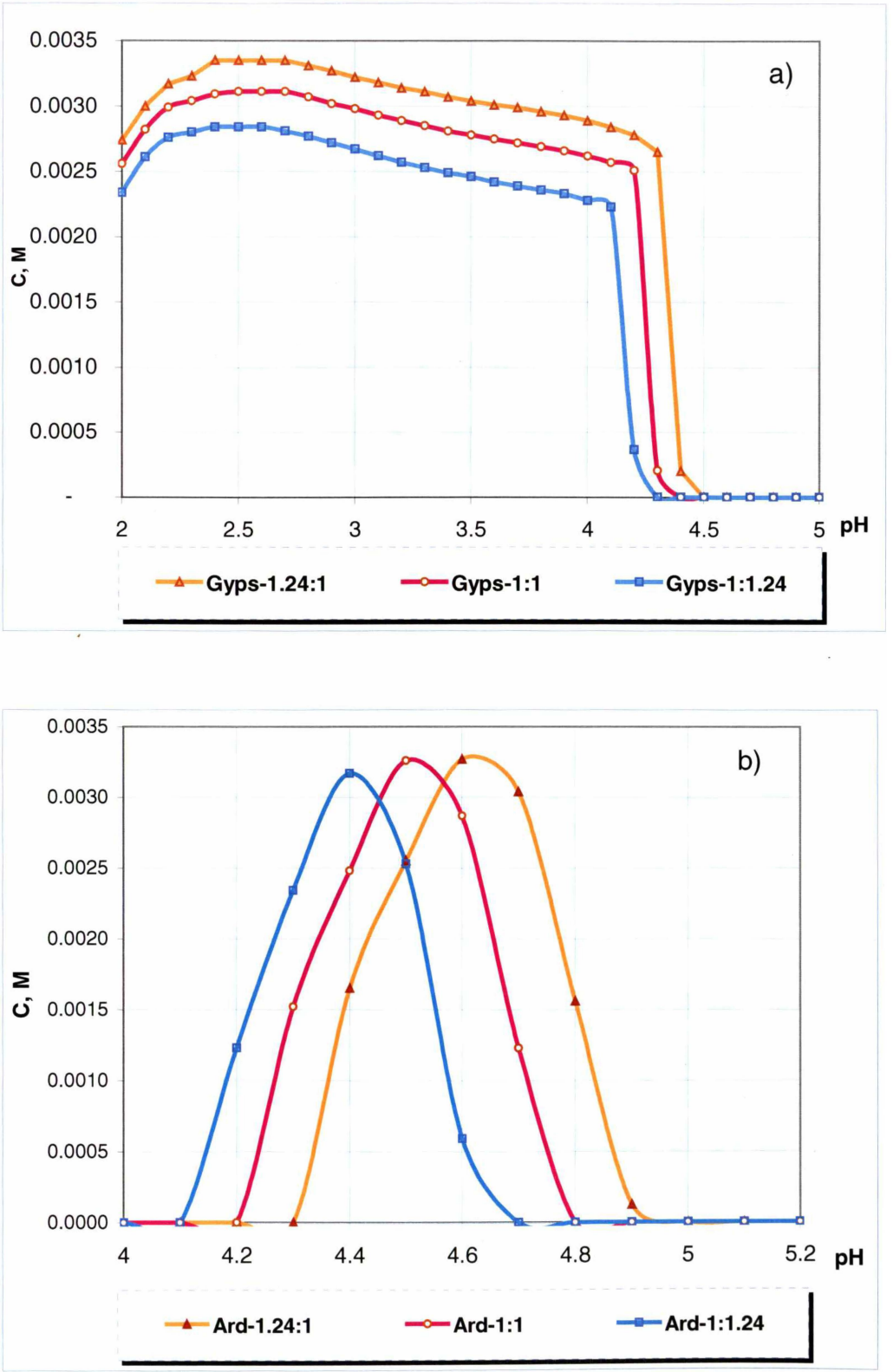

Figure 5-30: Influence of Ca:P molar ratio on: a) Gypsum and b) Ardealite formation. Ca:P molar ratios were varied from 1.24:1 to 1:1.24.

Other Interesting Effects Arising from Changes in the Ca:P Molar Ratio

(i) In general, an increase in phosphate concentration extends the pH stability region for brushite formation to higher pH and consequently delays OCP formation (*cf* the effect induced by higher citrate concentrations) (see Figure 5-29).

(ii) It is also quite evident that an increase in phosphate concentration in this system suppresses the formation of gypsum solid at lower pH (see Figure 5-30a).

(iii) Another interesting observation is that an increase in phosphate concentration in these system causes a shift in the hypothetical ardealite formation boundary to lower pH and narrows its pH region of stability (see Figure 5-30b).

(iv) It is also important to note that an increase in phosphate concentration in the system suppresses the formation of the small amount of calcium citrate solid ($Ca_3Cit_2.6H_2O$) formation.

5.2.3(f) *Impact of varying Sulfate Concentration on the Precipitation of Calcium Phosphate*

Figure 5-31 summarises the effects of different Ca:S molar ratios in the whey permeate on the distributions of precipitating solids in the pH range 3.5-7.5. In general, it is clear that there is a significant increase in the level of gypsum formation in the low pH range of 3.5-4.6. For instance at pH=4.0 the concentration of gypsum is 2.89 mM when a Ca:S molar ratio of 1.13 (which is the typical level in a mid-season whey permeate) is used, and is 5.47 mM for a Ca:S molar ratio of 0.91 (corresponding to late season permeate). In addition, the pH stability region of gypsum is extended to higher pH values when the sulfate concentration is increased in the medium.

It has been reported (Bohner et al., 1995) that an excess of SO_4^{2-} inhibits the formation of brushite which is confirmed in the calculations (see Figure 5-29a). There is also a concomitant increase in the concentration of the hypothetical ardealite compound as sulfate levels increase in the medium.

For example at a Ca:S molar ratio of 1.13:1, the pH region in which ardealite is expected to form is narrower (4.3-4.9) and at lower pH values and the concentration of

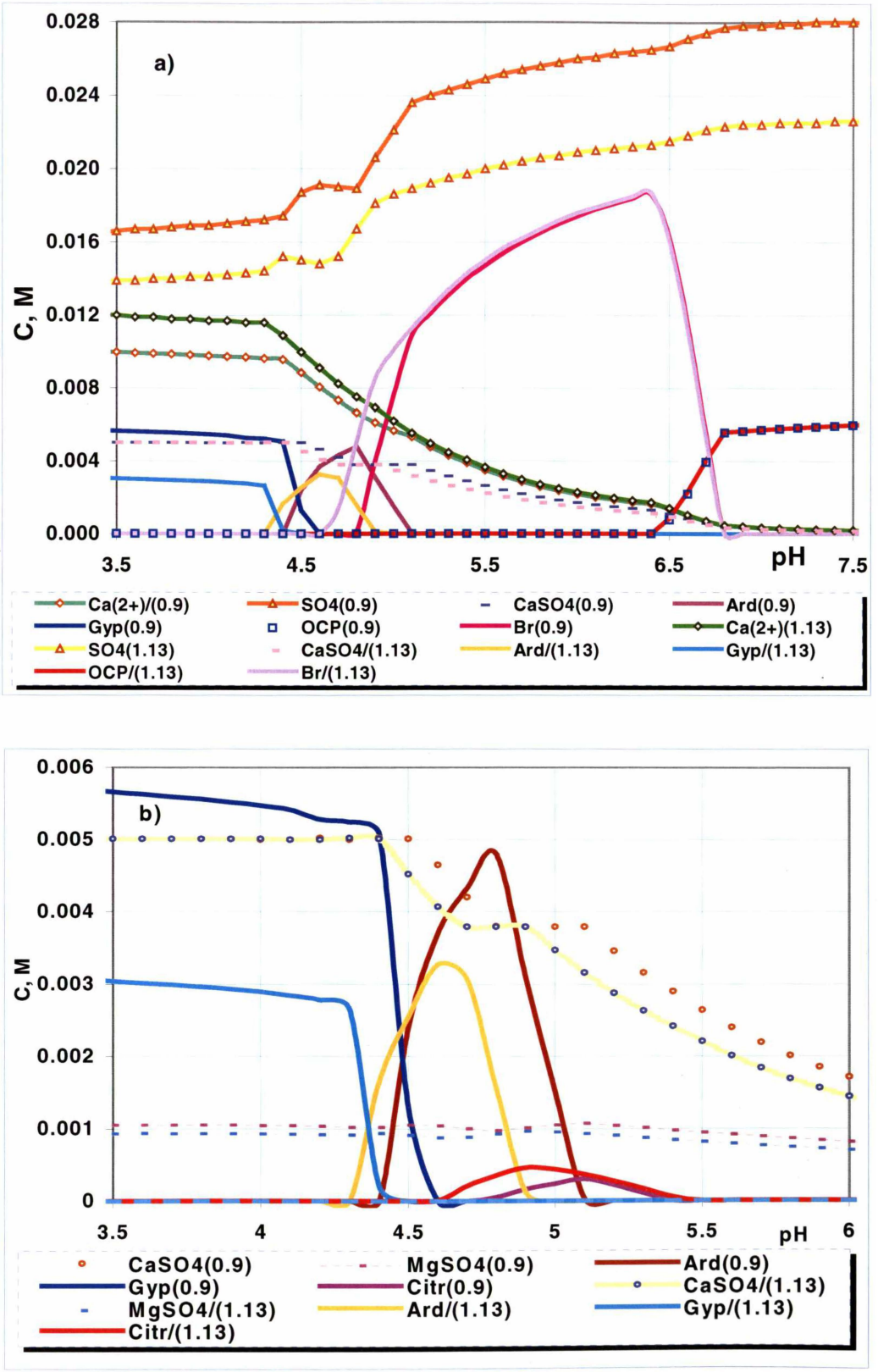

Figure 5-31: Distribution of ion and solid species depending on Ca:S ratio: a) main species and b) zoomed fragment, showing the formation of Gypsum, Ardealite, and Citrate ($Ca_3Cit_2.6H_2O$) as well as molecular $CaSO_4$ and $MgSO_4$ levels. The Ca:S ratio is indicated in brackets.

the compound is lower (3.27 mM maximum concentration achieved at pH 4.6) than at higher sulfate concentrations (Ca:S molar ratio of 0.9:1) where ardealite forms at higher pH and over a broader region (4.4-5.1). Moreover, it forms at higher concentrations (4.8 mM maximum concentration achieved at pH = 4.8). In addition, it was also found that increased sulfate levels suppress the formation of calcium citrate solid ($Ca_3Cit_2.6H_2O$) in the system (Figure 5-31b).

A Brief Word on Magnesium Speciation in the Sulfuric Acid Whey Permeate

It is of interest to discuss the speciation of magnesium in the whey permeate system as this element has some nutritional interest in the Dairy Industry. Figure 5-12b illustrates the fate of magnesium in the sulfuric acid whey permeate as a function of pH. The total magnesium in the typical sulfuric acid whey permeate is 3.45 mM. At very low pH (3-4), magnesium is present predominantly as free magnesium (Mg^{2+}) and the soluble, molecular ion-pair complex, $MgSO_4$, MgH_2Cit^+ and MgHCit complexes are also present but in minor amounts. After pH 4, the levels of Mg^{2+} and soluble $MgSO_4$ species start to fall due to the onset of formation of the $MgCit^-$ complex which increases significantly and reaches a maximum at pH 10. Thus, citrate is a major binding agent of free magnesium in the medium. The soluble magnesium levels as calculated by the SPE program are generally quite significant due to the fact that magnesium is not "formally" involved in any solid formation (in the SPE program input file). However, in reality, a small amount of magnesium does become incorporated into the hydroxyapatite crystal lattice by substitution for Ca^{2+} ions. Some interesting comparisons between lactic and mineral acid derived ALAMIN™ powders have been made with respect to magnesium levels determined by chemical analysis (see later). The kinetic role of magnesium in inhibiting the ACP precursor phase must also be considered in this permeate as in the lactic whey permeate. The SPE program does not take this into account since it does not "know" of the existence of either ACP or the ACP-Mg complex that forms in real-life precipitating solutions of calcium phosphate in the presence of magnesium ion. Due to time constraints, the development of a simulated sulfuric acid ultrafiltrate (SSWUF) buffer was not possible in order to test these trends predicted by the SPE program. However, some experimental evidence for the trends predicted was provided by IR spectra and ICP-OES analyses of the ALAMIN™ powders and whey permeates from the production process. These results are summarised in Chapter 6.

CHAPTER SIX

CHARACTERISATION OF WHEY PERMEATE AND ALAMIN™ POWDER FROM VARIOUS SOURCES

This chapter concentrates on studies in which commercial as received ALAMIN™ powder and its source whey UF-permeate from Kiwi Co-operative Dairies and Anchor Products Edgecumbe have been extensively characterised by a large suite of techniques. This was regarded as an important aspect of the overall research project because the chemical composition of actual whey permeate usually can vary considerably from batch to batch and from day to day and also from season to season. ALAMIN™ powder characteristics can also vary to an extent depending on the industrial conditions used and the nature of original whey UF-permeate. Industrially, this is crucial in that it sets a scientific standard and allows compilation of a range of "typical" data for the materials that can be used for reference.

6.1 Characterisation of the Commercial Lactic Whey Permeate and ALAMIN™ Powder by Chemical, Spectroscopic and Microscopic Techniques

6.1.1 Atomic Absorption Spectroscopy (AAS) Analysis of Ca Concentration in the Commercial Lactic Whey Permeate

Experimental. Initially, Flame Atomic Absorption Spectroscopy (GBC 909AA Spectrometer) was used to determine the concentration of calcium in samples of the commercial lactic acid whey permeate. Later elemental analyses made use of the more matrix-insensitive technique of ICP-OES (see 6.1.2: "Chemical Analysis of the Commercial Lactic Whey Permeate by ICP-OES"). AAS measurements were conducted using a GBC 909AA spectrometer employing an air-acetylene flame housed in the Chemistry Department. Calibration standard solutions of 5, 10, 15, 20, and 30 ppm Ca^{2+} were prepared by dilution using deionised water of a pre-supplied BDH analytical grade $CaCl_2.2H_2O$ (Ca^{2+}concentration=1000 ppm) stock solution. To each standard solution 4 mL of 0.125 M Na_2-EDTA solution was also added prior to analysis to reduce the well-known AAS interference caused by calcium phosphate formation in the flame. The typical dilution of whey permeate samples was 1:100 (or 1:50) using deionised water. 4 mL of 0.125 M Na_2-EDTA solution was also added to the whey permeate samples. Samples were then aspirated into the air-acetylene flame and the

concentration of calcium measured by measurement of the absorbance at wavelength = 422.7 nm. In the instrument, the absorbance readings (mean absorbance) for each sample were taken as three replicates and the results averaged. The calibration plot for the standards is shown in Figure 6-1:

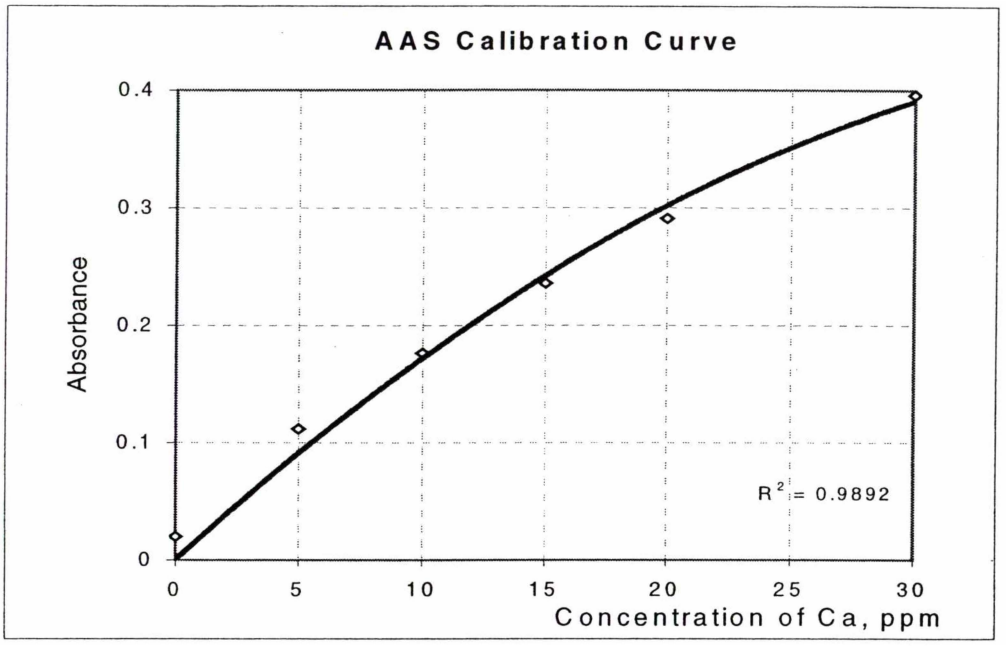

Figure 6-1: The AAS calibration plot for the standard solutions with varying Ca^{2+} concentration (0-30 ppm).

Results. The mean AAS absorbance for the diluted (1:100) commercial lactic whey permeate (as received from proprietary process on 14.05.98) sample was found to be 0.208 (mean between 0.208, 0.203 and 0.213). After accounting for dilution, this corresponds to a Ca^{2+} concentration of 1175 ppm (i.e. *ca.* 1.2 g L^{-1}). The second AAS measurement for the same the lactic whey permeate, diluted 1:100, carried out 1 week later, shows a Ca^{2+} concentration of 1179 ppm (i.e. *ca.* 1.2 g L^{-1}). The mean AAS absorbance for diluted (1:50) lactic whey permeate (as received on 26.06.98) sample was found to be 0.337 (mean between 0.338, 0.339 and 0.335). After accounting for dilution, this corresponds to a Ca^{2+} concentration of 1209 ppm (i.e. *ca.* 1.2 g L^{-1}). This is in good agreement with later ICP-OES analyses of lactic whey permeate (see 6.1.2: "Chemical Analysis of the Commercial Lactic Whey Permeate by ICP-OES"). AAS studies were also carried out on whey permeate serum (filtrate after separation of the solid) samples after stimulating calcium phosphate precipitation with the addition of sodium hydroxide solution. The results of these are summarised in Chapter 7.

6.1.2 Chemical Analysis of the Commercial Lactic Whey Permeate by ICP-OES

It was decided to follow up the AAS- studies on the whey permeates by performing ICP-OES analyses. ICP-OES as described in Chapter 3 (see 3.9: "Inductively Coupled Plasma (Optical Emission Spectroscopy/Mass) Spectroscopy (ICP-OES/MS)") is an elemental analysis technique which is freer of sample matrix complications than AAS. Given the sample matrix for whey permeates is quite complex and that no attempt was made to match it synthetically in the calcium ion standards prepared for calibration for the AAS studies, it was decided to repeat elemental determinations using ICP-OES to check on the authenticity of the results from AAS. From an analytical point of view, ICP-OES is thus far superior and can, moreover, carry out multiple analyses of various elements other than Ca such as Mg, P, Na and K in the commercial lactic acid whey permeate.

Experimental. ICP-OES studies were conducted using a range of instruments. Initial studies were carried out by commissioning outside laboratories (Hill Laboratories Ltd, Hamilton and AgResearch Soil Fertility Service, Ruakura Research Centre, Hamilton) to run samples sent to them, by using ICP-OES and AAS methods. In the latter stages of this project, the University of Waikato Chemistry Department acquired a radial configuration GBC OPTIMA3000 (Perkin-Elmer, Norwalk, CT USA) ICP-OES, which was used to repeat studies carried out using AAS (see section 6.1.1) as well as samples that had been sent off to outside laboratories (see Appendix A1). The work reported in this section is derived from use of the GBC OPTIMA 3000 and used the following parameters for ICP-OES analyses (see Tables 6-1 and 6-2).

Table 6-1: ICP-OES parameters for all ion determinations.

Parameters	Data
Plasma height (mm)	6.0
Nebuliser flow (L min^{-1})	0.5
Pump (rpm)	10.0
Power (W)	1200
PMT (volts)	600
Auxiliary gas flow (L min^{-1})	0.5
Plasma gas (L min^{-1})	10.0
Replicates	3

Table 6-2: Characteristic wavelengths, used for the ICP-OES measurements.

Element	Wavelengths (nm)
Ca	422.6
Mg	285.2
K	766.5
Na	588.9
P	177.5

The calibration standard solutions were prepared by dilution of the appropriate stock solutions with deionised water. Calibration of the instrument required the preparation of only two standard solutions with the following concentrations for the element in question: 50 and 2.5 ppm (Ca), 50 and 5 ppm (K), 5 and 0.5 ppm (Mg), 20 and 2 ppm (Na), 100 and10 ppm (P). Standard solutions were prepared by dilution of stock $Ca(NO_3)_2$ (1000 ppm), K_2CO_3 (10000 ppm), $Mg(NO_3)_2$ (1000 ppm), Na_2CO_3 (10000 ppm) and $(NH_4)H_2PO_4$ (10000 ppm) solutions. These standards were in turn referenced against accepted reference materials obtained via the Laboratory of the Government Chemist (UK), viz., GBW08501 (Peach Leaves) and GBW08509 (Milk Powder) by ICP-OES. The concentration deviation for all standards solutions against the standard reference material concentrations was ± 0.1%.

Lactic acid whey permeate samples were prepared by diluting 2 mL of an as received lactic acid whey permeate sample to 100 mL by using deionised water. ICP-OES analyses were made on the commercial lactic whey UF-permeate (as received on 3.03.2000).

Results. Table 6-3 (column 1) represents the ICP-OES data obtained for the commercial lactic whey permeate. For comparison, Table 6-3 (column 2) contains data for the commercial lactic whey permeate that had extra UF treatment to remove proteins. The ICP-OES measurements show that Ca, Mg, Na, K, and P concentrations in this commercial lactic whey permeate batch are as follows: Ca concentration is 1.210 g L^{-1} (30.2 mM), Mg concentration is 0.1030 g L^{-1} (4.2 mM) and P concentration is 0.716 g L^{-1} (23.1 mM). The concentration of Na and K is 0.319 g L^{-1} (13.9 mM) and 1.577 g L^{-1} (40.3 mM) respectively:

Table 6-3: ICP-OES data of the chemical composition for a typical commercial lactic whey permeates. Data from three replicate measurements plus the average of these are given.

Lactic whey permeate			Lactic whey permeate, extra UF treated		
Ca concentration			Ca concentration		
ppm	g L^{-1}	g L^{-1} average	ppm	g L^{-1}	g L^{-1} average
1192.00	1.192		1150.38	1.150	
1227.05	1.227	1.210[1]	1162.52	1.162	1.155[1]
1212.36	1.212		1154.35	1.154	
1311.78	1.312		1131.37	1.131	
1171.53	1.172		1113.57	1.113	
1233.43	1.233	1.238[2]	1146.55	1.146	1.131[2]
1238.29	1.238				
Mg concentration			Mg concentration		
101.88	0.1018		103.12	0.1031	
103.12	0.1031	0.1030[1]	100.86	0.1008	0.102[1]
104.21	0.1042		100.70	0.1007	
K concentration			K concentration		
1537.70	1.537		1389.49	1.389	
1579.63	1.579	1.577[1]	1376.02	1.376	1.367[1]
1614.75	1.614		1385.88	1.385	
Na concentration			Na concentration		
311.01	0.311		301.17	0.301	
323.10	0.323	0.319[1]	280.33	0.280	0.289[1]
323.77	0.324		287.05	0.287	
P concentration			P concentration		
723.14	0.723		683.57	0.683	
711.34	0.711	0.716[1]	670.23	0.670	0.670[1]
714.98	0.714		658.99	0.658	

1 Analyses were made on 22.03.2000;
2 Analyses were made on 9.03.2000.

In general, the ICP-OES determined values for calcium ion are in agreement with those determined by AAS (see section 6.1). It is interesting to note that lactic whey permeate Cas-1 starter, extra UF treated (see Table 6-3, column 2) exhibits lower concentrations of the all elements Ca, Mg, Na, K and P elements in comparison with the lactic whey permeate not subjected to the extra UF treatment. This implies that the extra UF treatment to "polish" the lactic whey permeate (i.e. by removing extra whey protein) is leading to the removal of a small amount of salts possibly by association of, for instance, calcium ions with the removed proteins.

6.1.3 Electrospray Mass Spectrometric Analysis (ESMS) of the Commercial Lactic Whey Permeate

Electrospray Mass Spectrometry (ESMS) was considered as a novel *in situ* technique for characterising the inorganic and organic components present in the commercial lactic whey permeate before and after the precipitation of calcium phosphate. In this section, the ESMS spectrum of the source whey permeates alone will be discussed. Chapter 7 will describe ESMS studies of the lactic whey permeate after CaP precipitation.

Exprimental. ESMS analyses were carried out using a VG Platform II mass spectrometer. Control of the ESMS system was by a computerised MassLynx^{TM} data system. Preparation of the sample was relatively simple. A drop of fresh lactic whey permeate was placed into a test tube and mixed with *ca.* 5 drops of a 50% aqueous solution of acetonitrile. The sample solution was then injected into an HPLC column via a 10 μL loop. The sample flow rate through the column was 0.02 mL min^{-1} before it passed through to the nebuliser electrospray cone. The applied cone voltage was ± 25 V, depending on the ion mode of detection selected (see section 3.7: "Electrospay Mass Spectrometry (ESMS)" for theoretical details relating to this technique).The spectrum was then allowed to acquire for 1-2 minutes before it was presented as a plot of intensity versus mass/charge (m/z). Both positive and negative ion mode spectra were acquired.

Results. The *negative ion mode* ESMS spectrum (at –25 V) of the commercial as received lactic whey permeate is shown in Figure 6-2. A peak at m/z 89.3 was assigned to the presence of *Lactate*$^{-}$ ion. The peak at m/z 137.3 consisted of a mixed solvent-species peak (these are common in ESMS and are a result of ion-solvent combination in he cone and are in no way representative of bulk solution species) which was assigned

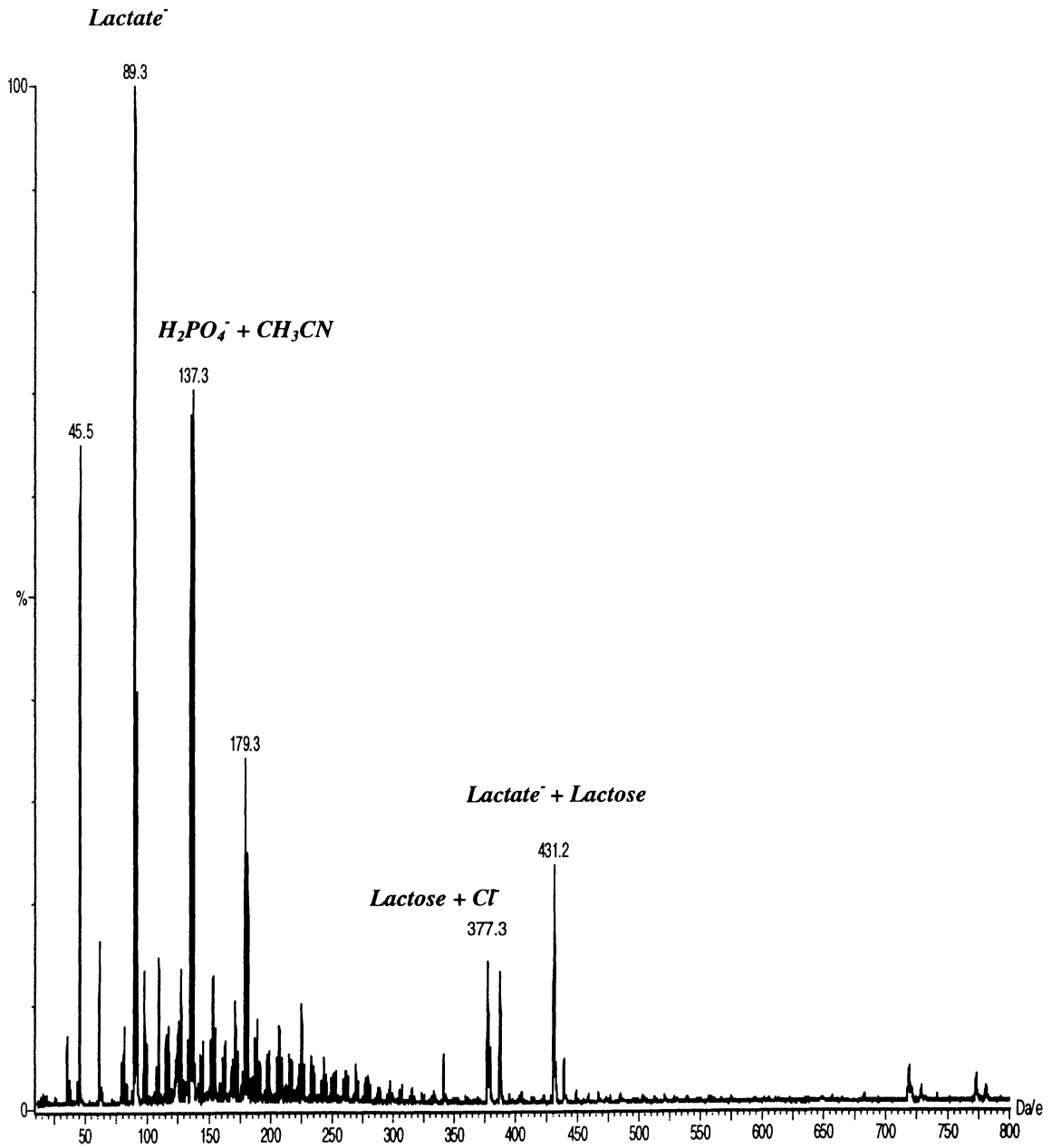

Figure 6-2: Negative ion mode ESMS spectrum (-25 V) for the commercial as received lactic whey UF-permeate.

to a $H_2PO_4^-$ + CH_3CN combination. Other weak peaks at m/z 377.3 and 431.2 were assigned to ion combinations of *Lactose* + Cl^- and *Lactose* + *Lactate*$^-$ respectively.The *positive ion mode* ESMS spectrum (at +25 V) of the commercial as received lactic whey permeate (obtained 3.11.99) is given in Figure 6-3. The peak at m/z 39.3 and 80.2 is representative of the potassium ion present in the lactic whey permeate since it corresponds to K^+ and the K^+ + CH_3CN ionic species respectively. A peak at m/z 143.3 was tentatively assigned to an ion combination corresponding to *Lactic acid* $+2H_2O+H_3O^+$. More minor peaks at m/z 362.3 and 381.1 are due to the combinations of *Lactose* + Na^+ and *Lactose* + K^+ ion species respectively.

A very weak peak at m/z 18.7 (z = 2) was thought to correspond to the Ca^{2+} ion although this assignment is a little tenuous (Figure 6-4). A peak at m/z 23.5 can be confidently assigned to the presence of Na^+ ion in the lactic whey permeate.

Discussion. Thus from the positive and negative ion mode of the ESMS spectra, the presence of calcium, magnesium, potassium, and sodium could be deduced. *Lactose* along with the moderate levels of *Lactate*$^-$ ion, were also important features in the commercial lactic whey permeate. When ESMS spectra of the samples of commercial lactic whey permeate from different batches (as received on 16.06.98 and 3.11.99) were compared, some differences in the intensities of peaks associated with *Lactate*$^-$ and *Lactose* were noted. The most recent batch (as received on 3.11.99) of lactic whey permeate featured a relatively stronger peak at m/z 89.3 due to *Lactate*$^-$ and a relatively weaker peak at m/z 377.3 due to *Lactose* compared to the samples (as received on 16.06.98) of the commercial lactic whey permeate which were discussed and illustrated above. Although this technique is qualitative in nature with some caution needed in interpreting spectra and relative ion intensities, these results suggest that lactic whey permeate sample (batch from 3.11.99) exhibited a higher conversion of *Lactose* to *Lactate*$^-$ in the states of the samples when they were examined by ESMS. Whether this was a result of the original starter bacteria or a result of further bacterial degradation in the permeate on standing before analysis is difficult to ascertain. It, however, shows one possible application of ESMS (after future work has been carried out to investigate quantitation by this technique) to determine the degree of *Lactose* to *Lactate*$^-$ conversion in individual whey permeate samples. Other studies relating to the use of ESMS in following changes in the whey permeate as a result of precipitation of calcium phosphate are described in Chapter 7.

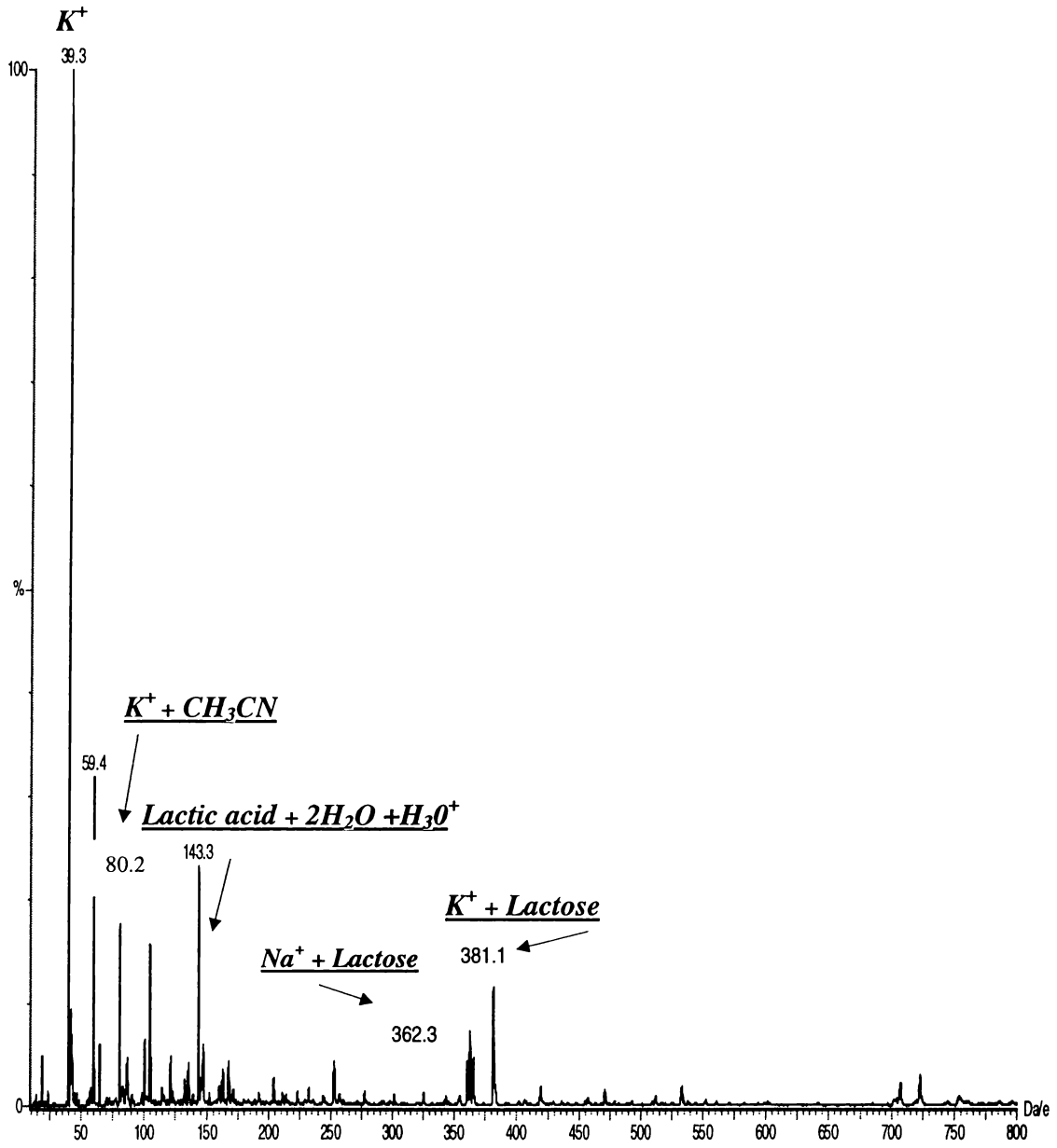

Figure 6-3: Positive ion mode ESMS spectrum (+25 V) for the commercial as received lactic whey UF-permeate.

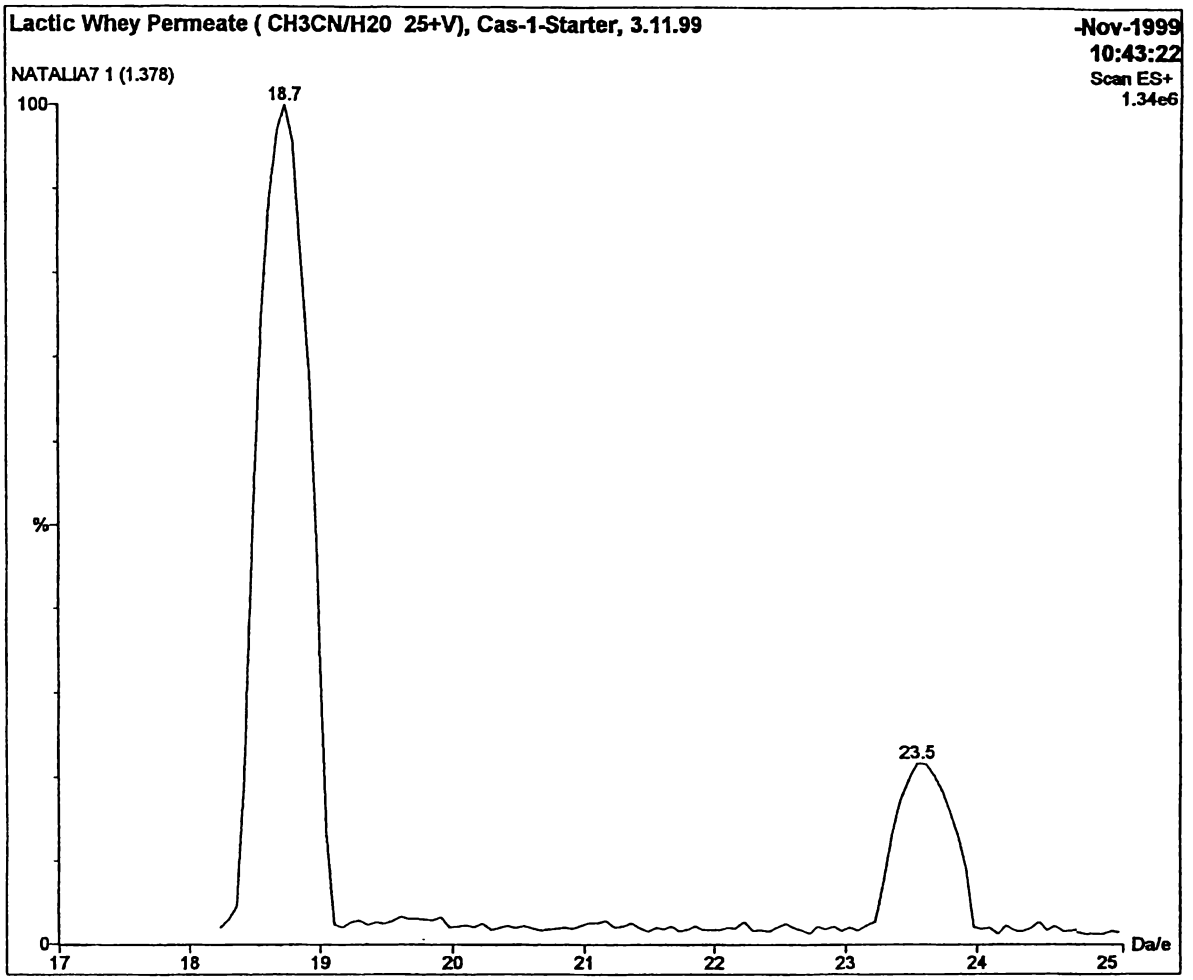

Figure 6-4: Expansion of positive ion mode ESMS spectrum (+25 V) region from m/z 17 to 25 for the commercial as received lactic whey UF-permeate.

6.1.4 Fourier Transform Infrared Spectroscopy (FTIR) Analyses of the Commercial ALAMIN™ Powder, produced from Lactic Whey Permeate

FTIR Spectroscopy was found to be an important technique for the characterisation of ALAMIN™ and other calcium phosphate solids generated or received for study in this project as it gave valuable information with regard to phase compositions and impurities in the calcium phosphate powders investigated (see Chapter 4).

Experimental. FTIR spectra of the different commercial grades of the commercial ALAMIN™ powder were recorded as KBr (oven dried BDH grade) discs. The disks were prepared by grinding a few mg of sample in an agate mortar and pestle and then adding oven dried KBr followed by further grinding and pressing at 5-7 tons on a disk press to produce semi-transparent disks. Spectra of the disks were obtained using a Digilab FTS-40 FTIR Spectrometer. 16 scans were acquired between 4000-400 cm^{-1} at 4 cm^{-1} resolution.

Results. The typical FTIR spectra for calcium phosphate solids have already been covered in previous Chapter 4 (section 4.5: "Fourier Transform Infrared Spectroscopy (FTIR) Analysis of the CaP Precipitates obtained from the SLWUF Buffers"). As has been noted in this chapter the final precipitate, obtained from the "standard" SLWUF buffer, has an FTIR spectrum which is practically identical to that expected for semi-crystalline apatitic calcium phosphate. For purposes of comparison, the FTIR spectra of the commercial ALAMIN™ powder (in the region 4000-400 cm^{-1}) will be formally described. In general, five major peaks can be identified (see Figure 6-5) which have been assigned as follows:

6.1.4 (a) Assignment of Peaks in the 500-1200 cm^{-1} Region

Peak 1 is a split band at 562 and 601 cm^{-1} and can be assigned to the ν_4 (O-P-O) bending vibration of the PO_4^{3-} unit. *Peak 2*, is an intense peak with some structure at 1032 and 1099 cm^{-1} corresponds to the ν_3 (P-O) asymmetric stretching vibration of the PO_4^{3-} unit (Elliot, 1994). Both *Peak 1* and *Peak 2* are fundamental vibrations of the PO_4^{3-} unit and are at values consistent with semi-crystalline hydroxyapatite when it is compared with an FTIR spectrum of pure *Fluka*-brand hydroxyapatite (Figure 6-6). The ALAMIN™ FTIR spectrum differs from the FTIR spectrum of hydroxyapatite because it does not

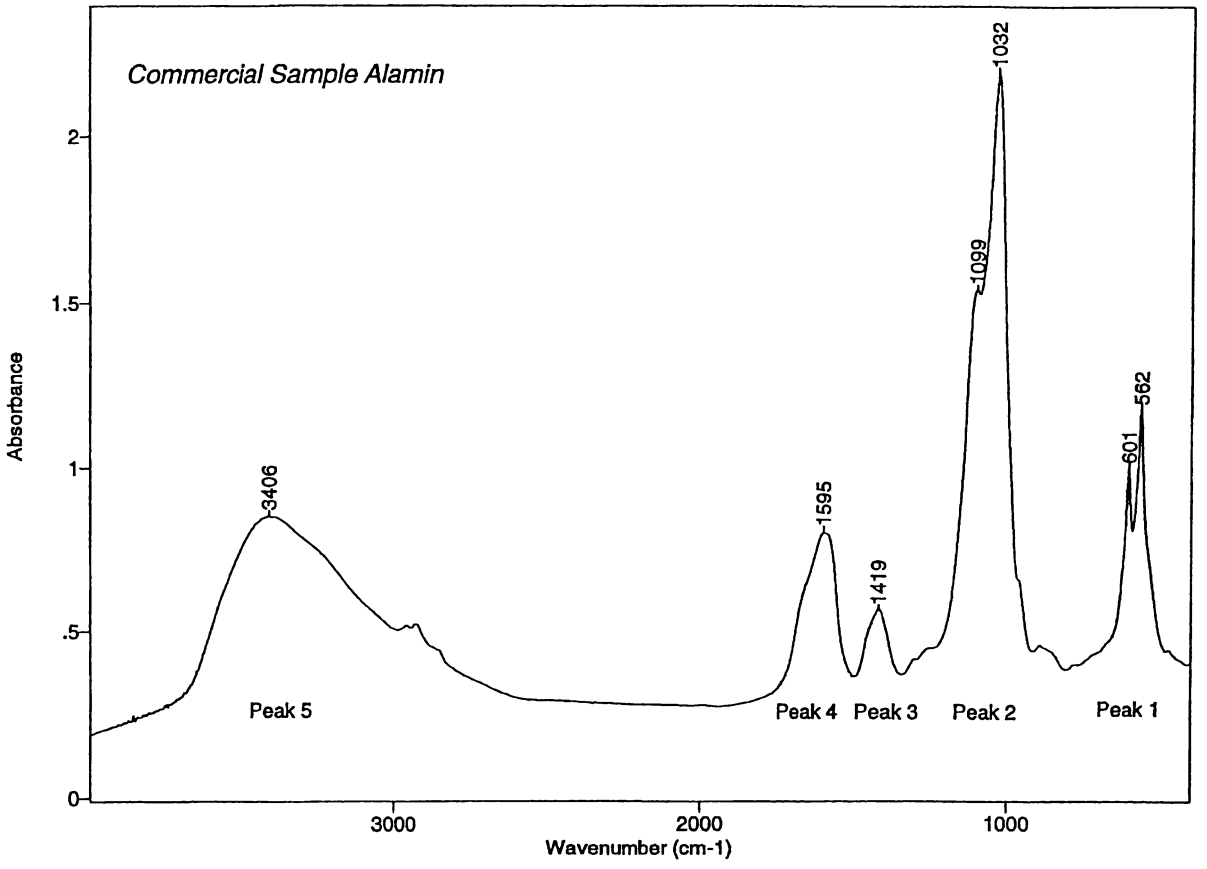

Figure 6-5: FTIR spectrum of the typical commercial lactic ALAMIN™ powder.

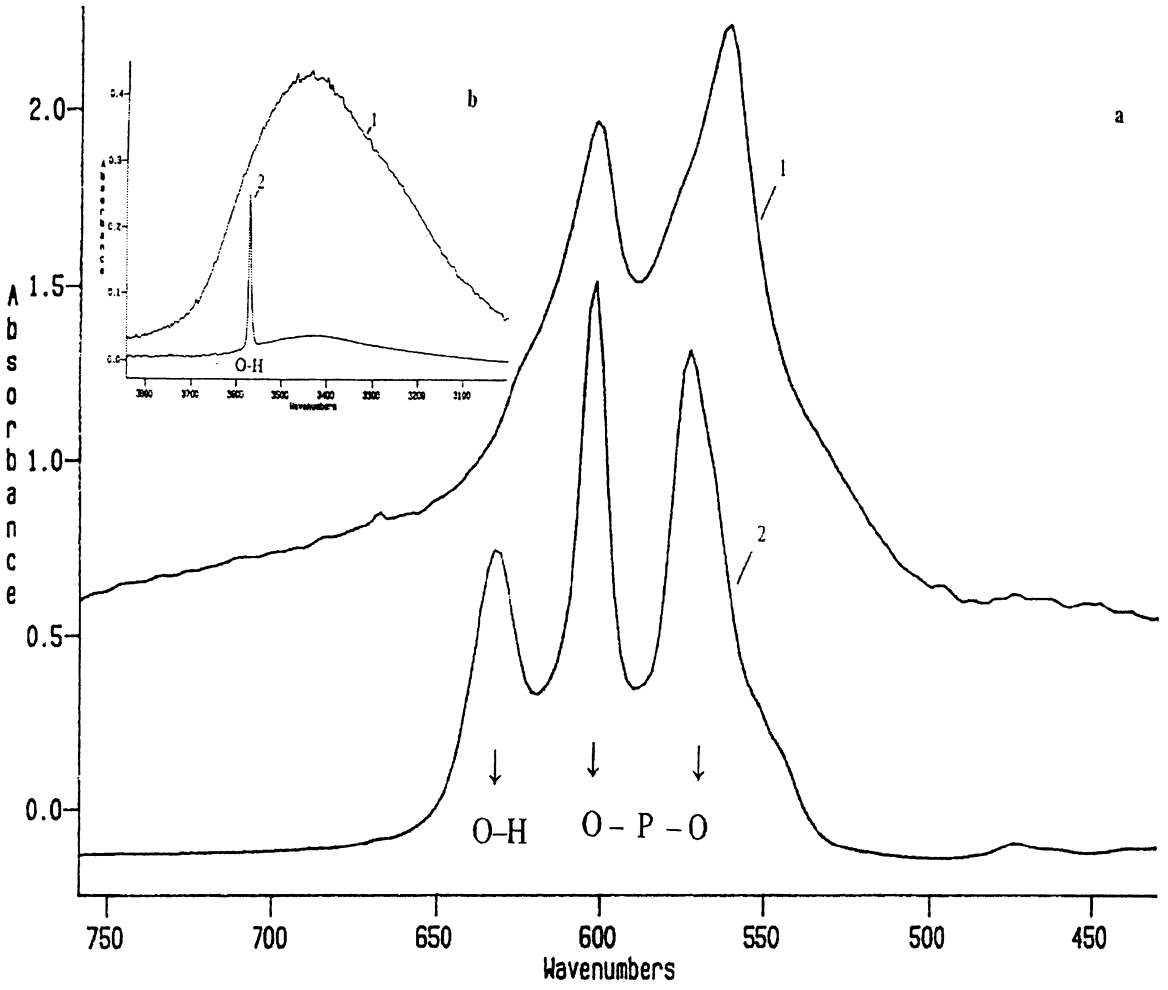

Figure 6-6: Comparison of the FTIR spectra of commercial lactic ALAMIN™ powder (1) with *Fluka*-brand hydroxyapatite (2): a) region showing "Peak 1" and b) (inset) region showing "Peak 5" (see Figure 6-5).

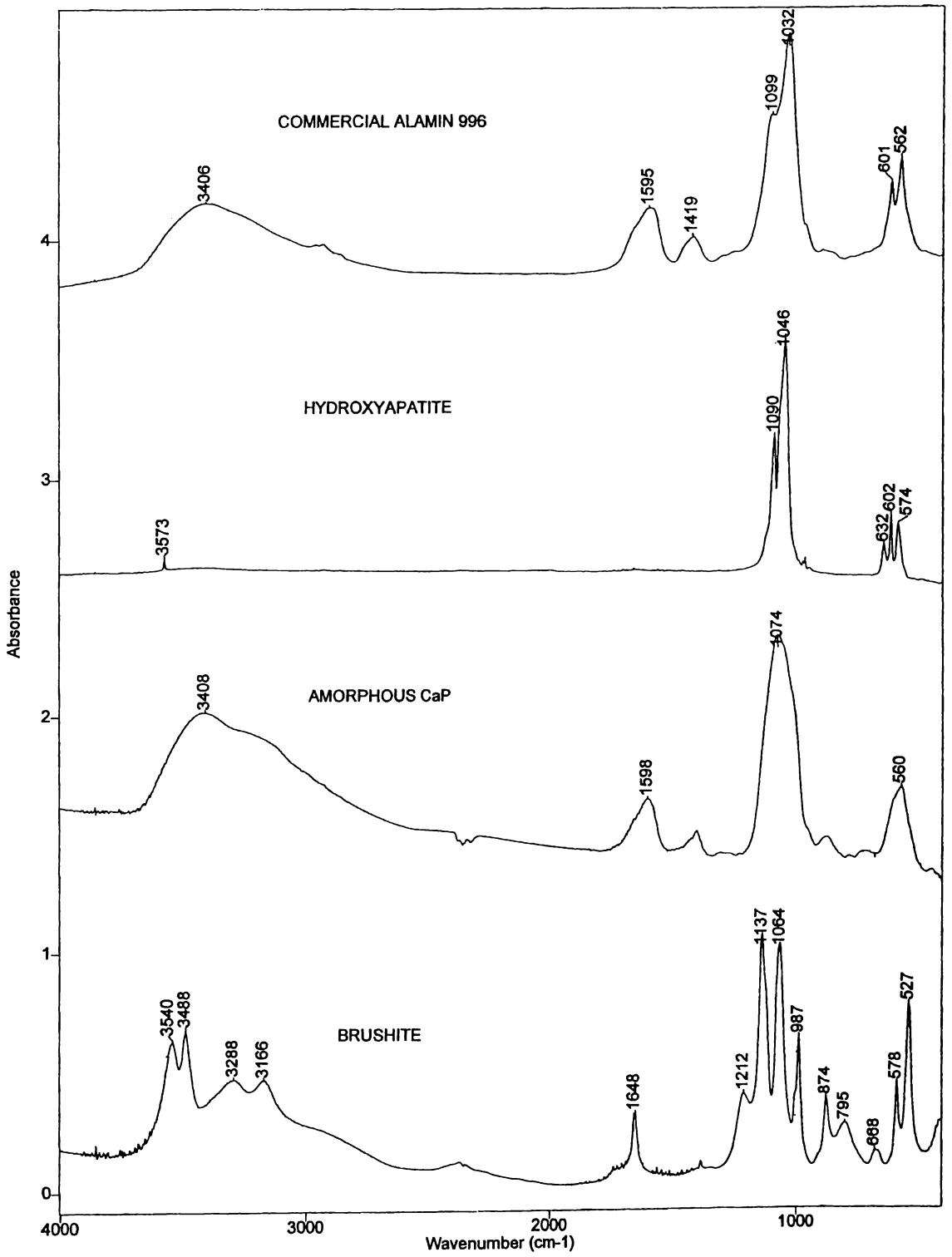

Figure 6-7: FTIR spectra of the typical commercial lactic ALAMIN™ powder and different calcium phosphates.

contain a sharp peak at 3572 cm^{-1} due to ν (O-H) stretching from the hydroxyl group contained in hydroxyapatite (see Figure 6-6). The absence/reduced intensity of the 3572 cm^{-1} ν (O-H) stretching peak in ALAMIN™ FTIR spectrum is correlated with a similar absence/reduced intensity of a peak at 632 cm^{-1} appearing on the shoulder of the peaks at 562 and 601 cm^{-1} which is known to be due to an OH vibrational mode (Elliot, 1994). The absence of the OH peak in the ALAMIN™ FTIR spectrum can be generally attributed to the semi-amorphous state of the apatitic phase comprising the ALAMIN™ sample.

6.1.4(b) Assignment of other Non-phosphate related Peaks in the 4000-1300 cm^{-1} Region

A broad and sometimes intense peak observed at 3406 cm^{-1} (*Peak 5*, Figure 6-5) in ALAMIN™ FTIR spectra is the O-H stretching mode of water (moisture) contained in the sample. This peak is always accompanied by a sharper peak at 1595 cm^{-1} (*Peak 4*, Figure 6-5) which is due to H-O-H bending vibration. These peaks are always detected in ALAMIN™ powders which have not been completely dried or which have been exposed to moist air especially if there is protein contained in the ALAMIN™ (see later) which has a tendency to retain water. It has to be mentioned that the 1595 cm^{-1} band is much broader than can be expected if water was contributing to it alone and is hence due to other species present in the ALAMIN™ powder (to be explained later). These other species are responsible for the other unassigned peaks in the ALAMIN™ FTIR spectrum (Figures 6-5 and 6-7). *Peak 3* at 1419 cm^{-1} was initially thought to be carbonate incorporated in the hydroxyapatite lattice given the ease with which this ion can enter the HAP lattice on the basis of earlier reports (Elliott, 1994). However the absence of the 812 cm^{-1} peak (a bending mode of carbonate) proved that it cannot be due to carbonate and suggests some other species is present. In general, it has already been demonstrated in the SLWUF FTIR studies (see section 4.5: "Fourier Transform Infrared Spectroscopy (FTIR) Analysis of CaP Precipitates obtained from SLWUF Buffers") that a partial contributor to this peak is a vibrational mode due to citrate (which also partially contributes to the 1595 cm^{-1} peak). Chronologically this revelation about citrate (as well as protein) being partial contributors to the 1419 cm^{-1} and 1595 cm^{-1} peaks was made on the basis of additional FTIR characterisation work (done prior to the SLWUF IR work which confirmed the revelation about citrate and protein) that was carried out on pure compounds reasoned to be components in the ALAMIN™, viz., citrate salts, lactose, lactate and some whey proteins. FTIR spectra of all these solids were recorded as KBr (oven dried BDH grade) disks.

Figure 6-8 shows the comparison of the FTIR spectra of the citrate salts: tri-sodium citrate dihydrate ($Na_3Cit.2H_2O$) and tri-calcium dicitrate tetrahydrate ($Ca_3Cit_2.4H_2O$) with the FTIR spectrum of the commercial ALAMIN™ powder. In the 1600-1300 cm^{-1} region of FTIR of the $Na_3Cit.2H_2O$ salt, there is an intense peak at 1592 cm^{-1} and a weaker complex peak at 1419 cm^{-1} (with an additional peaks at 1395 and 1441 cm^{-1}), which occur approximately at the frequency expected for the 1595 and 1419 cm^{-1} bands in the ALAMIN™ FTIR spectrum. Despite their complex nature (and the lack of structure plus partial obscuring of the corresponding putative citrate bands observed in the ALAMIN™ FTIR spectra), there is strong evidence that these bands are what are being observed in the ALAMIN™

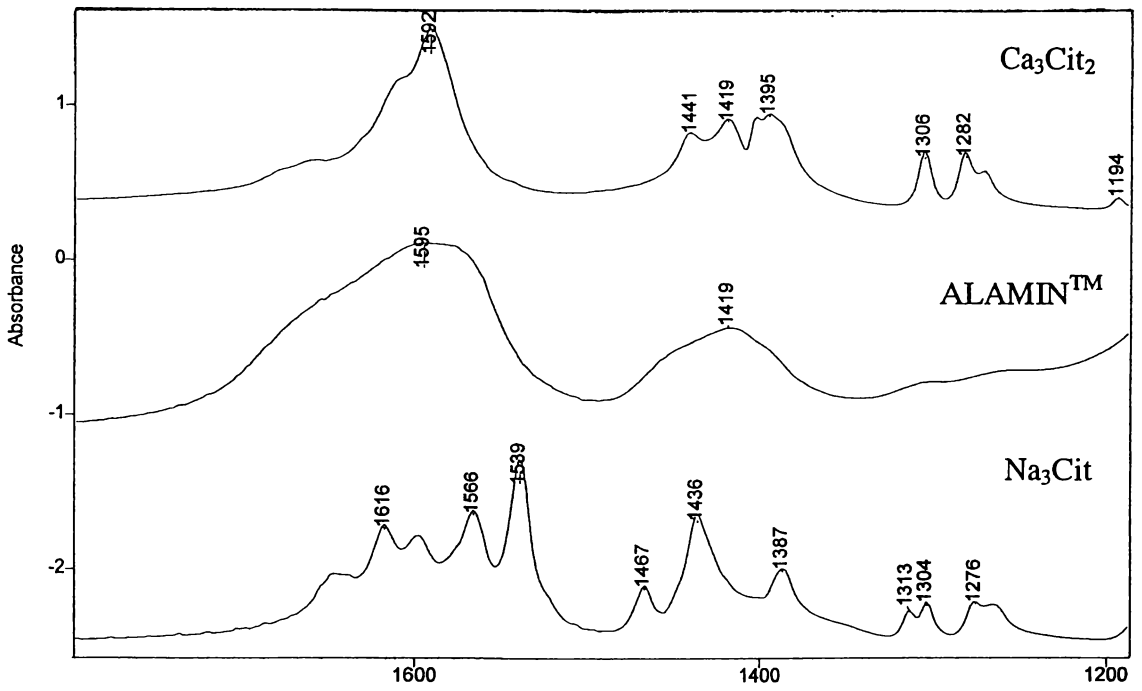

Figure 6-8: Comparison of the FTIR spectrum of commercial lactic ALAMIN™ powder with FTIR spectra of Ca_3Cit_2 and Na_3Cit.

This assignment was further strengthened by reference to a study by Tenhuisen et al (Tenhuisen et al., 1994) who recorded FTIR spectra of hydroxyapatite prepared in the presence of citrate which contained the same broad featureless band at *ca.* 1419 cm^{-1}. In addition, it has been shown by Marković et al (Marković et al., 1993) et al. that a series of calcium phosphates based on the OCP structure can be prepared in which citrate is

incorporated into the lattice structure. The IR spectra of these compounds show the same tendency to exhibit the featureless band at 1419 cm^{-1}. The strongest evidence that this band was due to citrate was well demonstrated by studies of precipitates derived from the SLWUF buffer model solutions in this project. When these spectra of SLWUF-derived CaP precipitates are compared with the band at 1419 cm^{-1} in the ALAMIN™ FTIR spectra, it is obvious that there is *another* component in the ALAMIN™ which is contributing to the 1419 cm^{-1} band. The most likely contributor is reasoned to be whey protein co-deposited with the calcium phosphate in the ALAMIN™.

This was demonstrated by the recording of FTIR spectra of KBr disks of solid mixed whey protein samples obtained from the New Zealand Dairy Research Institute consisting of β-lactalbumin and α-lactoglobulin in the following proportion: 85 and 9 % (PT6378 batch) and also 13 and 69 % (PT3886 batch) mixture respectively. These IR spectra (see Figure 6-9) illustrate that the most significant contribution of the whey protein to the FTIR spectra is the "amide I region" (1620-1700) cm^{-1} which is in agreement with previous IR investigations (Boye et al., 1997). The next most significant IR peak for both whey proteins is at 1541±1 cm^{-1} which corresponds to the amide II band (1550 cm^{-1}). This band arises from -CONH vibrations of the peptide backbone. Hence these spectra show that whey proteins will not only give a contribution to the 1419 cm^{-1} band in the IR spectra but also to the 1595 cm^{-1} band so that this band in the ALAMIN™ FTIR spectrum has *three species* contributing to it in total.

These results show the potential power of IR spectroscopy, a relatively simple spectroscopic technique in indicating the quality of the ALAMIN™ product. Product quality industrially may be regarded as being degraded when appreciable levels of protein from leakage through the UF membrane contaminate the ALAMIN™ product. This may be picked up by a simple FTIR spectrum of the product.

6.1.4(c) FTIR Spectra of the Other Commercial Products of Potential Use as ALAMIN™ Supplements

During the project, samples of products similar to ALAMIN™ manufactured in dairy factories overseas became available. These samples of other commercial products, viz., LACPRODAN (manufactured in Denmark) and LACTOVAL (manufactured by DMV in the Netherlands) were analysed by FTIR and compared to ALAMIN™ FTIR spectra.

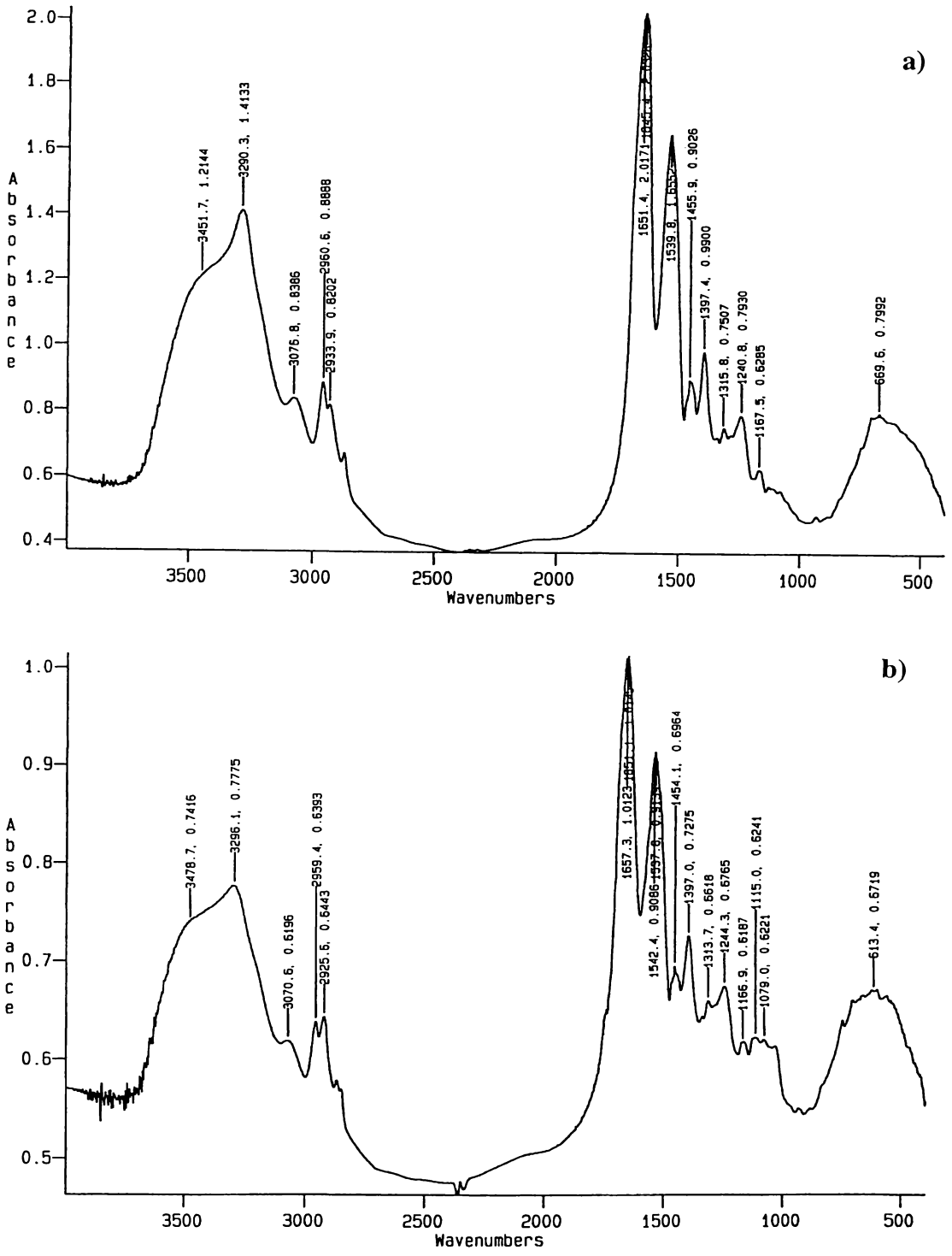

Figure 6-9: FTIR spectra of KBr disks of the whey proteins:

a) FTIR spectrum of β-lactalbumin and α-lactoglobulin mixture (85 and 9 %) and

b) FTIR spectrum of β-lactalbumin and α-lactoglobulin mixture (13 and 69 %).

At the time these experiments were being considered, ALAMIN™ was in short supply due to a large demand for it overseas and hence supplementation by overseas sources was being considered.

The FTIR spectrum of LACPRODAN is shown in Figure 6-10a. This was found to be very similar in appearance to ALAMIN™ although LACPRODAN appeared to show peaks at 1259 and 892 cm^{-1} which suggested elevated levels of some organic impurity such as lactose. This agreed with the supplied chemical analysis of this other commercial product (see Appendix B) which stated that the product contained 23.04 wt. % of lactose. In contrast, ALAMIN™ contains lactose levels at about 4 wt. %.

In contrast, the FTIR spectrum of LACTOVAL (see Figure 6-10b) was completely different in appearance from that of ALAMIN™. The spectrum of LACTOVAL powder contained an intense peak centred at *ca.* 1570 cm^{-1} which had much fine structure associated with it. A medium intensity peak centred at 1435 cm^{-1} also had some shoulders and structure in its overall peak shape. In addition, the phosphate-associated IR fundamental peaks at *ca.* 1060 and 566/603 cm^{-1} were slightly distorted in shape from the corresponding peaks customarily observed in ALAMIN™ FTIR spectra. The IR features observed appeared reminiscent of the presence of a large amount of citrate-containing material in the product. This was also in agreement with the supplied chemical analysis of the product which indicated 18.6 wt. % citric acid (Appendix B).

The conclusion to these studies of other commercial products is that each manufacturing site overseas making ALAMIN™ "look-alike" products must use slightly different manufacturing conditions as well as different starting materials, most notably the starting whey permeate. This thus results in different levels of minor whey components co-depositing with the calcium phosphate.

6.1.5 Scanning Electron Microscopy (SEM) and Transmission Electron Microscopy (TEM) of the Commercial ALAMIN™ Powder, produced from Lactic Whey Permeate

Scanning Electron Microscopy (SEM) and Transmission Electron Microscopy (TEM) are widely used techniques for characterising the morphology of calcium phosphates.

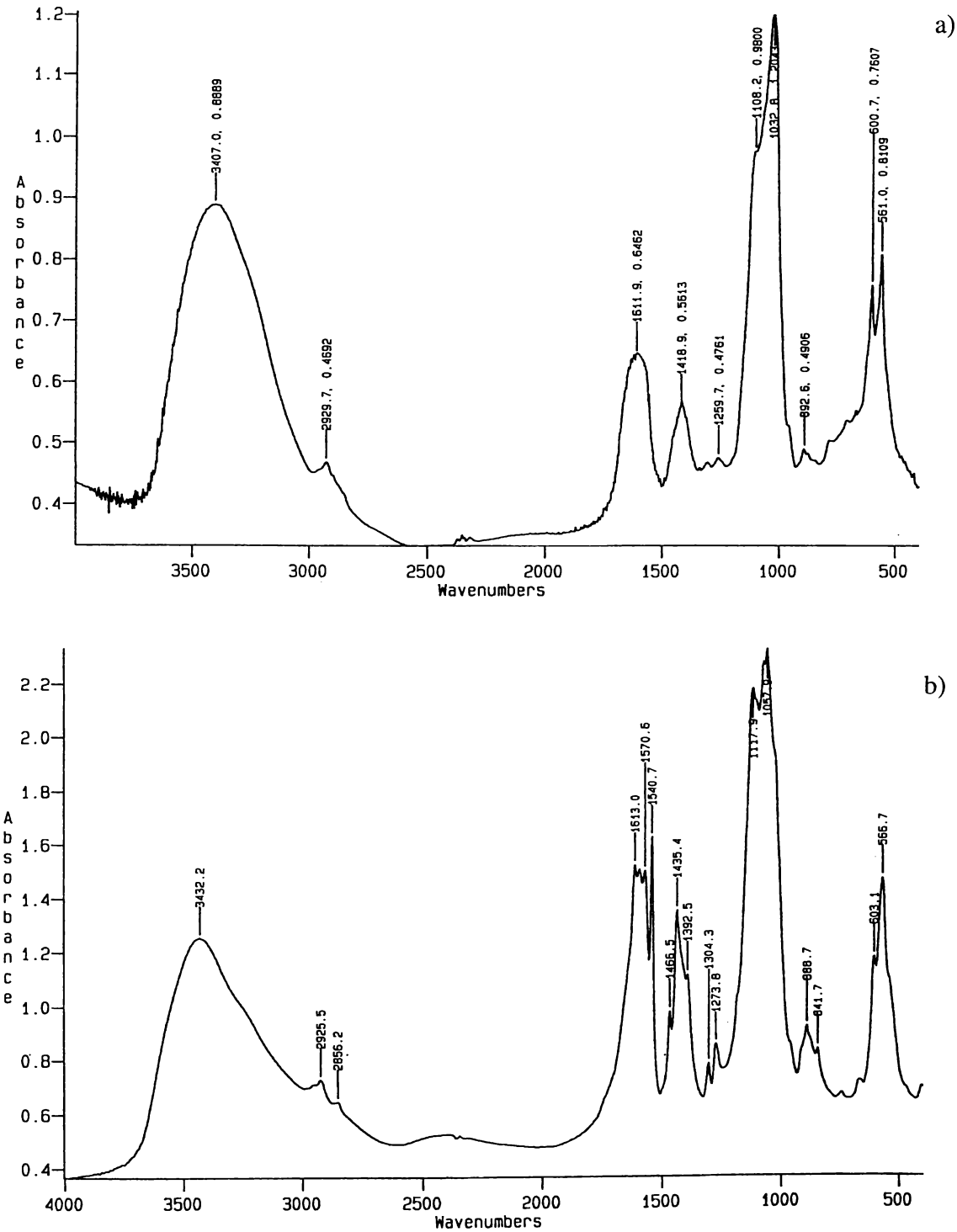

Figure 6-10: FTIR spectra of: a) LACPRODAN and b) LACTOVAL powders.

Particle form and shape is regarded as a critical factor in the manufacture of ALAMIN™ and in particular with regard to overall filterability of the product after precipitation and maturation time in the holding tank. The purpose of the present PhD investigation was to provide an idea of the general appearance of ALAMIN™ particles manufactured under standard industrial conditions.

6.1.5 (a) Particle Morphology

Experimental. Scanning Electron Microscopy (SEM) analyses were undertaken using a *Hitachi S4000 Scanning Microscope*. SEM photomicrographs were taken at the typical accelerating voltage 5 kV at varying magnifications. ALAMIN™, being a calcium phosphate, is partially insulating and thus has to be coated with a conductive layer to carry away the negative electrical charge that builds up on the sample by adsorption of electrons from the primary electron beam. A small amount of ALAMIN™ powder was placed on double sided sticky carbon tape affixed to the top of a sample stub. Samples were then placed into a *Hitachi E1030 Ion Sputter Coater* which was pumped down. When the vacuum reached 20 Pa, the chamber was purged with Argon and a coating of Pt-Pd (20 nm) was sputtered onto the sample. The specimen stub with coated particles of ALAMIN™ powder was subsequently mounted on a sample holder and placed on the stage of the specimen chamber of the SEM instrument where it was pumped down to a pressure of 2×10^{-7} Pa.

Results. Commercial ALAMIN™ powder (as produced from lactic whey UF-permeate) typically gave SEM micrographs as illustrated in Figures 6-11, 6-12 and 6-13:

It was apparent from the micrographs that commercial ALAMIN™ powder is a highly complex material with a wide distribution of particle sizes (particles ranging in size from 1-150 μm). The particles are irregularly shaped and have a chunky nature although are approximately spherical in character. Also it is important to mention that the form of the commercial ALAMIN™ powder agglomerates are not always uniform in nature: as an example see the following SEM photos (Figures 6-11, 6-12 and 6-13). It appears that they can exist as an aggregation of smaller particles in one conglomerate, as was observed even for the finest fraction of ALAMIN™ powder (see Figure 6-12).

a)

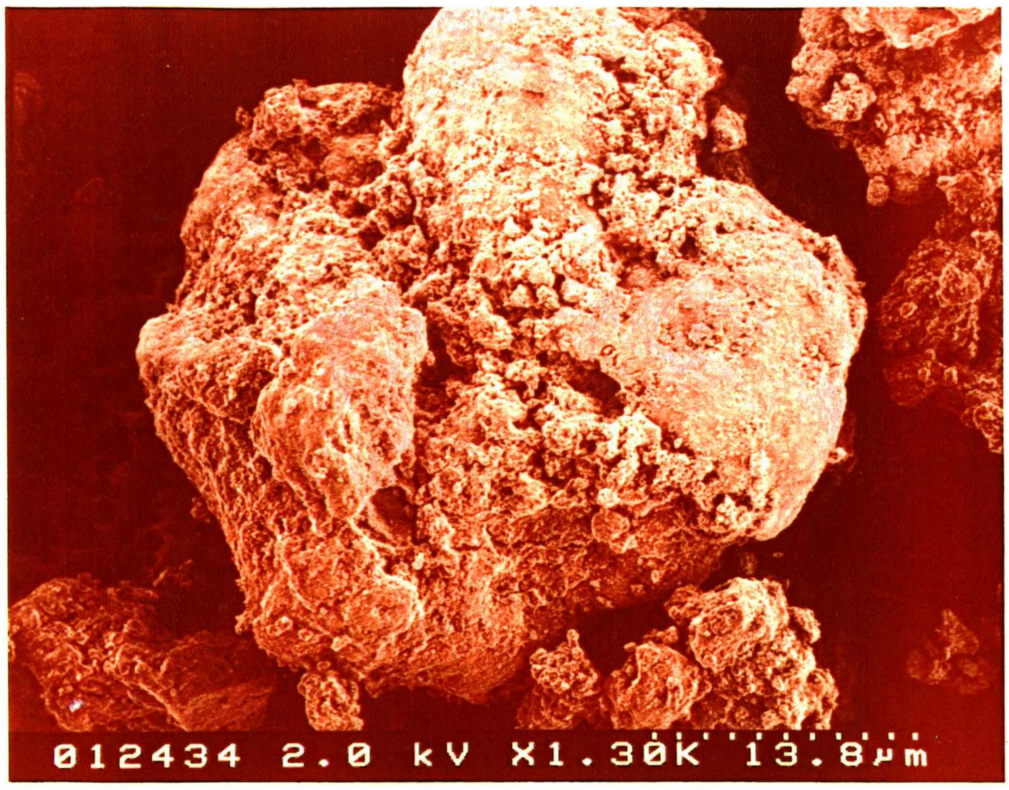

b)

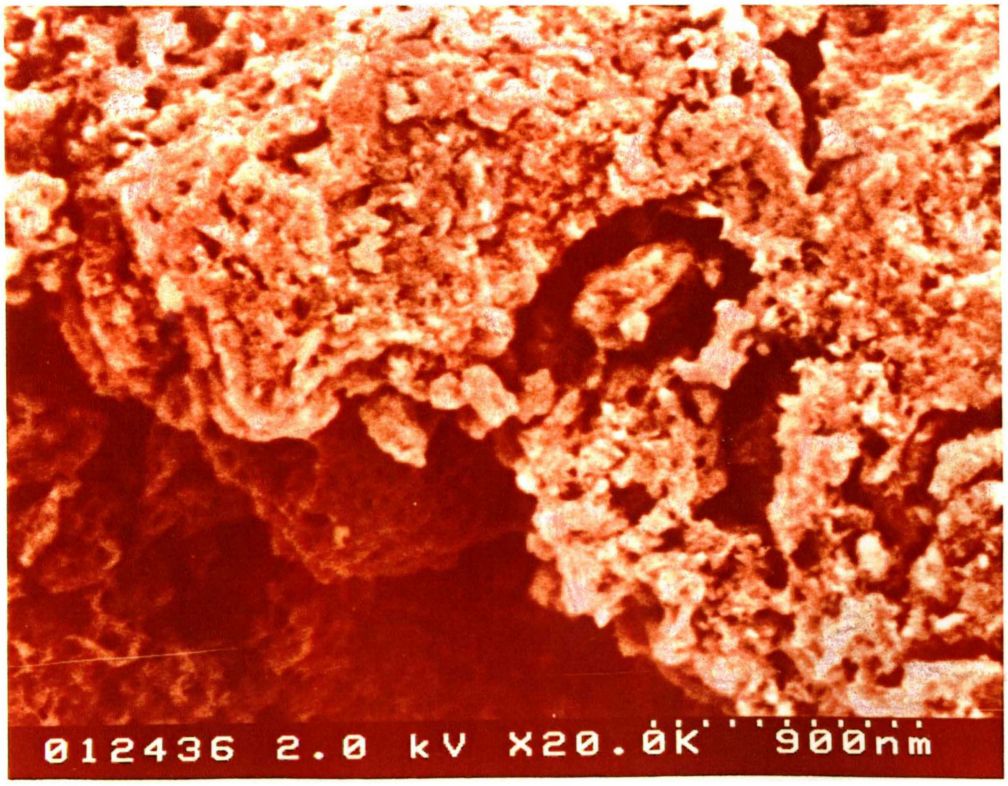

Figure 6-11: SEM micrographs of the commercial lactic ALAMIN™ powder: a) typical particle at the magnification x 1 300 and b) at the magnification x 20 000.

a)

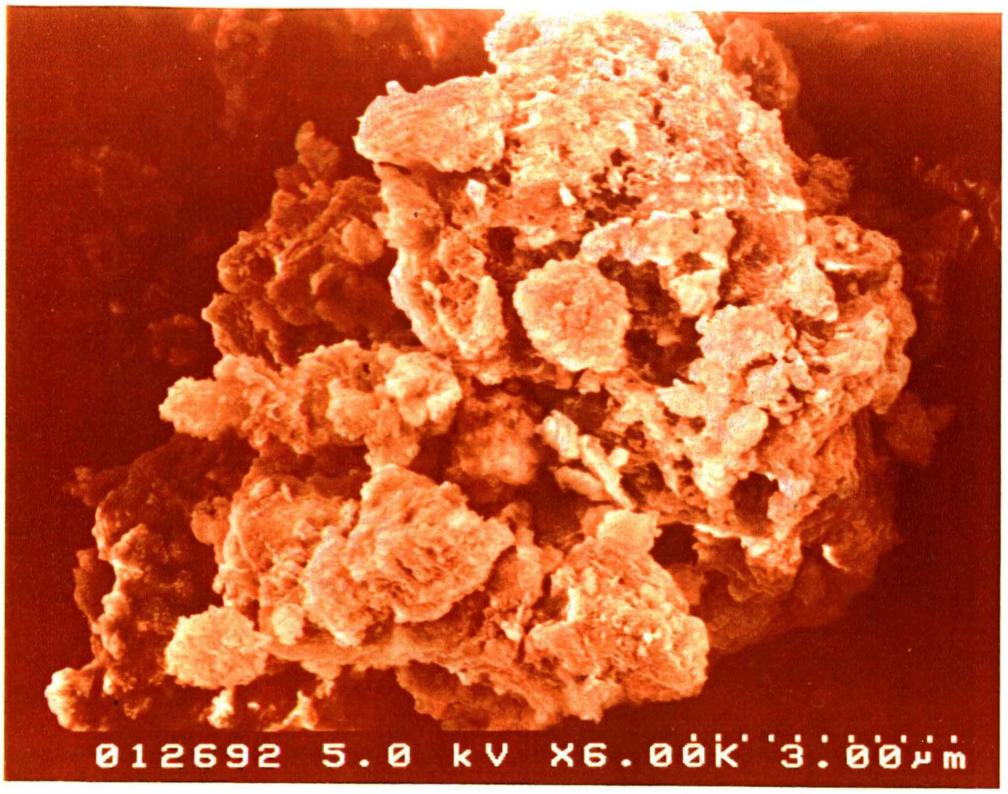

b)

Figure 6-12: SEM micrographs of the commercial lactic ALAMIN™ powder (*finest fraction*): a) typical particle at the magnification x 6 000; b) at the magnification x 20 000.

a)

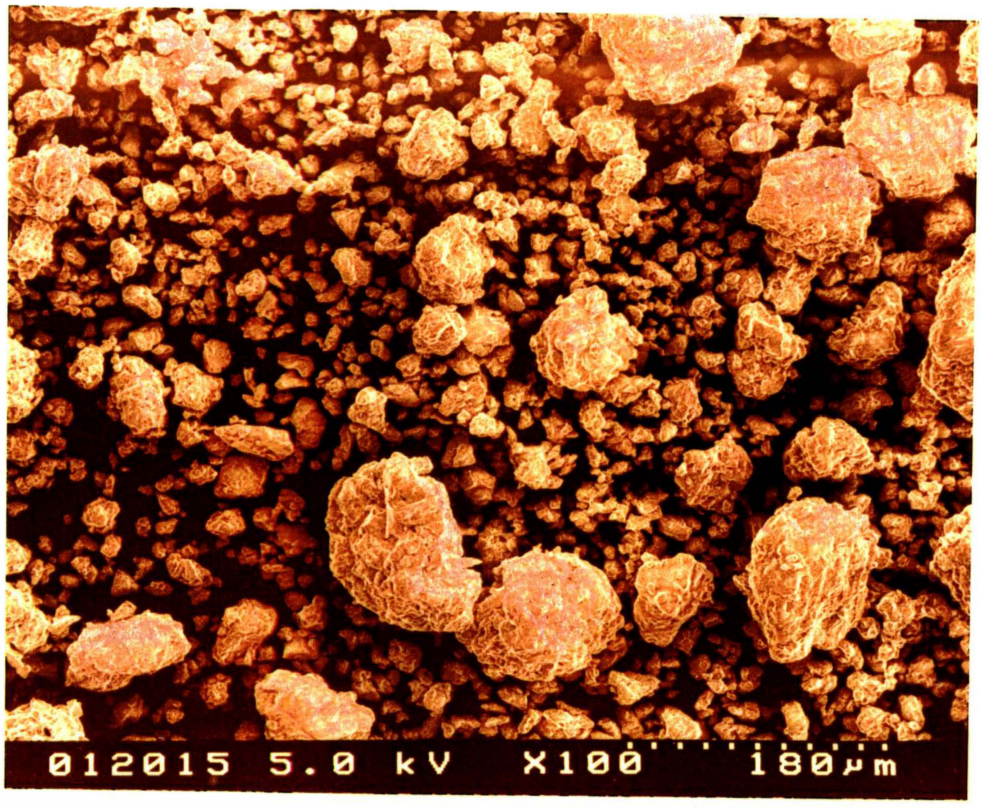

b)

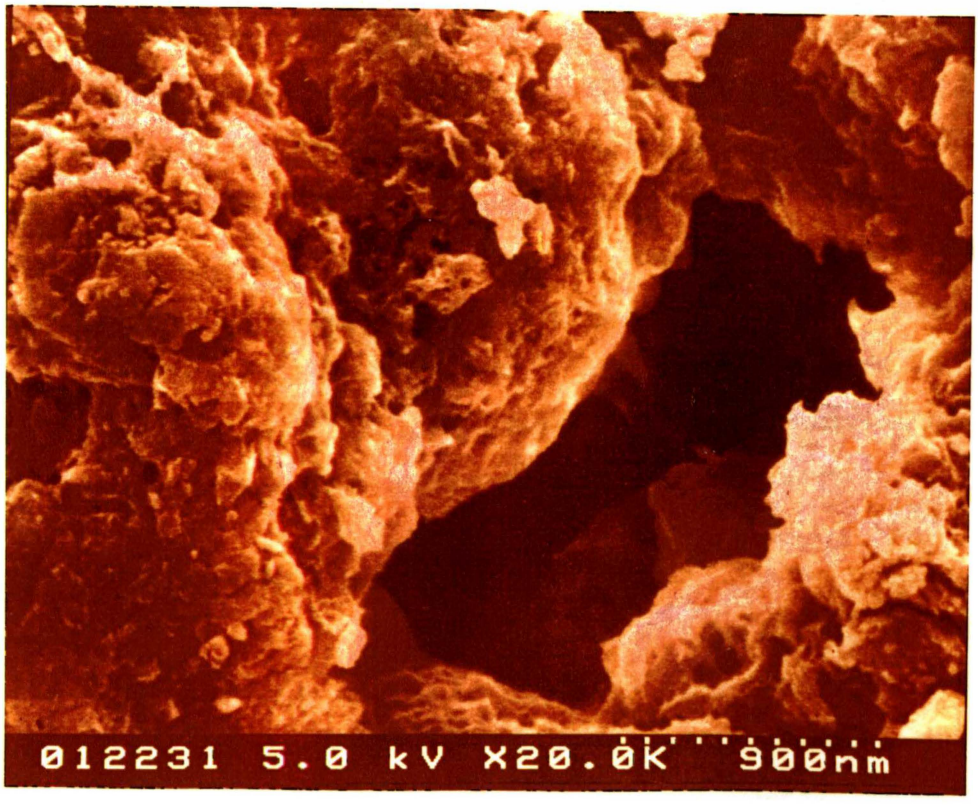

Figure 6-13: SEM micrographs of the commercial lactic ALAMIN™ powder: a) typical particle at the magnification x 6 000 and b) at the magnification x 20 000.

The SEM investigation of different samples of the commercial ALAMIN™ powder shows that at high magnification the surface of the typical ALAMIN™ particle is quite porous in nature with gaps and voids (Figures 6-13) and has 'layer like' structural features caused probably by coating with protein film. The surfaces of particles appear uniformly amorphous in character with an absence of ordered crystalline cell features compared to commercial well crystallised pure samples of calcium phosphate like *Fluka*-brand HAP (see Figure 6-14) and without the needle-like structure as is classically observed for fine nanocrystalline hydroxyapatite (*BABI*-brand hydroxyapatite supplied as a suspension of nanosized HAP in an aqueous solution from laboratories at the University of California at Berkley (see Figure 6-15).

A transmission electron microscopy (TEM) analysis of the finest grade of ALAMIN™ powder was undertaken on a specially prepared cross-section of particles (length ca. 3-4 microns) embedded in a resin matrix. This showed additional evidence of the porosity within the ALAMIN™ particles and apparent amorphous features in the cross sections (Figure 6-16).

In general, most of the ALAMIN™ samples had these chunky non-descript aggregated features. It is likely that the drying process used industrially to desiccate the ALAMIN™ as well as the co-deposition of other whey components such as lactose and proteins in particular can heavily influence the degree of aggregation and indeed "hardness" of the resultant material. Generally, particle morphology of manufactured ALAMIN™ was very different from any precipitates produced in the laboratory from bench-scale CaP precipitations from whey permeate (see Figure 7-7 in Chapter 7) or from artificial SLWUF buffers (see Figures 4-29 to 4-32 in Chapter 4). This is additional evidence that the industrial drying process has a strong influence on particle morphology.

6.1.5(b) SEM Analysis of Other Commercial Products

Samples of the other commercial products LACPRODAN (manufactured in Denmark) and LACTOVAL (manufactured by DMV in the Netherlands) were also analysed by SEM and compared to ALAMIN™ (New Zealand) to complement the earlier FTIR study of these products and to compare it with that observed for ALAMIN™ as described above.

a)

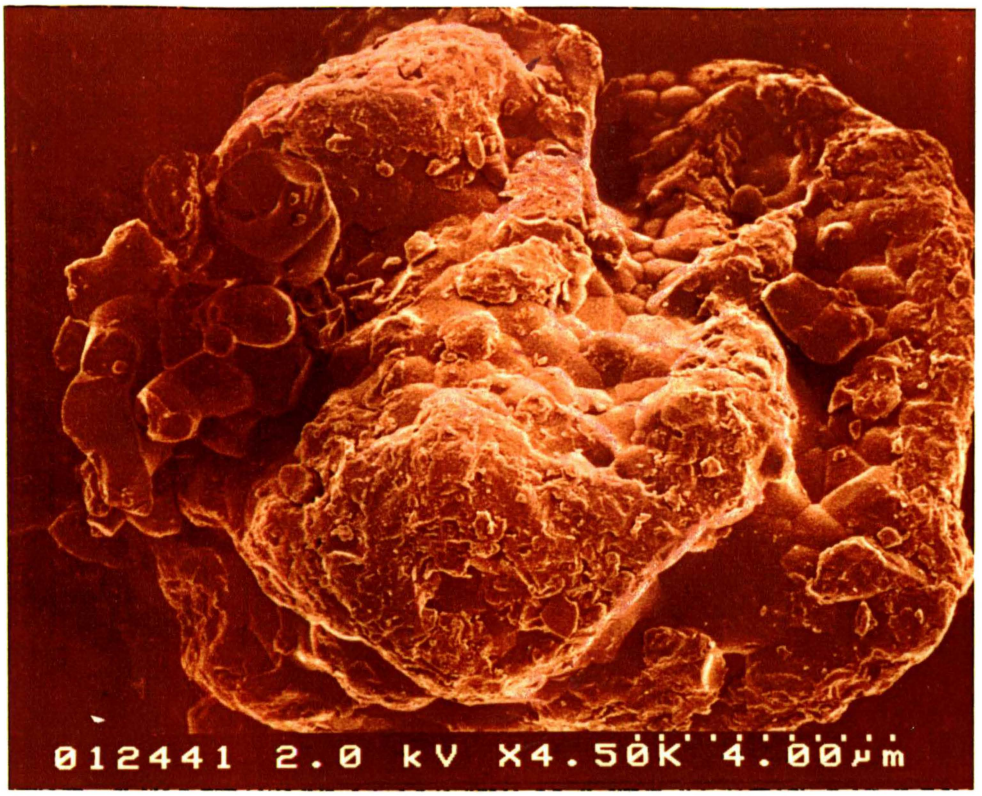

b)

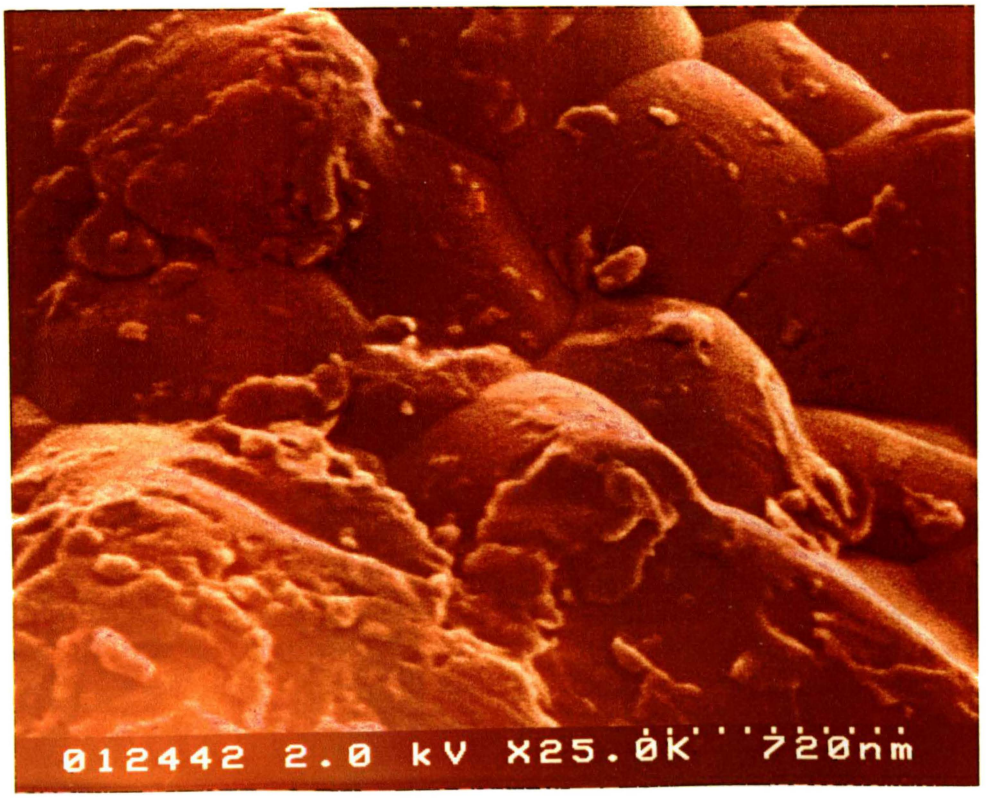

Figure 6-14: SEM micrographs of *Fluka*-brand HAP powder: a) typical particle at the magnification x 4 500 and b) surface of particle at the magnification x 25 000.

a)

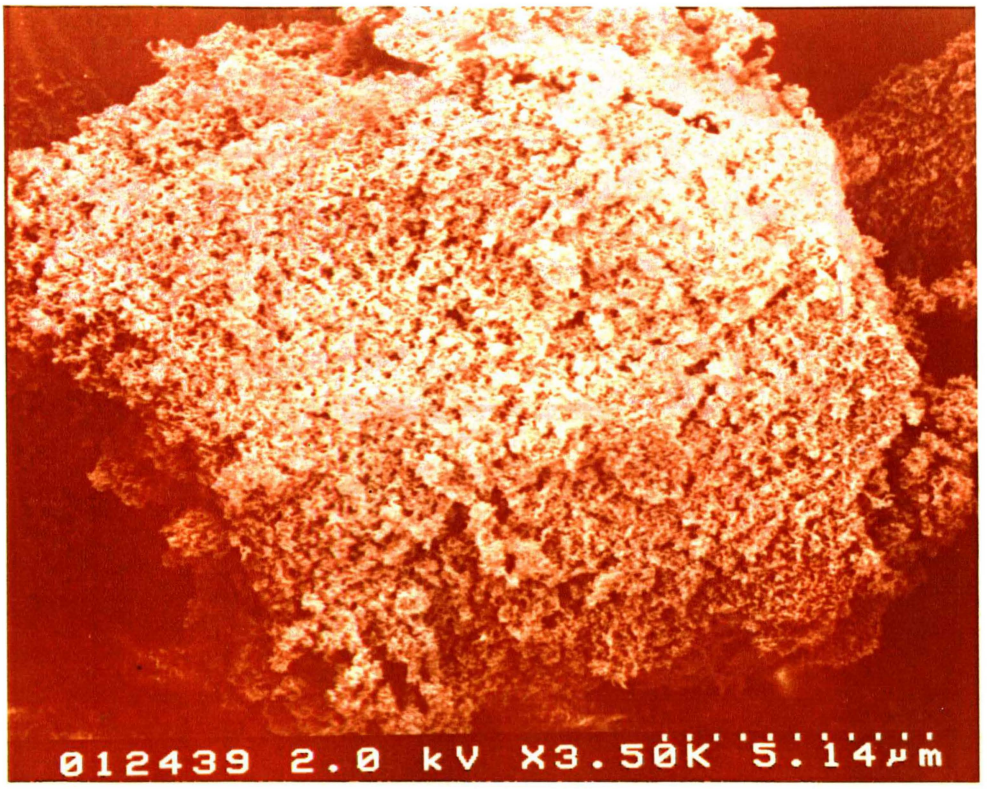

b)

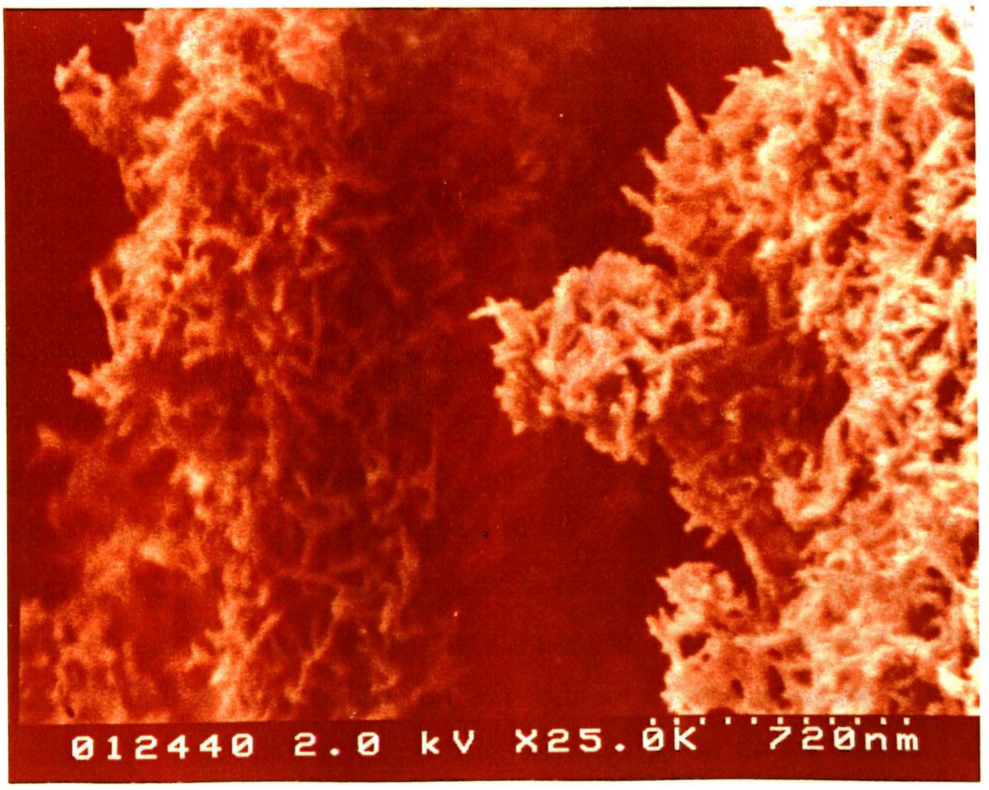

Figure 6-15: SEM micrographs of *BABI*-brand HAP powder: a) typical particle at the magnification x 3 500 and b) surface of the particle at magnification x 25 000.

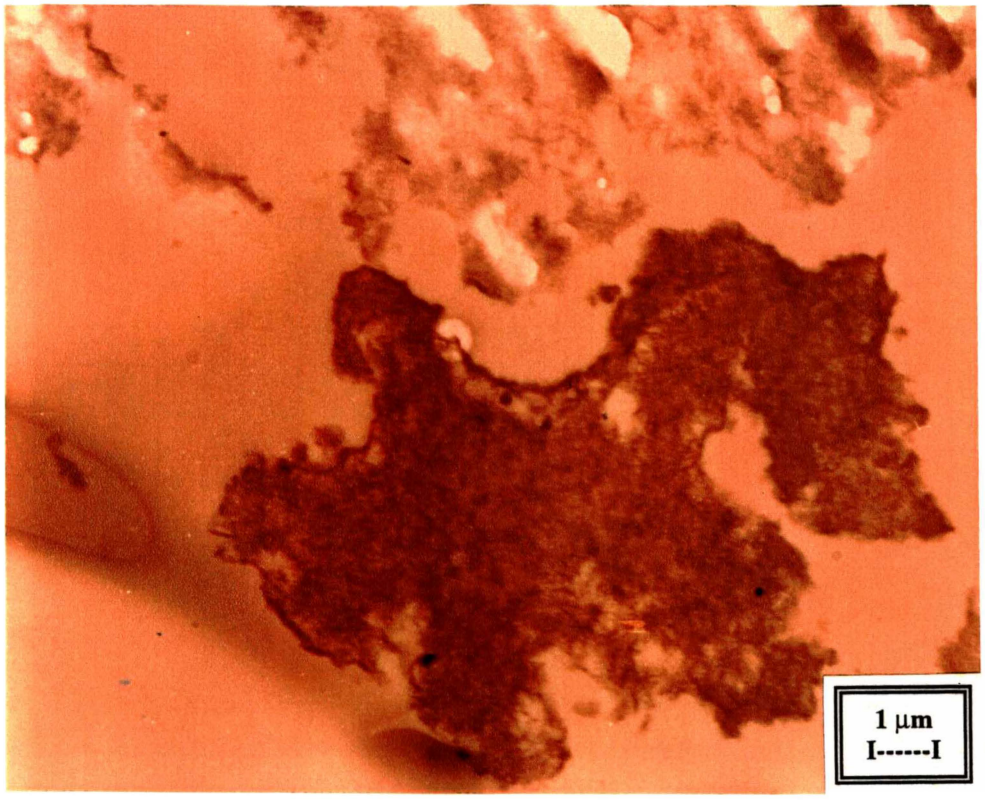

Figure 6-16: TEM micrograph of the cross-section of commercial lactic ALAMIN™ powder (finest fraction) at the magnification x 18 300.

SEM confirmed that the morphology of LACPRODAN resembled that more of ALAMIN™ than the LACTOVAL powder (see Figures 6-17 and 6-18) in that the same chunky non-descript appearance for particles was observed. This was despite the higher analysed lactose and lower calcium (20 wt. %) that was found to exist in LACPRODAN compared to ALAMIN™. In contrast, LACTOVAL was completely different in morphology. LACTOVAL particles appeared to have a large degree of layering in the particles, which gave it a more hetereogeneous appearance than the more spherically shaped LACPRODAN particles. The difference in appearance could be linked to the high level of citric acid (18.6 wt. %) in LACTOVAL. These studies therefore showed that the levels of minor (whey) components present can significantly alter the particle morphology especially if there are inclusions of foreign phases (e.g. calcium citrate) in the product.

a)

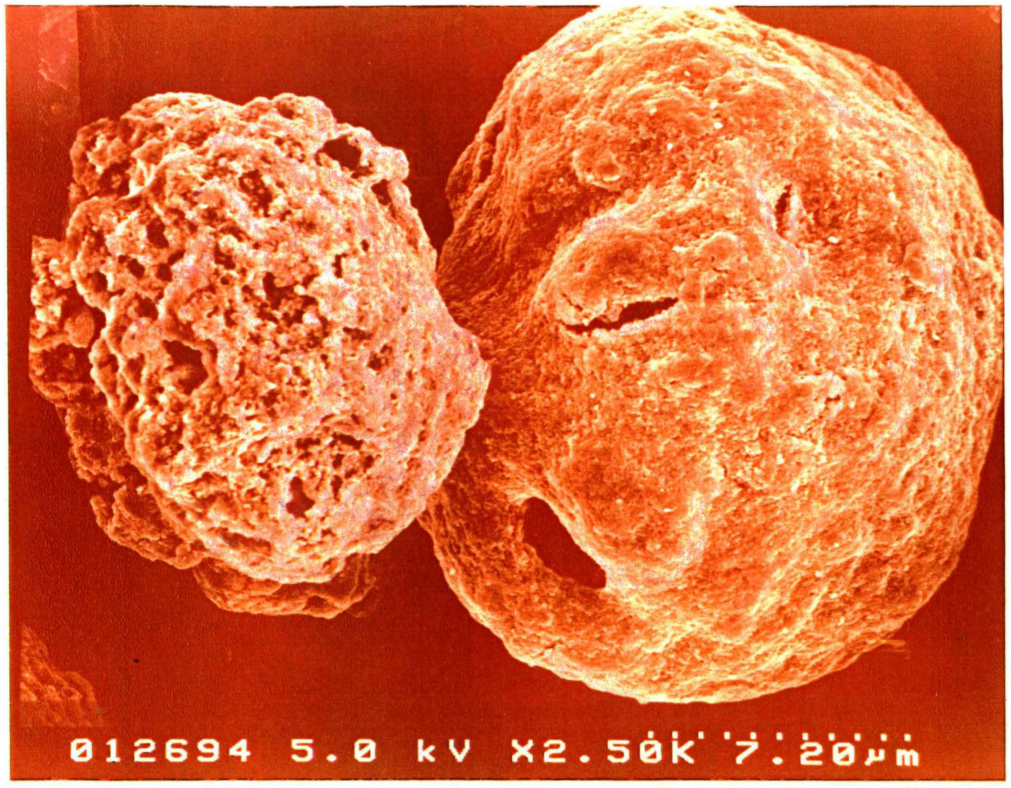

b)

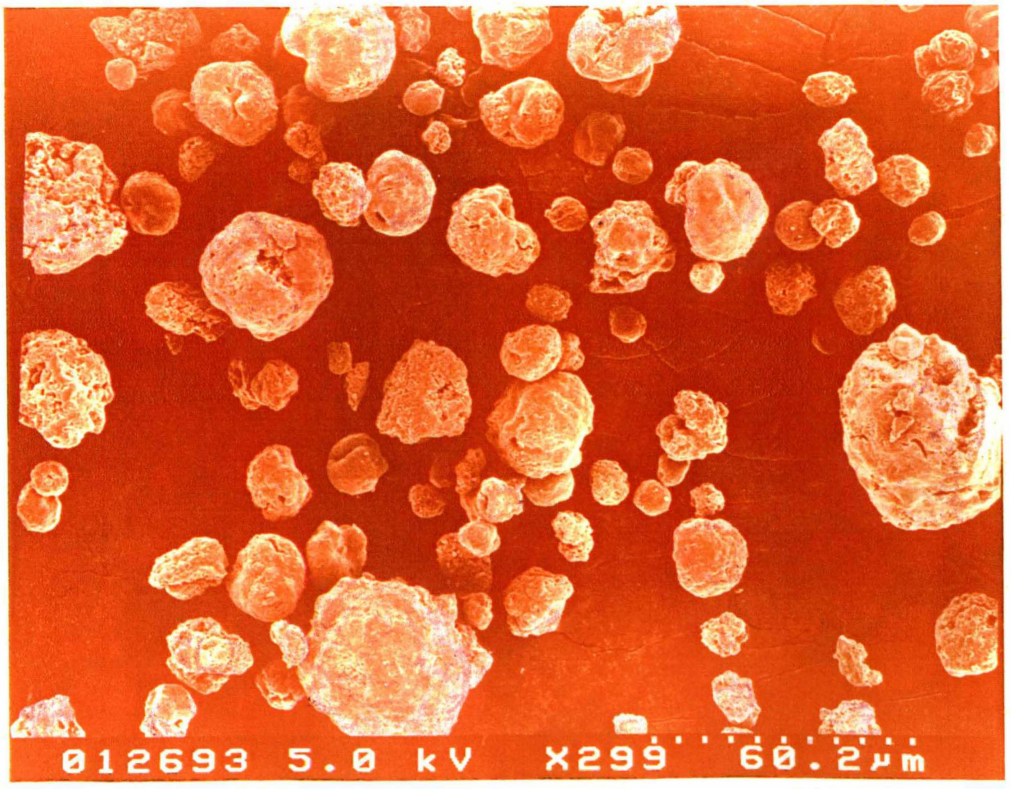

Figure 6-17: SEM micrographs of LACPRODAN powder: a) typical particle at the magnification x 2 500 and b) at the magnification x 299.

a)

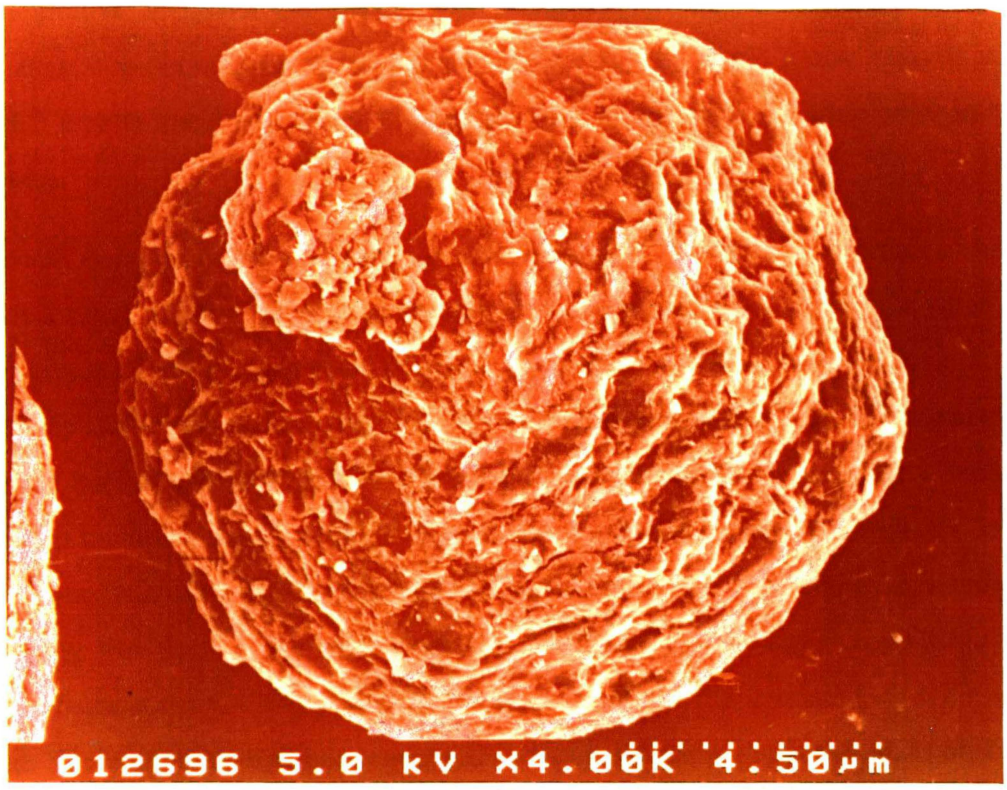

b)

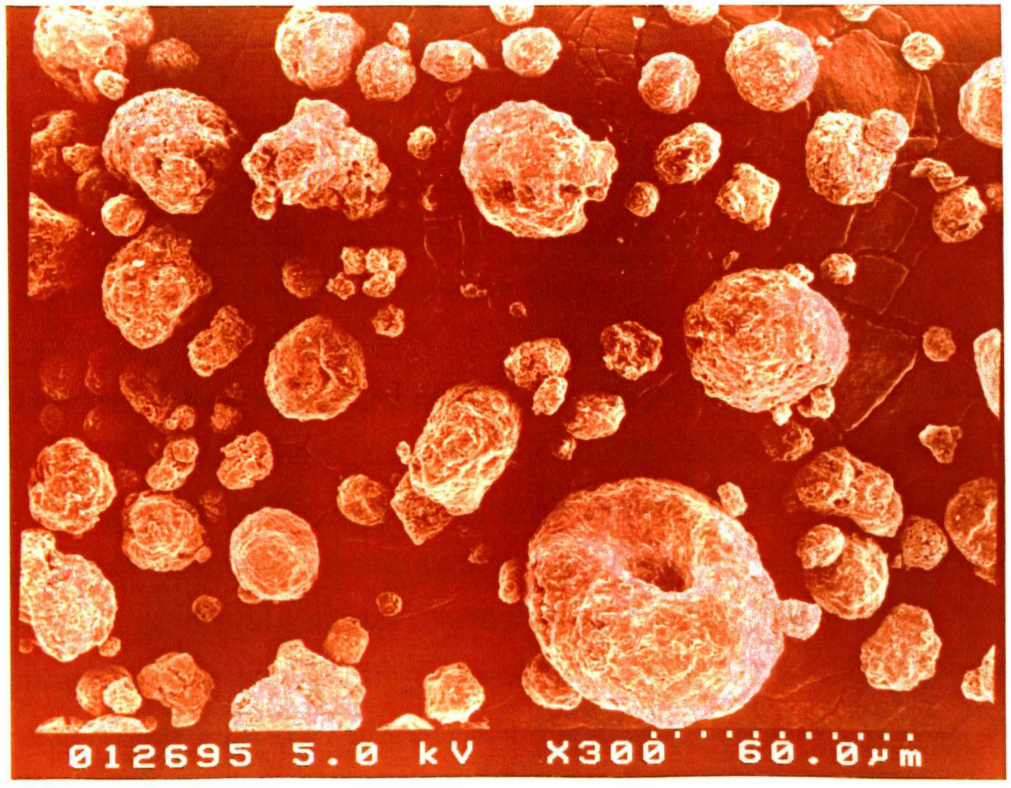

Figure 6-18: SEM micrographs of LACTOVAL powder: a) typical particle at the magnification x 4 000 and b) at the magnification x 300.

6.1.5 (c) Energy Dispersive X-ray Analysis (EDX) of ALAMIN™ Powder

X-ray quantitative microanalysis (EDX) was performed in conjunction with the SEM analyses as a non-destructive technique for measuring the Ca:P molar ratio in the ALAMIN™ powders and also to see if elements such as Mg, Na, etc. are present in the solid phases.

Experimental. Samples of standard commercial ALAMIN™ powder were prepared by a vacuum disk press method. In general enough of the powder was added to the press in order to produce a disk of about 1 cm diameter. This was carried out in order to obtain a sample with a surface smooth enough for quantitative microanalysis. All EDX analyses were carried out on a Hitachi S4000 scanning electron microscope at 20 keV with a beam sample incidence angle of 90.0 degrees and an X-ray emergence angle of 29.5 degrees. *Kevex Quantex* software was used for determining the Ca:P ratios. A standard for measuring the Ca:P molar ratio consisting of fluorapatite ($Ca_5(PO_4)_3(F,Cl,OH)$) (Registered Standard no: 4269, prepared by Micro-Analysis Consultants Ltd, UK) was purchased. These samples had been mounted in an epoxy resin, sectioned and polished to produce an optically flat surface. Usually the standard was analysed first and then the ALAMIN samples in order to provide referenced data on relative Ca and P intensities. A "ZAF correction via magic V" algorithm was used to produce atomic percent values From these the Ca:P molar ratio was determined from simple rationing of these atomic percent values for the various grades of ALAMIN™. In addition, samples of *Fluka* HAP and TCP were analysed by EDX for comparison. The ALAMIN™ and *Fluka* calcium phosphate samples were also sent down to Industrial Research Limited, Lower Hutt for a check on EDX analyses performed at Waikato.

Results. In general, industrial grade ALAMIN™ gave a wide range of Ca:P molar ratios from 1.45-1.65. The pure calcium phosphate samples gave Ca:P molar ratios lower than expected for the stoichiometry of these compounds (e.g. *Fluka* TCP gave a Ca:P molar ratio of 1.47±0.01 which is lower than its theoretical value of 1.50) which implied that this technique is not the most reliable for determining Ca:P molar ratios. Nevertheless, the values obtained for the ALAMIN™ samples are mostly less than the Ca:P molar ratio for stoichiometric calcium hydroxyapatite which has a theoretical Ca:P molar ratio equal to 1.67. This indicates that ALAMIN™ can be described as a *calcium deficient* hydroxyapatite, a term commonly used in the literature (see Chapter 2) to describe precipitated HAPs, which contain sub-stoichiometric amounts of calcium.

Comparison of EDX and ICP analyses of powders as a means of determining Ca:P molar ratios

Given the above results, especially with regard to attempts to measure Ca:P molar ratios for the pure calcium phosphate phases, TCP and HAP, EDX is not regarded as the most ideal method for analysis of Ca:P molar ratios due to the need for appropriately matched standards which is not always achievable. In addition, EDX is very sensitive to the surface morphology which thus imparts a large uncertainty ±10% to the measurements. Conventional chemical analyses in which the sample is digested and analysed for total calcium and phosphorus content are, therefore, regarded as the more reliable means of measurement of Ca:P molar ratio as long as the sample being analysed is reasonably phase pure. Comparison of the EDX-measured Ca:P molar ratios from various samples of ALAMIN™ (see Table 6-4 for their designations) with conventional chemical analyses of the same ALAMIN™ powders, (i.e., ICP-OES measurements on solutions of acid digested ALAMIN™ powders, see Appendix A2) were made and found to be in reasonable agreement to within ±10% of each other. Thus EDX could be useful as a quick alternative method for estimating Ca:P molar ratios without destroying the sample.

Table 6-4: Comparison of Ca:P molar ratios, determined by EDX and ICP-OES for the commercial ALAMIN™ powders.

ALAMIN™ Samples[1]	Ca:P molar ratio (EDX)	Ca:P molar ratio (ICP)	Ca, wt. % (ICP)	P, wt. % (ICP)	Ca:P molar ratio (EDX, Wellington)
Fraction >150 μm	1.65	1.62	27.00	12.90	
Fraction <150 μm	1.53	1.59	27.20	13.20	
ALAMIN™ (Batch A)	1.50	1.59	26.00	12.60	1.50
ALAMIN™ (Batch B)	1.45	1.55	27.30	13.60	1.44
Finest fraction	1.55	1.61	25.00	12.00	
ALAMIN™ (1996)	1.60	1.62	25.60	12.20	1.61

[1]The designations of various grades of ALAMIN™, Batch A and B refers to two batches of manufactured of ALAMIN™ powder, labels of other forms of ALAMIN™ (e.g."< 150 μm", "ALAMIN™ (1996)" refer merely to size fractions sorted after drying or years in which the commercial ALAMIN™ sample was obtained.

6.1.6 X-Ray Photoelectron Spectroscopy (XPS) of the Commercial ALAMIN™ Powder, produced from Lactic Whey Permeate

As has been discussed in Chapter 3, XPS is useful for surface analysis of many different kinds of materials. This technique was used to characterise the general surface characteristics of ALAMIN powder to see if any useful information could be obtained.

Experimental. XPS spectra were recorded on a KRATOS XSAM-800 X-ray photoelectron spectrometer (Figure 6-19), located at the Research Centre for Surface & Material Science, Auckland University.

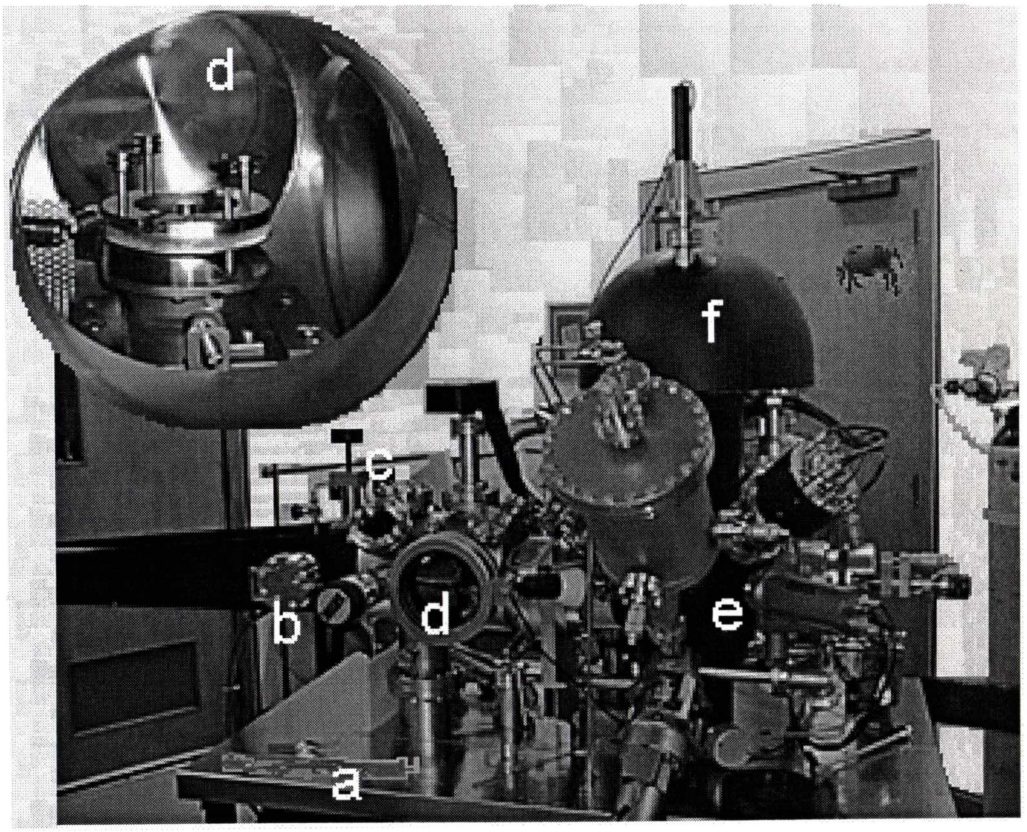

Figure 6-19: Photograph of the XPS spectrometer employing a hemispherical electron energy analyzer and a non-monochromatic X-ray source:

Key to Figure 6-19:

a) Sample stub holder used to transfer the samples into introduction chamber.
b) Introduction port through which samples enter the introduction chamber.
c) Isolating tap between introduction chamber and preparatory chamber.
d) Preparatory chamber. (Inset: the 4 stub carousel inside preparatory chamber).
e) Analytical chamber (pumped to ca. 10^{-12} torr).
f) Hemi-spherical energy analyser.

A sample of the commercial lactic ALAMIN™ powder was pressed into indium foil and attached to a sample stub. After introduction through a series of pumped down chambers it was positioned in the XPS target chamber and irradiated with non-monochromatised MgKα X-rays.

A wide scan from 0-1000 eV was run followed by narrow scans of the C 1s and N 1s regions. The following parameters (see Tables 6-5 and 6-6) were set up in the software for the acquisition of the XPS spectra.

Table 6-5: XPS operational parameters for the wide scan spectrum.

Parameters	Data
Collection (dwell) time	2.0 s per eV
X-ray excitation energy	MgKα (1253.6 eV)
Analyser mode	FAT
Scan type	Regular
Pass energy	65 eV
Magnification	High

Table 6-6: XPS operational parameters for the narrow scan spectrum.

Parameters	Data
Collection (dwell) time (s)	2.0 s per eV
X-ray excitation energy	MgKα (1253.6 eV)
Analyser mode	FAT
Scan type	Regular
Pass energy	38 eV
Magnification	High

Results: Wide scan XPS analysis of commercial lactic ALAMIN™ powder. The wide scan spectrum of the commercial lactic ALAMIN™ powder is illustrated in Figure 6-20. As expected, photoelectron peaks due to Ca (2s and 2p), P (2s and 2p), O (1s) were detected. These are similar in binding energy to peaks observed for hydroxyapatite (Konishi et al., 1987).

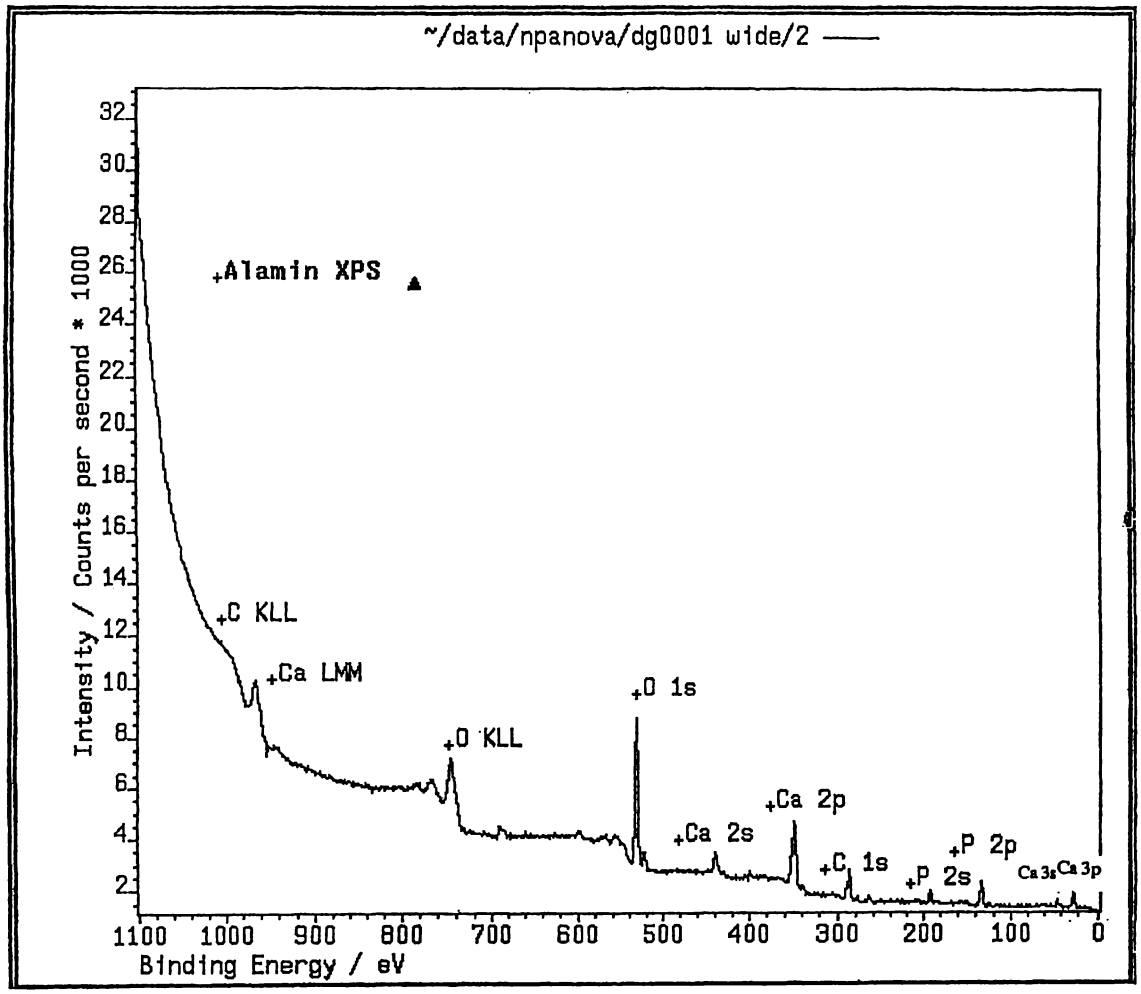

Figure 6-20: Typical XPS wide-scan spectrum of the commercial lactic ALAMIN™ powder.

In addition, to these peaks, carbon C (1s) and N (1s) peaks were detected. One of these (C 1s) is due to adventitious hydrocarbons adsorbed on the surface of the sample. Most XPS samples exposed to the atmosphere prior to their analysis show this carbon contamination peak. However, part of the peak intensity must also be due to C-containing minor whey components associated with the ALAMIN™ such as citrate and protein. The N 1s peak though weak is likely to be associated with co-deposited whey proteins in the ALAMIN™. A standard quantitative analysis using "QUANT" software in the instrumental operating system software allowed determination of atomic and mass concentrations of elements in the ALAMIN™ sample from the XPS spectrum. These were determined by defining "windows" in the spectrum usually placed around the termini of the most intense of XPS peaks for a particular element (e.g. Ca 2p for Ca, O 1s for O, P 2p for P etc) and then allowing the QUANT program to run for determination of the concentrations (see Table 6-7).

Table 6-7: XPS peaks analysis for the commercial lactic ALAMIN™ powder.

Peak	Position, EV	Sensitivity Factor	Atomic Mass	Mass Conc. %	Atomic Conc. %
O 1s	534.00	0.660	16.00	39.50	48.99
P 2p	136.00	0.390	31.00	17.62	11.28
Ca 2p	350.00	1.580	40.10	25.88	12.80
C 1s	288.00	0.250	12.00	24.21	14.64
N 1s	403.00	0.420	14.00	1.58	2.24

C 1s and N 1s narrow scan XPS analyses in the commercial lactic ALAMIN™ powder

A narrow scan was run over the C 1s region in order obtain a profile with improved resolution which would lead to some insights into what components were actually contributing to the observed profile. The narrow scan run using the conditions detailed in Table 6-6 is illustrated in Figure 6-21a. The spectrum consists of two superimposing peaks. The higher intensity component at lower binding energy can be attributed to adventitious hydrocarbons adsorbed on the specimen. The lower intensity component at higher binding energy is due according to published literature on binding energy shifts (Wagner, 1990) to a carboxyl type carbon, e.g. the C=O as expected in an amide linkage for proteins or the carboxyl carbon such as what exists in citrate.

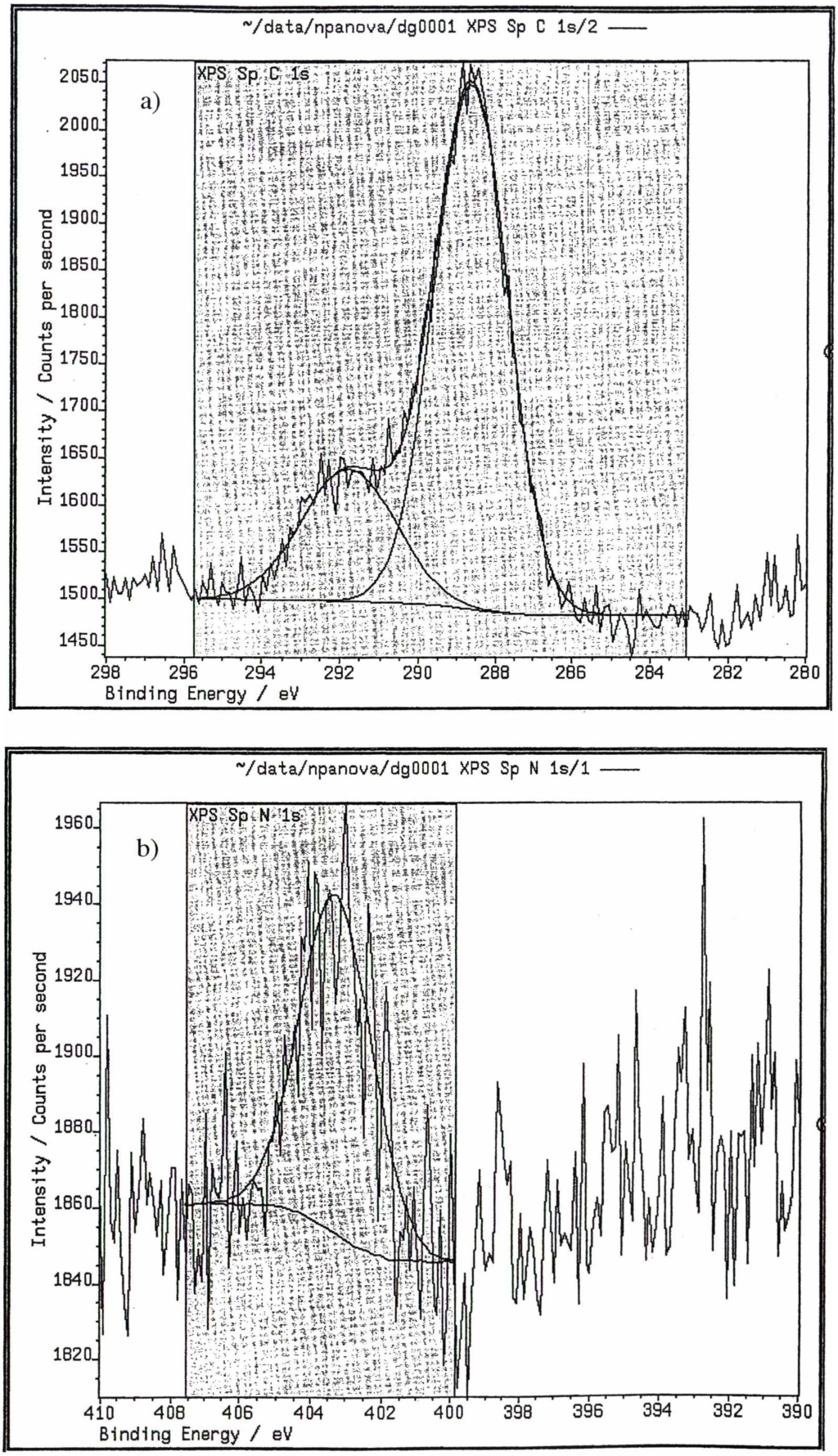

Figure 6-21: Typical XPS narrow-scan spectra for the commercial lactic ALAMIN™ powder in the region: a) C 1s and b) N 1s.

The observation of a N 1s peak in the wide scan XPS spectrum of ALAMIN™ powder (see Figure 6-21b) is strong evidence that protein is co-deposited and exists on the surface of the ALAMIN™ particles as this would arise from amide linkages in the proteins.

6.1.7 X-ray Diffraction (XRD) Investigation of the Commercial ALAMIN™ Powder, produced from Lactic Whey Permeate

6.1.7(a) Phase Identification of ALAMIN™ Powder

Experimental. Samples of the commercial ALAMIN™ powder were prepared for XRD analysis by grinding to a fine powder and placing in an aluminium rectangular sample holder with a small depression in the centre where they were examined using a Philips X'PERT X-Ray Diffractometer. Comparison was also made with X-ray data, obtained of the same samples on an X-ray Diffractometer (Philips PW 1130 high voltage generator and Cu anode X-ray tube), housed at the University of Auckland. The diffractograms of the commercial ALAMIN™ powder were recorded from $2\theta = 2^{o}$ to $2\theta = 100\text{-}150^{o}$ using Cu-K_{α} radiation ($\lambda = 1.5405$ Å).

Results. The typical ALAMIN™ powder X-ray diffractogram ($2\theta = 2\text{-}100^{o}$) exhibited nine major peaks (Figure 6-22). The search/match process of ALAMIN™ powder diffractograms was performed using an installed JCPDS database (PC-APD Diffraction Software) which showed that the *major* d-values in the XRD of ALAMIN™ powder were closely related to the crystal structure of hydroxyapatite, especially in the region $2\theta = 22\text{-}52^{o}$ (see table below). The most intense lines exhibited by a pure hydroxyapatite spectrum (JCPDS cards 01-1008 and 24-0033) were as follows:

d, Å	*h k l*	Intensity, %
3.44	0 0 2	40
2.79	2 1 1	100
1.94	2 2 2	20
1.84	2 1 3	20
1.71	0 0 4	16

Table 6-8 summarises the XRD data for ALAMIN™ and compares it to XRD data that would be exhibited by samples of pure HAP and OCP. OCP has been included as it has been stated to be a precursor phase to HAP in studies by previous researchers in this area (see Chapter 2). It was of interest to see whether any traces of OCP existed in ALAMIN™ after processing.

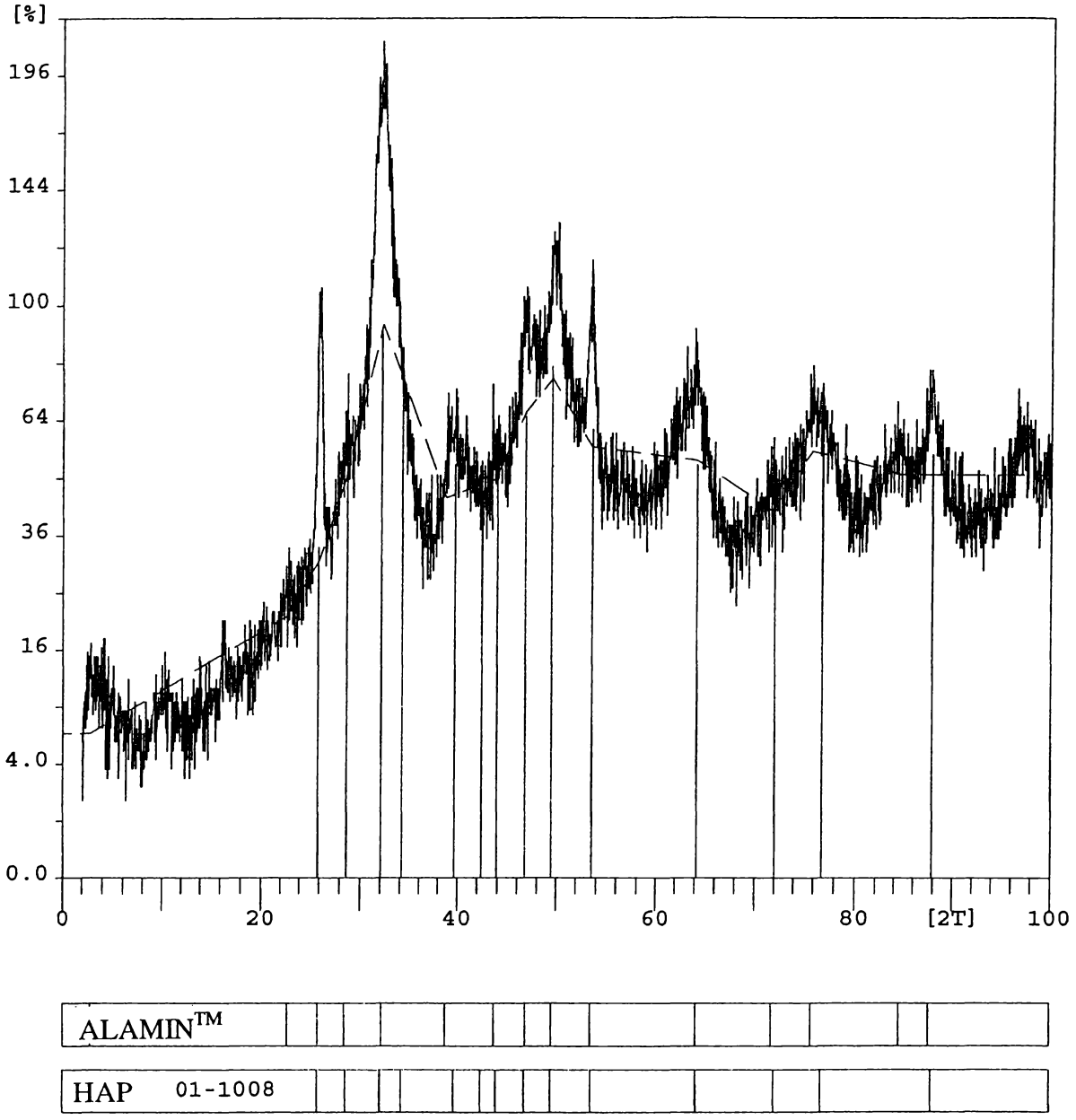

Figure 6-22: XRD patterns of the commercial lactic ALAMIN™ powder.

Table 6-8: Comparison XRD data of the commercial lactic ALAMIN™ powder and crystals of HAP and OCP.

ALAMIN™				HAP		OCP	
No	Angle, 2θ	*d* space, Å	Int., %	d, Å/ hkl	Int., %	d, Å / hkl	Int., %
1	2.39	36.9	91				
2	3.53	25.0	62				
3	4.76	18.5	89			18.60/ 100	100
4	25.91	3.44	71	3.44/ 002	40	3.43/ 002	100
5	31.97	2.79	100	2.79/ 211	100	2.84/ 420	100
6	46.70	1.94	33	1.94/ 222	20	1.95/ 822	80
7	49.34	1.84	40	1.84/ 213	20	1.84/ 642	90
8		1.71		1.71/ 004	16		
9		1.45		1.45/ 323	8		
10		1.24		1.24/ 513	4		
11		1.11		1.11/ 514	8		

On the basis of the above data, the XRD confirms that ALAMIN™ is essentially a semi-crystalline phase of HAP (crystal system: *hexagonal*, space group $P6_3/m$). The typical HAP crystal structure is shown in Figure 6-23. This assignment is further strengthened by the observation of additional *minor* structural peaks at (d, Å): 3.111, 2.621 and 2.270, which are also assignable to a HAP-type crystal structure.

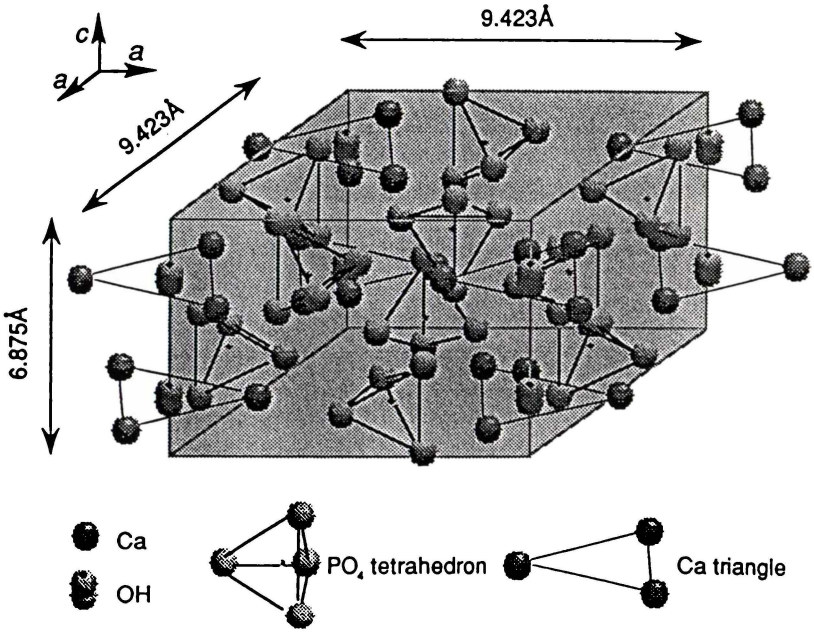

Figure 6-23: Schematic of the crystal structure of hydroxyapatite (Aoki H., 1994).

OCP was considered briefly as a phase in ALAMIN™ due to the once only observation of an intense feature at $2\theta = 4.76°$ in an XRD recorded on the Auckland instrument. This was believed to correspond to OCP given this phase of calcium phosphate exhibits a very characteristic peak at that approximate position in the XRD. Unfortunately further samples of the commercial ALAMIN™ powder run on the same instrument did not show the same feature.

6.1.7(b) Crystallite Sizes of ALAMIN™ Powder

X-ray powder diffraction can be used to determine mean crystallite sizes in semi-crystalline powders. A "crystallite" could be taken to mean the primary particle that makes up a powder or aggregate. The mean crystallite size, D, of the commercial ALAMIN™ powder has been estimated from the corresponding half-height width ($\beta_{½}$) of the 002 diffraction XRD peak using the Scherrer equation:

$$D = \frac{57.3\ K\ \lambda}{\beta_{1/2}\cos\theta}$$

where D = the dimension (lengthwise) of an apatite crystallite, K is the crystal shape factor constant (0.9), $\beta_{½}$ is the width at half height of the 002 peak, λ is the X-ray wavelength in Ångstroms, and θ is one-half of the scattering angle measured as 2θ.

For the 002 peak of apatite θ has a value of 12.93°. The 002 diffraction peak is an appropriate choice of peak for determining crystallite size because it is a well separated and distinct feature in the XRD pattern. Table 6-9 summarises the results of these determinations of crystallite size. It was found that for the different samples of manufactured ALAMIN™ powder the mean crystallite size (D) data were quite constant 203.3±0.5 Å (see Table 6-9). As evidenced by the constancy of the $\beta_{½}$ values, the "mean crystallite size" of the commercial ALAMIN™ powder appears to be essentially invariant between manufacturing runs. Whether this measured value is independent of the degree of aggregation of individual particles in the sample is not known. Some degree of caution must be exercised in interpreting these results absolutely given the Scherrer formula is assumed to apply to a perfect single crystal.

Table 6-9: Data from XRD analysis: width at half height ($\beta_{1/2}$) of the 002 diffraction peak and crystallite size, *D*.

ALAMIN™ Samples	$\beta_{1/2}$, 2θ	*D*, Å
ALAMIN™ (Batch A)	0.417	203.8
ALAMIN™ (Batch B)	0.419	202.8
ALAMIN™ (1996)	0.418	203.4
ALAMIN™ (fraction >150 μm)	0.418	203.3
ALAMIN™ (finest fraction)	0.512	165.9

Impact of Heating on the XRD of Commercial Lactic ALAMIN™ Powder

In order to investigate the temperature effect on the ALAMIN™ structure the samples of fine commercial powders were placed in a Platinum sample holder and inserted to the high temperature XRD camera. An appropriate X-ray diffractograms were recorded for the temperatures 200-800°C using a Philips X'PERT X-Ray Diffractometer. The stacked plot of XRD patterns of the commercial lactic ALAMIN™ powder as a function of temperature (from 200-800°C) showed the following trends (Figure 6-24):

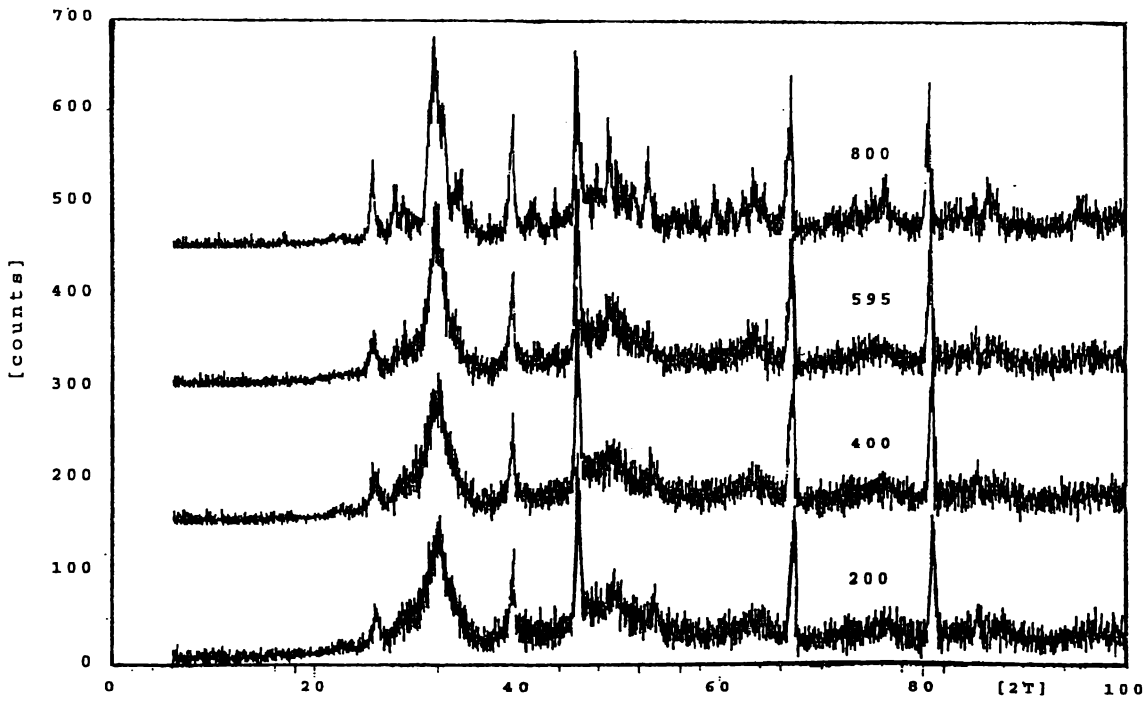

Figure 6-24: Stacked plot of XRD patterns of the commercial lactic ALAMIN™ powder as a function of temperature (T=200, 400, 595 and 800°C).

In general, heating of the ALAMIN™ powder from room temperature up to 800°C led to an increase in the intensities of XRD peaks assigned to HAP phases, especially for the 002 and 211 diffraction peaks. This shows that there is predictably an increase in the degree of crystallinity as the ALAMIN™ powder is heated. Additionally it was noticed that the X-ray diffraction patterns for ALAMIN™ powder at 800°C featured a few more XRD peaks relative to the pattern at room temperature. In general, changes were observed in the 101, 102, 210, 112, 300 and 202 peaks in contrast with ALAMIN™ powder, examined at room temperature. Moreover, the width of the XRD peaks decreased with increasing temperature showing the formation of long-range order in the atom arrangement in the crystal structure as a result of crystallisation. This cursory examination of the heating behaviour of the commercial ALAMIN™ powder thus served to show that there is a gradual transformation of the ALAMIN™ powder from a partially amorphous/ crystalline to a generally more crystallised apatitic phase.

As was mentioned in section 2.18: "Solid State Interconversions of Calcium Phosphate Compounds"), heating of some calcium hydroxyapatite compounds can lead to solid state phase interconversions caused mostly by the dehydroxylation of hydroxyapatite. HAP is known to dehydroxylate and undergo a phase change to TCP at a temperature of 1300-1460°C (Ruys et al., 1992). However, it has been shown by many researchers that HAP begins to lose its OH groups at a much lower temperature (e.g. 770°C) than that at which the phase change occurs. These temperatures are well above the temperature at which the ALAMIN™ powder is dried in the proprietary process (~200°C), so that dehydroxylation of HAP to form TCP is not likely to occur. Further information on the behaviour of ALAMIN™ on heating has been provided by a DSC analysis which is dealt with later in this chapter.

6.1.8 Malvern (*Mastersizer*) Determination of Particle Sizes on Various Grades of Commercial ALAMIN™ Powders, produced from Lactic Whey Permeate

Experimental. Light scattering Malvern particle size measurements were undertaken to determine the particle sizes of commercial ALAMIN™ powders, using the Laser Diffraction Particle Sizer (The Malvern *Mastersizer-S).* The ALAMIN™ powder particles to be measured were added into the sample dispersion unit, which contained a litre of tap water (18-20°C) which was circulated through a flow cell which illuminated by a 2 mW power HeNe laser with wavelength 0.63 μm laser light.

System Details. The parameters used for performing Malvern (*Mastersizer*) experiments on the ALAMIN™ powder samples are summarised in Table 6-10.

Table 6-10: Typical Malvern (*Mastersizer*) parameters, used for the ALAMIN™ particle size measurements.

Parameters	Data
Range Lens (μm)	300RF[1] (0.05-880 μm)
Analysis Model	Polydisperse
Presentation	3PHD
Beam Length (mm)	2.40[2] mm
Particle R.I.	(1.5960, 0.1000)
Dispersant R.I.	1.3300

[1]Range Lens: The lens that was fitted for the analysis performed, e.g. 300RF gives a range of analysis from 0.05 to 880 μm.
[2]Beam Length: The distance that the beam travels through the sample in the course of a measurement. For a sample in liquid suspension, 2.4 mm is the distance between the windows in the flow cell.

So in this experimental work the light scattering Malvern particle size measurement were undertaken to determine the particle sizes of commercial as received ALAMIN™ powders at the same laser beam pathlength (2.40 mm) and particle refractive index (1.5960, 0.1000) while keeping the obscuration *ca.* 20%. As mentioned earlier (see section 3.6.2: "Basic Procedure for Malvern (*Mastersizer*) Particle Size Determination"), the obscuration, also known as turbidity, is a measure of the amount of sample added to the tank. Unscattered light is focused onto the obscuration detector (see Figure 3-1). If there is no sample present then the obscuration is zero. When the sample is introduced some of the light is absorbed, reflected, diffracted, scattered, etc and an obscuration number is obtained. The instrument works with obscuration values between 10% and 30% which ensures sufficient signal-to-noise for good measurements and eliminates the possibility of multiple scattering.

Results. The full printouts of the laser particle size (Malvern) measurements for the different grades of commercial lactic ALAMIN™ powder, including the fractions < 150 and > 150 μm and the finest grade can be found in the Appendix C. In general, the manufactured grades of ALAMIN™ powder are complex material with a wide distribution of particle sizes, D[4, 3] (the most common parameter used in this technique for quoting the general particle size) = 5-190 μm (Table 6-11).

Table 6-11: Malvern (*Mastersizer*) particle size data[1] for various grades of commercial ALAMIN™ powders, produced from lactic whey permeate.

ALAMIN™ Samples[2]	D [4, 3], μm	D (v, 0.9), μm	D (v, 0.5), μm	D (v, 0.1), μm	D [3, 2], μm
Fraction >150 μm	189.00	293.14	193.44	54.09	30.15
Fraction <150 μm	29.95	60.76	23.66	6.26	29.95
ALAMIN™ (Batch A)	28.20	58.00	21.51	4.39	28.19
ALAMIN™ (Batch B)	18.50	35.07	16.38	4.12	18.49
"Typical" ALAMIN™	27.41	58.85	20.41	2.62	4.93
Finest fraction	5.20	10.90	3.79	1.45	5.23

[1] measured mean diameters are:

D[4, 3]- the volume weighted mean diameter. The diameter of the sphere having the same volume as the real ALAMIN™ particle.

D[3, 2]- the surface weighted, or Sauter, mean diameter. The diameter of the sphere having the same surface area as the real ALAMIN™ particle. Apart from the mean diameters D[4, 3] and D[3, 2] the result (Table 6-11) has listed the 10%, 50% and 90% volume percentile, expressed as D[v, 0.1]-means that 10% of the distribution is below this value, D[v, 0.5]- 50% volume percentile, or median of the volume distribution, and D[v, 0.9]- 90% of the distribution is below this value.

[2]The various batches of manufactured ALAMIN™ used in this study.

In general, approximately symmetrical unimodal type distributions were obtained for each sample with some tailing to the particle size end. The widths of these distributions were generally quite broad indicating a wide range of particle sizes (see Appendix C).

6.1.9 Differential Scanning Calorimetric Analysis (DSC) of ALAMIN™ Powder, produced from Lactic Whey Permeate

Differential Scanning Calorimetric (DSC) analysis was also carried out on as received ALAMIN™ powders as part of the suite of characterisation techniques that have been applied to this material. DSC was used to investigate the thermal properties of the commercial grades of ALAMIN™ powder (i.e. processes occurring when the solid material is heated). This complements the cursory XRD investigation performed on this powder as described in section 6.1.7: "X-ray Diffraction (XRD) Investigation of ALAMIN™ Powder, produced from Lactic Whey Permeate". As a comparison, the

other commercial products, LACTOVAL, and LACPRODAN as well as pure samples of likely contaminants in ALAMIN™ such as lactose, whey proteins and citric acid were also subjected to DSC analysis.

Experimental. In a typical DSC experiment, each powder was placed in aluminium pans, which were hermetically sealed and weighed accurately before analysis. DSC analysis was carried out using two instruments. The first instrument on which preliminary measurements had been taken was a Perkin Elmer DSC-6 Differential Scanning Calorimeter. This scanned in the temperature interval 25-400°C at a preset heating rate of 10°C min^{-1}. The second DSC instrument used was a TA instruments DSC 2920 which could be taken beyond 400°C (the maximum temperature of the DSC-6) up to 640°C using a heating rate of 10°C min^{-1} with an air flow of 50 cm^3 min^{-1}. Most data presented have been recorded on the TA Instruments DSC unit.

Results and Discussion. Figure 6-25a shows the typical DSC curves of the commercial lactic ALAMIN™ powder, heated from 25 to 640°C. The positions of the endothermic and exothermic peaks of the DSC thermograms for the commercial ALAMIN™ powder, LACPRODAN and LACTOVAL powders are shown in Table 6-12.

For comparative purposes, DSC curves were also recorded of pure materials known to be associated with ALAMIN™ powders such as whey proteins (α-lactalbumin and also β-lactoglobulin), lactose and citric acid (see Table 6-13).

Table 6-12: Positions of the DSC thermogram peaks for the commercial ALAMIN™, LACPRODAN and LACTOVAL powders.

Samples	*Endothermic* DSC thermogram peaks, °C	*Exothermic* DSC thermogram peaks, °C
ALAMIN™, derived from lactic whey permeate	121	500
ALAMIN™, derived from sulfuric acid whey permeate	116	395
LACPRODAN, produced in DENMARK	127	395, 589
LACTOVAL, produced in NETHERLANDS	121	593

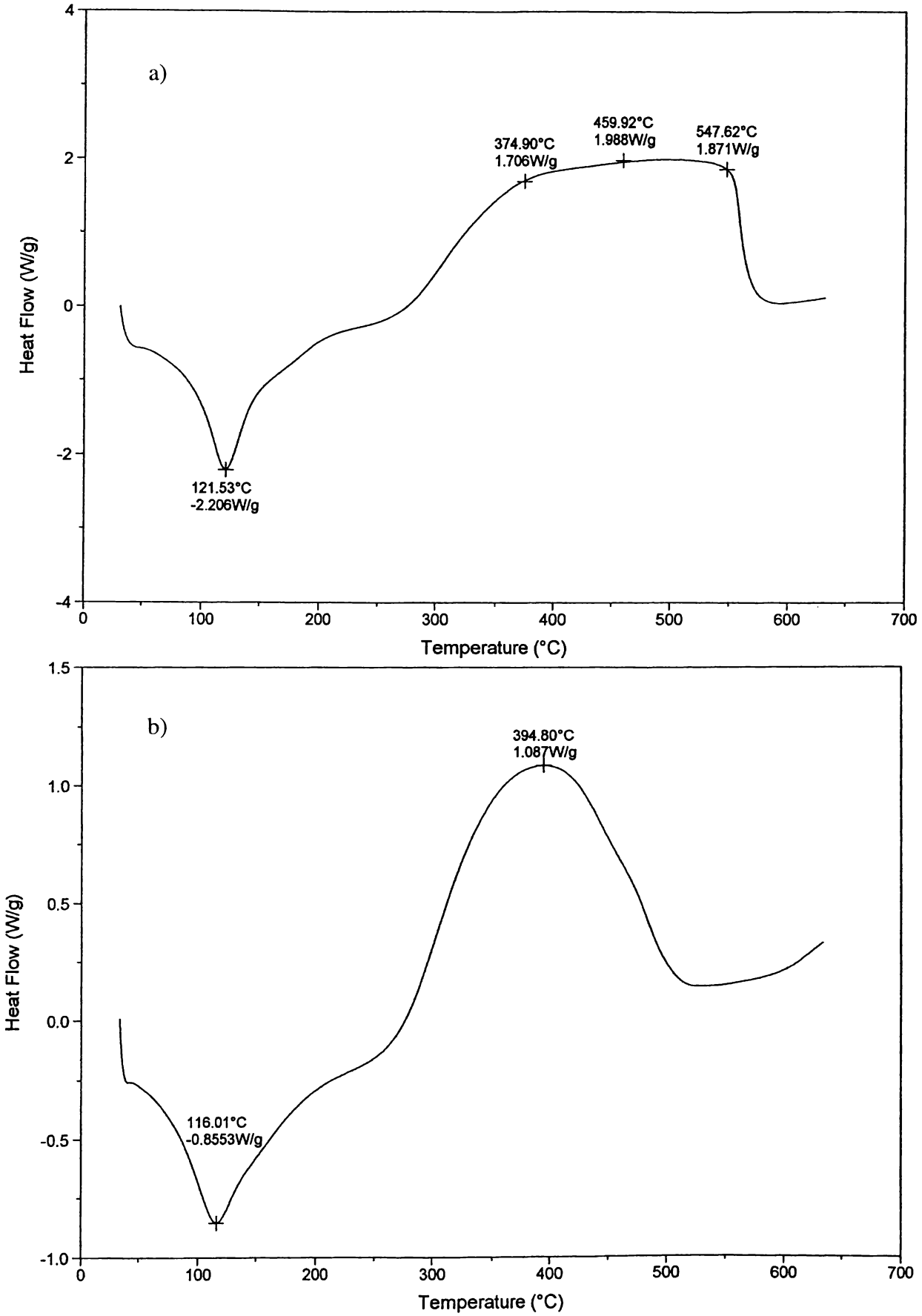

Figure 6-25: Typical DSC curves for the commercial heated from 25 to 640°C ALAMIN™ powders, derived from: a) lactic whey permeate; b) sulfuric acid whey permeate.

Table 6-13: The positions of the DSC thermogram peaks for whey proteins, lactose and citric acid.

Samples	Endothermic DSC thermogram peaks, °C	Exothermic DSC thermogram peaks, °C
Whey proteins (α-lactalbumin-β-lactoglobulin)	115-119	600-607
α-Lactose monohydrate	148	384, 542
Citric acid	72, 130	454

In general, comparison of the DSC profiles obtained for ALAMIN™ with those for the pure proteins, citric acid and lactose was difficult due to the great variability between profiles of the different samples. Only some general suppositions could be made regarding the origin of peaks observed in DSC profiles.

The main *endothermic* DSC peak (116-121°C) for the commercial, as received ALAMIN™ powders (and also LACPRODAN and LACTOVAL products) is associated with the dehydration of the powder samples. The shift to higher temperatures than would be expected for the dehydration of water (i.e. 100°C) could be due to dehydration of water chemically bound with lactose. It was found by Drapier-Beche et al. (Drapier-Beche et al., 1997) that a dehydration step of α-lactose (monohydrate) form is occurring at 144°C, as was shown in their DSC investigations of the transition temperatures of the different α and β-lactose forms.

There is also a possibility that citrate-associated thermally-induced transformations could be in some way giving rise to this profile. Mahmood (Mahmood et al., 1986) reported in their DSC study of citric acid that the thermal decomposition of this compound was due to melting (melting point *ca.* 153°C) and dehydration to give aconitic acid (II) on heating at 175°C.

The next prominent DSC peak observed in samples of ALAMIN™ was an *exothermic peak* which occurred over the 300-600°C region. This region is associated generally with the pyrolysis or combustion of organic-type compounds. Thus in ALAMIN™ it could be associated with thermal decomposition of the citrate and lactose contained in the powders (see Figure 6-26). An example of the citrate decomposition mechanism

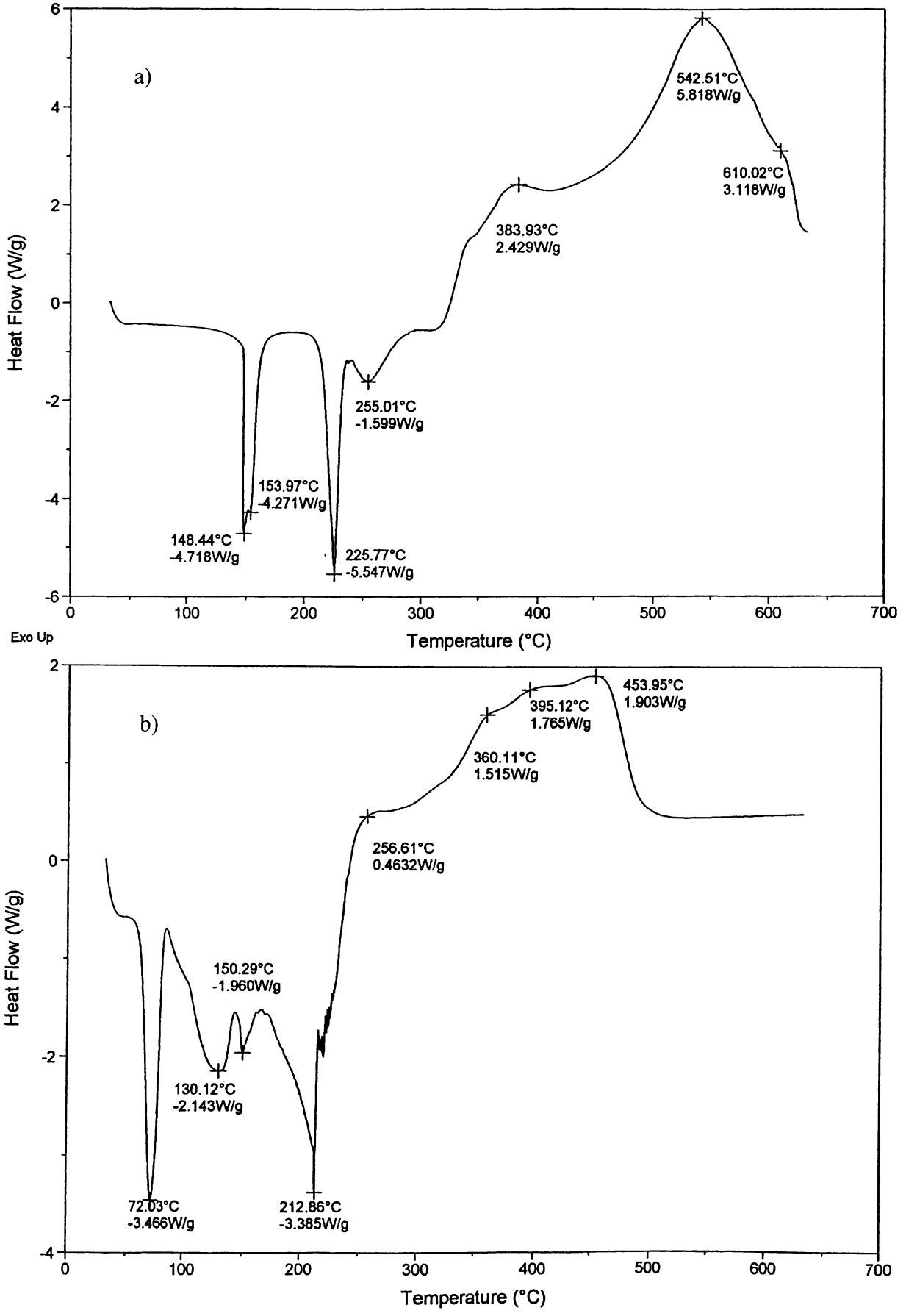

Figure 6-26: DSC curves for: a) lactose and b) citric acid, heated from 25 to 640°C.

that could occur is its transformation to acetone dicarboxylic acid which results in the elimination of CO_2.

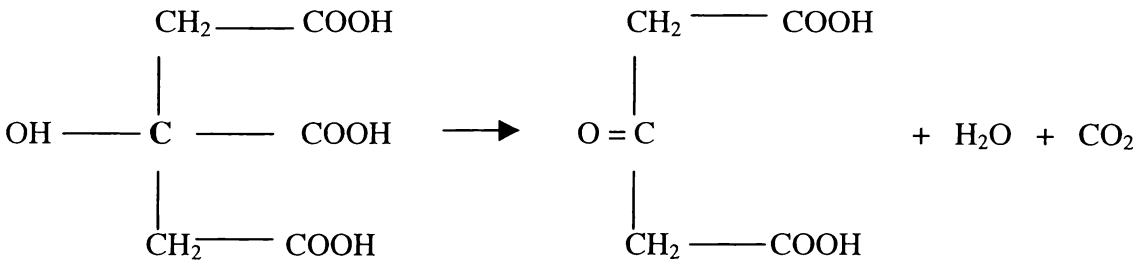

Further decomposition of the acetone dicarboxylic acid to acetone could then proceed at higher temperatures (Mahmood et al., 1986).

In addition, the influence of whey proteins co-deposited with the ALAMIN™ cannot be overlooked. These will also denature and decompose in the 300-600°C region. Under such conditions, a Maillard-type reaction could occur which results in the samples of ALAMIN™ developing an overall brown colour at the end of the experiment.

In general the differential scanning calorimetric analysis for ALAMIN™ powder suggests that a mixture of components could be giving rise to the observed profile such as moisture and varying proportions of organic material like citrate, lactose, and whey proteins which are intimately associated with the CaP powder particles. Further work on this area involving thermogravimetric analysis coupled with mass spectrometry and FTIR of the heated product would probably be needed to provide more information.

6.2 Characterisation of the Commercial Sulfuric Acid Whey Permeate and ALAMIN™ Powder by Chemical, Spectroscopic and Microscopic Techniques

6.2.1 Fourier Transform Infrared Spectroscopy (FTIR) Analyses

FTIR spectra were recorded of solid samples as KBr disks on a Digilab FTS-40 FTIR Spectrometer from 4000-400 cm^{-1} at 4 cm^{-1} resolution. Solids analysed were commercial sulfuric acid whey permeate-derived: ALAMIN™ powder, unwashed and washed ALAMIN™ cake, BDH grade gypsum ($CaSO_4.2H_2O$) and BDH grade anhydrous calcium sulfate ($CaSO_4$). Some of these results have been used as a partial confirmation of trends predicted in the chemical speciation calculations described in Chapter 5 for this whey permeate system.

Commercial Sulfuric Acid ALAMIN™ Powder, Unwashed and Washed CaP Cake

Figure 6-27 is an FTIR spectrum of the commercial ALAMIN™ powder, derived from sulfuric acid whey permeate. Figure 6-5 (see section 6.1.4: "Fourier Transform Infrared Spectroscopy (FTIR) Analyses of ALAMIN™ Powder, produced from Lactic Whey Permeate") is an FTIR spectrum of a sample of ALAMIN™ powder obtained by precipitation from lactic acid whey permeate as carried out in the proprietary process. It is obvious that the two spectra are practically identical to each other so that the character of the CaP phases present in each of the powders closely resemble each other.

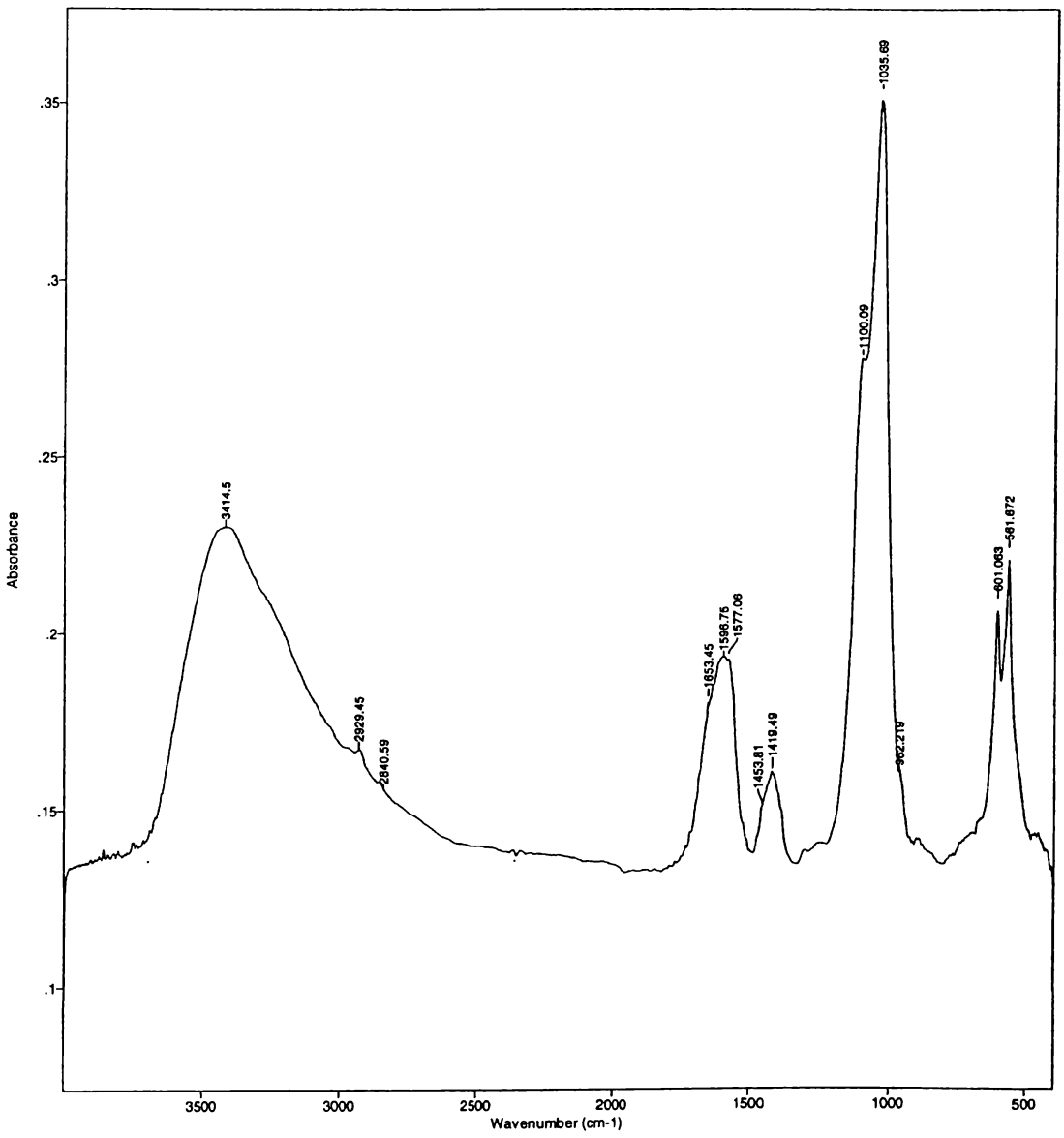

Figure 6-27: FTIR spectrum of the commercial sulfuric acid ALAMIN™ powder.

Figures 6-28(a) and (b) are IR spectra of washed and unwashed CaP cake respectively from the sulfuric acid ALAMIN™ industrial proprietary process.

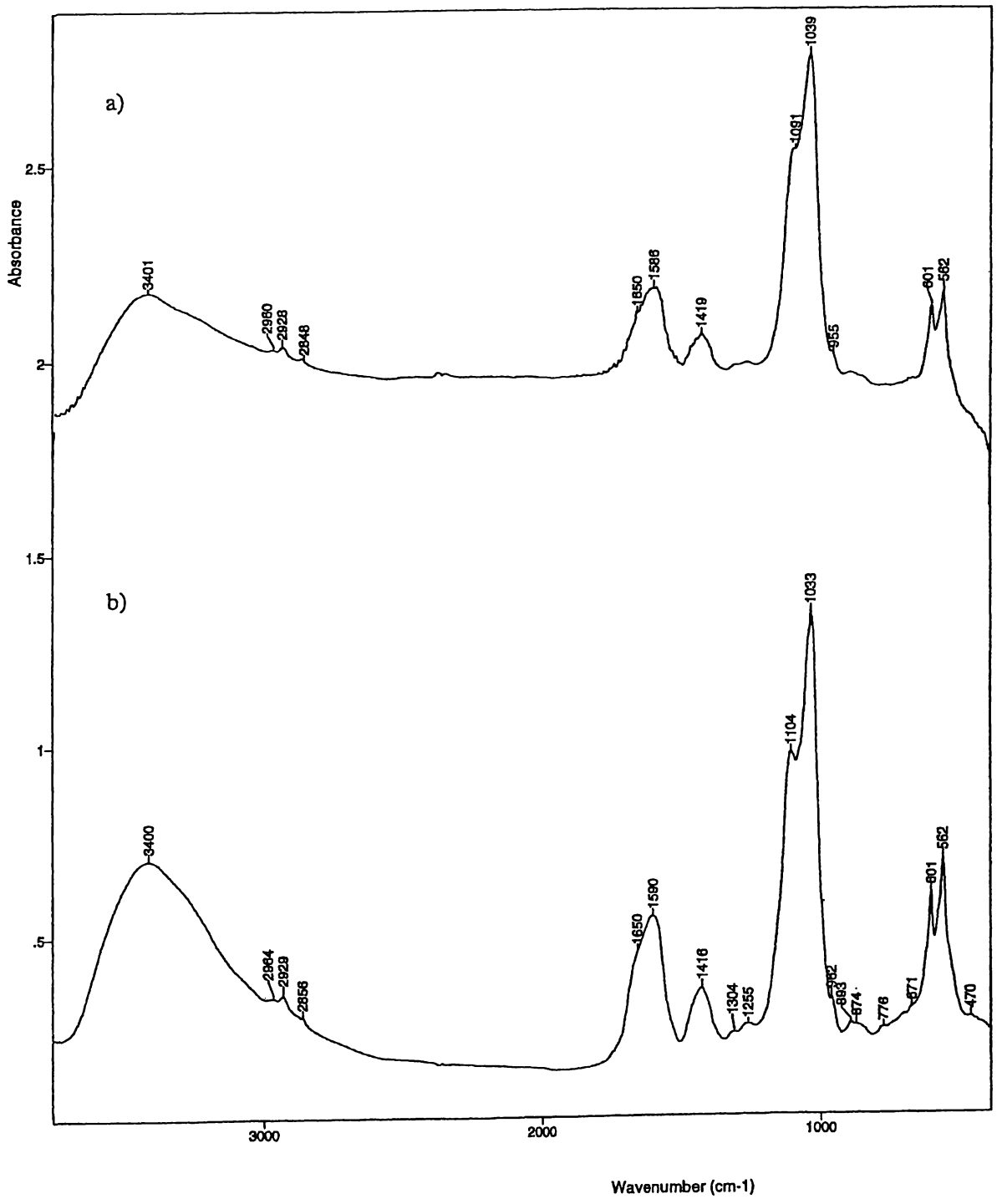

Figure 6-28: FTIR spectrum of the commercial sulfuric acid derived a) washed and b) unwashed CaP cake.

CaP cake samples were examined by FTIR in order to ascertain whether there were any entrained solid phases of calcium sulfate present in the product. Unwashed cake, especially, should show any contamination by sulfate in the product. However, when

the two spectra were compared, it was evident that they were practically identical except for the presence of some minor peaks at 1304, 1255, 893, 874 and 776 cm^{-1} which are possibly associated with higher levels of protein and lactose/citrate before washing. This is confirmed when one examines the FTIR spectrum of the washed cake which shows a diminution in these peaks. For comparative purposes, FTIR spectra were also acquired of pure calcium sulfate from various sources.

Figure 6-29 is an IR spectrum of "naturally occurring" gypsum, Figure 6-30 is a spectrum of calcium sulfate hemihydrate ($CaSO_4.1/2H_2O$) and Figure 6-31 is a spectrum of anhydrous calcium sulfate ($CaSO_4$). Since SO_4^{2-} and PO_4^{3-} are both tetrahedral anions, they exhibit similar IR spectra with different stretching and bending frequencies due to the differences in the mass of P and S atoms. These stretching and bending frequencies characteristic of sulfate and phosphate anions can be summarised in the table below (Table 6-14).

Table 6-14: Fundamental vibrational frequencies (Nakamoto, 1986) of the tetrahedral five-atom molecules $SO_4^{2-}$and PO_4^{3-} (in cm^{-1}) in FTIR spectra.

Ions	ν_1	ν_2	ν_3	ν_4
SO_4^{2-}	983	450	1105	611
PO_4^{3-}	938	420	1017	567

For calcium sulfate phases containing waters of crystallisation in their structural lattice (e.g "natural" gypsum and the hemihydrate), additional peaks due to the stretching vibrations of water will also be present at 3549, 3406, 1685, 1622 cm^{-1} (in natural gypsum) and at 3611, 3550 and 1619 cm^{-1} in the hemihydrate.

Comparison of the spectra in Figures 6-29 to 6-31 with Figure 6-28 show that there is no detectable sulfate present in the cakes as shown by the complete absence of any readily discernible sulfate-associated peaks in the spectra. If a low level of a calcium sulfate solid phase or (the more likely scenario of) calcium sulfate solution trapped in pores were present, its IR peaks would be hidden/strongly overlapped by the more intense calcium phosphate-associated peaks.

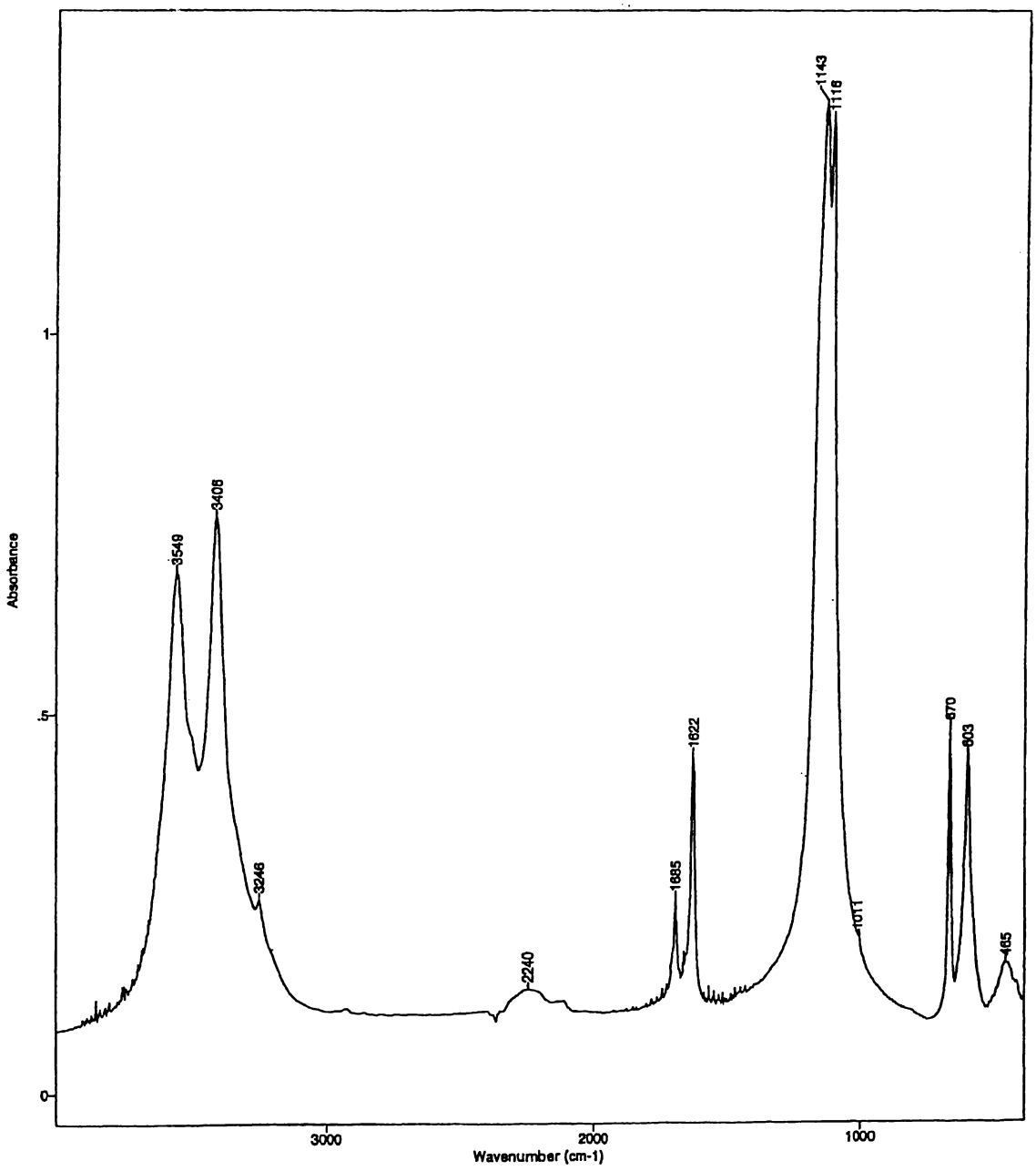

Figure 6-29: FTIR spectrum of naturally occurring gypsum (geological sample).

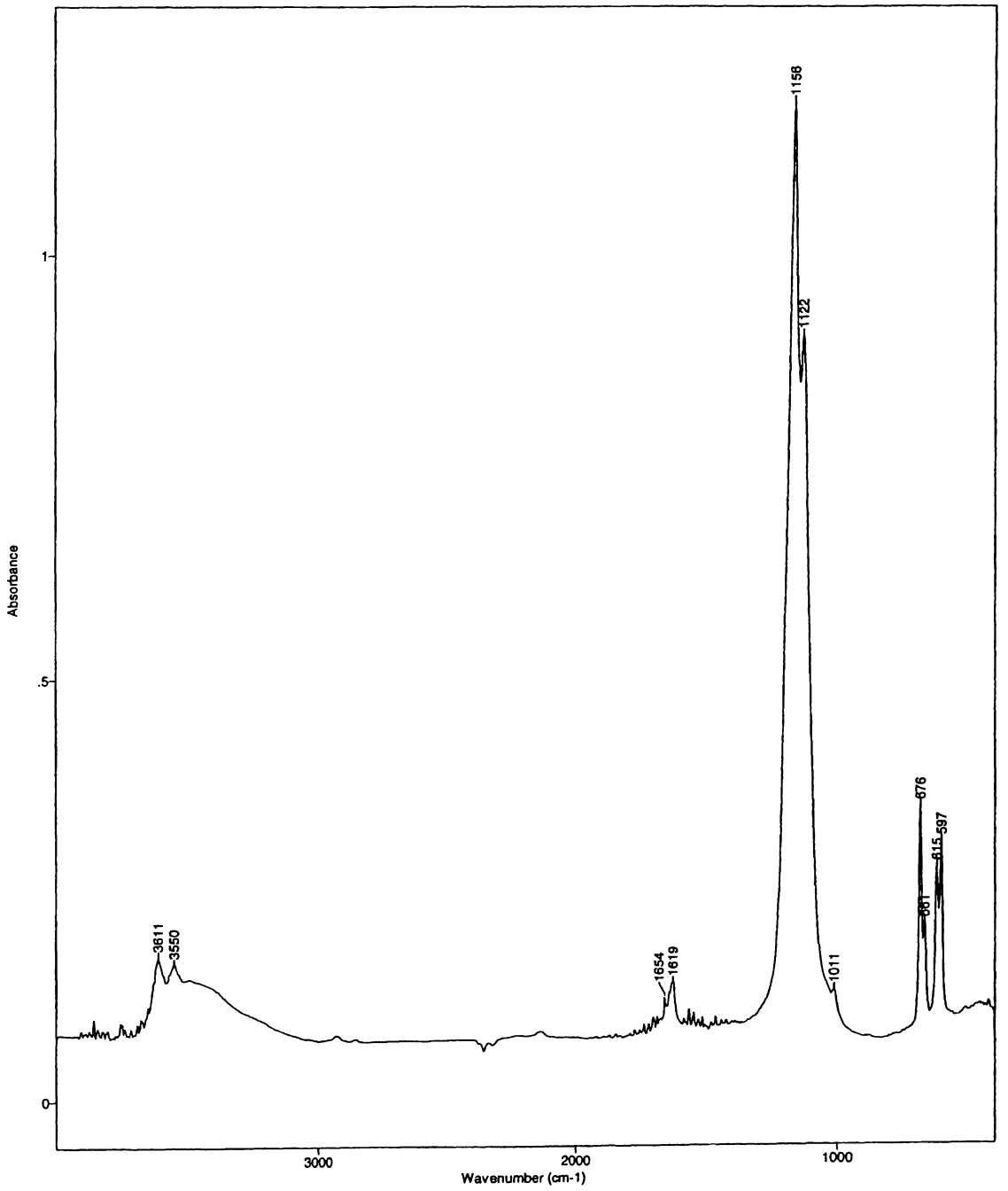

Figure 6-30: FTIR spectrum of calcium sulfate hemihydrate ($CaSO_4.1/2\ H_2O$).

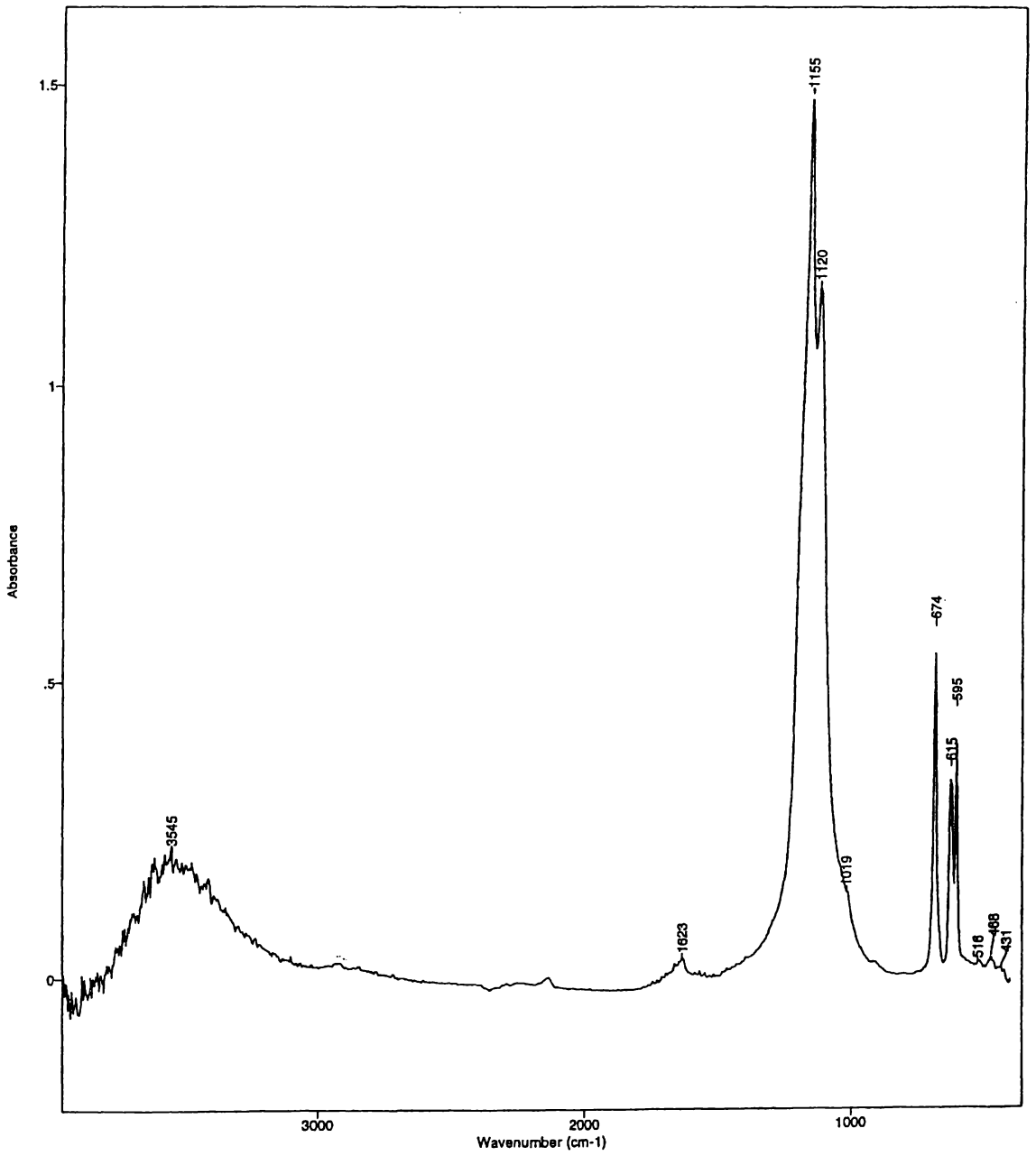

Figure 6-31: FTIR spectrum of anhydrous $CaSO_4$.

This is especially so if the weight percent of sulfate was less than 1% (see later chemical analyses). Even though IR cannot detect the presence of any sulfate in the product, chemical analyses have shown that the "background" sulfate level in the sulfuric acid ALAMIN™ is higher than that in the lactic ALAMIN™ (see section 6.2.3: "Chemical Analysis of ALAMIN™ Powders and Cakes by ICP-OES").

6.2.2 Scanning Electron Microscopy Characterisation of ALAMIN™ Solids, produced from Sulfuric Acid Whey Permeate

A small SEM study was conducted to investigate the typical morphological characteristics of sulfuric acid whey permeate-derived: ALAMIN™ powders, unwashed and washed CaP cake. Figure 6-32(a) and (b) represent SEMs of unwashed CaP cake from the industrial proprietary process. What is immediately evident is the porous, "pumice-like" nature of the unwashed cake surface. The clumps look as if they are composed of large aggregates formed from the amalgamation of many smaller particles. Figures 33(a) and (b), in contrast represent SEMs of washed CaP cake. These particles differ from those seen in unwashed cake in that they have a "washed out" look. In other words, they have a more dendritic and apatitic-looking structure, which perhaps become more visible after the washing out of various minor (whey) components such as protein and lactose etc. Larger channels and pores in the washed cake are more evident due perhaps to the washing process. Figure 6-34(a) and (b) are a SEM micrographs of the commercial sulfuric acid ALAMIN™ powder (after being dried). The structural characteristics of the particles making up the powder are broadly similar to those of lactic ALAMIN™ powder when examined under the SEM, i.e. they exhibit layer-like structure with pores and channels and voids evident in the particle. In general, owing to caking processes that occur upon drying of the cake, the individual commercial ALAMIN™ powder particles exhibit a somewhat denser nature (despite some particles having some visibly large channels) than those particles comprising the ALAMIN™ cakes.

6.2.3 Chemical Analysis of ALAMIN™ Powders and Cakes by ICP-OES

Table 6-15 summarises the analyses by ICP-OES of acid-digested samples of the sulfuric acid whey permeate-derived washed and unwashed CaP cake (and also washed lactic CaP cake and ALAMIN™ powder). Analyses were made for Ca, Mg, P, S, Na, and K. The wt. % of Ca and P were similar between all samples analysed showing consistency of product.

a)

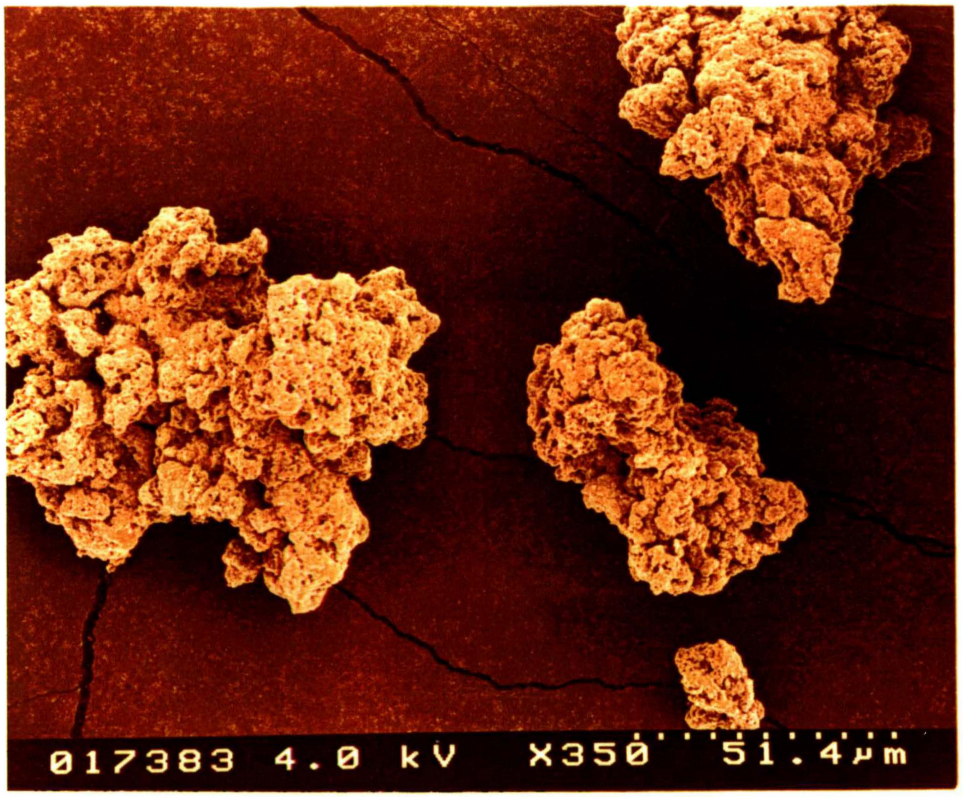

b)

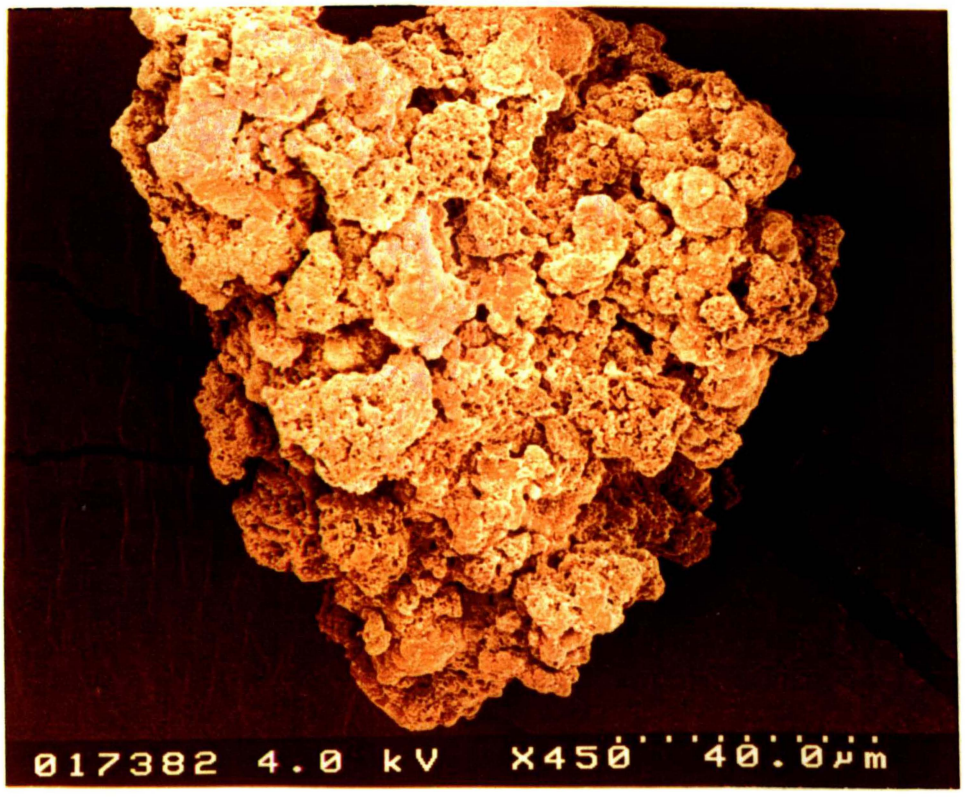

Figure 6-32: SEM micrographs of unwashed CaP cake powder at the magnification of: a) x 350 and b) x 450.

a)

b)

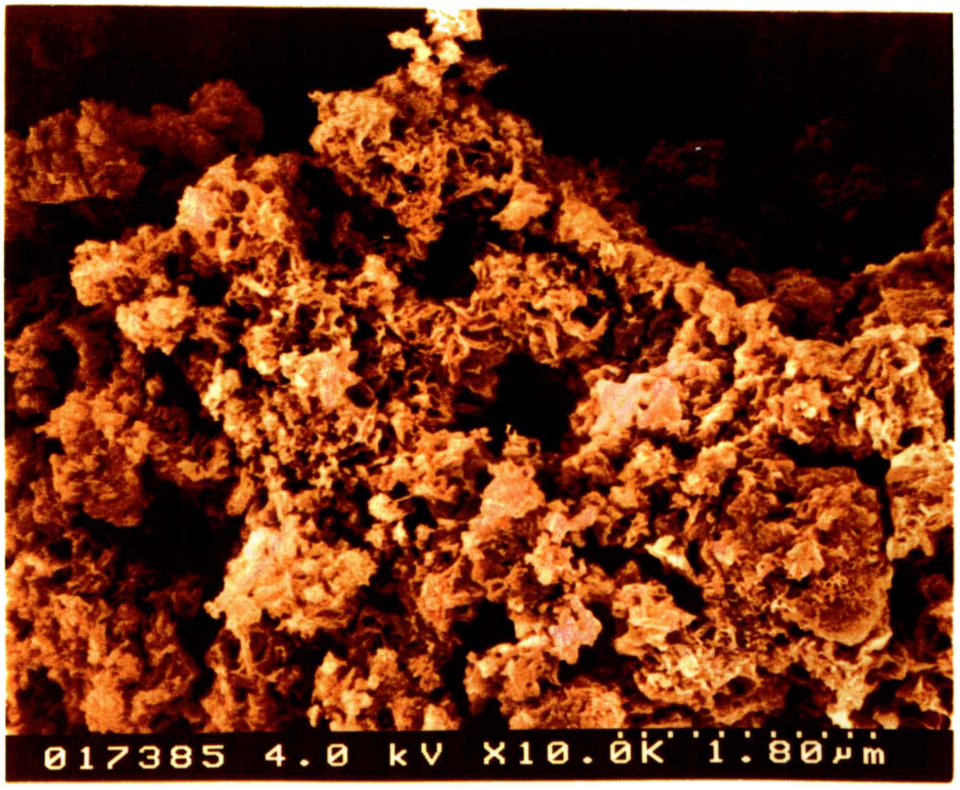

Figure 6-33: SEM micrographs of: a) unwashed and b) washed CaP cake powder, produced from the sulfuric acid whey permeate.

a)

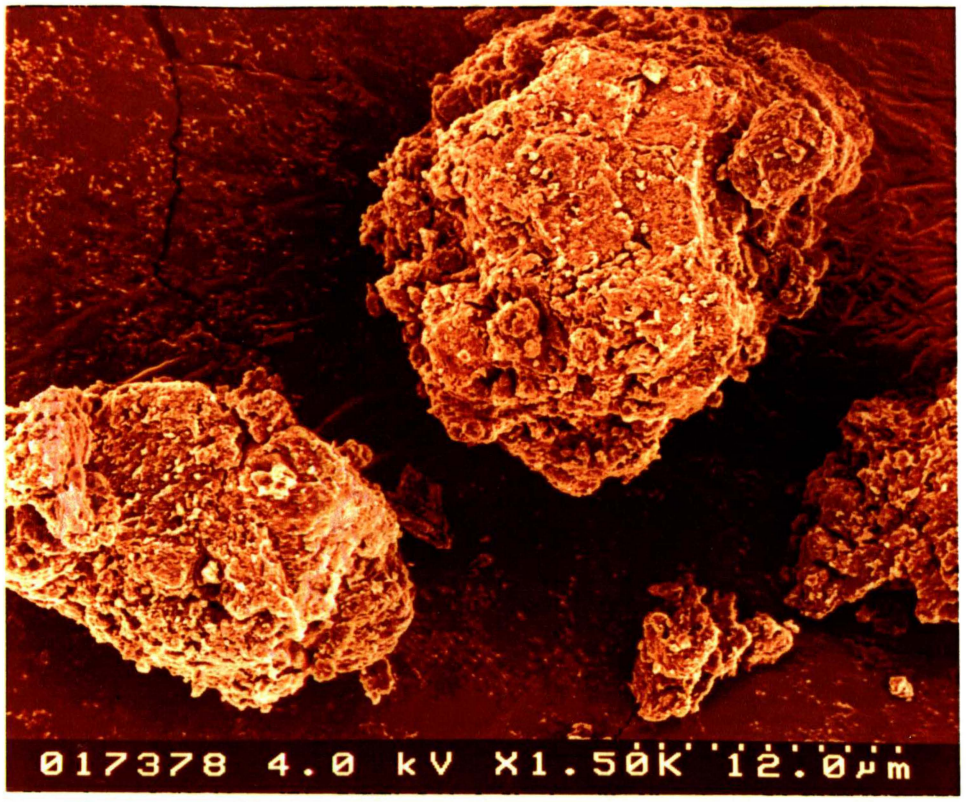

b)

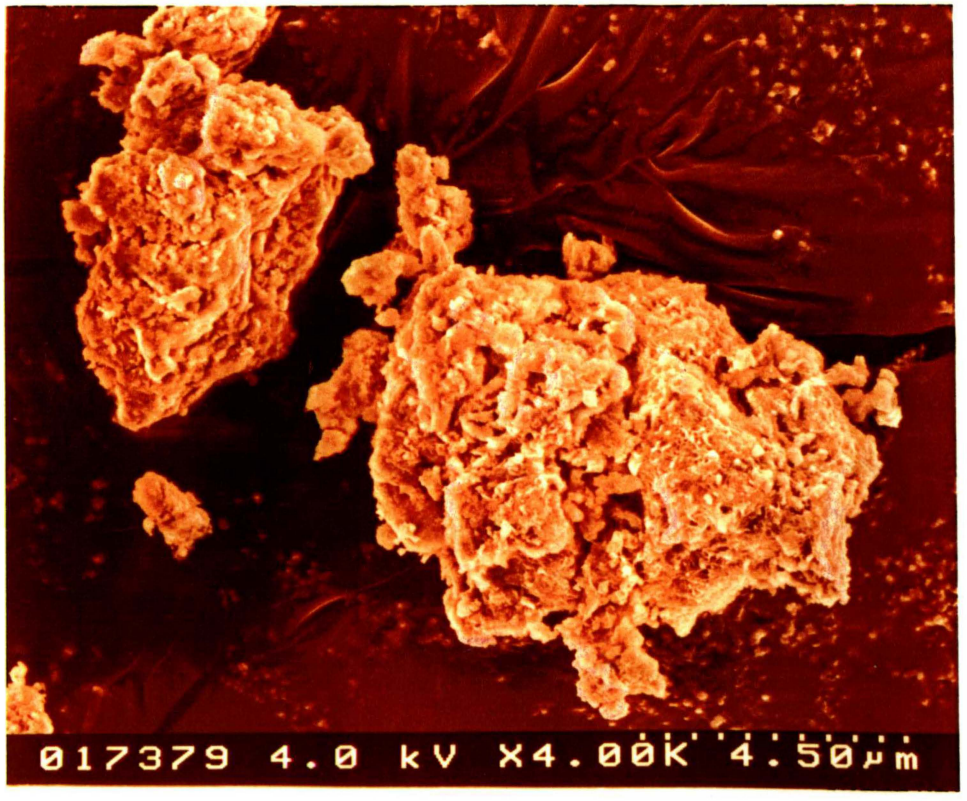

Figure 6-34: SEM micrographs of the sulfuric acid ALAMIN™ powder: a) typical particles at magnification x 1 500 and b) at magnification x 4 000.

Table 6-15: Chemical ICP-OES analyses[1] of acid-digested samples of the sulfuric acid whey permeate-derived washed and unwashed CaP cake (and also washed lactic CaP cake and ALAMIN™ powder).

Commercial sample	P wt. %	S wt. %	Mg wt. %	Ca wt. %	Na wt. %	K wt. %
CaP cake *unwashed* (from sulfuric acid whey permeate)	10.0	0.26	0.51	23	0.43	0.34
CaP cake *washed* (from sulfuric acid whey permeate)	10.7	0.13	0.50	25	0.28	0.18
CaP cake *washed* (from lactic whey permeate)	10.3	0.04	0.77	22	0.39	0.19
ALAMIN™ (from lactic whey permeate)	10.4	0.06	0.86	24	0.47	0.25

[1] as received from AgResearch Soil Fertility Service, Hamilton (Laboratory Reference 99/B/2299-2302, 12.04.99): Method used was a total digestion on all samples using Nitric/Perchloric acid mixture. Analyses by ICP-OES were used for P, S, Mg and Ca. Analysis by Atomic Absorption was used for Na and K.

It should be mentioned that ICP-OES chemical analyses give the most consistent data for the Ca wt. % values, however, the data for P wt. % values are very inconsistent. The difference in P wt. % were more than 3 % for the same sample when it was analysed by two independent laboratories using the *same* digestion method and the *same* technique (ICP-OES).

At the last moment, colorimetric methods, that were brought in to analyse for phosphate gave *slightly higher* values for P in most of the ALAMIN™ samples analysed (see Table 6-16, Hills Laboratories report), an observation which confirms the need to be somewhat wary about analysed P readings by ICP-OES.

The wt. % of Na in the unwashed CaP cake (from sulfuric acid whey permeate) was higher (0.44 %) than in the washed CaP cake (0.31 %). K and S also decreased upon washing. The wt. % of Mg remained the same between washed and unwashed CaP cake indicating it was an intimate structural component in the apatite lattice making up ALAMIN™ and was thus not susceptible to removal by washing.

Table 6-16: Colorimetric (for P) and ICP-OES data of acid-digested samples of the sulfuric acid whey permeate-derived washed and unwashed CaP cake (and also washed lactic CaP cake and ALAMIN™ powder).

Commercial sample	P, wt. %	S, wt. %	Mg, wt. %	Ca, wt. %	Na, wt. %	K, wt. %
CaP cake *unwashed* (from sulfuric acid whey permeate)	13.2	0.27	0.48	24.3	0.44	0.39
CaP cake *washed* (from sulfuric acid whey permeate)	14.2	0.15	0.47	26.3	0.31	0.26
CaP cake *washed* (from lactic whey permeate)	13.5	0.05	0.73	23.5	0.36	0.22
ALAMIN™ (from lactic whey permeate)	13.3	0.05	0.68	24.0	0.46	0.29
ALAMIN™ (from sulfuric acid whey permeate	13.2	0.17	0.47	26.6	0.34	0.30

[1] as received from Hill Laboratories, Hamilton (Laboratory Reference 129051, 13.04.99): Method used was a total digestion on all samples using Nitric/Perchloric acid mixture. Analyses by ICP-OES were used for S, Mg, Ca, Na and K. Analysis by Colorimetry was used for P.

The most significant observation from these analyses (Tables 6-15 and 6-16) is the fact that the analysed S level (although low) in the CaP cake (both washed and unwashed, derived from sulfuric acid whey permeate industrial process) is significantly higher than corresponding ALAMIN™ samples derived from the lactic whey permeate commercial process.

For example (see Table 6-15), the level of S in unwashed CaP cake (from sulfuric acid whey permeate industrial process) is over four times higher (at 0.26 wt. %) than the level detected in washed CaP cake and commercial ALAMIN™ powder (0.04 wt. % and 0.06 wt. % respectively), manufactured from lactic whey permeate. Even in washed CaP cake (from sulfuric acid whey permeate industrial process), the level of detected S (0.13 wt. %) is twice that in washed CaP cake (0.04 wt. %), manufactured from lactic whey permeate. This indicates that in the unwashed cake, much of the sulfate is present in an easily removable form and as such indicates that it is mostly in the form of a

soluble salt. This is supported by the speciation calculations to a large extent (see Chapter 5) as these showed that sulfate exists largely as free solution sulfate in the commercial precipitation region (i.e. CaP solid phases are thermodynamically more stable than calcium sulfate solid phases in this region).

However, it is evident that the level of sulfate in the sulfuric acid ALAMIN^{TM} product is somewhat higher than that in lactic ALAMIN^{TM} powder (see Table 6-16) which requires explanation. This is believed to be due to the fact that at sulfuric acid ALAMIN^{TM} is being precipitated from a sulfate-rich medium, so that some sulfate will inevitably be taken up by the hydroxyapatite lattice upon formation. This is due to the fact that the hydroxyapatite lattice is very "hospitable" one which allows the substitutions of many other ions. So, substitutions in the structure of various cations and anions for (Ca^{2+}), (PO_4^{3-}) or (OH^-) groups many occur often without changing the structural integrity of solid significantly. Thus the sulfate could have been taken up in the structure upon precipitation.

However, *another* possibility is that sulfate is adsorbed on the surfaces of the evolving apatitic precipitate. It is known that the chemical structure and size of the sulphate ion (SO_4^{2-}) are quite similar to those of the phosphate ion (PO_4^{3-}). In fact the interatomic distance between S and O (0.149 nm) in sulfate anion is almost the same as that between P and O (0.155 nm) in phosphate anion. Yet another possibility for the inherently higher sulfate level found in (washed) CaP cake can be due to the industrial process used to produce the ALAMIN^{TM} from the commercial sulfuric acid whey permeate. Yaminskii (Yaminskii et al., 1991) has commented that in the formation of precipitated phosphogypsum, the combination of particles in aggregates can be caused by the formation of adhesive nuclei in the contacts between particles.

CHAPTER SEVEN

CHEMISTRY OF CALCIUM PHOSPHATE PRECIPITATION FROM WHEY PERMEATES

7.1 Bench-Scale Experimental Investigation of the Precipitation of Calcium Phosphate from Whey Permeates

7.1.1 The Precipitation Reaction: Experimental Procedure

In general, the investigation of any given precipitation reaction of calcium phosphate from whey permeates was carried out following the flowchart illustrated below (see Figure 7-1). Lactic or sulfuric acid whey UF-permeate was customarily supplied in 20 L plastic containers directly from the commercial production sites. When received, this was stored at 4°C storage fridge until use. Because of the distance of both factories from the University of Waikato, the whey UF-permeate could not always be investigated in a fresh state. It was also not possible in the case of the lactic whey UF-permeate to always know which starter bacteria were used in its manufacture. Hence the aim of these bench scale experiments was to provide an overall understanding of the *general trends in the chemistry* of calcium phosphate precipitation from whey permeates and not to look for differences between different starters. In addition, most data in this thesis pertain to precipitation reactions performed with lactic whey UF-permeate due to its greater availability. In a typical precipitation experiment, 500 mL of whey permeate was placed in a round-bottomed quickfit flask equipped with a reflux condenser, thermometer, magnetic stirring bar and pH electrode (see Figure 7-2). The pH electrode was attached to a Radiometer PHM pH meter previously calibrated between pH=4.005 and 6.865 at 75°C using Standard IUPAC (*Radiometer*) buffers. The entire flask was immersed in a heated water bath which was used for bringing the temperature of the whey permeate to 75°C before base addition. The initial pH of the lactic whey UF-permeate was typically 4.6 and was adjusted to pH 6.8 by a single addition of 10% NaOH solution via syringe. This resulted in immediate precipitation of a white solid. The vessel was then left for 30 minutes (with stirring) to allow development of the precipitate. Unlike the pH-stat experiments in Chapter 4, no further NaOH was added to maintain pH at 6.8. pH readings of the pH-adjusted precipitating permeate were than taken every minute during the 30 minutes standing time and a plot generated (see Figure 7-3). After 30 minutes,

the reaction mixture was then cooled to room temperature in an ice bath and the solid filtered. The serum (filtrate) was saved for further analysis.

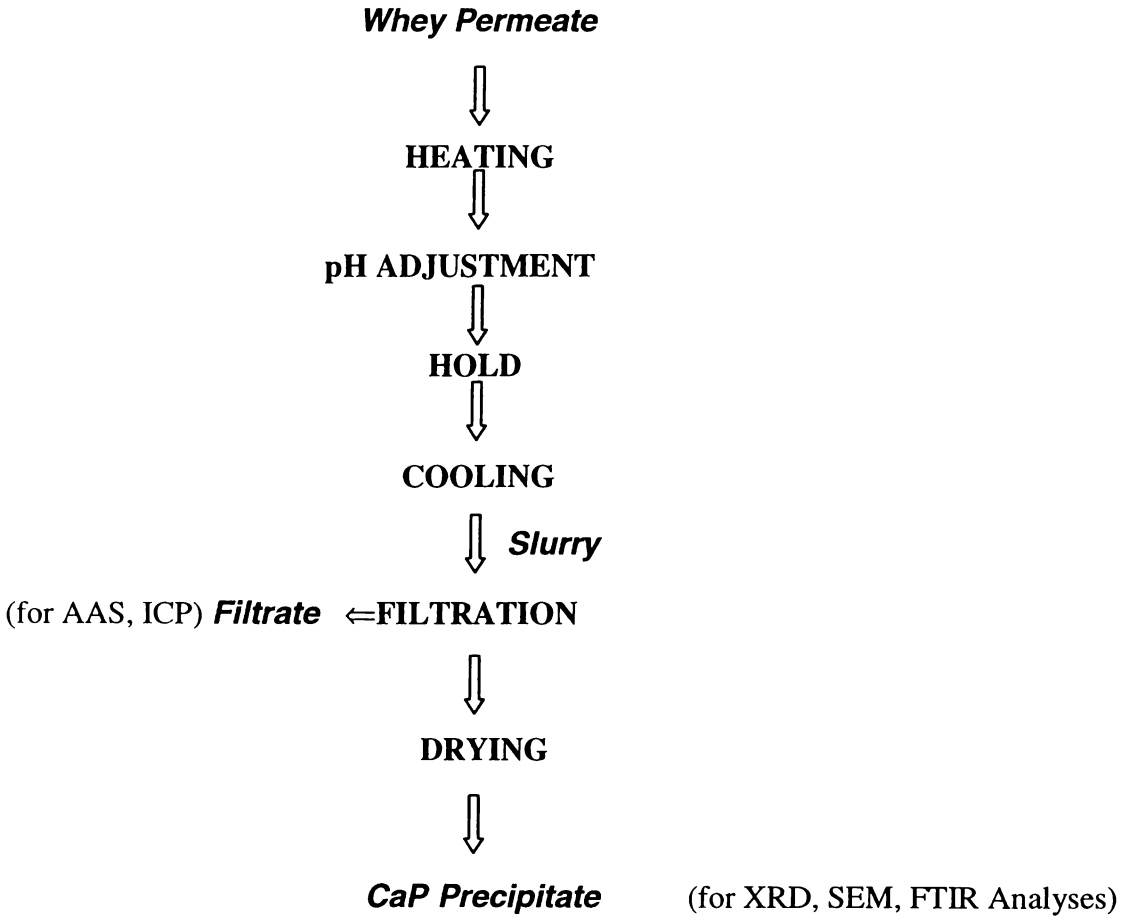

Figure 7-1: Flowchart for the experimental bench-scale precipitation reaction of calcium phosphate from the commercial whey UF-permeate.

Analysis of the starting materials and products of the precipitation reaction from whey permeates. The precipitation reaction described above was studied in tandem using a combination of techniques. For example, Atomic Absorption Spectroscopy (AAS) and Electrospray Mass Spectrometry (ESMS) were used to study the starting permeate and the serum after precipitation. The calcium phosphate precipitates (isolated at different times after base addition) were characterised using X-ray diffraction (XRD), scanning electron microscopy (SEM) coupled with energy dispersive X-ray analysis (EDX), transmission electron microscopy (TEM) and Fourier transform infrared spectroscopy (FTIR). The experimental details involved with the use of these techniques are described in later sections of this chapter.

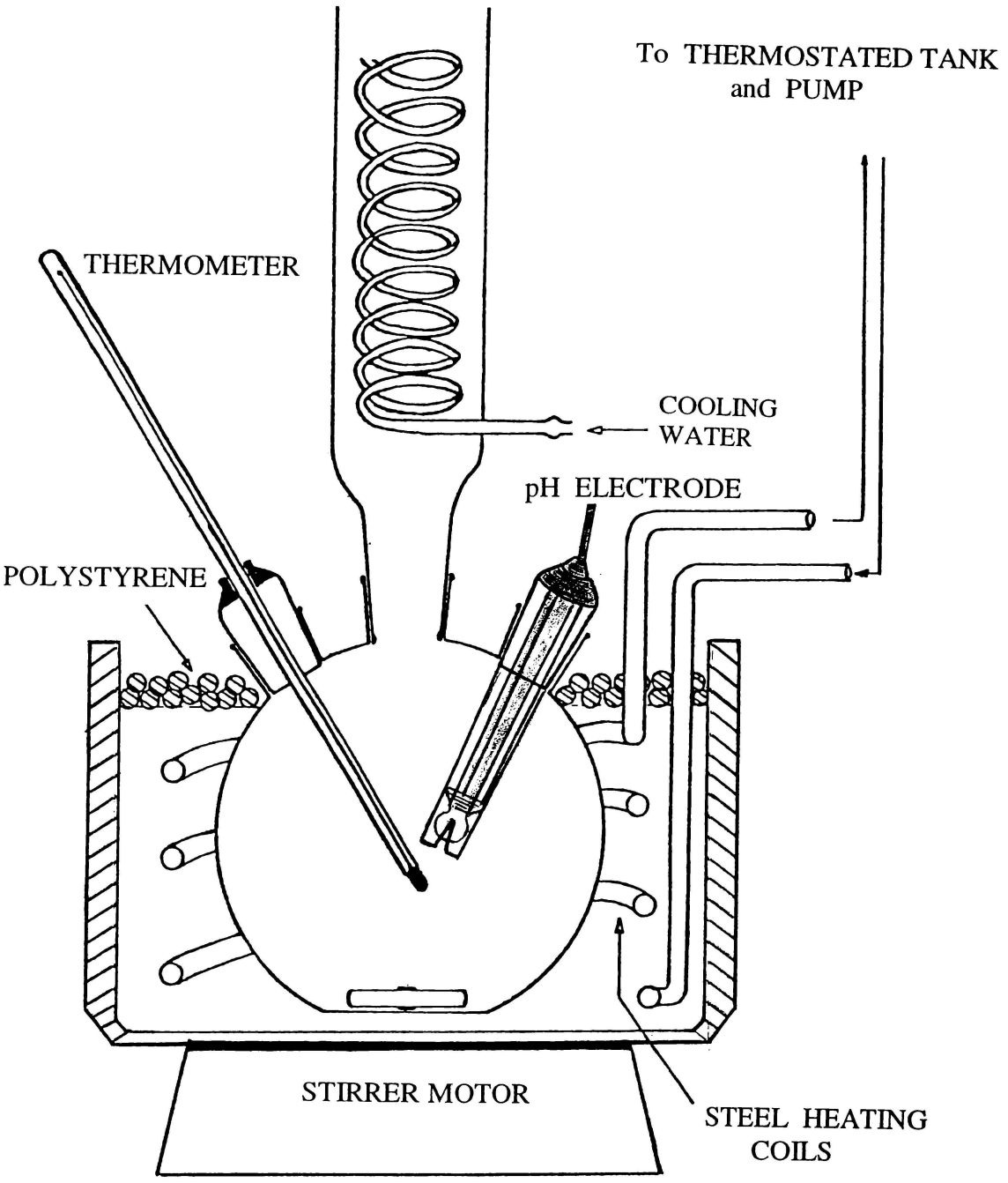

Figure 7-2: Apparatus used for the experimental bench-scale precipitation reaction of CaP from the commercial whey UF-permeate.

7.1.2 pH Study of the Precipitation Process from Whey Permeates

7.1.2(a) Results of the pH Study of the Precipitation Process from Lactic Whey Permeate

A curve of pH versus time for precipitating CaP from lactic whey permeate is illustrated in Figure 7-3. In general, the resultant curve showed that pH in the reaction medium decreased as a function of time after the single pH adjustment to pH 6.8. Literature reports on calcium phosphate precipitation (see Chapter 2) have shown that the first calcium phosphate precipitate to separate is usually "amorphous calcium phosphate" (ACP) which then "develops" over time into hydroxyapatite via a solvent mediated phase transformation mechanism. The phase transformation process leads to an overall production of H^+ which causes a drop in pH. In the whey permeate, it is highly likely that a similar mechanism of precipitation is being followed (as has been shown by pH stat experiments on model solutions in Chapter 4), hence the downward trend in pH with time. It can thus be assumed that in the whey permeate, ACP is being initially produced which phase-transforms over time to OCP and then to HAP with resultant consumption of base and calcium ions, viz. (Holt, 2001):

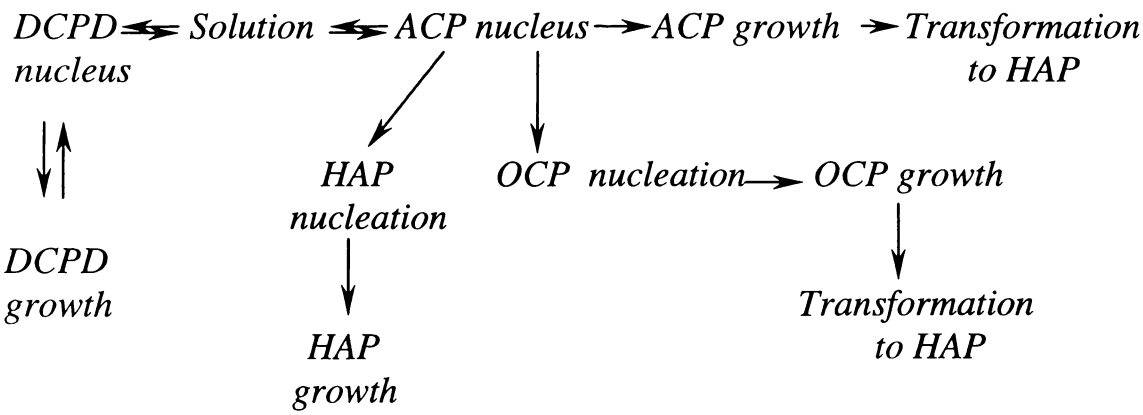

7.1.2(b) Results of the pH Study of the Precipitation Process from Sulfuric Acid Whey Permeate

Figure 7-4 represents a pH vs. time plot for a precipitation reaction using sulfuric acid whey permeate from the industrial proprietary process. In contrast to the curve given by the lactic whey permeates, pH did not initially start decreasing immediately after adjustment of pH to 6.8 by NaOH but instead exhibited a plateau for ca. 10 minutes before decreasing to a final pH of 6 after ca. 40 minutes. The reason for this difference

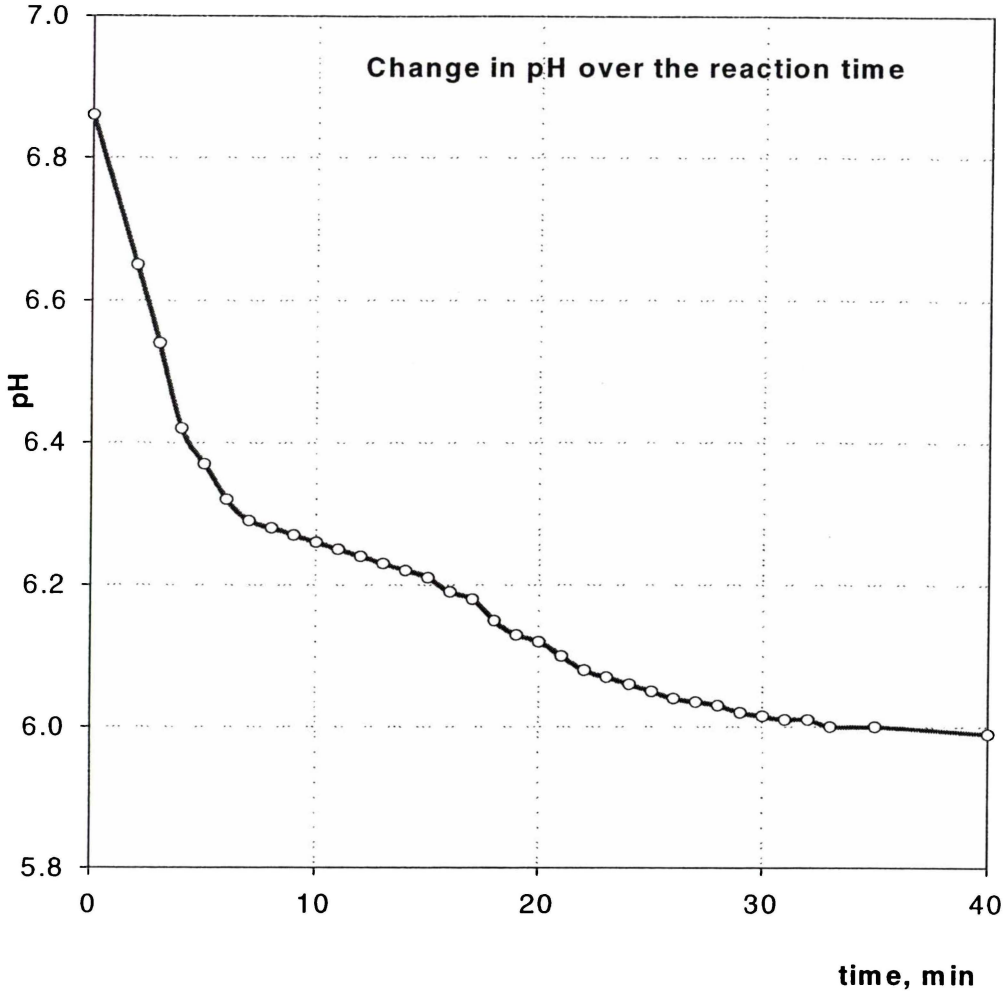

Figure 7-3: Change in pH over the reaction time for CaP precipitation process from heated (T=75°C) lactic whey UF-permeate.

is most likely to be due to the larger buffering capacity of the sulfuric acid whey permeate compared to the lactic acid whey permeate. This higher buffering capacity in the sulfuric acid whey permeate may be caused by the higher level of citrate (at most 9 mM which is the level present in milk) compared to lactic whey permeates (possibly 0-2 mM citrate). The lower citrate level in lactic whey permeates is due the use of starter bacteria which convert lactose to lactic acid and consume citrate released from the casein micelles. Citrate can delay the formation of CaP precipitates as was shown by the pH-stat measurements on SLWUF buffers.

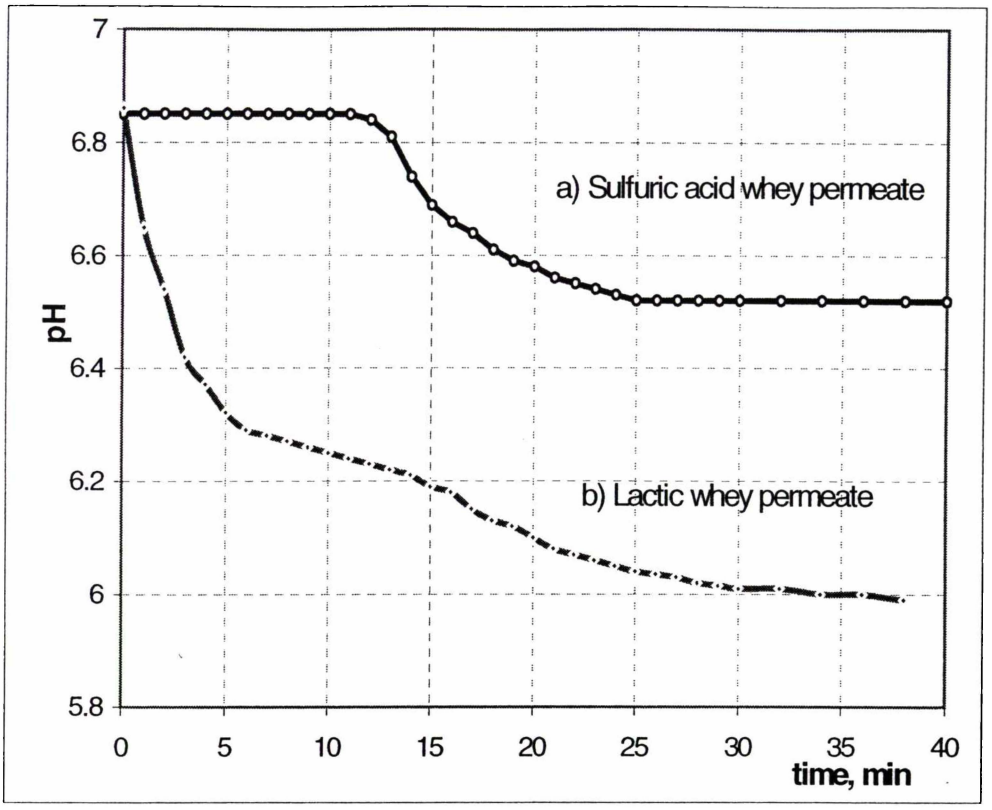

Figure 7-4: pH as a function of the reaction time for heated (T=75°C) whey permeates: a) sulfuric acid whey permeate; b) lactic whey permeate.

7.1.3 Atomic Absorption Spectroscopy (AAS) Study of Ca Concentration in the Whey Permeate Sera obtained after Precipitation of Calcium Phosphate

Atomic absorption spectroscopy (AAS) was initially used as a technique for the analysis of change in total calcium in the whey permeates during the precipitation reaction. In the later stages of the project, an ICP-OES instrument was used to repeat these measurements.

Experimental. During any given precipitation reaction, 30 mL aliquots of serum containing precipitated solid were withdrawn from the reaction mixture using a plastic syringe. It was important to extract both solids and liquid simultaneously from the reaction mixture due to the unstable nature of the initially separated calcium phosphate precipitates. The sample withdrawal procedure deliberately included both solid and liquid in each aliquot to ensure simultaneous sampling. These were then centrifuged and the solids separated by filtration. The transparent clear liquid filtrates were then stored

in plastic containers for analysis by AAS. The solids after filtration were washed, freeze dried and kept for later analysis by SEM, XRD and FTIR.

All AAS analyses of calcium concentration were performed using a GBC 909AA Spectrometer with an air-acetylene flame as employed for the analysis of the untreated whey permeates (see Chapter 6).

Results. AAS analyses of lactic whey permeate samples before and after precipitation. Figure 7-5 shows the calcium drop in a lactic whey permeate as a function of time after pH adjustment to pH 6.8.

In general, the initial AAS-determined concentration of calcium ions in the whey permeate medium is around 1200 ppm (*ca.* 30 mM Ca, see Chapter 6). After base addition, calcium phosphate precipitates which immediately resulted in a large drop in calcium ion concentration. The calcium ion concentration then fell off gradually after this point reaching a constant value of 3–4 ppm after 25 minutes, depending on the initial pH at which precipitation was stimulated, and remaining at an approximately constant level for the rest of reaction (see Figure 7-5).

The slow decrease in calcium with time after the large initial drop was likely to be due to the influence of the phase transformation reaction undergone by the precipitate, which results in consumption of calcium ions. This was confirmed by Ca ISE measurements on SLWUF buffer solutions which showed a large drop of free calcium and a subsequent sigmoidal decrease in the remaining calcium ion left in solution.

Unfortunately, the use of AAS for monitoring the fall in calcium ion concentration with time after base addition is a rather qualitative technique as it is largely insensitive to the subtle changes caused to the solution medium by the phase transformation of the precipitating solid. AAS monitors changes in *total* calcium rather than actual *free, available* calcium. This is better followed using calcium ion selective electrode (see section 7.1.7: "Free Ca^{2+} ion Measurements using a Calcium Ion-Selective Electrode (ISE) Method").

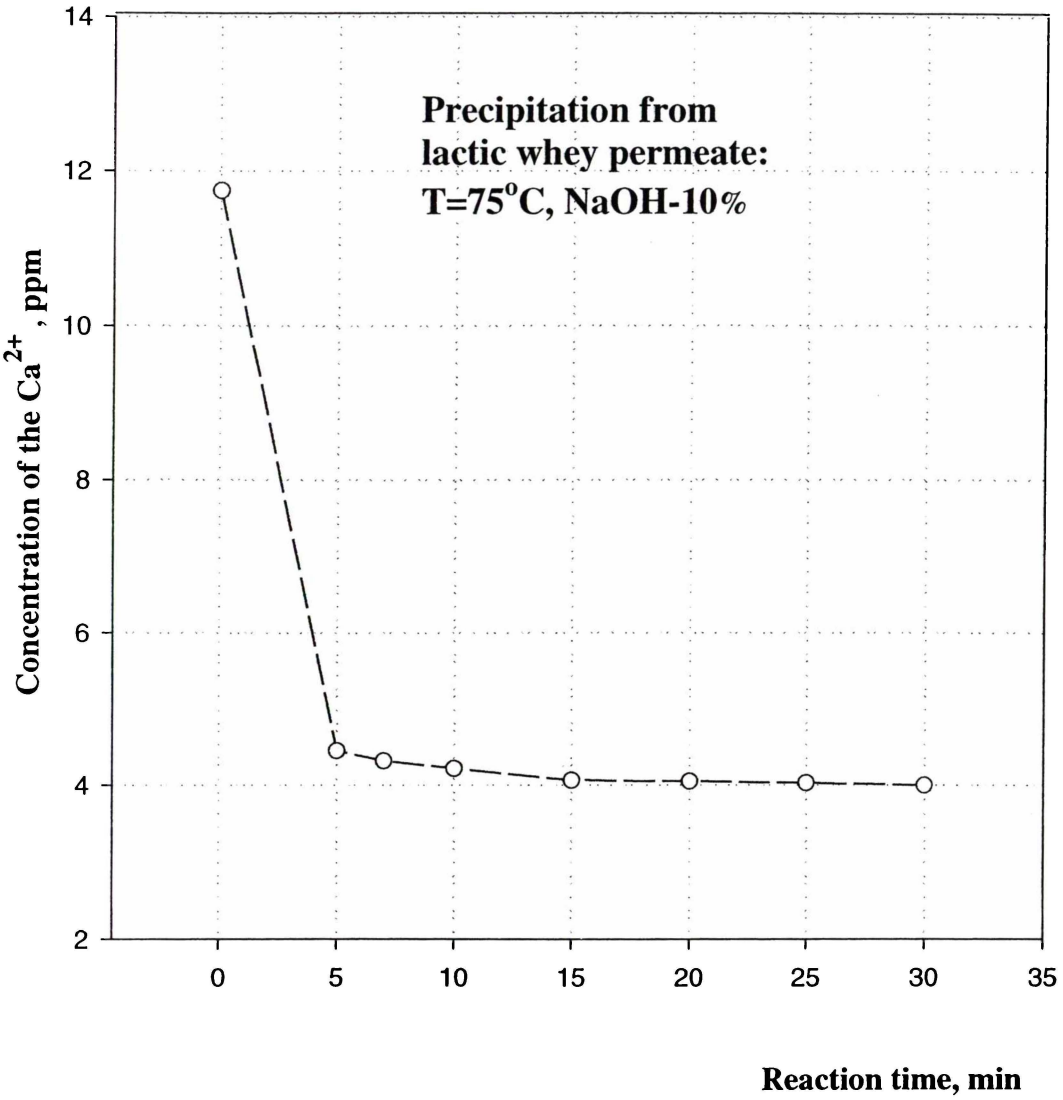

Figure 7-5: Concentration of the Ca^{2+} as a function of the reaction time, as measured by Atomic Absorption Spectroscopy.

7.1.4 Chemical Analysis of Serum by ICP-OES

Experimental. The experimental details for the analysis of the precipitating whey permeates as a function of time after base addition by ICP-OES were the same as those

outlined in Chapter 6 for the analysis of untreated whey permeate. The sampling procedure was identical to that described for the AAS analyses. The advantage of ICP-OES over AAS is that it can do multi element analyses in a very short time compared to AAS which is more time consuming and more prone to solution matrix influences. In addition, chemical interferences are relatively low and the element P (which is not analysable with AAS and hence must be determined using a spectrophotometric technique) can be directly determined with ICP-OES. Three whey permeate serum samples were analysed by ICP-OES, viz., serum samples extracted 3, 15 and 30 minutes after base addition. The samples were analysed for Ca, Mg and P.

Results. Table 7-1 represents the ICP-OES data of the chemical composition of the serum, extracted after 3, 15 and 30 min after the onset of the precipitation process from lactic whey permeate. Concentrations of the Ca, Mg and P are given as average of three aspirations ± standard deviation. There is a drop from the initial value in the lactic whey permeate concentrations of Ca, P and Mg. Initial concentration of Ca in the lactic whey permeate was 1210 ppm. After 3, 15 and 30 min of the precipitation process, concentration of the Ca has been accordingly changed to 207.8, 146.5 and 142.8 ppm. Initial concentrations of P in the lactic whey permeate were of the order of 716 ppm. During the precipitation process, the concentration of P dropped to 116.7 ppm (3 min), 72.51 ppm (15 min) and 71.30 ppm (30 min). This shows the uptake of these components into the apatitic precipitate over time. The initial concentration of Mg in the lactic whey permeate was 103.0 ppm. After 3, 15 and 30 min of the precipitation process, concentration of the Mg has been accordingly changed to 46.0, 72.87 and 80 ppm. So the comparison of Mg concentration results show that after the NaOH addition the Mg concentration dropped significantly over the first 3 minutes of the precipitation process and then there is a small increase 15 and 30 minutes after initiation of the precipitation. The same tendency was found for Mg concentration for whey permeate (UF extra treated): from initial value 101.5 ppm till 48.3 ppm (3 min), 81.4 (15 min) and finally to 88.1 ppm (30 min). It shows that during the precipitation time Mg is partially released from the CaP precipitates. The release of magnesium from the precipitates is an interesting phenomenon. Given that magnesium stabilises the amorphous calcium phosphate state, perhaps it becomes initially bound in the ACP but is then released later when the more thermodynamically stable HAP formation sets in. It could be a topic for further study.

Table 7-1: ICP-OES data of the chemical composition of the serum, derived from the lactic whey permeate after removal of the CaP precipitate obtained at T=75°C and pH=6.8.

Time after NaOH addition, min	Concentration[1], ppm		
	Ca	P	Mg
0	1210.5 ± 0.8	716.0 ± 1	113.0 ± 0.9
3	207.8 ± 0.9	124.6 ± 5	46.5 ± 0.1
15	146.5 ± 0.2	72.5 ± 5	72.9 ± 0.4
30	142.8 ± 1	71.3 ± 3	80.7 ± 0.9

[1]Analyses were made on 22.03.2000.

7.1.5 Fourier Transform Infrared Spectroscopy (FTIR) Analyses of the Precipitated CaP Solids

FTIR spectra were acquired of the evolving calcium phosphate precipitates generated in the bench-scale precipitation experiments described earlier (see section 7.1.1: "The Precipitation Reaction: Experimental Procedure") as a function of time (after addition of base to adjust pH to 6.8) by isolating solids, freezing them with liquid nitrogen and vacuum drying in a desiccator using a water vacuum desiccator. All FTIR spectra were recorded of solid samples as KBr disks using a Digilab FTS-40 FTIR Spectrometer with a DTGS detector and scanning from 4000-400 cm^{-1} at 4 cm^{-1} resolution.

Figure 7-6 represents FTIR spectra of the evolving precipitating calcium phosphate from lactic whey permeate. In the spectrum of the sample collected 3 minutes after base addition, a shoulder at 525 cm^{-1} on peaks at 601 and 561 cm^{-1} corresponding to O-P-O phosphate bending vibrations was observed (see Figure 7-6a) which appeared to be coincident with a similar peak observed in the IR spectrum of pure OCP (Posner et al., 1984). The peak was not observed in spectra of precipitates collected 15-30 minutes after the precipitation had started. Spectra of these later precipitates, indeed, indicated a solid that more closely resembled hydroxyapatite in character (see Figure 7-6b and 7-6c).

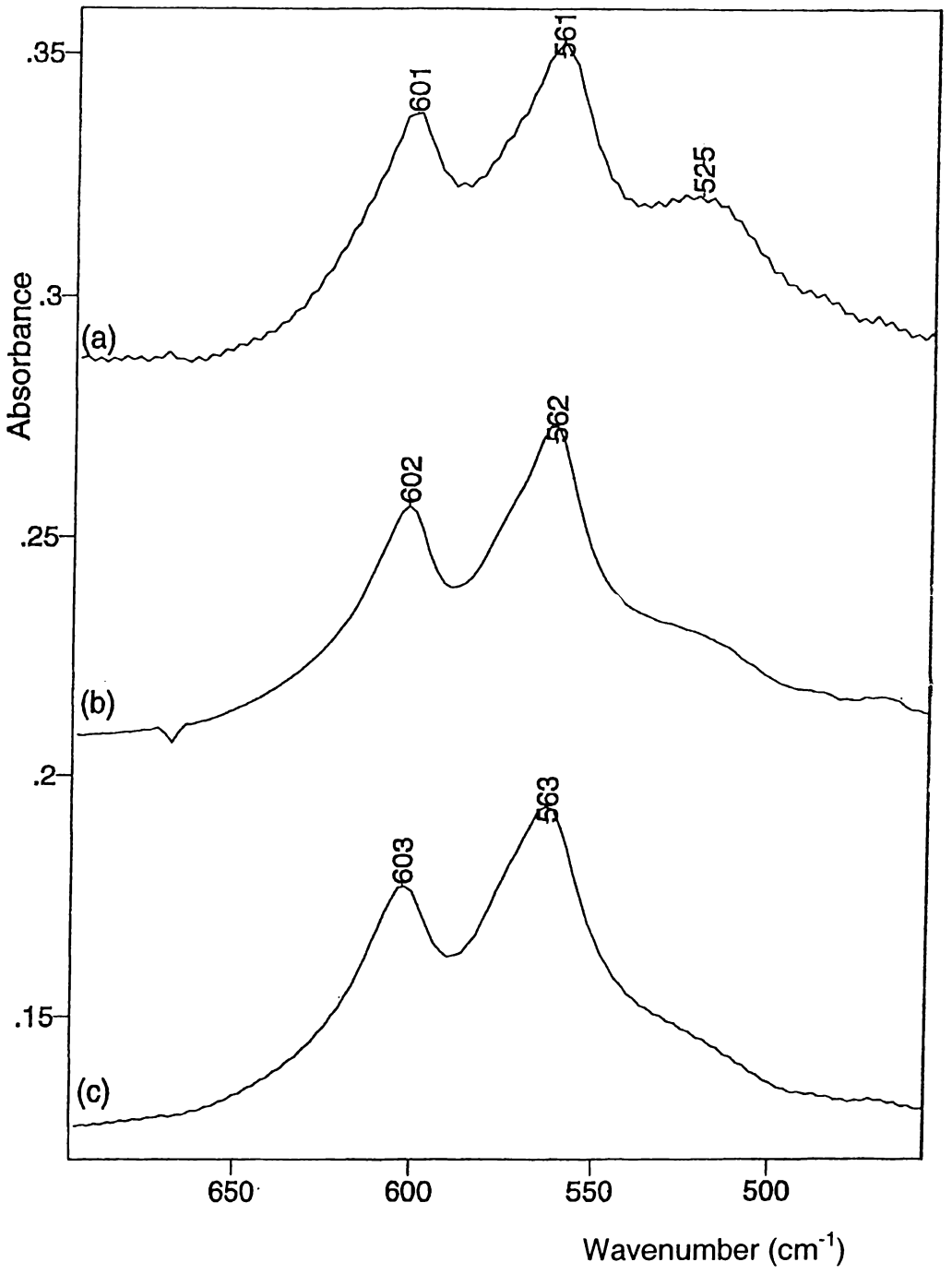

Figure 7-6: FTIR spectra of the CaP solids, collected after: a) 3 min; b) 15 min; c) 30 min after the onset of the spontaneous precipitation process from lactic whey permeate.

Because this research chronologically preceded the precipitation studies from the SLWUF buffer in this project, it was assumed that this peak at 525 cm^{-1} was due to OCP being formed as an intermediate solid in the CaP precipitate from phase transformation of the ACP through to HAP. However, in the later model solution FTIR studies of the evolving CaP precipitates from the SLWUF buffers (see Chapter 4) it was found that this peak is more close to the peak of brushite (at 527 cm^{-1}). In fact, the only phases that were ever observed in such studies were ACP, brushite and HAP which indicates possibly that OCP is far too transient a species to be detected under the experimental conditions.

It appears evident from the IR spectra, that the final product of precipitation from the whey permeate is hydroxyapatite as illustrated by the SLWUF studies in Chapter 4 and that the precipitate goes through a similar phase transformation mechanism before developing into its thermodynamically most stable phase, viz., HAP.

7.1.6 Scanning Electron Microscopy (SEM)/ Transmission Electron Microscopy (TEM) Analyses of the Precipitated CaP Solids

7.1.6(a) SEM Studies of Calcium Phosphate Precipitates

Experimental details. SEM micrographs of calcium phosphate precipitates derived from the bench-scale experimental investigations of precipitation from whey permeates were obtained using the procedures and scanning parameters as described in previous Chapters 3 and 4.

Results. Figure 7-7 is an SEM of the vacuum-dried precipitate particles derived from a lactic whey permeate reacted at 75°C and allowed to precipitate for 30 minutes. The most obvious observation to make on this system is that the particle morphology of the particles is very different from that of the commercial ALAMIN™ samples. In contrast to the chunky non-descript nature of the commercial ALAMIN™ particles (see Chapter 6), the particles shown in Figure 7-7 were of a more open structure and possessed dendritic character. The basic crystal morphology was the fine crystals as characteristic of apatitic calcium phosphate. The reason for the difference can be understood in terms of the drying process, which are naturally very different for the laboratory and commercial samples. In the commercial samples, ring drying is employed and high temperatures which can influence how the particles stick together especially if there are temperature sensitive organic components such as lactose present in the powders.

a)

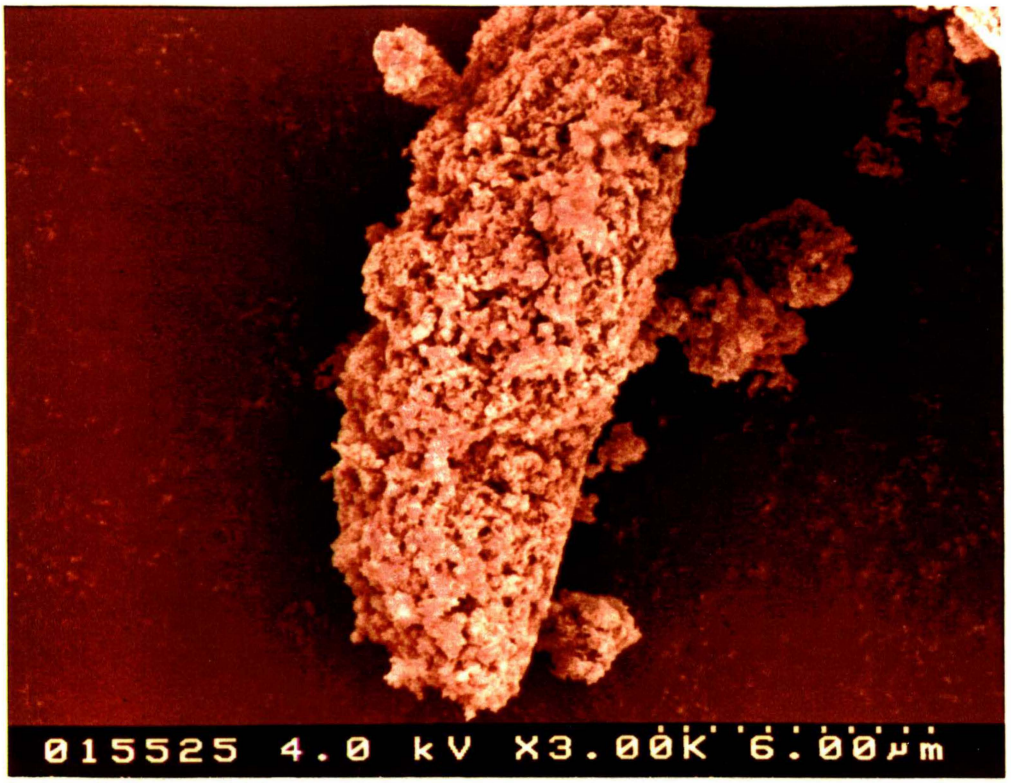

b)

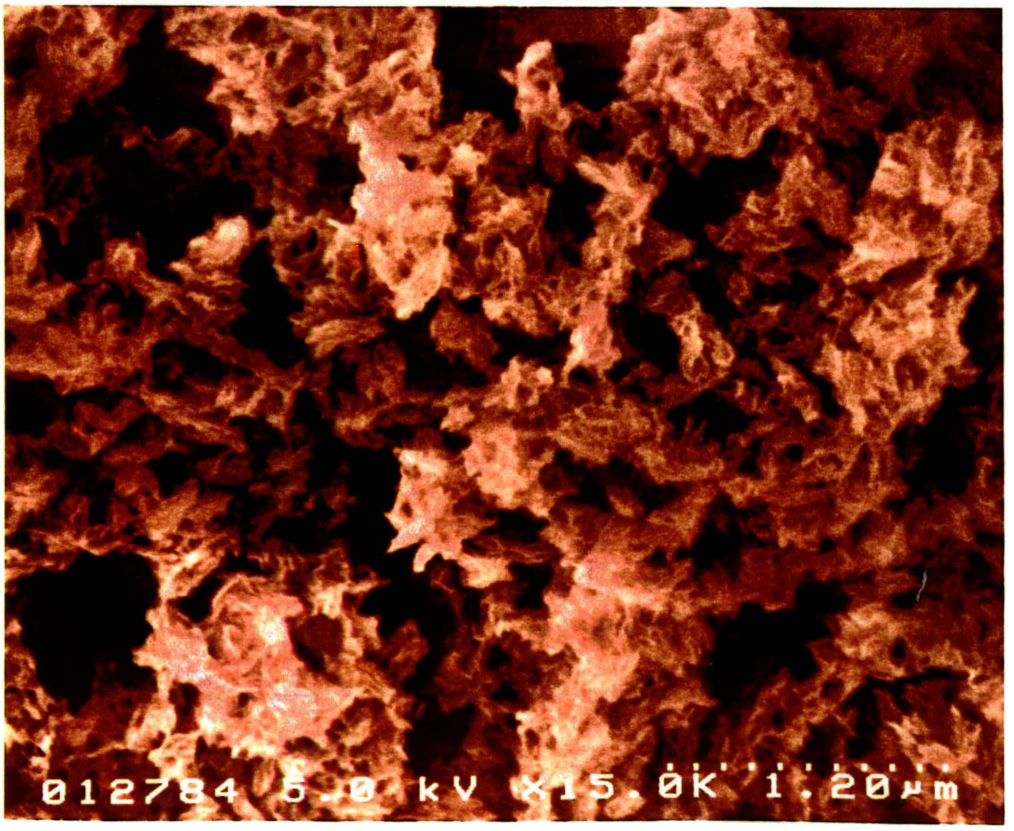

Figure 7-7: SEM micrographs of the vacuum dried CaP precipitate, isolated from the precipitating lactic whey permeate 30 minutes after base addition: a) typical particle at magnification x 3 000; b) at magnification x 15 000.

7.1.6(b) TEM Studies of Calcium Phosphate Precipitates

Experimental details. TEM studies were undertaken to investigate the morphological features of precipitated calcium phosphate solids as a function of time after base addition to gain insights into the phase transformation from ACP to HAP. All TEM micrographs were recorded using *Philips* Transmission Electron Microscope. The samples for TEM analysis were precipitated calcium phosphate from the lactic whey permeate and were collected at 5, 15-20, and 30 minutes after base addition which represented the initial, intermediate and final stages of the precipitation process. Drops of initially formed solid/liquid suspensions were placed on Formvar–carbon coated copper grids conventionally used for TEM analysis, with excess solution removed, dried and then taken for placement inside the Transmission Electron Microscope (which was at an external location). Micrographs of the deposited solids were then acquired using a 100 kV beam.

TEM studies of CaP precipitates derived from the bench-scale experimental investigations of the calcium phosphate precipitation from lactic whey permeate:

Results and Discussion. Figure 7-8 is a TEM of the solid isolated from the precipitating lactic whey permeate 5 minutes after base addition. The micrograph indicates a large amount of fine highly aggregated material with no apparent shape or form. Large hollow spheres are also evident in the micrograph around which the highly aggregated material is collected. It is believed that these are due to bubbles that form as a result of the action of the electron beam on the formvar film. The lack of structure in deposited material in the TEM is strong evidence that the solid material could be due to amorphous calcium phosphate (ACP) which is well known from the careful TEM studies done by Eanes et al. (Eanes et al., 1973) on evolving calcium phosphate precipitates. In that particular study spherical and structureless "blobs" of calcium phosphate material were observed in micrographs of initially precipitated calcium phosphate solids. Due to the highly aggregated nature of the material and clustering around imperfections in the formar film on, it is difficult to quantify the size of these solid particles.

Figure 7-8: TEM micrograph of the CaP solid, isolated from the precipitating lactic whey permeate 5 minutes after base addition (magnification x 228 000).

Figure 7-9 is the TEM of precipitated solid isolated 20 minutes after base addition. This shows large aggregates of dense material with evidence of needles adhering to the perimeters of the aggregates. This observation is similar to ones made by Eanes (Eanes, 1998) who postulated on the basis of TEM micrographs that apatitic needle-like crystals grew on the perimeter of the initially formed ACP. The needles observed in Figure 7-9 could thus well be representative of HAP nucleating on the perimeter of initially formed ACP presumably after it had undergone a phase transformation to OCP. In the absence of spectroscopic data on this particular sample, it is difficult to state exactly what the phases are in this micrograph. The most that can be said on morphological grounds is that HAP appears to be forming as a function of time in the precipitate from the lactic whey permeate which provides further evidence that precipitation of calcium phosphate from the whey permeate is following a similar phase transformation mechanism as reported in earlier fundamental studies on calcium phosphate precipitation.

Figure 7-10 represents a TEM micrograph of precipitated solid from the lactic whey permeate isolated 30 minutes after base addition which effectively represents the final stages of the precipitation process. In this, collections of needle like crystals are observed which are similar in morphology to those reported for HAP crystals (Eanes, 1998). This indicates that HAP is the final product of the precipitation of calcium phosphate from lactic whey permeate as has been shown by FTIR.

7.1.7 Free Ca^{2+} ion Measurements in Reacting Whey Permeates using a Calcium Ion-Selective Electrode (ISE) Method

Experimental. In earlier sections, AAS and ICP-OES were used as a way of monitoring calcium levels in the reacting whey permeates before and after precipitation of calcium phosphate. These techniques were, however, recognised as being rather qualitative techniques for monitoring calcium levels since they are only reflective of absolute calcium levels in the permeates and sera and take no account of the amount of *free calcium ion* which is the species which reacts directly with phosphate to generate calcium phosphate. To this end, calcium ion selective electrode (Ca ISE) measurements were carried out on lactic whey permeate samples to determine the trends in *free* calcium ion concentrations in the sera as a function of time after precipitation of calcium phosphate. All calcium ion- selective measurements including preparation of standard solutions were performed using the procedure described in Chapter 4.

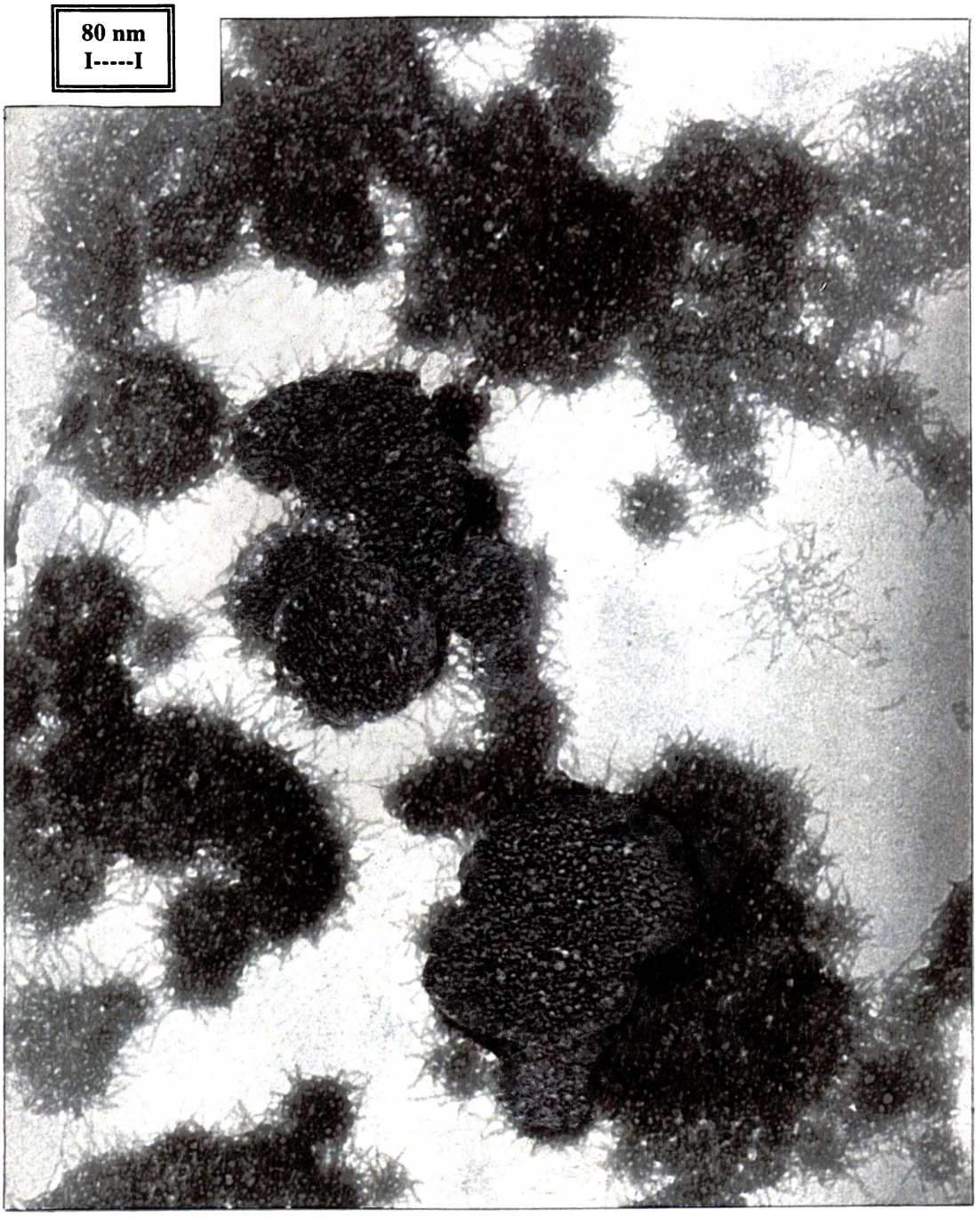

Figure 7-9: TEM micrograph of the CaP solid, isolated from the precipitating lactic whey permeate 20 minutes after base addition (magnification x120 000).

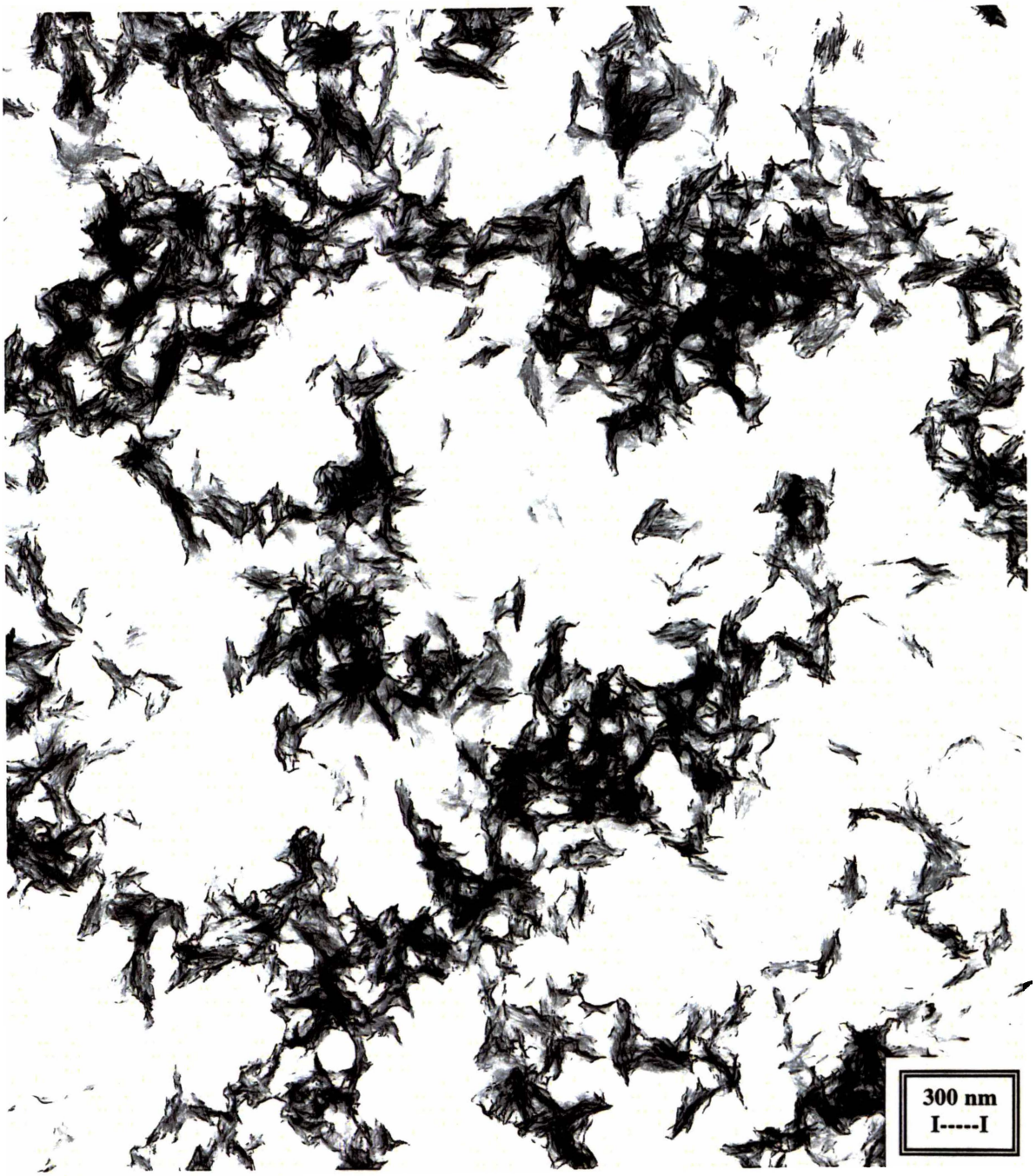

Figure 7-10: TEM micrograph of the CaP solid, isolated from the precipitating lactic whey permeate 30 minutes after base addition (magnification x 30 000).

In a typical experiment, precipitation of calcium phosphate from the lactic whey permeate at 75°C was induced by adjustment of the pH to 6.84 by addition of 10% NaOH solution. Initial experiments involved continuous immersion of the Ca ISE in the precipitating whey permeate and measurement of the potential with time. However, this was found to lead to a constant reading of the mV value on the pH meter indicating that the electrode had become temporarily impaired by fouling of the surface from the precipitating solid. Hence an alternative experimental procedure which avoided this situation was adopted in which samples of the precipitating reaction mix were separated 1, 3, 5, 7, 10, 15, 20, 25, 30, 35 and 40 minutes after base addition. The Ca ISE was then immersed in the sera obtained after filtration of the solid phases in order to obtain readings corresponding to the level of free calcium ion. This experimental procedure was found to generate a satisfactory data set and the phenomenon of constancy of mV readings did not occur.

Results and Discussion. Figure 7-11 is a plot of the concentration of free calcium ion versus time after base addition to a lactic whey permeate.

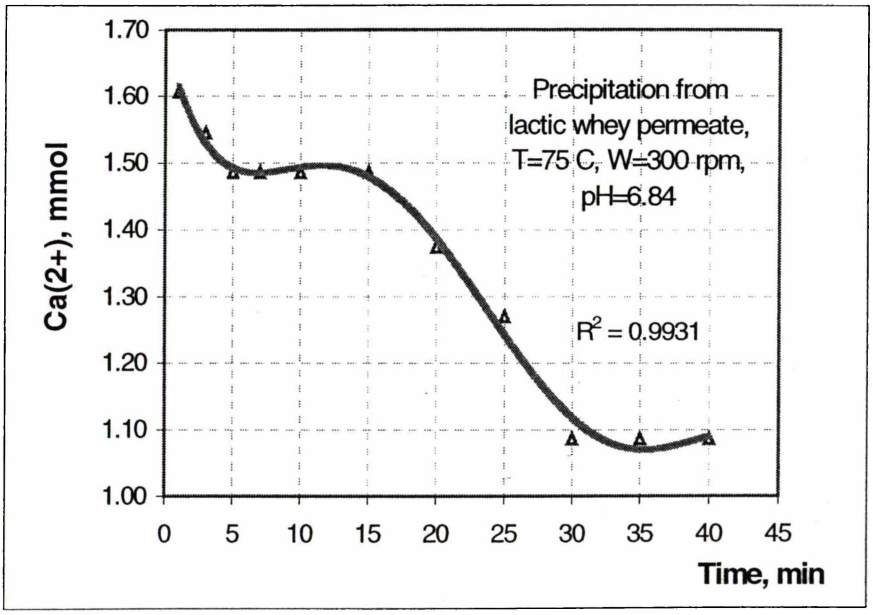

Figure 7-11: Free Ca^{2+} ion concentration in the sera after NaOH addition as measured by a Ca ISE method (expanded).

At zero time (i.e. before base addition, pH 4.6), the initial free Ca^{2+} ion concentration in the lactic whey permeates was found to be *ca.* 8 mM. The free calcium ion concentration is lower than the expected absolute calcium concentration for the whey permeate (i.e. 31 mM) due to the various chemical equilibria which involve chelation of calcium ion in

various complexes. In speciation calculations predicting the distribution of solid and dissolved species in whey permeate as a function of pH using industrially supplied concentration parameters (see Chapter 4), a value of 10 mM free calcium ion concentration was predicted to exist in the permeate when at pH 4.6. The lower value observed experimentally in the Ca ISE measurements could be due to a variety of reasons. For one, the parameters (relating to concentrations of calcium ion, magnesium, phosphate etc in the permeate) used by the SPE program to generate the speciation plots in Chapter 5 were average typical values from accumulated industrial data and so were subject to natural and seasonal variation from permeate to permeate. A second possibility for the non-agreement between experimental and theoretical prediction is that some loss of solution calcium by settling could have occurred. Whey permeate over time tends to develop a turbidity over time which could be due to a variety of factors such as settling out of calcium and mould growth. Given that the use of aged permeate was unavoidable at times during this project, the second possibility could be an important factor.

Free calcium ion levels after base addition in the lactic whey permeates. The calcium ion concentration dropped sharply from ca. 8 mM to 1.6 mM 1 minute after addition of base and levelled off in the sera samples at 3-15 minutes after base addition (see Figure 7-11) before decreasing further and stabilising at 1.10 mM 30 minutes after base addition. This behaviour in the calcium ion concentration is similar to the "sigmoidal type" behaviour observed in experiments in which Ca ISE measurements were made in sera of precipitating SLWUF buffer model solutions at pH 6.8 (see Chapter 4). The plateau observed at 3-15 minutes is believed to be due to an offsetting of the drop in free calcium ion by precipitation by release of free calcium ion from the dissolving ACP precipitate as it transforms into a crystalline apatitic product. It is believed that these trends exhibited in Figure 7-11 above are a further indication that the phase transformation process is occurring in the whey permeate of calcium phosphate precipitates in homogeneously precipitating systems in which dissolution of the initially formed amorphous calcium phosphate is occurring followed by reincorporation by reprecipitation of the calcium so released into the final apatitic CaP product.

7.1.8 Electrospray Mass Spectrometry of Serum (ESMS)

Electrospray Mass Spectrometric analysis was trialed as a novel technique in this study for analysing changes in the whey permeate as a result of precipitation of calcium phosphate. Electrospray Mass Spectrometric analyses of lactic whey permeate were

discussed earlier (see 6.1.3: "Electrospray Mass Spectrometric Analyses (ESMS) of Lactic Whey Permeate").

Exprimental. ESMS analyses were carried out using VG Platform II mass spectrometer as described in Chapter 6. Precipitation experiments to generate serum samples for analyses by ESMS from the lactic whey permeate were carried out following the procedure outlined in section 7.1. Generally samples were isolated from the precipitating system at 2, 15, 30 and 40 mins after base (10%) addition, the solids filtered off and then prepared for ESMS as per the following procedure. A drop of each serum sample was placed into a plastic vial and mixed with a 50% acetonitrile/water solvent with 50-70% dilution. The sample solution was then injected into the ESMS instrument following the general procedure described in Chapter 6. Two series of sera solutions were examined by ESMS, i.e. sera, obtained after the precipitation from lactic whey permeates at 75°C (batches from 3.11.99 and 16.06.98). Both positive and negative mode ESMS spectra were acquired.

Results and Discussion. Figure 7-12 is the *negative ion mode* of the ESMS spectrum (at a cone voltage of -25 V) of a sample of the lactic whey permeate serum (collected 3.11.99) 2 minutes after base addition. Figure 6-2 is the ESMS spectrum of the lactic whey permeate before base addition which is shown for comparison. In Figure 7-12, it was apparent that the peak corresponding to $H_2PO_4^-$ at m/z 137 as observed in Figure 6-2 had completely disappeared which confirmed its assignment to this species and furthermore indicating its consumption during the precipitation to form calcium phosphate solid. The m/z peaks at 89.4, 377.2 and 431.2 due to *Lactate*$^-$ ion and *Lactose* (which were also observed in the ESMS spectrum of lactic whey permeate before base addition) were also detected in the ESMS spectrum of the serum. Significant reductions in these species are not expected due to the high solubility of calcium lactate solid phases compared to calcium phosphate phases and the low stability constant for these complexes compared to that for calcium phosphate (i.e. ACP, brushite, HAP etc). In serum samples isolated 15–40 minutes after base addition, the ESMS spectra show similar features.

Figure 6-3 (see section 6.1.3: "Electrospray Mass Spectrometric Analyses (ESMS) of Lactic Whey Permeate) is the *positive ion* ESMS (at cone voltage +25 V) spectrum of lactic whey permeate (collected 3.11.99, from Cas-1 starter) before base addition. This

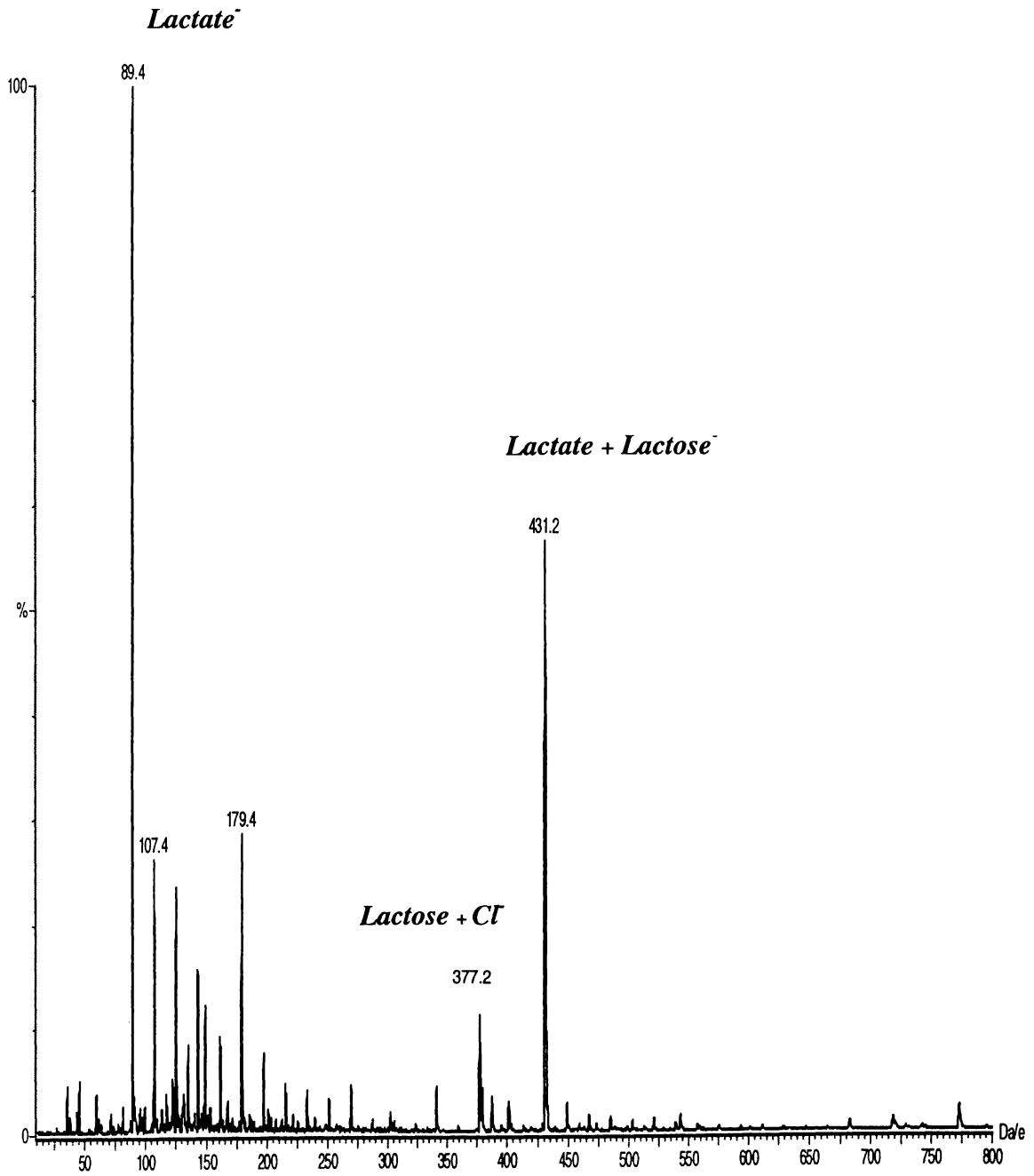

Figure 7-12: Negative ion mode ESMS spectrum (-25 V) for the lactic whey permeate serum, collected 2 min after the onset of CaP precipitation process.

spectrum indicated the presence of K^+, Ca^{2+}, and Na^+ ions in the whey permeate as expected. The ESMS peak due to K^+ ion was particularly dominant although absolute intensities in ESMS must be interpreted with caution as these are related more to ion formation efficiencies in the instrument rather than to absolute concentrations of the ions in the sample matrix being investigated.

Figure 7-13 is the positive ion mode ESMS spectrum of the lactic whey permeate 2 minutes after base addition. Some obvious changes in the ESMS spectrum were noted. Compared to the ESMS spectrum of lactic whey permeate before base addition (Figure 6-3), an apparent increase in intensity of the peaks due to sodium ion (i.e. peaks at m/z 64.4, m/z 105.2 and m/z 365.3) was observed which is correlated to the use of NaOH for adjusting pH to 6.8. ESMS peaks due to potassium ion were observed at m/z 39.3, 80.3, 121.2 and 381.8.

For ESMS spectra of the samples isolated 15-40 minutes after base addition all observed negative ion mode spectra looked similar to each other. ESMS spectra in the positive mode exhibited little differences in the intensities of peaks at m/z 80.3 and 105.2 associated with potassium and sodium ions.

In general, the capacity of ESMS to offer specific information on the whey permeate after precipitation is limited. For information on the relative levels of inorganic ions in the permeate as a function of time after base addition, the use of ICP-OES, AAS and Ca ISE measurements are recommended. These techniques allow for much greater control of experimental conditions and offer far more quantitative and reliable information.

7.1.9 X-ray Diffraction Study of Precipitated CaP Solids

Experimental. Samples of precipitated CaP solids, collected from the precipitation process (time 3, 15 and 30 minutes) from lactic whey permeate were prepared for XRD analysis by grinding it to a fine powder. Then these samples were placed in an aluminium rectangular sample holder with a small depression ion in the centre where they were examined using a Philips X'PERT X-Ray Diffractometer. The XRD patterns of the precipitated CaP solids were recorded from $2\theta = 2^\circ$ to $2\theta = 100^\circ$ using Cu-K_α radiation ($\lambda = 1.5405$ Å).

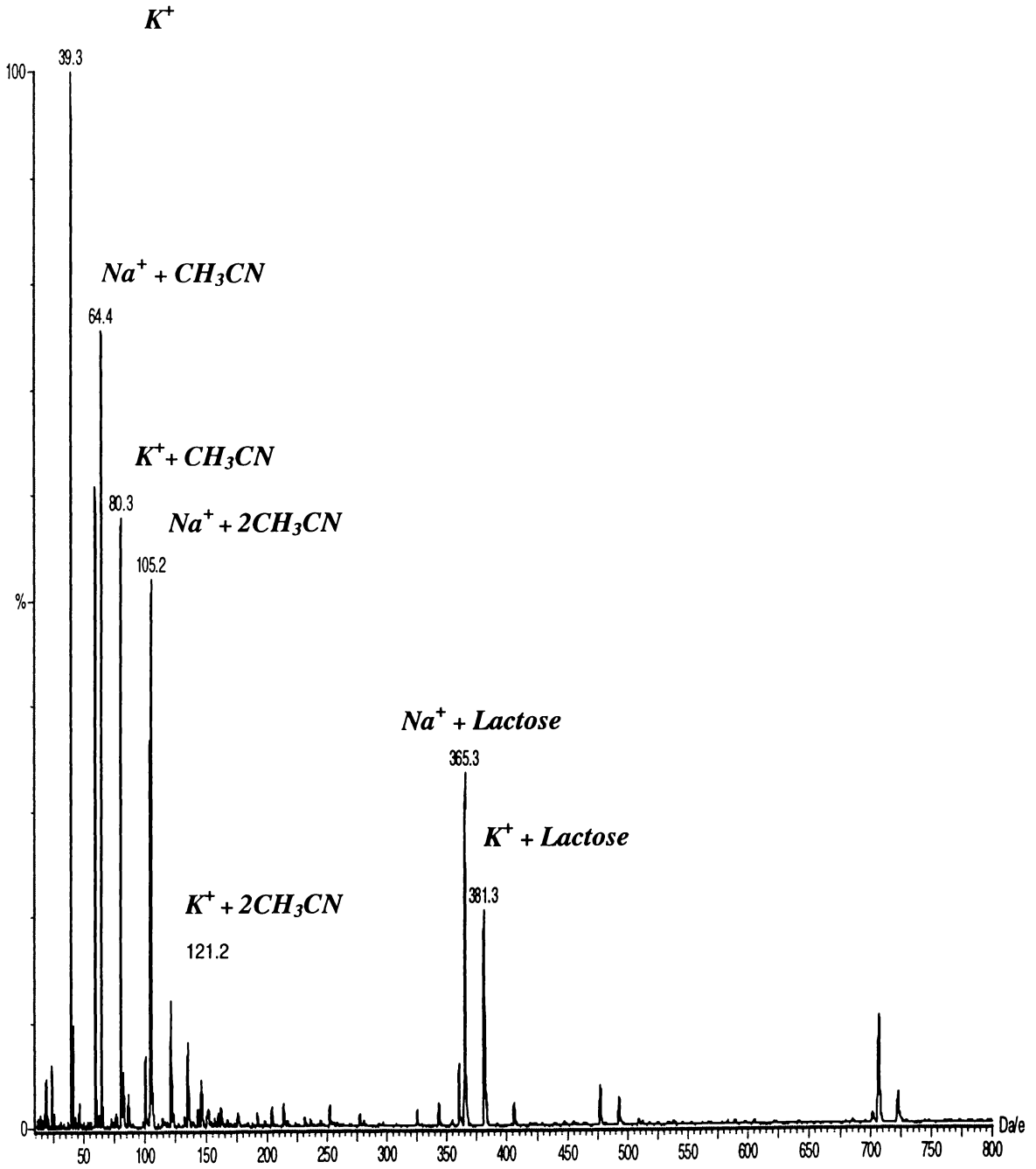

Figure 7-13: Positive ion mode ESMS spectrum (+25 V) for the lactic whey permeate serum, collected 2 min after the onset of CaP precipitation process.

Results. Figure 7-14a shows the XRD patterns for CaP precipitate, collected at the final stage of the precipitation process (30 min). Comparison of XRD CaP precipitate patterns was made with XRD patterns for fine nanocrystalline hydroxyapatite (*BABI*-brand hydroxyapatite) supplied as a suspension of nanosized HAP in an aqueous solution from laboratories at the University of California at Berkley (see Figure 7-14b).

The acquisition of XRD diffractograms for the CaP collected solid (collected time was 30 min), using PC-APD Diffraction Software, showed that the most intense 10 diffraction lines correspond to the crystallographic planes of nanocrystalline *BABI*-brand hydroxyapatite: [100], [002], [211], [310], [312], [210], [004], [502], [304] and [215, 513].

The XRD patterns of the CaP solids, collected at the early stages of the precipitation process, illustrate the same apatitic kind of structure as for the sample isolated 30 minutes after precipitation and showed that the precipitate was of low crystallinity as can be expected from solids isolated from aqueous solution. Given this solid was isolated 3 minutes after precipitation was initiated, a broad featureless profile should have been expected given that an ACP-like solid would be present at this stage of the precipitation (as gauged from studies on model solutions in Chapter 4). Unfortunately, some time elapsed before the sample could be properly freeze dried hence it is likely that the sample may have phase transformed during the time before freeze-drying could take place. This highlights the difficulty of working with unstable nascent calcium phosphate precipitates.

7.2 Aqueous ALAMIN™ Suspension Study

One of the earlier tasks of this project was to gain a greater understanding of the behaviour of industrially produced calcium phosphate powder when dispersed in water and in the presence of various additives. This information is of use when using commercial CaP powder in foodstuffs where its prolonged dispersal in aqueous or dairy media is imperative to a long shelf life for the product. This led to a series of experiments in which aqueous ALAMIN™ suspensions were exposed to a variety of additives such as CO_2 gas and casein protein and their effects on the ALAMIN™ particles probed by Malvern (*Mastersizer*) laser light scattering, FTIR and SEM.

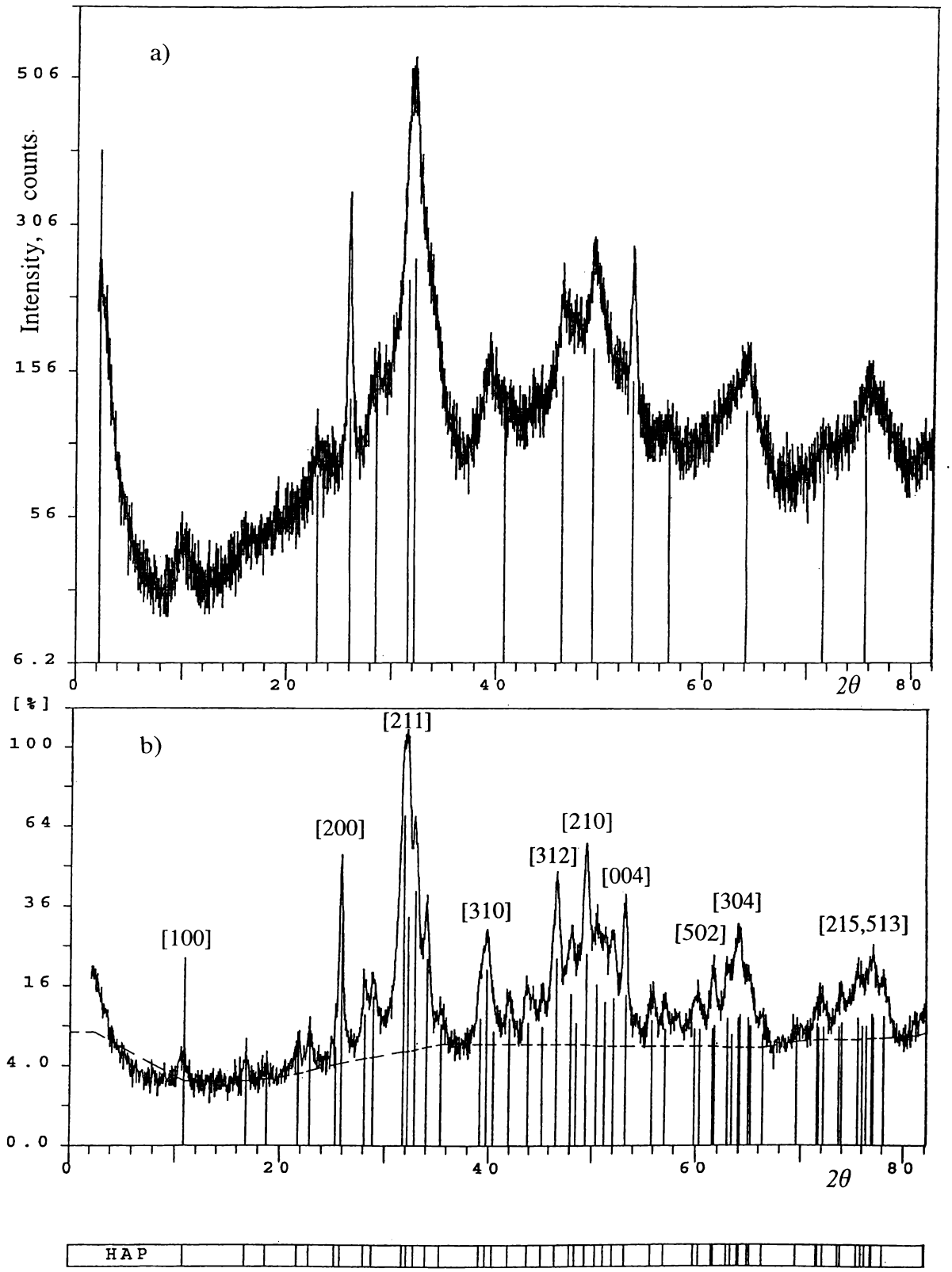

Figure 7-14: Comparison of XRD patterns: a) for CaP precipitate, collected at the final stage of the precipitation process (30 min) with b) for fine nanocrystalline HAP (*BABI*-brand).

It should be stressed that these experiments were qualitative in nature and were carried out with the general intention of obtaining broad trends that could be of use to industry.

Experimental. All Malvern laser light scattering data were carried out on the Malvern Mastersizer-S as previously described in Chapter 6. SEM micrographs were obtained using the Hitachi SEM instrument also described in Chapter 6.

Before each experiment, batches of commercial ALAMIN^{TM} powder of various size and industrial classification grades (i.e. ALAMIN^{TM} (>150 μm), and ALAMIN^{TM} (<150 μm) which had been manufactured in 1996) were ultrasonicated in double distilled water for 2 hours at 25°C in an ultrasonic bath (ULTRAsonic104X) at the maximum power setting. The point of this was to break up the clusters of particles in the ALAMIN^{TM} which had aggregated together as a result of industrial spray drying processes. The following experiments were then performed:

CO_2 gas bubbling. CO_2 gas (BOC gases, food grade) was bubbled via a Drechsel bottle into a suspension containing various amounts of ALAMIN^{TM} in water. The suspension was examined on the Malvern laser light scattering instrument usually 20-30 minutes after the sample was prepared. SEM micrographs of the solids after filtration of the water were obtained afterward.

Results and Discussion. Bubbling of the ALAMIN^{TM} suspension with CO_2 gas appeared to result in an increase of transparency of the initially "milky-looking" ALAMIN^{TM} suspension with subsequent sedimentation after 30-40 minutes on standing. Bubbling with CO_2 gas not surprisingly led to a slight decrease in solution pH from *ca.* 7.0 to 6.5. Malvern measurements conducted on the ALAMIN^{TM} suspensions bubbled with CO_2 gas are summarised in Table 7-2. For each ALAMIN^{TM} powder type examined, comparison with a reference suspension of ALAMIN^{TM} powder not exposed to CO_2 gas was made. It can be seen from the change in volume-weighted mean diameter (D[4, 3]) that bubbling of CO_2 gas tends to lead to a decrease in average particle size of the ALAMIN^{TM} particles While this effect on particle size is almost marginal in the case of the ALAMIN^{TM} particles < 150 μm, it is very prominent for the aqueous suspension of the largest ALAMIN^{TM} powder fraction (>150 μm) (see Table 7-2) where an almost halving of the volume-weighted mean particle diameter is observed. Also it was

observed that the process of bubbling CO_2 gas through the ALAMIN™ suspension is accompanied by a decrease in pH (see column 1 at Table 7-2).

Table 7-2: The particle size of ALAMIN™ powder before/after bubbling of CO_2 gas through the aqueous suspension. pH before/after bubbling is also given in parentheses.

Sample	D [4, 3], μm	D [v, 0.5] μm	D [v, 0.9], μm
ALAMIN™ (>150 μm), pH (7.02/6.43)	26.22 / 12.38	13.52 / 9.30	66.27 / 27.07
ALAMIN™ (<150 μm), pH (7.11/6.51)	17.18 / 13.91	14.79 / 11.64	34.60 / 28.58

The drop in particle size could be the result of two factors: the mechanical action of bubbling, which leads to the breakdown of aggregates, and the partial dissolution of ALAMIN™ particles. The second factor may arise from the well-known CO_2 - H_2O equilibrium in water which is responsible for the slight acidity existing in distilled water exposed to the ambient atmosphere.

$$CO_2 + H_2O \rightleftarrows \text{“}H_2CO_3\text{“} \rightleftarrows H^+ + HCO_3^- \rightleftarrows H^+ + CO_3^{2-}$$

Calcium phosphates are known (Dorozhkin, 1997) to become increasingly soluble in water as pH falls, although any dissolution of ALAMIN™ at pH 6.5 is probably marginal.

Another possibility for the increased dispersibility of the ALAMIN™ in CO_2-bubbled water is an interaction of the carbonates with the calcium phosphate solid. The hydroxyapatite structure is known for its hospitality in accepting atoms other than calcium and phosphate or hydroxide into its crystal lattice by ion exchange. Hence entry of carbonate or bicarbonate from solution into the HAP crystal lattice could well influence the properties of the suspended ALAMIN™ solid. So-called “carbonate apatites” are known to exhibit greater solubility than pure apatites (Elliot, 1994).

In fact an FTIR spectrum recorded of the ALAMIN™ solid before and after CO_2 gas treatment revealed the development of a slight shoulder in the 1420 cm^{-1} peak which has been assigned to citrate and protein co-deposited with the ALAMIN™ solid (see Chapter 6). The position at which the shoulder developed (due to a reduction in intensity of the overall peak at this wavenumber (*ca.*1450 cm^{-1}) suggests that some protein (see 6.1.4(b): "Assignment of other Non-phosphate related peaks in the 4000-1300 cm^{-1} Region") has dissolved out of the ALAMIN™ solid by dispersal in water.

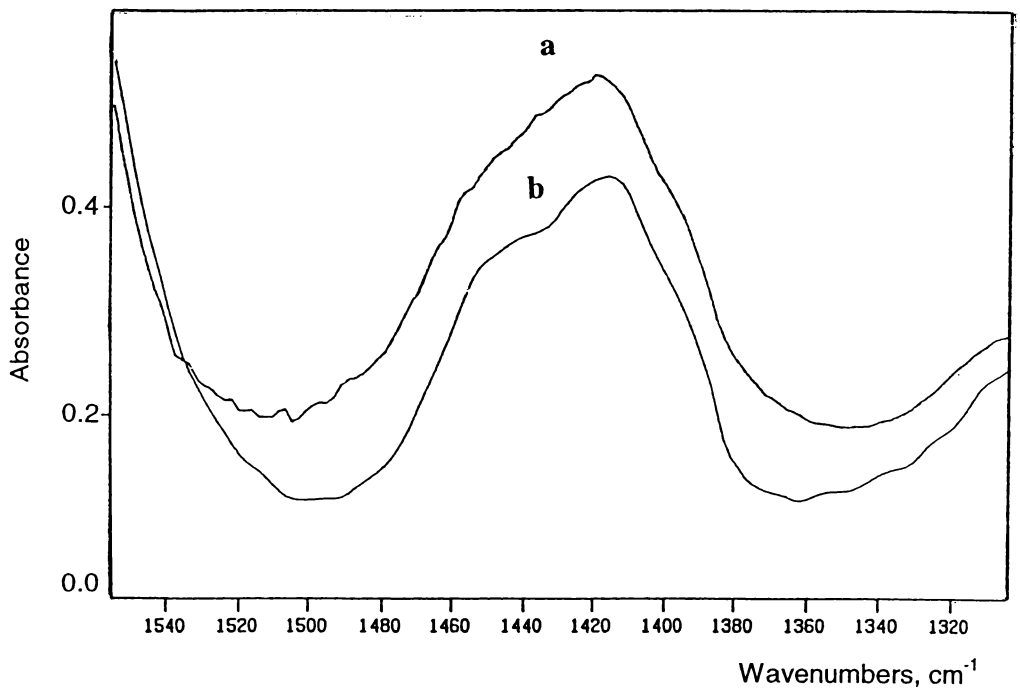

Figure 7-15: FTIR spectrum recorded of the lactic ALAMIN™ solid: a) before and b) after CO_2 gas treatment in the IR band at 1320-1540 cm^{-1}.

When examined by SEM (Figure 7-16), micrographs of the ALAMIN™ particles appear to indicate that CO_2 gas bubbling has caused the formation of many small particles and an overall increase in porosity in the solid. Hence CO_2 gas appears to influence ALAMIN™ dispersions. The exact reason for this is not completely understood given the absence of extra data of further experimentation, however it is an effect that could be exploited industrially for increasing dispersion/solubility of ALAMIN™ in product formulations. Another effect on the structural characteristics which cannot be overlooked is possible dissolution of any co-deposited phases such as citrate, lactose and protein from the ALAMIN™ by simple dispersal in water and the change in pH.

a)

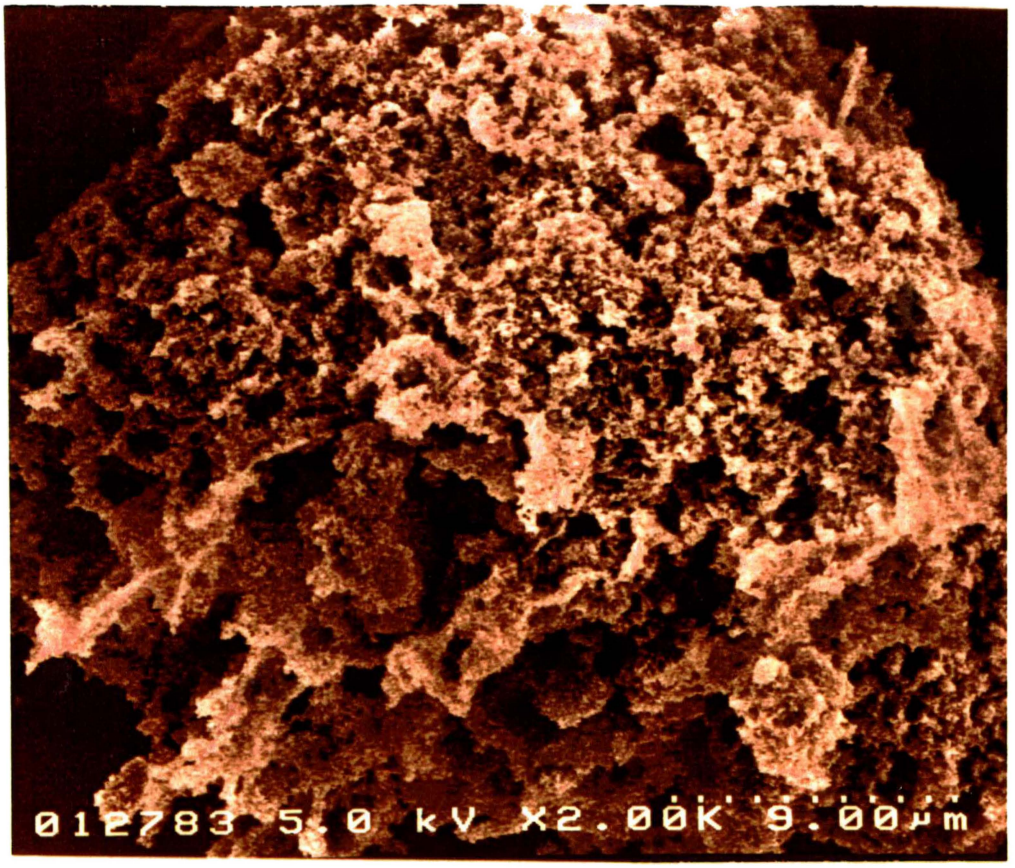

b)

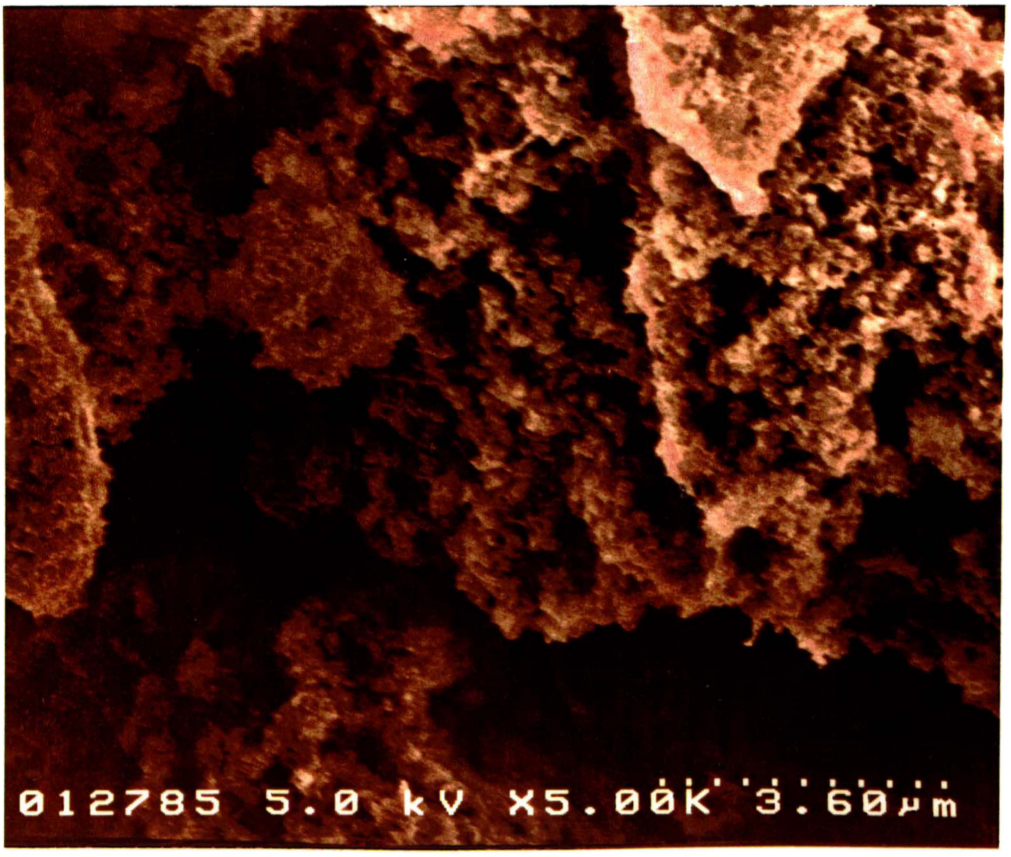

Figure 7-16: SEM micrographs of the typical CaP particle, derived from lactic ALAMIN^{TM} suspension after CO_2 gas treatment: a) at the magnification x 2 000; b) at the magnification x 5 000.

When casein (BDH, light white soluble) was added to an aqueous suspension of ALAMIN™ and SEM micrographs acquired, the casein was found to have an aggregating effect on the ALAMIN™ particles (see Figure 7-17), acting as a flocculant/ binder.

"Grape-like" aggregates of particles suggesting gluing together of particles by casein were observed. This effect is probably not surprising in view of the fact that the casein/ALAMIN™ mixture when filtered from solution and dried acquired a somewhat sticky consistency as can be described by a following scheme:

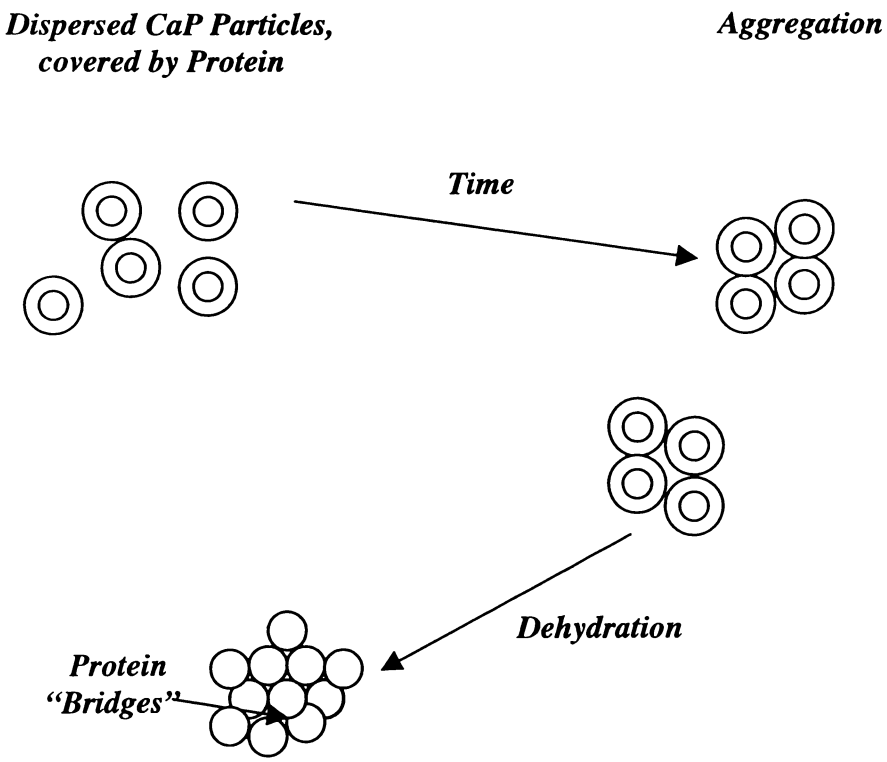

a)

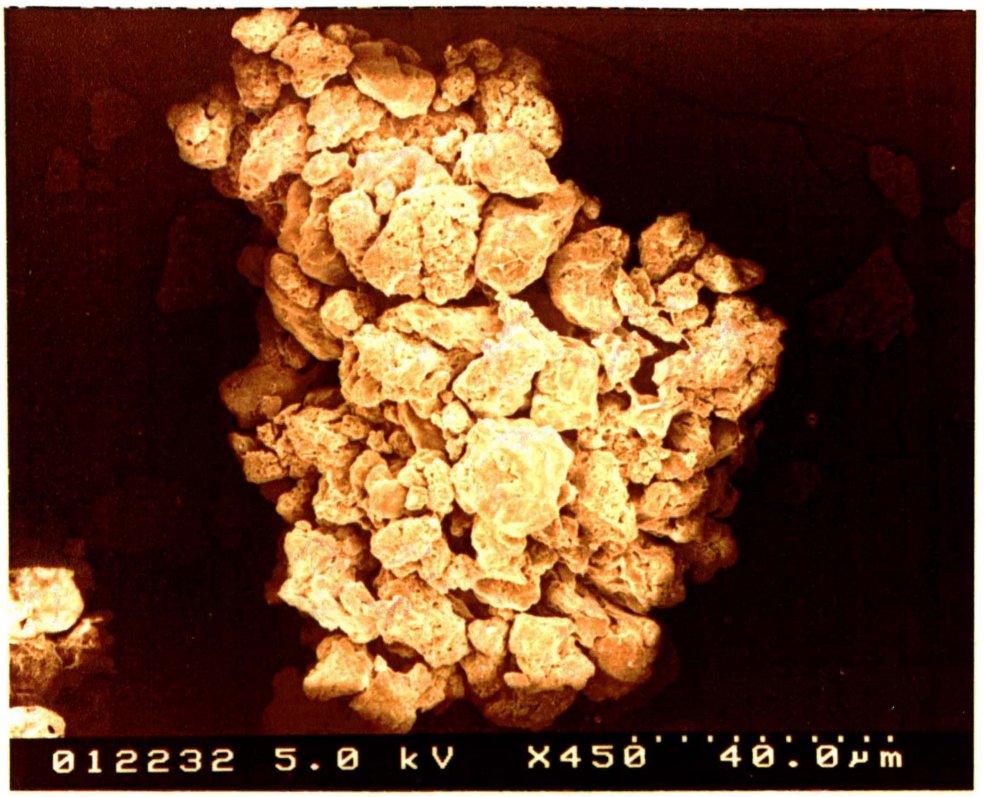

b)

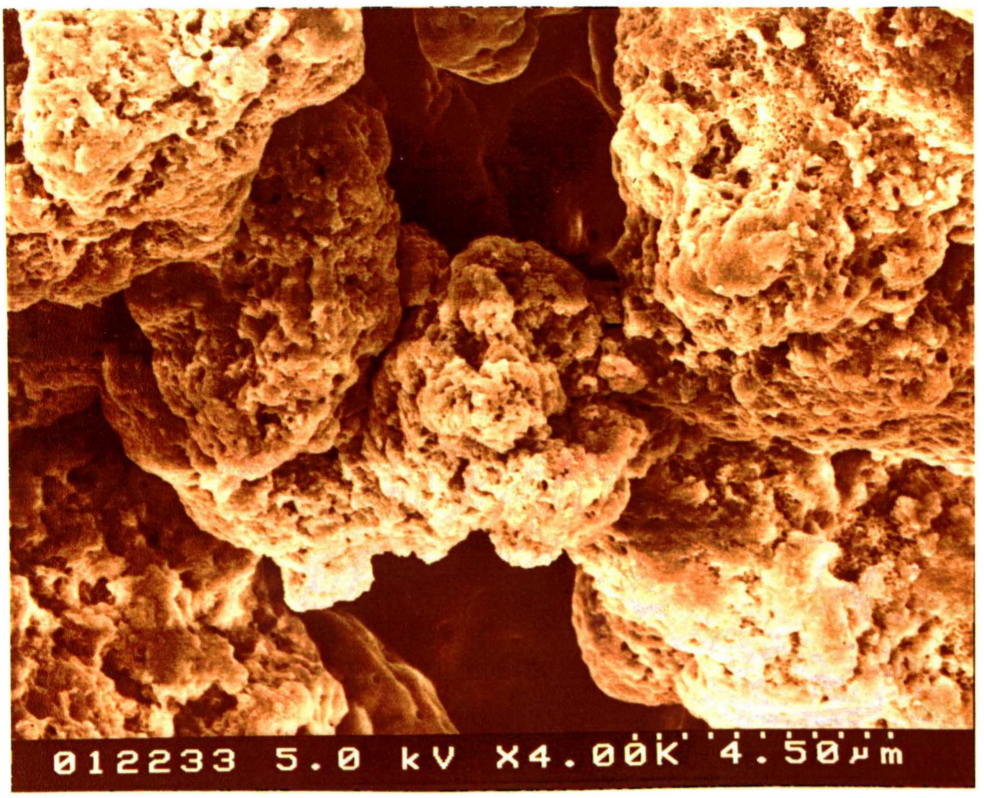

Figure 7-17: SEM micrographs of the ALAMIN™ powder, enriched by casein (10 %): a) typical particle at the magnification x 450; b) it's surface at the magnification x 4 000.

7.3 Measurement of Adsorption Isotherms of Whey Proteins on the Surface of Commercially Synthesised (Pure) Hydroxyapatite

This study represents a stand-alone investigation in which the surface activity of pure hydroxyapatite was assessed with respect to whey proteins, β-lactoglobulin and α-lactalbumin which are known to be proteins adsorbed to the surface of the commercial calcium phosphate precipitates. Hydroxyapatite is well-known for its surface activity towards proteins, a fact heavily exploited in the manufacture of liquid chromatography columns for the purification of proteins. In the present investigation, a small UV/Vis study was executed in order to measure simple adsorption isotherms of the protein on commercially supplied (*Fluka* Biochemica) hydroxyapatite. The reason this was used instead of actual ALAMIN™ was because commercial ALAMIN™ already has protein adsorbed to its surface which would render the quantitative measurement of uptake of *additional* protein on its surface a difficult task owing to the complexities associated with possible surface desorption of existing protein when suspending the ALAMIN™ in aqueous media so constituting the risk of spurious influences on the UV/Vis absorbance. The experimental method used was based on one used in a simple undergraduate Physical Chemistry experiment at the University of Waikato (Mucalo, 1997) which related to the adsorption of dyes on sand assuming a Langmuir Adsorption Isotherm model.

Experimental. Pre-weighed (~ 1.000 g) samples of *Fluka* hydroxyapatite (pre-sieved to ensure particle sizes were < 250 μm) were placed into ten 50 mL beakers and shaken for 2 hours on a mechanical shaker containing varying volumes (10-35 mL) of protein (β-lactoglobulin/ α-lactalbumin of weight ratio 9.4 being batch PT3886 from the New Zealand Dairy Research Institute) stock solutions (with initial concentrations of 1 g L^{-1} (6 samples) and 2 g L^{-1} (4 samples)) which had been pipetted in previously. After 2 hours, the slurries were centrifuged for one hour to remove suspended solid and the supernatant was analysed by UV-visible spectroscopy using a CARY 1 UV-Visible Spectrophotometer to monitor the change in absorbance of between the original protein solutions (before any shaking was performed with HAP) and the solutions after shaking with HAP of the protein-associated UV at 291.5 nm. This was then used to determine the equilibrium concentration of protein remaining in solution after shaking with HAP by dividing by the slope of the linear Beer's Law plot that had been previously determined by measuring the absorbance of accurately known concentrations of protein in g L^{-1}.

The change in absorbance was then inputted into the following equation in order to calculate x, the amount of protein adsorbed in mg per g of adsorbent (this being HAP) and this was then plotted with x on the y axis and C (the equilibrium concentration of protein left after shaking with HAP) on the x axis:

$$x = \frac{\Delta C \times V}{W}$$

where V-volume of the protein solution, W-mass of the HAP powder. The resultant plot is given in Figure 7-18. The plot shows a smooth curve with an obvious inflection point at *ca.* 0.3 g L^{-1} protein. This appears to correspond to a "levelling off" feature which in the graphical definition of a Langmuir type adsorption indicates the formation of the first monolayer of protein on the hydroxyapatite surface. After this inflection point, the adsorption appears to increase further. This can be taken to indicate a multilayering phenomenon of protein on the hydroxyapatite surface.

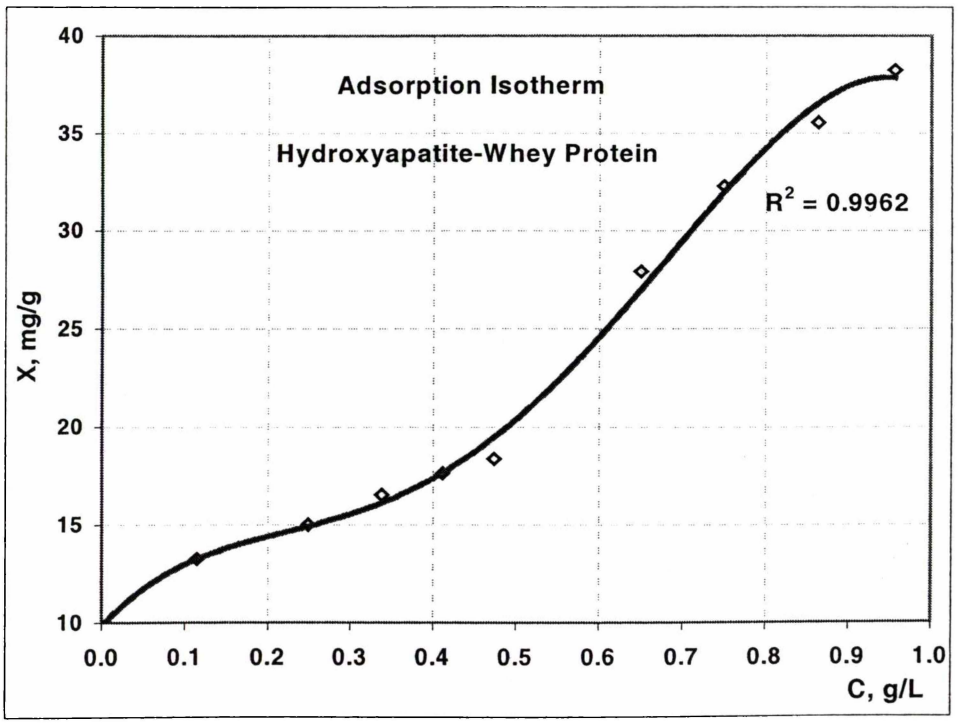

Figure 7-18: Adsorption isotherm for whey proteins (β-lactoglobulin/α-lactalbumin of weight ratio 9.4) on the surface of *Fluka*-hydroxyapatite powder particles at T=25°C.

Multilayering of proteins on hydroxyapatite surfaces has been observed by previous workers (Hambling et al., 1992, Brew et al., 1992, Boye et al., 1997). In general, the whey proteins, β-lactoglobulin and α-lactalbumin exhibit the potential to give multilayer adsorption on the surface of HAP. β-lactoglobulin, the major protein constituent of

whey, is a globular protein with a MW of 36000 Da which exists as a dimer of a MW 18,000 Da monomer unit cross-linked by two disulphide bonds. α-lactalbumin, on the other hand, is essentially a monomer and has a MW of 14000 Da; it contains four disulphide bonds (Hambling et al., 1992, Brew et al., 1992, Boye et al., 1997). Both whey proteins like any typical protein consist of long chains of amino acids (Hudson, 1992) and some of these amino acids carry side-chain carboxyl or amino groups which remain free and exposed to the solvent when the protein is dissolved in solution. Therefore, dissociation is possible in aqueous solution, a process strongly dependent on pH (see Figure 7-19 below), resulting in $-COO^-$ and $-NH_3^+$ ions covalently attached to the protein macromolecule. In acidic solution, for instance, a typical protein will be positively charged because of the presence of $-NH_3^+$ and (unionised) COOH groups. In basic solution, the protein exhibits a negative charge due to COO^- and (unionised) $-NH_2$ groups. At the isoelectric point, there is an equal proportion of positive and negative charges (zwitterion) and the net charge is zero (see Figure 7-19). Indeed this phenomenon is exploited for producing the lactic and sulfuric wheys for the production of commercial calcium phosphate. A sorbent surface like hydroxyapatite will contain multiple binding sites to which the proteins with their multiply ionised groups could bind (see Figure 7-20). Once coating the HAP surface, further protein could then interact with this adsorbed monolayer by *cooperative adsorption* (Luo et al., 1998). Hence this mechanism could explain the multilayering of the whey proteins on the commercial HAP surface and could be extended to ALAMIN™. Although there was not sufficient time in this study, it would be of interest to carry out further investigations in this area given that addition of protein could be considered as a means of enhancing the dispersion of ALAMIN™ in dairy product formulations.

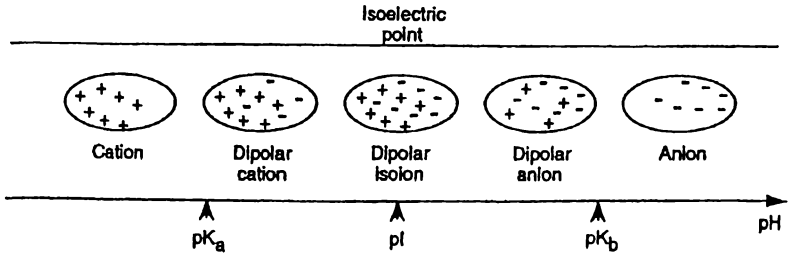

Figure 7-19: Schematic representation of the variation of charge with pH for a protein.

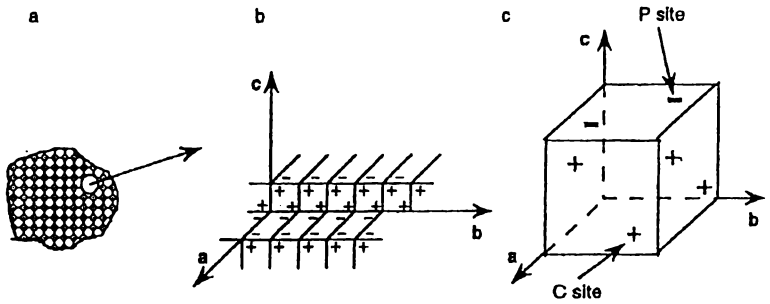

Figure 7-20: Schematic representation of the surface charge of hydroxyapatite in the crystal state: a) hydroxyapatite particle; b) expanded area of hydroxyapatite; c) crystal unit cell of hydroxyapatite (from Luo et al., 1998).

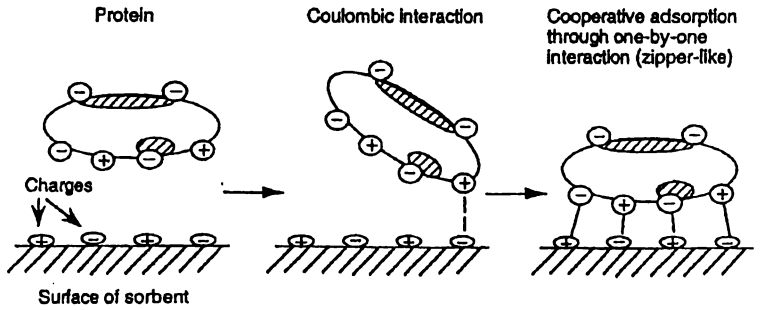

Figure 7-21: Schematic representation of the cooperative adsorption between protein and surface (from Luo et al., 1998).

7.4 Malvern Laser (*Mastersizer*) Determination of the Particle Sizes over the Course of Precipitation Reaction

From an industrial point of view, the final particle sizes of the resultant calcium phosphate precipitate were seen as important to the smooth running of the industrial process. Particle size and shape were believed to influence filterability of the final CaP cake when it was being filtered. The interest in this was the impetus for the study into the effect of agitation rate on the particle sizes of calcium phosphate derived from lactic

whey permeate. Bench-scale precipitations of calcium phosphate from lactic whey permeate were thus carried out following the procedure outlined in section 7.1: "Bench-scale Experimental Investigation of the Precipitation of Calcium Phosphate from Whey Permeates" with the use of known agitation rates to investigate the effect on the calcium phosphate produced. For this purpose, the technique of Malvern laser light scattering (as discussed in Chapter 3) was used to monitor the particle sizes of the precipitate directly in the precipitation medium.

7.4.1 Effect of Agitation Rate on CaP Particle Sizes

Experimental. Bench-scale experimental work was carried out following the procedure outlined in section 7.1.1: "The Precipitation Reaction: Experimental Procedure". Lactic whey permeates were heated to 75°C and treated with 10 % sodium hydroxide solution to stimulate CaP precipitation. Experiments were performed using agitation rates of 3-1000 rpm. Agitation rate was controlled by means of an IKA® stirrer (RW20DZM.n) motor which employed a digital readout. The vessel in which agitation was carried out is shown schematically below (see Figure 7-22). The agitation system used consisted of two propellers oriented at 90° to each other.

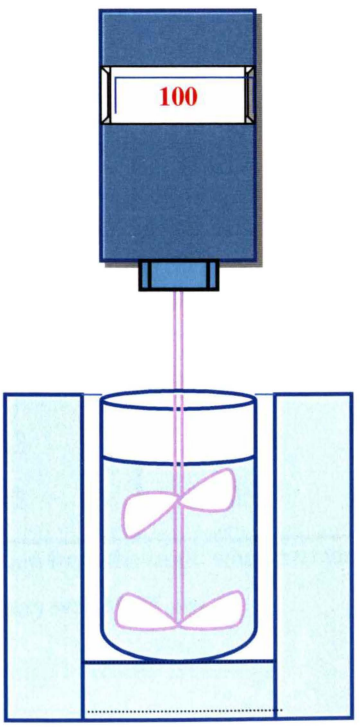

Figure 7-22: Reaction vessel illustrating the agitator propellers used in the agitation rate precipitation experiments.

The ratio of diameters of the containment vessel (which was a 400 mL cylindrical jacketed cell (as used in the pH-stat studies) with a vessel: agitator propeller diameter of 1.7. The vessel was heated to the required temperature by way of water circulated through the jacket from a thermostatted water bath accurate to within ±0.2°C. The precipitation experiments were carried out in a neighbouring laboratory to the Malvern (*Mastersizer*) so that samples could be quickly injected into the instrument at certain times after precipitation had been initiated. The length of each precipitation experiment was 30-40 minutes.

7.4.1(a) The Influence of Agitation Rate on the Particle Sizes of CaP precipitated from Heated Whey Permeates

Malvern Laser Particle Size analyses at the agitation rate 3-150 rpm. The Malvern (*Mastersizer*) results from 5 separate precipitation experiments run for 30 minutes each in which agitation rate was varied from 3-150 rpm are displayed in Table 7-3. These data show a clear tendency for particle size to increase with increasing agitation rate. Thus it appears that agitation appears to bring about an acceleration of the particle growth process in precipitating whey permeate

Table 7-3: Malvern (*Mastersizer*)-determined final particle sizes in CaP slurries[1] precipitated from lactic whey permeate.

Agitation rate, rpm	D [4, 3], μm	D (0.9, v), μm	D (0.5, v), μm
3	29.4	53.5	26.9
27	37.5	67.4	33.9
54	38.1, 40.1	68.7, 72.5	34.2, 36.3
100	51.3	100.0	42.6
150	55.2	105.8	46.8

[1]Reaction time=30 min, precipitation from the lactic whey permeate (as received 14.05.98) at T=75°C. Initial particle size in slurry was 19.75 μm.

7.4.1(b) Flocculation Kinetics

The profile of the observed particle size distributions from the Malvern *Mastersizer-S* became more monodisperse and shifted to larger particle diameters as the reaction time progressed (see Figure 7-23). This indicated that particle size growth by aggregation

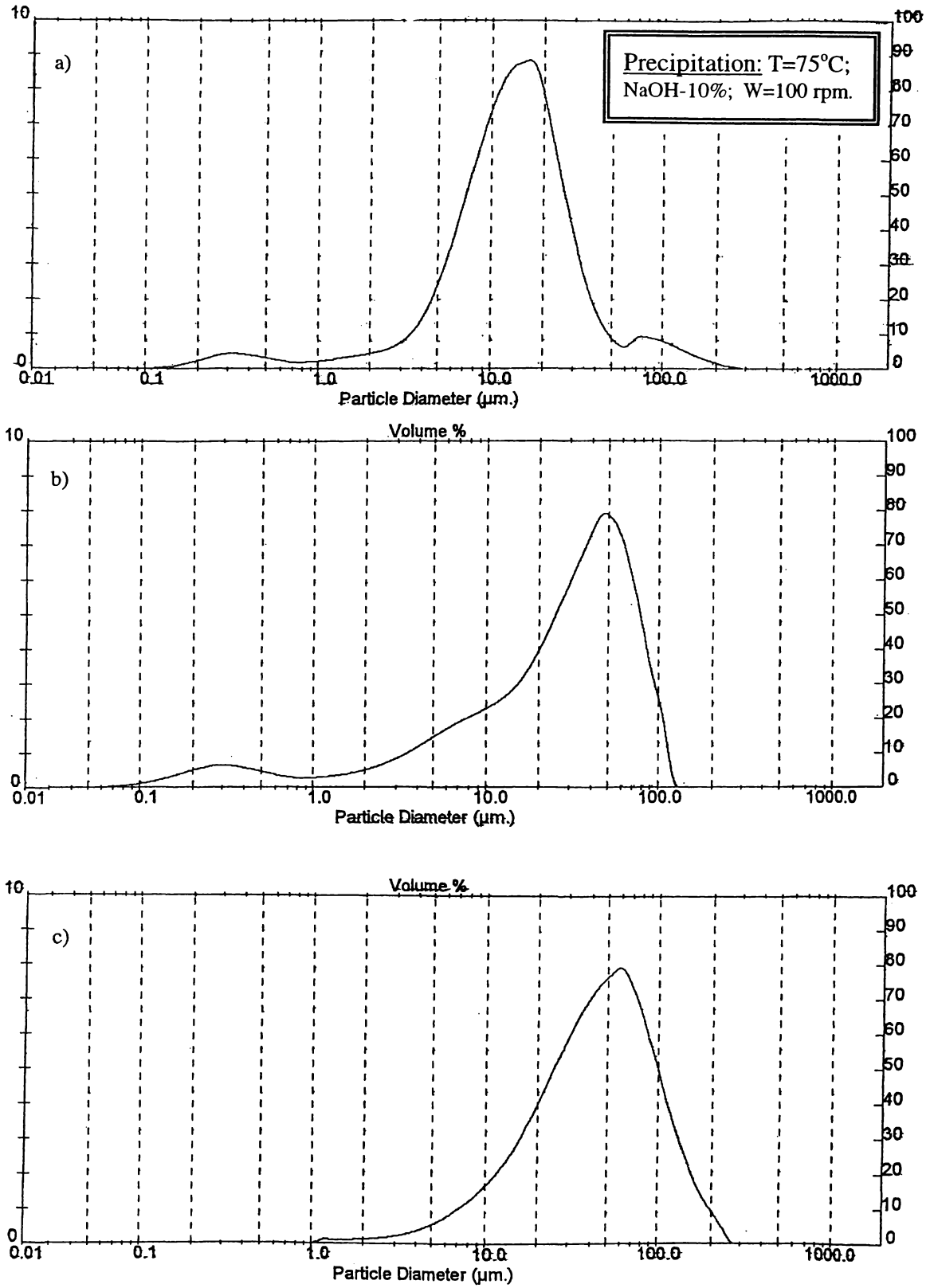

Figure 7-23: Malvern particle size distributions for the precipitation of CaP from lactic whey permeate at T=75°C and W=100 rpm as a function of the reaction time: a) initial (1 min); b) 5 min; c) 30 min.

was occurring. It has been shown that for *agitated* systems (Chander et al., 1987) the mean floc size x varies as:

$$x = x_o \, exp \, (0.23 \, t/t_{1/2})$$

while for systems where the collisions arise primarily from *Brownian motion*, the mean floc size varies approximately as:

$$x = x_o \, (1 + t/t_{1/2})^{1/3}$$

where x_o is the primary particle size and $t_{1/2}$ is the flocculation half-life defined as the time for the total number of particles to be reduced to one half of the original value. What this means is when flocculating particles are agitated, the increase in particle size increase exhibits a much sharper (exponential) increase (see Figure 7-23) than particles whose only source of "agitation" is via Brownian motion.

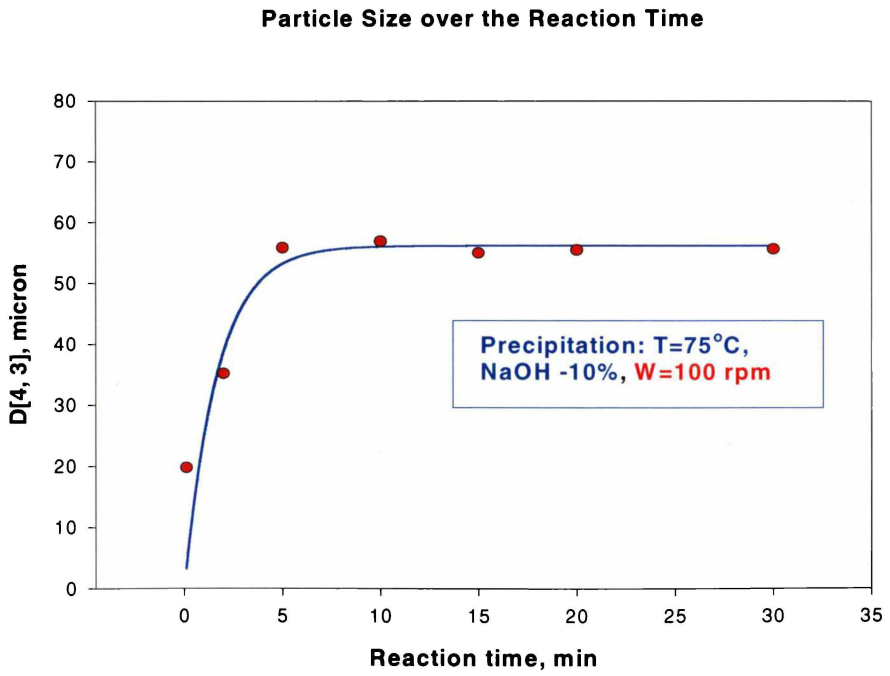

Figure 7-24: Plot of D[4, 3] versus precipitation reaction time for precipitation of CaP from lactic whey permeate at T=75°C at an agitation rate, W=100 rpm.

This is clear evidence that even mild agitation can result in a substantial growth rate. In light of the present study, it was found that during the precipitation time (*ca.* 30 minutes), the mean Malvern-determined floc diameter D[4, 3] increased in almost

exponential fashion over the first 15 minutes of the precipitation reaction before reaching a maximum value at which point it stabilised (Figure 7-24).

7.4.1(c) Additional Malvern Particle Size Analyses at more Vigorous Agitation Rates

Low-angle light scattering measurements were carried out to determine the effect of more vigorous stirring rate (>150 rpm) on CaP precipitate particle size from lactic whey permeate. For this purpose bench-scale reactions where agitation rate was varied from 34 to 1000-1200 rpm were performed. Lactic whey permeate (Cas1-starter, as received 3.11.99) was heated to 75°C and treated with 10% NaOH to stimulate calcium phosphate precipitation at pH 6.8. A graph of D[4, 3] μm vs W (agitation rate, rpm) (see Figure 7-25 below) shows that the size of the particle aggregates depends on the agitation rate. This curve has a maximum value of D[4, 3] (particle diameter) of 82 μm at W=300 rpm. Further increase in the agitation rate from 300 to 1000 rpm results in a gradual *decrease* in aggregate size from a maximum of 82 μm at W=300 rpm to a minimum of 14.7 μm at W=1000 rpm.

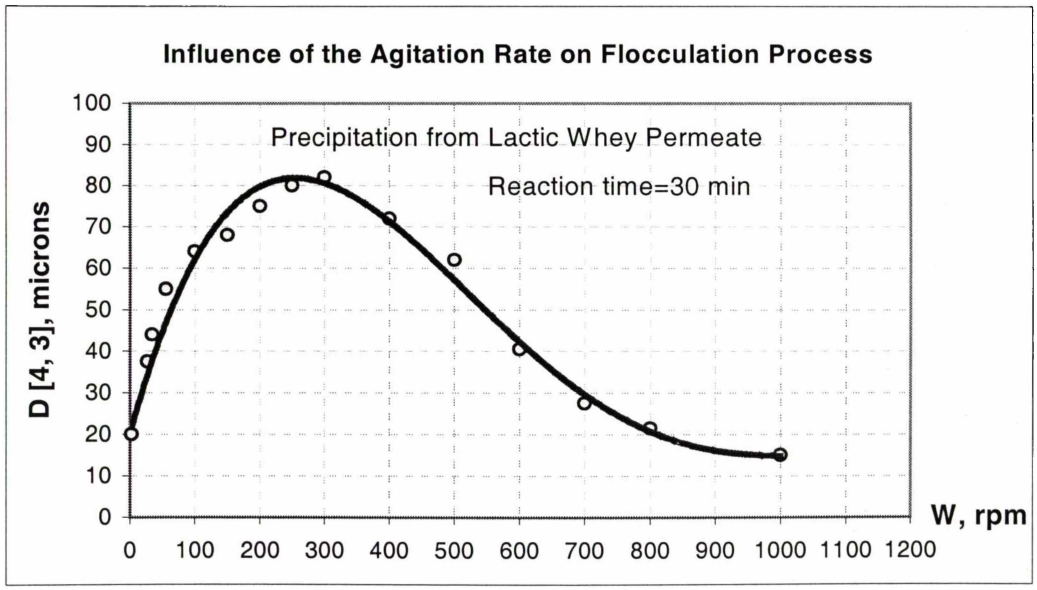

Figure 7-25: Relationship between Malvern-determined particle diameter D[4, 3] of CaP particles and the agitation rate (W) during the precipitation from lactic whey permeate. This represents data from 16 separate CaP precipitation experiments and covers a wide range of agitation rates. The particle size quoted in the graph relates to particle sizes in suspensions after 30 minutes of reaction time.

Figure 7-26 demonstrates the change of the profile of Malvern particle size distributions for the precipitation of CaP from lactic whey permeate at T=75°C at varying agitation rates W=34, 100, 300, 600 and 1000 rpm.

a)

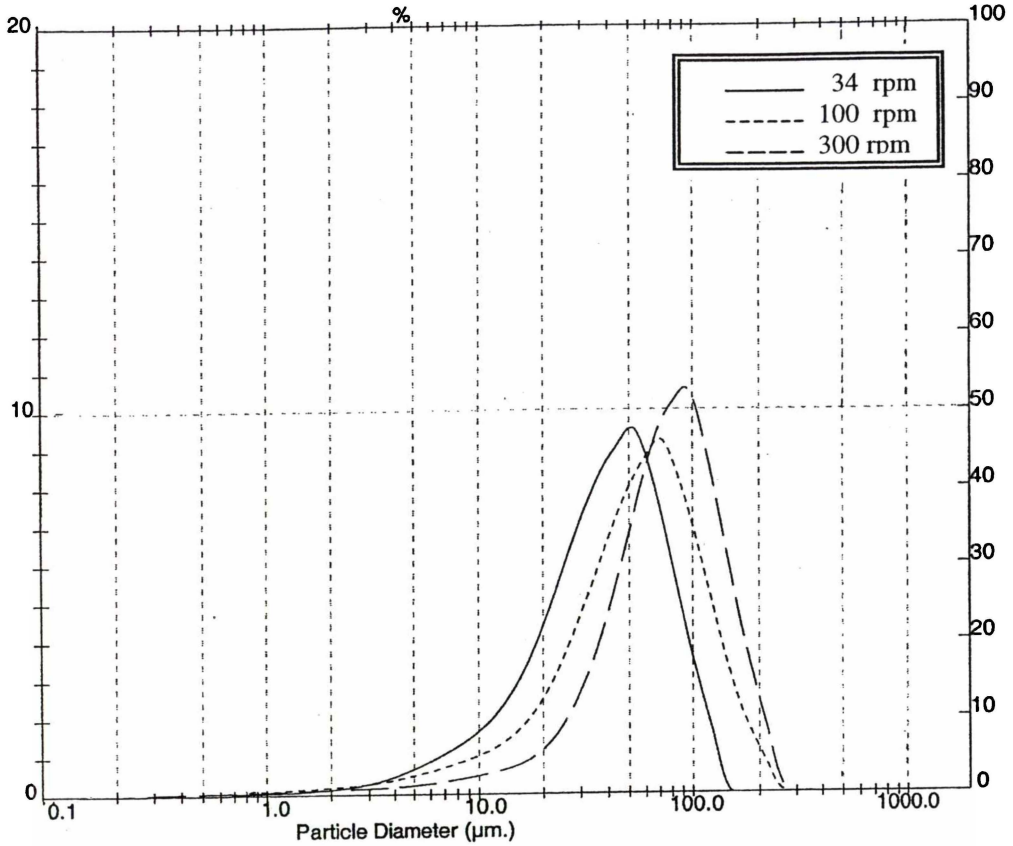

b)

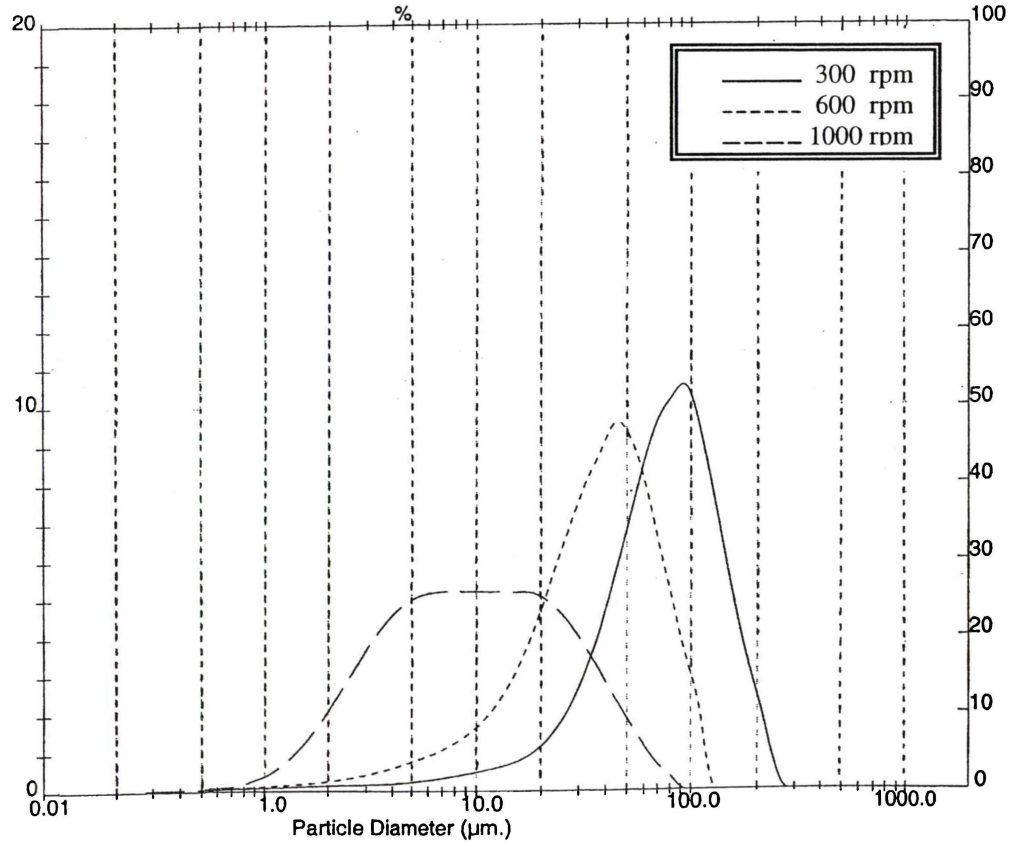

Figure 7-26: Malvern particle size distributions for the precipitation of CaP from lactic whey permeate at T=75°C at varying agitation rates (W): a) increase in W from 34 to 300 rpm; b) increase in W from 300 to1000 rpm.

These experiments were carried out with the principal aim of giving the wider scenario as regards the effect of agitation rate on the precipitation of CaP from lactic whey permeates. In general, it is clear that for agitation rates up to 300 rpm, that final particle sizes reach a maximum value of 82 μm. When using agitation rates in excess of 300 rpm, it is clear that final particle sizes in precipitates begin to show a decrease. At 1000 rpm, a particle size of only 14.7 μm is observed. In general, this effect can be described in terms of an orthokinetic (shear-induced) agglomeration process.

Orthokinetic coagulation is the generation of larger aggregates from hydrodynamically induced collisions of smaller particles (Kramer et al., 1999). The interparticle bonds that hold real aggregates together during precipitation are not obviously uniform within the structure of forming flocs (Mumtaz et al.; Kramer et al., 1999). For isotropic Newtonian fluid, the deviatoric stress, acting on the forming flock, can be calculated by equation:

$$\tau_{lm} = 2\mu \left(\frac{\partial U_l}{\partial X_m} + \frac{\partial U_m}{\partial X_l} \right)$$

where l and m are the direction (1, 2 or 3) indices, μ is a fluid viscosity. The deviatoric stress tensor is symmetric and composed of both shear (off diagonal) and normal (diagonal) components of stress. These two basic directions of stress that may act on an aggregate are depicted in Figure 7-27:

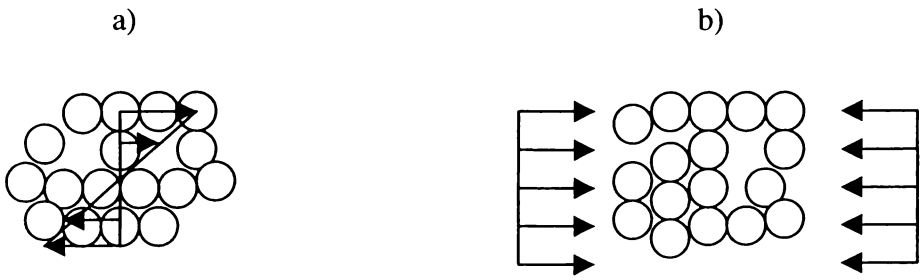

Figure 7-27: Stress acting on an aggregates: a) shearing stress; b) normal stress (Kramer et al., 1999).

It was established by British engineer Osborne Reynolds that there were two types of viscous flow. At *low velocities* flow is streamlined and *laminar* and the pressure drop is

proportional to the velocity. At *higher velocities,* the flow breaks up into eddies and becomes *turbulent.* The transition from laminar to turbulent flow in the fluid system is a function of a single prominent parameter, known as the Reynold's number:

$$\mathrm{Re} = \frac{\nu D l}{\eta}$$

where ν is the tip speed (ν = rotational speed x radius of agitator), D *is* the fluid density, l is the characteristic length of flow, η is the fluid viscosity.

Thus in the present study, it can be concluded that mild agitation (such as W≤300 rpm) accelerates the aggregation process so leading to larger particle aggregate sizes, whilst more aggressive agitation (for W>300 rpm) of the precipitating mixture causes the break up of particle aggregates by shearing which leads to smaller particle sizes. In addition, the particle size distribution profiles become broader reflecting a loss in monodispersity for the particles formed in 1000 rpm agitated suspensions (see Figure 7-26).

In the precipitating whey permeate, it is known that protein is present. There could be thus some influence of this on the calcium phosphate precipitation process. It is well-known (Gregory, 1987) that polymeric flocculants can give very much stronger flocs than more conventional agents, presumably because of the formation of polymer bridges between particles with many points of attachment.

The entire schematic diagram showing the bridging mechanisms of CaP flocs formation with long chain polymer (e.g. whey proteins) can be described as a process (Gregory, 1987), involving: a) mixing of the flocculant molecules among the particles (CaP) to give a uniform distribution, b) adsorption of them on the surface of the particles, c)- re-conformation of the adsorbed chains to give (eventually) an equilibrium configuration of particles, d) collision between destabilised particles to form aggregates (flocs) and e) break-up of flocs (see Figure 7-28). Thus this could be a factor in the precipitating whey permeates.

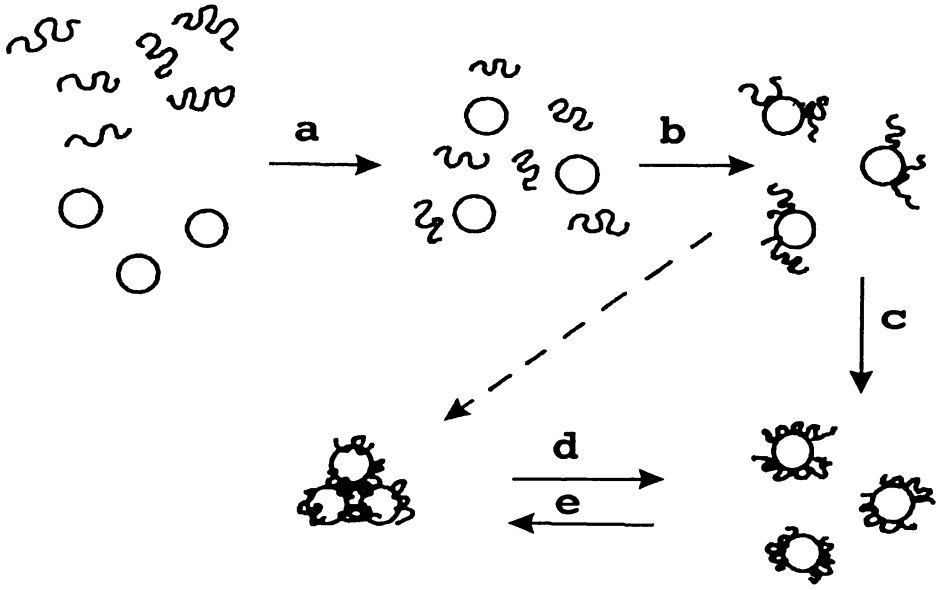

Figure 7-28: Schematic diagram showing: a) mixing; b) adsorption; c) re-arrangement of the adsorbed chains to give an equilibrium conformation of particles; d) collisions between destabilised particles to form flocs and e) break-up of flocs (from Gregory, 1987).

7.4.2 Log-Normal Distribution Analyses of the Particle Size Distributions

7.4.2(a) Log-Normal Distribution Analysis

Previously the low-angle light scattering measurements were carried out to determine the effect of stirring rate on CaP precipitate particle size, precipitated from lactic whey permeate. Bench-scale reactions where agitation rate was varied from 34 to1000 (1200) rpm were performed. Lactic whey permeate was heated to 75°C and treated with sodium hydroxide to stimulate calcium phosphate precipitation at pH=6.8.

The resolution of particle size distributions data into several log-normal populations was undertaken to consider and describe mathematically the shape of the Malvern particle size distribution curves (Pearce, 1999). The reason for this was to determine how particle size populations changed in reacting precipitates of calcium phosphate as a function of time at the different agitation rates employed.

The resolution problem involves fitting a continuous equation containing one or more normal distribution curves to the discrete Malvern size-fraction data. The Malvern (*Mastersizer*) reports the size distribution as the volume fraction of material in each of 64 size intervals with the total volume fraction = 100%.

$$\sum_{1}^{64} y_i = 100$$

Thus:

where y_i is the volume fraction of particles in the *i'th* size class having width Δx (Δx = 0.031569) for the 100 mm Malvern lens). The area (=100%) under the Malvern size

$$Area = \sum_{1}^{64} y_i \Delta x = 100 \Delta x$$

distribution curve is given by:

$$Norm = 1 = \frac{1}{s\sqrt{2\pi}} \int_{-\infty}^{\infty} \exp\left(\frac{1}{2}\left(\frac{\bar{x}-x}{s}\right)^2\right) dx$$

The area under a Log-Normal curve is given by the following equation:
The area under the Malvern curve can be resolved into several normal curves:

$$Area = 100\Delta x = c_1 Norm_1 + c_2 Norm_2 + c_3 Norm_3 = c_1 + c_2 + c_3$$

where c_i is the volume fraction of particles belonging to Log-Normal distribution *i*.
The constant values are: 100 Δx = 3.1569 and $\sqrt{(2\pi)}$ = 2.5066. Different Malvern lenses produce different Δx. In the case of the Malvern (*Mastersizer*) 2000, Δx = 0.0500 and 100 Δx / $\sqrt{(2\pi)}$ = 1.9947. The value of Σc_i for a regression provides a further measure of the goodness of fit.

7.4.2(b) Log-Normal Analyses of the Experimental Malvern Particle Distribution Curves for Precipitation Experiments conducted with varying Agitation Rates

Sigma Plot was used to fit up to two overlapping Log-Normal distributions (described by a function f, see equation below) of the Malvern size data with each distribution having a characteristic mean diameter (d_i) standard deviation (s_i) and volume fraction (c_i). Thus these parameters were used for fitting the following equation:

$$f = \sum_{i=1}^{n} c_i \times 2.646 \times \exp(-0.5(d - d_i)\text{^}2 / s_i\text{^}2) / s_i$$

The results of this fitting exercise are described in Figures 7-29, 7-30, 7-31 and Table 7-4. The most significant result from these calculations was that an increase in the particle aggregation for reactions performed at agitation rates, W ≤ 300 (rpm) range is associated with the development of two particle size populations possessing particle diameters d1 and d_2 values (with $d_2 > d_1$). Both d_1 and d_2 show an increase with agitation rate. The "concentration" of the population with larger particle diameter, d_2, tends to be the dominant contributor to the particle size distributions. If agitation rate is increased, the partial contribution of the second population with particle diameter, d_2 progressively increased (as is shown by increases in the volume fraction, c_2 while the population given by d_1 decreased (as is shown by the decrease in volume fraction c_1) (see Table 7-4).

Table 7-4: Overall Malvern Laser (*Mastersizer*) particle distribution curve fitting data as a function of agitation rates W ≤ 300 rpm for the precipitation of calcium phosphate (reaction time=30 min) from lactic whey permeate.

W (rpm)	Log (d_1)	Log (d_2)	s_1	s_2	c_1	c_2	R^2	Norm
34	1.318	1.681	0.3281	0.3281	0.396	0.600	0.9962	1.3313
55	1.361	1.774	0.3618	0.2115	0.336	0.657	0.9963	1.2903
100	1.369	1.801	0.3907	0.2343	0.283	0.711	0.9977	1.0008
200	1.507	1.883	0.3408	0.2015	0.260	0.733	0.9959	1.4829
300	1.592	1.917	0.3078	0.2060	0.262	0.718	0.9969	1.2865

7.4.2(c) Log-Normal Analyses of the Experimental Malvern Particle Distribution Curves in a given Precipitation Experiment as a Function of the Precipitation Time

In this fitting calculation, the precipitation reaction of calcium phosphate from lactic whey permeate conducted at W=34 rpm was studied to see what kinds of particle populations are present as the reaction proceeds with time. In contrast to the last section where 2 particle size populations were fitted, this experiment required the use of three Log-Normal curves to describe particle size populations. The results for this are illustrated in Figures 7-30 and 7-31.

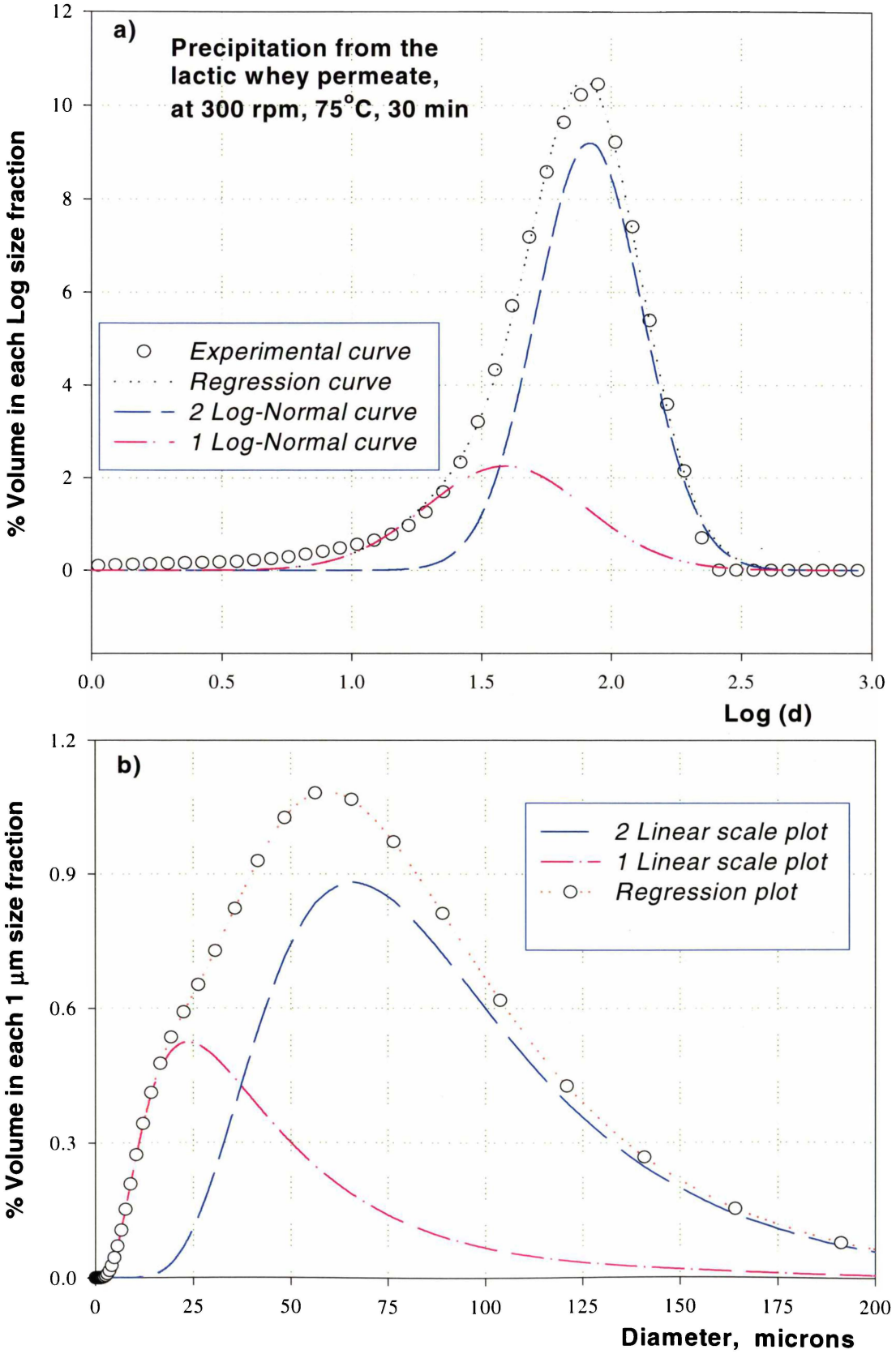

Figure 7-29: 2 Log-Normal populations fitted to the experimental Malvern particle size distribution curves: a) Log scale plot; b) Linear scale plot.

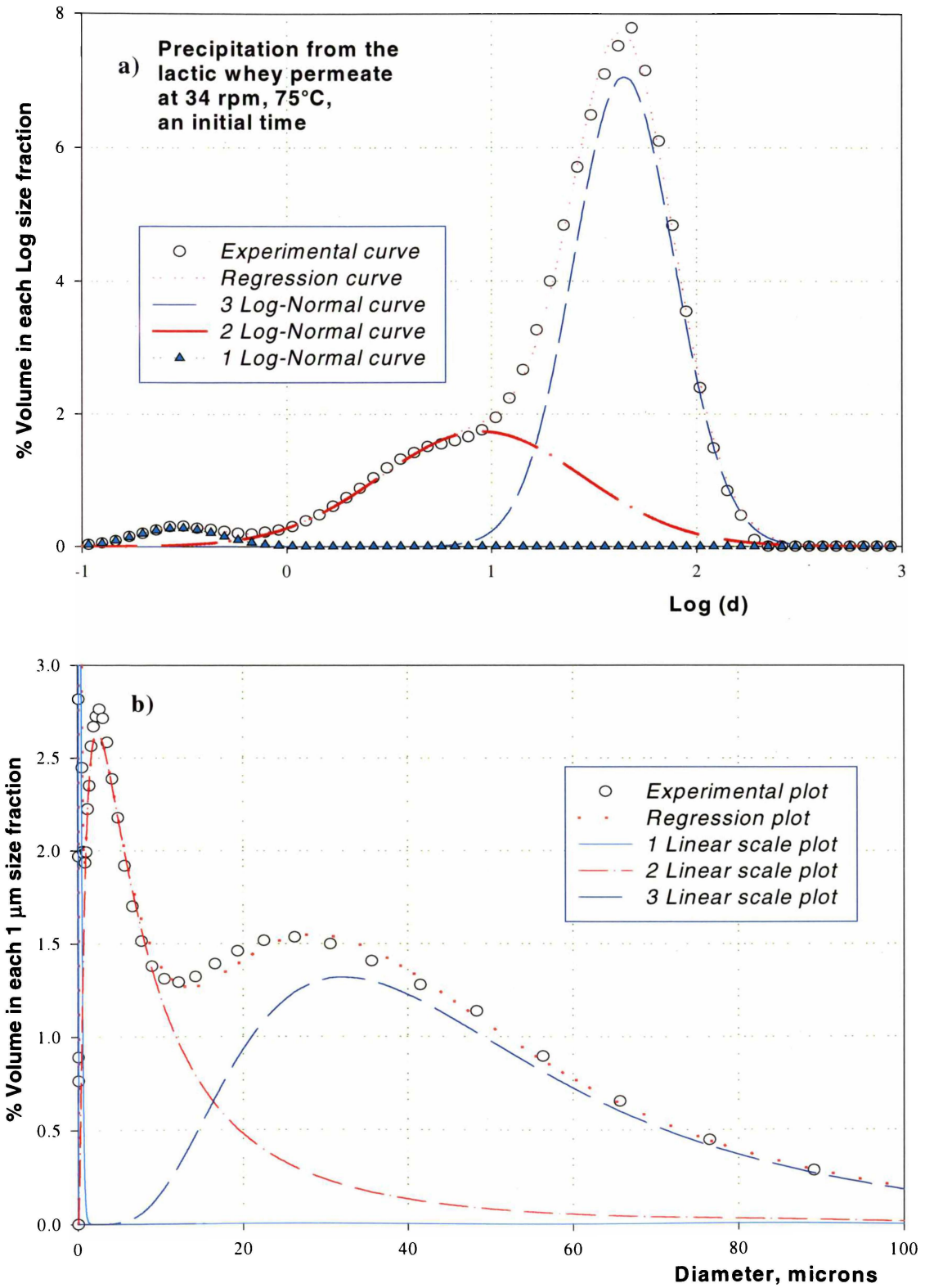

Figure 7-30: 3 Log-Normal populations fitted to the experimental Malvern particle size distribution curves: a) Log scale plot; b) Linear scale plot.

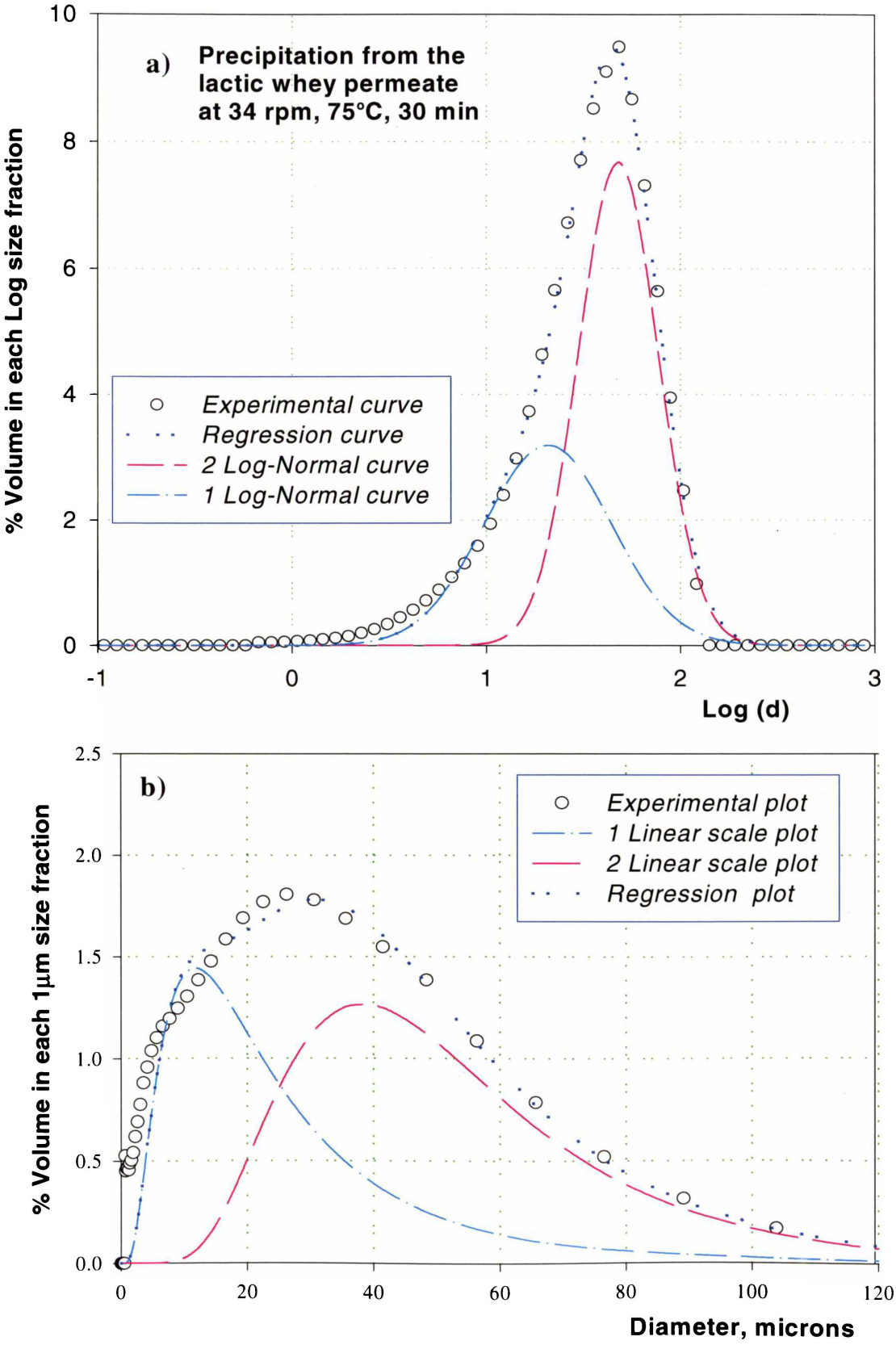

Figure 7-31: 2 Log-Normal populations fitted to the experimental Malvern particle size distribution curves: a) Log scale plot; b) Linear scale plot.

In general, these calculations showed that there was a reduction in numbers of discrete populations of particles as the precipitation reaction progressed (see Figures 7-30 and 7-31). Initially (after 1-2 minutes after precipitation was initiated) the experimental data (% Volume in each Log size fraction, see Figure 7-30) could be described as a set of 3 Log–Normal distributions showing three particle size populations with a parameters $Log(d_1)$ = -0.5285 (d_1 = 0.296 μm), $Log(d_2)$ = 0.9509 (d_2 = 8.93 μm), $Log(d_3)$ = 1.6477 (d_3 = 44.4 μm), s_1 = 0.2023, s_2 = 0.4962, s_3 = 0.2471, c_1 = 0.0217 and c_2 = 0.3257, c_3 = 0.6599.

After 30 minutes there were only 2 main particle populations discernible with the fitting software that had the following parameters: $Log(d_2)$ = 1.316 (d_2 = 20.7 μm), $Log(d_3)$ = 1.681 (d_3 = 47.97 μm), s_1 = 0.3281, s_2 = 0.328 and c_1 = 0.396, c_2 = 0.600 (see Figure 7-31). Thus the first (small population) characterised by a $Log(d_1)$ value of -0.5285, s_1 = 0.2023, c_1 = 0.0217 had disappeared in this calculation and the second population had undergone an increase in particle size after 30 minutes of reaction time with d_2 increasing from 8.93 to 20.7 μm while the particle size of d_3 had more or less remained static (cf 44.4 μm with 47.97 μm). It may then be concluded that particle size distributions become more monodisperse in nature after 30 minutes of precipitation and associated with 2 particle size populations.

In conclusion, it can be stated that orthokinetic (shear-induced) particle aggregation is occurring during the precipitation of CaP from commercial lactic whey permeate. An increase in particle aggregates ($W \leq 300$ rpm) is clearly discernible even under conditions of mild agitation. The effects of agitation are reasoned to occur in the initial stages of the reaction as is shown by Log-Normal distributions which show a change in particle populations with time. Flocs grew to some limiting size at which growth and breakage were essentially balanced in the agitated medium. The largest flocs break most readily since they are subject to the highest stresses and are probably the most fragile. More vigorous agitation ($W > 300$ rpm) clearly results in the breakage of the forming CaP flocs due to turbulent flow in the reaction vessel which is expected at the higher agitation rates.

CHAPTER EIGHT
CONCLUSIONS

8.1 Review and Evaluations of Objectives

The purpose of the work in this project was to undertake a general investigation of the chemistry related to the production of ALAMIN™, a calcium phosphate salt derived in a commercial process from whey UF-permeates in the New Zealand Dairy Industry. The industrial rationale for this project, which represented a collaborative effort between University of Waikato and the Dairy Industry, was to understand more thoroughly the chemistry of calcium phosphate precipitation. To achieve this aim, the project involved work summarised under the following subheadings:

1) Extensive literature search on the existing industrial processes and trials relating to the manufacture of ALAMIN™ in New Zealand and review on the analytical techniques that could offer useful information on calcium phosphate precipitation.

2) Theoretical speciation studies which modelled precipitation of calcium phosphate from a simulated lactic whey ultrafiltrate (SLWUF) buffer.

3) Experimental confirmation of the trends predicted by theoretical speciation (SPE) calculations on the SLWUF buffer.

4) Extensions of the ion speciation calculations using ionic compositions corresponding very closely to those existing in the commercial whey permeates and experimental confirmation of some of these trends by spectroscopic, microscopic and chemical characterisation of some typical ALAMIN™ samples.

5) Experimental work on actual industrial whey permeate streams and as received ALAMIN™ solids:

   (a) *Characterisation by spectroscopic, microscopic and chemical analysis techniques of commercial as received ALAMIN™ powders and whey permeates*;
   (b) *Bench-scale precipitation experiments on industrial samples of whey UF-permeate and analysis of results using a combination of spectroscopic, chemical, microscopic and computer fitting techniques.*

1) Extensive Literature Search on the existing Industrial Processes and Trials relating to the Manufacture of ALAMIN™ in New Zealand and Review on the Analytical Techniques that could offer useful Information on Calcium Phosphate

The literature review of work carried out so far in the New Zealand Dairy Industry recognises that recovery of CaPs from dairy fluids is a commercially important process. It also recognised that little rigorous scientific attention internationally has been directed to studying the precipitation of calcium phosphate from whey permeates hence providing an impetus for this project. The literature review on the fundamental chemistry of calcium phosphate precipitation showed that calcium phosphate can form a large range of solids and that its chemistry was exceedingly complex especially that of hydroxyapatite. It was shown that when calcium phosphate salts precipitate from aqueous solution, the precipitate initially formed is unstable in nature and transforms by a dissolution-reprecipitation process via a series of solid phases in accordance with Ostwald's Law of Stages before ultimately forming the thermodynamically most stable phase, hydroxyapatite. This "phase transformation" as it was so termed was found to depend on many factors such as pH, ionic strength, and additives in the precipitating medium, temperature, supersaturation, time and seeding. To add to this complexity, the final product, hydroxyapatite could also have a structure whose composition depended on what was present in the medium from which it precipitated due to the substitutional lability of lattice ions in the hydroxyapatite structure.

It was also shown that a large number of *spectroscopic, microscopic* and other *instrumental/ analytical* techniques could be readily applied to study calcium phosphate precipitation and yield useful results.

2) Theoretical Speciation Studies which modelled Precipitation of Calcium Phosphate from a Simulated Lactic Whey Ultrafiltrate (SLWUF) Buffer

For this purpose, a "SLWUF" buffer solution was developed which was of similar composition to that of natural lactic whey permeates. Ion complexation and solids equilibria within this system were studied using a proprietary computer speciation program, SPE in order to understand how the system behaved over the pH range 2-12. Variations to the SLWUF buffer composition were made by varying certain components such as citrate levels, Ca:P molar ratio and magnesium levels in order to simulate what

effect seasonal variations would have on the chemistry of calcium phosphate precipitation from the SLWUF. In general it was found that as pH increases from the whey permeate pH of 4.6, an increasing amount of calcium becomes involved in the formation of solid calcium phosphate phases such as brushite and OCP (HAP) and that this solid phase formation effectively dominates the speciation distribution of calcium for pH above 5.

In general, *free calcium ion concentration* was found to be the fundamental factor affecting calcium phosphate precipitation and yields of calcium containing solids in the SLWUF buffer. *Free calcium ion concentration* was dependent on a number of factors such as *citrate* concentration, *Ca:P molar ratio* and to a lesser extent *magnesium* and *lactate* ion concentrations. *Citrate*, for instance, was predicted to act as a moderate chelator of free calcium ion so influencing the overall level of this ion in the medium. Lactate ion to some extent was also a chelating agent but to a much lesser extent due to the weak ion complex between calcium and lactate ions. The addition of extra phosphate to the SLWUF buffer (and consequent change in Ca:P molar ratio) was associated with a greater overall utilisation of calcium in the SLWUF due to the formation of extra calcium phosphate solid. This was recognised as being important from an industrial point of view given that extra phosphate addition to the whey permeate, for instance may lead to the realisation of improved yields. In other words, phosphate was perceived as being a *limiting reagent* in the precipitation of calcium phosphate. The speciation calculations underestimated the effect of magnesium ion in the SLWUF. According to the calculations, magnesium ion merely competed with calcium ion for citrate and phosphate but in reality it is well known from previous studies that magnesium has a fundamental effect on kinetics of the phase transformation process of CaP solids in solution.

3) Experimental Confirmation of the Trends predicted by Theoretical Speciation (SPE) Calculations on the SLWUF Buffer

pH-stat studies on the precipitation of calcium phosphate from the SLWUF buffers were then conducted in order to provide some experimental evidence for the predictions made on calcium phosphate precipitation from the SLWUF buffers by SPE.

In general, the typical pH-stat profile of precipitation of calcium phosphate from a SLWUF buffer at pH 6.8 was a sigmoidal shape which demonstrated that the precipitation of calcium phosphate was controlled by kinetic factors and involved the well documented phase transformation of an initially amorphous calcium phosphate precipitate to an apatitic final product after passing through an autocatalytic stage characterised by the steep rise in hydroxide consumption on the pH-stat profile. pH stat-controlled experiments performed on SLWUF buffer formulations which differed from the "standard" formulation were carried out to observe whether any changes occurred in the sigmoidal profile. In particular the times taken for the onset of the autocatalytic stage and development of the final apatitic product (where hydroxide consumption levelled off) were used for determining how fast or slow the precipitation reaction progressed. In these cases, the change in *kinetics* (caused by change in calcium ion concentration for instance) was taken as *indirect evidence* of the predictions made on thermodynamic grounds by SPE.

In general, these experiments and their results can be summarised as follows: Experiments in which the Ca:P molar ratio in the SLWUF was varied from 1.55 to 1.0 were found to lead to an overall acceleration of the calcium phosphate precipitation process as evidenced by the shorter time it took for the final apatitic product to be produced for the buffer with Ca:P molar ratio 1:1 (30 mM phosphate) compared to that which had a Ca:P molar ratio of 1.55:1 (20 mM phosphate). This indicated that phosphate was an accelerating reagent from a kinetic point of view but also that a greater extent of reaction had occurred with the extra phosphate present as predicted from speciation calculations. This alone was not evidence to prove the speciation calculations that predicted differences in free calcium ion concentration. Ca ISE experiments provided this data (see later).

pH-stat experiments involving the precipitation of calcium phosphate from SLWUF buffers in the presence of varying concentrations of *citrate* (0-8 mM) demonstrated an increasing *delay* in the formation of the final apatitic product with increasing concentrations of *citrate* in the medium. The slower kinetics caused by increasing citrate concentrations is undoubtedly due to the decrease in concentration of free reactive calcium ion, which is bound up as citrate complexes in the medium. This proves the result derived from the speciation calculations that predicted decreases in

free calcium ion concentrations and increases in the pH stability region of various CaP containing solids as citrate concentration increases.

pH-stat experiments involving the precipitation of CaP from SLWUF buffers in the presence of varying concentrations of magnesium ion did not support or agree with the results of the speciation calculations. These experiments showed that as magnesium ion concentration increased, the time for formation of the final apatitic product *increased.* The reason for this is due to the well-known effect of magnesium ion, which inhibits the kinetics of the phase transformation process of the calcium phosphate precipitate. The speciation program did not have any data relating to this process hence it could only make predictions based merely on the distribution of magnesium in various complexes and solids involving citrate and phosphate.

Other pH-stat experiments associated with confirming trends predicted by SPE calculations involved conducting the precipitation of calcium phosphate from SLWUF buffers at pH values at which brushite and OCP are expected to form in order to confirm the presence of these phases (by FTIR spectroscopy) in the precipitate. When the precipitation was conducted at pH 6.0 for 40 minutes, the final solid phase isolated from the reaction mixture was found by FTIR to be brushite. This agrees with speciation calculations that predict the existence of this phase at pH 6.0. OCP has never been unequivocally identified in precipitates due perhaps to its unstable nature and the difficulty in collecting samples in the so-called "autocatalytic" region where the precipitate is undergoing rapid change.

Ca ISE measurements were also undertaken to obtain a measure of the free calcium ion concentration in the SLWUF buffers as a function of pH and to gauge the effects of components such as citrate and phosphate on the concentrations of free calcium ion. They thus constituted additional experimental evidence for confirmation of trends predicted by the computer speciation calculations. Ca ISE measurements for five SLWUF buffer formulations with different citrate concentrations (0, 2, 4, 6 and 8 mM) show clearly that the concentration of free calcium ion decreases from 7 mM for the SLWUF buffer with 0 mM citrate to *ca.* 4.4 mM for the SLWUF buffer with 8 mM citrate. This agrees with what was predicted from the speciation calculations that demonstrated an overall suppression in free calcium ion concentration with increasing citrate concentration in the buffer.

In general, Ca ISE experiments which followed changes in calcium ion concentration *after* precipitation was initiated in the SLWUF buffers were used to confirm trends predicted by the ion speciation calculations with regard to the addition of extra phosphate in the buffers. When these precipitation experiments were carried out under pH-stat control at pH 6.8 and 25°C in combination with Ca ISE monitoring of the filtrates, it showed that the typical curve of free calcium ion ($[Ca^{2+}_{(aq)}]$) concentration left in the SLWUF filtrates as a function of time after precipitation is a sigmoidal type curve which mirrors the typical pH-stat profile curve for NaOH consumption as a function of time. This confirms that free calcium ion is intimately associated with the phase transformation process of the precipitate and is subject to a sharp uptake in the autocatalytic region (i.e. that the kinetics of the process is mirrored in the free calcium ion concentration changes).

Most importantly, Ca ISE measurements on the filtrates from CaP precipitation from SLWUF buffers prepared with different concentrations of phosphate showed a distinct overall *decrease* in free calcium ion over all pH values as the phosphate concentration in the buffer *increased.* This effectively confirmed the prediction made by the speciation calculations which demonstrated that a higher concentration of phosphate in the SLWUF buffer would result in more effective calcium utilisation (in the form of precipitated calcium phosphate) and hence lead to a lower level of calcium ion in the medium. Overall, this lends experimental weight to the prediction from the speciation calculations that phosphate is a limiting reagent for the CaP precipitation process occurring in the SLWUF buffer solutions.

4) *Extensions of the Ion Speciation Calculations using Ionic Compositions corresponding very closely to those for a Typical Commercial Whey Permeates; Experimental Confirmation of some of these Trends by Spectroscopic, Microscopic and Chemical Characterisation of some typical ALAMIN™ Samples*

Extensions to the speciation calculations involved using input files for the program in which the composition was typical for lactic whey permeate. An additional ion speciation calculation was performed using an input file containing concentrations of components relevant to sulfuric acid whey permeate. This was carried out with the specific aim of determining whether solid calcium sulfate was a solid phase that could appear in the calcium phosphate product.

The results of the speciation calculations on the system with ion concentrations equivalent to lactic whey permeate were predicably practically identical to the results of speciation calculations performed on the SLWUF. As pH increased from the whey permeate pH of 4.6, an increasing amount of *calcium* becomes involved in the formation of solid calcium phosphate phases such as brushite and OCP (HAP) and that this solid phase formation effectively dominates the speciation distribution of calcium for pH above 5.

Similar trends with respect to free calcium ion concentrations and influences on it were noted. The only difference in these speciation calculations and those carried out for the SLWUF was that a "NaOH titration curve" for the system, which was taken to symbolise caustic demand, was calculated. This was carried out with regard to the industrial precipitation process as it helped to elucidate the factors that may be responsible for increased caustic demand in the vicinity of the pH at which the industrial precipitation is carried out. This is especially important for understanding what effects seasonal variations in the permeate could have on the amount of NaOH needed to carry out the precipitation. A titration curve calculation was performed to compare the level of caustic demand for a permeate with 2 mM citrate and for one with 8 mM citrate and this revealed, perhaps not suprisingly, that a higher titre of NaOH was required to bring about the endpoint in the "titration". This could be understood very basically in terms of there being a higher level of protonated citrate to deprotonated.

In contrast to the lactic whey permeate, the sulfuric acid whey permeate exhibited slightly different results because of the presence of sulfate ion in the medium instead of lactate ion. In this modelled system, consideration of the possible solid phases that can precipitate indicated that solid calcium sulfate species such as gypsum is stable at very low pH (<5). At higher pH, a hypothetical mixed calcium sulfate-phosphate complex known as “ardealite” was considered to form over a narrow pH range (4.4-4.9) as an intermediate phase between gypsum and brushite. However, over the pH region 4.7-6.7, trends similar to those observed in the SLWUF and lactic whey permeates were observed in that the major calcium phosphate solid phase to appear in this modelled system is brushite ($CaHPO_4.2H_2O$) with OCP ($Ca_8H_2(PO_4)_6.5H_2O$) appearing and dominating the speciation diagram after pH 6.5. The most significant result from these calculations are that *no* solid calcium sulfate phases are predicted to appear in any calcium phosphate precipitation product from this modelled system on thermodynamic grounds.

FTIR spectra and ICP-OES analysis of samples of washed and unwashed CaP cake from sulfuric acid whey permeate effectively provided experimental proof to backup the predictions from the speciation calculations with regard to calcium sulfate. FTIR confirmed that no calcium sulfate phase was present in the commercial ALAMIN™ powders. However, ICP-OES analyses showed a slightly elevated level of analysed S in unwashed CaP cakes from the sulfuric acid whey permeate relative to lactic-derived samples, which reduced by 50% when washed and were analysed by ICP-OES. This proved that the sulfate present in sulfuric acid ALAMIN™ was easily washable surface-adsorbed sulfate only from the medium. An interesting observation from the ICP-OES analyses was the consistently lower level of analysed magnesium in the final ALAMIN™ products. A tentative explanation for this trend could be derived from the speciation calculations which predict that citrate is a major binding agent of free magnesium ion in the medium. Given that the citrate concentration in the sulfuric acid whey permeate is significantly higher than in the lactic whey permeate, it is not unreasonable to assume that citrate is complexing magnesium ion and preventing its incorporation into the final ALAMIN™ product. In summary the results demonstrate the tremendous power of the ion speciation calculations in predicting the actual chemistry of complex solutions in which there are multiple equilibria coexisting between many ions.

5) *Experimental Work on actual industrial Whey Permeate Streams and as received ALAMIN™ Solids*

a) Characterisation by Spectroscopic, Microscopic and Chemical Analysis Techniques of as received ALAMIN™ Powders and Whey Permeates

For the characterisation of ALAMIN™ powder and commercial whey permeates from various industrial sources, 14 techniques were involved such as: X-ray Diffraction (XRD), Scanning Electron Microscopy/Energy Dispersive X-ray analysis (SEM/EDX), Transmission Electron Microscopy (TEM), Fourier Transform Infrared Spectroscopy (FTIR), X-ray Photoelectron Spectroscopy (XPS), Malvern *(Mastersizer)* Laser Light Scattering analysis, Electrospray Mass Spectrometry (ESMS), Atomic Absorption Spectroscopy (AAS), Inductively Coupled Plasma Spectroscopy (ICP-OES), pH-stat method, Calcium Ion-Selective Electrode (ISE) method, UV-Visible Spectroscopy and Differential Scanning Calorimetry.

For the ALAMIN™ powders, it is evident that the manufactured grades of commercial ALAMIN™ are complex composite materials consisting of partially crystalline non-stoichiometric hydroxyapatite with some co-deposited citrate, denatured whey protein and lactose as confirmed by FTIR spectroscopy. The particles are manufactured with a wide distribution of size diameters ranging from 5–190 μm, as was found by Laser Particle Sizer (Malvern) studies. XRD results confirm that the ALAMIN™ contains poorly crystalline HAP as a major structural component with individual "crystallite" (i.e. the so-called fundamental primary particle which is undergoing the X-ray diffraction) sizes of *ca.* 0.0203 μm. The general morphology of the commercial dried ALAMIN™ particles are irregularly shaped with a chunky and aggregated, porous nature as illustrated in SEM micrographs. Lamination observed in the particles was perceived as being due to protein layers. EDX analyses on the SEM samples of ALAMIN™ powder for measurement of Ca:P molar ratio gave values ranging from 1.50-1.65 which confirmed that ALAMIN™ was a Ca-deficient non stoichiometric hydroxyapatite compound. The DSC profiles of ALAMIN™ powder suggest a mixture of organic components intimately associated with the calcium phosphate are giving rise to the observed thermal transitions, namely citrate, lactose and denatured whey proteins. Some characterisation was also undertaken of some other commercial calcium phosphate products from overseas manufactures. These showed the powders to be of similar composition to ALAMIN™ but with a higher level of co-deposited impurities such as citrate and lactose.

For the whey permeate streams, AAS and ICP-OES studies indicated that the absolute concentration of calcium in the whey permeates before any precipitation occurs was in the vicinity of 1200 ppm (*ca.* 30 mM Ca). In contrast Ca ISE analyses of the whey permeate before precipitation gave a value of *ca.* 8 mM at pH 4.6 corresponding to free calcium ion in the permeate. The difference is due to the involvement of the calcium ion in various ion-ion or ion-molecule complexes as predicted by the ion speciation calculations.

ESMS characterisation of the lactic acid permeates merely showed that lactose, lactate, potassium and calcium ions were present in the permeate. The comparison of two different lactic whey UF-permeates showed a reduction in the relative intensity of the lactose peak relative to the lactate peak. This prompted the suggestion that ESMS may

be useful in ascertaining the degree of bacterial degradation of the permeate though this technique should be used with caution.

b) Bench-scale precipitation experiments on industrial samples of whey permeate and analysis of results using a combination of spectroscopic, chemical, microscopic and computer fitting techniques

Some simple bench-scale precipitation work on the natural lactic and sulfuric acid whey permeates covered three distinct aspects: 1) pH-time studies on the precipitation of calcium phosphate from whey permeates at pH 6.8 not under pH-stat control, 2) Elemental analysis of these reaction solutions by AAS and ICP-OES, 3) Examination of the precipitates using XRD, SEM and FTIR. The pH versus time curves for calcium phosphate precipitation (when the permeate was adjusted without pH-stat control to pH 6.8) showed two regions of discontinuity perceived to be associated with phase transformations in accordance with Ostwald's Law of Stages. The first region of discontinuity could represent transformation of an amorphous calcium phosphate (ACP) to intermediate phase (Brushite/OCP) while the second region could represent the final transformation to apatitic CaP. FTIR spectra of the evolving precipitating phase suggests tentatively that a change in the precipitate is taking place as a function of time. AAS and ICP-OES data show that the bulk of the precipitation of the CaP in whey permeate is over after the first few minutes. Ca ISE data on the sera obtained from precipitating whey permeates also show a drop in free calcium ion concentration from 8 mM to 1.5 mM with a gradual further drop to 1.10 mM after 40 minutes which suggests extra calcium ion being taken up as a function of time by the precipitate. TEM data of CaP precipitates from lactic whey permeate as a function of time also suggest a change in the structural characteristics of the precipitate as a function of time after precipitation.

In general, most of these observations suggest that precipitation of calcium phosphate from natural whey permeates follow a process in which the precipitate is evolving over time in a phase transformation process. This agrees with the general experimental results from SLWUF pH-stat controlled precipitation work, the theoretical computer speciation calculations for SLWUF and lactic whey permeate. The phase transformation process can be generally stated by reference to the following scheme: (Figure 8-1). Calcium phosphate precipitates from the whey permeate as an initially amorphous phase (i.e. ACP) and then evolves via a series of dissolution-reprecipitation reactions into the

most stable final phase known as hydroxyapatite (HAP). The calcium phosphate phases intermediate between ACP and HAP are reckoned to be brushite/OCP as deduced from the precipitation studies on the SLWUF buffers and for lactic whey permeates. This unique study has thus shown that precipitation of CaP from whey permeates is a very interesting and complex system about which a lot more information has been discovered as a result of the extensive investigations carried out in this thesis.

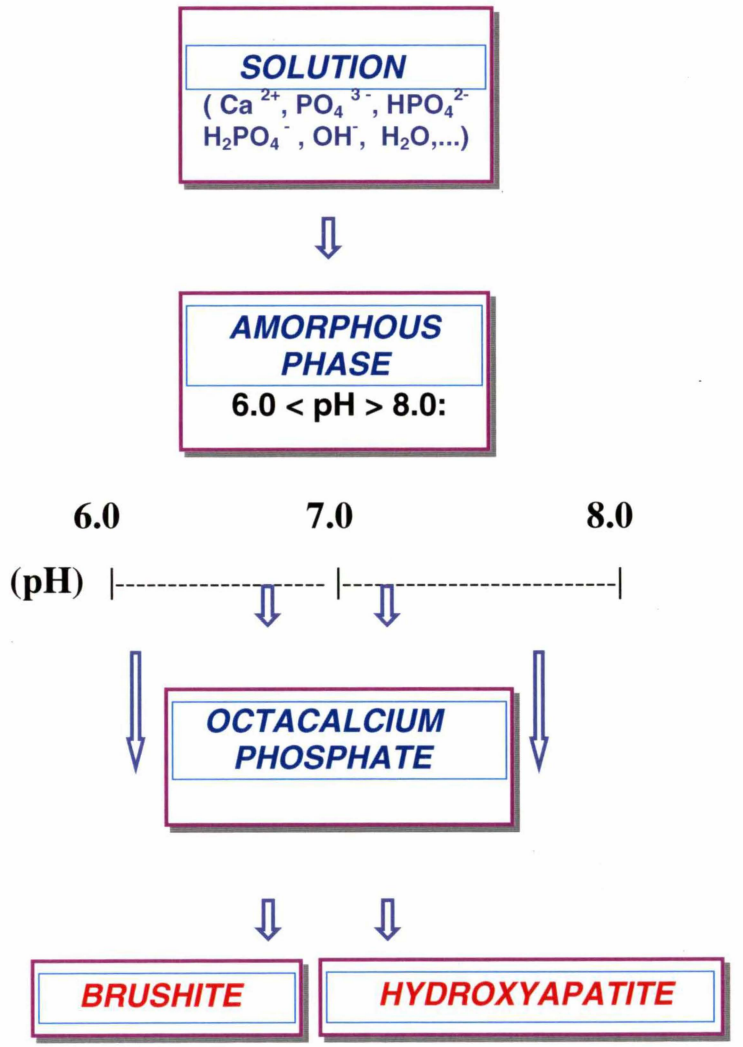

Figure 8-1: General scheme showing the phase transformation of calcium phosphate precipitating from lactic whey permeate solution.

In addition, an attempt was made to investigate the mechanism of formation and flocculation process of CaP phases precipitated from heated whey permeates and to identify how potentially important industrial parameters such as agitation rate affects particle size and particle growth processes and what distinct populations of particles develop during the precipitation process. This work was performed using Malvern laser light scattering measurements on heated precipitating whey permeates over various times and at different agitation rates.

The overall conclusions from this investigation were that for agitation rates up to 300 rpm, final particle size of any precipitates produced increases with increases in the agitation rate.

This showed clearly that orthokinetic (shear-induced) particle aggregation was occurring during the precipitation of CaP from commercial lactic whey UF-permeate. In other words, the effects of agitation were reasoned to occur in the initial stages of the reaction with flocs growing to some limiting size at which growth and breakage were essentially balanced in the agitated medium. The largest flocs would then break most readily as they are subject to the highest stresses and are probably the most fragile. Precipitation from whey permeate agitation rates > 300 rpm were found by Malvern laser light scattering studies to results in final particle diameters which were *smaller* than the maximum particle diameter observed for agitations < 300 rpm. This trend was believed to be due to the breakage of the CaP flocs with the size reduction being associated with the turbulence in the vessel that occurs at these high agitation rates.

8.2 Recommendations for Further Study

The results from this study highlighted a number of aspects that suggests potential for further research due to the broad nature of this topic and the fact that many techniques can be used to study it, several of the aims could not be fully investigated. Suggestions for continued work in these areas have been mentioned previously throughout the text. Some of the broader topic areas include:

- Continuation of the SLWUF precipitation work in order to elucidate the influence of whey proteins, lactose, magnesium and citric acid on the physico-chemical properties and morphology of the precipitated CaP particles. Additional work on measuring the solid yield should also be carried out.

- Providing a full characterisation of the composition (of both organic and inorganic components) of ALAMIN™ so that a standard material could be prepared.

- To study in detail the impact of various temperatures and the different starters on the CaP precipitation process.

- Completion of the study into the effect of agitation rate in which the influence of different flocculating agents (e.g. proteins) are investigated.

- To use a combination of scanning electron and confocal microscopy which is especially useful for looking at protein layers on the commercial ALAMIN™ powder.

- Investigation of the mechanical properties of ALAMIN™ product.

- Extension to the X-ray Photoelectron analyses of ALAMIN™ but in the presence of various dispersal agents such as protein to monitor surface uptake.

- Investigation of where a magnesium-enriched calcium phosphate can be formed.

- Development of a simulated sulfuric whey ultrafiltrate permeate (SSWUP) for performing pH-stat controlled precipitations to provide experimental proof of the trends predicted by the ion speciation calculations on sulfuric acid whey permeate.

- Finding unequivocal chemical tests to accurately analyse for levels of citrate and lactate/lactose in the lactic whey permeate given the importance of some of these components a calcium phosphate precipitation.

Investigation into these areas could give new and innovative ways to creating value from ALAMIN™ product, which is currently manufactured in New Zealand. In addition, some insight was needed into how the chemistry of calcium phosphate precipitation would change if the whey permeate changed as a result of, for instance, seasonal variations.

REFERENCES

(Abbona et al., 1990): F. Abbona and M. Franchini-Angela, "Crystallisation of calcium and magnesium phosphates from solutions of low concentration", *J. Cryst. Growth,* **104**, 661.

(Adami et al., 1968): A. Adami and M.J. Ridge, "Observation on calcium dihydrate formed in media rich in phosphoric acid. 1. Precipitation of calcium sulphate dihydrate", *J. Appl. Chem.*, **18**, 361.

(Allen, 1981): T. Allen, in *Particle size measurement* (Chapmen & Hall, London), 103.

(Aoba et al., 1984): T. Aoba and E.C. Moreno, "Preparation of hydroxyapatite crystals and their behaviour as seeds for crystal growth", *J. Dent. Res.*, **63**, 874.

(Aoki, 1994): H. Aoki, in *Medical applications of hydroxyapatite*, (Ishiyaku EuroAmerica Inc., Tokyo) 222.

(Aslaninan et al., 1982): S. Aslaninan and D. Stoilova, "Study of ardealite, an intermediate member of the gypsum-brushite series", *Bull. Mineral.*, **105**, 621.

(Atkins, 1996): P.W. Atkins in *The elements of physical chemistry, second edition* (Oxford University Press, Oxford, England).

(Atkins, 1998): P.W. Atkins in *Physical chemistry, sixth edition* (Oxford University Press, Oxford, England) 625.

(Bachra et al., 1965): B.N. Bachra, O.R. Trautz, and S.L. Simon, "Precipitation of calcium carbonates and phosphates-III. The effect of magnesium and fluoride ions on the spontaneous precipitation of calcium carbonates and phosphates", *Arch. oral Biol.,* **10**, 731.

(Bachra et al., 1969): B.N. Bachra and H.R.A. Fischer, " Effect of some inhibitors on nucleation and crystal growth of apatite", *Calcif. Tiss. Res.*, **3**, 348.

(Balenzano et al., 1984): F. Balenzano, L. Dell'Anna, J. M. Di Pierro, S. Fiore, "Ardealite $CaHPO_4CaSO_4.4H_2O$: A new occurrence and new data", *Neues Jahrb. Mineral., Monatsh*, **10**, 461.

(Barr, 1994): T.L. Barr in *Modern ESCA. The principles and practice of X-ray photoelectron spectroscopy,* (CRC Press, Ann Arbor).

(Berry et al., 1972): E. E. Berry, "Some Observations on the Setting of Calcium sulphate hemihydrate in the presence of phosphoric acid and hydrated lime", *J. Appl. Chem. Biotechnol.*, **22**, 667.

(Bespalov et al., 1994): A.V. Bespalov, A.V. Mikhailov, E.Y. Shinkovskaya, "Precipitation of an industrial calcium sulfate dihydrate slurry", *Khimicheskaia Promyshlennost (Moscow)*, **9**, 598.

(Bohner et al., 1995): M. Bohner, J. Lemaître, K. Ohura, P. Hardouin, "Effect of sulfate ions on the in *vitro* properties of β–TCP-MCPM-Water Mixtures. Preliminary *in vivo* results", *Bioceramics: Materials and Applications*, **48**, 245.

(Boye et al., 1997): J.I. Boye, I. Alli, A.A. Ismail, "Use of differential scanning calorimetry and infrared spectroscopy in the study of thermal and structural stability of α-lactalbumin", *J. Agric. Food Chem.*, **45**, 1116.

(Blumenthal et al., 1972): N.C. Blumenthal, A.S. Posner, and J.M. Holmes, "Effect of preparation conditions on the properties and transformation of amorphous calcium phosphate", *Mater. Res. Bull.*, **7**, 1181.

(Blumenthal et al., 1975a): N.C. Blumenthal, F. Betts, and A.S. Posner, "Nucleotide stabilisation of amorphous calcium phosphate", *Mat. Res. Bull.*, **10**, 1055.

(Blumenthal et al., 1975b): N.C. Blumenthal, F. Betts, and A.S. Posner, "Effect of carbonate and biological macromolecules on formation and properties of hydroxyapatite", *Calcif. Tiss. Res.*, **18**, 81.

(Bowen et al., 1975): D.K. Bowen and C.R. Hall in *Microscopy of Materials* (Macmillan press, London).

(Boskey et al., 1973): A.L. Boskey and A.S. Posner, "Conversion of amorphous calcium phosphate to microcrystalline hydroxyapatite. A pH-dependent, solution-mediated, solid-solid conversion", *J. Phys. Chem.*, **77**, 2313.

(Boskey et al., 1974): A.L. Boskey and A.S. Posner, "Magnesium stabilisation of amorphous calcium phosphate: A kinetic study", *Mat. Res. Bull.*, **9**, 907.

(Boskey et al., 1976): A.L. Boskey and A.S. Posner, "Formation of hydroxyapatite at low supersaturation", *J. Phys. Chem.*, **80**, 40.

(Brecevic et al., 1979): Lj Brecevic and H. Furedimi, "Precipitation of calcium phosphates from electrolyte-solutions. 5. Influence of citrate ions", *Calcif. Tiss. Int.*, **28**, 131.

(Brew et al., 1992): K. Brew, J.A. Grobler, "α-Lactalbumin" in *Advanced Dairy Chemistry. - Volume 1: Proteins*, P. F. Fox, ed. (Elsevier Applied Science), 191.

(Brothersen et al., 1982): C.F. Brothersen, N.F. Olsen, and T. Richardson, "Recovery of calcium phosphate from ultrafiltration permeates", *J. Dairy Sci.*, **65**, 17.

(Brown et al., 1984): W.E. Brown, M. Mathew, and L.C. Chow, "Roles of octacalcium phosphate in surface chemistry of apatites" in *Adsorption on and surface chemistry of hydroxyapatite,* D. N. Misra, ed. (Plenum Press, New York) 13.

(Budz et al., 1998): J. Budz, A.G. Jones, J.W. Mullin, "Effect of selected impurities on the continuous precipitation of calcium sulphate (gypsum)", *J. Chem. Tech. Biochnol.* **36**, 153.

(Bűchner et al., 1989): W. Bűchner, R. Schliebs, G. Winter, K.H. Bűchel in *Industrial inorganic chemistry* (Weinheim; Basel (Switzerland); Cambridge; New York, NY: VCH).

(Calcium Electrode, Operating Instructions, 1998): Manual accompanying the ISE25 Ca ion-selective electrode (Radiometer Analytical S.A., France).

(Chander et al.,1987): S. Chander, R. Hogg, Sedimentation and consolidation in destabilized suspensions. Flocculation in Biotechnology and Separation Systems, edited by Attia Y.A., (Elsevier Science Publishers B.V., Amsterdam) 279.

(Chaplin, 1984): L.C. Chaplin, "Studies on micellar calcium phosphate: composition and apparent solubility product in milk over a wide pH range", *J. Dairy Res.*, **51**, 251.

(Cheng et al., 1983): P-T. Cheng and K.P.H. Pritzker, "Solution Ca/P ratio affects calcium phosphate crystal phases", *Calcif. Tiss. Int.*, **35**, 596.

(Christoffersen et al., 1989): J.C. Christoffersen, M.R. Christoffersen, W. Kibalczyc, and F.A. Andersen, "A contribution to the understanding of the formation of calcium phosphates", *J. Cryst. Growth*, **94**, 767.

(Cole, 1997): R.B. Cole in *Electrospray ionisation mass spectrometry: fundamentals, instrumentation application* (Wiley-Interscoience, New York).

(Currie, 1990): I.E.L. Currie, "Optimisation of the primary extraction of calcium phosphate precipitate from lactic whey UF permeate" Diploma of Dairy Science and Technology Dissertation, Massey University, January 1990.

(Daufin et al., 1993): G. Daufin, F. Michel, J.P. Labbé, A. Quémerais, and A. Grangeon, "Ultrafiltration of defatted whey: improving performance by limiting membrane fouling", *J. Dairy Res.*, **60**, 79.

(Davies, 1962): C.W. Davies in *Ion Association* (Butterworths, London, 1962).

(De Robertis et al., 1995): A. De Robertis, P. De Giacomo, and C. Foti, "Ion-selective electrode measurements for the determination of formation constants of alkali and alkaline earth metals with low-molecular-weight ligands", *Analytica Chimica Acta*, **300**, 45.

(Dorozhkin, 1997): S.V. Dorozhkin, "An elaboration of the new dissolution mechanism for apatite", *Bioceramics*, **10**, 187.

(Drapier-Beche et al., 1997): N. Drapier-Beche, J. Fanni, M. Parmentier, M. Vilasi, "Evaluation of lactose forms by nondestructive analysis", *J. Dairy Sci*, **80**, 457.

(Eanes et al., 1965a): E.D. Eanes, I.H. Gilllessen, and A.S. Posner, "Intermediate states in the precipitation of hydroxyapatite", *Nature*, **208**, 365.

(Eanes et al., 1965b): E.D. Eanes and A.S. Posner, "Kinetics and mechanism of conversion of noncrystalline calcium phosphate to crystalline hydroxyapatite", *Trans. N.Y. Acad. Sci.*, **28**, 233.

(Eanes et al., 1968): E.D. Eanes and A.S. Posner, "Intermediate phases in the basic solution preparation of alkaline earth phosphates", *Calcif. Tiss. Res.*, **2**, 38.

(Eanes et al., 1973): E.D. Eanes, J.D. Termine, and M.U. Nylen, "An electron microscopic study of the formation of amorphous calcium phosphate and its transformation to crystalline apatite", *Calcif. Tiss. Res.*, **12**, 143.

(Eanes, 1976): E.D. Eanes, "The interaction of supersaturated calcium phosphate solutions with apatitic substrates", *Calcif. Tiss. Res.*, **20**, 75.

(Eanes et al., 1977): E.D. Eanes and J.L. Meyer, "The maturation of crystalline calcium phosphate precipitates in aqueous suspensions at physiologic pH", *Calcif. Tiss. Res.*, **23**, 259.

(Eanes et al., 1981): E.D. Eanes and S.L. Rattner, " The effect of magnesium on apatite formation in seeded supersaturated solutions at pH 7.4", *J. Dent. Res.*, **60**, 1719.

(Eanes, 1998): E.D. Eanes, "Amorphous calcium phosphate: thermodynamic and kinetic considerations" in *Calcium phosphates in biological and industrial systems*, Z. Amjad, ed. (Kluwer Academic Publishers Group), 21.

(Elliot, 1994): J.C. Elliot in *Structure and chemistry of the apatites and other calcium orthophosphates* (Studies inorganic chemistry 18 series, Elsevier, Amsterdam).

(England, 1991): B.M. England, "Scanning electron microscopy" in *The Mineralogical Record,* **22**, 123.

(Evenhuis et al., 1957): N. Evenhuis and Th. R. de Vries, "The condition of calcium phosphate in milk IV", *Neth. Milk Dairy J.*, **11**, 180.

(Feenstra, 1979): T.P. Feenstra," A note on the calculation of concentrations in the case of many simultaneous equilibria", *J. Chem. Educ.*, **56**, 104.

(Feenstra et al., 1979): T.P. Feenstra and P.L. de Bruyn, "Formation of calcium phosphates in moderately supersaturated solutions", *J. Phys. Chem.*, **83**, 475.

(Feenstra et al., 1981): T. P Feenstra, P.L. de Bruyn, "The Ostwald rule of stages in precipitation from highly supersaturated solutions: a model and its applications to the formations of the nonstoichiometric amorphous calcium phosphate precursor phase", *J. Coll. Interface Sci.*, **84**, 66.

(Freiser, 1980): H. Freiser in *Ion-selective electrodes in analytical chemistry, volumes 1 and 2* (Plenum Press, New York).

(Fulmer et al., 1998): M.T. Fulmer and P.W. Brown, "Hydrolysis of dicalcium diphosphate dihydrate to hydroxyapatite", *J. Mat. Sci. Materials in Medicine*, **9**, 197.

(Furedi-Milhofer et al., 1971): H. Furedi-Milhofer, B. Purgaric, Lj. Brecevic and N. Pavkovic, "Precipitation of calcium phosphates from electrolyte solutions", *Calcif. Tiss. Res.*, **8**, 142.

(Goldmann et al., 1992): D. Goldmann and D.E. Hartmann, "Method for sweet whey permeate reprocessing to recover lactose", German patent DE 41 13 836 A 1, 1992 (in German).

(Gregory 1987): J. Gregory " Kinetic aspects of polymer adsorption and flocculation" in "Flocculation in Biotechnology and Separation System, Y.A. Attia, ed. (Elsevier Science Publishers B.V., Amsterdam), 31.

(Hambling et al., 1992): S.G. Hambling, A.S. McAlpine, L. Sawyer, "β-Lactoglobulin",

in Advanced Dairy Chemistry-Volume 1: Proteins, P.F. Fox, ed. (Elsevier Applied Science), 141.

(Hamdona et al.,1993): S.K. Hamdona, R.B. Nessim, S.M. Hamza, "Spontaneous precipitation of calcium sulphate dihydrate in the presence of some metal ions", *Desalination*, **94**, 69.

(Heughebaert et al., 1984): J.C. Heughebaert and G.H. Nancollas, "Kinetics of crystallisation of octacalcium phosphate", *J. Phys. Chem.*, **88**, 2478.

(Hobman, 1992): P.G. Hobman, "Ultrafiltration and manufacture of whey protein concentrates", in *Whey and lactose processing*, J.G. Zadow, ed. (Elsevier Science Publishers Ltd, London) p.195.

(Holt et al., 1981): C. Holt, D.G. Dalgleish, and R. Jenness, "Calculation of the ion equilibria in milk diffusate and comparison with experiment", *Anal. Biochem.*, **113**, 154.

(Holt, 1982): C. Holt, "Inorganic constituents of milk. III The colloidal calcium phosphate of cow's milk", *J. Dairy Res.*, **49**, 29.

(Holt et al., 1982): C. Holt, S.S. Hasnain, and D.W.L. Hukins, "Structure of bovine milk calcium phosphate determined by X-ray absorption spectroscopy", *Biochim. et Biophys. Acta*, **719**, 299.

(Holt, 1985): C. Holt, "The milk salts: their secretion, concentrations and physical chemistry", in *Developments in dairy chemistry -3. Lactose and Minor constituents*, P.F. Fox, ed. (Elsevier Applied Science Publishers, London) p.143.

(Holt et al., 1989): C. Holt, M. J.J.M. van Kemenade, L.S. Nelson, L. Sawyer, J.E. Harries, R.T. Bailey, and D.W.L. Hukins, "Composition and structure of micellar calcium phosphate", *J. Dairy Res.*, **56**, 411.

(Holt et al., 1996a): C. Holt and D. S. Horne, "The hairy casein micelle: Evolution of the concept and its implications for dairy technology", *Neth. Milk Dairy J.*, **50**, 85.

(Holt et al., 1996b): C. Holt, N. M. Wahlgren, and T. Drakenberg, "Ability of a β-casein phosphopeptide to modulate the precipitation of calcium phosphate by forming amorphous dicalcium phosphate nanoclusters", *Biochem. J.*, **314**, 1035.

(Holt, 1997): C. Holt. The milk salts and their interaction with casein in *Advanced Dairy Chemistry. volume 3: Lactose, Water, Salt and Vitamins*, P.F. Fox, ed. (Elsevier Applied Science, London).

(Holt, 2001): C. Holt. Recommendations from the examiner's report.

(Hoppenbrouwers et al., 1988): P.M.M. Hoppenbrouwers and F.C.M. Driessens, "The effect of lactic and acetic acid on the formation of artificial caries lesions", *J. Dent. Res.*, **67**, 1466.

(Hudson, 1992): B.J.F. Hudson in *Biochemistry of Food Proteins* (Elsevier Applied Science Publishers Ltd, London).

(Inskeep et al., 1988): W.P. Inskeep and J.C. Silvertooth, "Kinetics of hydroxyapatite precipitation at pH 7.4 to 8.4", *Geochim. et Cosmochim. Acta*, **52**, 1883.

(Ishikawa et al., 1993a): K. Ishikawa, K. Asaoka, and N. Kuwayama, "Hydrolysis of octacalcium phosphate to hydroxyapatite in the presence and absence of fluoride, magnesium and hydroxyapatite", *Chemistry Express (Kinki Chemical Society, Japan),* **8**, 433.

(Ishikawa et al., 1993b): K. Ishikawa, P. Ducheyne, and S. Radin, "Determination of the Ca/P ratio in calcium deficient hydroxyapatite using X-ray diffraction analysis", *J. Mat. Sci. Materials in Medicine,* **4**, 165.

(Jenness et al., 1962): R. Jenness and J. Koops, "Preparation and properties of a salt solution which simulates milk ultrafiltrate", *Neth Milk Dairy J.,* **16**, 153.

(Kazak et al., 1981): V.G. Kazak, A.G. Kostyuk, "Precipitation of calcium and strontium sulfates from solution containing both", *J. Appl. Chem. of the USSR*, **54**, 1563.

(Kebarle et al., 1993): P. Kebarle and L. Tang, "From ions in solution to ions in the gas phase. The mechanism of electrospray mass spectrometry", *Anal. Chem.,* **65**, 972A.

(Kieswetter et al., 1994): K. Kieswetter, T.W. Bauer, S.A. Brown, F. Van Lente, and K. Merritt, "Characterisation of calcium phosphate powders by ESCA and EDXA", *Biomaterials,* **15**, 183.

(Konishi et al., 1987): K. Konishi, M. Kambara, H. Noshu, and M. Uemura, "X-ray photoelectron spectroscopic (ESCA) study on the surface of hydroxyapatite", *J. Osaka Dent. Univ.,* **21**, 1.

(Koutsoukos et al., 1980): P. Koutsoukos, Z. Amjad, M.B. Thomson, and G.H. Nancollas, "Crystallisation of calcium phosphates. A constant composition study", *J. Am. Chem. Soc.,* **102**, 1553.

(Koutsoukos et al., 1981): P. G. Koutsoukos and G.H. Nancollas, "Crystal growth of calcium phosphates-Epitaxial considerations", *J. Cryst. Growth*, **53**, 10.

(Kramer et al., 1999): T. A. Kramer and M. M. Clark, "Incorporation of Aggregate Breakup in the Simulation of Orthokinetic Coagulation", *J. Coll. Interface Sci.*, **216**, 116.

(Kronman et al., 1981): M.J. Kronman, S.K. Sinha, and K. Brew, "Characteristics of the binding of Ca^{2+} and other divalent metal ions to bovine α-lactalbumin", *J. Biol. Chem.,* **256**, 8582.

(LeGeros et al., 1983): R.Z. LeGeros and M.S. Tung, "Chemical stability of carbonate and fluoride-containing apatites", *Caries Res.,* **17**, 419.

(LeGeros et al., 1989): R.Z. LeGeros, G. Daculsi, R. Kijowska, and B. Kerebel, "The effect of magnesium on the formation of apatites and whitlockites" in *Magnesium in health and disease,* Y. Itokawa and Y. Durlach, eds. (John Libbey) 11.

(LeGeros et al., 1993): R.Z. LeGeros and J.P. LeGeros, "Dense hydroxyapatite", in *An introduction to bioceramics (Advanced series in ceramics, volume 1)*, L. Hench and J. Wilson, eds. (World Scientific, Singapo) 139.

(López-Macipe et al., 1998): A. López-Macipe, J. Gomez-Morales, R. Rodrigues-Clemente, "The Role of pH in the adsorption of citrate ions on hydroxyapatite", *J. Colloid and Interface Sci.*, **200**, 114.

(Luo et al., 1998): Q. Luo and J.D. Andrade, "Cooperative adsorption of proteins onto hydroxyapatite", *J. Coll. Interface Sci.*, **200**, 104.

(Lyster, 1979): R.L.J. Lyster, "The equilibria of calcium and phosphate ions with the micellar calcium phosphate in cow's milk", *J. Dairy Res.*, **46**, 343.

(Lyster, 1981): R.L.J. Lyster, "Calculation by computer of the individual concentrations in a simulated salt solution. II. An extension of the previous model", *J. Dairy Res.*, **48**, 85.

(McDowell et al., 1971): H. McDowell, W.E. Brown, and J.R. Sutter, "Solubility study of calcium hydrogen phosphate. Ion pair formation", *Inorg. Chem.*, **10**, 1638.

(Madsen et al., 1991): H.E.L. Madsen and F. Christensson, "Precipitation of calcium phosphate at 40°C from neutral solution", *J. Cryst. Growth,* **114**, 613.

(Mahmood et al., 1986): M.B. Mahmood and D.A. Al-Sammerrai, "Thermal decomposition of citric acid", *Thermochim. Acta*, **98**, 119.

(Mann, 1988): S. Mann, "Molecular recognition in biomineralisation", *Nature*, **332**, 119.

(Marković et al., 1993): M. Marković, B.O. Fowler, W.E. Brown, "Octacalcium phosphate carboxylates. 2. Characterization and structural considerations", *J. Chem. Mater.*, **5**, 1406.

(Marshall, 1982): K.R. Marshall, "Industrial isolation of milk proteins: whey proteins", in *Developments in Dairy Chemistry-1,* P.F. Fox, ed. (Applied Science Publishers, London) 339.

(Martell et al., 1992): A.E. Martell and R.J. Motekaitis in *Determination and use of stability constants* (VCH Publishers, New York).

(Meyer et al., 1978): J.L. Meyer and E.D. Eanes, "A thermodynamic analysis of the secondary transition in the spontaneous precipitation of calcium phosphate", *Calcif. Tiss Res.*, **25**, 209.

(Mile et al., 1982): B. Mile, A.T. Vincent, C.R. Wilding, "Studies of the effects of electrolytes on the rates of precipitation of calcium sulphate dihydrate using an ion-selective electrode", *J. Chem. Tech. Biotechnol.*, **32**, 975.

(Moreno et al., 1968): E.C. Moreno, T.M. Gregory and W.E. Brown, "Preparation and solubility of hydroxyapatite", *J. Res. NBS (Phys. and Chem.),* **72A**, 773.

(Moreno et al., 1984): E.C. Moreno, M Kresak, and D.I. Hay, "Adsorption of molecules of biological interest onto hydroxyapatite", *Calcif. Tiss. Int.*, **36**, 48.

(Moulder et al., 1995): J.F. Moulder, W.F. Stickle, P.E. Sobol, and K.D. Bomben in *Handbook of X-ray Photoelectron Spectroscopy* (Physical Electronics, Inc, USA).

(Mucalo et al., 1991): M.R. Mucalo, R.P. Cooney and J.B. Metson, "Platinum and palladium hydrosols: characterisation by X-ray photoelectron spectroscopy and transmission electron microscopy", *Colloids Surfaces,* **60**, 175.

(Mucalo et al., 1995a): M.R. Mucalo, M. Toriyama, Y. Yokogawa, T. Suzuki, Y. Kawamoto, F. Nagata, and K. Nishizawa, "Growth of calcium phosphate on ion-exchange resins pre-saturated with calcium or hydrogenphosphate ions: an SEM/EDX and XPS study", *J. Mat. Sci. Materials in Medicine,* **6**, 409.

(Mucalo et al., 1995b): M.R. Mucalo, Y. Yokogawa, M. Toriyama, T. Suzuki, Y. Kawamoto, F. Nagata, and K. Nishizawa, "Growth of calcium phosphate on surface modified cotton", *J. Mat. Sci. Materials in Medicine,* **6**, 597.

(Mucalo et al., 1995c): M.R. Mucalo, Y. Yokogawa, T. Suzuki, Y. Kawamoto, F. Nagata, and K. Nishizawa, "Further studies of calcium phosphate growth on phosphorylated cotton fibres", *J. Mat. Sci. Materials in Medicine,* **6**, 658.

(Mucalo, 1997): M.R. Mucalo "0771.302 Physical Chemistry Laboratory Manual", The University of Waikato.

(Mullin, 1993): J.W. Mullin in *Crystallization, third edition* (Butterworth - Heinemann, London) 286.

(Mumtaz et al., 1997): H.S. Mumtaz, M.J. Hounslow, N.A. Seaton, W.R. Paterson," Orthkinetic aggregation during precipitation: a computational model for calcium oxalate monohydrate", *J. Trans. I. Chem. E,* **75**, 152.

(Myers, 1987): H.M. Myers," Structure-activity-relationships (SAR) of hydroxyapatite-binding molecules", *Calcif. Tiss. Int.,* **40**, 344.

(Nakamoto, 1986): K Nakamoto in *Infrared and Raman spectra of inorganic and coordination compounds, fourth edition* (Miley - Interscience Publication).

(Nancollas et al., 1974): G.H. Nancollas and B. Tomazic, "Growth of calcium phosphate on hydroxyapatite crystals: effect of supersaturation and ionic medium", *J. Phys. Chem.,* **78**, 2218.

(Nelson et al., 1986): D.G.A. Nelson, H. Salimi, and G.H. Nancollas, "Octacalcium phosphate and apatite overgrowths: A crystallographic and kinetic study", *J. Coll. Interface. Sci.,* **110**, 32.

(Nelson et al., 1989): L.S. Nelson, C. Holt, and D.W.L. Hukins, "Phosphopeptide dissociation from micellar calcium phosphate preparations does not induce crystallinity", *J. Dairy Res.,* **56**, 669.

(Nylen et al., 1963): M.U. Nylen, E.D. Eanes, K.A. Omnell, "Crystal growth in rat enamel", *J. Cell Biol.,* **18**, 109.

(Ostwald, 1897): W. Ostwald, *Z Phys. Chem.,* **22**, 289.

(Pach et al., 1996): L. Pach, S. Duncan, R. Roy, and S. Komareni, "Morphological control of precipitated calcium carbonates and phosphates by colloidal additives", *J. Mat. Sci.,* **31**, 6565.

(Packter, 1974): A. Packter, "The precipitation of calcium sulphate dihydrate from aqueous solution", *J. Crystal Growth*, **21**, 191.

(Pearce, 1997): K N Pearce, NZDRI, Personal communications and unreported results relating to the determination of free calcium in cheese and rennet casein sols using an Orion™ or similar calcium ion-selective electrode.

(Pearce, 1998): K.N. Pearce, NZDRI, Personal communications and unreported results relating to the speciation calculations in dairy products, an outline of procedures and selected acidity, stability and solubility constants for dairy speciation calculations.

(Pearce, 1999): K.N. Pearce, NZDRI, Personal communications and unreported results relating to the log-normal particle size distribution data for the CaP precipitation process from whey permeate.

(Posner et al., 1961): A.S. Posner in *Phosphorus and its compounds, Volume II: Technology, biological functions and applications*, J.R. Van Wazer, ed. (Interscience, New York).

(Posner et al., 1984): A.S. Posner, N.C. Blumenthal, and F. Betts, "Chemistry and structure of precipitated hydroxyapatites", in *Phosphate Minerals*, J.O. Nriagu and P.B. Moore, eds., (Springer, Berlin) 362.

(Pouliot et al., 1991): Y. Pouliot, J. Landry, and J. Giasson, "Induction of calcium phosphate precipitation in sweet whey permeate", *Lait*, **71**, 313.

(Puech et al., 1982): J. Puech, J.C. Heughebaert, and G. Montel, "A new mode of growing apatite crystallites", *J. Cryst. Growth*, **56**, 20.

(Pyne et al., 1960): G.T. Pyne and T.C.A. McGann, "The colloidal phosphate of milk. II Influence of citrate, *J. Dairy Res.*, **27**, 9.

(Reference Manual, Malvern Instruments Ltd, 1996) Manual accompanying the instrument at the University of Waikato, Earth Sciences Department.

(Rhee et al., 2000): S-H Rhee and J. Tanaka, "Hydroxyapatite formation on cellulose cloth induced by citric acid", *J. Material Science: Materials in Medicine*, **11**, 449.

(Rogers, 1998): A.J. Rogers, NZDRI and University of Waikato Chemistry Department, Personal communications and unreported results relating to Malvern data identifying the phase transition of ACP to apatitic calcium phosphate in whey permeates, confocal microscopy data on protein adsorption on ALAMIN™ particles, SLWUF buffer model solution work, IR data relating to the "trapping" of amorphous calcium phosphate precipitate from whey permeate by freeze drying.

(Rowles, 1968): S.L. Rowles, "The precipitation of whitlockite from aqueous solutions", *Bull Soc. Chim. Fr.*, 1797.

(Ruys et al., 1992): A.J. Ruys, K.A. Ziegler, O.C. Standard, A.A. Brandwood, B.K. Milthorpe, and C.C. Sorrell, "Hydroxyapatite sintering phenomena: densification and dehydration behaviour", in *Ceramics, adding the value, Volume 2, Proceedings of the international ceramic conference, Australia, 1992* (Ed., Michael J. Bannister, CSIRO publications, Melbourne).

(Sakae et al., 1978): T. Sakae, H. Nagata, and T. Sudo, "The crystal structure of synthetic calcium phosphate-sulfate hydrate, $Ca_2HPO_4SO_4.4H_2O$ and its relation to brushite and gypsum", *American Mineralogist*, **63**, 520.

(Sarig et al., 1982): S. Sarig and J.W. Mullin, "Effect of trace impurities on calcium sulphate precipitation", *J. Chem. Tech. Biotechnol*, **32**, 525.

(Schmidt, 1982): D.G. Schmidt, "Association of caseins and casein micelle structure". Developments in Dairy Chemistry-1, P.F. Fox, ed. (Applied Science Publishers, Esse), 61.

(Schmidt et al., 1987a): D.G. Schmidt and P. Both, "Studies on the precipitation of calcium phosphate. I. Experiments in the pH range 5.3 to 6.8 at 25°C and 50°C in the absence of additives", *Neth. Milk Dairy J.*, **41**, 105.

(Schmidt et al., 1987b): D.G. Schmidt, P. Both, S. Visser, K.J. Slangen, and P.J. van Rooijen, "Studies on the precipitation of calcium phosphate. II. Experiments in the pH range 7.3 to 5.8 at 25 and 50°C in the presence of additives", *Neth. Milk Dairy J.*, **41**, 121.

(Sime, 1998): J. Sime, "The natural choice", *Chemistry in Britain*, **34**, 26.

(Singer et al., 1988): J.K. Singer, J.B. Anderson, M.T. Ledbetter, I.N. McCave, K.P.N. Jones and R. Wright: "An assessment of analytical techniques for the size analysis of fine-grained sediments", *Jnl. Sed. Petrol.*, **58**, 3, 534.

(Sleigh et al., 1979): R.W. Sleigh, T.B. Sculley, and A.G. McKinlay, "The binding of β -casein to hydroxyapatite: the effect of phosphate content and location", *J. Dairy Res.*, **46**, 337.

(Slosarczyk et al., 1996): A. Slosarczyk, E. Stobierska, Z. Paszkiewicz, and M. Gawlicki, "Calcium phosphate materials prepared from precipitates with various calcium:phosphorus molar ratios", *J. Am. Ceram. Soc.*, **79**, 2539.

(Smith et al., 1998): R. M. Smith, A.M. Martell and R.J. Motekaitis. NIST Critically selected stability constants of metal complexes database, US Department of Commerce, National Institute of Standards and Technology, Gaithersburg, Maryland.

(Tenhuisen et al., 1994): K.S. Tenhuisen and P.W. Brown, "The effects of citric and acetic acids on the formation of calcium deficient hydroxyapatite at 38°C", *J. Mat. Sci., Materials in Medicine,* **5**, 291.

(Termine et al., 1970): J.D. Termine, R.A. Peckauskas, and A.S. Posner, "Calcium phosphate formation *in vitro*. II Effects of environment on amorphous-crystalline transformation", *Arch. oral Biol.*, **140**, 318.

(Termine et al., 1972): J.D. Termine and E.D. Eanes, "Comparative chemistry of amorphous and apatitic calcium phosphate preparations", *Calcif. Tiss. Res.*, **10**, 171.

(Tomazic et al., 1975): B. Tomazic and G.H. Nancollas, "The seeded growth of calcium phosphates. Surface characterisation and the effect of seed material", *J. Coll. Interface Sci.*, **50**, 451.

(Toschev, 1973): S. Toschev, "Homogeneous nucleation" in *Crystal Growth: an introduction*, P. Hartman, ed. (North Holland Publ. Co).

(Tung, 1998): M.S. Tung, "Calcium phosphates: structure, composition, solubility, and stability" in *Calcium phosphates in biological and industrial systems*, Z. Amjad, ed. (Kluwer Academic Publishers Group), 1.

(Ure et al., 1994): A.M. Ure and C.M. Davidson *in Chemical Speciation in the Environment* (Blackie Academic & Professional) 86.

(van Kemenade et al., 1987): M.J.J.M. van Kemenade and P.L. de Bruyn, "A kinetic study of precipitation from supersaturated calcium phosphate solutions", *J. Coll. Interface Sci.*, **118**, 564.

(van Kemenade et al., 1989): M.J.J.M. van Kemenade and P.L. de Bruyn, "The influence of casein on the precipitation of brushite and octacalcium phosphate", *Colloids Surfaces,* **36**, 359.

(Wahlgren et al., 1990): N. M. Wahlgren, P. Dejmek, and T. Drakenberg, *J. Dairy Res.*, **57**, 355.

(Wahlgren et al., 1993): N. M. Wahlgren, P. Dejmek, and T. Drakenberg, "Binding of Mg^{2+} and Ca^{2+} to β-casein-A^1: a multi-nuclear magnetic resonance study", *J. Dairy Res.*, **60**, 65.

(Walstra, 1984): P. Walstra and R. Jenness in *Dairy Chemistry and Physiscs* (John Wiley and Sons, New York).

(Willard et al., 1988): H.W. Willard, L.L. Merritt, J.A. Dean, and F.A. Settle in *Instrumental Methods of Analysis, seventh edition* (Wadsworth Publishing Company, California).

(Wong et al., 1993): A.T-C. Wong and J.T. Czernuszka, "Transformation behaviour of calcium phosphate. 1. Theory and modelling", *Colloids Surfaces A: Physiochem. Eng. Aspects,* **78**, 245.

(Yamamoto et al., 1992): K. Yamamoto, H. Kumagai, and T. Yano, "Effect of alginate on the formation of calcium phosphate", in *Apatite volume 1, Proceedings of the first international symposium on apatite, Mishima, Japan, July 1991* (Japanese association of apatite science, March, 1992) 59.

(Yaminskii et al., 1991): V.V. Yaminskii, K.B. Yaminskaya, A.V. Pertson, E.D. Shchukin, "Correlation of nucleation and coagulation in crystallization from solution", *Colloid Journal of the USSR*, **53**, 77.

APPENDICES

APPENDIX A

Standard Chemical Analyses of Whey Permeate and ALAMIN™ carried out by Commissioning outside Laboratories

Appendix A1

AgResearch
New Zealand Pastoral Agriculture Research Institute Limited
Soil Fertility Service

N Panova / M Mucalo
Chemistry Department
The University of Waikato
Private Bag 3105
HAMILTON

02 February 1999

Dear Client,

LABORATORY REPORT-

Chemical ICP-OES analyses of the sulfuric acid and lactic whey permeate

Commercial sample	P, %	S, %	Mg, %	Ca, %	Na, %	K, %
Sulfuric acid whey permeate	0.07	0.08	0.01	0.12	0.03	0.14
Lactic whey permeate	0.07	<0.01	0.01	0.14	0.04	0.15

Please Note: Method used was a total digestion on all samples as received using Nitric/Perchloric acid mix. Analysis by ICP-OES was used for P, S, Mg, Ca and Ba. Analysis by Atomic Absorption was used for Na and K.

Please do not hesitate to contact us if we can be of further assistance.

Yours faithfully

S J Harrison

ANALYST

99/B/262

While all care is taken with analysis, the Soil Fertility Service will not accept any responsibility for their resulting use. These results have been obtained from the sample "as received" at the laboratory and may not be representative of the bulk material. This report may not be reproduced except in full.

Ruakura Agricultural Centre, Private Bag 3123, Hamilton, Phone (07) 838 5920 or 0800 655 126, Fax (07) 838 5160

Appendix A2

SOIL FERTILITY SERVICE
SCIENCE YOU CAN RELY ON

ENVIRONMENTAL LABORATORY

Chemistry Department
University of Waikato
Private Bag
HAMILTON

Attention: Natalia Panova / Michael Mucalo

18 March, 1998

Dear Client,

LABORATORY REPORT -

The results for your samples received on **10/03/98** are given below.

Sample Description Powders
Your Reference
Our Reference 98/B/2607

		P	Mg	Ca	Na
Alamin (Fraction >150)	%	12.9	0.74	27.0	0.39
Alamin (Fraction <150)	%	13.2	0.84	27.2	0.40
Alamin Finest	%	12.0	0.63	25.0	0.46
Alamin QC 1	%	12.6	0.73	26.0	0.37
Alamin QC 2	%	13.6	0.99	27.3	0.36
Commercial 1996, Kiwi	%	12.2	0.61	25.6	0.47

Please do not hesitate to contact us if we can be of further assistance.

Yours faithfully

S Harrison

ANALYST

98/B/2607

Appendix A3

R J Hill Laboratories Limited

incorporating Analytical Services Laboratory

Address:
1 Clyde Street,
Private Bag 3205,
Hamilton, New Zealand

Telephone:
+64 (7) 858-2000
Facsimile:
+64 (7) 858-2001

Email:
mail@hill-labs.co.nz
Internet:
www.hill-labs.co.nz

Client: *University of Waikato*
Address: *Private Bag 3105, HAMILTON*
Contact: *Natalia Panova*

Laboratory No: *115528*
Date Registered: *16/03/98*
Date Completed: *20/03/98*
Page Number: *1 of 1*

The results for the analyses you requested are as follows:

Sample Type: Biological Materials, Dairy Product

Sample Name	Lab No	Protein*
(1) Alamin Commercial 1996	115528/1	3.4
(2) >150um Alamin	115528/2	6.4
(3) <150um Alamin	115528/3	5.3
(4) Finest Alamin	115528/4	4.5
(5) QC1 Alamin	115528/5	5.7
(6) QC2 Alamin	115528/6	7.9

* This test is not accredited by International Accreditation New Zealand.

Summary of Methods Used and Detection Limits

The following table(s) gives a brief description of the methods used to conduct the analyses for this job.
The detection limits given below are those attainable in a relatively clean matrix. Detection limits may be higher for individual samples should insufficient sample be available, or if the matrix requires that dilutions be performed during analysis.

Substance Type: Biological Materials

Parameter	Method Used	Detection Limit
Protein*	Protein. Calc by Total N x 6.25	0.6 g/100g .

* This test is not accredited by International Accreditation New Zealand.

Analyst's Comments:

These samples were collected by yourselves and analysed as received at the laboratory.

Samples are held at the laboratory for three months (where appropriate) after reporting of results. After this date they are discarded unless otherwise advised by the submitter.

This report must not be reproduced, except in full, without the written consent of the signatory.

R. M. Haslemore

Roger Haslemore B.Sc., Ph.D., MNZIC
Non-Routine Section Manager

APPENDIX B

Chemical Analyses of other Commercial Products:
LACPRODAN (manufactured in Denmark) and
LACTOVAL Q (manufactured by DMV in the Netherlands)

Appendix B1

F A C S I M I L E M E S S A G E

Fax No 04 471 8601

New Zealand Dairy Research Institute

Private Bag 11 029
Palmerston North
New Zealand
Phone +64-6 350 4649
Fax +64-6 356 1476

Lacprodan MM-0519 ex MD Foods

We are still waiting for completion of the mineral analysis (Mg), but below is the proximate and mineral composition of the above sample. Note the high chloride level, indicative of an HCl acid casein whey source. Calcium is lower (20%) than in ALAMIN, and another major difference is the high lactose content (23%).

Component	%,w/w
Protein (TN x 6.38)	4.08
Fat	0.85
Lactose (monohydrate)	23.04
Ash	56.04
Moisture	5.21
Sodium	0.94
Potassium	1.03
Calcium	20.20
Magnesium	
Total P	10.66
Phosphate	28.91
Chloride	1.10
Sulphate	0.06
Citrate	0.43

Particle size distribution is shown in the attached figure. Although the d(0.9) was 47μm, only 10% of the particles were less than 12μm. Thus, it is unlikely that this sample of Lacprodan would have better calcium suspendability properties than ALAMIN. This will be tested next week. We won't do any sensory analysis until we receive the Garuda and the DMV products. Let me know if you require any further information.

Appendix B2

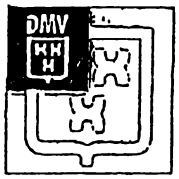

DMV INTERNATIONAL

TYPICAL ANALYSIS
Lactoval Q

	SPECIFICATION	TYPICAL
CHEMICAL		
Minerals - hydrous		92.1 %
Protein (Nx6.38)	Max. 6.0%	1.0%
Moisture		5.5%
Lactose	Max. 3.0%	1.0%
Fat		0.4%
pH (10% dispersion, 20°C)		6.0
MICROBIOLOGICAL		
Standard Plate Count	Max. 10.000/g	1.000/g
Coliforms	neg. in 1g	neg. in 1 g.
Yeasts	Max. 25/g	10/g
Moulds	Max. 25/g	10/g
Sulphite Reducing Clostrida	Max. 10/g	<10/g
E. coli	neg. in 1g	neg. in 1 g
Staphylococcus aureus	neg. in 1g	neg. in 1 g
Salmonella	neg. in 100g	neg. in 100g
NUTRITIONAL PROFILE		**PER 100G**
Energy value		290 kJ
Minerals - anhydrous		83.0 g
Calcium	Min. 21.5	24.5 g
Phosphate		36.2 g
Citric acid		18.6 g
Sodium		2.7 g
Potassium		0.03 g
Magnesium		0.4 g
Chloride		0.6 g
PHYSICAL AND SENSORIC		
Colour		white
Flavour		bland/salty
Odour		neutral
Mouthfeel		sandy
Particle size		95% < 100 µm
Sedimentation in liquids		fast
Bulk density		700 g/l

APPENDIX C

Malvern (*Mastersizer*) Analysis Reports
of the Commercial as Received Lactic ALAMIN™ Powder

Appendix C1

MALVERN INSTRUMENTS MASTERSIZER

Result: Analysis Report

Sample Details

Sample ID: Alamin, QC1
Sample File: NATALIA
Sample Path: C:\SIZERS\DATA\
Sample Notes:

Run Number: 8
Record Number: 55

Measured: Wed, 10 Dec 1997 17:48
Analysed: Wed, 10 Dec 1997 17:48
Result Source: Analysed

System Details

Range Lens: 300RF mm
Presentation: 3PHD
Analysis Model: Polydisperse
Modifications: None

Beam Length: 2.40 mm
[Particle R.I. = (1.5960, 0.1000); Dispersant R.I. = 1.3300]

Sampler: MS17

Obscuration: 18.9 %
Residual: 0.757 %

Result Statistics

Distribution Type: Volume
Mean Diameters:
D [4, 3] = 28.19 um

Concentration = 0.0227 %Vol
D (v, 0.1) = 4.39 um
D [3, 2] = 6.68 um

Density = 1.000 g / cub. cm
D (v, 0.5) = 21.51 um
Span = 2.492E+00

Specific S.A. = 0.8980 sq. m / g
D (v, 0.9) = 58.00 um
Uniformity = 7.970E-01

Size Low (um)	In %	Size High (um)	Under%	Size Low (um)	In %	Size High (um)	Under%
0.05	0.00	0.06	0.00	6.63	2.18	7.72	16.08
0.06	0.00	0.07	0.00	7.72	2.79	9.00	18.86
0.07	0.00	0.08	0.00	9.00	3.52	10.48	22.38
0.08	0.00	0.09	0.00	10.48	4.35	12.21	26.73
0.09	0.01	0.11	0.01	12.21	5.24	14.22	31.97
0.11	0.01	0.13	0.02	14.22	6.09	16.57	38.06
0.13	0.02	0.15	0.04	16.57	6.81	19.31	44.87
0.15	0.04	0.17	0.08	19.31	7.29	22.49	52.16
0.17	0.06	0.20	0.14	22.49	7.47	26.20	59.63
0.20	0.09	0.23	0.23	26.20	7.36	30.53	66.99
0.23	0.13	0.27	0.36	30.53	7.08	35.56	74.06
0.27	0.17	0.31	0.53	35.56	6.14	41.43	80.20
0.31	0.20	0.36	0.73	41.43	5.07	48.27	85.27
0.36	0.22	0.42	0.95	48.27	4.03	56.23	89.30
0.42	0.25	0.49	1.20	56.23	3.09	65.51	92.39
0.49	0.29	0.58	1.49	65.51	2.30	76.32	94.69
0.58	0.33	0.67	1.82	76.32	1.69	88.91	96.38
0.67	0.39	0.78	2.21	88.91	1.24	103.58	97.62
0.78	0.45	0.91	2.66	103.58	0.92	120.67	98.54
0.91	0.51	1.06	3.17	120.67	0.70	140.58	99.24
1.06	0.57	1.24	3.74	140.58	0.48	163.77	99.72
1.24	0.62	1.44	4.36	163.77	0.25	190.80	99.97
1.44	0.66	1.68	5.02	190.80	0.03	222.28	100.00
1.68	0.68	1.95	5.70	222.28	0.00	258.95	100.00
1.95	0.70	2.28	6.40	258.95	0.00	301.68	100.00
2.28	0.73	2.65	7.13	301.68	0.00	351.46	100.00
2.65	0.77	3.09	7.90	351.46	0.00	409.45	100.00
3.09	0.84	3.60	8.74	409.45	0.00	477.01	100.00
3.60	0.95	4.19	9.69	477.01	0.00	555.71	100.00
4.19	1.12	4.88	10.81	555.71	0.00	647.41	100.00
4.88	1.37	5.69	12.18	647.41	0.00	754.23	100.00
5.69	1.72	6.63	13.89	754.23	0.00	878.67	100.00

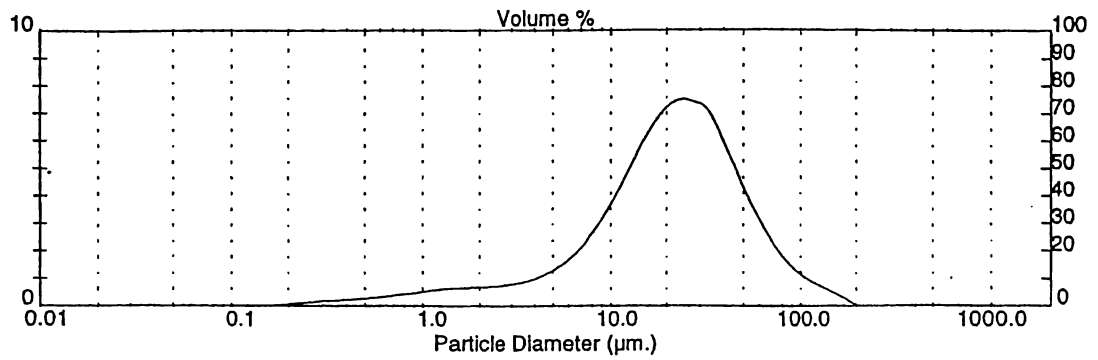

Appendix C2

MALVERN INSTRUMENTS MASTERSIZER

Result: Analysis Report

Sample Details

Sample ID: 12
Sample File: NATALIA
Sample Path: C:\SIZERS\DATA\
Sample Notes: ALAMIN < 150

Run Number: 19
Record Number: 24

Measured: Thu, 20 Nov 1997 16:47
Analysed: Wed, 26 Nov 1997 08:32
Result Source: Analysed

System Details

Range Lens: 300RF mm
Presentation: 3PHD
Analysis Model: Polydisperse
Modifications: None

Beam Length: 2.40 mm
[Particle R.I. = (1.5960, 0.1000); Dispersant R.I. = 1.3300]

Sampler: MS17

Obscuration: 20.7 %
Residual: 0.621 %

Result Statistics

Distribution Type: Volume
Mean Diameters:
D [4, 3] = 29.95 um

Concentration = 0.0288 %Vol
D (v, 0.1) = 6.26 um
D [3, 2] = 7.44 um

Density = 2.650 g / cub. cm
D (v, 0.5) = 23.66 um
Span = 2.304E+00

Specific S.A. = 0.3041 sq. m / g
D (v, 0.9) = 60.76 um
Uniformity = 7.279E-01

Size Low (um)	In %	Size High (um)	Under%
0.05	0.00	0.06	0.00
0.06	0.00	0.07	0.00
0.07	0.00	0.08	0.00
0.08	0.00	0.09	0.00
0.09	0.00	0.11	0.01
0.11	0.01	0.13	0.02
0.13	0.02	0.15	0.04
0.15	0.03	0.17	0.07
0.17	0.05	0.20	0.12
0.20	0.09	0.23	0.21
0.23	0.13	0.27	0.34
0.27	0.17	0.31	0.51
0.31	0.20	0.36	0.71
0.36	0.22	0.42	0.93
0.42	0.25	0.49	1.19
0.49	0.29	0.58	1.48
0.58	0.32	0.67	1.80
0.67	0.36	0.78	2.16
0.78	0.40	0.91	2.56
0.91	0.43	1.06	2.99
1.06	0.46	1.24	3.45
1.24	0.47	1.44	3.91
1.44	0.46	1.68	4.38
1.68	0.45	1.95	4.83
1.95	0.44	2.28	5.27
2.28	0.45	2.65	5.71
2.65	0.47	3.09	6.19
3.09	0.53	3.60	6.72
3.60	0.63	4.19	7.35
4.19	0.80	4.88	8.14
4.88	1.04	5.69	9.18
5.69	1.39	6.63	10.57
6.63	1.85	7.72	12.42
7.72	2.46	9.00	14.88
9.00	3.21	10.48	18.09
10.48	4.08	12.21	22.16
12.21	5.03	14.22	27.19
14.22	5.98	16.57	33.17
16.57	6.82	19.31	39.99
19.31	7.45	22.49	47.44
22.49	7.79	26.20	55.23
26.20	7.83	30.53	63.06
30.53	7.68	35.56	70.74
35.56	6.82	41.43	77.56
41.43	5.77	48.27	83.33
48.27	4.69	56.23	88.02
56.23	3.66	65.51	91.68
65.51	2.75	76.32	94.44
76.32	2.00	88.91	96.44
88.91	1.42	103.58	97.85
103.58	0.99	120.67	98.84
120.67	0.69	140.58	99.53
140.58	0.39	163.77	99.92
163.77	0.08	190.80	100.00
190.80	0.00	222.28	100.00
222.28	0.00	258.95	100.00
258.95	0.00	301.68	100.00
301.68	0.00	351.46	100.00
351.46	0.00	409.45	100.00
409.45	0.00	477.01	100.00
477.01	0.00	555.71	100.00
555.71	0.00	647.41	100.00
647.41	0.00	754.23	100.00
754.23	0.00	878.67	100.00

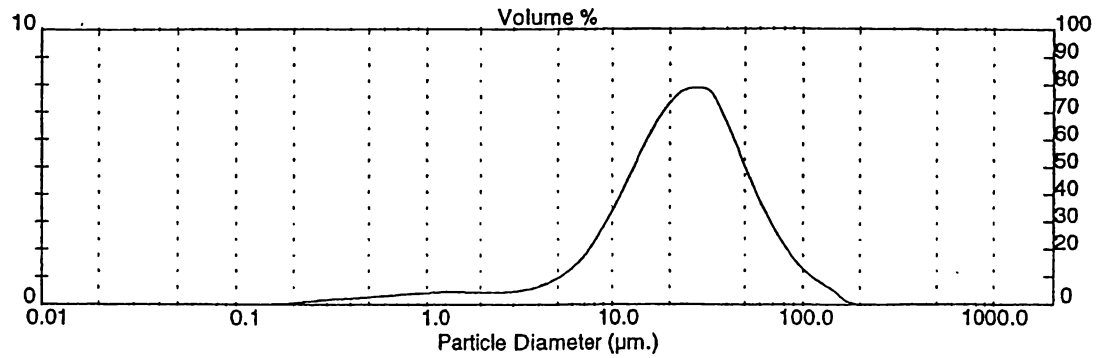

Appendix C3

MALVERN INSTRUMENTS MASTERSIZER

Result: Analysis Report

Sample Details

Sample ID: 13
Sample File: NATALIA
Sample Path: C:\SIZERS\DATA\
Sample Notes: ALAMIN > 150

Run Number: 20
Record Number: 25

Measured: Thu, 20 Nov 1997 16:56
Analysed: Wed, 26 Nov 1997 08:32
Result Source: Analysed

System Details

Range Lens: 300RF mm
Presentation: 3PHD
Analysis Model: Polydisperse
Modifications: None

Beam Length: 2.40 mm
[Particle R.I. = (1.5960, 0.1000); Dispersant R.I. = 1.3300]

Sampler: MS17

Obscuration: 18.3 %
Residual: 1.233 %

Result Statistics

Distribution Type: Volume
Mean Diameters:
D [4, 3] = 188.94 um

Concentration = 0.0752 %Vol
D (v, 0.1) = 54.09 um
D [3, 2] = 30.15 um

Density = 2.650 g / cub. cm
D (v, 0.5) = 193.44 um
Span = 1.236E+00

Specific S.A. = 0.0751 sq. m / g
D (v, 0.9) = 293.14 um
Uniformity = 3.398E-01

Size Low (um)	In %	Size High (um)	Under%	Size Low (um)	In %	Size High (um)	Under%
0.05	0.00	0.06	0.00	6.63	0.46	7.72	6.32
0.06	0.00	0.07	0.00	7.72	0.40	9.00	6.72
0.07	0.00	0.08	0.00	9.00	0.36	10.48	7.08
0.08	0.00	0.09	0.00	10.48	0.33	12.21	7.41
0.09	0.00	0.11	0.00	12.21	0.33	14.22	7.75
0.11	0.00	0.13	0.00	14.22	0.35	16.57	8.10
0.13	0.00	0.15	0.00	16.57	0.38	19.31	8.48
0.15	0.00	0.17	0.00	19.31	0.39	22.49	8.87
0.17	0.00	0.20	0.00	22.49	0.37	26.20	9.24
0.20	0.00	0.23	0.00	26.20	0.32	30.53	9.55
0.23	0.00	0.27	0.00	30.53	0.23	35.56	9.79
0.27	0.00	0.31	0.00	35.56	0.15	41.43	9.93
0.31	0.00	0.36	0.00	41.43	0.04	48.27	9.97
0.36	0.00	0.42	0.00	48.27	0.04	56.23	10.02
0.42	0.00	0.49	0.00	56.23	0.12	65.51	10.13
0.49	0.00	0.58	0.00	65.51	0.31	76.32	10.45
0.58	0.06	0.67	0.06	76.32	0.73	88.91	11.18
0.67	0.08	0.78	0.14	88.91	1.58	103.58	12.76
0.78	0.11	0.91	0.25	103.58	3.28	120.67	16.04
0.91	0.15	1.06	0.40	120.67	6.39	140.58	22.44
1.06	0.20	1.24	0.60	140.58	10.85	163.77	33.28
1.24	0.27	1.44	0.87	163.77	15.16	190.80	48.44
1.44	0.33	1.68	1.20	190.80	17.65	222.28	66.09
1.68	0.38	1.95	1.59	222.28	14.90	258.95	81.00
1.95	0.45	2.28	2.03	258.95	10.55	301.68	91.54
2.28	0.49	2.65	2.52	301.68	6.17	351.46	97.71
2.65	0.54	3.09	3.06	351.46	2.29	409.45	100.00
3.09	0.57	3.60	3.63	409.45	0.00	477.01	100.00
3.60	0.58	4.19	4.21	477.01	0.00	555.71	100.00
4.19	0.58	4.88	4.79	555.71	0.00	647.41	100.00
4.88	0.55	5.69	5.35	647.41	0.00	754.23	100.00
5.69	0.51	6.63	5.86	754.23	0.00	878.67	100.00

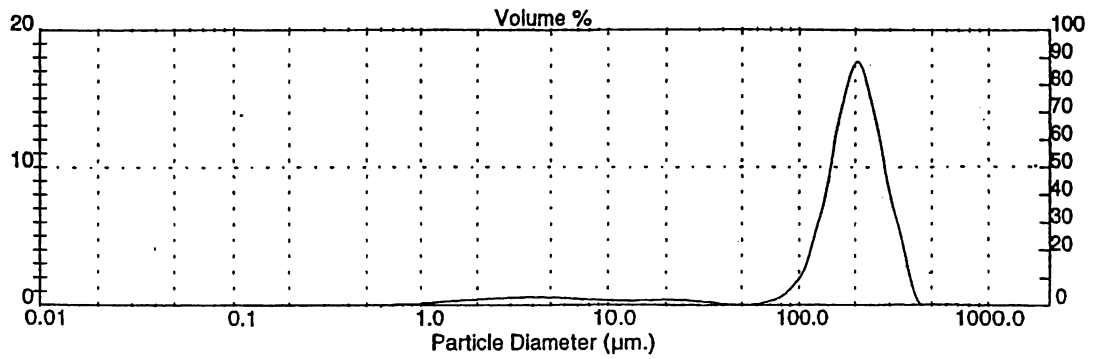

Appendix C4

MALVERN INSTRUMENTS MASTERSIZER

Result: Analysis Report

Sample Details

Sample ID: 14
Sample File: NATALIA
Sample Path: C:\SIZERS\DATA\
Sample Notes: ALAMIN FINEST

Run Number: 21
Record Number: 26

Measured: Thu, 20 Nov 1997 17:02
Analysed: Wed, 26 Nov 1997 08:32
Result Source: Analysed

System Details

Range Lens: 300RF mm
Presentation: 3PHD
Analysis Model: Polydisperse
Modifications: None

Beam Length: 2.40 mm
[Particle R.I. = (1.5960, 0.1000); Dispersant R.I. = 1.3300]

Sampler: MS17

Obscuration: 27.1 %
Residual: 0.254 %

Result Statistics

Distribution Type: Volume
Mean Diameters:
D [4, 3] = 5.23 um

Concentration = 0.0111 %Vol
D (v, 0.1) = 1.45 um
D [3, 2] = 2.95 um

Density = 2.650 g / cub. cm
D (v, 0.5) = 3.79 um
Span = 2.491E+00

Specific S.A. = 0.7681 sq. m / g
D (v, 0.9) = 10.90 um
Uniformity = 7.802E-01

Size Low (um)	In %	Size High (um)	Under%
0.05	0.00	0.06	0.00
0.06	0.00	0.07	0.00
0.07	0.00	0.08	0.00
0.08	0.00	0.09	0.00
0.09	0.00	0.11	0.00
0.11	0.00	0.13	0.00
0.13	0.00	0.15	0.00
0.15	0.00	0.17	0.00
0.17	0.00	0.20	0.00
0.20	0.00	0.23	0.00
0.23	0.00	0.27	0.00
0.27	0.00	0.31	0.00
0.31	0.00	0.36	0.00
0.36	0.00	0.42	0.00
0.42	0.00	0.49	0.00
0.49	0.09	0.58	0.09
0.58	0.28	0.67	0.37
0.67	0.58	0.78	0.95
0.78	1.13	0.91	2.08
0.91	1.78	1.06	3.86
1.06	2.55	1.24	6.41
1.24	3.40	1.44	9.81
1.44	4.32	1.68	14.13
1.68	5.26	1.95	19.39
1.95	6.11	2.28	25.50
2.28	6.86	2.65	32.36
2.65	7.37	3.09	39.73
3.09	7.63	3.60	47.36
3.60	7.60	4.19	54.97
4.19	7.30	4.88	62.27
4.88	6.82	5.69	69.08
5.69	6.24	6.63	75.32
6.63	5.41	7.72	80.73
7.72	4.59	9.00	85.32
9.00	3.83	10.48	89.14
10.48	3.12	12.21	92.27
12.21	2.49	14.22	94.75
14.22	1.90	16.57	96.66
16.57	1.39	19.31	98.05
19.31	0.95	22.49	98.99
22.49	0.60	26.20	99.59
26.20	0.34	30.53	99.93
30.53	0.07	35.56	100.00
35.56	0.00	41.43	100.00
41.43	0.00	48.27	100.00
48.27	0.00	56.23	100.00
56.23	0.00	65.51	100.00
65.51	0.00	76.32	100.00
76.32	0.00	88.91	100.00
88.91	0.00	103.58	100.00
103.58	0.00	120.67	100.00
120.67	0.00	140.58	100.00
140.58	0.00	163.77	100.00
163.77	0.00	190.80	100.00
190.80	0.00	222.28	100.00
222.28	0.00	258.95	100.00
258.95	0.00	301.68	100.00
301.68	0.00	351.46	100.00
351.46	0.00	409.45	100.00
409.45	0.00	477.01	100.00
477.01	0.00	555.71	100.00
555.71	0.00	647.41	100.00
647.41	0.00	754.23	100.00
754.23	0.00	878.67	100.00

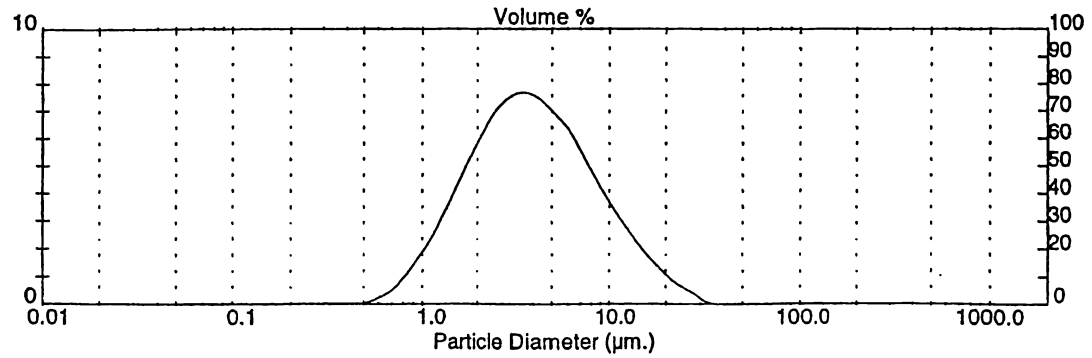

Appendix C5

MALVERN INSTRUMENTS MASTERSIZER

Result: Analysis Report

Sample Details

Sample ID: 16
Sample File: NATALIA
Sample Path: C:\SIZERS\DATA\
Sample Notes: ALAMIN QC2 (HIGH ASH)

Run Number: 23
Record Number: 53

Measured: Thu, 20 Nov 1997 17:14
Analysed: Wed, 26 Nov 1997 08:32
Result Source: Analysed

System Details

Range Lens: 300RF mm
Presentation: 3PHD
Analysis Model: Polydisperse
Modifications: None

Beam Length: 2.40 mm
[Particle R.I. = (1.5960, 0.1000); Dispersant R.I. = 1.3300]

Sampler: MS17

Obscuration: 19.3 %
Residual: 0.704 %

Result Statistics

Distribution Type: Volume
Mean Diameters:
D [4, 3] = 18.49 um

Concentration = 0.0201 %Vol
D (v, 0.1) = 4.12 um
D [3, 2] = 6.03 um

Density = 2.650 g / cub. cm
D (v, 0.5) = 16.38 um
Span = 1.890E+00

Specific S.A. = 0.3758 sq. m / g
D (v, 0.9) = 35.07 um
Uniformity = 5.800E-01

Size Low (um)	In %	Size High (um)	Under%	Size Low (um)	In %	Size High (um)	Under%
0.05	0.00	0.06	0.00	6.63	3.14	7.72	18.40
0.06	0.00	0.07	0.00	7.72	4.18	9.00	22.57
0.07	0.00	0.08	0.00	9.00	5.35	10.48	27.93
0.08	0.00	0.09	0.00	10.48	6.57	12.21	34.50
0.09	0.00	0.11	0.00	12.21	7.67	14.22	42.16
0.11	0.00	0.13	0.01	14.22	8.51	16.57	50.68
0.13	0.01	0.15	0.02	16.57	9.06	19.31	59.73
0.15	0.02	0.17	0.04	19.31	9.37	22.49	69.10
0.17	0.04	0.20	0.08	22.49	8.52	26.20	77.62
0.20	0.07	0.23	0.15	26.20	7.20	30.53	84.82
0.23	0.12	0.27	0.27	30.53	5.64	35.56	90.45
0.27	0.17	0.31	0.44	35.56	4.07	41.43	94.53
0.31	0.22	0.36	0.66	41.43	2.69	48.27	97.22
0.36	0.26	0.42	0.91	48.27	1.60	56.23	98.82
0.42	0.31	0.49	1.23	56.23	0.83	65.51	99.65
0.49	0.38	0.58	1.61	65.51	0.35	76.32	100.00
0.58	0.43	0.67	2.04	76.32	0.00	88.91	100.00
0.67	0.51	0.78	2.55	88.91	0.00	103.58	100.00
0.78	0.56	0.91	3.11	103.58	0.00	120.67	100.00
0.91	0.62	1.06	3.73	120.67	0.00	140.58	100.00
1.06	0.67	1.24	4.40	140.58	0.00	163.77	100.00
1.24	0.70	1.44	5.10	163.77	0.00	190.80	100.00
1.44	0.70	1.68	5.80	190.80	0.00	222.28	100.00
1.68	0.68	1.95	6.48	222.28	0.00	258.95	100.00
1.95	0.66	2.28	7.14	258.95	0.00	301.68	100.00
2.28	0.65	2.65	7.79	301.68	0.00	351.46	100.00
2.65	0.67	3.09	8.46	351.46	0.00	409.45	100.00
3.09	0.75	3.60	9.20	409.45	0.00	477.01	100.00
3.60	0.91	4.19	10.12	477.01	0.00	555.71	100.00
4.19	1.20	4.88	11.32	555.71	0.00	647.41	100.00
4.88	1.65	5.69	12.97	647.41	0.00	754.23	100.00
5.69	2.29	6.63	15.26	754.23	0.00	878.67	100.00

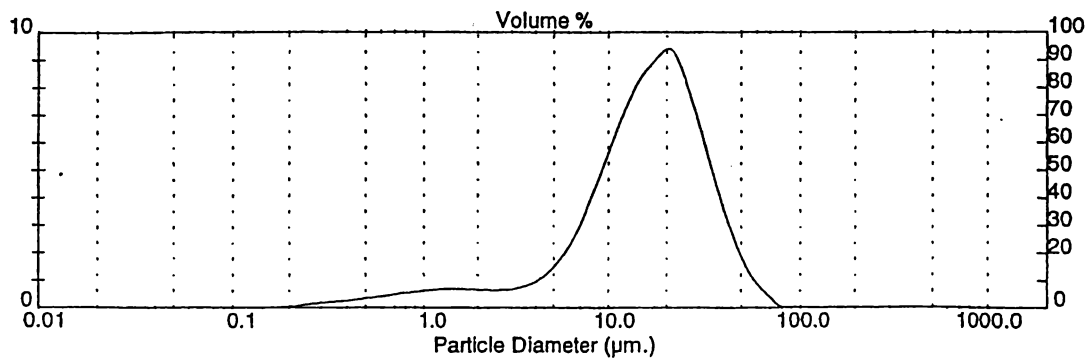

REVIEWS, CONFERENCES ABSTRACTS AND PUBLICATIONS ARISING FROM THE WORK

1. The Influence of Agitation Rate on the Particle Size of Calcium Phosphate Precipitated from Supersaturated Solutions. - N.N. Panova, M.R. Mucalo. - Annual New Zealand Engineering and Technology Postgraduate Student Conference. Massey University, Palmerston North, 26 & 27 November 1998, 139.

2. Phase Transformation of Calcium Phosphate Derived from Supersaturated Solutions. - N.N. Panova, M.R. Mucalo. - Annual New Zealand Engineering and Technology Postgraduate Student Conference. Massey University, Palmerston North, 26 & 27 November 1998, 55.

3. Review of the Chemistry of Calcium Phosphate Precipitation with regard to the Production of ALAMIN™ in the New Zealand Dairy Industry. - M.R. Mucalo, N.N. Panova, A.J. Rogers. - Confidential to the New Zealand Dairy Industry, 1998. -128 p. *On Campus* staff newsletter of the University of Waikato, Staff publication Supplement, October 1998, **12**(8), 6.

4. Formation and Flocculation of Calcium Phosphate Phases Precipitates from Heated Whey Permeates.- N.N. Panova, M.R. Mucalo, K.N. Pearce.- 21st Australian Colloid & Surface Chemistry Student Conference hosted by the University of Newcastle in Morpeth on the 27 September –1 October 1999, 32.

5. A Better Understanding of ALAMIN Properties and the ALAMIN Process. - A.J. Rogers, K.N. Pearce, M. R. Mucalo, N.N. Panova. - Confidential Report NZDRI-1999. -58 p.

6. The Effect of the Multicomponent Equilibria on the Precipitation of Calcium Phosphate from Simulated Whey Permeate Solutions. - N.N. Panova, M.R. Mucalo, A.J. Rogers, K.N. Pearce.- New Zealand Institute of Chemistry Conference 1999 hosted by the Victoria University of Wellington, 21-24 November 1999, IA7.

7. A Chemical Speciation Calculation Study on the Industrial Precipitation Process of ALAMIN™ from Sulfuric Acid Whey Permeate at Anchor Products Edgecumbe (APE).- N.N. Panova.- Industrial Report, April 1999. - 57 p.